Biosourced Coating Systems for Metallic Substrates

Lydia Alexandra Heinrich

N°d'ordre NNT : 2017LYSE1004

THESE de DOCTORAT DE L'UNIVERSITE DE LYON
opérée au sein de
l'Université Claude Bernard Lyon 1

Ecole Doctorale N° 206
Chimie, Procédés, Environnement

Spécialité de doctorat : Chimie
Discipline : Chimie verte

Soutenue à huis clos le 23/01/2017, par :
Lydia Alexandra Heinrich

Biosourced Coating Systems for Metallic Substrates

Devant le jury composé de :

Mme PINEL Catherine	Directrice de Recherche	CNRS Lyon	Présidente
M. CAILLOL Sylvain	Chargé de Recherche – HDR	CNRS Montpellier	Rapporteur
Mme DRAYE Micheline	Professeure des Universités	Université Savoie Mont Blanc	Rapporteur
Mme ROQUETA Corinne	Chercheure	ARKEMA Verneuil en Halatte	Examinatrice
M. ANDRIOLETTI Bruno	Professeur des Universités	Université Lyon 1	Directeur de thèse
Mme GOUX-HENRY Catherine	Maitre de Conférences	Université Lyon 1	Encadrante
M. COGORDAN Frank	Ingénieur	ARKEMA Verneuil en Halatte	Invité

UNIVERSITE CLAUDE BERNARD - LYON 1

Président de l'Université	**M. le Professeur Frédéric FLEURY**
Président du Conseil Académique	M. le Professeur Hamda BEN HADID
Vice-président du Conseil d'Administration	M. le Professeur Didier REVEL
Vice-président du Conseil Formation et Vie Universitaire	M. le Professeur Philippe CHEVALIER
Vice-président de la Commission Recherche	M. Fabrice VALLÉE
Directrice Générale des Services	Mme Dominique MARCHAND

COMPOSANTES SANTE

Faculté de Médecine Lyon Est – Claude Bernard	Directeur : M. le Professeur G.RODE
Faculté de Médecine et de Maïeutique Lyon Sud – Charles Mérieux	Directeur : Mme la Professeure C. BURILLON
	Directeur : M. le Professeur D. BOURGEOIS
Faculté d'Odontologie	Directeur : Mme la Professeure C. VINCIGUERRA
Institut des Sciences Pharmaceutiques et Biologiques	Directeur : M. X. PERROT
Institut des Sciences et Techniques de la Réadaptation	Directeur : Mme la Professeure A-M. SCHOTT
Département de formation et Centre de Recherche en Biologie Humaine	

COMPOSANTES ET DEPARTEMENTS DE SCIENCES ET TECHNOLOGIE

Faculté des Sciences et Technologies	Directeur : M. F. DE MARCHI
Département Biologie	Directeur : M. le Professeur F. THEVENARD
Département Chimie Biochimie	Directeur : Mme C. FELIX
Département GEP	Directeur : M. Hassan HAMMOURI
Département Informatique	Directeur : M. le Professeur S. AKKOUCHE
Département Mathématiques	Directeur : M. le Professeur G. TOMANOV
Département Mécanique	Directeur : M. le Professeur H. BEN HADID
Département Physique	Directeur : M. le Professeur J-C PLENET
UFR Sciences et Techniques des Activités Physiques et Sportives	Directeur : M. Y.VANPOULLE
Observatoire des Sciences de l'Univers de Lyon	Directeur : M. B. GUIDERDONI
Polytech Lyon	Directeur : M. le Professeur E.PERRIN
Ecole Supérieure de Chimie Physique Electronique	Directeur : M. G. PIGNAULT
Institut Universitaire de Technologie de Lyon 1	Directeur : M. le Professeur C. VITON
Ecole Supérieure du Professorat et de l'Education	Directeur : M. le Professeur A. MOUGNIOTTE
Institut de Science Financière et d'Assurances	Directeur : M. N. LEBOISNE

Biosourced Coating Systems for Metallic Substrates - Abstract

Moving away from petroleum and towards biobased materials not only leads to greater sustainability and lower dependence on diminishing fossil resources, but can also catalyse the discovery of new properties. Aliphatic polyesters based on renewable resources have already started to replace traditional products. Within the Sorago project, a fully biobased resin for interior coil coatings has recently been proposed on the market (Estetic® Bio Air, Arcelor Mittal).

In order to extend the possible use of the biobased product to exterior applications, an improvement of its resistance to humidity and UV radiation is crucial. This presents two challenges: The limited availability of monomers which provide rigidity in the resin structure and the relationship between the resin composition and its weatherability.

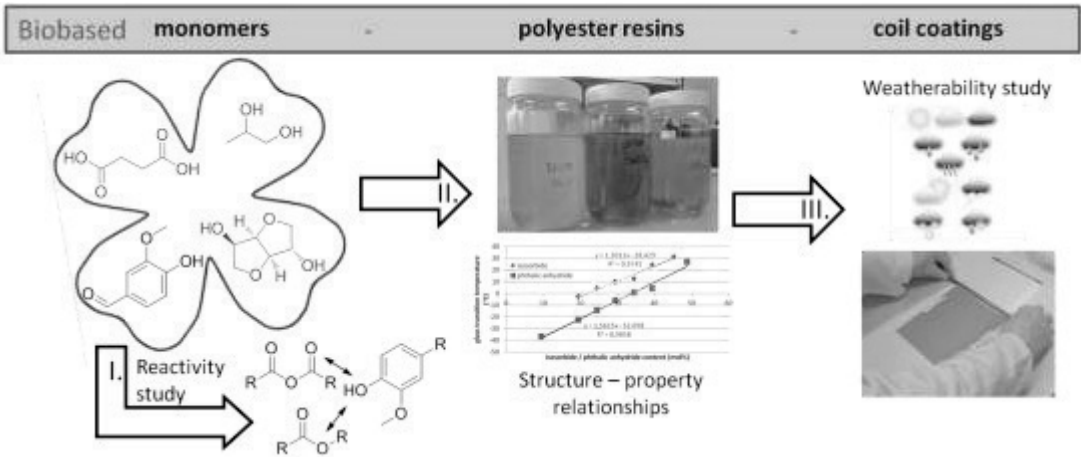

Scheme 1: Biobased Coating Systems for Metallic Substrates

Vanillin was chosen as a possible extension to the range of rigid, biobased monomers for polyesterification reactions. The transformation of its aldehyde and its reactivity was studied in terms of catalytic activation and through a series of copolymerisations which revealed the influence of the reaction conditions on the composition of the product.

A structure-property relationship concerning the coating glass transition temperature and visco-elastic behaviour of the coating was furthermore established for the renewable monomers isosorbide, 1,2-propanediol, 1,3-propanediol, glycerol, succinic acid and sebacic acid, and contrasted with phthalic anhydride. Series of prototypes with a wide variety of properties were then subjected to accelerated weathering tests. Their degradation was followed directly by gloss retention and different mechanisms were revealed using FTIR, µ-hardness and film thickness measurements.

While the performance of the biobased coating was subpar, no evidence linking its degradation to the presence of renewable monomers was found, suggesting that the creation of a sufficiently durable and renewable exterior coating will be possible.

Revêtements biosourcés pour substrats métalliques – résumé de thèse en français

Dans le cadre de l'étude de synthèse de revêtements biosourcés sur des surfaces métalliques, le remplacement de monomères d'origine pétrosourcée par des analogues biosourcés est un nouvel enjeu. Cela permettra de diminuer la dépendance aux ressources fossiles et de découvrir de nouvelles caractéristiques et propriétés pour ces nouveaux monomères. Les polyesters aliphatiques biosourcés ont déjà partiellement remplacé certains produits traditionnels. Dans le contexte du projet Sorago, une résine entièrement biosourcée pour les revêtements de prélaquage des produits intérieurs a déjà été introduite sur le marché (Estetic® bio Air, Arcelor Mittal).

Pour permettre l'utilisation de ces types de résines dans des applications extérieures, la résistance à la lumière UV et à l'humidité sont à améliorer. Cela pose deux problèmes : Une disponibilité limitée de monomères pouvant introduire de la rigidité dans la résine et la relation entre la structure de la résine et sa dégradation.

Dans une première partie, représentée dans le Scheme 2 en bas, la vanilline a été choisie comme synthon : monomère rigide biosourcé. C'est un rare exemple de composé aromatique qui est déjà disponible à grande échelle à partir des ressources renouvelables. En plus, ce composé possède une fonction phénol qui peut réagir pour former un ester.

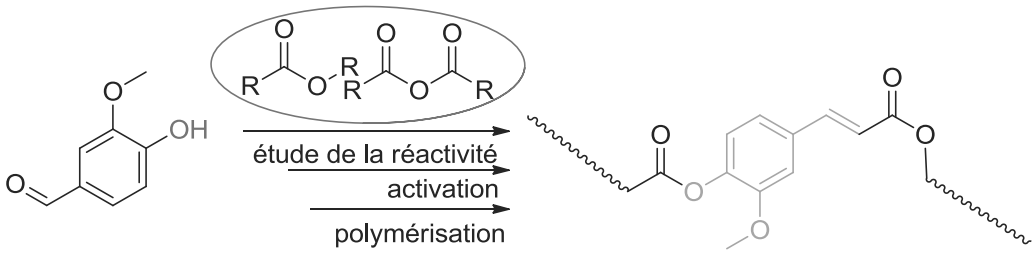

Scheme 2: Stratégie pour la création des polymères aromatiques biosourcées

Nous avons étudié la réactivité du phénol en présence de nombreux catalyseurs et avec des substrats différents comme les anhydrides et les esters en utilisant une « réaction modèle » avec le guaiacol. Malgré la présence du groupement methoxy en position *ortho*, qui diminue l'accessibilité du groupement hydroxy par rapport à celle des phénols, l'estérification a été réalisée en utilisant des anhydrides.

De plus, la vanilline a été transformée par la réaction de Perkin et hydrogénée en suivant l'exemple de Mialon *et al.* pour donner de l'acide dihydroferulique acétylé.[1] La polymérisation de ce produit ainsi que celle de l'acide ferulique, qui peut être obtenu des plantes, a été réalisée avec des co-monomères différents et avec des conditions variées. Les produits ont été ensuite caractérisés grâce à la chromatographie d'exclusion stérique, spectroscopie RMN, spectrométrie de masse et

calorimétrie différentielle à balayage pour donner des informations sur le comportement des monomères lors de la formation de la résine et sur les propriétés qui peuvent être obtenues pour ce type de résine.

Dans la deuxième partie du projet, une résine biosourcée pour des produits intérieurs proposée par Arkema a été modifiée afin d'établir une relation structure-propriétés concernant la température de la transition vitreuse et la viscoélasticité.

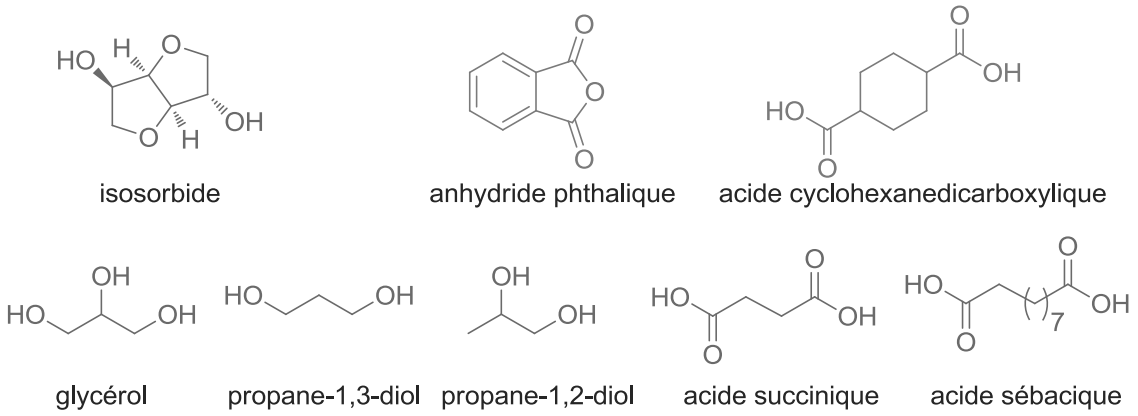

Scheme 3: Monomères utilisés pour la synthèse des résines

Les quantités de plusieurs monomères biosourcées utilisées, montrés en Scheme 3 en haute en vert et de deux monomères petrosourcées, montrés en rouge, ont été modifiées systématiquement pour élucider leurs effets sur les propriétés de la résine, et pour définir des possibilités de composition de résines entièrement et partiellement biosourcées. Une relation linéaire entre la quantité des monomères rigides et la température de transition vitreuse de la résine a été par exemple mis en évidence, montrée en figure 1 en bas.

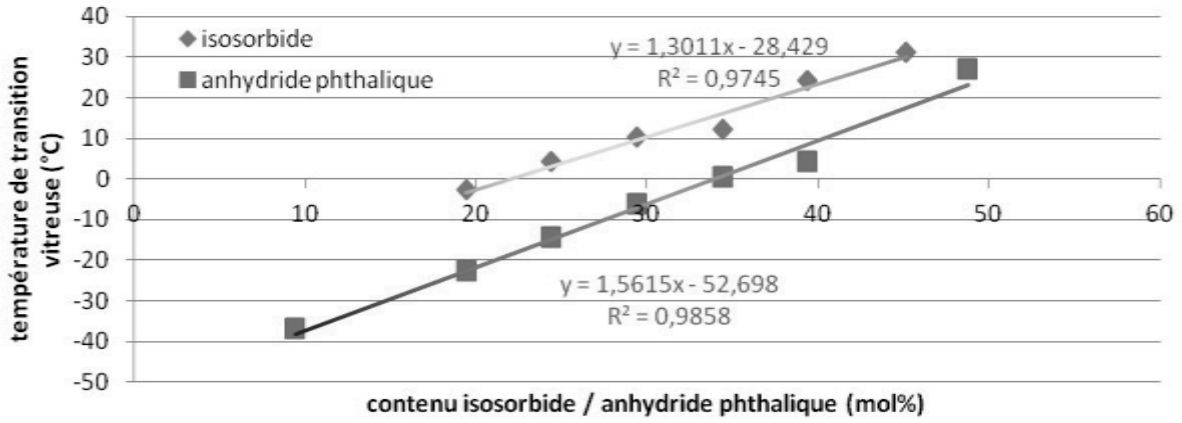

Figure 1: La dependence de la température transition vitreuse au contenu d'isosorbide et anhydride phthalique

Plusieurs séries de prototypes ont été ensuite introduits dans des formules de peinture et transformés en revêtements par la cuisson avec une résine mélamine formaldéhyde. L'analyse

mécanique dynamique et un test de microdureté ont été utilisés pour définir la densité de la réticulation et le comportement viscoélastique des films réticulés formés.

Finalement, les prototypes ont été soumis à un test de vieillissement rapide dans lequel ils étaient exposés à la lumière UV, à des températures élevées et à l'humidité. Leur dégradation a été suivie sur la base de leur rétention de brillance, par FTIR, par des tests de µ-dureté et d'épaisseur des films et en microscopie optique, montré en figure 2 en bas.

Figure 2: Image microscopique des revêtements exposés pour 2000 h

Les formules des résines ont été modifiées pour comprendre l'influence de chaque monomère sur le vieillissement, et pour ensuite être capable de proposer une résine compatible avec les exigences d'un revêtement pour l'extérieur.

Concernant le mécanisme de dégradation, une combinaison de perte des bouts de chaines par scission hydrolytique des liaisons, avec la formation de nouvelles connections entre chaines grâce aux radicaux formés a été observée. La présence d'isosorbide semble accélérer le premier mécanisme, tandis que la présence d'anhydride phtalique favorise le deuxième.

Malheureusement, malgré la synthèse variée de résines, aucun des prototypes examinés biosourcés ne semble avoir une résistance à la dégradation proche de celle dite standard. Par contre, la performance des différents prototypes biosourcés en rétention de brillance après 2000 h de vieillissement était assez proche. Un facteur structurel semble déterminant dans la dégradation des résines et non pas seulement un facteur concernant leurs compositions. Aucune corrélation entre la dégradation élevée et la présence de monomère biosourcé utilisé n'a été observée.

Pour ces raisons, la création d'une résine biosourcée et adaptée pour l'extérieur sera possible si la structure du revêtement sera relativement proche à celle du standard utilisé en ce moment.

1 Designing exterior coil coating resins based on biosources within the Sorago project

What does it take to preserve the environment while making competitive products? Uniting two research universities and five industrial partners, the Sorago project aims to produce a realistic and applicable solution for the French coating industry. Coil coating, with a global market of 940 kilotons (2014), is a field in which more sustainable products can make a large difference.[2]

This thesis explores the design of a polyester resin based on renewable resources for use in a melamine crosslinked coil coating film with sufficient weathering resistance for outdoor applications within the Sorago project. That includes both the synthesis of the resin from new monomers as well as testing of the applied film to establish a structure-weatherability relationship.

After giving a brief overview of the Sorago project objectives as well as the different components of a coil coating paint, and the requirements on the formulation, the current choice of available biobased monomers and their uses in polyester products will be presented. The available knowledge of factors that can influence the deterioration of coatings due to exterior influences will then be discussed.

Different strategies of the incorporation of vanillin in a polyester, which has been unexplored for this type of application to this point, will be evaluated. Furthermore, a series of resin prototypes based on biobased monomers is introduced and evaluated. Lastly, the results of accelerated ageing tests performed on biobased films as well as conclusions about possible ways to improve the weatherability of biobased coatings to make them suitable for exterior applications will be discussed.

Table of contents:

1.1 The Sorago project

Sorago stands for **s**ubstrate with **o**rganic covering **ra**n**g**e from bi**o**sources, and was launched in France in 2013 under the leadership of the Swedish company Beckers.[3] Disposing of € 4,1 million, of which a part is publicly financed, it aims to develop industrial paint formulations for the general industry as well as for the coil coating industry during the three years of its duration. The official poster is shown in figure 3.

1.1.1 Objectives

One of the incentives for the project is the prospect of enabling the French industry to remain competitive with regards to imported products. The development of innovative products which are not available elsewhere, especially if French agricultural resources are utilised, can ensure the continued presence of production in the country.

A second motivation is the prophylactic preparation for environmental legislation, which is increasingly imposing restrictions with the aim of moving towards more sustainable products. The project is also a response to consumer wishes. As the environmental awareness in the general public increases, demand rises for products which can advertise their sustainability. For this reason, one of the objectives defined for the project is the certification of the final product with an environmental label.

Lastly, the rise of petroleum prices predicted due to the limited nature of oil resources is making it attractive to decrease dependency on non-renewable materials.

Figure 3: Official Sorago poster

The success of the project is measured by the amount of biosourced carbon incorporated in the final product, which can be assessed by radiocarbon, or ^{14}C dating. While in general, a maximum use of renewable carbon content is envisioned, minimum targets were set for three different application areas. For coil coating, the target for interior paints was set at 75% renewable carbon content, and at 65% for exterior paints, recognising the higher demands on the latter. The general industry paints are targeted to contain 80% renewable carbon. Only the organic fraction, which makes up about 75% of the total paint, is considered in this calculation, excluding any mineral additives and pigments.

Concerning the product quality, an equivalent or better performance with regard to the current petroleum based product was targeted. This includes compliance with all customer requirements as

well as a 10 year guarantee. A price increase of 30% for the resin, 10% for the paint and 1% for the final product was deemed acceptable.

1.1.2 Partners

The partners involved in the Sorago project comprise representatives of the entire value chain of coil coating products and are shown in figure 4. Monomer production and resin synthesis is represented by Arkema, a French specialty chemicals and advanced materials company.[4] Arkema was founded in 2004 after Total restructured its business and currently employs 19 000 people generating €7.7 billion of annual sales revenue. 24% of its business is dedicated to coating solutions, and in the Sorago project, Arkema is involved in the formulation and synthesis of resins for interior coil coating applications as well as for the general industry.

The research on renewable solvents is managed by Activation, a Lyon based start-up founded in 2003 by CEO Dr. Vivien Henryon specialised in process research, catalysis and green chemistry.[5] The formulation of the coil coating paint is the responsibility of Beckers, the leading supplier of coil coating paints globally, with a research centre in Montbrison, France.[6]

The French industrial paint manufacturer Prospa, founded in 1926 and currently employing 33 people, is responsible for the formulation and application of the general industry paints.[7] The last industrial partner, responsible for the actual production of the coated sheets, is Arcelor Mittal, the world's leading steel and mining company with several production sites in France and an office in Paris.[8]

Figure 4: Sorago project partners

Two academic partners also contribute to the Sorago project. One is the CREIDD (Centre de recherches et d'études interdisciplinaires sur le développement durable), where the PhD student Annie Leal-Meza is working on a life cycle analysis under the direction of Dr. Junbeum Kim at the Charles Delaunay institute of the Technological University Troyes.[9] The second partner is our group, the CASYEN laboratory at the ICBMS institute at the University of Lyon under the direction of Bruno Andrioletti.

Our task was defined as the development of a resin for exterior coil coating applications. This initially involved close collaboration with Arkema, as their resin for interior coil coating applications as well as their petroleum based resins can be used as a basis for our project. Furthermore, close collaboration with both Activation and Beckers were necessary to evaluate the compatibility of prototypes with solvents and paint formulation.

In this chapter, the coil coating process as well as the different components of coil coating products will be introduced to illustrate the requirements and possibilities of the resin design. The information presented is common knowledge in the coil coating business, and is therefore not specifically referenced for each detail. All of it can be found in the works of Deligny *et al.*, Brock *et al.*, Holmberg *et al.* or on the website of the European Coil Coating Association.[10-14]

1.2 Coil coating products

Coil coating, according to the definition of the European Coil Coating Association ECCA, is "a method in which an organic coating material is applied on a rolled metal strip in a continuous process".[13] The metal is generally supplied in coils, and the final product is also referred to as prepainted metal.

1.2.1 Applications and requirements

The most important properties for the paint are compatibility with the coil coating line, i.e. the ability to be uniformly distributed on the metal and a short curing time, and enough flexibility for the metal to be processed afterwards without causing damage to the paint. The ability of the paint to protect the metal and to comply with functional and aesthetic requirements determines its quality. The coated metal plates are used for various purposes and hence take on a wide variety of forms and have to withstand many different types of stress.

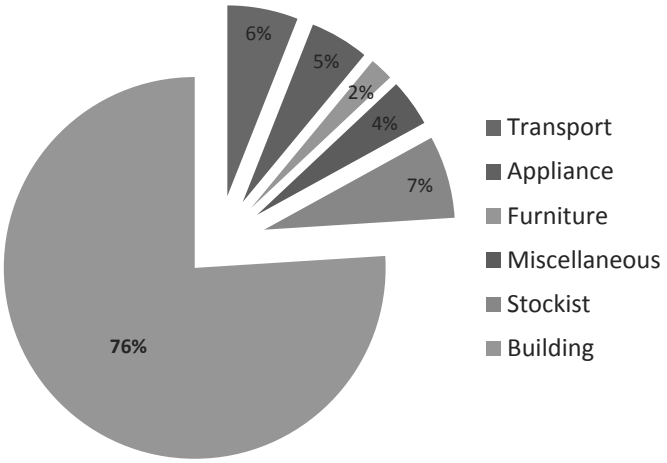

Figure 5: 2012 sales of prepainted metal in Europe

As shown in figure 5, their primary application is the construction industry, where they are used as cladding panels and structures, trapezoidal sheeting, garage doors, entry doors and as partitions.[15] Prominent buildings in France constructed with coil coating products include the "Centre Pompidou" in Metz, the city hall in Gauchy and the "Pôle agro-alimentaire du Grand Lyon".[16] Secondary users are the automotive industry, where prepainted metal might serve as caravan or commercial vehicle superstructure.[11] White goods, i.e. large domestic appliances, and housings for electronic equipment may also be made from contain coil coated metal.

1.2.2 Advantages of the coil coating process

The main advantages of coil coating over traditional coating techniques as promoted by ECCA derive from the efficient application of the paint to the metal. This generates both financial and

sustainability benefits through the reduction of waste. As the line is highly automated, consistent quality and low safety risk for workers are ensured. Further benefits are the durability and recyclability of the products, and the fact that it saves users and processers from setting up their own coating application shop.

1.2.2.1 The coil coating plant and materials

A typical coil coating line, as represented in figure 6 below, can generate from 3000 to 200,000 tons of coated metal from 15 to 250 cm width. After being uncoiled, the metal is pre-treated and levelled to ensure consistency of the coating layer.

The pre-treatment consists of cleaning and application of a conversion coating. Both serve the protection of the metal and the adhesion of the organic coatings applied afterwards. As most organic coatings can be penetrated by small amounts of water and air, the conversion coating is necessary to stop oxidation, especially if cracks are formed in the organic coating layer.

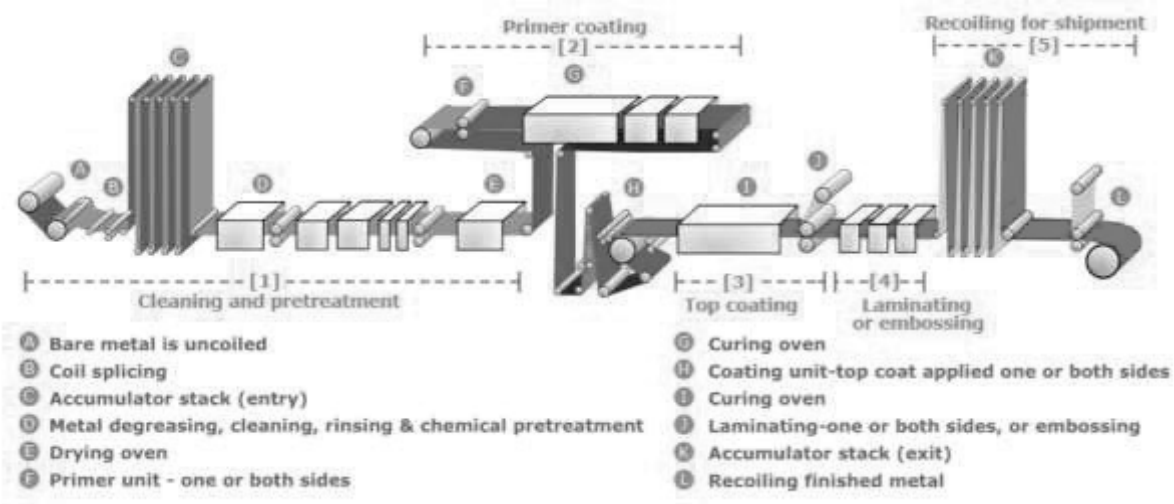

Figure 6: Coil coating process (European Coil Coating Association)

The cleaning removes oils using alkaline or in the case of aluminium acidic solutions; and carbon or rust particles by brushing. The conversion coating is formed through a reaction of the surface of the metal and is thus integral to the metal strip. The different types of coatings include zinc, iron and chromium phosphate as well as alkaline, chromium and titanium/zinc oxides; and are selected depending on the requirements of flexibility, adhesion and corrosion resistance as well as on the substrate. Some of them require an additional rinsing step after their application.

Depending on the type of product, several layers of coating can be applied. First, primer and backing coats are applied to both sides, followed by curing. Then, a top coat is applied above and is again passed through an oven for curing. Primers thickness can be between 5 – 35 µm, while top coats are 15 – 200 µm thick. Overall, top coats represent the largest market share with 59%, as shown in figure 7.[15]

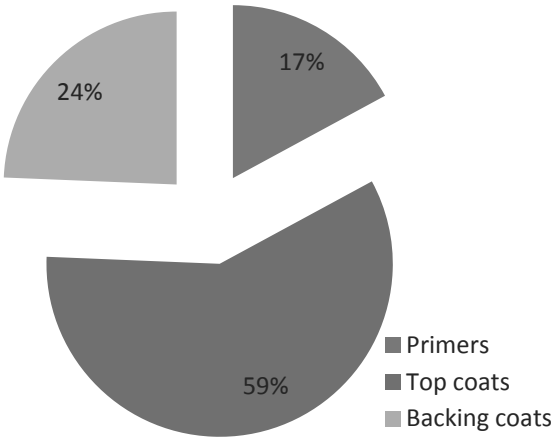

Figure 7: Paint systems in 2012

After each curing, the metal is cooled in water and blow dried. The solvent which evaporates during the curing process is combusted to generate energy to heat the oven. This means that there is little evaporation of solvent after the product leaves the line, and that the inherent energy of the solvent is recovered.

The requirements to organic coating and coating line vary depending on the type of metal, which is either steel or aluminium.[I] In 2012, steel made up 84% of the market which was 5 317 kilotons in total.[15]

The properties of steel plates depend on their carbon content, the metals other than iron present and the method of treatment. Generally, low carbon steel is used for coil coating material. The most common types include cold reduced steel, hot dip galvanised steel and electrozinc steel. The latter two are protected with a layer of zinc. The second is the most commonly used, while the first is suitable for low corrosion applications and the last for applications which require high surface quality.

1.2.2.2 Aspects of coil coating sustainability

Using coil coating for the application of paint has some inherent benefits to the environment compared to other application techniques. As mentioned above, it minimises the emission of solvents into the atmosphere, as they are immediately burned for energy recovery during the curing process. Other waste is also minimised since it is a highly precise technique, and the high quality increases the life time of the product, for which warranties for up to 30 years can be offered.[17] Functional coatings, which can for example deflect sunlight and help to preserve cold temperatures within buildings, can increase sustainability by reducing the energy demand of air conditioning.

[I] For more information on aluminium based coil coating materials, see annexe.

Other trends within the business to increase sustainability during the last 20 years concerned the reduction of solvents in the formulation, causing a move towards high solid paints (non-volatile content of over 60%) or powder coatings, as well as the phasing out of toxic components.

Pigmented paints still contain metal components which are often mined in processes with very high energy demands. However, heavy metals such as lead and cadmium have been eliminated from the formulations. Hexavalent chromium used previously for corrosion protection, such as chromic acid, CrO_3, $SrCrO_4$ and dichromium trischromate, is no longer used in primers and is projected to be completely phased out by 2017.[15] This has mostly been motivated by the restriction of harmful chemicals imposed by REACH, a 2006 European Union legislation concerning the **r**egistration, **e**valuation, **a**uthorisation and restriction of **ch**emicals.

1.2.3 Formulation of a coil coating paint

The coil coating paint consists of pigments, solvents, the binder and a small amount of additives. The different components are mixed in a batch process, using a high speed stirrer or a bead mill. When pigments are used, they are first broken up and mixed with a part of the resin. Only once all of the particles are finely dispersed and covered in binder, the rest of the components are added. Finally, solvent and pigments are used to adjust viscosity and colour to the target values. In the following section, options for and properties of the different components will be discussed.

1.2.3.1 The film former or resin

The film former, often also called binder, is a polymeric substance which makes up the largest part of the paint formulation and is also the main determining factor for its properties. While there are many different types of resins that can be used as film formers in different coating formulations, only a small selection are used in coil coating. Because the paint is applied rapidly, at speeds of up to 220 m/min, and cured fast and at high temperatures (6 – 60 s at 210 – 250 °C), not all polymers are suitable. Generally, only amorphous polymers are used in coatings as crystallinity impedes solubility, can hinder the flow and result in cloudy appearance.

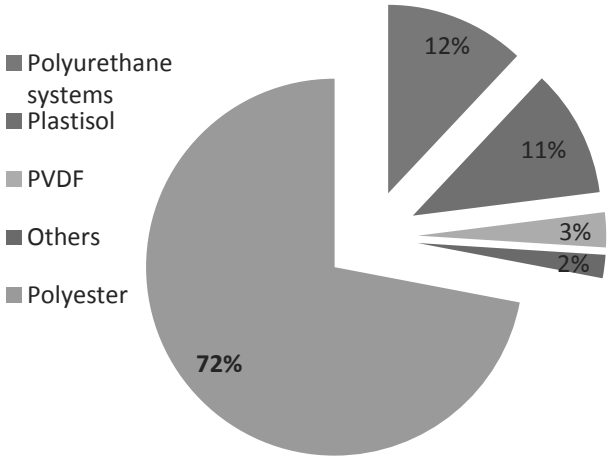

Figure 8: Top coat paint systems in 2012

1.2.3.1.1 Polyester resins

The by far most popular resins in coil coating are polyester resins, as shown in figure 8. Polyester resins are made by condensing di- and trifunctional alcohols with organic acids or

anhydrides. Generally, a slight excess of alcohols is used in the reaction, so that a hydroxy functionalised polymer is produced. It is then crosslinked with a melamine resin to produce the thermosetting coating.

1.2.3.1.1.1 Crosslinking with a melamine resin

Melamine resins are synthesised by the reaction of melamine with formaldehyde and low molecular weight alcohols as shown in scheme 4, and are therefore sometimes referred to as melamine formaldehyde resins.

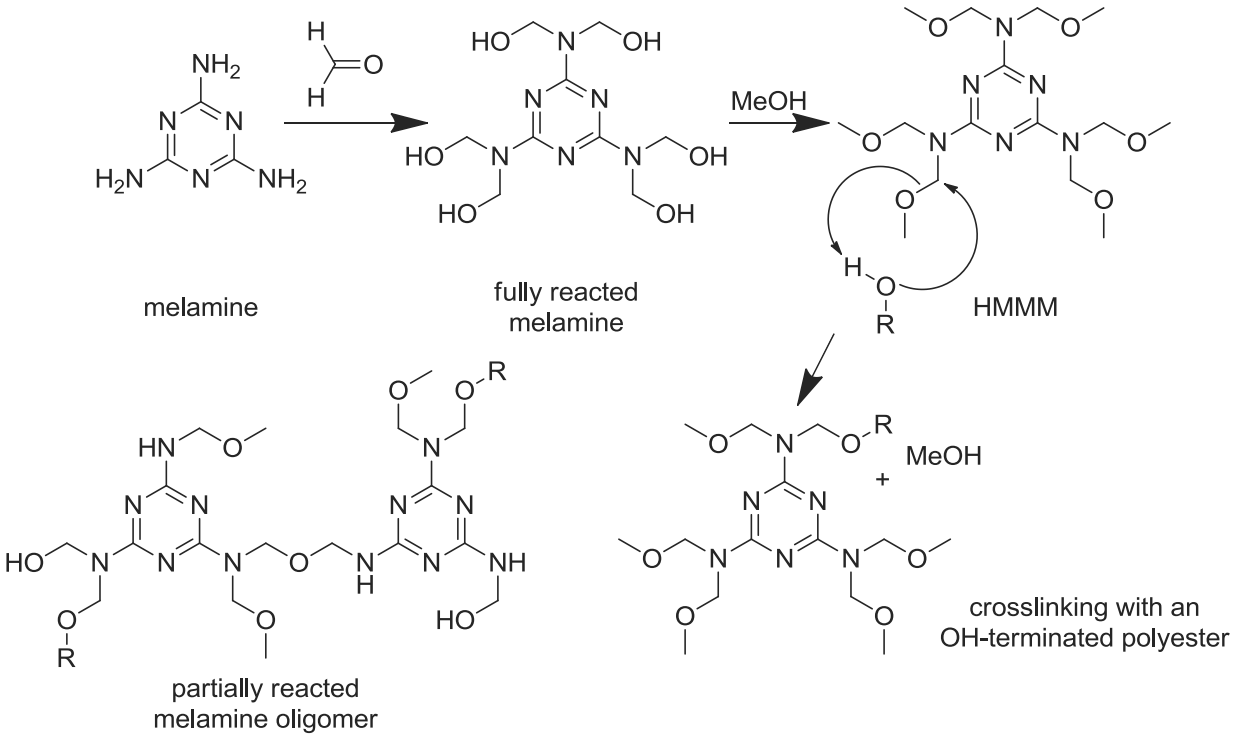

Scheme 4: Melamine resins

In the first step, the amine groups are partially or fully converted by reaction with formaldehyde. Afterwards, they are etherified with methanol or butanol to improve their solubility in organic solvents and their compatibility with the resins. During this reaction, crosslinking also takes place between different melamine groups, and oligomers are formed. The products are classified depending on the amount of substitution on their amine groups. The most commonly used melamine resin, hexamethoxymethylmelamine, or HMMM, has two substituents on each amine group.

The ratio of melamine resin to polyester resin can be from 30:70 to 10:90, depending on which crosslinking density is required. Catalysts such as *p*-toluene sulfonic acid are also added to the paint to accelerate the crosslinking.

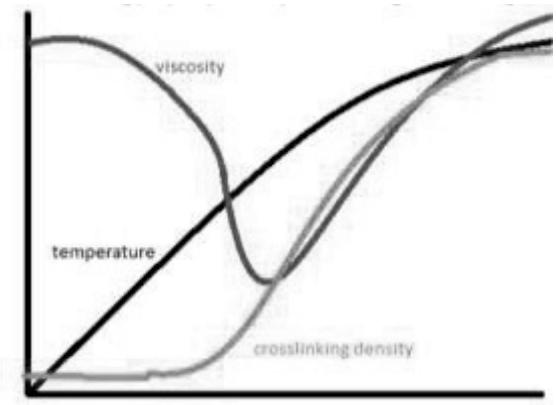

Figure 9: Coating property development during stove curing

During the crosslinking, the viscosity of the resin first drops due to the temperature increase. As shown in figure 9, as the crosslinking density increases, it begins to counteract the temperature effect on the viscosity, which reaches a minimum and rises again. The crosslinking can continue until completion or until the mobility of the chains does not permit any more reactions.

While theoretically, hexamethoxymelamine could crosslink at six points, in reality the reaction of only three of those is usually achieved. Furthermore, an agglomeration of melamine moieties within the resin space during the curing process has been observed.[18]

1.2.3.1.1.2 Typical monomers used in the resin synthesis

The properties of the polyester resin as well as of the crosslinked film can be governed by the choice of monomers in the resin synthesis. Some typical monomers are presented below in scheme 5, 6 and 7.

In order to introduce aromaticity, which brings hardness due to the strong π-stacking interactions between rings, terepthalic acid, isophthalic acid or the related phthalic anhydride are commonly used. Terephthalic acid is not as reactive as the other two, and also causes low polymer solubility because of its symmetrical structure.

The flexibility can be improved by using its aliphatic counterpart, cyclohexanedicarboxylic acid, or the partly hydrogenated tetra- and hexahydrophtalic anhydrides. Long, saturated fatty acids such as isononanoic and isooctanoic acid are also good for the flexibility, and can be used to decrease the average molecular weight as they act as chain terminators. However, in going from aromatic to cycloaliphatic to linear monomers, a decrease in hardness has to be taken into account.

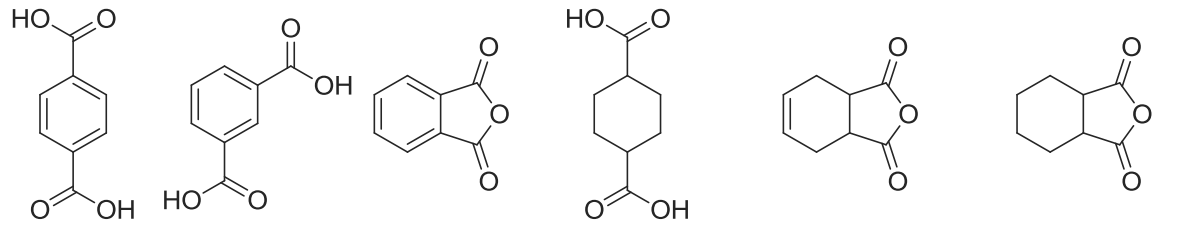

Scheme 5: Examples of rigidity inducing monomers

Neopentyl glycol is a monomer used when good stability is needed, as it has no β-hydrogens and two methyl groups providing steric hindrance to chemical attack. Its symmetric structure also generates a high T_g and low viscosity. As an alternative, trimethylpentanediol is available.

Both monomers improve the solubility as the methyl groups keep the chains apart, but the latter induces a higher viscosity. It is also less reactive and can lower the hardness due to its unsymmetrical structure. Similarly, 2-butyl-2-ethyl-1,3-propanediol can be used to reduce the viscosity and density and improve the solubility, and hydrogenated bisphenol A is used to improve solubility and chemical resistance.

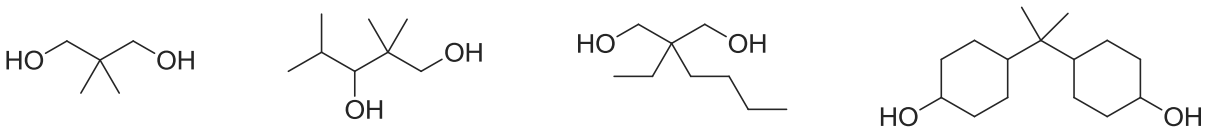

neopentyl glycol | 2,2,4-trimethyl-pentane-1,3-diol | 2-butyl-2-ethyl-1,3-propanediol | hydrogenated bisphenol A

Scheme 6: Examples of diol monomers

In order to introduce branching into the polymer, monomers with a functionality higher than two, such as glycerol, are employed. However, attention has to be paid to the reactivity: Glycerol's secondary hydroxyl group is a little less reactive than the primary ones. Therefore, it only reacts after them. An alternative, which results in a lower crosslinking density and therefore a lower viscosity, is trimethylolpropane. Trimethylolethane also exists, and is preferable to the former if high thermal resistance is required. Lastly, pentaerythritol, which has four hydroxyl groups, is known for its high durability as well as its good reactivity.

glycerol | trimethylolpropane | trimethylolethane | pentaerythritol

Scheme 7: Examples of triol monomers

Of the monomers commonly used for resin synthesis, only glycerol and pentaerythritol are currently available from biosources.

A variety of catalysts, mostly based on titanium, tin, germanium or antimony are used in polyester synthesis, and are chosen depending on the substrates and product requirements.[19] [II]

[II] For examples and more information about the different types of catalysts used, please see annexe.

1.2.3.1.1.3 Other uses for polyester resins

Depending on their structure, polyester resins have many other applications outside of coil coating. Linear, high molecular weight polyesters are used for example in can coating, packaging and printing applications, while low molecular weight as well as branched polyester resins are used in automotive and industrial coatings. Both branched hydroxy- and branched carboxylic acid functionalised resins are suitable for powder coating applications.

1.2.3.1.2 Other resins suitable for coil coating

The second most common resins used in coil coating applications after polyesters are polyurethane resins.[14] They are obtained from the reaction of alcohol and isocyanates, and can be based either on one or two component systems. In one component systems, monomeric diols and isocyanates are reacted directly, while in the more common two component systems, a polyol is simply crosslinked with oligomeric polyisocyanates. An isocyanate group as well as a polyurethane unit are shown in scheme 8.

Scheme 8: Polyurethane structure

Polyurethane films can be thicker than polyester-melamine based films and provide better weathering and corrosion resistance. Their lower popularity may partially stem from the fact that isocyanates can be harmful to human health, but is probably mostly due to the fact that they are more expensive than the polyester equivalents.

Polyvinylidene fluoride (PVDF) resins have very good toughness and flexibility, and furthermore do not absorb UV light. Therefore, they have great weathering resistance and are primarily used in sunny areas. However, in order to also protect the primer underneath from UV light, which can pass through the PVDF coating, absorbing pigments must be used, which limits the possible colour range for this type of coating.

Another class of resins with possible application in the coil coating industry are epoxy resins, shown in scheme 9. They are characterised by their free epoxy chain ends, which can be crosslinked with a variety of compounds, including amines and anhydrides, but also urea or melamine resins. Epoxy resins can provide good adhesion and hence good corrosion resistance, but are used less and less due to their limited flexibility.

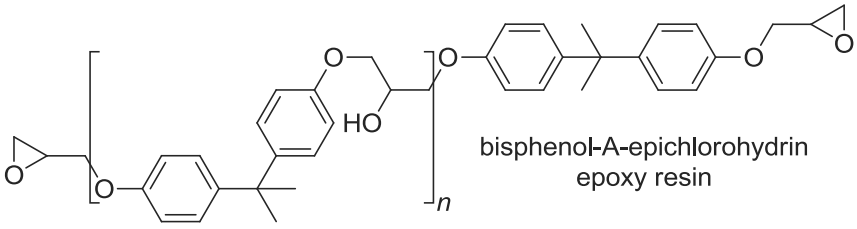

Scheme 9: Example of an epoxy resin

Lastly, polyvinyl chloride plastisols are specialty resins which can be embossed with patterns while still hot, and generate very thick and thus resistant films.

1.2.3.1.3 Other coating binders

Three of the most common resins used in coatings, but not suitable for coil coatings, are unsaturated polyesters, alkyds and acrylic resins. Their principle applications are listed below.

Unsaturated polyester coatings are mostly used for wood and furniture coatings, as their adhesion to metal is not sufficient. They have good hardness and resistance to scratches and chemical damage and confer high gloss, but their weatherability is only moderate.

Alkyd resins, which are self curing, are classed depending on their oil content, i.e. the amount of fatty acid incorporated into their structure. Long oil alkyds are used as decorator's paints or DIY (do-it-yourself) paints, while medium oil alkyds are used for industrial coatings of machines, vehicles, domestic appliances and sometimes as primers or undercoats.

Lastly, acrylic resins can be used in a wide variety of applications. They are strong and display excellent weatherability properties, and are therefore used for example in automotive coatings.

1.2.3.2 Other components

While the resin is the most important component of the formulation, solvents, pigments and additives are equally necessary to adjust the application properties and colour and can also impact on the overall performance.

1.2.3.2.1 Solvents

Solvents are used to modify the viscosity of the binder to suit application purposes; generally it has to be between 0,05 and 1 Pa*s. The nature of the solvent as well as its interaction with the resin determines the flow of the paint on the substrates, and therefore its quality. The wrong solvent choice can lead to defects in the paint surface, lowering its gloss and also its resistance to penetration by water, air and other adverse influences.

Polar solvents are often used to dissolve the resin, followed by the addition of non-polar solvent which dilute the mixture. The solvent mixture has to be adjusted to each specific resin.

The solubility of the resin depends on its molecular weight, structure, and the chemical similarity with the solvent. As a rule, high molecular weight chains can entangle more easily, leading to poorer solubility. Branched structures are more soluble than linear chains because the branches keep the polymer chains apart. On the other hand, linear chains and long branches can lead to the

entanglement of different chains, which can prevent chain-solvent interactions and therefore lower the solubility. This can partially be explained with the entropy gain upon solubilisation. Where the motion of the network is restrained by crosslinking or entanglement, the energy gain upon solubilisation remains low.

The compatibility of resin and solvent can be estimated using the Hansen parameters, which evaluate the dispersion forces, polarity and hydrogen bonding potential of each component.[20] While completely accurate predictions of solubility are difficult, the distance between a resin and a solvent in the three dimensional Hansen space can be a good first indicator of their compatibility.

The dissolution of polymers differs from that of small organic molecules. It is a gradual process, as the polymer begins to swell first, gradually binding solvent molecules to the chains and forcing them apart, before complete dissolution, which means free movement of the chains, is achieved. This also means that precipitation generally doesn't take place when solvent is removed, as the polymer just goes back to the swollen state.

A distinction can be made between bonded solvent, which is in direct contact with the polymer chain, and free solvent. This is significant due to a phenomenon called solvent retention, which means that bonded solvent will evaporate much more slowly than its free counterpart.

The evaporation behaviour of the solvent is the most important factor other than its capability to dissolve the resin and adjust its viscosity. The volatility is partially dependent on the boiling point, but differences in solvent-solvent interactions also have to be taken into account, as intramolecular hydrogen bonds can slow the evaporation. The speed of evaporation is sometimes estimated using the evaporation index, which describes the time needed for a quantity of solvent to evaporate compared to an equal quantity of diethyl ether. However, this time changes when solvent mixtures are used, as well as where resins are involved due to the additional interactions.

Generally, the formulation should be adjusted so that the solubilisation improves progressively as evaporation occurs. If the most solubilising part of the solvent mixture is also the least volatile, it can aid homogeneous merging of the particles on the surface, leading to high gloss.

Lastly, the surface tension, toxicity, odour, combustibility, environmental compatibility and cost of the solvent are also properties considered for its choice.

1.2.3.2.2 Pigments and fillers

Pigments provide colour and opacity, but can also contribute to the durability and corrosion resistance of the system. Both inorganic and organic pigments are used, with the former providing

advantages of cost, opacity and stability and the latter being aesthetically favourable. Important properties are the size and crystal structure of the pigments, as well as their interaction with light.

Fillers are also inorganic substances such as $CaCO_3$, SiO_2, silicic acids, silicates and sulphates, which are added to the paint. Their purpose is to fill empty spaces left by pigments and resins in the structure and thus provide a reinforcing skeleton and better strength. Furthermore, they can be used to control the gloss, where a matted aspect is desired, and reduce the overall cost.

1.2.3.2.3 Additives

Additives are products added in small quantities to improve coating properties and performance. One important group are surface-active additives, which are used to prevent flow defects during the curing process.

As the solvent evaporates during the curing process, the top layers become more concentrated, and as a consequence more viscous. Then the lower layers, which begin to flow up, create high density regions at the top and low density regions at the bottom. The heavier top then sinks back down, thus a constant flow is taking place, which results in the formation of a honeycomb structure referred to as Bénard's cells. Pigments and other particles can be entrained in different quantities by this flow, depending on their size and structure. This in turn creates regions of low surface tension and regions of high surface tension. If the difference is too large, the paint will concentrate in the low surface tension areas, resulting in holes in the final structure.

The purpose of surface active additives is to provide even surface tension throughout the film. Depending on the resin, fluorinated compounds, silicone oils, and modified polysiloxanes can be used.

While lowering the surface tension between substrate and paint, surface additives can have the negative side effect of also lowering the surface tension between paint and air. This can result in the encapsulation and trapping of air, and the creation of foams. As the coating is heated, the bubbles of trapped air can then violently burst, leading to surface defects.

In order to prevent that, defoaming additives such as polysiloxanes are used. Their compatibility with the resin needs to be adjusted carefully, as too compatible defoamers are not effective, while incompatible substances can lead to cratering in the film. Antifoaming additives may also lose their efficiency over time, and should be checked after long storage.

A further negative consequence of surface tension lowering additives can occur if they get trapped in the top layer of the coating. Optimal wetting occurs when there is a maximum difference between the surface tension of the paint and the surface tension of the substrate. Very low surface tension on the surface of for example the primer can therefore impede good flow of the following top coat.

Other additives used include biocides, rheological agents which can further adjust the viscosity, light stabiliser and UV absorbers.

1.2.3.3 Design criteria

The most important decisive critera which determine the successful design of a coating are summarised below. The viscosity of the resin is particularly important as it is crucial for the compatibility with the coil coating line. Furthermore, the significance and modification of the glass transition temperature, the surface appearance, the viscoelastic response to stress and the coating hardness and flexibility will be discussed.

1.2.3.3.1 Viscosity

Foremost, the viscosity of a resin solution depends on the hydrodynamic volume of the polymer, which describes the flow dynamical resistance to movement. Where the solvent interacts strongly with the polymer and can disrupt the dispersion forces, hydrogen bonds and polar attraction between the chains, the chains will form extended coils, which can easily entangle and resist movement. Therefore, high compatibility between solvent and polymer leads to a high viscosity. Where, on the other hand, the interactions between the chains are stronger than with the solvent, the chains form contracted coils, leading to a low viscosity. However, where the interactions are too weak, strong bonds can form between the different chains, which can again raise the viscosity.

Other factors influencing the viscosity are the molecular weight and structure of the resin, the amount of solvent present and the temperature.[III]

1.2.3.3.2 Glass transition temperature

One of the most important characteristics both of a resin and of a crosslinked coating is their glass transition temperature (T_g). Above the T_g, the polymer is very flexible, as there is enough energy to permit translational motion of entire molecules, which causes flow, and rotational motion, i.e. wriggling of segments of 40-50 carbons. This results in flexing and uncoiling. Below the T_g, only motion of 5-6 atoms or side groups and vibrational motion is possible and the polymer becomes brittle and glassy.

The energy in the system is distributed statistically in a Boltzman fashion. As the temperature is lowered, some bonds will start not having enough energy to move. The chains connect many bonds with each other, so as the number of non-rotating bonds increases, a point is reached at which the whole structure is blocked. This is the critical temperature, i.e. the T_g, which is characteristic for each polymer.

Because of this, it is dependent on the average energy required to rotate the bonds. The bond rotation energy is determined by the conformation, the bulk on the chain and the polarity and hydrogen bonding ability of the groups. A symmetrical structure in monomers facilitates attraction and therefore typically leads to a high T_g. Rigid groups generally hinder rotation, but ether linkages in place of carbon atoms can ease rotation. The same is true for inserted double bonds, which result in a 120° angle instead of a tetrahedral angle and therefore reduce the clash between adjacent methyl groups. Similarly, stiff or long chains cause a high glass transition temperature, and short chains and large free volume in the polymer lower it. It has also been found that the T_g is higher for even numbers of methyl groups than for an uneven number.

High molecular weight and a high crosslinking density also increase the T_g, as both restrict chain movement. The higher the crosslinking density of a polymer, the more pronounced is its glass transition.

1.2.3.3.3 Surface appearance

The appearance of the coating surface is governed by the behaviour during the curing, or the flow. Defects can be characterised either as orange peel or as craters.

Good flow depends on the substrate wetting, even spreading of the paint, uniform solvent evaporation and a uniform level of surface tension. The viscosity of the paint is of course an important factor in these properties. Wetting describes the spreading of a liquid on a surface, and can be estimated from the angle between a drop of liquid and that surface.

Orange peel generally occurs when solvents with too high volatility are used. Their premature evaporation can lead to elevated viscosities, which causes irregular flow.

Lastly, the occurrence of craters, or cratering, can be caused by a variety of factors. Bad wetting, caused by uneven surface tension or impurities is a main factor. Both soluble impurities, such as fats, oils or lubricants, which create areas of low surface tension, and insoluble impurities, such as dust or other particles, which create areas of high surface tension that cannot be completely covered by the paint, can lead to this type of defects.

Cratering can also be caused by volatile solvents which are trapped in the lower coating layers if the top layers harden too quickly, and burst out later on, destroying the surface.

[III] For more details on the different factors influencing the viscosity, see annexe.

1.2.3.3.4 Viscoelastic response to stress

The response to stress of a coating is called viscoelastic, and can be described by the spring and dashpot model, shown in figure 10. Under moderate tensile stress, vibrations are inhibited, which leads to a parallel alignment of chains and consequently to a stretch of the material. When the stress is relieved, chain vibrations starts again and the chains contract back to their original state. This explains the spring, or elastic response.

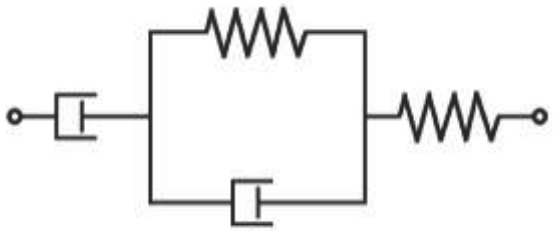

Figure 10: The spring and dashpot model for viscoelasticity

Where the stress is big enough and the crosslinking permits it, chains can slip past each other, in the viscous, or dashpot type of response. This is inhibited by attraction between chains, and entanglement caused by large molecular weight. Where the crosslinking density is high enough to prevent any flow, permanent plastic deformation takes place instead.

The degree of elastic, viscous and viscoelastic deformation can be examined using the μ-hardness indentation test but also dynamic mechanical analysis, as the storage modulus E' is a measure of elastic deformation and the loss modulus E'' of viscous behaviour.

1.2.3.3.5 Flexibility and hardness of the coating

Flexibility, hardness and weatherability are important properties of a coating, but cannot be directly observed in the resin. However, experience with different types of structures can be used as guidance in the formulation of the resin.

Flexibility means that the chains can rotate successively out of the way of pressure. This is inhibited for example by crystallinity, and high crosslinking density. If the chains are however crosslinked at few enough points, it can be favourable as it prevents the polymer from falling apart when it is stretched without inhibiting the motion of the chains. Linear chains, saturated linear monomer structures as well as cycloaliphatic monomers increase the flexibility. Additionally, it has been found that the low molecular weight fraction also has a positive impact compared to the heavier parts of the polymer.

On the contrary, the hardness is improved by the high molecular weight fraction. Regions with higher density are also more able to support stress. Therefore, linear chains are favourable. Strong dipole interactions can also induce hardness in a polymer.

1.2.3.3.6 Property summary for resin design

A summary of factors that can be modified through resin formulation and which have an influence on important coating properties is given below in table 1.

Table 1: Summary of factors influencing important coating properties

	increase	**decrease**
solubility	steric hindrance	linear chains, high aliphatic content (in aromatic solvents), high $M_{\bar{w}}$, high crosslinking density
	increase	**decrease**
T_g	high bond rotation energy and secondary forces: rigid groups, long and stiff chains, polarity, H-bonds, bulk, small bond angle, symmetrical structure, even number of CH_3 groups	low bond rotation energy and secondary forces: ether linkage in place of carbons, double bonds in place of single bonds, large free volume, little clash, large bond angle, short chains, odd number of CH_3 groups
viscosity	high $M_{\bar{w}}$, low solvent level, strong interactions with solvents, strong interaction between chains, large amount of hydrogen bond donors and acceptors, crosslinking	low $M_{\bar{w}}$, high solvent level, weak interaction with solvents, symmetrical monomers, bushy branches, rigid chains with double bonds
flexibility	facile chains rotation, linear chains, saturated linear monomers, cycloaliphatic monomers, low $M_{\bar{w}}$ fraction	bulk rigidity, crosslinking, rigid monomers
hardness	high $M_{\bar{w}}$ fraction, linear chains, strong dipole interactions	replacing aromatic monomers with linear, saturated monomers

1.3 Research scope

The aim of this work is the design of a coil coating resin suitable for exterior applications. The scope was limited to aliphatic-aromatic polyester resins not containing further double bonds or heteroatoms other than oxygen. Crosslinking was only done using melamine resins, more specifically HMMM, and properties were mostly tested on clear coats. The influence of pigments and other additives on the stability was not included in the investigations for a start except for where it enabled conclusions about the resin behaviour.

Furthermore, in order to enable compliance with current equipment, only direct condensation reactions not involving activated functional groups such as acid chlorides were used. Catalysis of the polyesterification reaction was limited to homogeneous catalysts, as they are generally added in very small quantities and not removed by purification. No other type of polymerisation reaction was evaluated.

At the beginning of the project, a fully biosourced resin for use in interior coil coating products was already available, designed by Arkema. Its weatherability had however been found to be insufficient for use in exterior applications. Therefore, alternative formulations for a biosourced or partially biosourced resin which display better weatherability need to be investigated.

The following two chapters will therefore firstly present the state of the art on available biosourced monomers, their use in polymerisation reactions as well as the properties that they impart on the resulting polyester products, and secondly explore the current knowledge on weatherability and methods to improve it.

2 State of the art biopolymers

2.1 Introduction

The word biopolymer has many different meanings, as there are several ways to obtain polymeric materials from biomass, and several approaches to convert them into useful products, including the use of natural polymeric materials. The following section will provide a brief overview of the main approaches to obtain sustainable polymers: they are the use of recycled polymer waste, bacterial polymerisation of biomass, composites of synthetic material and polymeric material present in nature and the chemical polymerisation of monomers sourced from biomass.

As the last approach provides the highest design flexibility, and is therefore the easiest way to achieve replacement of petroleum based products with biomass based products of equal quality, the different sources of biomass, and the monomeric compounds that can be derived from them will be discussed in the second section. An overview of the most important available monomers will conclude the first part of the chapter.

Finally, an overview will be provided of biomass based polyesters reported in the literature that are relevant to coil coating products. Particular attention will be paid to the synthesis and properties of isosorbide and vanillin derivate containing products, as they have the rare potential to introduce rigidity in the polymer structure.

2.1.1 Waste as a sustainable source of polyester products

One sustainable way to synthesise polyesters is by using recycled materials. While these are not per definition a renewable source of material, and the carbon content will still be derived from petroleum, their use will be sustainable as long as there is a sufficient waste stream to support the demand. Waste materials have an energetic advantage over freshly synthesised materials if some of the energy of polycondensation can be saved by conserving the molecular weight completely or partially. Additionally, the recycling of post-consumer stage polyester into new uses can help solving the waste problem that is currently threatening the ecology.[21]

A lot of attention has been paid to polyethylene terephthalate (PET) recycling, both due to its widespread use and due to its rigid, aromatic structure which impedes water uptake and thus hydrolytic and enzymatic degradation. PET can be recycled either mechanically, i.e. through melting and reforming, or chemically, which involves the breakdown of the polymer structure for example by hydrolysis, aminolysis or glycolysis.[22] The different steps and available methods for PET recycling have been reviewed for example by Al-Sabagh *et al.*, Park *et al.*, and Nikles *et al.* in detail.[23-25]

While the incorporation of recycled materials into coatings has been proven possible, their widespread use in coil coating applications is limited by the small choice of monomers. [IV] Furthermore, as will be presented later in the introduction, terephthalic acid displays only a limited stability to weatherability. The use of renewable monomers, which are available in greater diversity, is therefore preferred by the industry.[17]

2.1.2 Enzymatic polyester synthesis and polyhydroxyalkanoates

Other than degrading polymers, enzymes can also be used for their synthesis. Lipase enzymes are used in nature to break down fatty acids hydrolytically. However, due to the reversibility of the reaction, lipases can be used for ester bond formation if the conditions are controlled accordingly.

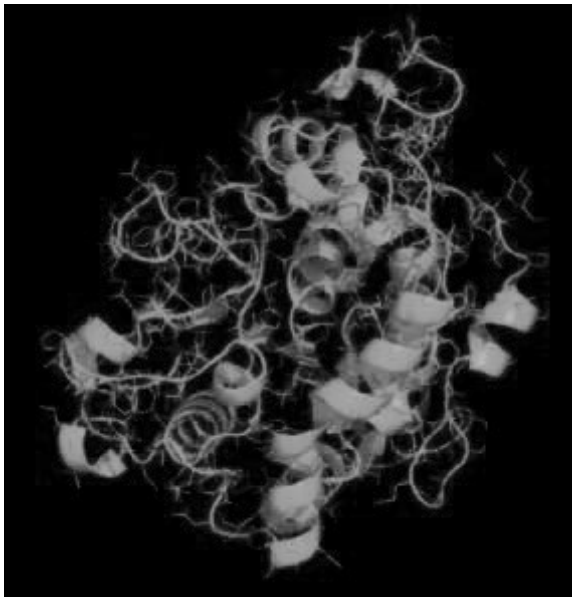

Figure 11: 3D structure of CALB (Kobayashi 2010)

The different enzymes, reactions and products available for and from enzymatic polyester synthesis have been reviewed by Kobayashi *et al.* amongst others.[26, 27]

One example of enzymes that can be used is candida antarctica lipase B, or CALB. It is shown in the illustration in figure 11, and consists of 317 amino acids, adding up to a molecular weight of 33 273 g/mol. The two main types of condensation reactions that can be catalysed by enzymes are ring opening polymerisation and the polyesterification between glycols and diacids.

Various linear glycols, including 1,4-butanediol, 1,8-octanediol and 1,10-hexanediol as well as various diacids such as adipic acid and sebacic acid have been used. The reaction conditions are generally mild, polyesterification can be achieved at as low as 60 °C. Molecular weights in the region of 10^4 g/mol have been achieved, and can be increased by increasing the pressure during the reaction. Compatibility of the enzymes with biosourced monomers is easily achieved, and the resulting polyesters are usually biodegradable. Disadvantages that have to be considered include the limited availability of lipases and the cost of the process.

The largest class of bacterially produced polyesters are polyhydroxyalkanoates (PHA). A general structure is shown below in scheme 10. They are a material used as a carbon and energy reserve by bacteria, and their structure, i.e. the size of the aliphatic chain x, the overall chain length n and the

[IV] For details concerning the different processes used for the recycling of PET, see annexe.

nature of the pendant group R, can be artificially modified either through the feedstock or through genetic modification of the bacteria.[28] The different available materials have been reviewed by Braunegg *et al.*, and by Tan *et al.* and Bugnicourt *et al.* more recently.[28-30]

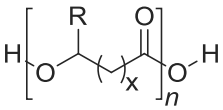

Scheme 10: PHA general structure

PHAs can be obtained by bacterial transformation of a variety of materials. They are particularly attractive because they include not only carbohydrate biomass, like glucose and sucrose, and vegetable oils, but also agricultural and industrial waste products such as glycerine from biodiesel production, olive mill food waste, and PET pyrolysis products. As PHAs are generally biodegradable, they contribute to solving the waste problem both by consuming it and by avoiding to create new waste.

More than 150 different PHAs are currently available, and include homopolymeric as well as copolymeric structures, unsaturated chains, aromatic pendant groups and end groups adapted to specialty applications.[28] In general, PHAs are thermoplastic, non-toxic and soluble in organic solvents but not water.[29] They display a good stability towards UV light, but a low resistance to thermal degradation, which can make processing under harsh conditions difficult. Additional problems are secondary crystallisation, which can take place in the amorphous phase during storage, and high cost which is not yet competitive with less sustainable alternatives.[30]

2.1.3 Biopolymers in composite applications

Nature already contains many polymeric materials, which can be used to replace or complement artificial plastic materials. Natural rubber is one example that has been in widespread use for a long time, but many new applications are being developed on the base of lignocellulosic biomass. Other examples of biopolymers include alginate, a plant based polysaccharide, chitin, a polysaccharide of animal origins, starch, tannins and proteins.[31, 32]

Biopolymers can be used to replace a petroleum based plastic fully or partially, or as a composite. [V] In a composite, two materials are mixed to allow a combination of their properties. For example, biopolymers can be used to replace mineral and inorganic fillers. This not only raises the renewable content of the material, but often also has benefits for the process safety and overall material weight.

One well known example of a renewably sourced filler is sawdust, but many different alternatives are reported. The fillers can be made from agricultural waste, and are therefore particularly attractive for regions that rely heavily on agriculture. The waste is often both abundant and cheap, and using it in higher value applications can bring financial gain in addition to a decrease in waste quantity and a sustainability benefit.

[V] For some examples of biopolymer composites, see annexe

Apart from their low price, low weight and low toxicity, biopolymers are also often easily degraded by fungi and bacteria. Since it is hard to separate the different components of composite materials, recycling them is not always possible, and biodegradability is therefore important. However, this low durability also means that their application is somewhat restricted to fast turnover products. One review suggests one time use materials, such as plastic cutlery, but also electronic goods with a short life, and some sports equipment, which have very specific demands but where failure does not pose a great risk.[32]

2.1.4 Renewable polymers synthesised from renewable monomers

A last alternative method to obtain polymers containing biosourced carbon is the incorporation of monomers from renewable sources into the synthesis. This is sometimes referred to as fungible replacement of the petroleum based material, as it offers a large degree of flexibility in the design, and partial replacement of the monomers is possible. Furthermore, the majority of the technology stays the same, as the overall process conditions can be retained. Due to the many possibilities in choice and combination of monomers, this route can enable the design and facile introduction of high performance materials. Unfortunately, it loses some of the advantages of the methods detailed above, such as mild process conditions, and the ability to transform waste.

The different routes to obtaining renewable monomers are detailed in the following section, as well as the choice of renewable monomers for polyester synthesis available. Afterwards, an overview over renewable polyesters obtained this way will be given.

2.2 Monomers from biomass feedstock useable in polyesterification reactions

Using biomass derived monomers for polyester synthesis can lower the final product carbon footprint, and limit its dependence on petroleum prices and availability. However, where products of equivalent quality can be made, the use of biomass has other advantages: It is abundant, often cheap, and the fact that it can be found anywhere in the world has the potential to improve resource equality from region to region.[33]

Biomass is defined as organic matter that is available on a renewable or recurring basis, including animal waste and other waste products.[34] Only 4% of the total biomass is currently used by humans for food and non-food purposes, so there is a large development potential.[35] While the first known polymers, such as natural rubber, were based on biomass, they came out of fashion due to the low oil prices associated with the petrochemical boom in the second half of the 20th century. With the exception of paper production, almost all biomass based technologies were replaced with cheaper, oil based alternatives. Very little research dedicated to this field was funded until a renewed interest

was sparked by the oil crisis in the 1970s, and an increase in environmental awareness. Therefore, the lack of technologies related to both biosourced monomers and polymers is not due to a lack of potential, but rather to a lack of investment.[36]

One major source of biomass is crop residue. Worldwide, approximately $1{,}55*10^{12}$ kg are produced annually (reported by Dale *et al.*, 2005).[33] Its origin is linked to different food sources, and production for the different continents can be seen in table 2 below. This suggests that food production and biomass production are intrinsically linked. Furthermore, additional plants such as algae and grass, which are not used for food at all, can be harvested for biomass. Therefore, if sufficiently advanced technology to convert this type of biomass into chemicals is developed, there will be no need for the sometimes feared competition for resources between energy, chemicals and food industries.

Table 2: Production of biomass on different continents (Dale 2005)[33]

Material ($kg*10^9$)	Africa	Asia	Europe	North America	Central America	Oceania	South America	Subtotal
corn stover	0	33,9	28,6	134	0	0,2	7,2	204
barley straw	0	2	44,2	9,9	0,2	1,9	0,3	58,5
oat straw	0	0,3	6,8	2,8	0	0,5	0,2	10,6
rice straw	20,9	668	3,9	10,9	2,8	1,7	23,5	731
wheat straw	5,3	145	133	50,1	2,8	8,6	9,8	354
sorghum straw	0	0	0,4	6,9	1,2	0,3	1,5	10,3
bagasse	11,7	74,9	0	4,6	19,2	6,5	63,8	181
subtotal	38	924	217	219	26,1	19,7	106	**1549**

Generally, biomass is derived either from annual plants, or from wood. Some biomass of animal origin, such as chitin, also exists, but will not be discussed because to the best of our knowledge, no monomers with possible use in a polyesterification reaction have been isolated.

Instead, the following section will provide an overview of diols, diacids and hydroxy acids derived from biomass, and address their production and availability. Furthermore, biosourced vanillin will be addressed due to the general lack of commercially aromatic moieties amongst the other biosourced compounds. Lastly, vegetable oils will be discussed both as a source of glycerol, and as starting materials for dimerisation, which can yield diacid monomers.

Compounds such as abietic acid, which can be extracted from rosin, and terpenes, a diverse class of aromatic ring structures synthesised by plants as an insect attraction and defence mechanism, will not be discussed due to their lack of condensable functional groups.

2.2.1 The biorefinery concept

Biosourced monomers can either be directly extracted from the biomass, as in the case of mono- and disaccharides and vegetable oils, or converted from the biomass feedstock by fermentation or chemical transformation in a biorefinery.

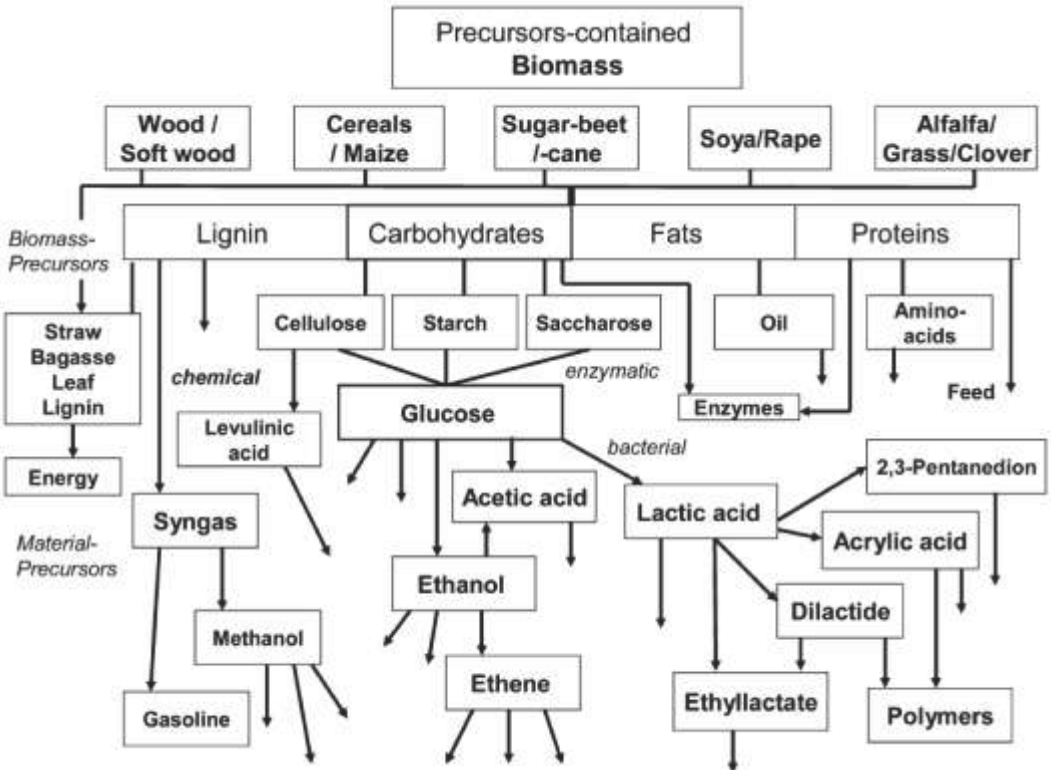

Scheme 11: Biorefinery for precursor containing biomass with preference for a carbohydrate line (Kamm 2004)

A biorefinery is defined by the "American National Renewable Energy Laboratory" as a facility that integrates biomass conversion processes and equipment to produce fuels, power and chemicals.[34] The concept is analogous to petroleum refineries, which produce multiple fuels and products from petroleum. An exemplary flowchart for a carbohydrate focused biorefinery is shown in scheme 11 above.[37]

As can be seen from the schematic, a large variety of starting materials can be used, and transformed to an equally large variety of compounds. The biorefineries are classed as first, second or third generation depending on the flexibility of materials and transformations that can be accommodated.

2.2.1.1 Fermentation of glucose

One of the key intermediates of carbohydrate conversion is glucose. Its fermentation can lead to a number of important platform chemicals which will be discussed in the next section.

Bacterial fermentation processes go through a variety of intermediates, all of which could theoretically be extracted and utilised as chemical products. A selection of molecules which are

intermediates and products in sugar fermentation are shown in scheme 12 below, but other processes, such as the citric acid cycle, also occur.[38] An infinite variety of molecules are present in nature as bacterial or fungal metabolites, intermediates and end products, but usually only produced in the quantity needed for survival by each organism. Therefore, in order to harvest a specific molecule in interesting quantities, defective or modified strains need to be used.

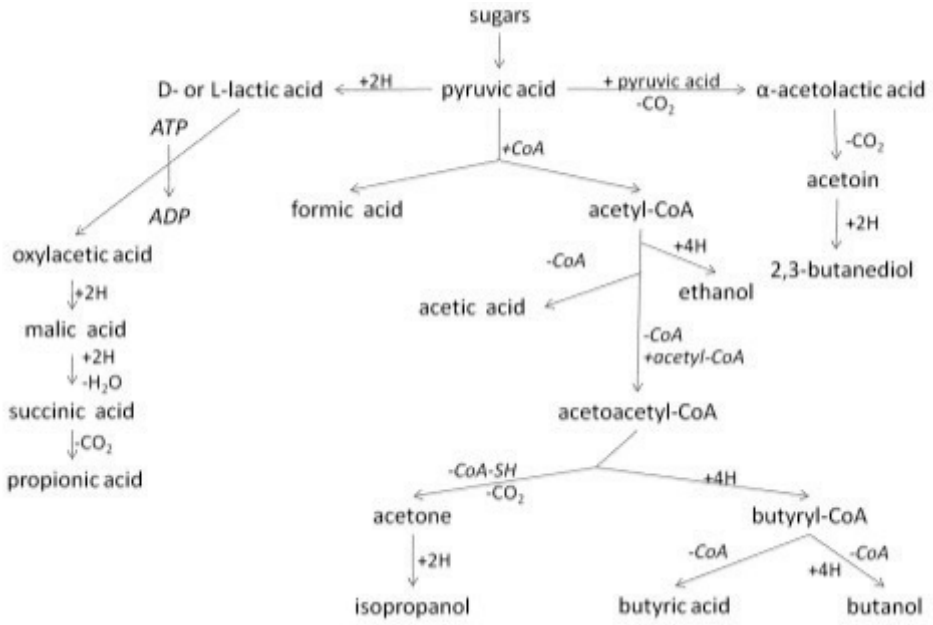

Scheme 12: Bacterial fermentation of sugars and possible production of monomers (Lindblad 2002)

Depending on the bacteria used, different fermentation pathways will take place, resulting in the production of different monomers. Usually, several monomers are produced by each strain.

Fatty acids, usually with an even number of carbons, can also be obtained through bacterial fermentation. However, they can be directly obtained from vegetable oil, as will be discussed below. The conversion of triglycerides present in the vegetable oil to fatty acid also yields glycerol, which is therefore available from two different routes.

2.2.1.2 Platform chemicals from glucose fermentation

The most important platform chemicals for polymer synthesis obtained from glucose fermentation as judged by Corma *et al.* are succinic acid, lactic acid, 3-hydroxypropionic acid, itaconic acid and glutamic acid.[35] An overview of the possible transformations of succinic, lactic and 3-hydroxypropionic acids is presented in scheme 13, 14 and 15. Itaconic acid and glutamic acid also serve as platform chemicals for various heterocyclic and amine compounds, but are not shown due to their irrelevance for polyesterification monomers. The product chemicals shown can each also serve as platform chemicals to be transformed into further derivatives of interest to the chemical industry.

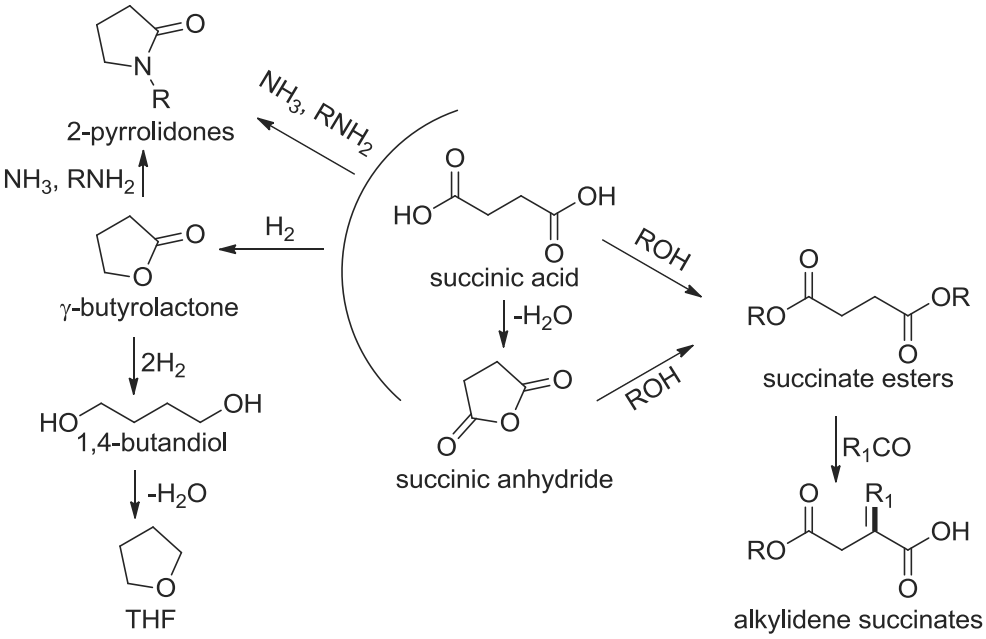

Scheme 13: Succinic acid platform (Corma 2007)

In terms of polyesterification, succinic acid, succinic anhydride and 1,4-butanediol are the most important chemicals that can be obtained from the succinic acid platform. However, succinate esters, as well as 2-pyrrolidones and γ-butyrolactone can also be important as solvents for dilute applications. While 2-pyrrolidones are unlikely to be part of a fully sustainable vision despite being excellent solvents for polyesters due to concerns about their toxicity, γ-butyrolactone has potential to replace the currently used *N*-methyl pyrrolidone (NMP).

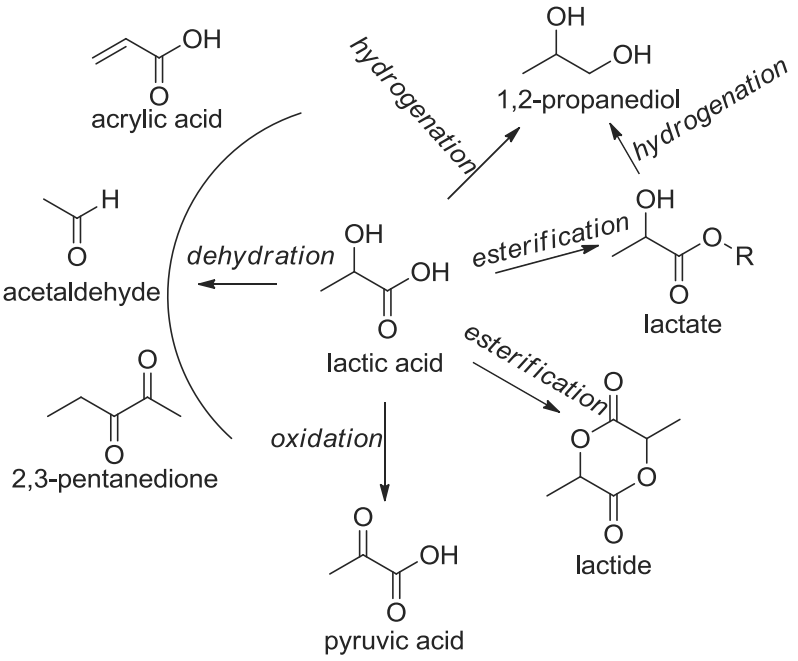

Scheme 14: Lactic acid platform (Corma 2007)

Aside from lactic acid and lactide, used in the synthesis of polylactic acid, 1,2-propanediol or propylene glycol is probably the most important derivative for polyesterification from the lactic acid platform.

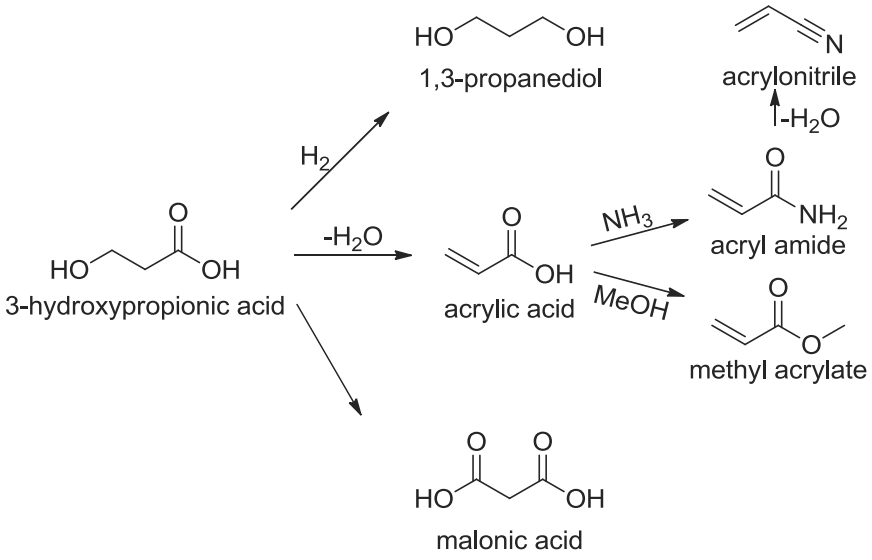

Scheme 15: 3-hydroxypropionic acid platform (Corma 2007)

Of the 3-hydroxypropionic acid platform, 1,3-propanediol, and also malonic acid and 3-hydroxypropionic acid can be used in polycondensation. 1,3-propanediol can also be obtained from the fermentation of glycerol. Either glycerol from vegetable oil origin or from glucose fermentation can be used for this, or the bacteria used for the glucose to glycerol conversion and the glycerol to 1,3-propanediol conversion can be combined to directly yield 1,3-propanediol from glucose.[39]

2.2.2 The lignocellulose based biorefinery

Lignocellulosic biomass is not linked as closely to food production as carbohydrate biomass, and is as a consequence less utilised. It contains lignin, hemicellulose and cellulose, and its importance lies in the potential to yield aromatic compounds. A flowchart of a biorefinery based on lignocellulosic feedstock is shown below in scheme 16.[37]

Lignin is the largest natural source of aromatics, but its exploitation to yield anything but vanillin is hindered by its complex structure, and the difficulty of extracting and separating individual compounds. Additionally, hemicellulose and cellulose have been used to make furanic monomers, including 2,5-furandicarboxylic acid (FDCA), which is the most important candidate for a renewable replacement of terephthalic acid.

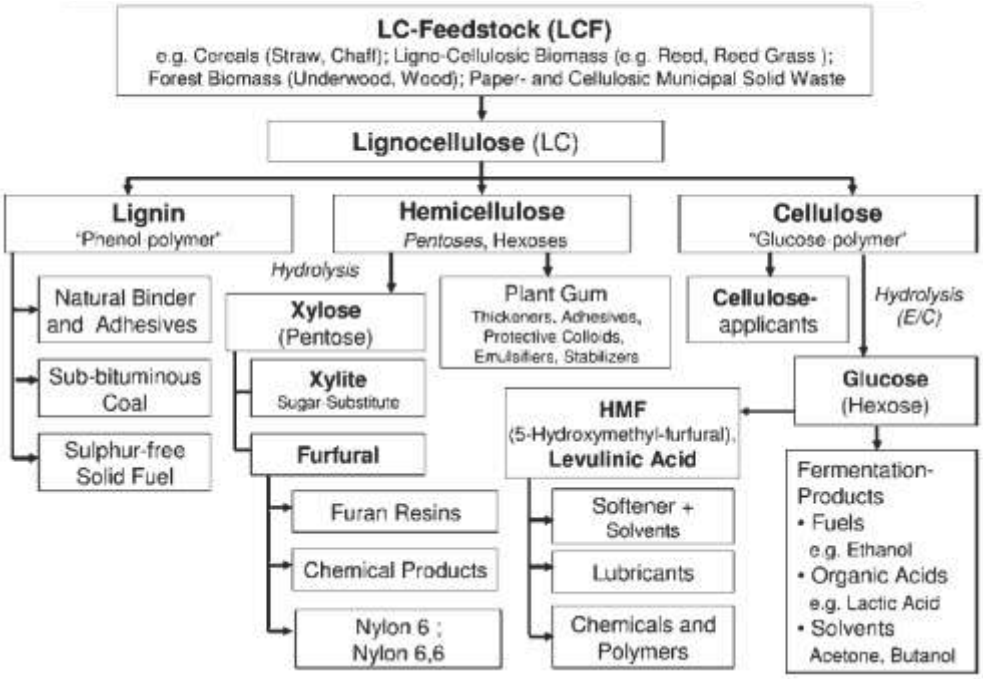

Scheme 16: Products of a lignocellulosic feedstock biorefinery (Kamm 2004)

2.2.2.1 Vanillin from biomass

Vanillin is not only one of the most used food flavourings, but also one of the only aromatic compounds commercially available from biomass. Natural vanilla is present in trace amounts in the woody tissue of many plants, and the highest concentration can be found in the beans of the vanilla orchid. The harvest is however long and complicated, and vanilla from this source, which is marketed as natural vanilla, is therefore very expensive and only represents a small fraction of commercial vanillin.

The conversion of guaiacol from petrochemical origin represents the largest source of vanillin in use today.[40] However, the extraction of vanillin from lignin has been commercialised as early as 1936. The Kraft process for pulp and paper production, which prevails in today's paper industry, yields a black liquor byproduct which contains around 30 – 34% vanillin.[41] It had originally been commercialised in an effort to valorise the paper mill waste stream, but was largely abandoned in the 1980's due to environmental concerns over the 160 kg of caustic waste produced for each kg of vanillin in the process. However, the process is still used today for example by Borregaard in Norway, the second largest vanillin supplier in the word.[41] Borregaard is using a biorefinery to convert 90% of wood biomass into cellulose, lignin, vanillin and bioethanol.[42]

Recently, the interest in vanillin from lignin sources was renewed in the context of the general efforts to move towards renewable materials, and an improved process for the extraction was proposed by Borges da Silva *et al.*,[VI] also yielding polyurethane and biofuel byproducts. [41]

An alternative for vanillin production from biomass is bacterial conversion. Ferulic acid, which is structurally close to vanillin and also has potential for use in polyesterification reactions due to its phenol and acid groups, can be extracted from plant cell walls.[39] It is present for example in corn fiber in 3% concentration, and in bran in 0.5-1% concentration, and can be converted to vanillin by fermentation. It is also possible to convert glucose directly to vanillic acid, which can then be enzymatically reduced to vanillin.[43]

2.2.2.2 Furfural and 5-hydroxy methyl furfural

The platform chemicals furfural[VII] and 5-hydroxymethylfurfural (HMF) can be obtained from agricultural and forestry waste products such as corn cobs, oat and rice hulls, olive stones and wood chips, which are available all over the world.[36] They can be obtained by chemical transformation from pentoses and hexoses respectively, and serve as precursors to a number of industrially interesting chemicals.[44] A representation of the HMF platform is shown below in scheme 17.

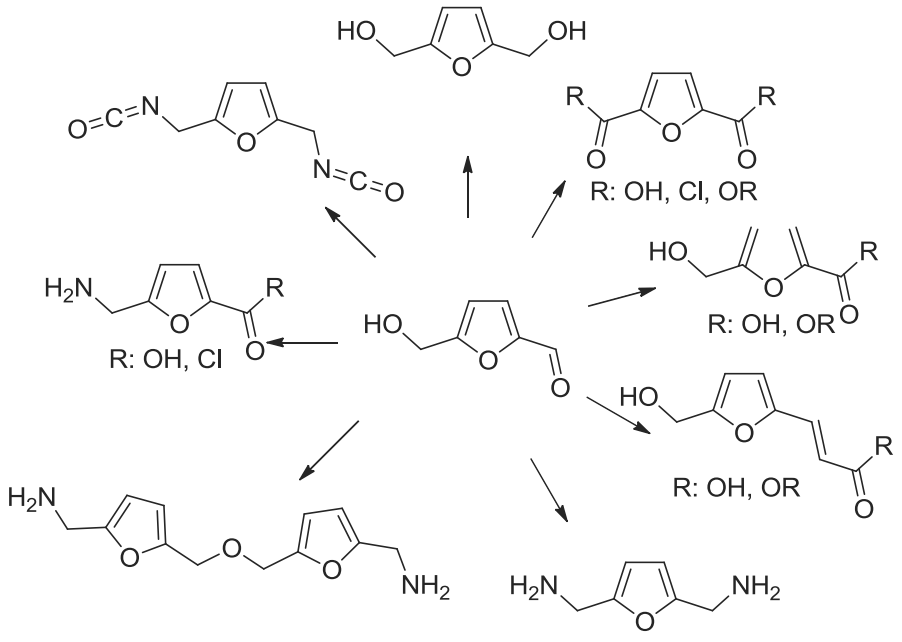

Scheme 17: HMF platform

Due to their versatility, much research has been dedicated to the development of furfural and HMF derivatives for use in polymer chemistry as well as in other fields, and has been extensively reviewed.[45-49] HMF is generally converted *in situ* due to its proneness to decomposition even in mild

[VI] See annexe for a process diagram of the valorisation of Kraft lignin proposed by Borges da Silva *et al*.

conditions. Its derivative, furandicarboxylic acid, is a very promising source for the introduction of rigidity and crystallinity in polyester resins. However, despite many promising developments in recent years, it is currently still only available at the astronomical price of 102,50€ for 5 g from Sigma Aldrich or alternatively for 215,00€ for 5 g from Alfa Aesar.[50, 51]

2.2.3 Other biomass derived products

Other biomass derived products that need to be taken into consideration for use in polyesterification reactions are vegetable oils, which contain glycerol and fatty acids, monosaccharides and derivatives which contain hydroxy groups and can be used directly in condensation reactions, and biomass derived terephthalic acid, which has been a focus of research into a fully biosourced PET.

2.2.3.1 Vegetable oils

Vegetable oils, shown in scheme 18, make up an important part of the available biomass, and about 80% of all oils, the other 20% being oils from animal origin. They are annually renewable, and are mostly used for animal and human consumption.

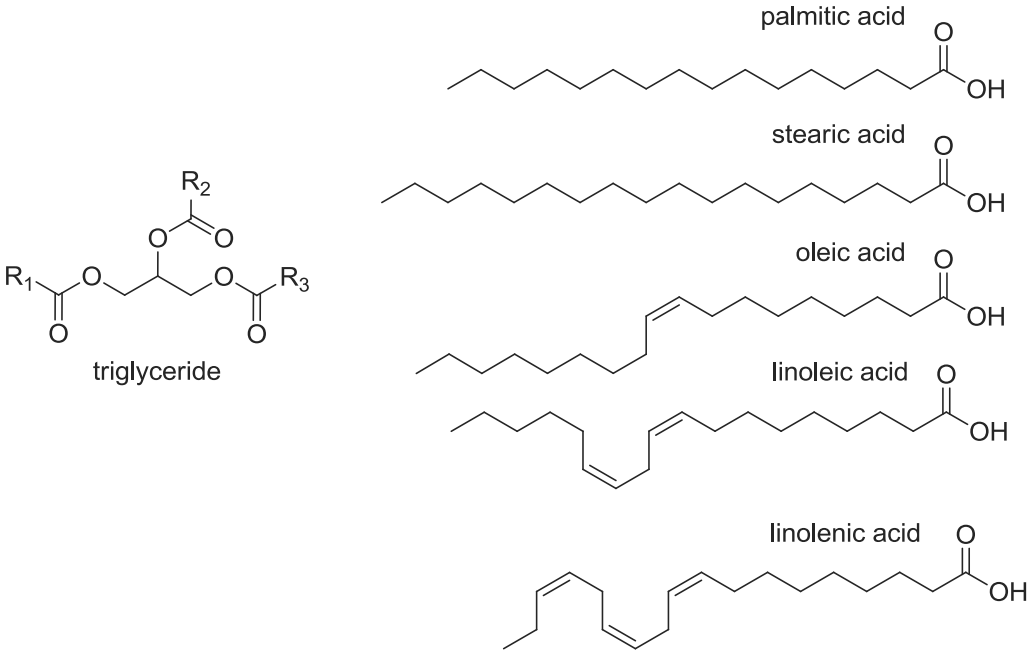

Scheme 18: Important vegetable oils

Vegetable oils are triglycerides, and hydrolysis of the ester bonds yields glycerol and a mix of fatty acid. Depending on the origin of the oil,[VIII] the fatty acids and average unsaturation vary.[52]

[VII] See annexe for a diagram of the furfural platform

[VIII] See annexe for details on the different fatty acid contents and unsaturations of important vegetable oils

Vegetable oils have been used in coatings since 1864, when linoleum, a floor coating on linseed oil basis, was commercialised. Nowadays, they are used for example in alkyd coatings, which are based on polyester resins made from a diacid or an anhydride, a triol like glycerol or pentaerithrytol, and fatty acids. The double bonds on the pendant fatty acid chains are used to crosslink the resin, and the number of unsaturations determines whether a resin is classed as drying, semi-drying or non-drying.

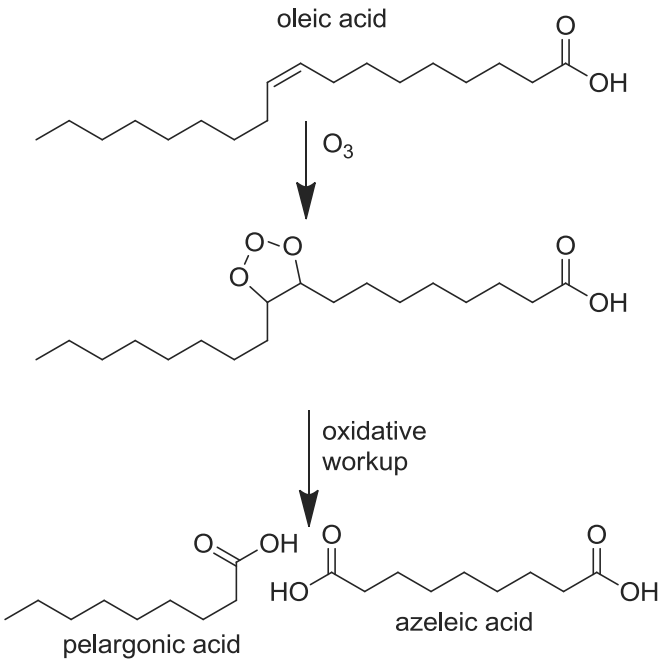

Scheme 19: Conversion of oleic acid to azaleic acid and pelargonic acid by ozonolysis

Current use of vegetable oil compounds in coatings as well as innovations towards 100% oil based polymers has been covered in several reviews.[53-55] Other than the traditional use as pendant groups in alkyd resins, vegetable oil based fatty acids have also been modified in different ways for use directly as monomers in polycondensation reactions. One possibility is for example the conversion of double bonds to hydroxy groups, for use in polyester-polyol resins.[56]

Sebacic acid, a diacid most often used in the production of polyamides, can be obtained from castor oil.[57] Oleic acid can be converted to azeleic acid, or nonane dioic acid, via an ozonolysis reaction, shown in scheme 19.[58]

Finally, fatty acids have been dimerised[IX] using different types of chemistry such as click additions and self-metathesis to give difunctional monomers for use in polycondensations.[59, 60]

2.2.3.2 Monomers from algae biomass

Algal biomass also contains oils, which are similar to those found in vegetable oils. Algal biomass is popular because it grows fast and is not in any competition with food products, and its use in polyester and polyurethane synthesis has been the subject of recent reviews.[61, 62]

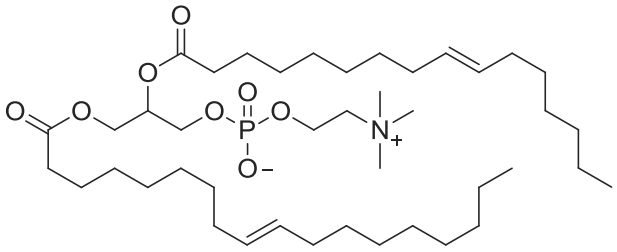

Scheme 20: Diacylglyceride from algae oil

The carbohydrate content of algae is at 75 – 80% significantly higher than that of lignocellulosic biomass, which contains only 30% carbohydrates.

[IX] For examples of dimerisations of fatty acids for polycondensation reactions, see annexe.

Other than via bacterial fermentation to important monomers such as furandicarboxylic acid and 1,2-propanediol, oil extracted from algal biomass can also be utilised for polyesterifications.

Contrary to the triglyceride form which can be found in vegetable oils, algae oil is generally present in diacylglyceride form, shown in scheme 20. Instead of a third fatty acid chain, the third glycerate chain is linked to a galactosyl or phosphate group. These oils can be transformed to diesters, as reported for example by Roesle *et al.*, and used as a monomers in polycondensation reactions.[63]

A potential problem associated with algal biomass is the large amount of energy required for drying, which can lead to high material prices.

2.2.3.3 Sugar monomers and natural polycarboxylic acids

Due to their multiple hydroxy groups, mono- and disaccharides can also be used directly in polycondensation reactions. However, their direct use is limited to applications in which either a large excess of free hydroxy groups or a large degree of crosslinking is wanted, as for example by Zamora *et al.*, who used the hydrophilicity of excess hydroxy groups to improve the hydrolysability of their materials.[64]

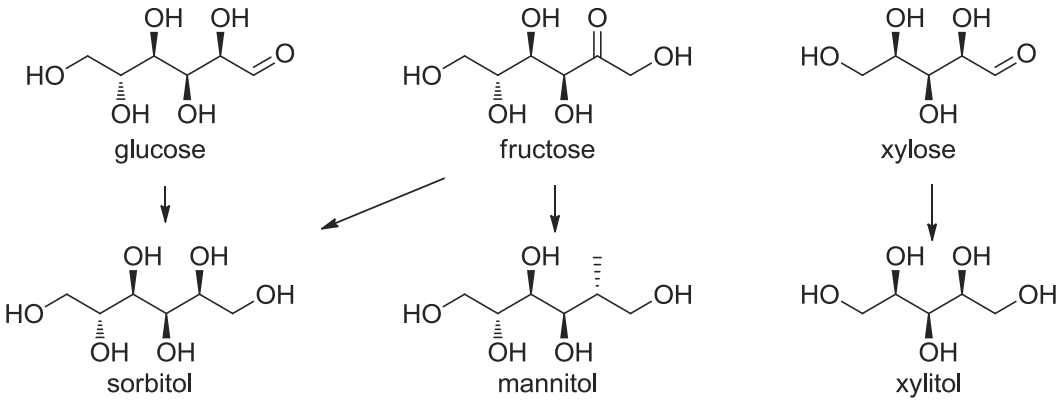

Scheme 21: Monosaccharide reductions

More importantly, glucose and related molecules can serve as platform chemicals.[X] While their oxidation can give rise to various hydroxy acids, the most important reaction in terms of polycondensation chemistry is, however, the reduction of glucose to sorbitol.[35] Some monosaccharide reductions are represented in scheme 21 above.

Sorbitol can be transformed into isosorbide in a double dehydration reaction, as shown in scheme 22 below. Due to its dicyclic structure, isosorbide is one of the rare biomass derived molecules that can introduce considerable rigidity into the polymer structure. It has been commercialised for example

[X] See annexe for an overview over the molecules that can be obtained from glucose oxidation

by the French company Roquette Frères since 2007, and the production capacity reached a volume of 20 000 t per year in 2015.[65]

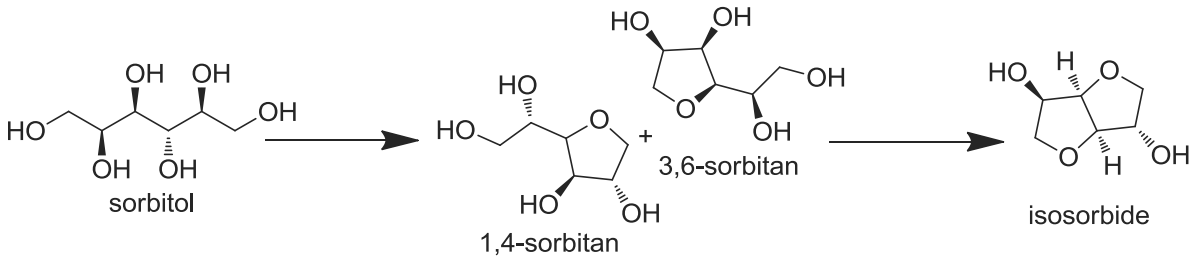

Scheme 22: Transformation of sorbitol to isosorbide

Similarly, natural polycarboxylic acids like citric acid and tartaric acid, shown in scheme 23 below, also contain both hydroxy- and carboxylic acid groups that can be used in polycondensation reactions. Citric acid and tartaric acid are present in fruits and vegetables, but can also be obtained from fermentation. The former[XI] is already exploited in many different applications such as food additives, cosmetics, pharmaceuticals and cleaning agent.[66, 67]

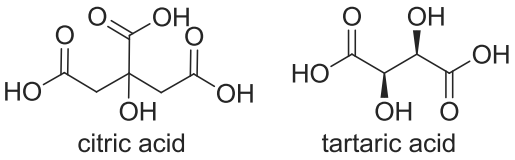

Scheme 23: Natural polycarboxylic acids

2.2.3.4 Biobased terephthalic acid

In parallel to the development of furandicarboxylic acid based alternatives to PET, many efforts have been devoted to the possibility of producing PET completely from biomass. While partially biobased PET, synthesised from petrochemical terephthalic acid and biomass based ethylene glycol, is already commercialised for example in the Coca Cola plant bottle, work on biobased terephthalic acid is still in progress. Backing the efforts is, for example, a collaboration of the US based companies Coca Cola, Heinz, Ford, Nike and Procter & Gamble.[68] It can therefore be supposed that biobased terephthalic acid will become commercially available in the not too distant future, also because a higher demand, leading to a decrease in price, would benefit the companies behind its development.[69]

The approach differs a little from those for most other monomers described above, as many of the different technologies to manufacture biobased terephthalic acid rely on the disintegration of biomass based molecules to simpler compounds, and their subsequent rebuilding, rather than on the utilisation of functionalities already present in biomass.

One method, shown in scheme 24 below, was patented by Gevo, and relies on a fermentation process to convert carbohydrate biomass to isobutanol, which can then be converted to *p*-xylene, a precursor of terephthalic acid.[70, 71] Similarly, Global Bioenergies developed a lab scale process employing enzyme modified bacteria to obtain isobutene gas from glucose biomass.[72]

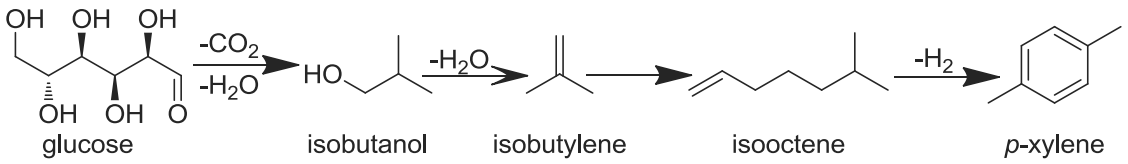

Scheme 24: Gevo's path to *p*-xylene from biomass

On the other hand, the companies Virent and Anellotech use thermomechanical approaches, also to obtain the precursor *para*-xylene. While Virent utilises an aqueous catalytic reforming process to degrade sugars to smaller hydrocarbon units, Anellotech employs a pyrolysis technique to turn lignocellulosic biomass into its aromatic components.[69, 73]

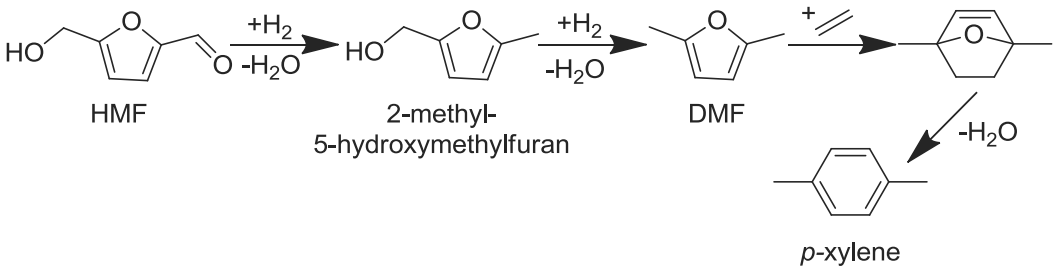

Scheme 25: Micromidas transformation of HMF to *p*-xylene

A different approach is followed for example by the company Micromidas, and exemplified in scheme 25 above, relying on the transformation of furan derivatives obtained from biomass to *para*-xylene. While a number of different variations of this endeavour have been published, it remains to be seen when it will become competitive and reach commercialisation stage.[74-76]

2.2.4 Biomass based monomers available for the synthesis of biosourced polyesters

A variety of renewable monomers from non-food competing biomass, both lignocellulosic and carbohydrate based, are available for use in polycondensation reactions. Below in scheme 26, an overview is given of the most important monomers for use in polycondensation reaction.

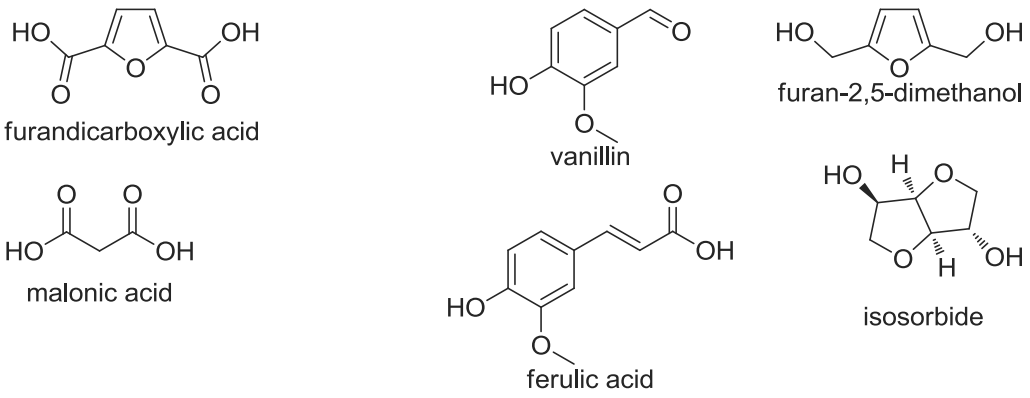

[XI] See annexe for some examples of tartaric acid derivatives in polycondensation reactions.

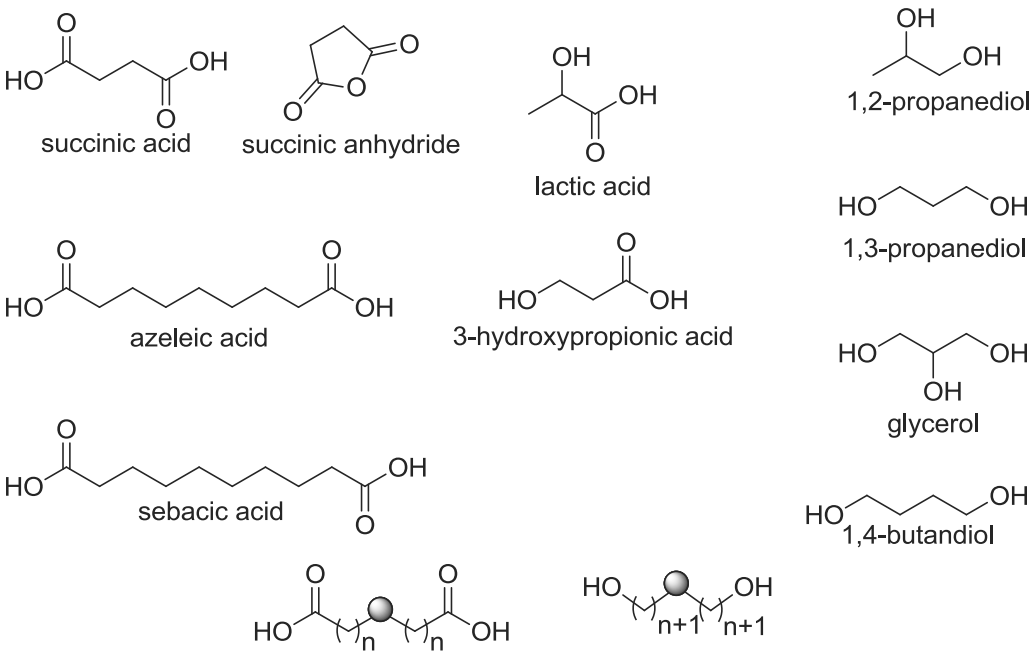

Scheme 26: Polycondensation monomers from biomass

With a view to the compatibility with coil coating resins, the selection was limited to di-and trifunctional acidic and hydroxy compounds, and monomers containing non-aromatic double bonds were excluded. Monomers which are not commercially available or unlikely to become commercially available on a large scale were also not shown. Due to the rarity of aromatic compounds, vanillin and ferulic acid are also included despite not fulfilling these criteria.

Table 3: Commercial availability of some biobased monomers (Hansen 2014)

monomer	volume (kt/year)
sebacic acid	15-20
FDCA	40
succinic acid	1
1,4-butanediol	>20
1,3-propanediol	90
lactic acid	300-400
ethylene glycol	500

The availability of some of the monomers in 2014 was reported by Harmsen *et al.* and is presented in table 3 on the left.[77] Overall, the selection of monomers available is sufficient to permit flexibility in the design, and is likely to increase in the near future as more monomers such as terephthalic acid become available. It should also be noted that some motives traditionally used in coil coating, such as methyl end groups present in trimethylol propane or neopentyl glycol, and rigidity provided by aliphatic carbon cycles or aromatic monomers are still sparse among renewable compounds.

2.3 Polymers from renewable monomers in the literature

A large amount of polymers based fully or partially on renewable monomers have been reported in the literature, and illustrate the variety of products that can be made from biomass. First, a selection

of linear aliphatic polyesters as well as some conclusions about their reactivity and about the possibilities for tuning their properties will be presented. Then, the introduction of more than bifunctional monomers to create functionalised or hyperbranched products will be discussed, followed by an overview of biobased thermosets and coating products present in the literature.

Lastly, the different means to introduce rigidity in a coating are discussed. The most explored options for this purpose are the incorporation of isosorbide and furandicarboxylic acid into the structure, but alternatives, such as the use of vanillin derivatives and other biobased rigid monomers exist.

After providing a short overview of furandicarboxylic acid based polyesters, and less prominent rigid monomers, the use of isosorbide in different types of polymers will be addressed. The main focus will be on the different properties influenced by the incorporation of isosorbide. In the end, use of vanillin and its derivates in polymers will be reviewed, concentrating on its reactivity and the potential in polymerisation reactions.

2.3.1 Linear polyesters from renewable monomers

One of the most prominent linear polyesters from biomass monomers is polybutylene succinate (PBS). Its reactivity has been investigated for example by Jacquel *et al.*, who investigated different catalytic systems to enable the synthesis of high molecular weight samples of polybutylene succinate despite its poor thermal stability, limiting reaction time.[78] The activity of organometallic catalysts based on metal was found to follow the order titanium >> zirconium ~ tin > hafnium > antimony > bismuth.

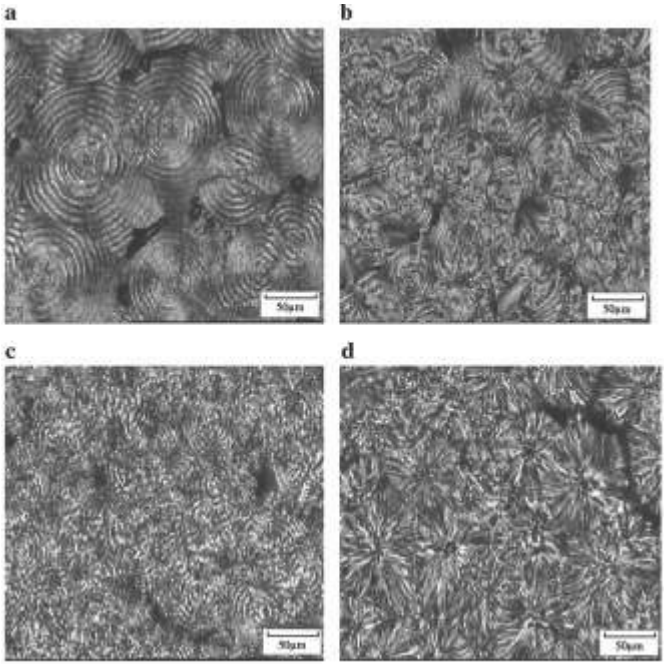

aPBS, **b**EG 5%, **c**EG 10%, **d**EG 15%

Figure 12: Polarisation optical microscopy (Zhou 2012)

Different modifications of polybutylene succinate have also been reported, and are shown in scheme 27, 28 and 29. For example, Zhou *et al.* synthesised copolymers from polybutylene succinate and polyethylene glycol (PEG), and found that they could change the thermal properties and morphology by changing the relative amount of ethylene glycol in the polyester chain.[79] Both the melting point and the crystallinity were decreased with increasing PEG content. This was also reflected in the crystalline morphology. The PEG inhibited the lamellar twisting growth, so that samples containing more

ethylene glycol displayed smaller spherulites than pure polybutylene succinate, as shown in figure 12 above.

Using a different type of modification, Yokohara *et al.* found that blending polybutylene succinate with polylactic acid could overcome some of the materials' inherent weaknesses, such as slow crystallisation behaviour, despite the immiscibility of the two materials.[80]

Xu *et al.* found that the melting and crystallisation temperatures of a copolymer from succinic acid with 1,4-butanediol and 1,3-propanediol could be decreased by increasing the propylene succinate content.[81]

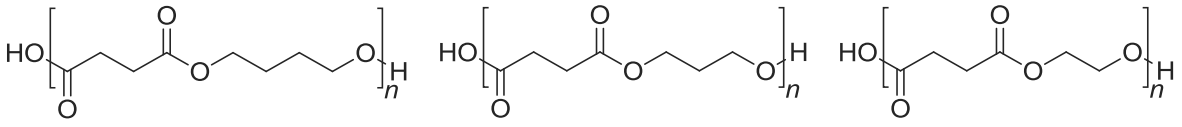

Scheme 27: Succinic acid based polyester units

On the other hand, Umare *et al.* synthesised copolymers from 1,3-propanediol with succinic acid, adipic acid and sebacic acid, in the hope that the different number of carbon atoms in the chain segments compared to polybutylene succinate and other 1,4-butanediol based aliphatic polyesters would lead to new properties.[82]

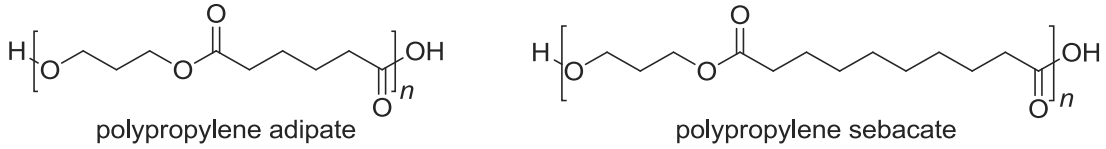

Scheme 28: 1,3-propanediol based polyester units

Tsai *et al.* also examined copolyesters from succinic acid and 1,3-propanediol with ethylene glycol in different ratios, and found that the crystallinity is decreased significantly with increasing content of 1,3-propanediol.[83]

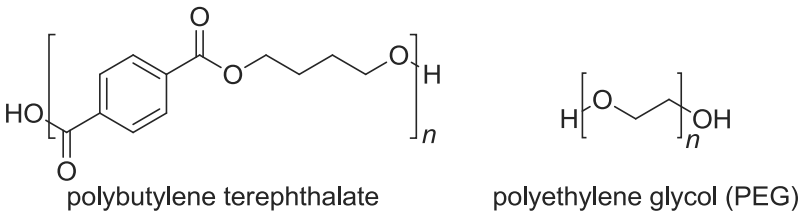

Scheme 29: PBT and PEG

An example of a partially biobased polyester was presented by Tachibana *et al.*, who synthesised partially biobased polybutylene terephthalate from 1,4-butanediol obtained from furfural, and confirmed that its melting point and molecular weight were equivalent to the petroleum based material.[84]

In terms of applications, an important area for biomass based polymers, due to their inherent biocompatibility and often good biodegradability properties are biomedical products. In order to

obtain a product with good drug release properties, Teomim *et al.* modified ricinoleic acid, which can be obtained from castor oil, with succinic acid or maleic acid, followed by a condensation reaction to yield polyanhydrides, as shown in scheme 30 below.[85]

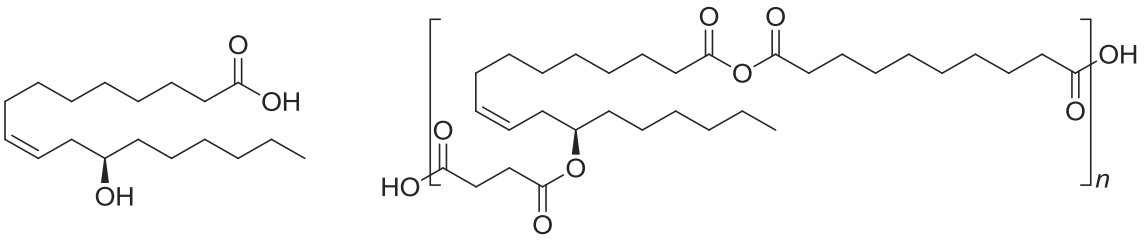

Scheme 30: Ricinoleic acid and ricinoleic acid based polyanhydride (Teomim 1999)

A different biomedical application, namely devices such as stents, was targeted by Guo *et al.*, who synthesised shape memory polymers from 1,3-propanediol, sebacic acid and itaconic acid.[86] The authors found that the polyester possessed excellent shape recovery and fixity properties, and that they could tune the switching temperature and shape recovery speed through the incorporation of different amounts of ethylene glycol into the structure.

2.3.2 Functionalised polyesters based on biomass

In order to be used as a thermosetting resin, some free chain functionality is necessary. In the case of polyester melamine thermosets, free hydroxy groups are used to crosslink the different chains via melamine rings. There are different ways to introduce free functionalities in the chains, and some examples from the literature are presented in the following section. [XII]

2.3.2.1 Hydroxy functionalised polyesters containing pentaerythritol or glycerol

The most common monomers to achieve hydroxy functionalisation are pentaerythritol and glycerol. Many reports of their use in polyesters exist. Below, some examples of their use together with biobased monomers are presented.

Brioude *et al.* for instance made hydroxy functionalised polyesters from adipic acid and glycerol, and investigated the effect of monomer ratio on their structure and stability.[87]

Kricheldorf *et al.* also investigated the polycondensation of dimethyl sebacate and pentaerythritol to obtain a hydroxy functionalised, branched network.[88] Equimolar amounts of both reagents or excess of pentaerythritol and optimised reaction conditions were used were used to avoid gelation.

[XII] One type of products that are not described are polymers for biomedical applications based on citric acid. See annexe for more details.

Lastly, Celli *et al.* introduced 0,5% to 2% of glycerol into a polybutylene dodecanoate network.[89] The authors obtained semi-crystalline polymers, and found that the quantity of glycerol introduced did not affect the melting temperature or level of crystallinity.

2.3.2.2 Unsaturated polyester resins and alkyd paints

One possibility to crosslink polyester networks is through the introduction of unsaturation, followed by radical crosslinking, for example through the incorporation of itaconic acid, which contains a double bond.

Barrett *et al.* used itaconic acid in a variety of aliphatic polyester compounds containing biosourced monomers, such as succinic acid and sorbitol, but also containing petroleum based monomers such as trimethylol propane and 1,4-cyclohexanedimethanol.[90] The polymers were cured with 0,1% of the photoinitiator diethoxyacetophenone, shown in scheme 31, and their mechanical properties were examined.

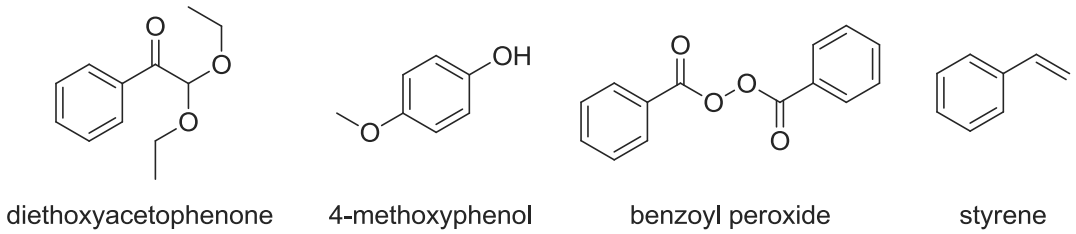

Scheme 31: Compounds used in the curing of unsaturated polyester resins

Itaconic acid was also used by Dai *et al.*, who incorporated it into a water soluble polyester for coating applications.[91] It was condensed with ethylene glycol, 1,4-butanediol or 1,6-hexanediol, and cured in the presence of 0,5% of the radical inhibitor 4-methoxyphenol, shown in scheme 31, under a mercury lamp. The mechanical properties of the resulting coatings were examined, and it was found that the pencil hardness decreased with increasing diol length, while the performance in the T-bend test improved.[XIII] Teramoto *et al.* also incorporated itaconic acid or maleic acid into the polybutylene succinate structure, shown in scheme 32, and crosslinked the resulting resin with benzoyl peroxide.[92]

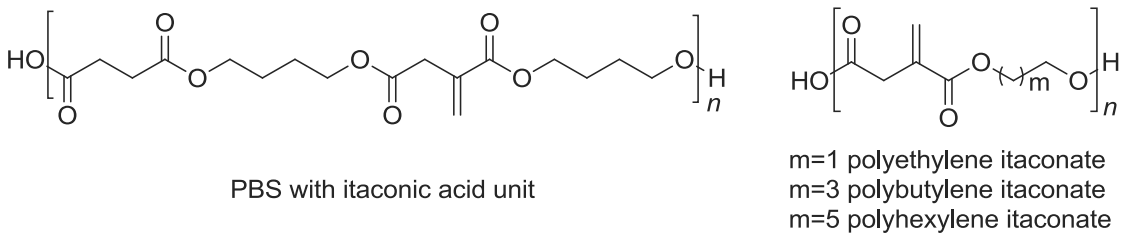

Scheme 32: Polyester containing itaconic acid

[XIII] T-bend test – A mechanical test to assess the behaviour of the coating upon deformation – see Chapter 7

A different biosourced monomer was used by Atta *et al.* to introduce unsaturation, namely the rosin based acrylopimaric and maleopimaric adducts shown below in scheme 33.[93, 94] It was condensed with different monomers such as 1,2-propanediol, ethylene glycol, phthalic anhydride, isophthalic acid, adipic acid and maleic anhydride as an additional source of unsaturation. The resulting resin was cured with styrene, and the influence of different monomer compositions on the mechanical performance was defined.

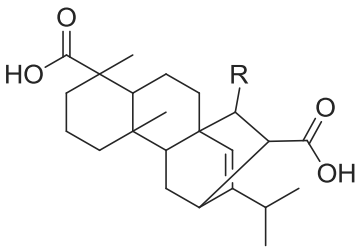

R = COOH - maleopimaric adduct
R = H - acrylopimaric adduct

Scheme 33: Rosin based adducts (Atta 2007)

Another class of unsaturated polyester coatings are alkyd paints. These are traditionally synthesised from fatty acids or triglycerides, and have therefore always contained biomass components. This field is still being developed for example through efforts to replace all present monomers by biomass based compounds, or to include new types of oils.[95] Several reviews detailing both the traditional uses and new innovations have been published recently.[96-98] Because there is a wide variety of fatty acids from different vegetable oils that can be used, and their function in alkyds as pendant groups for photocrosslinking is not really relevant to coil coating applications, they will not be addressed further in this section.

2.3.2.3 Polyurethane coatings based on biomass

Polyurethane coatings are based on hydroxy functional polyester or polyester polyol resins, and are crosslinked using isocyanates. Several strategies have been used to replace different parts in the polyurethane composition with biomass based material, and an overview will be given in the following section.[XIV]

Fungible replacement of petroleum based monomers was practiced for example by Anand *et al.*, who used sorbitol to introduce hydroxy functionality into their polyester polyol, and to a larger degree by Gubbels *et al.*, who prepared a hydroxy functionalised polyester resin from dimethylfurandicarboxylate, 2,3-butanediol and glycerol, pentaerythritol or trimethylol propane.

In a different approach Gustini *et al.* from the same group used lipase catalysed synthesis to obtain fully biobased polyurethane coatings.

Lastly, vegetable oils were used by Kong *et al.* and Gaikwad *et al.* in order to obtain polyol products. The former transformed canola oil, while the latter epoxidised karanja and cotton seed oil, followed by reaction with polyethylene glycol.

[XIV] For details about polyurethane coatings based on renewable monomers, see annexe.

2.3.2.4 HMMM crosslinked polyester coatings

Only very few examples of the use of renewable components in melamine crosslinked polyester coatings are reported. One example is the work of Siyab *et al.*, who synthesised two resins, one of which contained only biobased monomers, and another one which contained both biobased monomers and a petroleum based monomer.[17] The exact nature of the biobased monomers was not specified. The paper examines the performance of both coatings and finds that they are worse than the fully petroleum based resin, but promising.

Johansson *et al.* also incorporated renewable material into a melamine crosslinked polyester coating, but used it as a reactive diluent, to lower the resin viscosity. It was therefore only incorporated during the curing.[99] Rapeseed methyl ester, which mostly contains chains with 16 or 18 carbons and none to three unsaturations, was added in different quantities and with different cosolvents, and the effects on the curing and final film were evaluated. The incorporation caused a decrease of film T_g, and some oxidative crosslinking of the double bonds was detected. However, it also improved the levelling ability of the film, and overall, no quality deterioration was caused.

2.3.3 Introducing rigidity into the polyester structure

A rigid structure is important for a coating as it raises the glass transition temperature, which needs to be above the temperature of use, and provides hardness and impact resistance to the polymer film. There are several different ways in which rigidity can be introduced. Firstly, increasing the crosslinking density impedes molecular motion, which makes the overall network more rigid. However, it also stops the chains from moving with respect to each other, which can have a negative impact on the flexibility of the product.

The second possibility is the incorporation of smaller rigid segments into the chain, for example through the use of rigid monomers. While a certain amount of hardness can be achieved by introducing short chain monomers, such as ethylene glycol and succinic acid, the most effective and also traditionally preferred method is the use of aromatic compounds. Many aliphatic monomers based on biomass exist, and have been used successfully in various applications not requiring particularly rigid structures as demonstrated above. The replacement of aromatic compounds can however be a bit more difficult. Three of the most popular biomass based group of candidates are furan based monomers, isosorbide and vanillin derivatives that can be obtained from lignin. The following two sections are dedicated to the different examples reported of the use of the latter two in polyester compounds.

Furan based monomers are also very promising candidates, as they increase the hardness, water resistance and tensile strength compared to terephthalic acid, even though a colouration problem has been observed by several authors. Nevertheless, both partial and complete replacement in polyethylene terephthalate, as well as recycling of polyethylene furanoate (PEF) has been proven possible. Furan based monomers were not examined in this work due to the current high price of furandicarboxylic acid.[XV]

2.3.3.1 Isosorbide as a rigidity introducing monomer

Isosorbide is the most stable member of the isohexide family, which also contains its diastereomers isoidide and isomannide. Isohexides comprise two tetrahydrofuran cycles which are connected in a cis arrangement with a 120° angle between the two cycles, giving the molecule a concave shape. Each of the isohexides contains four chiral carbon atoms, and the diastereomers differ by the position of the hydroxy group, which can be either in an endo position, i.e. oriented towards the inside of the cavity, or in an exo position, oriented away from it, shown in scheme 34.[100]

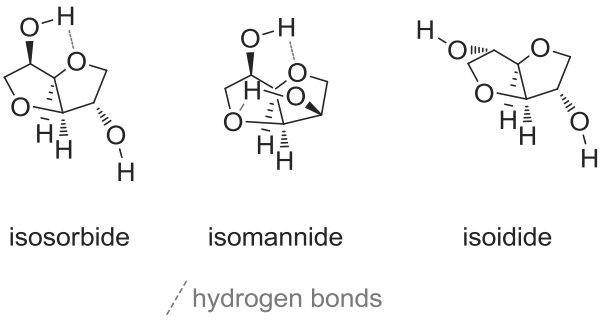

Scheme 34: Hydrogen bonds and conformations of isohexides

Hydroxy groups oriented in an endo fashion can form hydrogen bonds with the close by oxygen arom. This and the steric bulk of the two cycles cause the exo hydroxy to be significantly more reactive than the endo hydroxy. The difference was evidenced for example by Che *et al.*, who recorded the NMR shift of each hydroxy at different temperatures, as shown in figure 13 on the left.[101]

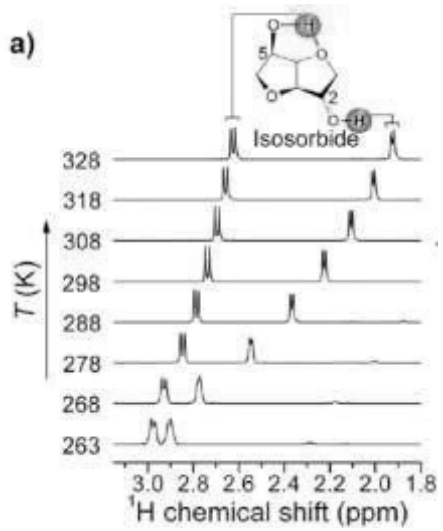

Figure 13: NMR signals of isosorbide hydroxylic hydrogens (Che 2015)

Isosorbide has been employed directly and in derivative form in a variety of polyester and coating products, and its capability to introduce rigidity is well documented. Its use has been reviewed by Kricheldorf *et al.*, and more recently by Fenouillot *et al.*, and Galbis *et al.*, too.[102-104]

In the following section, observations made by different authors concerning the incorporation of isosorbide as well as examples of different types of polymers containing isosorbide

[XV] For details of furan derivative containing polymers and their properties, see annexe.

that were reported are presented.

2.3.3.1.1 The effect of isosorbide on polyester properties

The effect of isosorbide on the T_g in a variety of aliphatic and aromatic products was studied as early as 1992. Braun *et al.* synthesised a series of polyesters based on isosorbide and aliphatic diacid chlorides with chains containing 4 – 14 carbons, and on isosorbide and aromatic diacids, shown in scheme 35 below.[105]

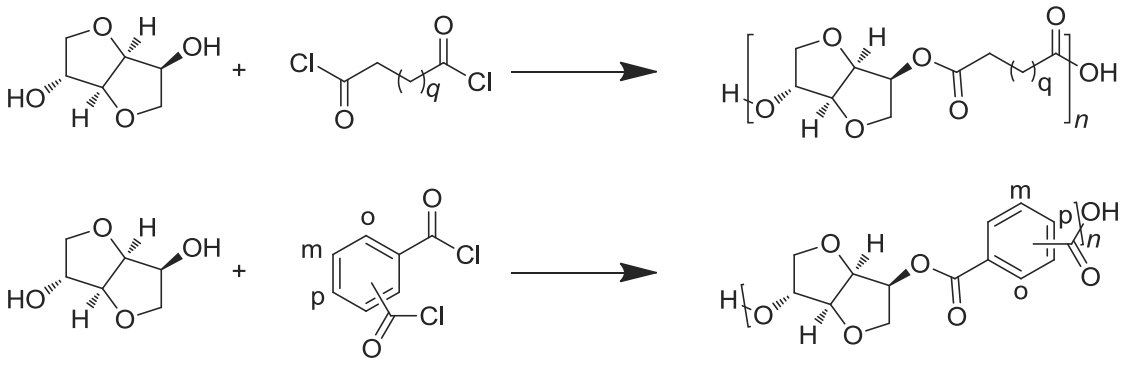

Scheme 35: Aliphatic and aromatic isosorbide polyesters (Braun 1992)

The molecular weight increased with longer chains and was biggest for the sebacic acid compound, at 23 000 g/mol. It decreased again until hexadecandiacid chloride to only 11 400 g/mol. Only very small sized molecules were obtained for the aromatic acids, between 2000 and 4000 g/mol. As shown in table 4 below, the glass transition temperature was significantly higher for the aromatic polyesters than for their aliphatic counterparts. Among the fully aliphatic compounds, the shortest chains had the highest glass transition temperatures.

Table 4: Glass transition temperatures of isosorbide polyesters (Braun 1992)

acid chloride		**T_g polyester**
name	**number of carbons q***	**°C**
succinic	1	65
adipic	3	25
suberic	5	11
sebacic	7	0
dodecanedioic	9	-2
tetradecanedioic	11	-4
thapsic	13	-4
	position	
phthalic	o	118
isophthalic	m	138
terephthalic	p	147

*see scheme 35 above

Solubility in organic solvents was improved with increasing chain length. Few differences were detected in the thermal stability of the polyesters, which decomposed between 330 °C and 490 °C. Stability was improved by 30 °C when the air was replaced with a nitrogen atmosphere during the synthesis.

Fumaric acid was then incorporated in the isosorbide sebacate product to make an unsaturated polyester resin, which was

subsequently crosslinked with styrene or methyl methacrylate and benzoyl peroxide initiatior. The final glass transition temperatures were, depending on the resin content, between 10 °C and 200 °C for the styrene compositions, and between 25 °C and 92 °C for the methylmethacrylate compositions. Both drying time and crosslinking density were found to be within a satisfying range. Polycarbonate resins and polyurethane resins were equally synthesised successfully.

Isosorbide terephthalate polyesters, albeit with longer chains, were shortly after studied in greater detail by Storbeck *et al.*, who also used terephthaloyl chloride for the synthesis.[106] A strong dependence of both the intrinsic viscosity and glass transition temperature on the molecular weight of the final product was observed as shown in table 5. Adding ethoxy side chains to the terephthalic acid ring caused the glass transition temperature to decrease by about 70 °C.

Table 5: Dependence of glass transition temperature and viscosity of isosorbide -terephtalates on $M_{\bar{n}}$ (Storbeck 1993)

$M_{\bar{n}}$	η	T_g
g/mol	**dL*g^{-1}**	**°C**
25600	0,67	205
23200	0,59	204
21300	0,52	203
14200	0,40	197
7900	0,29	187
6400	0,25	180
3200	0,13	158

In a separate publication, terephthalates containing varying quantities of isosorbide and ethylene glycol were examined.[107] A linear increase in glass transition temperature with increasing isosorbide content, as well as a slight increase in intrinsic viscosity and a decrease of crystallinity, were observed.

More recently, Moens *et al.* patented a method for the preparation of polyesters from isosorbide and recycled PET.[108]

The effect of the relative amount of isosorbide in a polyester has also been studied. Farrugia *et al.* patented the synthesis of isosorbide, succinic acid and azeleic acid copolyesters.[109] The composition was varied to achieve different glass transition temperatures, acid values and molecular weights, as shown in table 6 below.

Table 6: Characteristics of polyesters based on isosorbide, succinic acid and azeleic acid (Farrugia 2011)

relative amount of monomers			T_g	acid value	$M_{\bar{w}}$	$M_{\bar{n}}$
succinic acid	**isosorbide**	**azeleic acid**	**°C**	**mg KOH/g**	**g/mol**	**g/mol**
0,5	0,5	0	66	14,1	3800	2400
0,425	0,5	0,1	53	6,4	11500	4700
0,385	0,5	0,15	42	19,4	11002	4160
0,45	0,5	0,05	51	17,7	4699	2601
0,45	0,5	0,05	60	4,1	7444	4092

Similarly, Jacquel *et al.* studied the effect of incorporating 5, 10 and 20% of isosorbide into polybutylene succinate.[110] They observed a decrease in polyesterification rate, as shown in figure 14,

attributed to the low reactivity of the hydroxy group in the endo position, as well as a decrease of molecular mass compared to pure PBS.

An increase of glass transition temperature from -30 °C to -11 °C at 20% isosorbide content was also observed, which was larger than the increase observed when terephthalic acid or furandicarboxylic acid were incorporated into polybutylene succinate, even at up to 60%, as shown in table 7. An increase of elongation break was equally observed, which was attributed to the loss of crystallinity.

Table 7: Glass transition temperature increase by isosorbide, FDCA and terephthalic acid (Jacquel 2015)

	Tg (°C)	amount of comonomer incorporated			
	pure	5%	10%	20%	60%
PBS + isosorbide	-30	-28	-24	-11	
PBS + FDCA	-30	-31	-24	-17	-21
PBS + terephthalic acid	-30	-31	-28	-27	

Duan *et al.* incorporated 5% - 30% and 40% respectively of isosorbide or tartaric acid based 2,3-O-isopropylidene-L-threitol, shown in scheme 36, into polybutylene succinate, decreasing its crystallinity and increasing its glass transition temperature and hydrophilicity.[111] Isosorbide was found to be more effective than the tartaric acid derivative. Mechanical properties were equally assessed and it was found that tensile strength and elongation at break were highest for the copolymer containing 20% of isosorbide, and slightly lower for 30% isosorbide, as shown in table 8. The Young's modulus was seen to decrease with increasing isosorbide content.

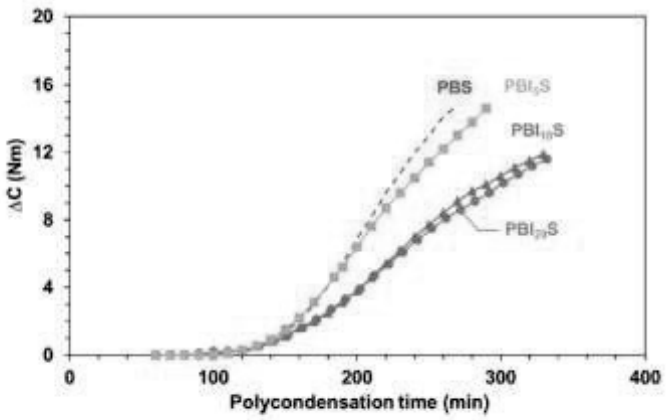

Fig. 2. Torque variation during the polycondensation of: --- PBS, ■ PBI_5S, ▲ $PBI_{10}S$ and ● $PBI_{20}S$ (temperature: 250 °C, Zr/diacid molar ratio: 1.8×10^{-3}).

Figure 14: Decrease of polyesterification rate with isosorbide content (Jacquel 2015)

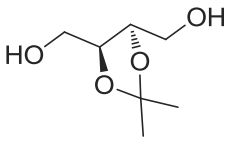

Scheme 36: 2,3-O-isopropylidene-L-threitol

Table 8: Dependence of mechanical properties on isosorbide content (Duan 2016)

isosorbide content	T_g	tensile strength	elongation at break	Young's modulus
%	°C	MPa	%	MPa
0	-34	40,6	382	339
5	-26	45,3	731	300
10	-21	47,5	925	289
20	-19	23,5	740	235

2.3.3.1.2 Isosorbide reactivity

The problem of low reactivity of the hydroxy group in endo position was addressed in different fashions by several authors. Feng *et al.* used isosorbide derivatives in a polyethylene terephthalate synthesis in order to counteract the poor secondary diol reactivity as well as the volatility of the isosorbide which led to only partial incorporation.[112] Isosorbide-2-terephthalate and isosorbide-5-terephthalate, shown in scheme 37, were synthesised and purified prior to polymerisation. The glass transition temperatures were 146 °C and 153 °C respectively, and both compounds were successfully incorporated at 15% into polyethylene terephthalate.

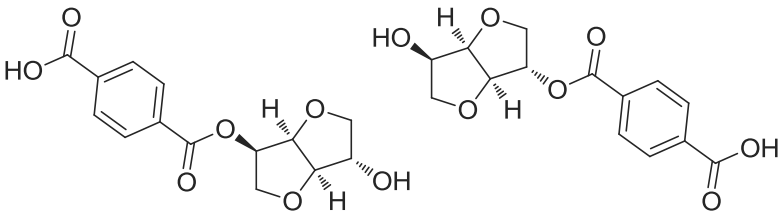

Scheme 37: Isosorbide 2- and 5- terephthalates

Yoon *et al.* also used an alternative strategy to solve react isosorbide.[113] The steric hindrance around the endo hydroxy group was reduced by *in situ* esterification with acetic anhydride, which was added to the reaction mixture, followed by transesterification. This method was successfully used to prepare high molecular weight polyesters with cyclohexanedicarboxylic acid, shown in scheme 38. However, it was found that the isosorbide ring was broken when too high quantities of acetic anhydride were added to the reaction.

Another solution for the low reactivity was proposed by Noordover *et al.*, who introduced citric acid into the resin.[114] Due to its capability of forming anhydride groups, citric acid was able to esterify both isosorbide hydroxy groups to a satisfying extent, so that isosorbide based resins could be used as acid functionalised powder coatings.

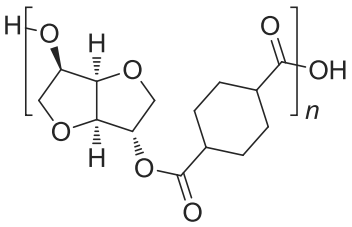

Scheme 38: Polyester from isosorbide and CHDA

On the other hand, Kricheldorf *et al.* attempted to produce cyclic monomers and dimers from isosorbide and various aliphatic diacid chlorides, but were not successful.[115] Instead, cyclic oligomers and polymers were synthesised, but deemed not suitable for use in ring opening polymerisations for example with lactones.

Later, the group succeeded in making copolyesters from isosorbide, lactide and isophthalic acid.[116] Isosorbide and lactide were first oligomerised and then reacted with isophthaloyl chloride. The resulting polyesters had high glass transition temperatures between 64 °C and 180 °C. It was furthermore observed that the thermal stability decreased with increasing lactide content.

Lastly, a completely different method for isosorbide based polyester synthesis was introduced by Habeych *et al.*, who compared the efficiency of the enzyme Candida Arctica Lipase B (CALB) in the polyesterification of isosorbide, isomannide and isoidide with succinic acid.[117] The endo hydroxyl group was found to be preferred by the enzyme, so that a conversion of 93,7% was achieved for isomannide.

2.3.3.1.3 Biodegradability of isosorbide compounds

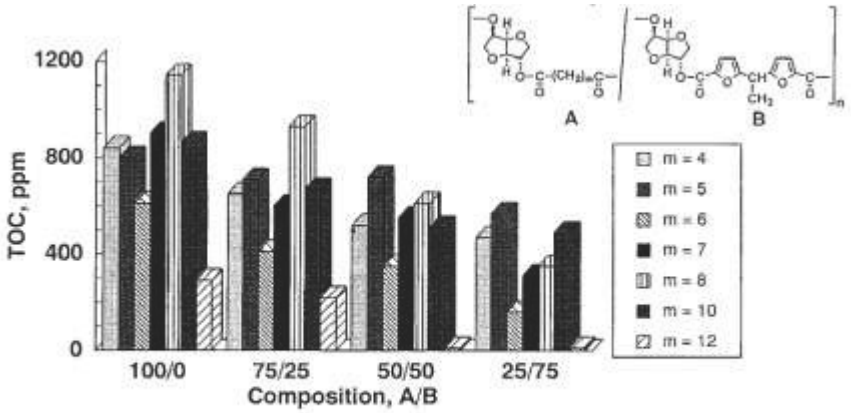

Figure 4 Enzymatic degradation of polyesters **5a–5g** by *P. pancreas* lipase. Conditions: lipase, 250 units; polyester, 25 mg; film thickness, 100 μm; phosphate buffer (pH 7.0), 2 mL; incubated at 80 strokes/min at 37°C for 24 h.

Figure 15: Enzymatic degradation of isosorbide polyesters with increasing aliphatic chains (Okada 1999)

The effect of isosorbide on biodegradability was examined by Okada *et al.*, who synthesised polyesters from isosorbide, a furan diester and aliphatic diesters with various chain lengths, shown in scheme 39, and studied their enzymatic degradation.[118] While the degradability decreased with increasing furanic content, no correlation between the chain length of the aliphatic monomer and degradability was observed, as shown in figure 15.

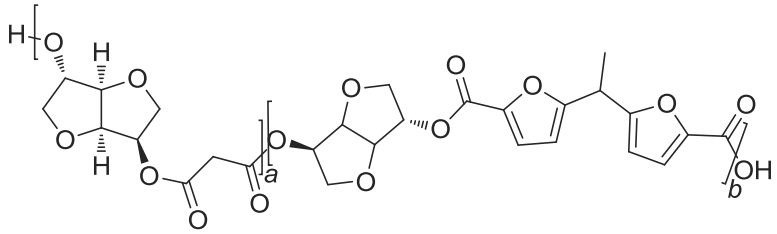

Scheme 39: Copolymer from isosorbide, furandiester and aliphatic diesters (Okada 1999)

2.3.3.1.4 Isosorbide containing polyurethane, epoxy and polycarbonate resins and unsaturated polyesters

Isosorbide has also been used as a monomer in a variety of thermosets, such as epoxy and polyurethane resins. Besse *et al.* for example developed isosorbide based polyhydroxyurethanes, an alternative to isocyanate based polyurethanes synthesised from dicyclocarbonates and diamines.[119] Monomeric and oligomeric dicyclocarbonates were crosslinked with four different diamines, and glass transition temperature, thermal stability and degradation products were assessed.

Polyhydroxyurethanes based on two different sized oligomers were compared. Both were amorphous, had low molecular weights at 7000 – 8000 g/mol and glass transition temperatures between 15 °C and 19 °C. 5% weight loss was detected at 242 °C and 237 °C, and the weakest bond was confirmed to be the urethane bond which is not affected by the presence of oxygen. By modifying the rigidity of the diamine, the T_g could be tuned from 0 °C to 59 °C.

Noordover *et al.* made hydroxy functionalised resins from isoidide or isosorbide with succinic acid and glycerol, 1,3-propanediol, 2,3-butanediol or trimethylol propane which were crosslinked to also make polyurethane resins.[120] Both powder and solvent borne coating techniques were used. The isosorbide resins were additionally acid functionalised with citric acid and crosslinked with an epoxy resin. The resulting coatings possessed good solvent resistance, hardness and impact resistance.

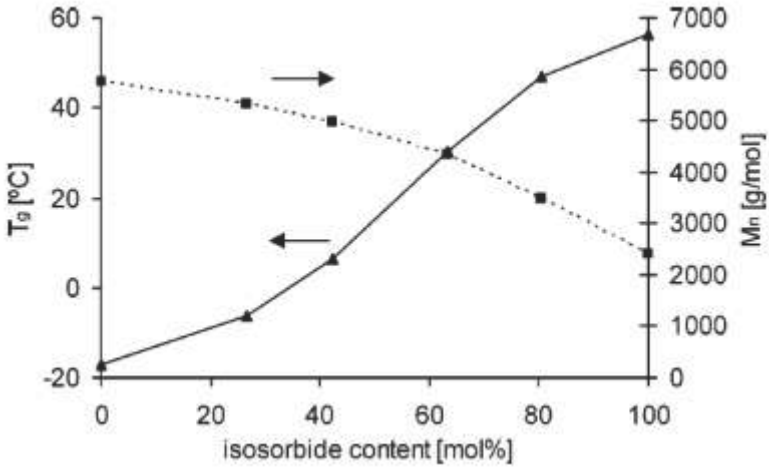

Figure 16: Development of T_g and M_n with isosorbide content (Noordover 2009)

The effect of isosorbide content on resin properties was also examined by the same authors.[121] Copolyesters were synthesised with neopentyl glycol and succinic acid, and a decrease of molecular weight as well as an increase of glass transition temperature was observed with increasing isosorbide content, as shown in figure 16. The resins were cured with isocyanates to obtain films, and a strong dependence of the coating colour, which ranged from colourless to slightly yellow, on the purity of the isosorbide was observed. Solvent resistance and mechanical performance was moderate but could be improved by the introduction of a branched structure.

Van Haveren *et al.* created powder coatings from isosorbide with a variety of bio- and petrosourced comonomers.[122] Linear biobased acids such as succinic acid were used, and other diols such as 2,3-butanediol, 1,3-propanediol and neopentyl glycol were incorporated. Decreasing the amount of isosorbide decreased the glass transition temperature and improved the resin colour. Citric acid and trimethylol propane were also incorporated in some of the resins, and both acid and hydroxy functional polymers were obtained. The resins were crosslinked with epoxy functionalised crosslinkers or blocked isocyanates respectively, and good hardness, solvent and impact resistance was observed.

Feng *et al.* mentioned above also developed an isosorbide based epoxy resin.[123] Isosorbide was transformed into di- and triglycidyl ethers, shown in scheme 40, and crosslinked with different amines. The water uptake of the resulting epoxy resin could thus be optimised to permit controlled biodegradation, for example for biomedical applications.

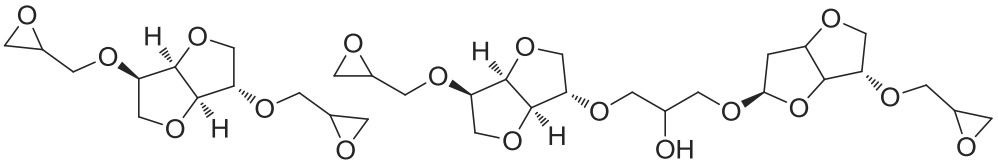

isosorbide diglycidyl ether biisosorbide triglycidyl ether

Scheme 40: Isosorbide glycidyl ethers

Hong *et al.* also used isosorbide diglycidyl ether as well as isosorbide diamine, shown in scheme 41, in combination with petroleum based components as epoxy and amine parts respectively in amine cured epoxy resins.[124] The properties of the isosorbide products were compared with those of the petroleum based epoxy and amine compounds.

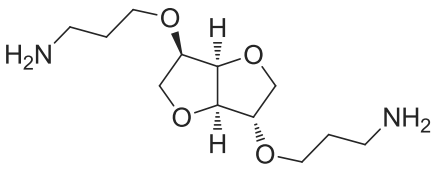

Scheme 41: Isosorbide di(3-aminopropyl ether)

Since a higher crosslinking density was achieved with the petroleum based epoxy resin, it also showed superior mechanical properties to the isosorbide based compound, but the isosorbide based diamine, displayed excellent mechanical qualities.

An acid functionalised resin was prepared by Gioia *et al.* from isosorbide, succinic acid, glycerol and recycled PET oligomers.[125] After crosslinking with an epoxy resin, it was found suitable for powder coating applications in gloss and impact strength tests.

Lastly, the glass transition temperature of a polyurethane from poly-3-hydroxybutyrate-co-3-hydroxyvalerate crosslinked with isocyanate was successfully raised from 5 °C to 34 °C by the incorporation of isosorbide.[126]

The same group also prepared films from diepoxy polyhydroxybutyrate-co-hydroxyvalerate, shown in scheme 42, and isosorbide diglycidyl ether.[127] A polycarbonate[XVI] based on isosorbide after reaction with bisphenyl carbonates was also reported.[128]

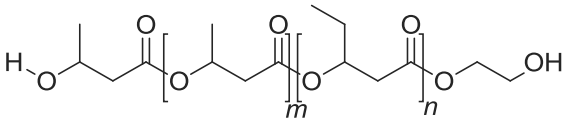

Scheme 42: Polyhydroxybutyrate-co-hydroxyvalerate

Several unsaturated resins based on isosorbide are also reported in the literature.[XVII] An increase in

[XVI] The structures of the polyurethane and polycarbonate containing an isosorbide unit can be found in the annexe

both viscosity and glass transition temperature was observed with increasing isosorbide, as well as an incompatibility with styrene.[129, 130] The group of Fonseca *et al.* also investigated the thermomechanical properties of an isosorbide containing resin, but no dependence of the degradation temperature on the chemical composition was observed.[131]

2.3.3.1.5 Use of isosorbide in crosslinker and spacer functions

Ma *et al.* reacted isosorbide with maleic anhydride to make a crosslinker which was used to make an epoxidised sucrose soyate based thermoset.[132] As the products had excellent flexibility, a molecular dynamics simulation was employed to sketch possible conformations of the isosorbide monomer, shown in figure 17 below. The conformation was found to be changing incessantly, and to be absorbing energy in the process, such as from an external applied force.

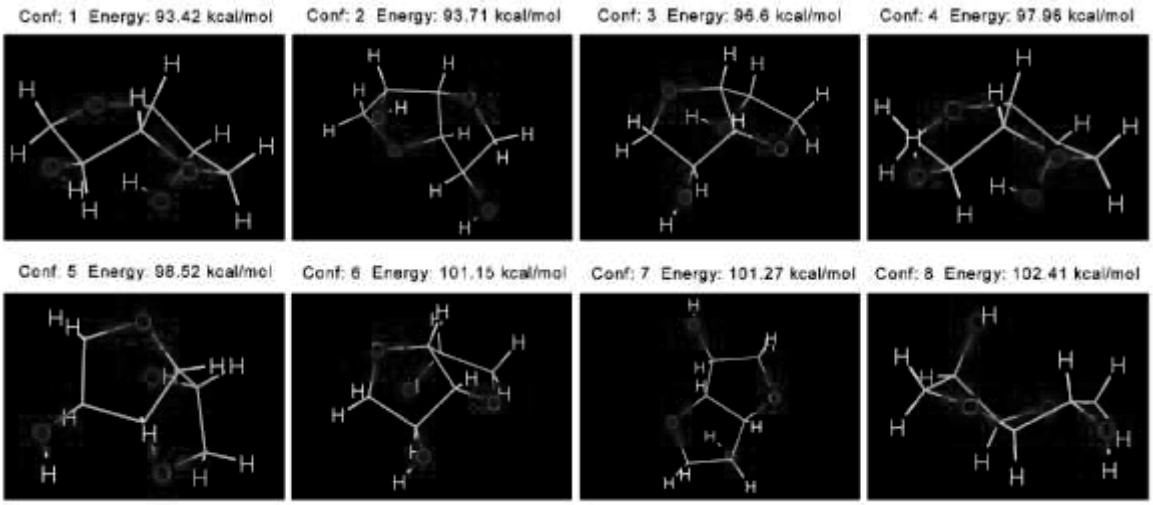

Figure 17: Molecular dynamics simulation of possible isosorbide conformations (Ma 2016)

Smiga-Matuszowicz *et al.* also used isosorbide as a crosslinker.[133] The group made isosorbide maleate oligomers and used them to cure an unsaturated poly(3-allyloxy-1,2-propylene succinate) resin, shown in scheme 43, in order to prepare a foam for bone tissue replacement.

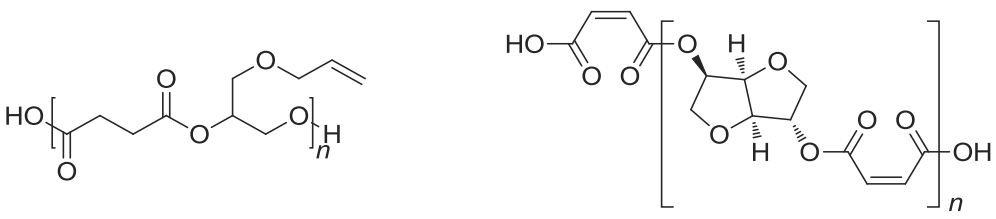

Scheme 43: poly(3-allyloxy-1,2-propylene succinate) (left) and isosorbide maleate oligomer (right) structures

Finally, isosorbide has also been used as a chiral spacer for photoreactive polyesters.[134]

[XVII] For a detailed description of the unsaturated polyester resins containing isosorbide and studies thereof, see annexe

2.3.3.1.6 Suitability of isosorbide for melamine crosslinked polyester resins for coil coating applications

Isosorbide has been used in a variety of thermosetting resins, which have displayed good mechanical properties when formulated with the right comonomers. The possibility to incorporate it in a large selection of structures and with different comonomers has also been proven. While some hydroxy functionalised resins have been synthesised, no crosslinking with melamine has been reported to the best of our knowledge. However, the results obtained for polyurethane, epoxy and unsaturated thermosetting resins suggest that it should be possible to obtain good quality products.

Furthermore, the increase in glass transition temperature, which is evidenced in many publications, and which is larger than that obtained for aromatic monomers such as furandicarboxylic acid and terephthalic acid, makes isosorbide a very promising candidate for the efficient introduction of rigidity into the resin structure.

Obstacles that need to be addressed when formulating isosorbide resins are the low reactivity of the endo hydroxy group as well as the possibility of colouration when high temperatures are used. However, several solutions proposed by different authors are available, and these problems are therefore far from unsolvable.

2.3.3.2 The potential of vanillin in polyester and resin products

Lignin is the largest natural source of aromatic molecules. It therefore has a huge potential as a source for environmentally beneficial biobased materials. The lignin structure principally contains three types of phenols, *p*-coumaryl alcohol, coniferyl alcohol and sinapyl alcohol, shown in scheme 44 below, that can be extracted and will hopefully become widely available once the right technologies are fully developed.[135]

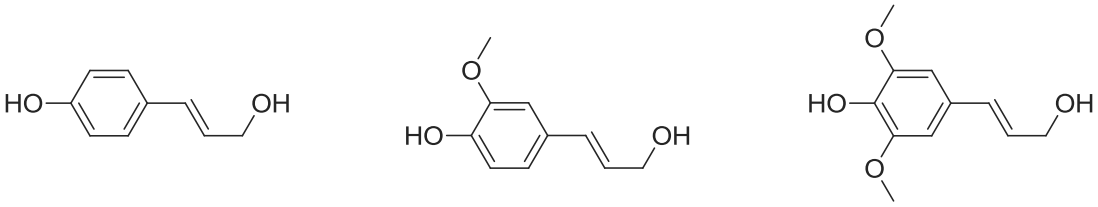

p-coumaryl alcohol coniferyl alcohol sinapyl alcohol

Scheme 44: Alcohols from the lignin structure

Until these compounds become available, vanillin, which is already to a significant degree produced from lignin, remains the most promising natural aromatic compound. While the field of vanillin based polymers is not as developed as for example that of furandicarboxylic acid based products and derivatives, a surge in interest has taken place in the last 5 – 6 years. Many publications have

appeared concerning polymers based on both vanillin and potential other aromatic lignin derivatives since 2010, and have been reviewed by Fache *et al.* as well as by Llevot *et al.* recently.[135, 136]

2.3.3.2.1 Phenol esterification

Theoretically, vanillin can be incorporated into polyester structures due to its phenol moiety. The aldehyde has good potential to be converted into a condensable group, either by reduction to vanillyl alcohol or by oxidation to vanillic acid. Furthermore, lignin derivatives such as ferulic acid, which already contain an alcohol and an acid group and can therefore be considered as bifunctional monomers for polycondensation reactions, are also available.

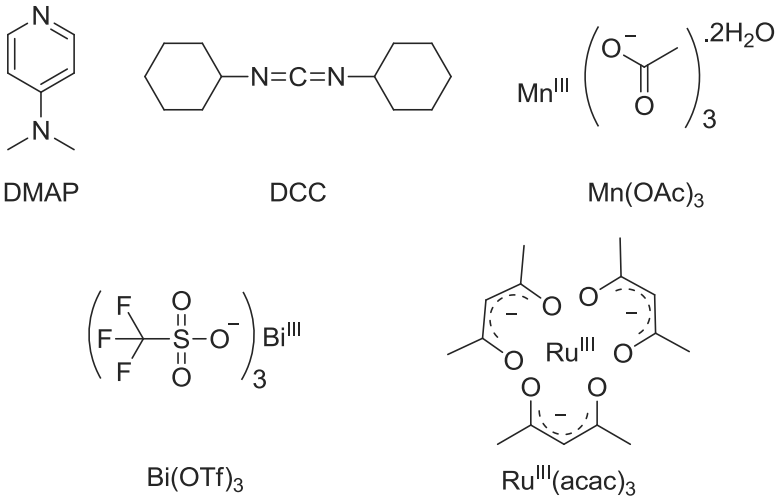

Scheme 45: Catalysts used in phenol esterification

However, due to steric bulk and the delocalisation of the nucleophilic electron pair from the oxygen onto the aromatic ring, direct esterification of phenols with simple carboxylic acids are, while not impossible, quite slow.[137] Traditionally, very harsh conditions or more reactive substrates such as acid chlorides or anhydrides can be used instead, but a few catalyst systems that can achieve the reaction have also been reported, and are shown in scheme 45 above.

One example of a direct esterification was reported by Brown *et al.*, who acetylated phenol and resorcinol in a large excess of acetic acid using high temperatures of 250 °C – 300 °C instead of a catalyst, as shown in scheme 46.[138]

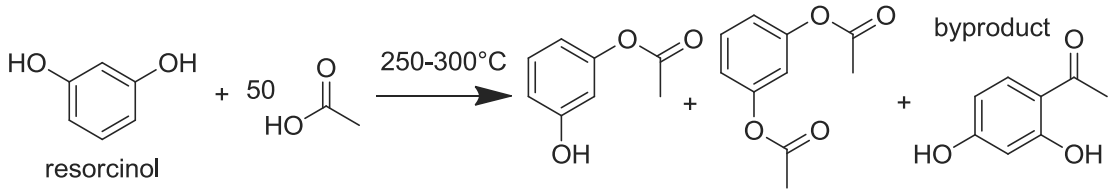

Scheme 46: Direct esterification of resorcinol (Brown 2000)

Methacrylic anhydride was successfully used by Stanzione *et al.*, who employed a dimethyl amino pyridine (DMAP) catalyst to esterify a variety of phenol derivatives with methoxy and hydroxy groups in *ortho* and *para* positions.[139] The authors then converted the product to a resin by radical polymerisation without purification, as represented in scheme 47 below.

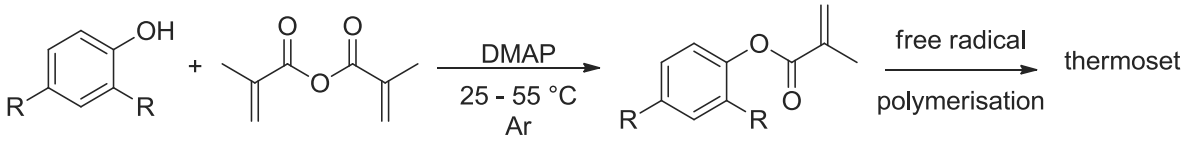

Scheme 47: Phenol esterification with DMAP and methacrylic anhydride (Stanzione 2013)

An example of a reagent with larger steric bulk was published by Harvey *et al.*, who created aromatic esters of a variety of fatty acids, for example phenyl docosahexaenoate.[140] A fatty acid anhydride was created using a 1,3-dicyclohexylcarbodiimide (DCC) catalyst, and subsequently reacted with the phenol compounds also using DMAP, as shown in scheme 48 below.

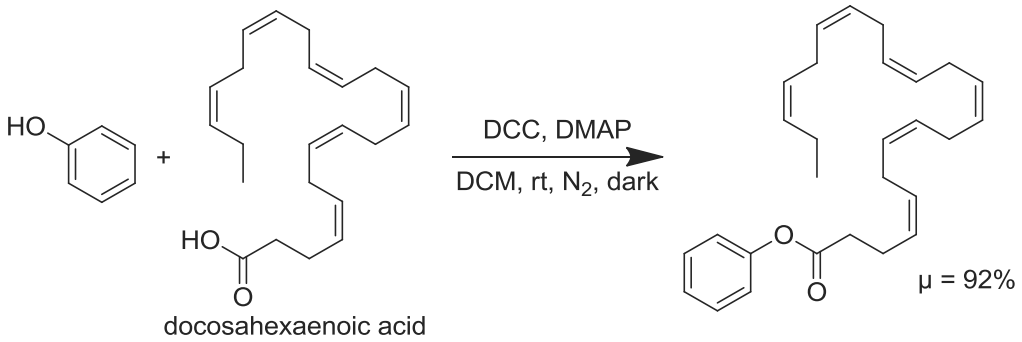

Scheme 48: Phenol esterification with long chain fatty acids (Harvey 2010)

Some examples of catalyst systems which can achieve direct esterification in milder conditions include a $Mn^{III}(OAc)_3.H_2O$ catalyst reported by Gowda *et al.*, different bismuth salts used by Mohammadpoor-Baltork *et al.* and a $Ru(acac)_3$ complex employed by Varala *et al.*, but the model esterifications were generally performed in medium to large excess of acetic acid, as shown in scheme 49 below.[141-143]

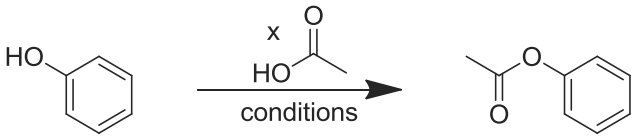

Scheme 49: Phenol esterification with excess acetic acid

In order to address the lack of reactivity, a variety of strategies have been used. The most common is the modification of vanillin, as for example the acetylation of the phenyl group.

Table 9: Conditions for phenol esterifications with excess acetic acid

author	concentration acetic acid	T	time	catalyst	concentration catalyst	yield
	x		min		%	%
Gowda *et al.*	1M	reflux	120	$Mn(OAc)_3.H_2O$	0,4	99
Mohammadpoor-Baltork *et al.*	0,3 M	reflux	80	$BiCl_3$	20	97
Mohammadpoor-Baltork *et al.*	0,3 M	reflux	60	$Bi(OTf)_3$	5	98
Varala *et al.*	1,1 equivalents	rt	120	$Ru(acac)_3$	2	78

In order to give an idea of the possibilities but also the challenges that can be expected, an overview of the different methods reported and products obtained is given in table 9 above. First, examples of direct condensations involving acetylated compounds, both *in situ* and after purification, will be presented. Then, polymers obtained through condensation with halogenated compounds, as well as some other modifications to the alcohol or acid functional groups which enable condensation reactions will be summarised. Lastly, a few vanillin containing resins from other types of reactions will be discussed for comparison.

2.3.3.2.2 Direct polycondensation of lignin derived aromatics using *in situ* condensation agents

A large number of publications deal with the use of ferulic acid (FER) or hydroxycinnamic acid (HC) for the synthesis of liquid crystalline polymers. In general, the monomers are polymerised in an acetic anhydride solution, which also acts as a so called condensation agent, creating an acetylated compound *in situ* and enabling a transesterification reaction.

Some AB type comonomers such as lactic acid, litocholic acid, cholic acid, *p*-hydroxybenzoic acid (*p*-HBA), shown in scheme 50, and glycolic acid are also incorporated, and the different hydroxycinnamic acid derivatives 3-hydroxycinnamic acid (3-HC), 4-hydroxycinnamic acid (4-HC) and 3,4-dihydroxycinnamic acid (3,4-DHC), shown in scheme 51, are examined.

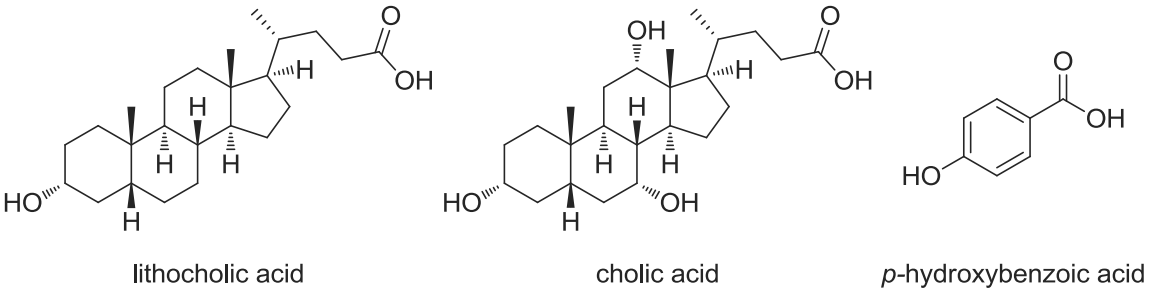

Scheme 50: Comonomers used in the synthesis of vanillin based liquid crystalline polymers

The reactions were conducted at high temperatures between 140 °C and 220 °C for up to 24 h. Generally, they were started at a lower temperature until the complete consummation or evaporation of the acetic anhydride had taken place. Then the temperature was raised until the completion of the reaction. Sodium or magnesium acetate were used as catalysts. In some cases, vacuum was applied at the end of the reaction.

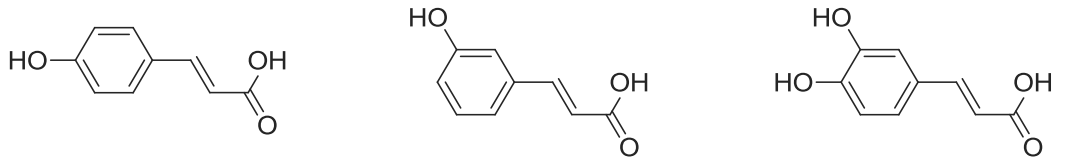

4-hydroxycinnamic acid or *p*-coumaric acid | 3-hydroxycinnamic acid or *m*-coumaric acid | 3,4-hydroxycinnamic acid or caffeic acid

Scheme 51: Coumaric and caffeic acids

For purification, the product was generally washed with organic solvent such as ethanol, acetone or pentafluorophenol (PFP). Jin *et al.* point out that the reaction is extremely temperature sensitive, as Fries rearrangements can take place if reaction temperatures are too low, and crosslinking of the double bonds occurs when they are too high.[144] Both prevent the formation of long chains, which can only happen in a narrow temperature window, and produce insoluble side products. The different conditions used by various authors are summarised in table 10 below.

Table 10: Conditions of condensation reactions involving vanillin derivatives using acetic anhydride

Source	main	co-	T – range	time	atm.	cat	purification	yield[a]
1st author	monomers		°C	h		M	solvent	%
Matsusaki[145]	4-HC	lactic acid	170 - 200	6	N_2, vac		acetone, Et_2O	45
Matsusaki[146]	4-HC	lithocholic acid	200	6		Na	PFP, EtOH	35
Jin[144]	4-HC	*p*-HBA, glycolic acid	170 - 218	5	N_2, vac	Mg	acetone, MeOH	90
Dong[147]	3,4-DHC	lithocholic acid	140 - 200	6	N_2, dark	Na	EtOH	78
Kaneko[148]	4-HC		220	24		Na	PFP, MeOH	90
Kaneko[149]	4-HC	3,4-DHC	220	24		Na	PFP, MeOH	90
Kaneko[150]	4-HC	lithocholic acid	220	24		Na	PFP, MeOH	52
	4-HC	cholic acid	220	24		Na	PFP, MeOH	7-84
Kaneko[151]	4-HC	cholic acid	150 - 200	7		Na	acetone	20
Kaneko[152]	4-HC	3,4-DHC	150 - 200	7		Na	acetone	80
Thi[153]	4-HC		200	6		Na	EtOH	69
	3-HC		200	6		Na	EtOH	69
	FER		200	6		Na	EtOH	69
Thi[154]	3,4-DHC	PLA	r.t.	24		py[b]	HCl, DCM, EtOH	93
	3,4-DHC	PEG	r.t.	24		py[b]	HCl, DCM, EtOH	81
	3,4-DHC	poly-ε-caprolactam	r.t.	24		py[b]	HCl, DCM, EtOH	92
Du[155]	FER		150 - 200	6	vac	Mg	acetone	-
	FER	*p*-HBA	150 - 200	6	vac	Mg	acetone	-
	FER	*p*-HBA, lactic acid	150 - 200	6	vac	Mg	acetone	-
Sun[156]	DAHMBA		150 - 200	3,5	vac	P[b]	$CHCl_3$, MeOH	-
	FER		150 - 200	3,5	vac	P[b]	$CHCl_3$, MeOH	-
	FER	DAHMBA	150 - 200	3,5	vac	P[b]	$CHCl_3$, MeOH	-
	4-HC	DAHMBA	150 - 200	3,5	vac	P[b]	$CHCl_3$, MeOH	-

[a]for copolymers, the yield of a 50:50 composition is reported, [b] non-metal cat.: pyridine or NaH_2PO_4

Matsusaki *et al.* also attempted the copolymerisation of lactic acid and 4-hydroxy cinnamic acid without an acetic anhydride condensation agent, but found that regardless of the relative quantity of each monomer, the resulting product was coloured brown.[145] This was attributed to the destruction of the double bond in 4-hydroxybenzoic acid, which was confirmed by NMR. On the other hand, the copolymers prepared with acetic anhydride were colourless or white, and the double bond was found intact. Yields increased from 31% for the copolymer containing 90% lactic acid to 85% for the copolymer with 75% aromatic content. However, the products containing over 20% 4-hydroxy cinnamic acid were no longer soluble in organic solvents (acetone, THF, DCM, $CHCl_3$, DMSO, DMF, MeCN).

Similarly, Kaneko *et al.* found the homopolymer of 4-hydroxybenzoic acid to be soluble only in pentafluorophenol, shown in scheme 52.[148] Thi *et al.* compared the compatibility with organic solvents of homopolymers from different hydroxycinnamic acids.[153] Polyferulic acid displayed the poorest solubility, as it was only soluble in pentofluorophenol, followed by poly-4-hydroxycinnamic acid, which could also be dissolved in a mixture of dichloromethane and trifluoroacetic acid. Poly-3,4-dihydroxycinnamic acid was additionally soluble in *N*-methyl pyrrolidone (NMP) and dimethylformamide (DMF), and the best solubility was displayed by 3-hydroxycinnamic acid, which was even dissolved by DMSO, THF and chloroform.

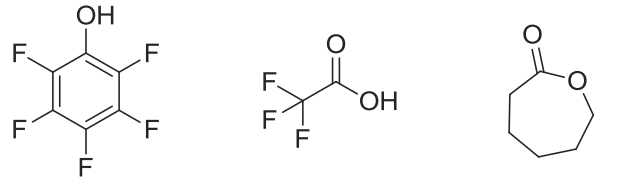

Scheme 52: Pentafluorophenol, TFA and ε-caprolactone

The same authors used 3,4-dihydroxycinnamic acid as an end group for aliphatic polymers such as polylactic acid, polyethylene glycol and poly-ε-caprolactone.[154] The thermal stability of the polymers in question was enhanced considerably through the blocking of the hydroxyl end group and the π-π stacking of the new chain ends.

A variety of comonomers were also employed to modify the properties of the final polymer. Jin *et al.* introduced glycolic acid to increase the hydrophobicity, and lithocholic acid was used by Dong *et al.* and by Matsusaki *et al.* to improve the solubility and biocompatibility.[144, 146, 147] Multifunctional comonomers such as cholic acid and 3,4-dihydroxycinnamic acid were used to create hyperbranched structure with improved mechanical properties and biodegradabilities.[150, 152]

Sun *et al.* introduced a divanillic comonomer in the polymerisation with 4-hydroxycinnamic acid and ferulic acid to make photofluorescent polymers.[156] Vanillin was oxidised to vanillic acid, followed by nitration and reduction to 5-aminovanillic acid hydrochloride. It was then converted to the final

divanillic imide monomer (DAHMBA) by reaction with 3,4-dimethoxybenzaldehyde, as shown in scheme 53 below.

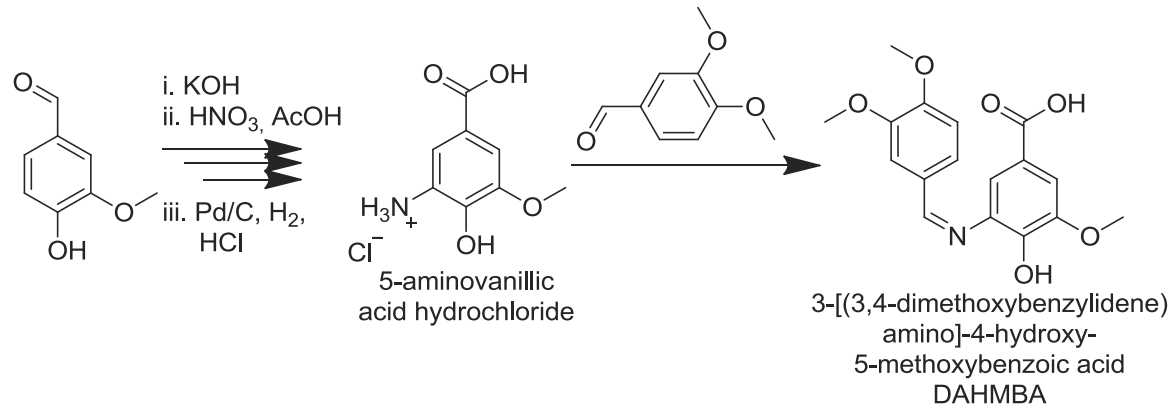

Scheme 53: Synthesis of DAHMBA divanillic monomer (Sun 2016)

The products obtained had relatively low molecular weights from $M_{\bar{w}}$ 2 000 g/mol to 10 300 g/mol. The DAHMBA monomer was the most reactive, followed by 4-hydroxycinnamic acid. Ferulic acid gave the shortest chains, which was attributed to the steric hindrance of the methoxy group *ortho* to the phenol. However, the ferulic acid products also showed the strongest photoluminescence, as shown in figure 18.

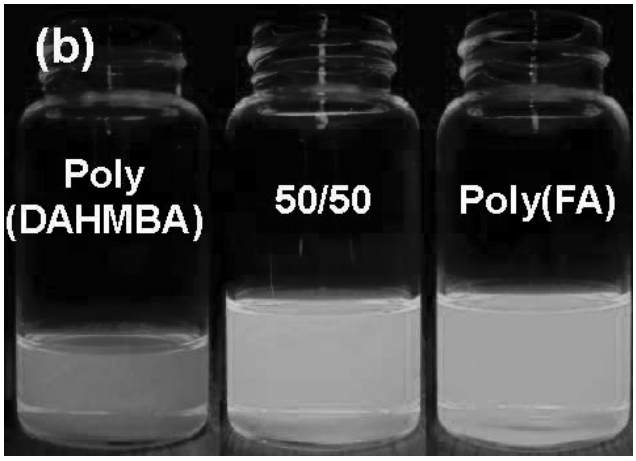

Figure 18: Photoluminescence of ferulic acid polymers (Sun 2016)

A wide range of molecular weights was measured in the other reactions, where solubilisation of the products was successful. Matsusaki *et al.* obtained products of only 3000 – 5000 g/mol, while Dong *et al.* observed chain length between 15 900 g/mol and 21 500 g/mol.[145, 147] The largest products were synthesised by Kaneko *et al.*, at 44 000 – 91 000 g/mol and by Thi *et al.*, at 70 000 g/mol.[149, 153]

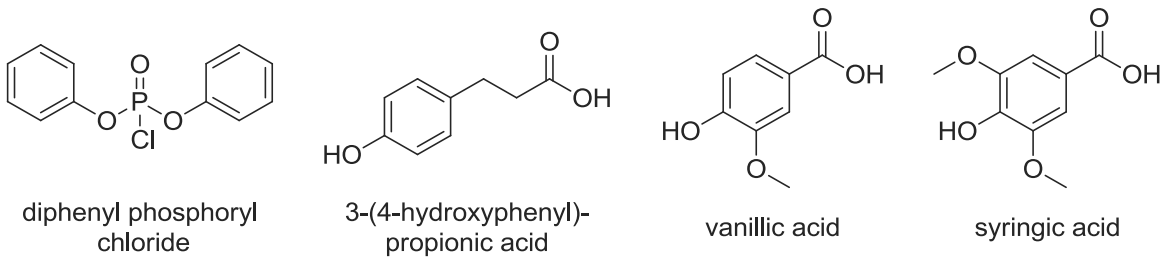

Scheme 54: Reagents used in condensation for vanillin derivate polymer (Nagata 2000)

A condensation agent different to acetic anhydride was used by Nagata *et al.* to make copolyesters from 3-(4-hydroxyphenyl)-propionic acid, and 4-hydroxybenzoic acid, vanillic acid or syringic acid, shown in scheme 54.[157] Direct condensation was achieved with a solution of diphenyl phosphoryl chloride in pyridine at 117 °C for 3 h. The presence of methoxy substituents on the aromatic ring was found to increase glass transition temperature and solubility, but decrease crystallinity and thermal stability.

2.3.3.2.3 Phenol acetylation

An alternative to the use of an excess of acetic anhydride as *in situ* condensation agent is the acetylation of the phenol prior to the reaction. This strategy was used for example by Wilsens *et al.*, who incorporated acetylvanillic acid into furandicarboxylic acid based thermotropic polyesters, shown in scheme 55.[158] Vanillic acid was acetylated using acetic anhydride, and incorporated into the polyester, which originally contained only *p*-acetoxybenzoic acid, to decrease the melting temperature. The high melting temperature had proven to be a problem due to crystallisation during the melt polymerisation, which prevented molecular weight build up. The melting temperature was successfully decreased from 336,6 °C to 230,3 °C by the incorporation of 20 mol% of acetylvanillic acid, which also led to an increase in T_g by 12,5 °C.

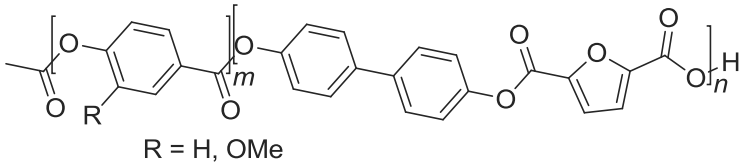

Scheme 55: Thermotropic vanillin based polyester (Wilsens 2014)

Mialon *et al.* synthesised and patented a homopolymer based on dihydroferulic acid starting from vanillin.[1, 159, 160] It was first transformed to acetylferulic acid in acetic anhydride with pyridine as a catalyst, following the protocol for a Perkin reaction published by Fosdick *et al.*, and then hydrogenated as shown in scheme 56 below.[161]

The polymerisation was carried out at 200 – 220 °C, first under nitrogen atmosphere for 2 h, and then under vacuum for 2 - 6 h. $Zn(OAc)_2$ and Sb_2O_3 were tested as catalysts, in addition to raising the temperature to 250 °C. While this was not very successful in increasing the yield obtained in a catalyst free reaction, the molecular weight determined by NMR end group analysis could be increased up to 17 800 g/mol.

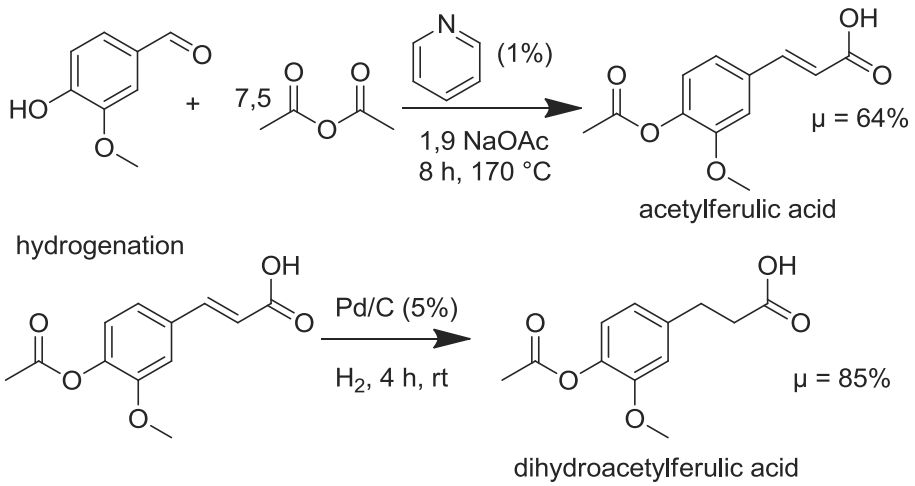

Scheme 56: Perkin reaction followed by hydrogenation (Mialon 2010)

In all cases except for where very low molecular weights below 3000 g/mol were obtained, the stirring of the reaction stopped after 30 – 90 min due to the consistency of the reaction mixture. Purification of the products was done by dissolving them in a mixture of dichloromethane and trifluoroacetic acid followed by precipitation through the addition of methanol. Glass transition temperatures around 70 °C and melting points around 230 °C, as shown in table 11, were observed for the products.

Table 11: Reaction conditions and product properties of polydihydroacetylferulic acid (Mialon 2010)

T_{max}	time melt	time vacuum	catalyst	yield	$M_{\bar{n}}$	T_g	T_m
°C	h	h	1 mol%	%	g/mol	°C	°C
220	2	2	none	83	4800	74	243
220	2	2	Sb_2O_3	67	4100	73	234
220	2	2	$Zn(OAc)_2$	82	6800	73	234
220	2	6	$Zn(OAc)_2$	91	8900	67	231
250	2	6	$Zn(OAc)_2$	68	17800	67	216
220	2	0,17	$Zn(OAc)_2$	75	3000	65	240
220	5	6	Sb_2O_3	5	630	-	-

Kricheldorf *et al.* also activated vanillic acid by acetylation of the phenyl group, or alternatively by trimethylsilylation of the acid group, as shown in scheme 57, in order to make thermotropic homo- and copolyesters as well as polyamides.[162, 163]

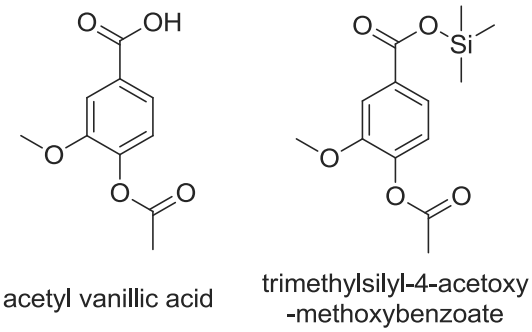

acetyl vanillic acid

trimethylsilyl-4-acetoxy-methoxybenzoate

Scheme 57: Activated vanillic acid

2.3.3.2.4 Reaction with halogenated alkyl chains

The most common alternative strategy for addressing the low reactivity of the phenol group to its acetylation is the use of halogenated compounds to create a more reactive ester or ether compound. Acyl chlorides were for example employed by Ouimet *et al.*, who made a ferulic acid adipate precursor, which was then polymerised to a polyanhydride ester using a triphosgene catalyst, as shown in scheme 58.[164]

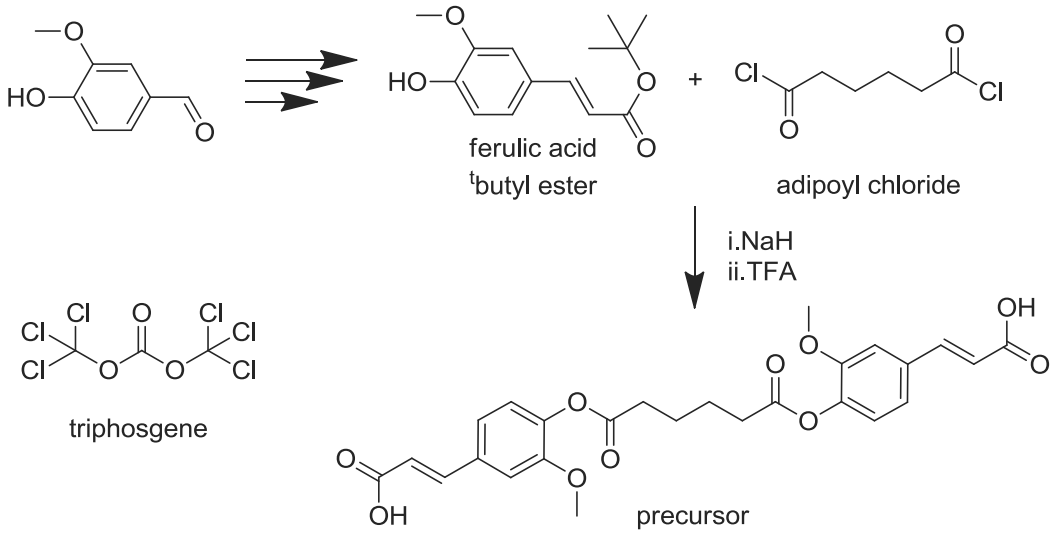

Scheme 58: Precursor synthesis from ferulic acid ^{t}butyl ester and adipoyl chloride (Ouimet 2013)

Vanillin was first converted to ferulic acid ^{t}butyl ester which was deprotected after the formation of the precursor. The product was successfully tested for controlled release through hydrolytic degradation of ferulic acid, which can be used as a photoprotective and antioxidant agent in biomedical and cosmetic products.

Nagata *et al.* used a similar precursor synthesised from *p*-hydroxy cinnamic acid and adipoyl chloride to make a series of copolyesters with various diols.[165-167] Thionyl chloride was used to convert the trimer to a diacid chloride before polymerisation with polyethylene glycol, poly-ε-caprolactam or aliphatic diols with chains of 6 to 10 carbon atoms to produce photocrosslinkable compounds, as shown in scheme 59 below.

Other than through esterification with an acyl chloride, the phenol moiety has also been transformed into a more reactive ether group, either by adding an alkyl chain with a more reactive, primary hydroxy group, or by creating a dimer with two acid groups.

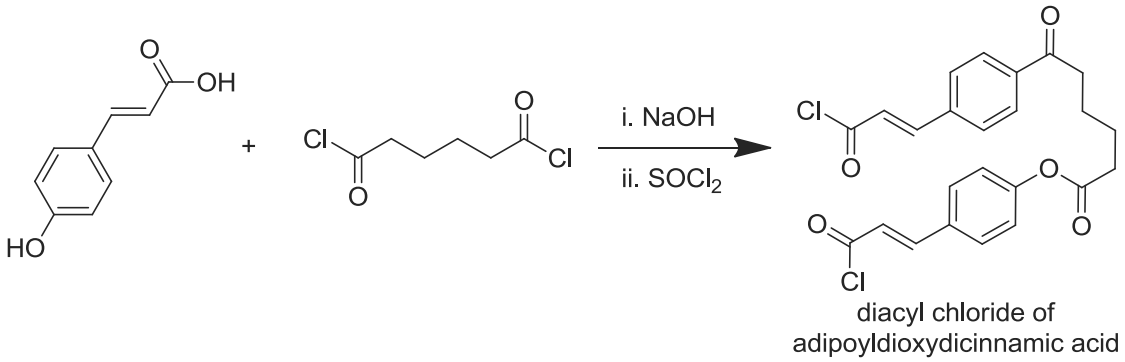

Scheme 59: Synthesis of diacyl chloride of adipoyldioxycinnamic acid (Nagata 2003)

Ethanol, ^{n}propanol and ^{n}hexanol ethers of 4-hydroxybenzoic acid, vanillic acid and syringic acid were prepared by Mialon *et al.*, followed by homopolymerisation at 200 – 250 °C for 1 h under N_2 and then 16 h under vacuum, as shown in scheme 60.[168] An antimony oxide catalyst was used. Molecular weights varied between 5 200 g/mol and 23 900 g/mol. Both methoxy substituents on the aromatic ring and additional carbons in the alkyl chain had a decreasing effect on the T_g.

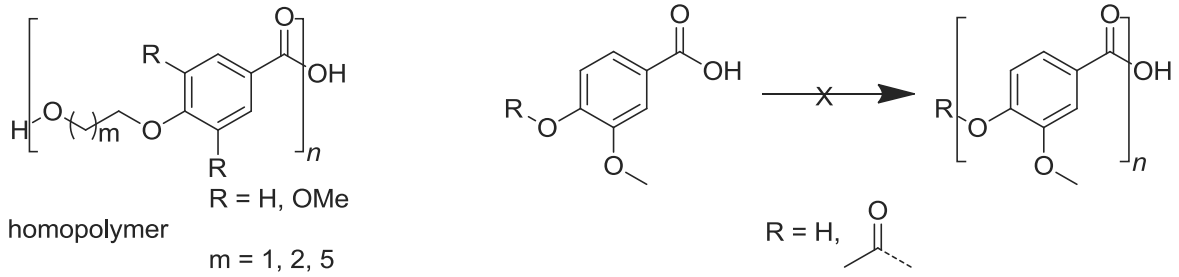

Scheme 60: Homo- and copolesters of vanillic and syringic acids (Mialon 2011)

Polymerisation of unsubstituted vanillic acid as well as acetyl vanillic acid using the same method was also attempted by the authors, but unsuccessful. Both reaction yielded insoluble materials, and the degree of polymerisation was estimated to be only 5-6 for the transesterification reaction based on the acetic acid side product collected.

Kreye *et al.* synthesised a similar monomer based on ferulic acid, as shown below in scheme 61.[169] After transformation to its methyl ester, the ferulate was reacted with bromoethanol followed by hydrogenation. An alternative, more sustainable route using ethylene carbonate for the etherification reaction after hydrogenation was also proposed by the authors. The resulting monomer was then homopolymerised as well as copolymerised at 130 °C for 24 h with a rapeseed fatty acid derived hydroxyester using 1,5,7-triazabicyclo-dec-5-ene (TBD) as a catalyst.

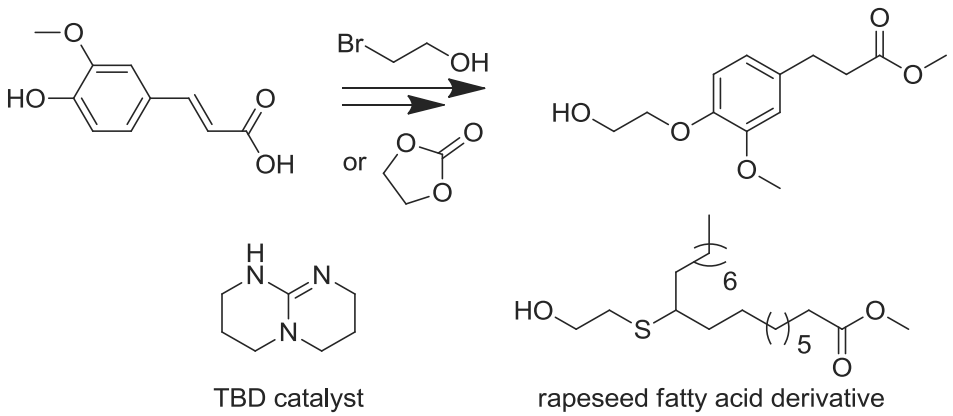

Scheme 61: Monomers for rapeseed based polyester (Kreye 2013)

The products obtained were soluble in THF and partially soluble even in methanol. By varying the relative amounts of both monomers, the glass transition temperature could be adjusted between -8,8 °C and -58,8 °C as shown in table 12. Using more ferulic acid derivative generally resulted in smaller molecular weights.

Table 12: Influence of ferulic acid content on $M_{\bar{n}}$ and T_g (Kreye 2013)

ferulic acid derivative	fatty acid derivative	$M_{\bar{n}}$	T_g
%	%	g/mol	°C
100	0	5 450	-27,1
20	80	15 300	-58,8
40	60	12 050	-50,3
60	40	10 100	-27,9
80	20	9 700	-8,8

Dimer compounds derived from vanillin have been used for polyester synthesis as early as 1950. Bock *et al.* converted vanillic acid to a diether using the Williamson ether synthesis.[170] Dibromides of ethylene glycol, 1,3-propanediol and 1,4-butanediol were used to create different sized linkers, and the resulting diacid was esterified with ethylene glycol prior to polymerisation to give a hydroxy acid. The polycondensation was performed uncatalysed at 275 °C – 280 °C under vacuum for 12 – 21 h, and yielded a brittle, glassy product, shown in scheme 62, which was "very resilient and not easily broken, but when broken with a hammer, the pieces tend to fly across the room".[171] With the exception of *m*-cresol, it was also insoluble in common organic solvents.

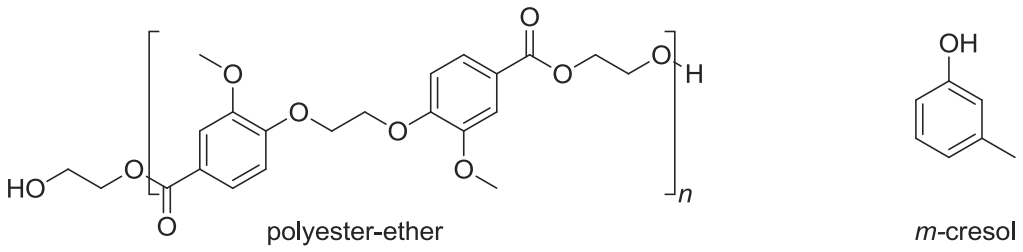

Scheme 62: Vanillic acid based polyester-ether and *m*-cresol

Later on, Lange *et al.* directly polycondensed a dimer made of vanillic or syringic acid and dibromoethane with ethylene glycol.[172] An alternative monomer synthesised using ethylene oxide, on the basis of different work of Bock as well as of Erä *et al.*, was also used in the condensation reactions, as shown in scheme 63.[173] The effect of the additional methoxy group as well as of different ratios of the aromatic monomers was tested. Molecular weights between 12 000 g/mol and 71 000 g/mol and glass transition temperatures from 45 °C to 69 °C were obtained. Furthermore, it was observed that vanillic acid based polymers exhibited greater crystallinity and considerably higher melting temperatures than the equivalent, largely amorphous syringic acid products.

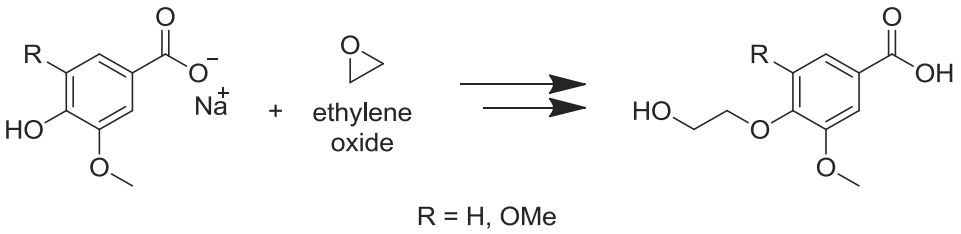

Scheme 63: Phenol etherification using ethylene oxide (Erä 1974)

Most recently, a similar strategy to those described above was used by Pang *et al.* to make polyester-ethers with varying aliphatic chain lengths.[174, 175] Chloroacetate and dibromobutane were used to make divanillate as well as monovanillate diacids or diesters, shown in scheme 64. These were then condensed with ethylene glycol, 1,3-propanediol, 1,4-butanediol, 1,6-hexanediol, 1,10-decanediol as well as with different fatty acid derived diols, made from 10-undecenoic acid using thiolene click chemisty.

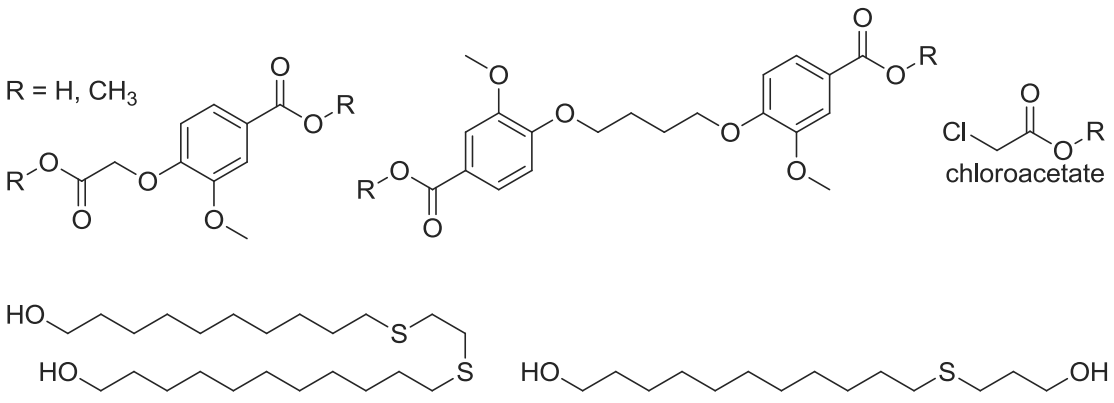

Scheme 64: Monomers used for the synthesis of polyester-ethers with varying chain lengths (Pang 2014, 2015)

The glass transition temperatures obtained from the condensation with aliphatic diols were between 5 °C and 67 °C. The monovanillin diacid monomer yielded higher T_g's compared to the dimer. Longer aliphatic chains also led to lower T_g's, with the lowest results obtained for the fatty acid derivatives between -12,7 °C and 13 °C.

2.3.3.2.5 Chemoenzymatic synthesis of vanillin based polyester products

Another route to reactive monomers was chosen by Llevot *et al.*, who transformed vanillin and vanillic acid into diol and diester monomers respectively using a laccase enzyme and some chemical transformations, as shown in scheme 65.[176] The thus obtained diol was condensed with sebacic acid and methyl sebacate. It was found that the transesterification yielded higher molecular weight products. Different catalysts were also evaluated.

The diester was reacted with 1,10-decanediol, and found less reactive than the vanillin diol. This was attributed to the conjugation and the steric hindrance of the ester group.

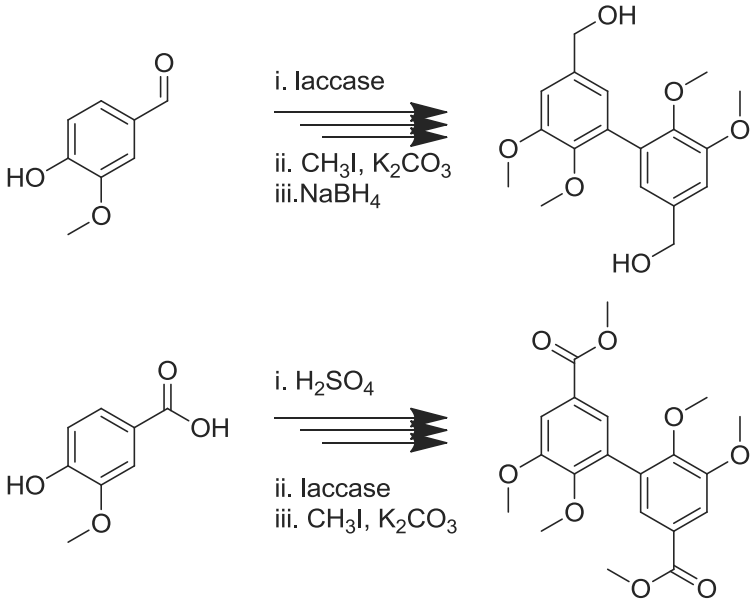

Scheme 65: Chemoenzymatic production of vanillin-based dimers (Llevot 2015)

A variety of polyesters were synthesised with different aliphatic chains, shown for example in scheme 66, aromatic moieties and also including a polyester entirely based on vanillin. The products obtained were amorphous and insoluble, with glass transition temperatures that could be varied from -5 °C to 139 °C, as shown in table 13. Minimum storage moduli were also obtained using point bending mode dynamic mechanical analysis (DMA).

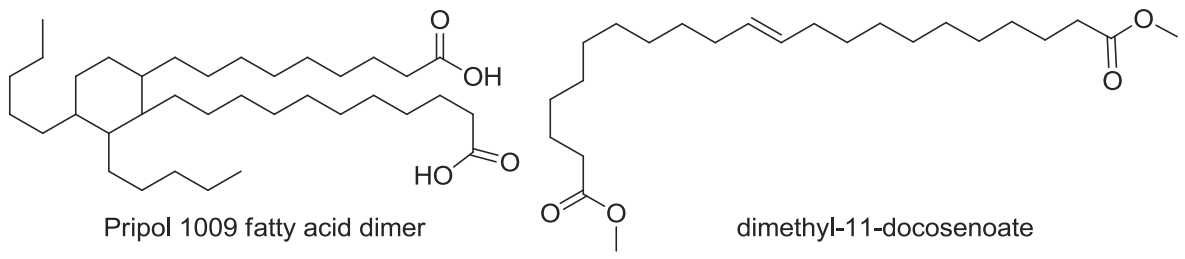

Scheme 66: Fatty acid based dimers

Table 13: T_g and crosslinking density of vanillin-dimers with various comonomers (Llevot 2015)

comonomer	T_g	E'
	°C	GPa
dimethyl sebacate	38	8,1
dimethyl-11-docosenoate	5	2,0
dimethyl succinate	68	5,1
fatty acid dimer Pripol 1009	-5	0,1
dimethyl terephthalate	102	2,0
furandicarboxylic methyl ester	139	1,4
vanillin diester	102	1,3

Similarly, Pion *et al.* created trimers based on dihydroferulic acid and isosorbide or 1,4-butanediol using the enzyme Candida Antarctica Lipase B (CALB), as shown in scheme 67.[177] These were reacted in a catalyst free polycondensation at 100 – 180 °C with succinyl and azelaoyl chloride. Polyesters with molecular weights $M_{\bar{w}}$ from 7 500 g/mol to 10 500 g/mol and glass transition temperatures ranging from 0,4 °C for the ^{n}butyl-azelaoyl derivative to 75,6 °C for the isosorbide succinyl derivative were obtained.

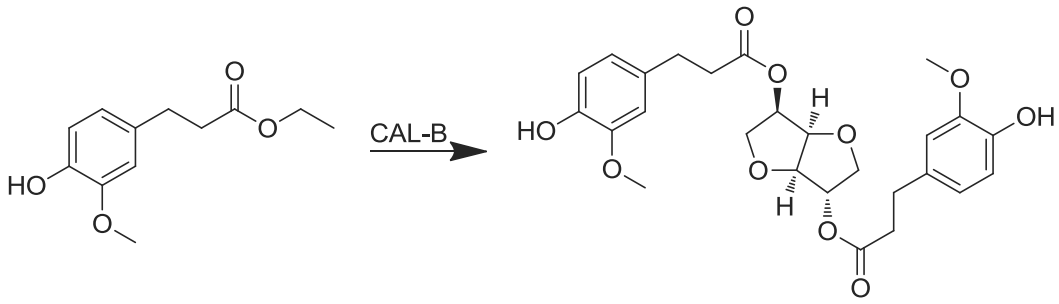

Scheme 67: Synthesis of dihydroferulic acid isosorbide trimer using CALB enzyme (Pion 2014)

2.3.3.2.6 Vanillin monomer platform

Aside from the pathways discussed above, there are many other ways to transform vanillin into a monomer for polymer production. This was illustrated for example by Fache *et al.*, who presented a platform of 22 different vanillin based products, shown in scheme 68 below.[178] Using vanillic acid, vanillic alcohol and methoxyhydroquinone as starting points, a range of diols, diacids, diepoxys, dicarbonate, diamines and diallyls was created.

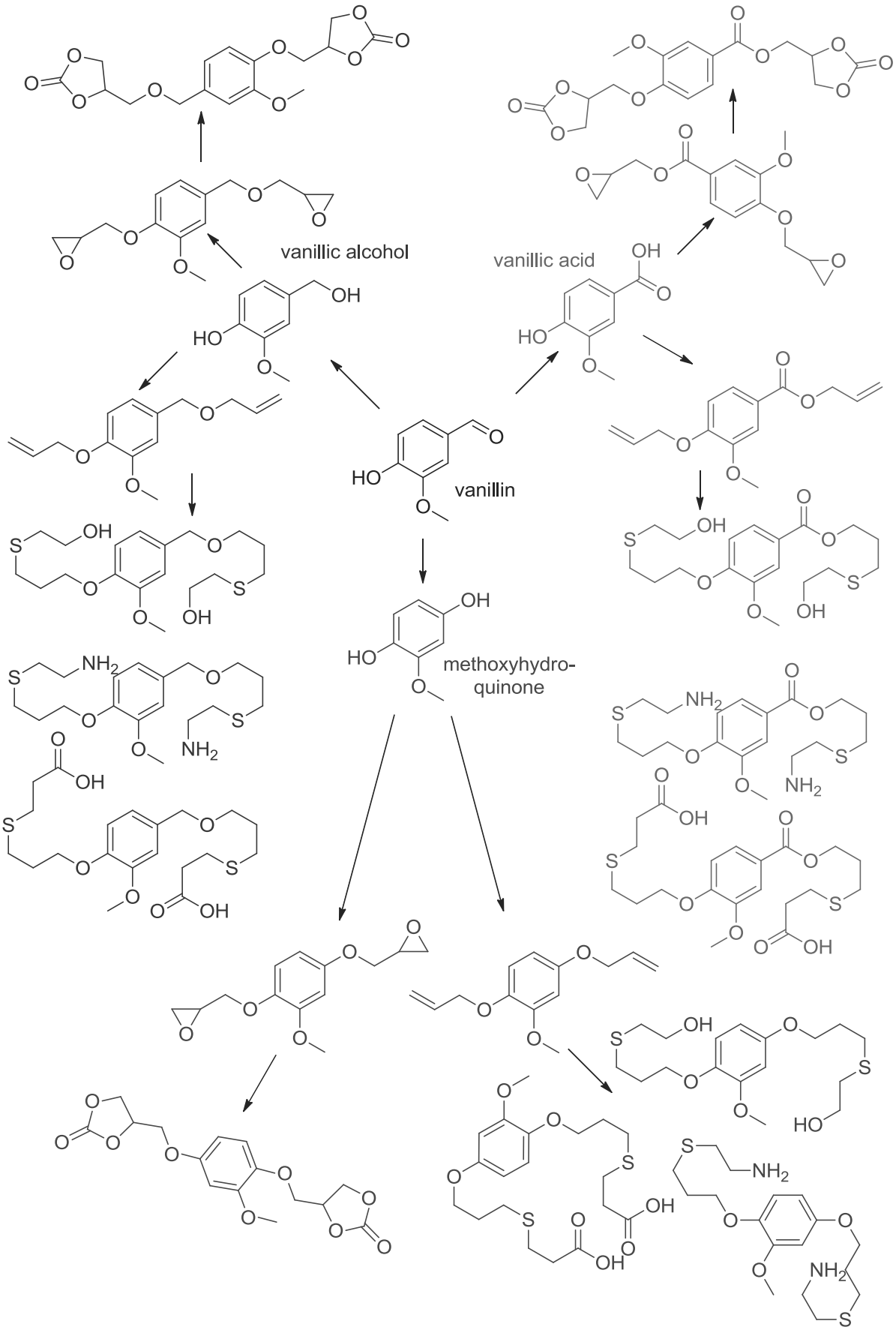

Scheme 68: Vanillin platform for polymerisation (Fache 2014)

A similar objective was pursued in the thesis work of Krause, who developed a platform of bivanillic monomers for polycondensation.[179] Both diols and diacids were synthesised, connecting the aromatic moieties with ether, carbonate or ketone links, as shown in scheme 69.

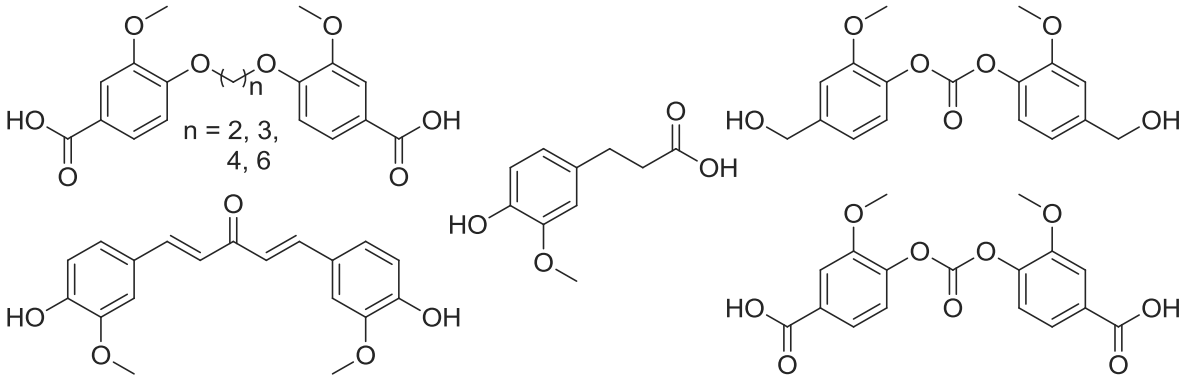

Scheme 69: Platform of bivanillic monomers (Krause 2012)

In the same group, the Tishchenko reaction for the transformation of aldehydes to ester groups, as shown in scheme 70, was studied by Schwolow to enable the incorporation of vanillin into polyester products.[180]

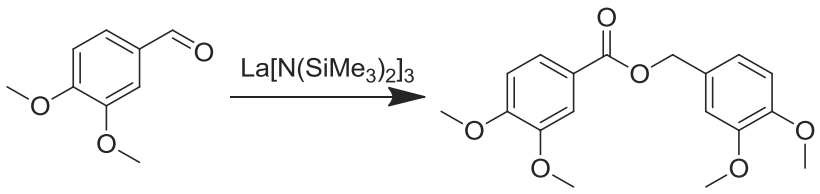

Scheme 70: Dimerisation of 3,4-methoxybenzaldehyde in a Tishchenko reaction

Based on these and other possible transformations, a large variety of vanillin based polymers can be synthesised.[XVIII]

2.3.3.2.7 Vanillin as a monomer for polyester resins

Introducing vanillin or its derivatives into a polymer structure can have many benefits, including rigidity, aromaticity, but also photoprotection and thermotropic properties. As evidenced by the discussion above, there are many different ways to achieve its incorporation. Due to the lack of reactivity of the phenol group, many of the methods reported utilise vanillin derivatives which are not at this point commercially available.

From our point of view, in order to simplify the material supply and to minimise impact on the environment, as few steps as possible between the commercially available compound and the monomer used in condensation are desirable. This makes the simultaneous conversion of the

[XVIII] See annexe for some illustrative examples of step growth and addition polymers.

aldehyde to an acid and acetylation of the phenol as seen for example in the Perkin reaction an attractive prospect, even though the yield reported in the literature is not optimal.

Furthermore, the unsaturation, especially where conjugated such as in the case of ferulic and *p*-coumaric acid, could potentially decrease the stability of its condensates towards UV light. Overall, while the potential of vanillin as a monomer in polyesterification reactions is undisputed, methods for the same still need to be optimised, and the potential for use in coil coating resins especially for exterior applications remains to be established.

2.3.3.3 Alternatives for introducing rigidity

Other than furandicarboxylic acid, isosorbide and vanillin based compounds, a couple of alternative monomers have been proposed to introduce rigidity into the polyester structure and will be reviewed in this section.

One candidate is resorcinol, which can be obtained by fermentation from glucose, even though it is currently produced petrochemically. There are two potential pathways available, one via inositol, shown in scheme 71, the other via triacetic acid lactone. Both can be converted into pyrogallol, which can then be reduced to resorcinol.[181]

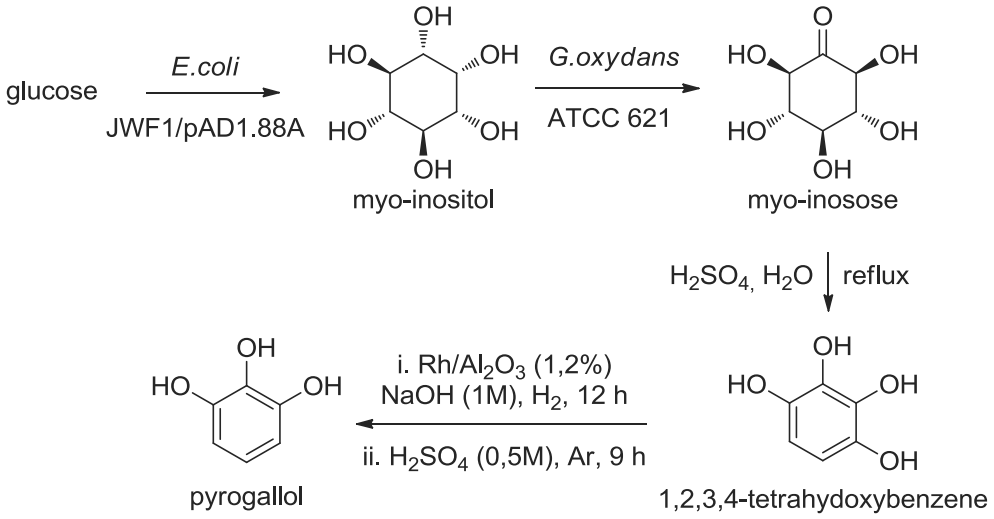

Scheme 71: Pyrogallol production from glucose (Hansen 2002)

One example of use of resorcinol in polycondensation was reported by Gioia *et al.*, who reacted resorcinol with ethylene carbonate to obtain a hydroxyethoxy resorcinol, as shown in scheme 72.[182] The new monomer was used in polycondensation with a variety of diacids and diesters, including the biobased monomers succinic acid and furandicarboxylic acid, but also petroleum based monomers cyclohexane dicarboxylic acid, dimethyl terephthalate, dimethyl isophthalate and cyclohexanedicarboxylic acid dimethyl ester.

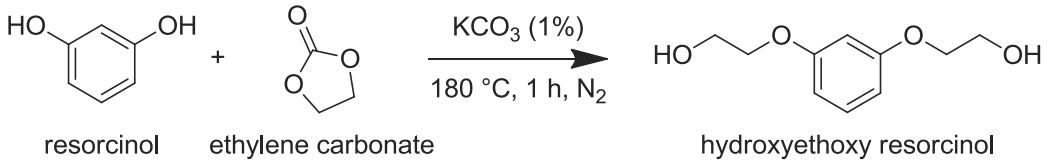

Scheme 72: Condensation of resorcinol and ethylene carbonate (Gioia 2015)

Another possibility is the tannin betulin, which can be isolated for example from birch crust, and contains a secondary and a primary hydroxy group, shown in scheme 73. Its use in a polycondensation was reported for example by Nemilov *et al.*, who studied the kinetics of the reaction with adipic acid, and confirmed that no reaction of the double bond was taking place.[183]

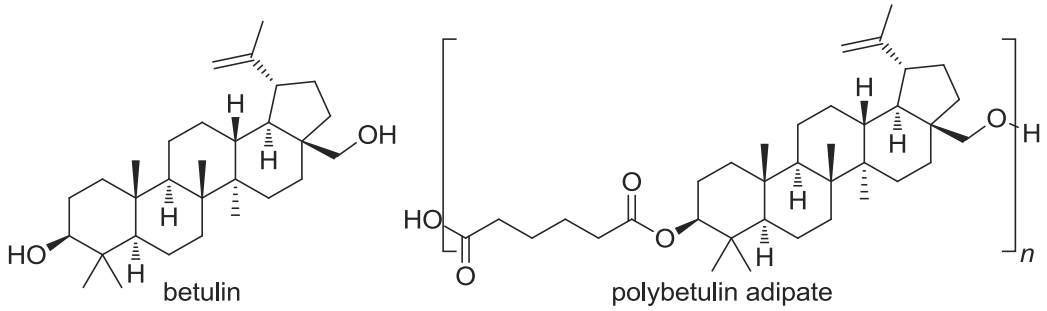

Scheme 73: Betulin and polybetulin adipate

3 Weatherability

3.1 Introduction to weatherability

In order to design a coating for exterior use, it is important to understand the different adverse influences it might encounter and their effect on its performance and aesthetic quality. Historically, much interest has been devoted to the degradation of polymers, as evidenced for example by the journal "Polymer degradation and stability" which counts more than 7 000 publications since 1979 (Web of Science search, July 2016). The main motivation behind the research is to prevent any degradation that could lead to failure, i.e. the polymer being unable to perform its original purpose.[184]

However, more recently, much work has also been devoted to the design of polymers with a finite end life that can be biologically degraded.[185, 186] The reason for this is growing concern about the accumulation of plastic waste in soil and aqueous environments and its adverse effects on ecology and human health.[21] Therefore, polymers which can degrade into less harmful substances by microbial and hydrolytic pathways are very interesting for products with a high turnover and the risk to end up in nature.

In the context of coil coating, biodegradability of the polymers used as binders in the paint is not a major concern. According to the European Coil Coating Association's sustainability report 2012, only 4% of coil coating products end up in landfill, while 65% are recycled and 31% incinerated, as represented in figure 19.[187] Due to the high cost of their production, both steel and aluminium have highly developed recycling industries; and the coil coating can last for up to 40 years. This makes it much less likely that the polymer will end up polluting the soil or the sea. Therefore, increasing the life time of the polymers by decreasing the susceptibility to degradation can have a positive impact on the environment, saving energy and material that would be used to renew the paint.

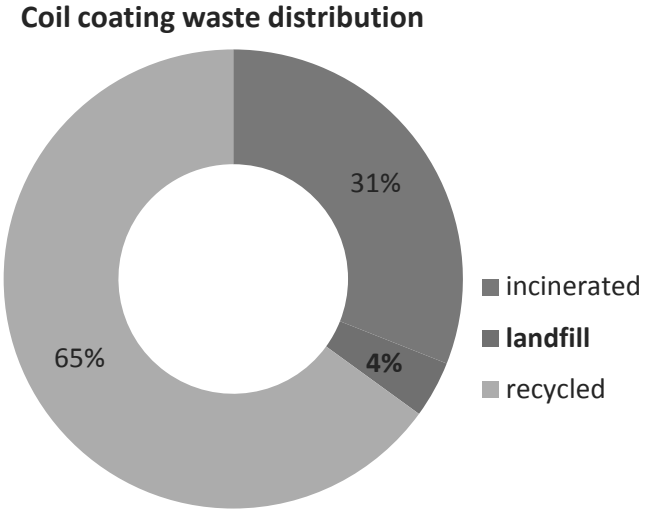

Figure 19: Coil coating waste distribution

The quality in a coating to withstand degradation can be referred to as its stability, durability or weatherability, and since the interest of this work is the development of a coating for exterior use, the latter term will be primarily employed from here on.

In order to predict the weatherability of a coating by other means than placing it in real life conditions for the full time of its intended use, three challenges need to be addressed: The variety and interaction between the different mechanisms of degradation, the multitude of influences to which the coating may be subjected, and the complexity of the substrate composition.

In the first part of this chapter, the different mechanisms of degradation, namely photolytic degradation, thermal degradation, hydrolytic degradation and physical ageing will be discussed. Exterior influences and different possibilities to model the weather and provide accelerated ageing will be presented and the question of the validity of prediction based on accelerated ageing will be addressed. The different components of the substrate which are likely to have a major influence on the weatherability such as the support, the nature of the binder and the crosslinker, pigments, catalysts and of course UV absorbers and stabilisers will be detailed.

In a second part, an overview of literature on the weatherability of melamine crosslinked polyester coatings will be presented. As only a limited amount of studies have been conducted on this specific subject, some results on the weatherability of related products such as polyester coatings crosslinked by different mechanisms and thermoplastic polyesters will also be presented, and their relevance to the project will be discussed.

Lastly, some interesting methods used in the study of the degradation of other coating types will be presented as an inspiration for further study.

3.2 Degradation mechanisms

Degradation mechanisms are generally categorised by the source of the degradation. Photolytic degradation proceeds by radical reaction pathways, and is caused by UV radiation. Since UV light is largely filtered out by glass windows, this pathway is much more important for exterior than for interior coatings. Thermal degradation is caused by heat, and hydrolytic degradation is caused by contact with water, either in the form of rain, condensation or as humidity in the air. Both can be encountered outdoors and indoors, and the degree of harshness depends on the specific use of the coated product. Lastly, physical ageing is a relaxation process present in any kind of plastic below its transition temperature. Except for the temperature, it is less dependent on exterior influences, but it can have an impact on the coating performance. While the mechanisms can be treated separately in theory, in practice synergies and catalytic effects between the different degradation products have to be taken into account, especially regarding photolytic and hydrolytic processes.

3.2.1 Photolytic degradation

Photolytic degradation is one of the most important and therefore most intensely studied pathways in polymer science.[184, 188-192] It is caused by the ultraviolet part of sunlight. While radiation between 100 nm and 380 – 400 nm wavelengths is generally qualified as ultraviolet, it is thought that radiation from 315 nm – 400 nm, called UVa, is most harmful to polymers as lower wavelengths are generally absorbed by moisture and small molecules in the atmosphere, and longer wavelengths are not energetic enough to cause damage.[184, 193]

Table 14: Bond dissociation energies and corresponding wavelengths

Bond	dissociation energy	wavelength
	kcal/mol	nm
C-C	85	336
C-H	95 - 100	286 - 301
C-O	80 - 100	286 - 357
O-O	35	817
O-H	85 -115	249 - 336

When exposed to heat, the energy of all atoms is increased simultaneously and in a step wise fashion. Bond scission occurs soon after the energy necessary is reached, and the scission products are energetically similar to their surroundings. Contrary to that, photolytic energy can selectively excite only certain bonds or functional groups, whose energy levels correspond to the wavelength emitted; and scission products can have a much higher energy than their surroundings.[190] This energy can be transformed into vibrational, rotational or translational motion.

As shown in table 14 above, the energy of UVa radiation is sufficient to break some of the bonds present in the polymer structure. Usually, ultraviolet radiation is first absorbed by so called chromophores present in the substrate. Chromophores are molecules which absorb at a certain frequency, and usually have π and lone pair (n) electrons. Some examples of chromophores and their different absorption maxima and corresponding coefficients are shown in table 15 below. The chromophores can absorb radiation if its energy corresponds to the difference between two electronic states (ΔE) of the molecule. These are usually an excited state and the ground state and the energy difference can be calculated according to the formula $h\upsilon=\Delta E$, where h is the Planck constant and υ is the frequency of the radiation. The frequency υ can be obtained using the formula $\upsilon=c/\lambda$, where c is the speed of light and λ is the radiation wavelength.

For organic molecules, the nearest transitions are of $^1(\pi\text{-}\pi^*)$, $^3(\pi\text{-}\pi^*)$, $^1(n\text{-}\pi^*)$ and $^3(n\text{-}\pi^*)$ character. Depending on which excited state is reached, the energy will be released in different transformations. For example, molecules excited in a singlet π-π* transition will undergo among others proton transfer reactions, twisting around double bonds or cyclic rearrangements, while molecules excited in triplet π-π* transitions will undergo hydrogen abstractions, addition to unsaturated bonds or radical rearrangements.[190]

Table 15: Absorption wavelengths and maxima of example chromophores

chromophore	compound	solvent	λ_{max}	$\varepsilon_{max}(\lambda)$
			nm	$mol^{-1}cm^{-1}$
	3-octene	hexane	185 230	8000 2
	acetone	hexane	188 279	900 15
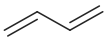	butadiene	hexane	217	20900
	benzene	ethanol	200 256	4400 226

The lowest excited state almost always has n-π* character, which leads to atom abstractions, electron abstractions or transfers, radical additions or α- and β-cleavages. However, the energies of the excited states as well as their order depend not only on the type of chromophores but also on their environment, and therefore on the type of polymer and its local structure. Hence, it is not possible to predict which degradation reactions will be caused by ultraviolet radiation without exact knowledge of the polymer in questions.

There are two different types of chromophores which can be present in the polymer and absorb ultraviolet radiation: internal and external. Internal chromophores can either be incorporated into the polymer chain by design, such as aromatic groups in polyethylene terephthalate or ester groups in all polyesters, or they can be the result of oxidation reactions which have occurred in the synthesis or during the life of the polymer. At temperatures above 80 °C, hydroperoxides can be formed even in the presence of small amounts of oxygen, and above 200 °C, they can thermally degrade to ketones and unsaturated bonds.

Table 16: Outdoors lifetime *vs.* UV cutoff of different polymer types

polymer	cutoff	outdoor lifetime
	nm	years
polyethylene	<180	0,5 - 1,0
polypropylene	<180	0,2
polyoxymethylene	<210	0,3
poly(vinyl chloride)	220	0,5
poly(methyl methacrylate)	240	>20
polyamide nylon 11	240	8
polystyrene	270	0
polycarbonate	280	0,5
poly(phenylene oxide)	280	<0,5
polyurethane	280	2
poly(ethylene terephthalate)	310	3
poly(m-phenylene isophthalamide)	340	0,2
poly(*p*-phenylene terphthalamide)	350	0,3

The second type is chromophores that are not part of the polymer chain. They are sometimes added on purpose, such as metals used as catalysts to aid the polymerisation or crosslinking reaction, pigments which can be metals or organic chromophores, or absorbing solvents. Accidentally added chromophores can include for example impurities such as metal debris from the reaction equipment.

While the capacity of absorption and therefore the susceptibility to degradation reactions of each polymer is evidently dependent strongly not only on its structure, but also on the production methods and additives in the formulation, the complexity of weatherability prediction is further evidenced by data reported by Carlsson *et al.* as presented in table 16 above.[191]

In this study, the UV cutoff, i.e. the wavelength at which a film of 10 µm thickness reached an absorbance of 1, was compared to the outdoor lifetime of a series of different polymers. The end of life was defined as a 50% loss of tensile, elongation or impact performance. The polymers are listed with increasing UV cutoff values, and it is clear that no direct correlation can be established concerning their lifetime.

3.2.1.1 Initiation reactions

After ultraviolet radiation has been absorbed by a chromophore in the polymer, radical chain reactions can be started by different types of initiation reactions. Carbon based radicals can be created for example near ester groups in a Norrish type I mechanism, resulting in polymer chain scission and creating two polymer based radicals, as shown in scheme 74. A similar reaction can occur near ketone and aldehyde groups.

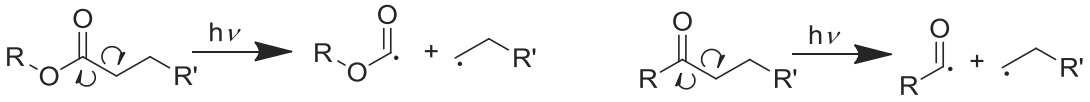

Scheme 74: Norrish type I degradation

Where hydroperoxides are already present in the chain, they can dissociate to create a variety of products as shown in scheme 75. After oxygen-oxygen bond cleavage, either two oxygen based radicals or one carbon and one oxygen based radical with an aldehyde are formed. The carbon based radical can recombine with the oxygen based radical to form a terminal double bond and a water molecule.

Carbon-oxygen bond cleavage can on the other hand result in the formation of a carbon based radical and a peroxy radical. Theoretically, the creation of one oxygen and one hydrogen radical would also be possible after oxygen-hydrogen bond cleavage. This is however seldom observed because of the bond energies, which are estimated at 42 kcal/mol (O-O), 70 kcal/mol (C-O) and 90 kcal/mol (O-H) respectively.

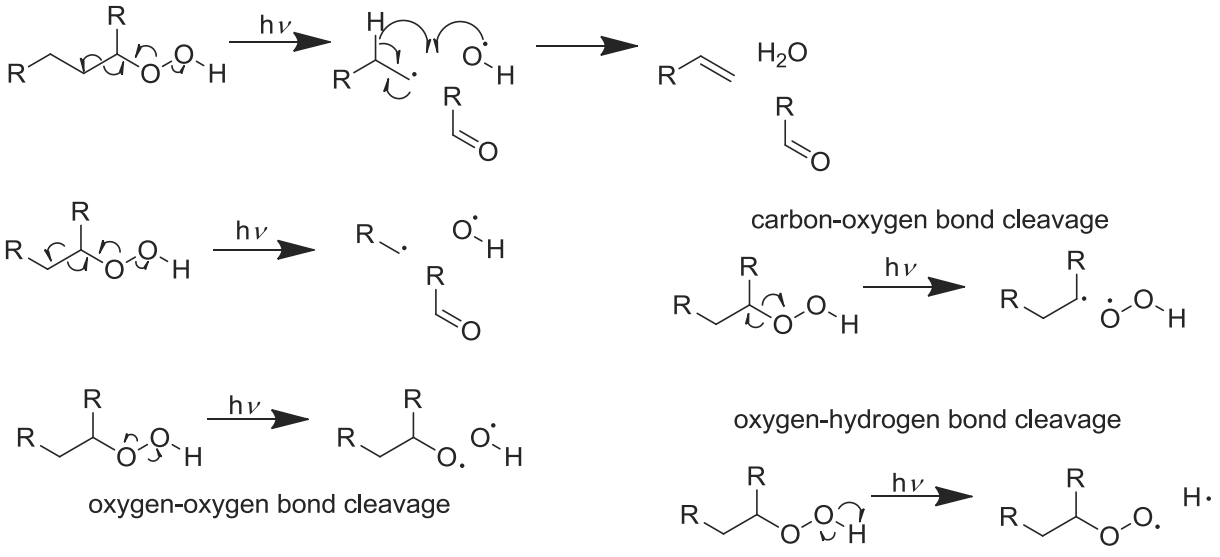

Scheme 75: Pathways of hydroperoxide dissociation

Transition metals such as for example Cu^{+}, Fe^{2+}, Cr^{2+} , V^{2+} or TiO_2 can act as catalysts for the decomposition of hydroperoxides into hydroxyl and peroxyl radicals in a one electron transfer reaction as described below.

$$M^{n+} + RO_2H \rightarrow M^{(n+1)} + RO^{\cdot} + OH^{-}$$

$$M^{(n+1)} + RO_2H \rightarrow M^{n+} + RO_2^{\cdot} + H^{+}$$

A third possibility is the formation of a charge transfer complex between a chromophore such as a metal or a ketone, and molecular oxygen. The oxygen can be excited into its more reactive singlet state and react with aromatic or allyl groups in the polymer chain as exemplified in scheme 76 below.

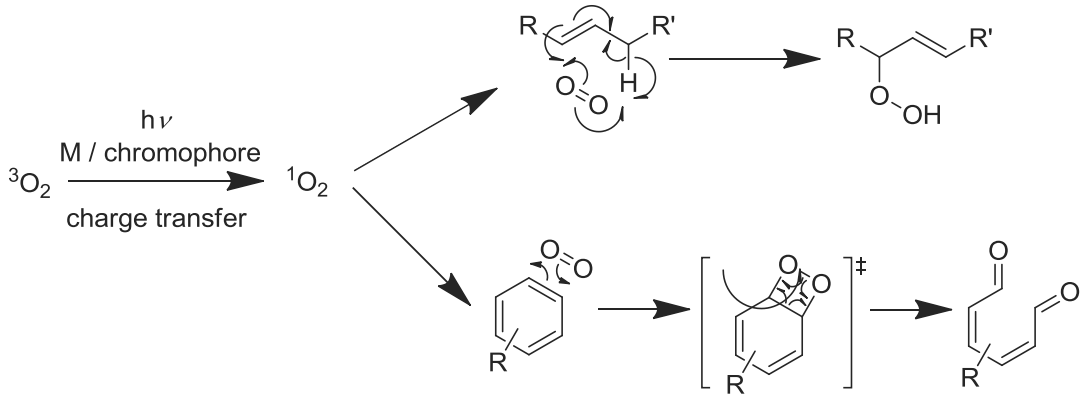

Scheme 76: Singlet oxygen reaction with allyl groups and aromatics

Lastly, where γ-hydrogen of the acid or β-hydrogen on the diol part are present in the structure, a Norrish type II mechanism can take place resulting in the formation of a terminal carbon-carbon double bond and a terminal carboxylic acid or ketone group, as shown in scheme 77.

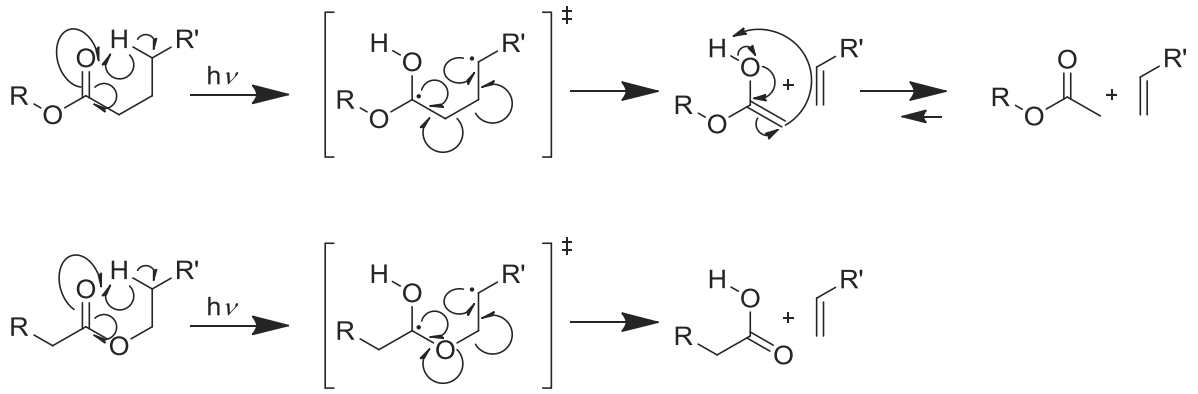

Scheme 77: Norrish type II degradation

Which of these initiation reactions is prominent, and at which rate they proceed depends largely on the individual polymer. Apart from the concentration of chromophores absorbing the radiation, the concentration of oxygen is rate determining for the pathway involving oxygen excitation (see Scheme above). For the Norrish type II pathway, a six-membered transition state has to be formed to enable the hydrogen transfer, making the geometry of the chain and its mobility key factors.

Finally, the reactions can take place either on the polymer backbone, on pendant groups or on organic solvent or pigment molecules. In each case, different rates and pathway preferences may be observed.

3.2.1.2 Propagation reactions

Following the initiation reactions, degradation is propagated in one or both of two ways. Firstly, radicals are created which continue to react either by hydrogen abstraction, as shown in scheme 78, or with oxygen. Secondly, the concentration of reactive groups such as peroxides, carbonyl groups and double bonds that can absorb radiation and partake in further initiation reactions, is increased.

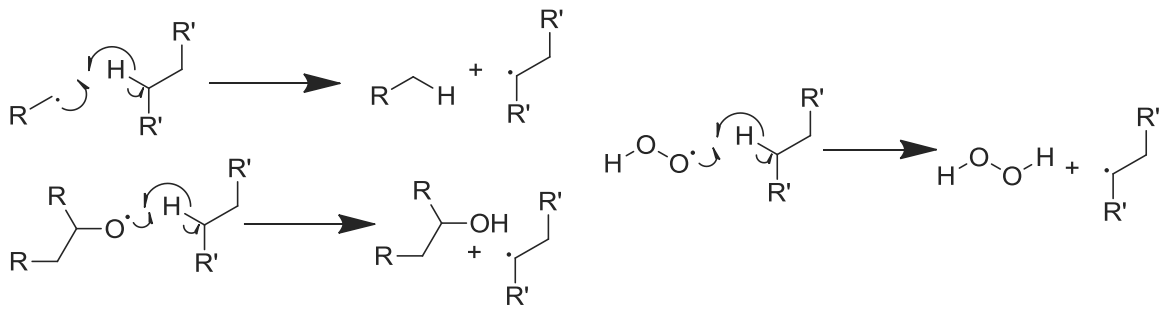

Scheme 78: Propagation reactions of carbon and oxygen based radicals

Both carbon and oxygen based radicals created in the mechanisms described above can propagate the radical chain reaction by abstracting hydrogen from another part of the polymer, thus creating a new radical. The availability of hydrogens for abstraction depends on the bond dissociation energy, which is largely influenced by electronic and steric influences of the neighbouring groups.

The transition state will generate a partial positive charge on the carbon from which the hydrogen is abstracted. Therefore, the energy of the transition state is lowered and the abstraction favoured by electron-donating groups, while the energy is increased and abstraction becomes less favourable in the presence of electron-withdrawing groups.

An approximate order of susceptibility to abstraction for several types of hydrogens, starting with the most vulnerable, has been provided by Wicks *et al.* and is reported in scheme 79 below.[188] Both the environment of hydrogens available in a polymer structure and their quantity can be an important factor for the rate and pathway of photodegradation.

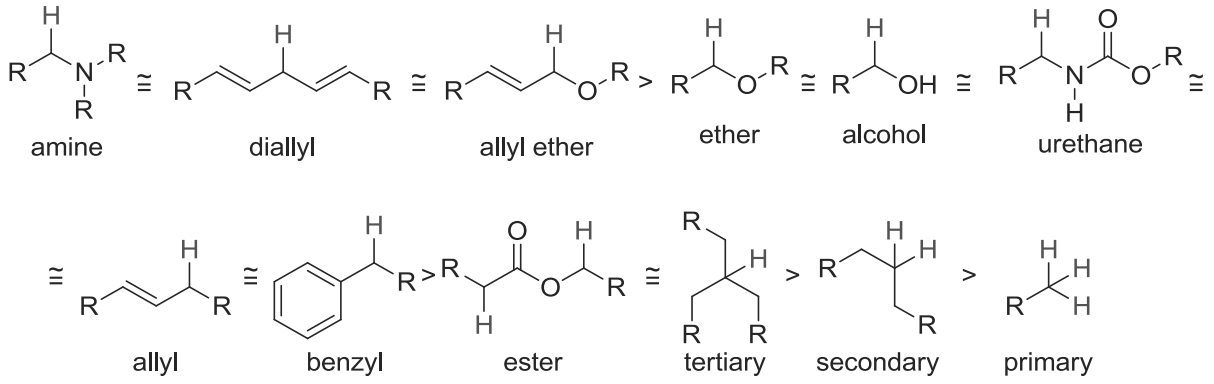

Scheme 79: Liability to abstraction of different hydrogen atoms

Oxygen based radicals can undergo β-scission reactions forming a ketone group and a radical chain end, as shown in scheme 80.

Carbon based radicals, as created for example in a Norrish type I mechanism or by hydroperoxide dissociation, can further react with molecular oxygen to create peroxyl radicals. These can abstract hydrogen to form hydroperoxides, or, if the radical was based on a carbonyl group, peracid groups, as shown in scheme 81. The hydroperoxides can then participate in further initiation reactions as described above.

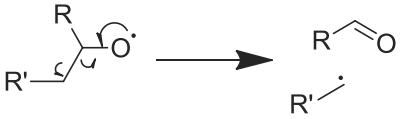

Scheme 80: β-scission of oxygen radicals

The reactivity of different functional groups towards peroxyl radicals was studied in by Carlsson *et al.* in the liquid phase.[191] The rate constant of the abstraction of different types of hydrogen is reported in $L.mol^{-1}.s^{-1}$ in table 17 below.

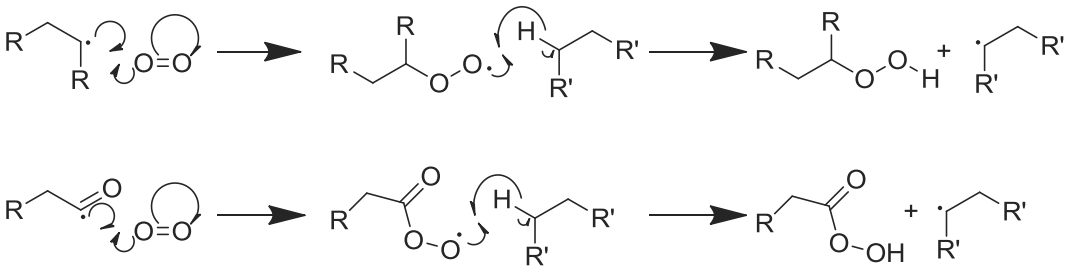

Scheme 81: Formation of hydroperoxides and peracids

It should be noted that while the liability towards abstraction of tertiary hydrogens was found to be 4600 times that of primary hydrogens, and the liability of secondary hydrogens 75 times that of primary hydrogens, this is somewhat compensated by the reactivity of the resulting hydroperoxides. Because primary and secondary peroxides react up 100 – 1000 times faster than tertiary peroxides, the final selectivity of hydrogen abstraction by peroxyl radicals is only 20 : 7 : 1 (tertiary : secondary : primary).

Table 17: Rate constant of abstraction of different type of hydrogen atoms in the liquid phase

structure	rate constant	structure	rate constant	structure	rate constant
	L/mol*s		L/mol*s		L/mol*s
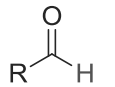	1 000	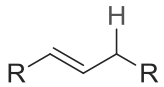	0,1 - 1	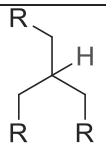	$5 – 10 * 10^{-3}$
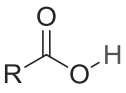	50 – 500	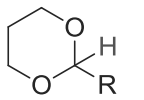	0,6 – 0,9	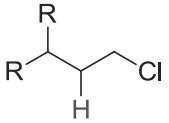	$4 * 10^{-3}$
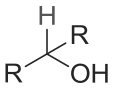	2	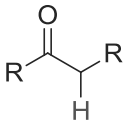	0,03 – 0,07	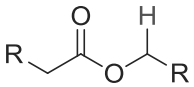	$2 * 10^{-3}$
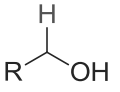	1	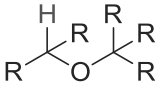	0,02 – 0,06	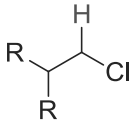	$6 * 10^{-4}$
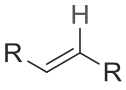	1	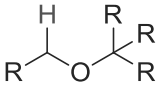	0,02	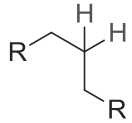	$1 – 5 * 10^{-4}$
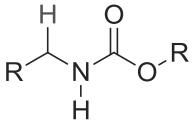	1	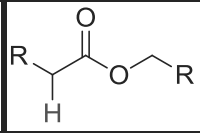	$10 * 10^{-3}$		$1 – 2 * 10^{-5}$

Overall, the rate constant for the reaction with peroxyl radicals agree with the theoretical bond strength reported above, and permit some degree of quantification. However, it must be kept in

mind that the radical reactions in polymers are often diffusion controlled, which is an important difference to the study conducted.

3.2.1.3 Termination reactions

The radical chain reaction is terminated when two radicals combine to give a stable product. The most likely combination is that of a peroxy and an alkyl radical, as shown in scheme 82. The combination of two alkyl radicals is also possible.

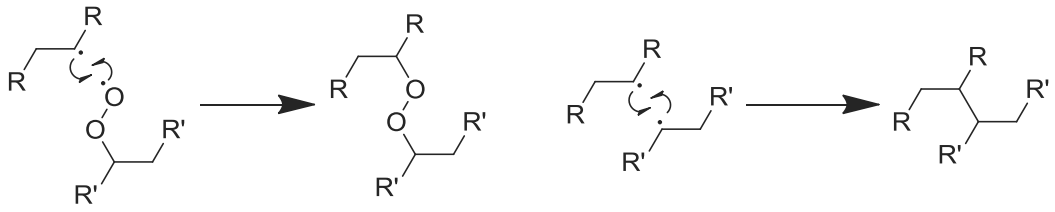

Scheme 82: Termination by combination of two radicals

Depending on the oxygen pressure, peroxy radicals can also combine, as shown in scheme 83. If the oxygen pressure is very high, one product is formed, whereas in lower oxygen pressure, the product will be a peroxide and molecular oxygen.

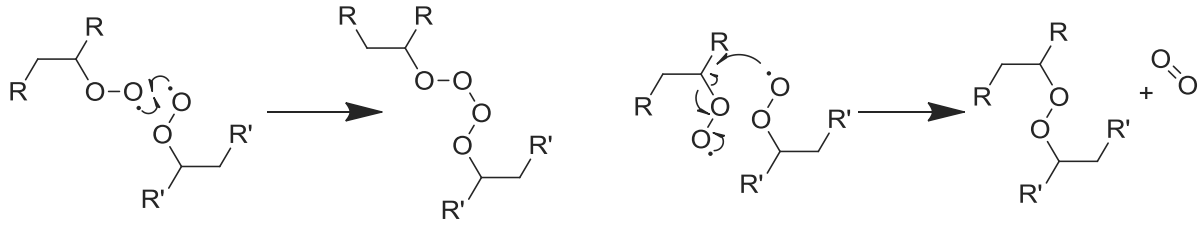

Scheme 83: Termination by combination of two peroxide radicals and formation of oxygen

Termination reactions often result in new crosslinks between chains. While it is hard to determine the exact nature of the reactions, it is possible to determine whether crosslinking reactions such as termination reactions or chain scission reactions are dominant by following the crosslinking density during the ageing process.

3.2.1.4 Factors influencing photolytic degradation

Aside from the influence of the chromophore concentration and the nature of hydrogen bonds described above, several other factors determine the rate and pathways of photolytic degradation.

The glass transition temperature (T_g) of the polymer determines if chains are mobile at any given temperature. Since the radical reactions are diffusion controlled, below the T_g, mostly small radicals such as hydroxyl radicals will react. Above T_g, polymer based alkyl radicals can react, and mechanisms such as the Norrish type II reactions can take place. The general mobility of the chains also

determines if radicals generated in an initiation reaction will be able to leave their cage and propagate the reaction, or if they will just recombine.

Similarly, the molecular weight and crosslinking density have an impact on chain mobility and need to be considered. Additionally, long chains are statistically more susceptible to chain scission, which will have a greater impact on their weight average molecular weight ($M_{\overline{w}}$). As degradation reactions are often found to be more efficient on pendant parts than on the main chain, the chain composition also needs to be considered.

Another important factor is the free volume, which is defined as the additional volume a polymer occupies at a given temperature compared to the volume it would theoretically occupy at a temperature of 0 K. Chain scission results in an increase of chain ends compared to polymer backbone. Since the former occupy more space, the free volume decreases in the course of the degradation, leading to strain on the overall polymer structure. Strain can lead to faster separation of radicals formed in initiation reactions, decreasing the amount of recombination. It can also increase the oxygen permeability.

On the other hand, through the reaction with oxygen, the overall hydrogen bonding capacity of the polymer increases, which can shorten distances between chains and decrease the oxygen permeability.

Lastly, the state of the polymer is important. As mentioned above, contrary to dissolved, liquid state polymers, the degradation in solid polymers is diffusion controlled. This is evidenced by the fact the degradation occurs localised and not equally distributed across the network.

3.2.1.5 Hindered amine light stabilisers

Hindered amine light stabilisers (HALS) are a type of radical trapping antioxidants which are commonly added to polymers intended for exterior use in order to increase their resistance to radical pathway photolytic degradation. They generally contain a di-tert-alkyl amine unit, and can interrupt the radical reaction via reaction with a peroxy radical to form a nitroxide. In a mechanism known as the Denisov cycle, the nitroxide radical reacts with an alkyl radical to form an alkoxyamine, which reacts with a further radical to regenerate the nitroxide. Therefore, each molecule can participate in several cycles of radical deactivation, and reach far above stoichiometric yields.[XIX]

As the efficiency of the HALS in a formulation depends on their ability to complete the Denisov cycle and regenerate themselves, it will also depend on the type of formulation. The diffusion and

[XIX] See annexe for details concerning the different mechanisms contributing to HALS action

solubility coefficients, the structure of the resin and the overall composition of the formulation can have an impact on the degree to which the HALS can decrease the radical induced degradation.

3.2.2 Thermal degradation

Thermal degradation is the oxidative degradation caused by temperature. Contrary to photodegradation, heat energy is more uniformly distributed in the coating, and less sensitive to depth. It results in chain breaking to yield smaller molecular weight fragments. The chain degradation can proceed through an unzipping mechanism, starting with an active chain end, or through random bond breaking. The former is typically observed for chain growth polymers, while the latter is more common for step growth polymers, such as polyesters.

The rate of thermal degradation depends on the rate of heating, and also on the removal of volatile products if any are formed. Possible products formed from polyesters include formaldehyde, acetaldehyde, formic acid, acetic acid, carbon dioxide and water.[189]

Possibly due to the difficulty of modelling thermal degradation, which is a combination of physical and chemical phenomena, or due to the complexity of products, the exact mechanism of thermal degradation is not completely understood.[194] It is thought to be caused in part by peroxyl radical formation, either through dissociation of peroxyl radicals present in the structure, or through an electron transfer process involving a metal catalyst. The thus generated radicals can propagate chain reactions identical to those described for the photodegradation process.

Additionally, pyrolysis, i.e. the decomposition in the absence of oxygen, and decarboxylation reactions at chain ends can occur. Examples of both are shown below in scheme 84 for a polyethylene terephthalate structure.[191, 192]

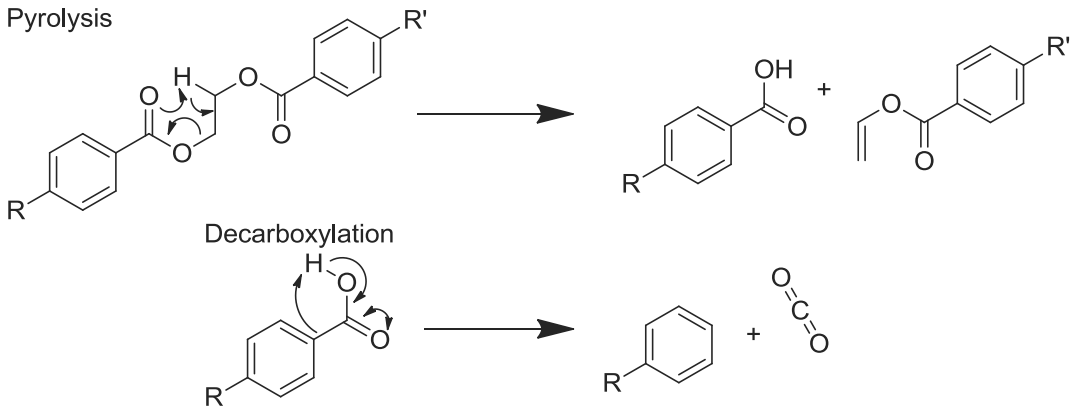

Scheme 84: Thermal degradation mechanisms

Synergistic effects that can be observed between thermal and photolytic degradation include the presence of radicals in both degradations, increased mobility of chains and radicals generated from

photolytic degradation at higher temperature and the increase of chromophores generated in thermal degradation.

3.2.3 Hydrolytic degradation

Hydrolytic degradation is the breaking of ester bonds by hydrolysis, reversing the polyesterification process and creating acid and alcohol end groups, as shown in scheme 85. Since the process is acid catalysed, it is accelerated both by the presence of acidic catalysts added for the polyesterification or the crosslinking, and by the reaction products.

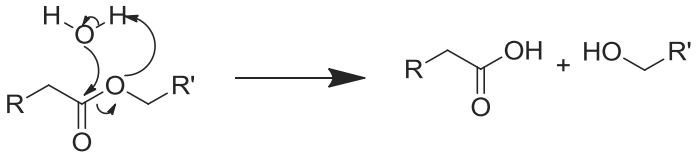

Scheme 85: Hydrolytic degradation

Factors affecting the rate of hydrolytic ageing are steric hindrances around the ester groups and the ability of water to permeate the structure.[188] For example, it has been found that a lower water solubility of the monomers results in a decreased rate of hydrolysis.[195] The chain length, T_g and surface tension also influence the permeability of the coating.

Water can also penetrate into the polymer network, particularly the pigment interstices where those are not completely wetted, and have a secondary effect on coating weatherability. This causes strain through swelling and disruption of hydrogen bonds between polymer chains.[184] The strain can be increased if episodes of wetting are followed by drying out of the water, which causes contraction of the network.

High temperatures, which accelerate the penetration of water into the polymer network, as well as photolytic degradation, which causes the formation of hydrophilic groups, increase the effect of hydrolytic degradation.

3.2.4 Physical ageing and other degradation mechanisms

Physical ageing is a relaxation process slowly transforming all polymers below their glass transition temperature.[196] When cooled down, the chain segments lose their mobility below the T_g, and cannot adjust to their optimum equilibrium position. This non-equilibrium situation is slowly resolved, resulting in a reduction of the free volume of the polymer. The process is reversible when the polymer is heated above its T_g.

Thermoset coatings, which are very rigid and contain a large free volume, are particularly affected by this relaxation. It can cause a decrease of flexibility and impact resistance, and an increase in hardness. Physical ageing can also be observed as a change in the relative storage modulus and loss tangent measured by dynamic mechanical analysis (DMA). The further away the ageing temperature

of the coating is from its T_g, the larger is the change in properties, and the slower is its progress. Furthermore, it was observed that the larger the free volume of the coating, the larger the effect of the physical ageing that can be observed. No influence of the pigment in the formulation was discovered.

Air pollutants such as SO_2, NO_x and HCl can also have an adverse impact on the coating.[197] They can diffuse into the surface of the polymer, react to form different products and diffuse further. Often, synergistic effects are observed if several pollutants are present, and in combination with ultraviolet light. High humidity can also accelerate the decomposition and penetrations of air pollutants in the material surface.

Other possible degradation mechanisms include the reaction of double bonds with ozone, mechanical degradation and biodegradation. Mechanical degradation is the generation of radicals from the homolytic cleavage of a carbon-carbon bond caused by strain. However, this is generally thought to occur in amorphous regions in between crystalline regions, which are not found in completely amorphous coatings. Biodegradation by microbes or enzymes generally requires a wet environment such as soil, or immersion in water, and is therefore not discussed here either.

Table 18: Resistance to different degradation pathways of different polymer types

polymer	photolytic	thermal	hydrolysis	ozone
polyethylene	poor	poor	excellent	excellent
polypropylene	very poor	very poor	excellent	excellent
polystyrene	poor	fair	excellent	excellent
poly(methyl methacrylate)	excellent	good	good	excellent
poly(tetrafluoroethylene)	excellent	excellent	excellent	excellent
polyamide (nylon 6 and nylon 6,6)	fair	fair	fair	-
polyacrylonitrile	good	poor	good	excellent
poly(vinyl chloride)	poor	very poor	excellent	excellent
poly(ethylene terephthalate)	good	good	good	excellent
polyoxymethylene	poor	poor	fair	fair
polycarbonate	poor	fair	good	good
poly(phenylene oxide)	fair	very poor	good	good
poly(ester urethane)	fair	fair	good	good
poly(ether urethane)	poor	poor	fair	good
poly(*m*-phenylene isophthalamide)	very poor	excellent	good	excellent
poly(*p*-phenylene terephthalamide)	very poor	excellent	good	excellent

Aside from the different synergies between degradation mechanisms, the relevance of each mechanism also differs depending on the nature of the polymer. This is illustrated by a ranking of importance of different degradation mechanisms presented by Carlsson *et al.* for different types of

polymer networks, shown in table 18. This kind of differences may also be observed for different formulations. Conditions effective in accelerating the degradation or principles useful for stabilising one type of coating can therefore not be assumed to automatically apply to other coatings.

3.3 Accelerated weathering

Accelerated weathering tests are used for two main purposes: To estimate the service life of a new product, or to compare the performances of two different products. They can be performed either outdoors, in locations with particularly harsh conditions, or in the laboratory, in an artificial weathering cabinet. Ideally, laboratory testing is used to study the effect of different types of exposure on a material, and to develop a model that can extrapolate the degradation observed over longer periods of time. Outdoor exposure[XX] is used to characterise the worst case exposure conditions, and to verify results from laboratory exposure in real life conditions. Since the design of the tests used has a large impact on the resulting prediction, it is also vital to understand which factors can cause variability.[197]

Where weathering cabinets for laboratory accelerated ageing are used, a choice has to be made as to which conditions are applied. Either, the conditions can be approximated to those of a specific location, and data concerning the humidity, temperature and sunlight spectrum measured at that location can be simulated. Another possibility is to select conditions to accelerate a specific type of degradation to be tested. Since ultraviolet light wavelengths, intensities, temperatures and humidity can be chosen freely in a weathering cabinet, harsher conditions and therefore a larger degree of acceleration as well as higher reproducibility can be achieved compared to outdoors tests. As results can be obtained in shorter time, cost is also generally lower than in outdoors tests.

Light, temperature and humidity may be applied in cycles in an artificial weathering chamber, in order to simulate variations in real weather such as day and night, and to capture degradation caused by for example repeated wetting and drying. Weathering chambers from the company Q-lab are often used, and denoted QUVa or QUVb, depending on whether the radiation is in the UVa or UVb region.[198]

3.3.1 Simulation of sunlight

Sunlight can be simulated by a xenon arc, a carbon arc, fluorescent lamps or mercury lamps. Since these light sources produce a different spectrum to the natural sunlight, filters based on borosilicates or quartz can be applied to adjust the wavelengths the sample is exposed to. In order to accelerate the photo degradation, fluorescent lights emitting in the UVb region have been employed. However,

[XX] For details on the different conditions used and parameters observed in outdoor exposure, see annexe

it has been observed that shorter wavelengths can cause degradation mechanisms not observed under exposure to natural light, and the faster degradation necessitates a trade off of prediction accuracy.

Intensity of light also has to be monitored and adjusted, especially since artificial lamps can lose intensity over time. The lamp either needs to be exchanged regularly, or the input power has to be adjusted.

3.3.2 Temperature inside a weathering chamber

As in outdoor weathering, both the ambient temperature of the weathering chamber and the actual surface temperature of the sample are important. The different response to the radiation used of samples for example with different colours needs to be accounted for.

3.3.3 Humidity

Different types of humidity such as fog and condensation, or immersion in water, can be produced in indoor weathering tests. The relative humidity of the chamber needs to be controlled as well as the input of water, since it can be affected by the humidity in the surrounding laboratory.

3.4 Prediction of weatherability

Many different factors influence the weatherability of a coating. As detailed above, a variety of degradation mechanisms can take place, and their rate and importance depends on the monomers used in the polymerisation, on the molecular weight and structure of the polymer, on the crosslinking agents used, on processing temperature and conditions and on the different ingredients of the final polymer formulation. The unpredictability of the weather and the variety of meteorological conditions found in different, even physically close places, adds difficulty to the predictions.

Much work has been done and many methods are available both for the elucidation of the different degradation mechanisms, and for the realistic simulation of weathering conditions. However, a large uncertainty is associated when transferring conclusions from one to a different product or from one set of test conditions to another. It has therefore been deemed necessary to directly perform tests on the products studied in this work to establish their absolute and relative weatherability.

3.4.1 Methods for weatherability assessment

There are many methods which can be used to assess coating weatherability, both where accelerated ageing was used, and the intention is to predict its performance in the long term, and where realistic natural exposure has taken place.

In general, the methods can be divided in two categories, depending on whether the performance is assessed directly or whether material properties are assessed which can then be extrapolated to evaluate the performance. An overview of the different techniques is presented in figure 20 below.[XXI]

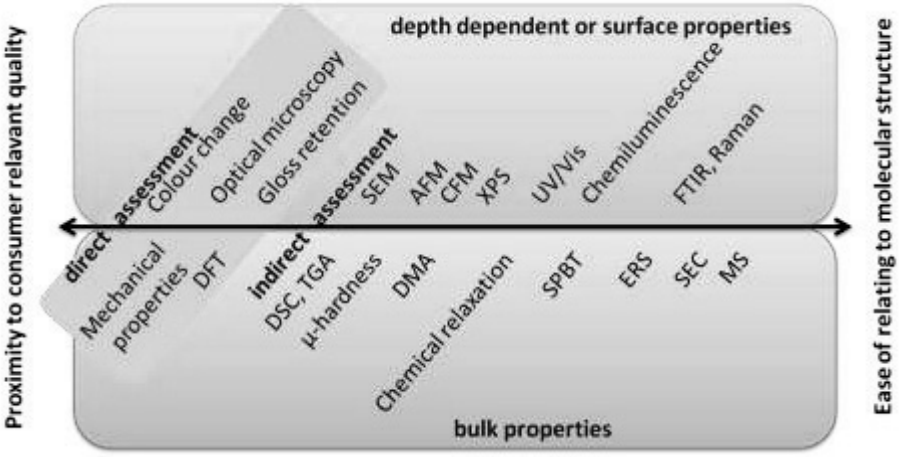

Figure 20: Approximate representation of different techniques involved in evaluating coating degradation and the compromise involved

3.4.2 Transferability of literature studies

While much research has been conducted to understand the mechanisms and factors governing coating degradation, care has to be taken when trying to transfer conclusions from one study to another. Both composition of the substrate and the design of the study can have a large impact on the result. Additionally, since many of the studies published were led by industrial researchers, the composition of the substrate is not always precisely reported to protect intellectual property.

The following three sections aim to provide an overview of work which is in some way relevant to the weatherability of thermosetting melamine crosslinked polyester films based on renewable monomers, indicating as clearly as possible all factors that could impact on the transferability of the conclusions drawn.

Firstly, some work on the importance of different degradation mechanisms and the impact of different wavelengths on the degradation of thermoplastic polyesters will be presented. Degradation studies on various renewable monomers used in thermoplastic polyesters are also included.

Numerous studies have been conducted on the hydrolytic, thermal and photodegradation of polyethylene terephthalate (PET).[199-202] However, the factors governing the degradation are likely to be quite different from those important for coil coatings for several reasons. Its structure containing the short diol and the terephthalate unit is much more rigid than that of polyester resins of interest for the coil coating industry. Furthermore, crystallinity, which is not present in fully amorphous coil coating resins, governs the density, mass transport and permeability in PET, which has a large impact on the degradation. Lastly, many studies focus on samples with a thickness well above 20 - 150 µm, and consequently a very different bulk to surface ratio. Work on PET has therefore not been deemed relevant to the question of weatherability addressed here.

The second and main part of the literature overview focuses on results obtained for comparable, i.e. melamine crosslinked polyester films. A summary of the different aspects studied, methods used and results obtained is presented.

Lastly, in the third part, some interesting work on films containing similar components such as polyester-polyols, polyester-urethanes and melamine crosslinked acrylic films is reviewed. Due to its relevance to the automotive industry, much research has been dedicated to understanding degradation of the latter.

Since the focus of this work is on resin design, studies about the efficacy of different UV absorbers and other stability modifying additives have not been included.

3.4.3 Literature studies on thermoplastic polyesters of interest

The main advantage of studying thermoplastic polyesters compared to thermosets is the fact that they can be solubilised. Therefore, a wider range of analytical techniques can be used and evidence for degradation mechanisms as well as products can be found more easily. This is demonstrated for example by a study of Carroccio *et al.*, who used MALDI-Tof spectrometry and UV/Vis spectroscopy to study the photodegradation of polybutylene succinate.[203] A summary of the different conclusions concerning the mechanisms and monomer susceptibility to degradation will be presented in this section.[XXII]

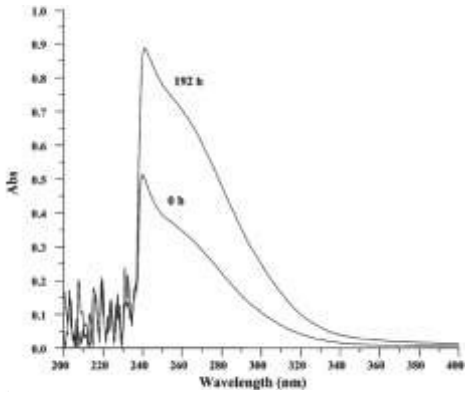

Figure 21: Broadening of the UV spectrum after degradation (Carroccio 2004)

Carroccio *et al.* obtained direct evidence of α-hydrogen abstraction and the Norrish type I degradation mechanism,

[XXI] See annexe for a description of each of the techniques and their role in weatherability testing
[XXII] See annexe for a more detailed description of the studies conducted.

as well as of an increase in chromophores with weathering, as shown in figure 21.[203] Oxidation of hydroxy groups into carboxylic acid groups was also observed, but β-hydrogen abstraction was concluded to be either absent as a degradation pathway, or not dominant compared to other reactions.

Shigemoto *et al.* used computational chemistry to study the mechanism of the β-hydrogen abstraction in polyterephthalates containing different aliphatic comonomers.[204] They successfully calculated the activation energy, but found no evidence of a catalytic effect on this degradation mechanism by metals present in the product.

The relative importance of different degradation mechanisms was studied by Nagai *et al.* in a thermoplastic polyester-polyether film.[205] They found that photolytic degradation occurs primarily in the ether parts of the chain, and that it is accelerated by temperature, but that temperature alone does not cause significant degradation.

The importance of different monomers was studied for example by Malanowski *et al.* comparing isophthalic and terephthalic acid.[206-208] They found that photolytic degradation in polyesters based on both proceeded in an identical Norrish type I mechanism, via three different radical intermediates shown in scheme 86 below. The rate of degradation was however considerably higher for the terephthalic acid containing product, which was attributed to the greater overlap of its absorption spectrum with the UV light compared to isophthalic acid.

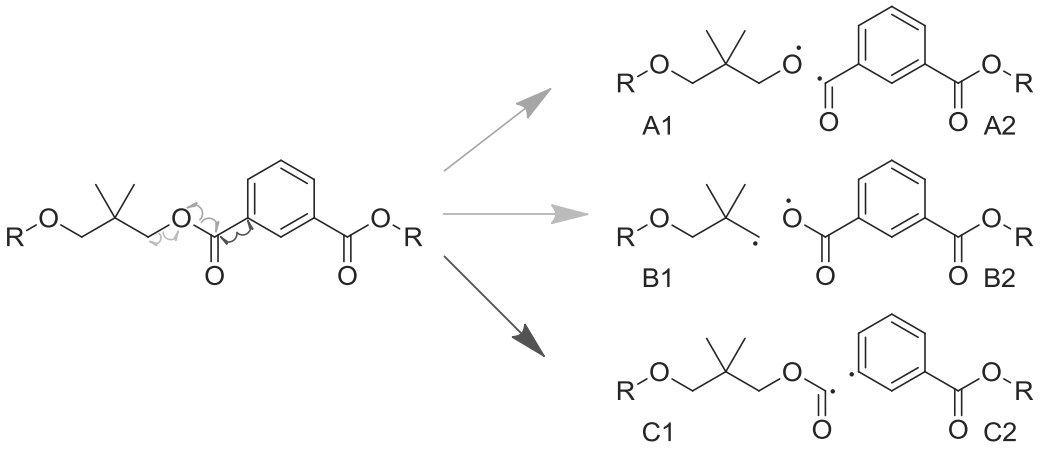

Scheme 86: Radical intermediates in Norrish type I degradation (Malanowski 2011)

When comparing different methods of weathering, the authors observed a larger degree of crosslinking when a QUVa weathering chamber with UV light with a peak of 240 nm was used, and a larger degree of chain scission when a xenon arc filter with UV light with a peak at 300 nm was used. This was explained with the penetration depth of the different light wavelengths. As the light emitted in the QUVa chamber was absorbed mostly at the surface, it created a higher concentration of

radicals in a small space, therefore favouring recombination reactions, which proceed at a second order rate. Chain scission reactions are first order with respect to radical concentration and are therefore favoured when the xenon arc light is used, which can penetrate into deeper layers.

The balance between chain scission and crosslinking was also studied by Commereuc *et al.*, who compared aliphatic and aromatic monomers.[209, 210] They concluded that chain scission is favoured in the presence of aliphatic monomers, while recombination is more prominent in the degradation of aromatic monomers. In the same group, Celli *et al.* observed that the incorporation of glycerol into the polyester not only increased the crosslinking density, but also favoured the chain scission mechanism upon photodegradation.[211]

Due to its importance to the biodegradability, the resistance to hydrolysis of biosourced polyesters has been studied by many authors. One example was presented by Zamora *et al.*, who studied the effect of various pentitols and hexitols on the degradation. While the difference between the biobased monomers was small and dependent on the other comonomers used, some insights on the mechanism of degradation could be gained.

It was found to proceed via an initially steep gradient, after which is slowed down considerably in each case. No acceleration when the pH was decreased from 7 to 4 was observed, but NMR revealed that chain scission took place primarily at ester groups adjacent to the pentitols and hexitols.

The hydrolytic stability of both isosorbide containing polyesters and polyesters based on *p*-hydroxycinnamic acid has also been investigated. The study of the former, conducted by Okada *et al.*, only examined the use of different chain lengths comonomers.[212] The latter however, published by Jin *et al.*, also compared the stability to terephthalic acid based polyesters and found that the water uptake, indicative of degradation, was significantly increased, as shown in figure 22.[144]

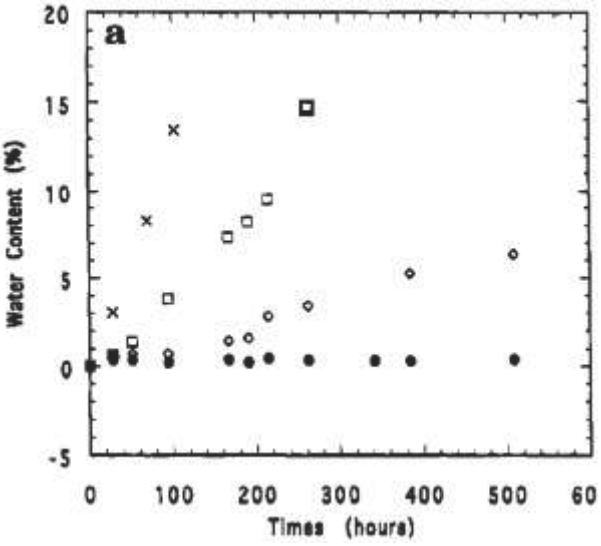

Figure 22: Water uptake dependency on $M_{\bar{w}}$ (Jin 1995)

The degradation was furthermore localised to take place near the ester bonds to the comonomer glycolic acid, and in the amorphous regions. An increase of degradation with lower molecular weight was also observed, as shown on the right.

3.4.4 Literature studies on thermosetting melamine crosslinked polyester films

A summary of the work to understand the degradation in polyester films crosslinked with melamine, shown in scheme 27, using indirect methods such as FTIR, and to correlate the results with observation from direct methods such as gloss retention measurements is summarised below.

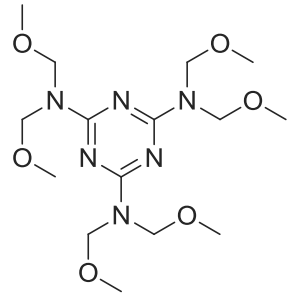

Scheme 87: Hexamethoxymethyl melamine (HMMM)

A mathematical correlation between the radical initiation rate and film thickness loss has been established by Lukey.[213] He used the chemiluminescence of several polyester melamine coatings as an indication of the hydroperoxide concentration in the coating, and proposed a correlation to the film thickness loss after natural weathering. He used the formula $[POOH]_t=k_1/(k_2-k_1)*C_0$ ($e^{-k1t} - e^{-k2t}$) to describe the concentration of hydroperoxides over time in terms of their rate constant of formation, k_1, their rate constant of decomposition, k_2, and the original chromophore concentration, C_0.

Four different melamine crosslinked polyester clearcoats were cured on an aluminium substrate at 280 °C for 40 s to reach a peak metal temperature of 232 °C and to give films of 20 µm thickness. They were then exposed in a QUVa chamber at 60 °C for up to 100 days and analysed periodically by heating at 10 °C/min from 50 °C to 250 °C and monitoring the photon count. Identical panels were exposed at an angle of 45° facing the sun in Rockhampton, Australia, in an area of high UV light intensity and high relative humidity for 4 years, and their film thickness was evaluated annually.

Assuming that the integrated intensity of chemiluminescence is representative of the total hydroperoxides concentration, the obtained curves were fitted to the formula to extract the individual parameters k_1, k_2 and C_0. It was found that the curve could be fitted to the data with a high confidence limit above 0,98 in each case. Furthermore, a good correlation was found for the hydroperoxides formation rate k_1 with the relative film thickness loss, indicating that this is a parameter important for the prediction of coating durability.

Table 19: Parameters to describe the degradation and correlation of hydroperoxides formation k_1 and film thickness loss (Lukey 2001)

Coating	k_1	k_2	C_0	r^2	dry film thickness decrease
A	0,147	0,036	4,81	0,989	Most (~100% after 4 years)
B	0,109	0,031	1,90	0,990	second most (~60% after 4 years)
C	0,079	0,031	4,16	0,991	third most (~40% after 4 years)
D	0,049	0,048	2,83	0,984	Least (~20% after 4 years)

Very similar parameters were found for the decomposition rate k_2 for the four films. The initial chromophore concentration C_0 was also not found to be predictive for the film thickness loss. The parameters obtained as well as a qualitative evaluation of the film thickness loss are shown in table 19 above.

Gamage *et al.*, of the same group, also used the radical concentration to investigate different factors impacting on the degradation, including melamine concentration, cure, oxygen in the atmosphere and strain, using electron spin resonance spectroscopy with a technique developed in the laboratory 11 years earlier.[214, 215] The polyester used was synthesised from isophthalic and adipic acids (6:4) and neopentyl glycol and trimethylol propane (9:1), with a molecular weight of 2500 g/mol. Also added to the paint were 5, 20, 20 or 50 % hexamethoxymethyl melamine (HMMM) and it was cured on silicone release-coated aluminium plates to a peak metal temperature of 215 °C, 232 °C or 245 °C using 30 s, 38 s, 26 s or 55 s in an oven at 252 or 280 °C respectively to give 20 µm thick free films. Radical formation was achieved by radiation with a 1000 W mercury/xenon lamp, with a water filter and a 280 nm UV cut-off filter to mimic the sunlight spectrum, and monitored with electron spin resonance (ESR) spectroscopy *in situ*.

The films were found to absorb between 290 nm and 310 nm with a peak at 295 nm. The types of radicals produced were found to be independent of irradiation intensity. Their quantity was observed to increase to a maximum followed by a decrease due to recombination.

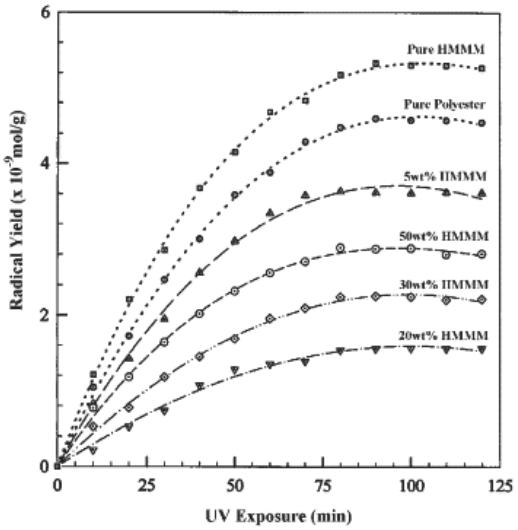

Figure 23: Rate of radical formation dependence on quantity of HMMM (Gamage 2003)

When the uncrosslinked polyester was irradiated, oxygen based radicals were observed despite the complete absence of oxygen from the atmosphere. The authors speculated that the signal could be due to carbonyl, alkyl dioxyl or alkoxyl radicals.

The authors also compared the ESR spectra of films crosslinked with different amounts of melamine. The shape of the spectra[XXIII] showed that the types of radicals formed were different from either pure polyester or pure HMMM, and depended on the chosen composition.

It was furthermore observed, as shown in table 20 below and figure 23, that the initial rate of formation of free radicals for melamine crosslinked polyester is lower than for that of each of the uncrosslinked components, and varies strongly depending on the melamine content and the curing conditions.

The optimum melamine content was 20%, which corresponds to a stoichiometric amount, and therefore to the lowest amount of free end groups. In comparing the different curing conditions, the longest cure at 55 s to reach the highest peak metal temperature of 245 °C resulted in the lowest amount of radical formation.

Table 20: Radical formation dependence on curing conditions and HMMM content (Gamage 2003)

curing conditions			HMMM content					
°C	°C	h	%					
PMT	oven T	time	0	5	20	30	50	1000
215	252	30		1,27	1,05	1,20		
232	252	38	1,41	1,21	0,52	0,73	1,08	1,64
245	252	55		1,18	0,49	0,70		
232	280	26		1,24	0,94	1,14	1,26	
predicted			1,41	1,42	1,46	1,48	1,53	1,64

This is attributed to both the completeness of the cure, and to the migration of HMMM to the coating surface, which can increase the formation of radicals and is accelerated by higher heating rates.

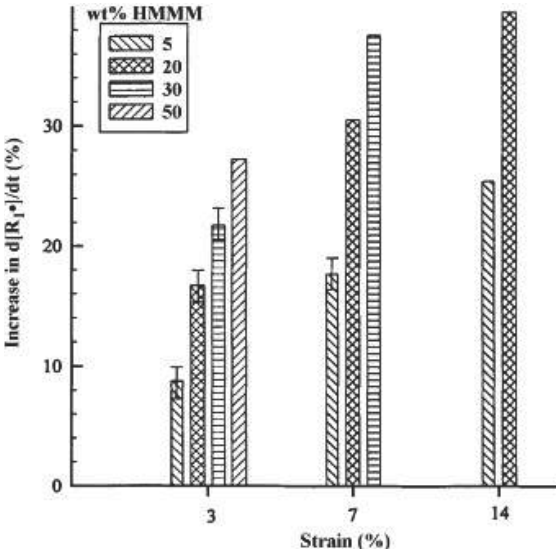

Figure 24: Radical formation dependence on strain and HMMM content (Gamage 2003)

The influence of strain on degradation was also investigated. It was found that above a melamine concentration of 5%, the rate of radical formation increases with strain and with melamine content, as shown in figure 24. New types of radicals were also observed compared to the unstrained sample. This was explained by strain hardening, which causes chain segments to orientate into lamella structures. This means that stress is no longer distributed uniformly and can cause different valence bonds to break depending on the affected area.

Because bond dissociation energies decrease proportionally to applied strain, the probability of UV excitation resulting in bond cleavage rather than local heating or luminescence is also increased. The dependency on the HMMM content is due to the elastically effective crosslinking density. As these crosslinks are responsible for load bearing, a higher strain is experienced by the material where a higher crosslinking density is present.

[XXIII] See annexe for the spectra obtained

Lastly, peroxy radical formation was observed directly in the clearcoat. The authors observed that the time needed to form peroxy radicals increased with increasing melamine content, and concluded that melamine has the ability to suppress some degree of photooxidation.

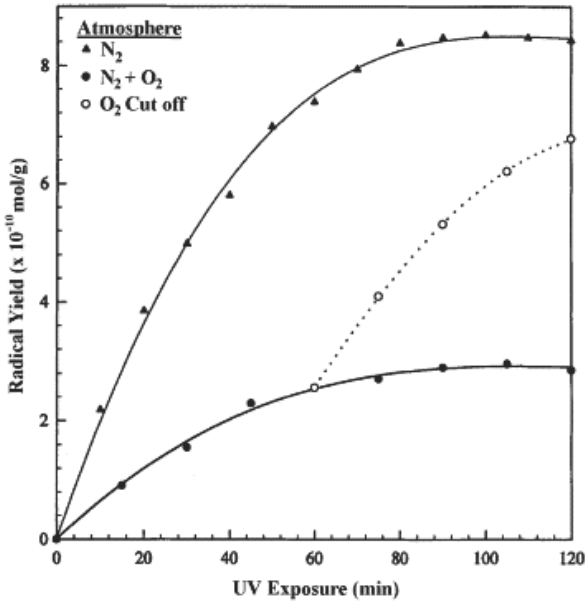

Figure 25: Radical formation in the absence of oxygen (Gamage 2003)

Furthermore, it was observed that the radical formation rate slowed down considerably when the experiments were performed in oxygen compared to nitrogen atmosphere. The accelerating effect of nitrogen was also observed where oxygen atmosphere was applied and then removed, as shown in figure 25. The decelerating effect of oxygen was attributed to the scavenging of radicals on the surface, implying that the radical reactions take place here rather than in the bulk.

A different strategy was used by Zhang *et al.*, who studied photolytic and hydrolytic degradation to relate weatherability to different parts of the formulation using FTIR.[216] They studied the degradation of a three layered coating system based on an aliphatic polyester resin crosslinked in a higher than stoichiometric ratio with melamine (4:1) depending on the depth in a clear coat layer and specific to the different melamine functional groups using step-scan photoacoustic FTIR and confocal Raman microscopy. The nature of the polyester was not further specified.[XXIV]

In order to characterise the degradation qualitatively and quantitatively, the absorption of the different peaks were characterised. On one hand, the OH peak at δ3000 – 3600 cm^{-1} and the carbonyl peak at δ1730 cm^{-1} were observed and normalised with the hydrocarbon peaks at δ3000 cm^{-1} and δ2700 cm^{-1}. The authors noted that the appearance of OH groups proceeded in three stages.

The fastest degradation was observed between 1000 h and 2000 h of exposure. In the first 1000 h, degradation was mainly caused by ultraviolet light, which penetrated all through the film and therefore caused degradation everywhere. In the second 1000 h, a sufficient level of degradation for moisture to penetrate the surface layer was reached, and the degradation was accelerated through hydrolysis and more prominent in the layers closer to the surface. Finally, the hydrolytically unstable groups were exhausted after 2000 h, and the overall degradation slowed down again.

[XXIV] See annexe for details of the coatings and weathering techniques used.

On the other hand, the changes in melamine peaks, more specifically that of the melamine aromatic ring peak at δ1550 cm^{-1} and the melamine side chain peaks at δ1085 cm^{-1} and δ913 cm^{-1} were also analysed. These peaks were normalised using hydrocarbon peaks at δ1450 cm^{-1} or δ1390 cm^{-1}.

Degradation in the melamine side chain as well as the formation of amine and amide groups, which show at δ1630 cm^{-1}, was found to be more likely than degradation of the aromatic ring. Furthermore, the degradation was observed to occur mostly in the top layers, and therefore concluded to be moisture enhanced. Lastly, the authors developed a model to reduce the number of scans necessary for a conclusive analysis.

The possibility of using tapping mode atomic force microscopy (AFM) to examine the behaviour of green-pigmented polyester melamine coatings under accelerated weathering conditions[XXV] was evaluated by Biggs *et al.*, and revealed information about the different steps of coating erosion.[217]

In comparing gloss retention and the root mean square of surface roughness, the authors found that higher gloss retention (24-30%) corresponds to lower surface roughness. A large error between measurements as well as a dependence on the number of scans performed was observed, which was attributed to the inherent surface heterogeneity.

Therefore, the authors examined a fixed area defined by microhardness indentations, and normalised the result over the initial hardness. This also made it possible to follow specific particles, and a mechanism of degradation as illustrated in figure 26 below was proposed.

Initially, the resin covering the different particles is degraded (a). This results in exposure of the pigments (b), which are eventually eroded (c). Lastly, more resin is degraded, decreasing the size of the hole made by the eroded pigment (d).

Figure 26: Erosion mechanism (Biggs 2001)

The authors also calculated the weathering rate based on the surface roughness increase after weathering, assuming that the increase is linear, and used it to compare different weathering methods. Specifically, the QUVb method described above was compared with a QUVa method, in which the radiation peak is at 340 nm instead of 313 nm, a Heraeus suntest, in which a 12 h cycle

[XXV] See annexe for details concerning the weathering technique used by Biggs *et al.*

consisting of 8 h of UV radiation from a xenon arc lamp at 500 mJ/m^2 at 75 °C and a 4 h cycle of immersion in water at 50 °C was used, and to exposure on a roof in Australia facing the sun at 45°.[218]

Table 21: Surface roughness increase rate for different radiation sources (Biggs 2001)

radiation source	roughness increase rate
	% per day
QUVb	8,30
QUVa	0,40
Xenon arc	7,00
Sun	0,08

As shown in table 21 on the left, very different results were obtained for the different methods. As the different rates of degradation correspond to the estimated harshness of each test, this was considered to confirm the validity of the measurement.

As with non-crosslinked, thermoplastic polyesters, several groups tried to establish a correlation between weatherability and single monomers in the resin. Unambiguous conclusions have however been rare, as often the results of different methodologies did not agree, even within a single study.

Several diacids with different levels of aromaticity were studied by Batista *et al.*, who also proposed a mechanism for the degradation of the melamine crosslinker, shown in scheme 88 and 89.[219] They conducted a weatherability study on four different polyester-melamine coatings, using FTIR, gloss measurements, optical microscopy and coating hardness to evaluate the result. Coatings were synthesised from 43,3% neopentyl glycol, 9,3% trimethylol propane and 16,4% adipic acid. The rigid acid component was varied between 31,1% isophthalic acid in the first resin, and 15,5% of hexahydrophthalic acid in combination with 15,6% terephthalic acid, phthalic anhydride or 1,4-cyclohexanedicarboxylic acid in the second, third and fourth resin respectively, as shown in table 22 below.

Table 22: Composition of resins used by Batista *et al.*

	resin composition (mol%)			
monomers	film 1	film 2	film 3	film 4
neopentyl glycol	43,3	43,3	43,3	43,3
trimethylol propane	9,3	9,3	9,3	9,3
adipic acid	16,4	16,4	16,4	16,4
isophthalic acid	31,1	-	-	-
hexahydrophthalic acid	-	15,5	15,5	15,5
terephthalic acid	-	15,6	-	-
phthalic anhydride	-	-	15,6	-
1,4-cyclohexanedicarboxylic acid	-	-	-	15,6

Resin T_g and acid number were measured, but the hydroxyl index and molecular weight were only calculated, not measured. In order to obtain films, resins were crosslinked with 11% hexa(methoxymethyl)melamine on glass panels at a peak temperature of 241 °C (160 s in 265 °C oven), to give films of 26 – 28 µm thickness. The panels were exposed to 150 cycles of 1 h of UV radiation from a carbon electrode without filter, at a relative humidity of 50% at 66 °C, followed by 1 h in darkness at a relative humidity of 100% at 29 °C.

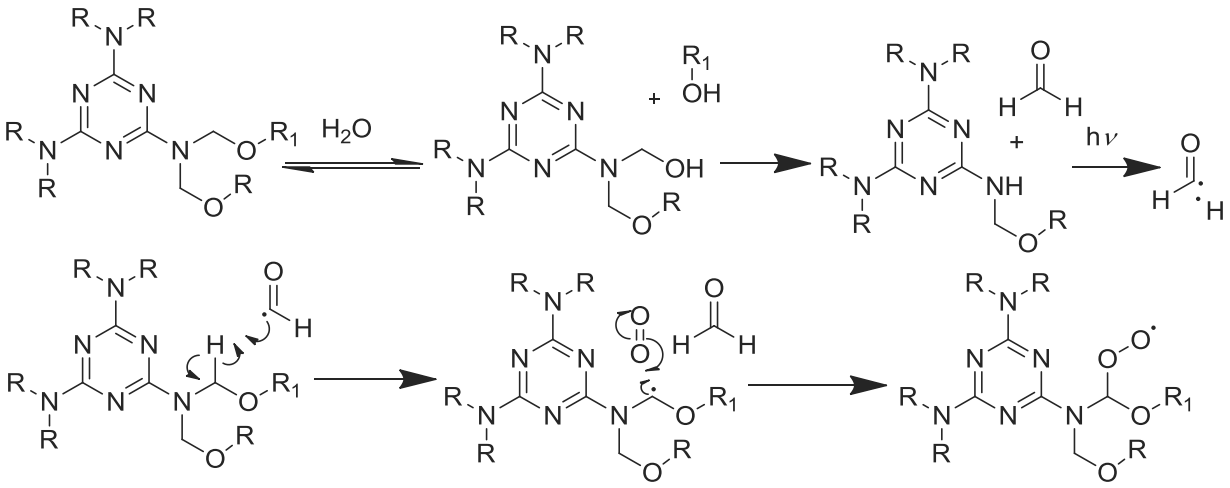

Scheme 88: Melamine degradation mechanism initiation (Batista 2011)

Fourier transform infrared spectroscopy (FTIR) was used to qualitatively and quantitatively examine the results of the degradation. The absorptions around 3431 cm^{-1} and 2965 cm^{-1} of OH and NH groups and CH groups respectively were reported before and after each set of 50 degradation cycles. The photo oxidation index was equally obtained using the formula below.

$$\mathbf{R_{abs}[(OH;NH)/CH]_t/R_{abs}[(OH;NH)/CH]_0}$$

Qualitatively, the decrease in intensity of the CH band was attributed by the authors to radical hydrogen abstraction from the polymer chain and the conversion of methylol groups to free formaldehyde. The increase in the region of 3431 cm^{-1} was attributed to the formation of amine groups, and the increase between 3380 cm^{-1} and 3520 cm^{-1} was attributed to the cleavage of alkoxy radicals into amide and amine groups, as shown in scheme 89 below.

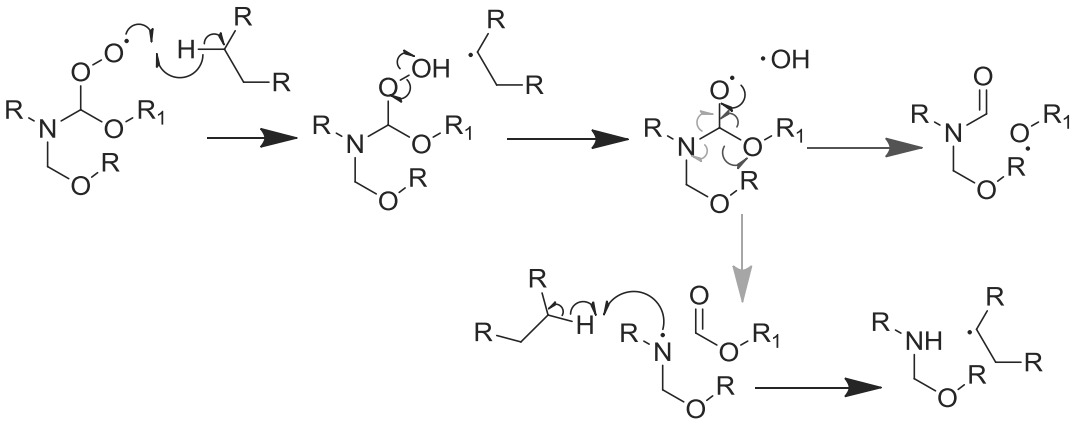

Scheme 89: Melamine degradation mechanism propagation (Batista 2011)

The initiation was attributed to the hydrolytic cleavage of melamine ether bonds. In optical microscopy analysis, localised degradation was observed. This was explained by the synergistic effect

of hydrolysis and photodegradation. In the absence of ultraviolet radiation, the hydrolysis was accelerated by the hydrophilic groups already formed in photodegradation.

Concerning the qualitative evaluation of the films, the first film containing isophthalic acid was concluded to have the best resistance to weathering, and the last film containing hexahydrophthalic acid and 1,4-cyclohexanedicarboxylic acid the least. The evaluation of the fourth film as suffering the greatest damage from degradation was consistent with the optical microscopy images, and the gloss measurements, shown in figure 27 below. Interestingly, it also showed the lowest film hardness (42 oscillations on an Erichsen Koenig device) and only a slight decrease in hardness during the weathering.

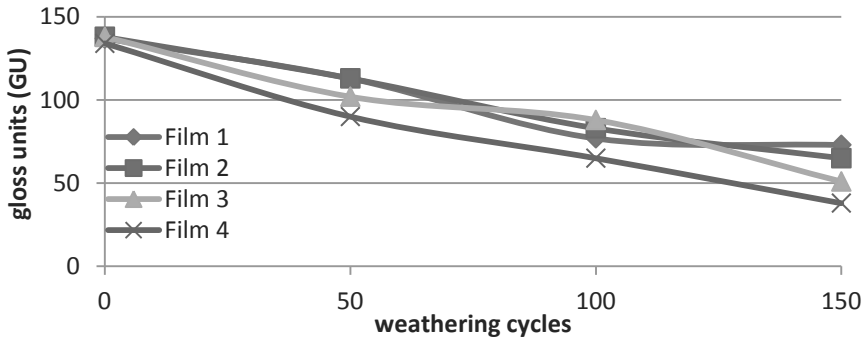

Figure 27: Gloss retention of different films (Batista 2011)

The evaluation of the first, isophthalic acid containing film to have the best resistance to weatherability was in accordance with the FTIR evaluation, shown in figure 28. However, its superiority was not evident from the gloss measurements. In general, the agreement obtained between gloss measurements and FTIR evaluation was not convincing.

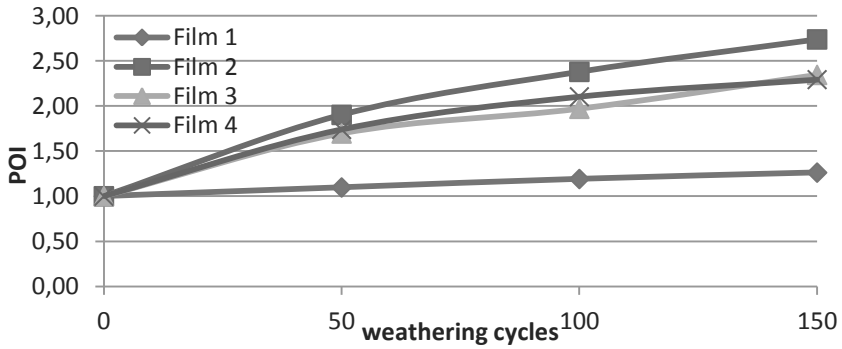

Figure 28: Photooxidation index of different films (Batista 2011)

Lastly, it is interesting to note that the three films containing some aromatic part were found to decrease in hardness considerably after 50 degradation cycles followed by a slow increase.

An even bigger disparity in results of different tests was encountered by Sullivan *et al.*, who compared the effect of different accelerated weathering tests on the gloss retention of melamine crosslinked polyester resins and performed frontier molecular orbital calculations to evaluate the reactivity of 2-methyl-1,3-propanediol (MPD) and neopentyl glycol (NG) through their diacetates.[220] Other monomers used in the formulation were 1,2-propanediol (1,2 PD), isophthalic acid (IPA), phthalic anhydride (PAN) and adipic acid (ADI).[XXVI]

The coatings containing 1:1 ratio of pigment and binder were cured at 245 °C for 75 s, and weathered separately using UVb-313 and UVa-340 bulbs in cycles of 12 h consisting of 8 h of radiation at 60 °C and 4 h of humidity at 50 °C, a xenon arc with borosilicate inner and outer filters in cycles of 2 h consisting of 102 min of radiation (0,35 W/M^2) at 63 °C and 50% relative humidity followed by 18 min of radiation and water spray, in an Emmaqua apparatus (ASTM D4141-82) and in Florida at a 26° angle (ASTM G7-89).

The reason to extend the study to several different ageing tests was that two identical studies conducted with QUVb-313 bulbs by the authors classed the coatings in reverse order from each other. In the QUVb-313 test reported in the paper, no conclusive ranking of the resins is observed until 400 h of ageing. Between 400 h and 1200 h, the fourth film performs best, followed by the second, first and third film in that order.

The QUVa-340 tests shows differences between the four films from 1500 h on, when the first and the third film are seen to lose gloss, without one clearly outperforming the other, whereas the second and fourth film show no degradation. In the xenon arc test, only the third film is seen to degrade, whereas the first, second and fourth film are increasing in gloss. Directly contrary, in the Emmaqua test the third film barely loses any gloss, while the first and second film degrade steeply after 20 weeks and the fourth film degrades steeply after 25 weeks, ending at the same level as the two former films. The Florida exposure shows only very small differences between the first and the fourth film after 20 weeks.

This disparity of results from the different test methods leads the authors to conclude firstly that there are only small differences between the films not relevant to long term stability. Secondly, it was concluded that a Norrish type II degradation mechanism, which would make the degradation rate strongly dependent on the presence of β-hydrogen, accelerating

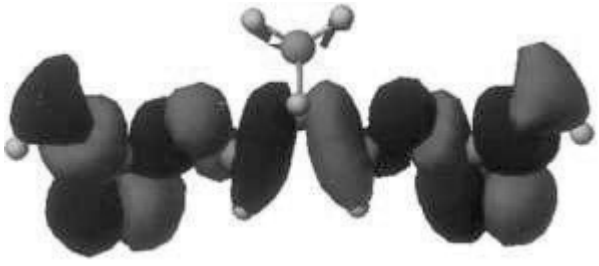

Figure 29: HOMO of MPD diacetate (Sullivan 1995)

[XXVI] See annexe for the exact composition of the resins used

more for 1,2-propanediol and 2-methyl-1,3-propanediol than for neopentyl glycol, is not prominent in this type of coatings.

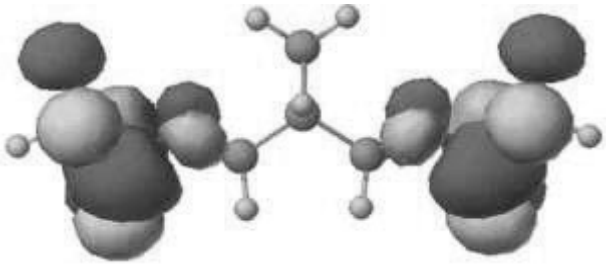

Figure 31: LUMO of MPD diacetate (Sullivan 1995)

Instead, the authors look for the relative liability of the hydrogen to abstraction to enable a prediction of weatherability based on the monomers used. In order to estimate this liability, MNDO-PM3 type frontier molecular orbital calculations are performed to model the highest occupied molecular orbital (HOMO), the lowest unoccupied molecular orbital (LUMO) and the frontier density contour map of 2-methyl-1,3-propanediacetate, as well as the frontier density contour map of neopentyl glycol.

Figure 30: FDCM of MPD diacetate (Sullivan 1995)

The molecular orbitals, presented in figures 30 – 33, show that the most reactive hydrogen in the structure are α to the ester group, and that the β-hydrogens have a very small coefficient, i.e. are not very reactive at all. The frontier density contour maps (FDCM) as well as the molecular orbital below the HOMO (HOMO1) show that when comparing the primary and the tertiary hydrogen, the tertiary is more reactive in accordance with previous assumptions.

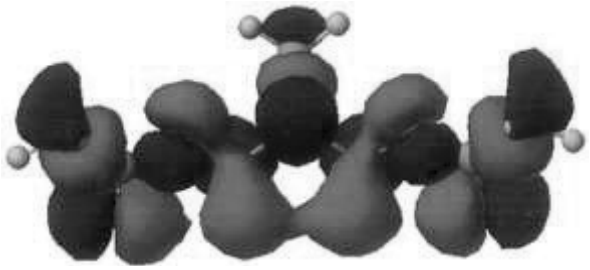

Figure 33: HOMO 1 of MPD diacetate (Sullivan 1995)

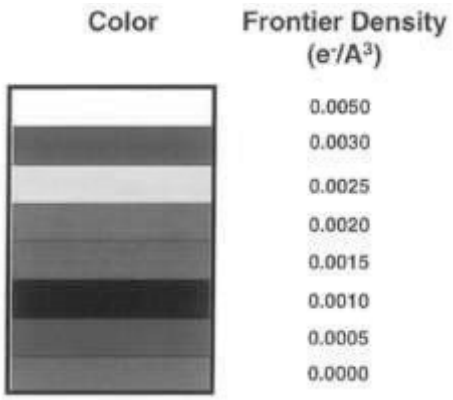

Figure 32: Colour legend for molecular orbital figures by Sullivan (Sullivan 1995)

Different diols were also studied by Narayan in two separate studies focusing on overall and thermal degradation. Firstly, Narayan *et al.* studied the degradation of melamine crosslinked polyester films based on different diols in accelerated weathering tests by dynamic mechanical analysis, X-ray photoelectron spectroscopy and scanning electron microscopy.[221] Polyester resins based on adipic acid, isophthalic acid, trimethylol propane and one of either neopentyl glycol, 1,4-cyclohexanedimethanol or 1,3-propanediol were crosslinked

in a 70:30 ratio with HMMM, cured at 140 °C on tin foil for 35 min followed by amalgamation to create free films of 200 µm thickness, and weathered in QUVa chambers using fluorescent UV lamps in 8 h cycles consisting of 4 h of radiation at 60 °C and 4 h of humidity at 50 °C. The effect of acetoacetylation of 30 % of the free hydroxy groups with ethyl acetoacetate prior to crosslinking, as shown in scheme 90, was also studied.

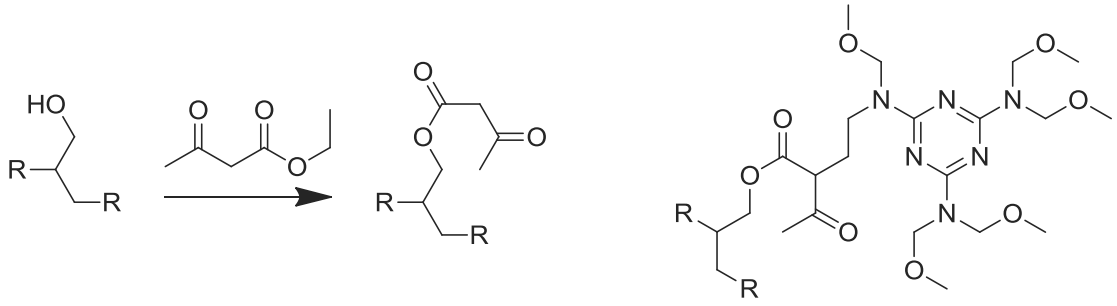

Scheme 90: Acetoacetylation of free hydroxy groups (left) and crosslink of acetoacetylated function (right) (Narayan 2005)

The resins obtained had a high theoretical hydroxy value of 240, and low molecular weights between 1000 – 2000 g/mol for both weight and number averages. Upon acetoacetylation, molecular weight decreased and polydispersity increased. T_g's of -4,3 °C, -33,5 °C and -47,4 °C were measured for the neopentyl glycol, 1,4-cyclohexanedimethanol and 1,3-propanediol containing resins respectively.

After weathering, no visible colour change was observed in the resins. As shown in table 23 below, in each film an increase of T_g and storage modulus and therefore crosslinking density was observed. The increase was most pronounced for the 1,3-propanediol containing film, and had a larger slope in the beginning of the degradation than in the end. The difference between the resins was attributed by the author to the increased chain flexibility of the straight chain of 1,3-propanediol, the increased interchain stiffness from the rigidity of 1,4-cyclohexanedimethanol and the decreased soft segment mobility from the steric hindrance of the additional methyl groups on neopentyl glycol.

Table 23: Influence of different diols on the degradation (Narayan 2005)

diol used	exposure time	T_g	E' at 150 °C	v_e
	h	°C	Pa*10^{-6}	(mol/cm^3) *10^{-5}
neopentyl glycol	0	80,9	1,30	12,3
	153	130,2	25,80	245,0
	450	148,1	62,60	593,0
cyclohexane-dimethanol	0	81,0	1,97	18,7
	365	94,1	66,00	625,0
	556	95,0 and 149,7	162,00	1535,0
1,3-propanediol	0	44,2	7,40	70,1
	450	167,6	218,00	2066,0

A decrease in peak height and increase in peak width of the tan δ curves was also observed with increasing exposure. In some cases, a second peak is observed in the tan δ curve, which is attributed to a layered structure, separating the highly oxidised surface from the less oxidised bulk.

After changing the angle of XPS from 0° to 45°, a higher concentration of nitrogen was observed at a 45° angle for the 1,4-cyclohexanedimethanol coating, suggesting that the melamine concentration is higher at the surface. This is explained by the lower free energy of the surface compared to the polyester bulk. Data for this weathered coating is not reported. However, in the acetoacetylated version, a large decrease of nitrogen was observed after weathering, as shown in table 24 below. For the same coating, the amount of carbon decreased and the amount of oxygen increased.

Table 24: Change of chemical composition after weathering and at different angles (Narayan 2005)

resin		XPS angle	C (%)	O (%)	N (%)
cyclohexane-dimethanol	unweathered	0	82,33	14,23	3,44
		45	77,29	18,63	4,08
cylcohexane-dimethanol acetoacetylated	unweathered	0	66,51	28,80	4,69
		45	70,84	25,64	3,52
	weathered (556 h)	0	65,62	33,72	0,66
		45	69,17	30,31	0,52

Scanning electron microscopy showed significant degradation of the outer layer after exposure.

In a separate paper, Narayan *et al.* also studied the thermal degradation by dynamic thermogravimetric analysis of the films described above.[222] The films were heated at a rate of 20 °C/min from 50 °C to 600 °C under nitrogen atmosphere and the initial degradation temperature (T_{id}) the temperature at which the maximum rate of weight loss occurred (T_{max}) and the final decomposition temperature (T_{fd}) were reported. The char yield % values at 300 °C and 450 °C were also analysed. Lastly, activation energies were calculated according to three different methods previously proposed by Broido, Coats-Redfern and Chang.[223-225] The results are shown in table 25.

Table 25: Thermal degradation of different diols (Narayan 2005)

	T_{id}	T_{max}	T_{df}	Conversion (%) at		E_a (kJ/mol)		
Diol	**°C**	**°C**	**°C**	**300 °C**	**450 °C**	**Broido[223]**	**Coats-Redfern[224]**	**Chang[225]**
neopentyl glycol	315	412	453	13,5	83,7	61,3	62,8	83,7
cyclohexane dimethanol	305	415	445	13,4	85,6	83,3	74,8	101,1
1,3-propanediol	322	392	452	11,8	85,2	64,5	65,4	93,6

A two step degradation was observed for the neopentyl glycol containing film. This was attributed by the authors to branch chain scission and steric hindrance due to the methyl groups. The different

degradation temperatures did not reveal an obvious ranking of the stability of the three diols used, but the char yields suggest that at 300 °C, the 1,3-propanediol containing film is the most stable, followed by the 1,4-cyclohexanedimethanol film, while at 450 °C, the neopentyl glycol film is the most stable, followed by the 1,3-propanediol containing film. The activation energies are lowest for the neopentyl glycol containing film and highest for the 1,4-cyclohexanedimethanol containing film in all three calculations.

Most recently, Siyab *et al.* compared the weatherability of melamine crosslinked polyester coatings containing resins based on renewable resources and petroleum in accelerated weathering tests using gloss retention measurements, FTIR, AFM, μ-hardness measurements and chemical force microscopy.[17] The petroleum based resin used contained aromatic and aliphatic monomers, and was compared to two different renewable resins. One contained cycloaliphatic and aliphatic renewable monomers, while the other contained about 50% renewable aliphatic monomers and 50% of a different petroleum based aromatic monomer. The resins were crosslinked with HMMM in a 4:1 ratio, with or without 21% TiO_2 pigment, and cured for 30 s on steel panels onto a primer to a peak metal temperature of 232 °C – 241 °C to give films of 18 – 20 μm thickness. The films were weathered in 12 h cycles consisting of 8 h UVa radiation at 0,87 W/m^2 with a peak at 340 nm at 60 °C followed by 4 h of humidity at 50 °C for a total of 3000 h.

As shown in figure 34 below, the partially biosourced resin displayed the best gloss retention performance in a clearcoat in the first 1500 h, but dropped below the petrosourced resin after that. The fully biosourced resin displaced the poorest gloss retention. Where TiO_2 pigment was added to the formulation, the partially biosourced resin performed in between the fully biosourced resin and the petrosourced resin.

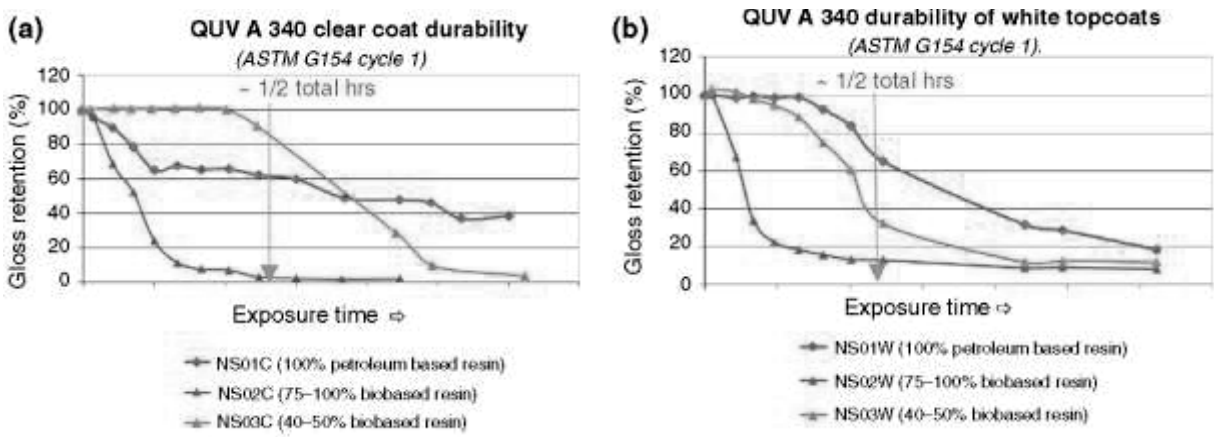

Figure 34: Gloss retention upon QUVa exposure of films with different biobased contents (Siyab 2016)

The partially biosourced (NS03C) and the petrosourced (NS01C) resin clearcoats were further examined with atomic force microscopy, to reveal the root mean square roughness, and with μ-

hardness measurements. Both confirmed the trend seen in gloss retention measurements, as shown in figure 35 and 37 below.

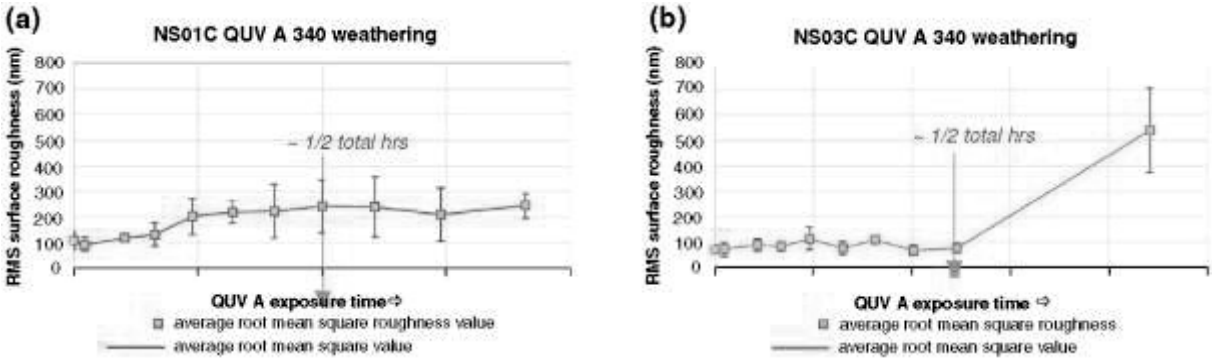

Figure 35: Surface roughness of petro- and biobased resin upon degradation (Siyab 2016)

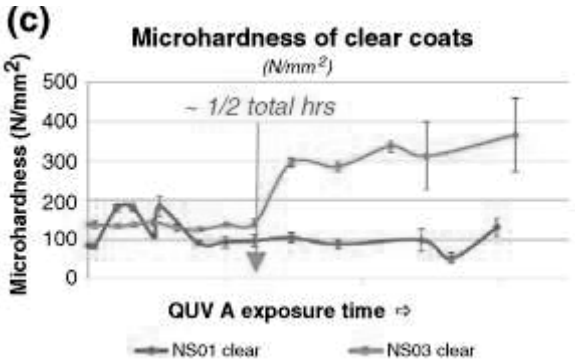

Figure 37: Microhardness upon degradation of petro- and biobased resins (Siyab 2016)

Photoacoustic FTIR measurements and chemical force microscopy mapping with an OH probe were used to further elucidate the degradation mechanisms. As shown in figure 38, infrared measurements showed that the increase of OH and NH stretching vibrations was more

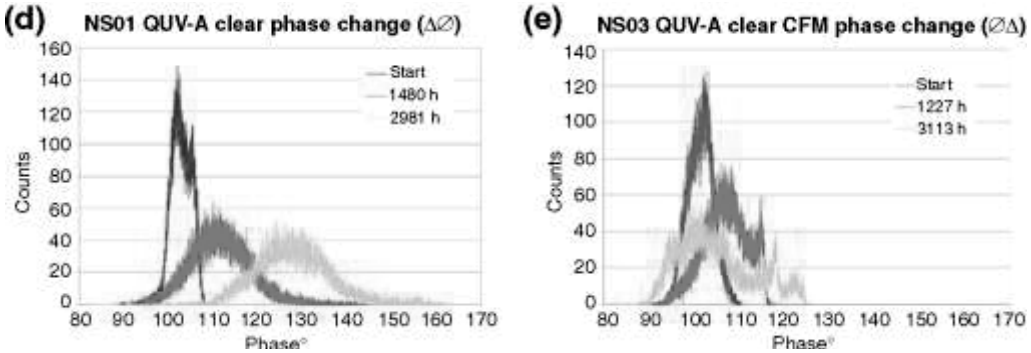

Figure 36: Chemical force microscopy measurements of surface polarity change upon degradation of petro- and biobased resins (Siyab 2016)

pronounced in the petrosourced resin compared to the biosourced resin, indicating a greater amount of photooxidation. However, the absorption of the melamine triazine ring as well as that of the melamine side chains decreased more rapidly for the partially biosourced resin. This indicates that while the partially biosourced monomers cause less susceptibility to photooxidation, the resulting crosslinks with melamine seem to be more sensitive.

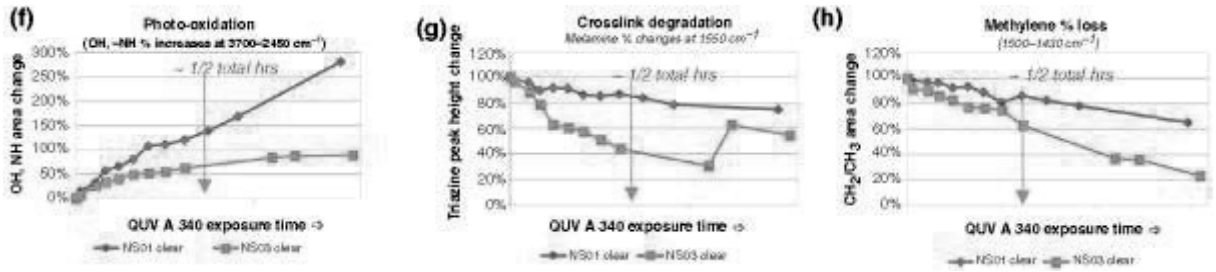

Figure 38: FTIR analysis of petro- and biobased resins upon degradation (Siyab 2016)

Lastly, the surface polarity was investigated using chemical force microscopy equipped with an OH probe. It was found that the surface polarity change, represented by the shift in peaks, as shown in figure 36, is much higher for the petroleum based resin, in accordance with the higher photooxidation observed in FTIR. Furthermore, it was observed that the phase angle measured for the partially biosourced resin underwent more broadening after the weathering process, indicating heterogeneity of the surface.

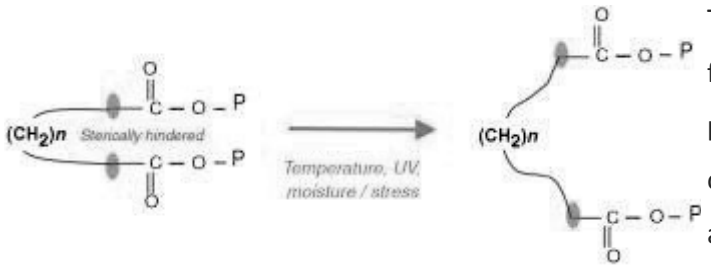

Figure 39: Conformation change of biobased long diacid (Siyab 2016)

The authors explain this behaviour as follows: The better stability of the partially biosourced resin in the first half of the weathering experiment is attributed to the better hydrolysis resistance of the aromatic acid used. The rapid decrease of the stability is explained by the replacement of a short aliphatic diacid in the petroleum based resin with a long aliphatic diacid. The long aliphatic chain is hypothesised to form a pseudo-cyclic conformation as shown in figure 39, increasing hydrophobicity and sterically shielding labile aliphatic hydrogens. This conformation is concluded to break up both in the presence of TiO_2 pigments and after longer exposure, causing a rapid decrease of weatherability.

This is consistent with the observations made with CFM and FTIR since the chain scission after abstraction of hydrogens from a long aliphatic chain will result in new, non-polar alkyl fragments.

While melamine is not a monomer used in resin synthesis, it is present in all above coatings, and a study of its degradation behaviour separated from the other compounds, is therefore of interest. Lukey *et al.* compared the degradation behaviour of two different melamine crosslinkers, hexamethoxymethylmelamine (HMMM) and trimethoxymethylmelamine (TMMM), shown in scheme 91, by trapping the radicals formed during the degradation at low temperature and observing the electron spin resonance (ESR) spectra.[226]

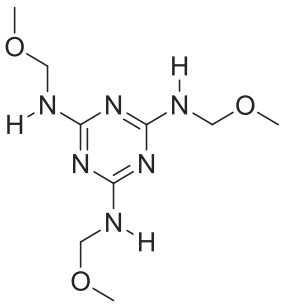

Scheme 91: Trimethoxymethylmelamine (TMMM)

While the radical intensity of TMMM after 30 min of irradiation was 9 times lower than that for HMMM, the radicals formed on HMMM were also observed to be considerably more stable.[XXVII]

Lastly, a study of Zhang *et al.* concerning the influence of different pigments on the coating weatherability illustrates the sometimes contradictory results observed when different methodologies are used.[227] Coatings containing titanium dioxide at different levels together with lead chromate, iron oxide or copper phthalocyanine pigments were studied in weathering chambers and under natural exposure using amongst other techniques[XXVIII] photoacoustic infrared spectroscopy.[XXIX]

In the QUVa weathering chamber, a higher degree of melamine degradation and lower gloss retention was observed for the copper phthalocyanine coating, while the lead chromate coating showed the highest degradation in the naturally weathered samples. This was attributed to the presence of acid rain during the natural weathering. The titanium dioxide was also observed to migrate to the surface, influencing the gloss retention and surface roughness measures in particular.

3.4.5 Literature studies on other thermoset films of interest

The following section describes studies of the weatherability of coatings similar to melamine crosslinked polyester coatings, such as melamine crosslinked acrylic paints, and polyurethane crosslinked polyester films. The degree to which the specific conclusions can be transferred to melamine crosslinked polyester films has to be evaluated in each case, but the methods used and general conclusions drawn can still be instructive for this study.

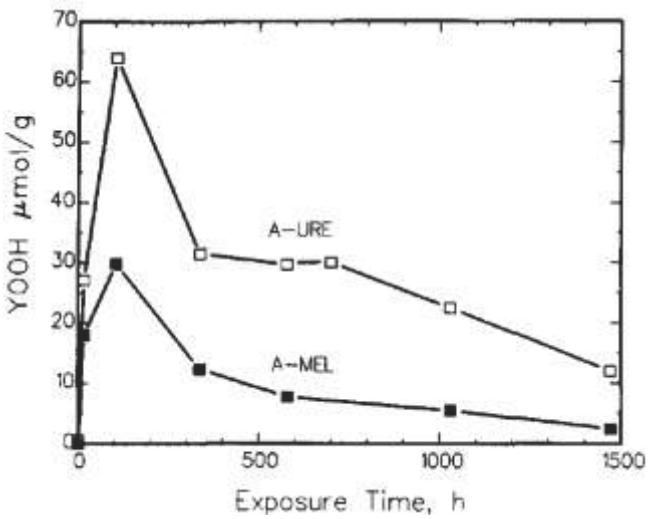

Figure 40: Hydroperoxide concentration upon degradation of acrylic urethane and melamine coatings (Mielewski 1991)

One example are Mielewski *et al.*, who used iodometric titration to determine the concentration of hydroperoxides upon weathering in acrylic melamine and acrylic urethane coatings, and to reveal some of the fundamental changes taking place in coating degradation.[228] They found that for both types of coatings, a steep rise of hydroperoxides was followed by a gradual decrease, as shown in figure 40. The assessment of coating durability thus

[XXVII] See annexe for details on the study and the proposed degradation mechanism
[XXVIII] See annexe for details concerning the different techniques used by Zhang *et al.*
[XXIX] The different techniques for IR measurements will be addressed in chapter 6

performed correlated well with the results of an assessment in which nitroxides were used to monitor the free radical formation.[XXX]

The same authors examined the relationship between ketones formed as a result of photooxidation on the hydroperoxides concentration.[229] After the peak in hydroperoxides concentration was reached, it was found that the ketone to hydroperoxides ratio remained constant for the rest of the ageing process. A formula to describe the relationship, assuming that all termination reactions result in the formation of ketones, was derived. It was furthermore observed that the presence of additional, non-ketonic chromophores can increase the steady state concentration of hydroperoxides.

They furthermore used the increase of carbonyl absorption detected by FTIR to estimate degradation and in particular to examine the efficacy and working mechanisms of hindered amine light stabilisers.[230-232]

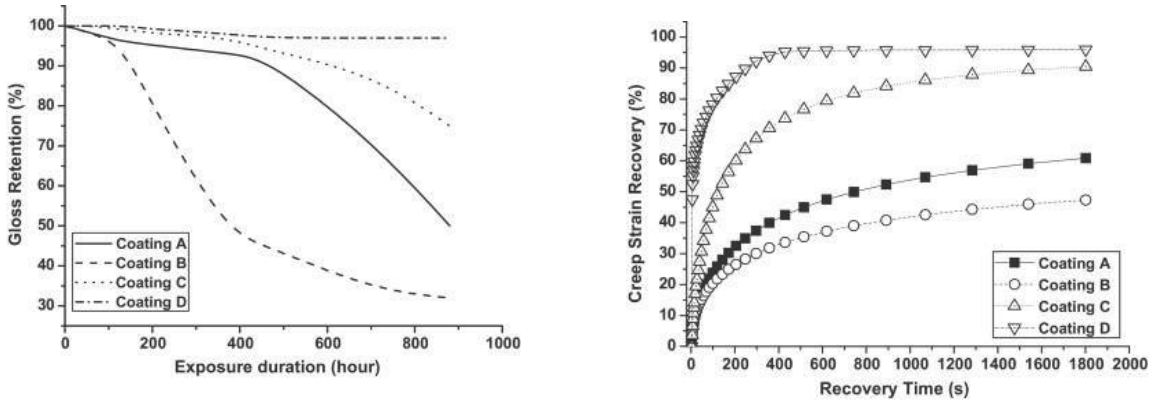

Figure 41: Correlation of gloss retention and creep recovery (Mitra 2014)

The changes in crosslinking density have been the interest of many publications. It was studied for example by Mitra *et al.*, who also observed a correlation between the creep recovery and gloss retention performance.[233] As shown in figure 41 above, both techniques classed the coatings examined in the order D>C>A>B.[XXXI]

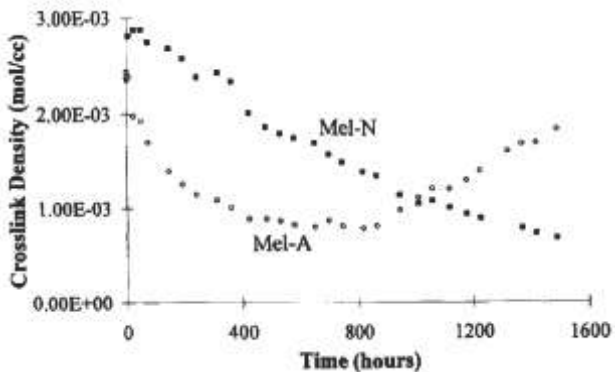

Figure 42: Crosslinking density change upon degradation (Nichols 1997)

Dynamic mechanical analysis, as well as chemical stress relaxation, was also used by Nichols *et al.* to study the crosslinking density upon degradation of two melamine crosslinked acrylate films synthesised with different initiators.[234] Free films of both were strained either continuously or intermittently and the load needed to maintain a fixed

[XXX] See annexe for a description of the nitroxide monitoring technique used
[XXXI] See annexe for details on the aim of the study and the nature of the coatings used

extension was measured over time, either in the dark or under fluorescent light. The two films showed different behaviour upon ageing: For one, the crosslink density briefly increased followed by a constant decrease, while for the other, the crosslink density decreased to a minimum followed by an increase, as shown in figure 42. The T_g of both films continually increased after weathering. These phenomena were attributed by the authors to the competition between chain scission and crosslinking, which govern both the crosslinking density and the T_g, and the degradation of chain ends and side chains, which influence the T_g only.

Chemical stress relaxation measurements and DMA measurements were in good agreement. Furthermore, the degradation was found to be substantially accelerated by the UV radiation, but not influenced by stress applied to the material.

Similarly, Richaud *et al.* examined the hydrolysis of a polyester resin synthesised from adipic acid, ethylene glycol and diethylene glycol crosslinked with benzene triisocynate.[235] The hydrolysis rate was followed by measurement of the uniaxial tension, from which the crosslinking density could be deduced using the elastic modulus. A decrease in crosslinking density was observed each time after exposure to different levels of relative humidity, and an equation was proposed to model the reaction.

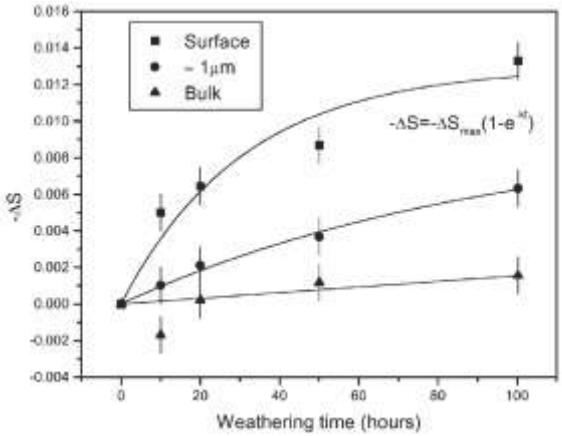

Figure 43: Free volume change upon weathering at different depths (Mallon 2002)

A different method related to the crosslinking density was employed by Mallon *et al.*, who used slow positron beam technique to detect the change in free volume and therefore the degradation in three different coatings exposed to natural and UVb weathering.[236] A polyurethane paint was compared with an epoxy and an acrylic paint. A loss of free volume was observed for each of the coatings with increasing weathering time. As shown for the polyurethane sample in figure 43, the loss was most pronounced on the surface, and least visible in the bulk. Furthermore, the difference between weathering rate after exposure to UVb light and after exposure to natural conditions was more pronounced in the bulk than in the surface of the coating.

An interesting result concerning the effect of hindered amine light stabilisers (HALS) was found by Nichols *et al.* upon the study of the same films described before.[237] They observed that the degradation was slowed down considerably by the HALS, preventing the formation of crosslinks and therefore preventing an overall increase in crosslink density. The retardation of photooxidation after the addition of HALS was also confirmed with FTIR measurements.

In order to improve the correlation between indirect and direct assessments of degradation as well as between different exposure sites and accelerated weathering, Zhang *et al.* proposed to use a peak fitting method to analyse the IR spectra obtained.[238]

The same ranking for three different crosslinkers examined[XXXII] was obtained using the peak fitting method for the two different natural exposures. Contrarily, using only the analysis of the hydroxy peak, the opposite ranking was obtained from one exposure site to the other. Neither method resulted in a good correlation between the accelerated weathering and the natural exposure, and both methods showed differences in the absolute degradation between the two natural exposure sites. Remarkably, one of the crosslinkers showed more degradation when left unexposed than when exposed after the peak fitting analysis.

Efforts have also been made to separate the effects caused by different degradation pathways. For this purpose, Larché *et al.* investigated the UV photolytic degradation of an acrylic melamine clearcoat in the presence of oxygen without added humidity by FTIR spectroscopy, GC-MS, µ-hardness measurements and dynamic mechanical analysis.[239] A good correlation between the increase in µ-hardness and the decrease in infrared absorption of the melamine either groups, shown as conversion in figure 44, was observed.

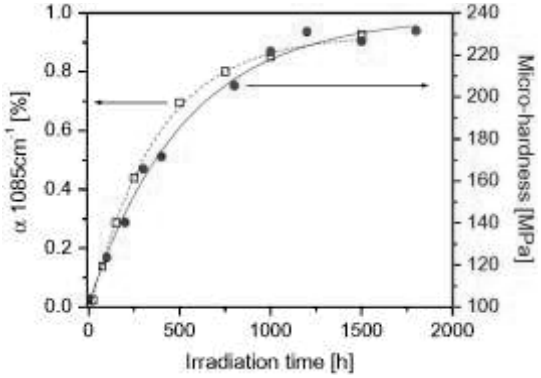

Figure 44: Microhardness increase upon degradation (Larché 2012)

Furthermore, an increase in T_g determined from the peak of tan δ and of the crosslinking density determined from DMA was also observed. The T_g measured in DSC also increased, but the T_g's measured from the two methods were not the same.[XXXIII]

In GC-MS analysis of volatile byproducts formed, butanol and butyl formate byproducts were observed. This is consistent with β-scission mechanisms on either side of alkoxy radicals since the melamine used as a crosslinker was butyl-oxylated. Lastly, the authors observed a correlation between the degradation observed in different depths of the film and the light penetration predicted by the Beer-Lambert law. From this, it was concluded that the degradation was not dependent on oxygen penetration of the film.

Another aspect, the hydrolysis in the absence of UV light, was studied by Nguyen *et al.* and Lee *et al.* from the same group.

[XXXII] See annexe for a description of the coatings and IR regions examined as well as for the exposure results
[XXXIII] See annexe for a graph of the glass transition temperatures measured by DMA and DSC

The water transport within coatings during hydrolysis is very complex due to the heterogeneous nature of the films, the variety of possible interactions and the slow kinetics that need to be observed. Its quantification was attempted by Lee *et al.* for a melamine crosslinked acrylic film in the absence of UV light.[240] The degradation was observed to be localised and autocatalytic. This was attributed to the presence of hydrophilic regions with low crosslinking densities and chain ends, containing low molecular weight products, and hydrophobic regions with high crosslinking densities, containing high molecular weight products. Water is thought to be transported only in the former regions. Interactions of water molecules with the film are complex, and very strong hydrogen bonding can be formed in the presence of O-H and N-H groups. This is further complicated by the fact that hydrolysis causes the formation of new, polar groups, which change the profile of each region.

In order to quantify the hydrolysis, it was assumed that one water molecule was consumed in each hydrolysis reaction. The reaction products were found to be primarily primary amines and formaldehyde formed from the hydrolysis of melamine side chains and crosslinks. Secondary oxidation of formaldehyde to carboxylic acids was also observed. The appearance of primary amines as well as the disappearance of the melamine ether groups was followed by FTIR spectroscopy.

Both the rate and the extent of the hydrolysis were found to increase with increasing relative humidity, and the rate was found to decrease over time. The authors derived an equation describing the degradation over time.

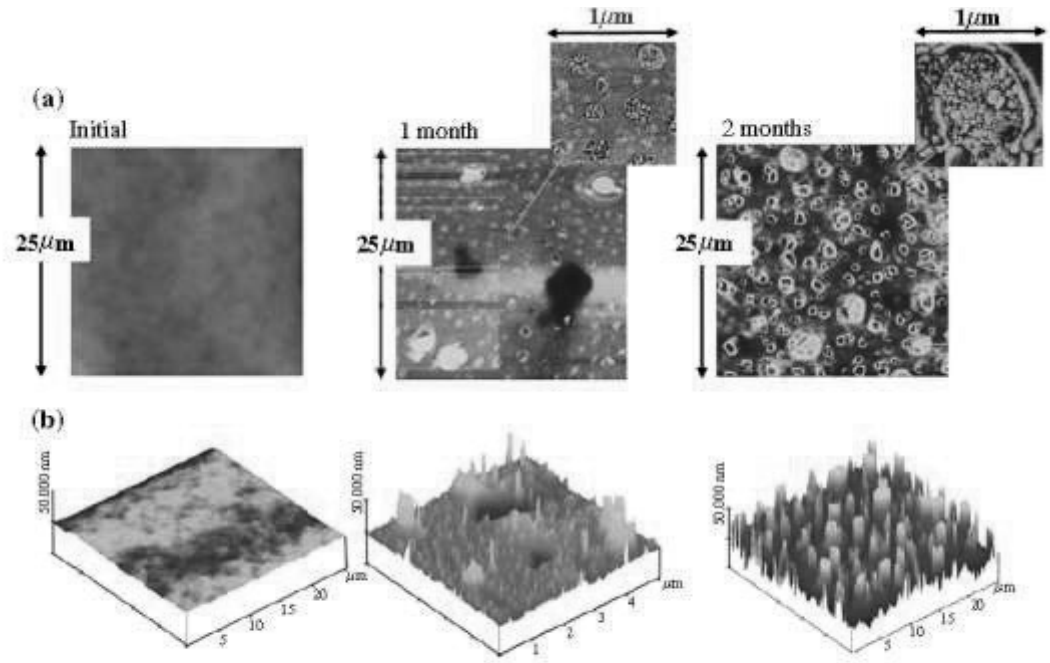

Fig. 3: 25 μm × 25 μm 2-D (a) and 3-D (b) AFM topographic images of the amine-cured epoxy before and after exposure to the outdoors in Gaithersburg, MD, for 1 and 2 months, started from the middle of July. Insets are high magnifications of the phase images

Figure 45: Pit formation upon degradation of amine cured epoxy coatings (Nguyen 2013)

The conclusions are mirrored in a publication by Nguyen *et al.* on the same topic.[241] They also concluded that hydrolysis increases with increasing humidity, and that the melamine methoxy groups as well as the crosslinks on monosubstituted amino chains are the primary target of attack, forming primary amines and formic acid. Disubstituted amino chains are found to hydrolyse more slowly. Furthermore, the hydrolysis is found to decrease in rate over time, and to proceed in an inhomogeneous, pit forming manner, as detected by AFM analysis.

A similarly heterogeneous degradation was observed by the same authors in a study of degradation in the presence of UV light for an acrylic melamine coating but also an amine cured epoxy and an acrylic urethane coating.[242] An example of the pit formation in the amine cured epoxy coating after one and two months outdoor exposure is illustrated in figure 45 above.

The authors also attributed the heterogeneity to the presence of hydrophilic domains within the network structure which contain unreacted chain ends, low molecular weight products and chromophores, as shown in figure 46 on the right.

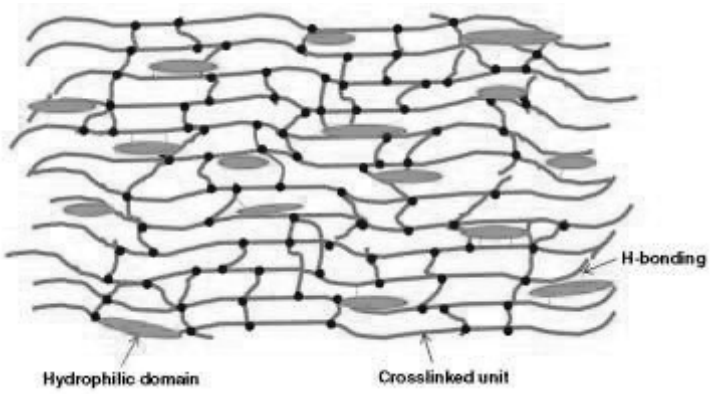

Figure 46: Heterogeneous distribution of hydrophilic and hydrophobic domaines in the polymer network (Nguyen 2013)

Lastly, the effect of different types of aromatics has been studied by several groups. More specifically, Osterhold *et al.* examined the influence of aromatic content in a melamine formaldehyde crosslinked polyol on the weatherability by studying surface tension, FTIR, gloss retention, surface topography, differential scanning calorimetry and dynamic mechanical analysis.[243] Three resins, formulated to clear coats without any stabilisers, containing no, medium and high aromatic content in the polyol, were investigated. All coatings showed a growth in surface tension, which was attributed to chain scission and confirmed by a decrease of ester groups and an increase of carbonyl groups in the FTIR spectrum.

The glass transition temperature increased 1,5 times more in the first 150 h of weathering for the two coatings containing aromatic monomers. The crosslinking density increased to a maximum in the first 100 h of weathering followed by a decrease back to the original level, but was not affected by the presence of aromatic units in the chains.[XXXIV]

[XXXIV] For details of the conditions used by Osterhold *et al.*, see annexe.

Maetens *et al.* studied the hydrolysis behaviour and the difference between terephthalic acid and isophthalic acid[XXXV] in a triglycidyl isocyanurate crosslinked polyester powder coating.[244] They confirmed the observation by Malanowski *et al.* that terephthalic acid is more susceptible to degradation than isophthalic acid, and observed that the hydrolysis caused leaching of low molecular weight compounds and the hydrolysis of anhydride groups in the coating.[208]

The authors furthermore concluded that the degradation process is unlikely to be of Norrish type I or Norrish type II nature because of the absence of β – hydrogens, and the fact that short wavelengths that could be absorbed by the films were not present in the weathering experiment. Instead, the degradation was attributed to the presence of a photoinitiatior radical R. The higher resistance to degradation of the isophthalic acid film was explained by different interactions with R, though R was not identified. The greater liability of the crosslinks in the terephthalic acid containing film towards β-hydrogen abstraction was offered as an additional explanation. Since oxygen and water permeability are similar for both films, they were excluded as the origin of the degradation.

3.5 How to design a more stable resin?

The following section will give an overview of the knowledge that can be drawn from the literature presented above, divided into three parts. Firstly, the influence of specific monomer and chain sections will be addressed. Secondly, the conclusions about which mechanisms take place concretely in melamine crosslinked polyester resins will be summarized. Thirdly, the insights about which methods work well for the prediction of weatherability and which issues can be encountered when assessing it will be presented.

3.5.1 Which monomers should be used in a more stable resin?

The melamine side chain is confirmed by several authors, including Zhang *et al.* and Batista *et al.* as the most labile part and therefore the origin of degradation.[216, 219] Larché *et al.* also observed products consistent with a β-scission mechanism adjacent to melamine side chain ether groups.[239] Additionally, Gamage *et al.* showed the influence of the degree of cure to be an essential factor for the degradation and both Lukey *et al.* and Nguyen *et al.* observed differences depending on the degree of melamine methylation.[214, 226, 241] The former observed that the cyclic mechanism of radical propagation was most effectively promoted in disubstitued cycles, while the latter found that steric hindrance in disubstituted cylces could contribute to the inhibition of hydrolytic degradation.

Concerning aromatic moieties in the film, Osterhold *et al.* found that the increase in T_g upon ageing was more pronounced for the higher the aromatic content.[243] Siyab *et al.* observed that aromatic

[XXXV] For details on the coating formulation and conditions used, see annexe.

monomers could shield the chain from hydrolytic attack, but also that overlap of the absorption of the aromatic ring with radiation could cause increased photolytic degradation.[17] In comparing several films with different amounts of aromatic and cycloaliphatic monomers, Batista *et al.* found the film containing only isophthalic acid to be the most stable.[219] This is mirrored by studies of Malanowski *et al.* and Maetens, who observed that isophthalic acid was significantly more stable than terephthalic acid.[208, 244]

Concerning cycloaliphatic monomers, Siyab *et al.* observed a significantly lower stability of a cycloaliphatic biosourced monomer compared to aromatic monomers.[17] They also found that long aliphatic chains could become vulnerable to scission after an induction period due to the formation and breaking up of aliphatic pseudo cycles.

Concerning different diols, Sullivan *et al.* concluded that there were only small differences in performance between the three diols neopentyl glycol, 1,2-propanediol and 2-methyl-1,3-propanediol.[220] Narayan *et al.* found that 1,3-propanediol was more susceptible to degradation than neopentyl glycol and cyclohexanedimethanol in moisture enhanced photolytic degradation.[221] The same ranking could however not be established in studies of thermal degradation.[222]

Nagai *et al.* observed that the ether part of a polyester-polyether was more susceptible to the degradation than the ester part.[205]

Lastly, the introduction of biosourced moieties such as glycerol, sugar hexitols and pentitols, isosorbide and isomannide or cinnamic acid has been found to increase polyester susceptibility to hydrolysis by Celli *et al.*, Zamora *et al.*, Okada *et al.* and Jin *et al.* respectively.[64, 144, 211, 212] While the ester link adjacent to the biosourced monomers was confirmed as the point of hydrolytic attack, and the increased hydrophilicity induced by oxygen rich monomers is certainly a factor that can induce susceptibility to degradation, it should be kept in mind that these studies were conducted on non-crosslinked thermoplastic films, and that the difference observed may not be as pronounced when the milieu is changed to a thermosetting, less permeable matrix.

3.5.2 Prevalent degradation mechanisms

In a thermoplastic coating, photolysis was observed by Nagai *et al.* to be the dominant mechanism causing degradation vis-à-vis thermal and hydrolytic pathways.[205] As observed by Zhang *et al.*, the situation is a little more complicated in thermosetting polyester melamine films, where photolysis dominates in the beginning, until sufficient water diffusion could take place and the degradation is accelerated.[216] This synergistic effect was also observed for example by Batista *et al.* and Nguyen *et al.* in the autocatalytic formation of heterogeneous surfaces.[219, 242]

Concerning the mechanism of photolytic degradation, both Mielewski *et al.* and Gamage *et al.* have observed a rise in peroxide species in the coating, the latter directly using ESR.[214, 228] Lukey also observed a dependence of degradation rate on the radical initiation rate.[213] This is also coherent with a dependence on light absorption and a rate increase with the presence of chromophores observed by Larché *et al.* and Gerlock *et al.* respectively.[239, 245]

Different propagation mechanisms are proposed by different authors. Carroccio *et al.* and Malanowski *et al.* both observed reaction products from a Norrish type I mechanism.[203, 208] Carroccio *et al.* also observed α-hydrogen abstraction products, but concluded that if β-hydrogen abstractions, or the Norrish type II mechanism, are taking place, they are not prominent. The same conclusion was reached by Sullivan *et al.*, whose computational study shows α-hydrogens to be considerably more labile than β-hydrogens.[220] Shigemoto *et al.* elucidated the β-hydrogen abstraction with a computational study, and found that it was not catalysed by metals.[204] On the other hand, Maetens concluded that neither Norrish type I nor Norrish type II mechanisms are responsible for the degradation, but an unidentified photoinitiator R.[244]

Where the balance between crosslinking reactions and chain scission reactions is concerned, different interpretations exists. While Nichols *et al.* reported an increase in T_g for all films tested, the crosslinking densities did not follow a linear behaviour. One film showed a decrease of crosslinking density, while the other showed a decrease followed by an increase. Commereuc *et al.* reported that the nature of the dominant mechanism depends on the presence of aliphatic or aromatic groups, and Nichols *et al.* reported that the crosslinking type mechanisms is interrupted by the presence of hindered amine light stabilisers.[209, 237]

On the other hand, Mallon *et al.* found that the decrease of free volume was more prominent at the surface compared to the bulk.[236] Malanowski *et al.* also reported that the dominance of either mechanism depended on the concentration of radicals, and thus on the amount of UV light penetrating, because the crosslinking mechanism is second order dependent on radical concentration while the chain scission mechanism is only first order dependent.[207] Finally, Richaud *et al.* reported a decrease of crosslinking density following hydrolysis.[235]

Concerning the autoacceleration of hydrolysis through a change in pH, neither Zamora *et al.* nor Jin *et al.* observed an acceleration of the hydrolysis rate when changing the pH from 7 to 4 or from 10 to 7 respectively.[64, 144]

Oxygen was also found by Gamage *et al.* to inhibit the photolysis rate by scavenging radicals.[214]

Finally, Biggs *et al.* showed that the degradation proceeds via the erosion of polymer layers followed by the erosion of particles and the flattening of the thus created holes.[217]

3.5.3 Methods and transferability of weatherability studies

While some methods employed for the assessment of weatherability described above were very successful in elucidating the degradation pathways and providing a means to time efficient predictions, others demonstrate that caution is needed when interpreting the results of such studies.

Examples of methods which worked well are the chemiluminescence study by Lukey, which permitted to distinguish between radical initiation and termination rates and chromophore presence, Zhang *et al.*'s use of FTIR to distinguish degradation of different functional groups at different depths of the coating and the use of CFM by Siyab *et al.* to distinguish polar and apolar degradation products.[17, 213, 216] Good correlation with gloss retention measurements was also obtained by Mitra *et al.* using the creep recovery, and by Siyab *et al.* using μ-hardness measurements and AFM surface roughness measurements.[233] Larché *et al.* also obtained a correlation between the μ-hardness results and the FTIR measurements.[239]

Contrarily, however, for Batista *et al.*, the results of gloss retention, μ-hardness measurements and FTIR measurements did not give the same ranking.[219] The study of Zhang *et al.* rated the influence of lead chromate and titanium dioxide completely differently depending on whether the tests were performed outdoors or in accelerated weathering, possibly due to the presence of acid rain in outdoors exposure.[227] Siyab *et al.* found that the increase in OH/NH group in the infrared increased significantly more for a petrosourced coating than for a biosourced coating, contrarily to the gloss retention, which correlated only to the decrease in melamine. Most obviously, the gloss retention test for three different diols gave the opposite ranking when it was run by Sullivan *et al.* twice, and no two weathering methods agreed on the ranking of those diols during further tests.[220]

While often the disparity of the results can be explained by the interaction of different conditions used for the accelerated weathering, as proven by Biggs *et al.* who found completely different results for the surface roughness depending on the light source, it is clear that both false positive and false negative evaluations can easily occur.[217] Fortunately, many different methods are available which can evaluate different aspects of a film such as the roughness of the surface, the rigidity and density of the crosslinked network as well as the presence of radicals and different functional groups which can help to confirm results or to indicate that further studies are needed before conclusions are drawn.

4 Incorporation of vanillin into a polyester resin

Vanillin is one of the only aromatic molecules widely commercially available from renewable resources, and while it has shown great promise as a monomer in various different types of polymers, it has to our best knowledge to this point not been used for the synthesis of polyester resins for coating applications. Therefore, we decided to study different routes to its incorporation into polyester products, both to explore its potential for exterior coil coating resins, and to expand the vanillin platforms to new applications, as illustrated in scheme 92.

Since the aim of the project is the transition from petroleum based to renewably sourced monomers, it is important to minimise the effort and cost involved and to make as little changes as possible to the currently used synthesis and processing methods. Because not only the use of renewable resources but also the creation of an overall more environmentally benign product is our motivation, green chemistry principles were used as guidance for the selection of reaction methods.

In this spirit, the use of acyl chlorides and the etherification using alkyl halides were avoided due to the unnecessary production of halogenated side products, and the associated need for an additional purification step. The introduction of an additional ether bond, which would also be possible for example using ethylene carbonate or ethylene oxide, as demonstrated by Erä *et al.* and Kreye *et al.*, was avoided due to the associated vulnerability to degradation reactions.[169, 173]

Therefore, a new method to solve the two challenges of incorporating vanillin into a polyester structure, namely the transformation of the aldehyde group to something esterifiable and the poor reactivity of the phenol group, had to be developed. In order to address the first, the works of Mialon *et al.* on the polymerisation of acetyldihydroferulic acid were used as an inspiration.[1] The authors used the Perkin reaction to transform vanillin into acetylferulic acid, achieving both the transformation of the aldehyde to a carboxylic acid and the activation of the unreactive phenol group by acetylation.

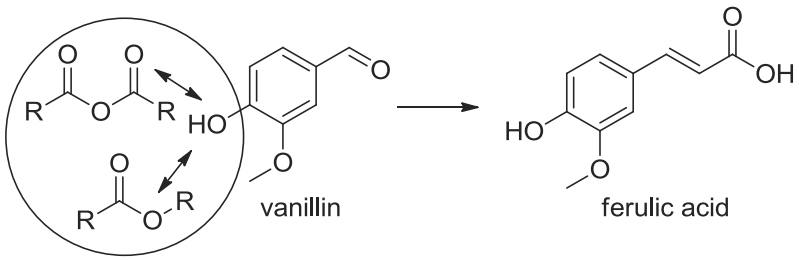

Scheme 92: Study of the reactivity and transformation of vanillin

While the yield of the Perkin reaction was problematically low at 64%, the reaction conditions at 170 °C are compatible with polyesterification equipment currently used, no metal catalysts are used and the byproduct acetic acid is relatively benign and would evaporate together with water and solvent under polyesterification conditions.[161]

One of the most attractive aspects of this strategy is that ferulic acid, albeit without the activated phenyl group, is present in plant cell walls, and can be directly obtained from renewable resources. It could be imagined as a substitute for vanillin derived acetylferulic acid prior to the optimisation and adaptation of the Perkin reaction to currently used polyesterification equipment, and enable the timely realisation of polyesters developed based on this strategy. While some attempts to increase the yield and atom efficiency of the Perkin reaction are detailed here, the polyesterification was prioritised for this reason.

Concerning the phenol reactivity, different strategies were explored. After screening a selection of catalyst systems reported in the literature, its reactivity towards a series of suitable anhydrides and methyl esters was also tested. Despite using high temperature and a large excess of the acid reagents, sufficiently high yields were not obtained.

Therefore, it was decided to turn to a method used by several authors including Jin *et al.* to obtain liquid crystalline polymers on the basis of phenolic vanillin derivatives such as *p*-hydroxy coumaric acid and ferulic acid.[144] As detailed in the introduction (Chapter 2, section 2.3.3.4.2), acetic anhydride was successfully employed by the authors as a condensation agent, yielding homo- and copolyesters of molecular weights ranging from 3000 g/mol to 91 000 g/mol. This method was also selected due to its compatibility with the Perkin reaction, which uses an excess of acetic anhydride, so that a one pot polycondensation without purification step is conceivable.

Lastly, in order to elucidate the mechanism and to explore the potential changes for the polyesterification, the effect of the different conditions used such as the nitrogen atmosphere, the order of addition of the monomers and the reaction temperature was tested.

4.1 Evaluation of phenol reactivity

In order to find suitable polyesterification reaction conditions for vanillin or vanillin derivatives, the reactivity of the phenol group was first explored. The default catalyst selected for the study was butylstannoic acid (Fascat 4100). It was chosen despite its incompatibility with green chemistry principles due to the toxicity of tin because it is a highly effective catalyst, used for example by Arkema in the synthesis of polyester resins at concentrations as low as 0,01%. After a model reaction was established, different catalysts reported in the literature as well as anhydride and methyl ester substrates were evaluated.

4.1.1 Establishment of a model reaction

The reactivity of the vanillin phenol group was evaluated in a model reaction, shown in scheme 95, instead of a polymerisation reaction for two reasons: Firstly, due to the polydispersity and size of the

reaction products, the yield in polyesterification reaction cannot be evaluated as precisely as in reactions resulting in low molecular weight products. Secondly, purification is not part of resin synthesis; therefore, the yield determined after purification of a polyester would not necessarily be representative of the target result.

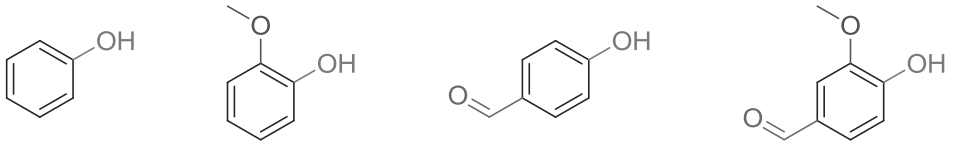

m.p.: 41 °C b.p.: 182 °C	m.p.: 28 °C b.p.: 204 °C	m.p.: 112 °C b.p.: 310 °C	m.p.: 81 °C b.p.: 285 °C
phenol	guaiacol	*p*-hydroxy benzaldehyde	vanillin

Scheme 93: Candidates for phenol model compounds

Several compounds were evaluated for a model reaction. Succinic acid was first chosen as a substrate due to its availability from renewable resources. Its reactivity towards phenol, guaiacol, *p*-hydroxy benzaldehyde and vanillin, shown in scheme 93, was tested in toluene solvent at 50 °C and 80 °C for up to 24 h. As none of the reactions yielded any product, the temperature was raised to 150 °C and succinic acid was replaced with hexanoic acid, shown in scheme 94. Its low melting and high boiling point permitted the reaction to be solvent free, and its aliphatic chain simulates the steric bulk, if not the electronic environment of succinic acid.

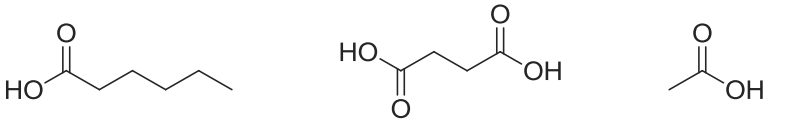

m.p.: -3 °C b.p.: 206 °C	m.p.: 118 °C b.p.: 235 °C	m.p.: 16 °C b.p.: 118 °C
hexanoic acid	succinic acid	acetic acid

Scheme 94: Candidates for acid model compounds

Of the different phenolic compounds, guaiacol was chosen. The presence of the *ortho* methoxy group permits to simulate the steric environment of the phenol in vanillin, while the absence of the aldehyde avoids side reactions which would not occur in the final polyesterification due to its transformation into an acid group. Lastly, its low boiling point facilitates the handling and homogenisation of the reaction milieu.

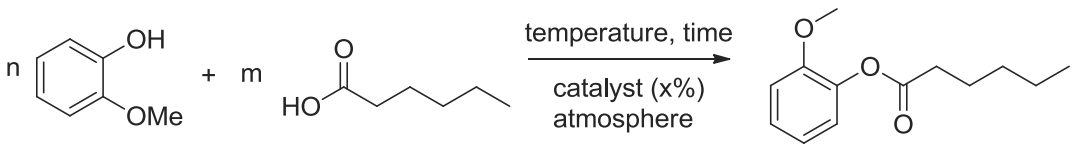

Scheme 95: Model reaction for phenol polyesterification

4.1.2 Tests of different catalyst systems for the esterification of guaiacol

A selection of metal catalysts reported in the literature for phenol acetylation reactions, shown in scheme 96, was tested in the model reaction. $Mn(OAc)_3.2H_2O$, which was used by Gowda *et al.* at 0,4% at 120 °C as well as $BiCl_3$ and $Bi(OTf)_3$, which were used by Mohammadpoor-Baltork *et al.* at 20% and 5% and 80 °C and 60 °C respectively were tested at 5% concentration at 150 °C.[141, 142] In each case, the yield reported in the literature was above 95%. Additionally, butylstannoic acid which is commercially sold as Fascat 4100, as well as *p*-toluene sulfonic acid (*p*TSA) and dimethylaminopyridine (DMAP), organocatalysts for esterification with acids and anhydrides, were used in those conditions. $Ru(acac)_3$, which was used by Varala *et al.*, was not tested due to its price.[143]

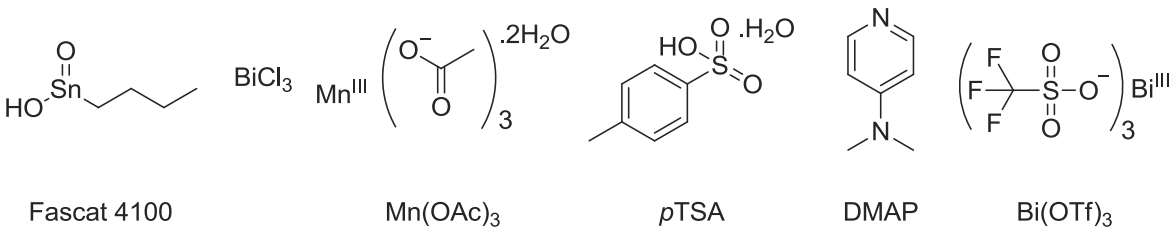

Scheme 96: Catalysts tested for phenol esterification

4.1.2.1 Reactivity towards hexanoic acid

Despite leaving the reaction for up to 24 h at temperatures up to 150 °C, only moderate yields were obtained with all catalysts tested, suggesting that the methoxyphenol is much less reactive than the phenol used in the literature. No product was observed when butylstannoic acid, $Mn(OAc)_3$ or $BiCl_3$ were used, even though they were added in up to 5% concentration with respect to the substrates. Increasing the amount of hexanoic acid to an excess of 10 equivalents as it was done with acetic acid in the literature also did not improve the result in any of the reactions, as shown in table 26.

Table 26: Conditions and results of the esterification of guaiacol using hexanoic acid

n	m	time	temp.	catalyst	x	atm	yield
mmol	equiv.	h	°C		mol %		%
10 - 12	1 - 3	2 - 8	120 - 150	Fascat 4100	0,5 - 5	air	no reaction
2 - 12	1	2 - 23	120 - 150	$Mn(OAc)_3$	0,5 - 5	air/Ar	no reaction
0,2 - 2	1 - 10	6,5 - 24	150	$BiCl_3$	5	air/Ar	no reaction
2 - 20	1 - 1,1	3 - 6,5	140 - 150	DMAP	5	air	no reaction
2	10	24	150	DMAP	5	Ar	no reaction
2	1	24	150	DMAP	5	Ar	15
2	1	6,5	150	$Bi(OTf)_3$	5	air	37
0,2	10	24	150	$Bi(OTf)_3$	5	air	30
2	1	6,5	150	*p*TSA	5	air	43

The most promising catalysts were *p*TSA and $Bi(OTf)_3$, which yielded the ester product in 43% and 37% respectively. The reaction catalysed by DMAP also resulted in a low yield of 15%, but only after 24 h. Using an inert argon atmosphere equally did not seem to help the reaction progress, suggesting that side reactions or degradations were not the cause of the lack of products.

4.1.2.2 Reactivity towards acetic acid

In order to determine whether the hydrophobicity or the steric bulk of the aliphatic chain on hexanoic acid is responsible for the lack of reactivity, the different catalysts were tested again using acetic acid as a substrate as shown in scheme 97.

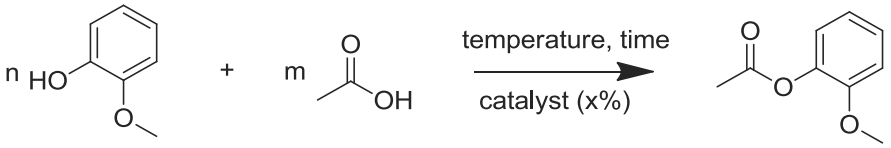

Scheme 97: Reaction of guaiacol with acetic acid

The conditions reported in the literature for each catalyst were also more closely observed in the second series of experiments. For example, $Mn(OAc)_3$ was used with an 175 equivalents excess of acetic acid, and $BiCl_3$ was used at a 20% concentration. Nevertheless, the results obtained were not better than with hexanoic acid as shown in table 27. No product was obtained for $Bi(OTf)_3$ and DMAP catalysts, and the yield of the reaction with *p*TSA decreased from 43% with hexanoic acid to 7% with acetic acid.

Table 27: Conditions and results of guaiacol esterification with acetic acid

n	m	time	temperature	catalyst	x	yield
mmol	**equiv.**	**h**	**°C**		**mol%**	**%**
2	2 - 10	24	100	Fascat 4100	5	no reaction
10 - 20	1,1 - 175	2 - 3	120 - 140	$Mn(OAc)_3$	4 - 5	no reaction
10	175	4	135	$Mn(OAc)_3$	4	31
1	53	1,3	120	$BiCl_3$	20	no reaction
20	1,1	3	140	$Bi(OTf)_3$	5	no reaction
20	1,1	3	140	DMAP	5	no reaction
20	1,1	3	140	*p*TSA	5	7

The decrease in yield can partially be explained by the high temperatures which were up to 20 °C above the boiling point of acetic acid. Despite the fact that a Vigreux column was used in the reaction, it is possible that some substrate was lost.

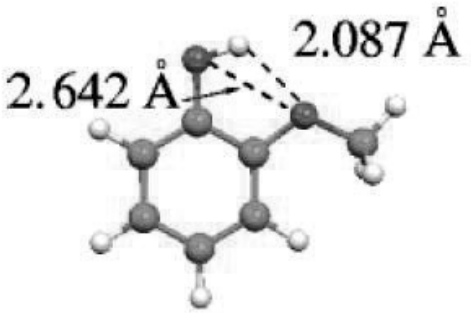

Figure 47: Intramolecular H-bond in guaiacol (Estacio 2004)

Only $Mn(OAc)_3$ showed a greater activity towards acetic acid with a yield of 31% at 135 °C, possibly due to the presence of acetate ligands or the large excess used. The large discrepancy observed between these results and the yields of phenol esterification from the literature, which were between 78% and 99% for shorter times and lower temperatures, must be due to the presence of the *ortho* methoxy group.[141-143]

An *ortho* methoxy group should by its nature be able to activate the phenol group through resonance. Furthermore, the electron density on the oxygen should be increased by the intramolecular hydrogen bond between the methoxy oxygen and the phenol hydrogen, which has an enthalpy of between 2,1 and 19,1 kJ/mol reported by Estacio *et al.* depending on the computational calculation method, shown in figure 47.[246] The steric bulk of the methoxy group is also generally oriented away from the phenol, as can be seen for example in the crystal structure of vanillin in figure 48, which was published by Velavan *et al.* and doesn't contain the above mentioned hydrogen bond.[247, 248]

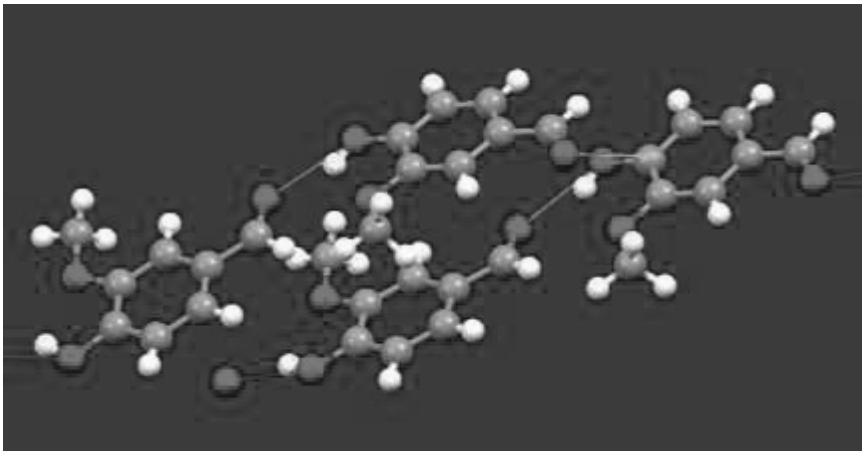

Figure 48: Vanillin I crystal structure with H-bonds (Velavan 1995, Cambridge structural database)

Nevertheless, no direct esterification of guaiacol with an unactivated substrate is reported to the best of our knowledge. This and the low yields of the reactions that otherwise result in 99% yield when phenol is used instead of guaiacol suggest that the presence of an oxygen only 2 Å from the phenol is sufficient to largely prevent the reaction with unactivated carboxylic acids. Therefore, the reaction with anhydrides and transesterification reactions were tested as alternatives.

4.1.3 Esterification of guaiacol with anhydrides

The use of anhydrides in the esterification of phenol derivatives is well established. Furthermore, anhydrides, for example phthalic anhydride, are also often used in polyesterification reactions and in

coil coating resins. Nonanoic anhydride and acetic anhydride were used to test both a bulky and a short chain substrate. As catalysts, DMAP, a well-known catalyst for the esterification of anhydrides as shown in scheme 98, and butylstannoic acid were compared.[249]

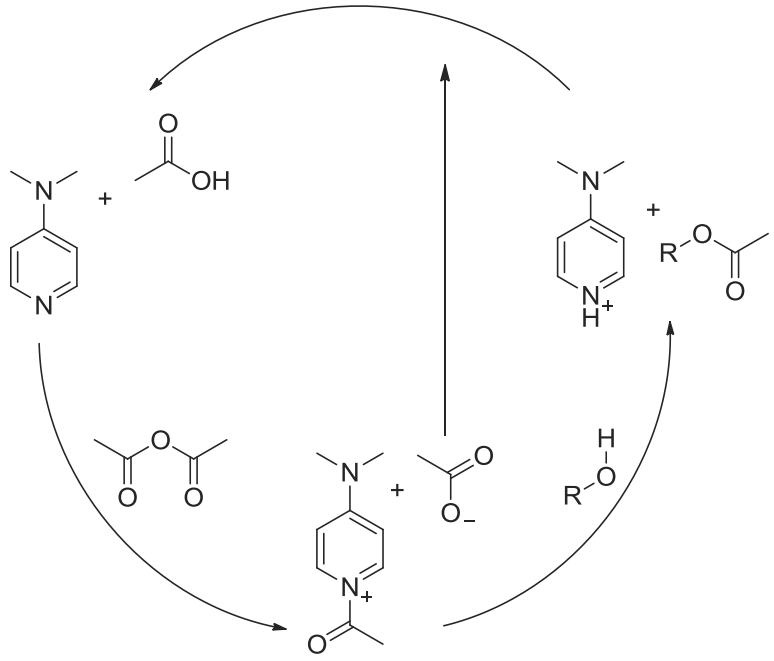

Scheme 98: DMAP catalytic cycle with acetic anhydride (Xu 2005)

4.1.3.1 Nonanoic and acetic anhydride

The esterification yields were markedly higher when anhydrides were used as shown in table 28. While no product was obtained with a butylstannoic acid catalyst and nonanoic anhydride after 5,5 h, 65% guaiacol nonanoate could be recovered when the reaction time was extended to 48 h. Using the DMAP catalyst, 53% and 66% yield could be obtained already after 3 h and 2 h for nonanoic and acetic anhydride respectively. High temperatures are clearly necessary for the reaction, as no product was obtained after 24 h of reaction at 50 °C and 100 °C with either catalyst.

Table 28: Conditions and results of the guaiacol esterifications using anhydrides

anhydride	n	m	time	temp.	catalyst	x	yield
	mmol	equiv.	h	°C		mol%	%
nonanoic	4	0,5	5,5	150	Fascat 4100	5	no reaction
nonanoic	4	0,5	48	150	Fascat 4100	5	65
nonanoic	20	0,55	3	140	DMAP	5	53
acetic	2	0,5	24	100	Fascat 4100	5	no reaction
acetic	10	5,3	2	140	DMAP	2	66
acetic	10	1,1	24	50	DMAP	2	no reaction

4.1.3.2 Citric acid

An alternative to the use of anhydrides is citric acid, a natural polycarboxylic acid widely available from biosources such as fruits and vegetables, and from fermentation. The neighbouring carboxylic acid groups can dehydrate *in situ* to form an anhydride group. This property has been used for example by Noordover *et al.* to accelerate the reaction with the comparatively inert secondary endo-hydroxy group of dianhydrohexitols, as shown in scheme 99.[114]

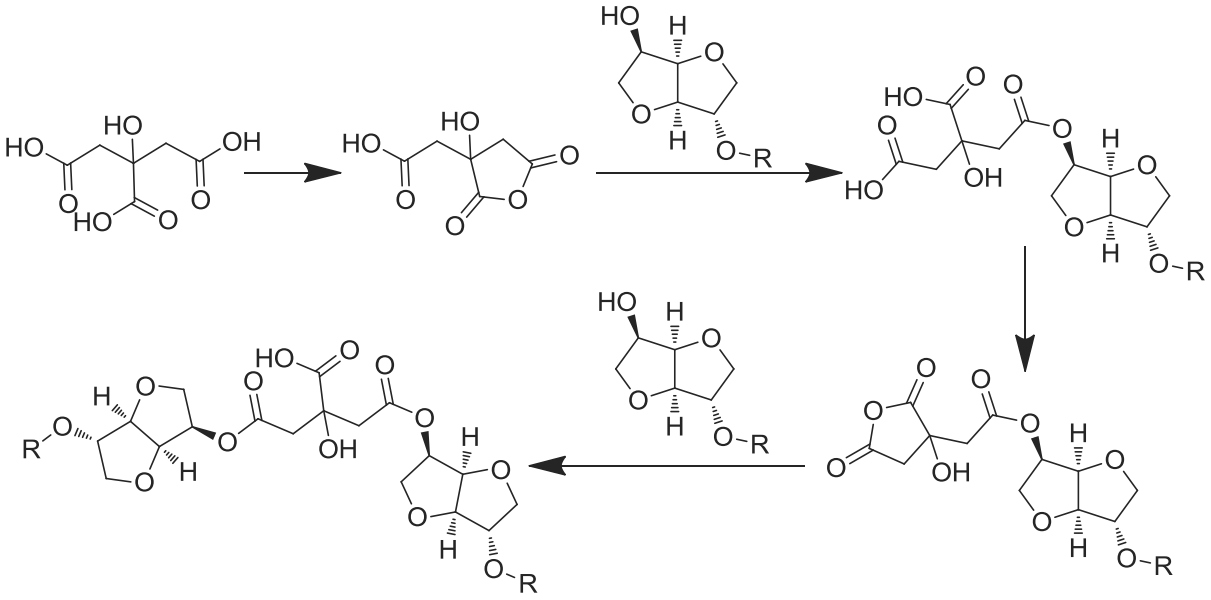

Scheme 99: Carboxylic acid functionalised polyesters from citric acid and dianhydrohexitols via anhydride formation (Noordover 2007)

Noordover *et al.* reported the importance of conducting the reaction between 140 °C and 160 °C, which is around the melting temperature of citric acid at 153 °C, to enable anhydride formation and avoid degradation. Therefore, guaiacol was reacted with citric acid at 160 °C as shown in scheme 100. Both $Ti(OBu)_4$, which was used for the esterification by Noordover *et al.*, and DMAP, as well as both catalysts together, were tested at 4%. However, no esterification product was observed.

This can probably be attributed to the lower reactivity of the phenol compared to the dianhydrohexitols, and the thermal decomposition of citric acid. Barbooti *et al.* studied the thermal decomposition behaviour of citric acid using DSC, and reported the initial decomposition temperature between 165 °C and 168 °C depending on the heating rate used and the particle size of the powder.[250]

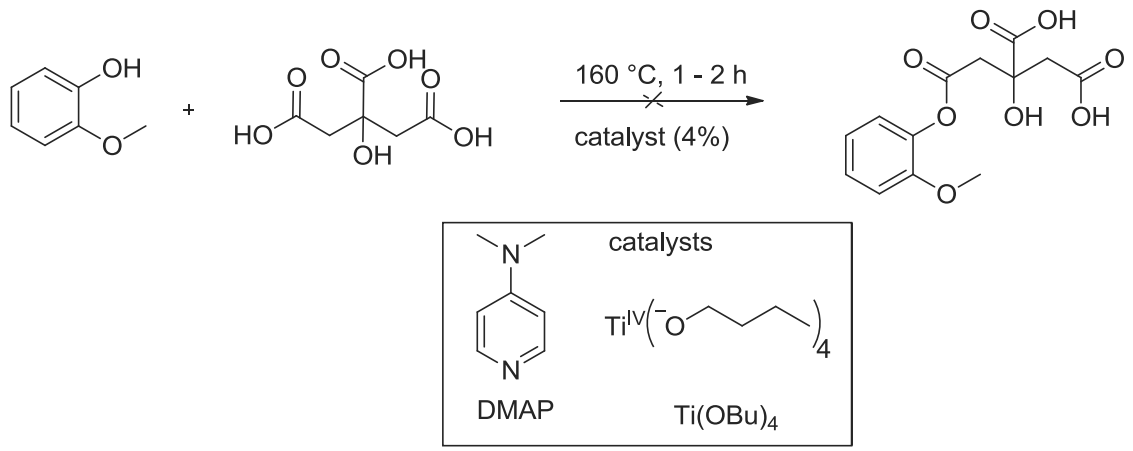

Scheme 100: Reaction of guaiacol with citric acid

The decomposition proceeds via two dehydrations followed by a decarboxylation resulting in itaconic anhydride and citraconic anhydride as shown in scheme 101.[251] This pathway is likely followed in the absence of the formation of esterification products. Isomerisation of trans-aconitic anhydride to its cis-isomer can also occur, but eventually results in the same decomposition products.

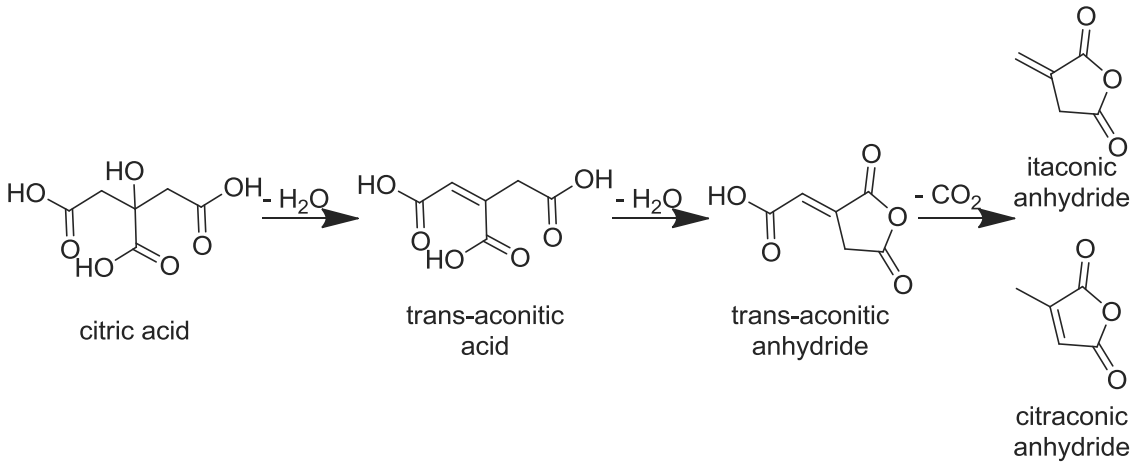

Scheme 101: Possible pathway of citric acid thermal degradation (Wyrzykowski 2011)

The product NMR spectrum showed a mixture of different compounds, shown in figure 49. Next to the starting materials, which were still present as a majority, new peaks around 6 ppm in the ^{1}H NMR and around 130 ppm in the ^{13}C NMR (both in DMSO^{d}) were observed.

Table 29: Comparison of new peaks to possible degradation product peaks from the literature

compound	^{1}H NMR	^{13}C NMR
reaction new peaks (DMSO^{d})	6,30; 6,29; 6,28; 6,24; 6,13; 6,12; 5,98; 5,88; 5,71	139,56; 135,80; 130,12; 127,93
citric acid (MeOH^{d4})[252]	2,74; 2,56	-
itaconic anhydride ($CDCl_3$)[253]	6,47; 5,86; 3,60	-
citraconic anhydride ($CDCl_3$)[254]	9,05; 6,05; 2,16	171,8; 169,6; 147,1; 122,7; 21,7

As illustrated in table 29 above, these are characteristic for conjugated double bonds. The proximity to the peaks of degradation products reported in the literature supports the hypothesis that citric acid underwent thermal degradation instead of esterification.[XXXVI]

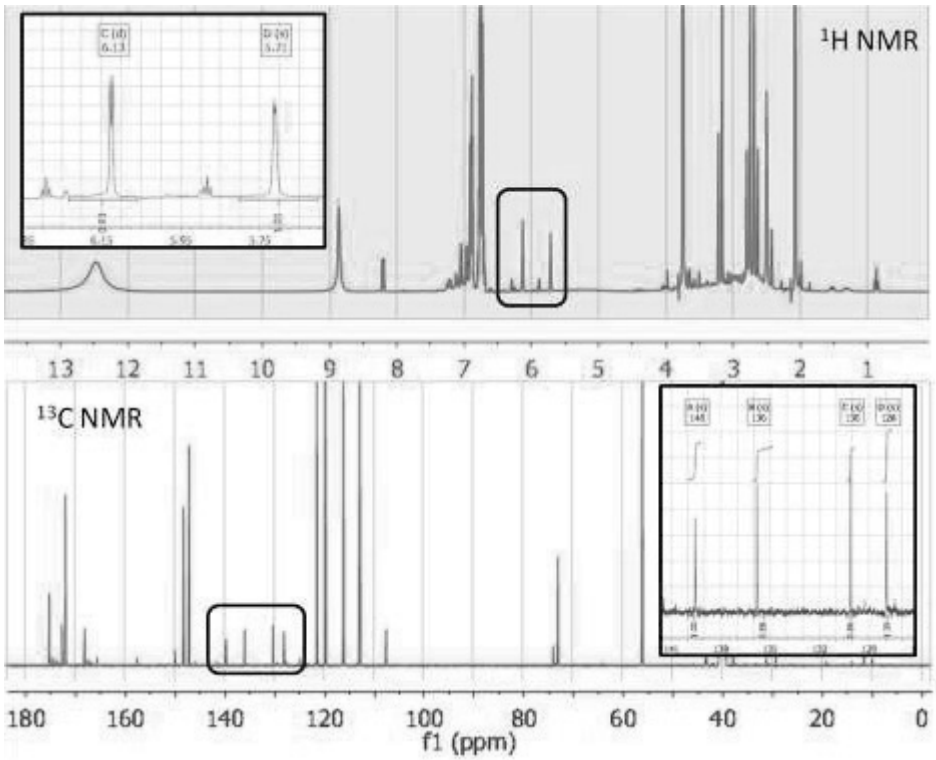

Figure 49: NMR of the reaction of citric acid and guaiacol showing new peaks possibly belonging to degradation products

4.1.4 Guaiacol transesterification with methyl hexanoate

Transesterification is often used in polyesterification due to the nature of the starting materials. For example, fatty acids are often supplied as triglycerides, and a transesterification is therefore used in alkyd synthesis. In the synthesis of polyethylene terephthalate, dimethyl terephthalate is also often used instead of terephthalic acid due to its higher solubility and lower boiling point, which makes it much easier to handle.

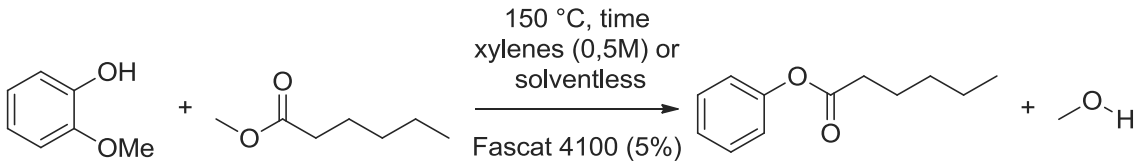

Scheme 102: Transesterification of methyl hexanoate with guaiacol

[XXXVI] NMR peaks of the other degradation products are not detailed in the literature, but their spectra can be found in the annexe, also showing peaks around 6 ppm in the ^{1}H NMR and around 130 ppm in the ^{13}C NMR.

In this case, the use of methyl hexanoate instead of hexanoic acid was tested, as shown in scheme 102. The presence of the ester group could be advantageous due to the lower boiling point of the formed methanol compared to water, which will move the equilibrium further to the product side due to its faster evaporation. Furthermore, the lower polarity of the ester group compared to an acid group could increase the chemical similarity and therefore the miscibility of both reagents.

Butylstannoic acid was used as a catalyst at a concentration of 5%. Only 5% of guaiacol hexanoate were obtained after 5 h, but the yield could be increased to 24% when the reaction was continued for 2 days. Furthermore, the addition of xylenes solvent increased the yield to 83%, as shown in table 30. This indicates that the improved compatibility between the reagents was the reason for the increase in yield compared to the reaction with hexanoic acid, and that the mixing of the reagents is a hindering factor for the esterification in addition to the steric bulk.

Table 30: Yields of the transesterification reactions of methyl hexanoate with guaiacol

n	time	solvent	solvent concentration x	yield
mmol	h		M	%
2	5,5	-	-	5
2	48	-	-	24
2	20	xylenes	0,5	83

4.1.5 Potential of the vanillin phenol group in esterification reactions

The study of guaiacol esterifications using different substrates and catalysts revealed a considerably lower reactivity compared to phenol, which was attributed to the steric hindrance imposed by the methoxy group and the low compatibility between the reagents. The latter hypothesis is supported by the fact that the transesterification yielded better results than the esterification, that the highest yield was obtained when xylenes solvent was added and that the reaction in acetic acid did not improve the yield compared to hexanoic acid despite its large excess.

While the steric environment of vanillin is well represented by guaiacol, its polarity is probably somewhat underestimated due to the absence of the aldehyde group. The addition of xylenes as a azeotrope forming solvent is also a possibility in polyesterification reactions, albeit not in 0,5M concentration with respect to the substrates.

The reaction of acid substrates was best catalysed by a *p*TSA catalyst. A $Bi(OTf)_3$ catalyst showed good activity for the hexanoic substrate but none for the acetic acid substrate, while the opposite was true for a $Mn(OAc)_3$ catalyst. Overall, however, the maximum yield obtained was 43%, which is too low for a successful polyesterification reaction.

The use of anhydrides with a DMAP catalyst made it possible to raise the yield to up to 66% regardless of their steric bulk. It also revealed that high temperatures of at least 140 °C are necessary for the reaction to proceed. This excluded the use of citric acid as a substrate, as it can form anhydrides *in situ* but degrades at high temperatures.

Overall, valuable conclusions about the reactivity of the phenol in vanillin could be drawn, but its reactivity could not be increased sufficiently for a polymerisation reaction through catalysis and the use of different substrates. The modification of the phenol group itself was examined next.

4.2 Transformation of vanillin to more reactive substrates

Several possibilities to increase the reactivity of the phenol group towards transesterification exist and are described in the introduction (*chapter 2*). Of these, acetylation was judged to be the most advantageous for this project because it doesn't introduce labile ether groups or other weak links and avoids the use of halide compounds. One of the possible pathways is the Perkin reaction, which was used for example by Mialon *et al.* in the synthesis of polydihydroferulic acid.[1]

4.2.1 The Perkin reaction on vanillin and its optimisation

The Perkin reaction on vanillin was first described by Fosdick *et al.* and involves the transformation to acetylferulic acid using a pyridine catalyst, sodium acetate and acetic anhydride as a reactive solvent.[161] The authors reported a yield of 64%. As the acetylation results in an activation of the phenol group towards esterification, and the reaction also transforms the aldehyde group into an acid, this reaction was studied as a potential intermediate step for the incorporation of vanillin into a polyester.

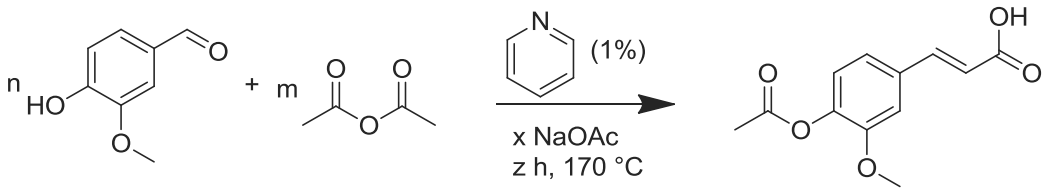

Scheme 103: Optimisation of the Perkin reaction

In an attempt to improve the yield, several modifications of the reaction procedure were made, as shown in scheme 103. The reaction time was increased from 6 h to 8 h and larger amounts of sodium acetate were added. In order to improve the efficiency of the reaction, the amount of acetic anhydride was decreased to two equivalents. In the end, however, the obtained yield stayed below 64%, the yield reported by Fosdick *et al.* The most effective way found to increase the yield was by upscaling of the reaction, as shown in table 31.

Table 31: Conditions tested for the optimisation of the Perkin reaction

vanillin n	acetic anhydride m	NaOAc x	z time	isolated yield
g	equivalents	equivalents	h	%
2	7,45	1,85	2,75	25
4	7,45	1,85	6	18
4	7,45	1,85	7	27
4,56	1,5	2	6,5	0
12	7,45	1,85	6,25	35
12	7,45	1,85	7,5	49
15	7,45	1,85	7	38
15	7,45	1,85	8	53

The purification of the product was done through recrystallisation from dilute acetic acid, therefore it is possible that part of the product remained dissolved and was lost. This explains the increase in yield when larger quantities were used, and could mean that higher yields are possible, particularly when the purification is modified or not at all performed.

However, as mentioned earlier, due to the possibility of substitution of acetylferulic acid from the Perkin reaction by ferulic acid from renewable resources, the optimisation of the reaction was not prioritised in this work. Factors which should be investigated for this purpose in the future include the replacement or complementation of pyridine with other organic or transition metal catalysts, the yield before purification, alternative purification methods and the effect of removing the product from the mixture during the reaction.

4.2.2 Reactivity of acetylferulic acid towards 1,3-propanediol

The suitability of acetylferulic acid for polyesterification reactions was tested by condensation with an excess of 1,3-propanediol, as shown in scheme 104. A black oil was obtained from which at least seven different products with very similar NMR spectra were isolated by column chromatography. The major product was identified as propane-1-ol-3-ferulate in a yield of 33%.

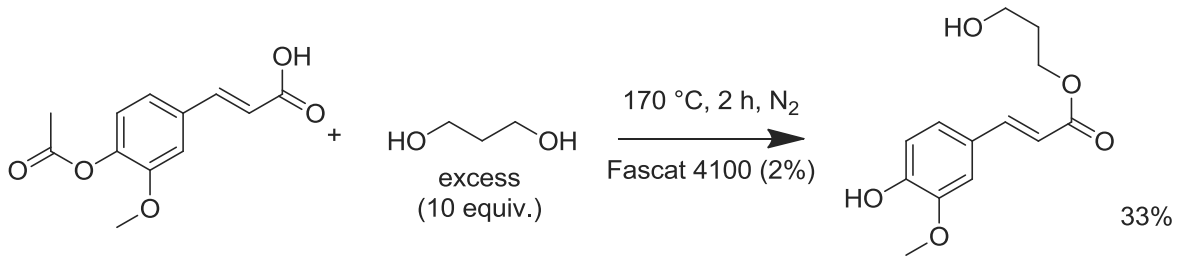

Scheme 104: Reaction of acetylferulic acid with 1,3-propanediol

Thus, the reactivity of the acid group as well as the possibility of liberation of the phenol group by transesterification was confirmed. However, due to the coloration of the product it was decided to follow the protocol proposed by Mialon *et al.* for the study of the polyesterification.

4.2.3 Hydrogenation of acetylferulic acid

Following the work of Mialon *et al.*, acetylferulic acid was hydrogenated using Pd/C as a catalyst, as shown in scheme 105. The product was obtained as a grey powder in up to 86% yield. Some of the remaining 14% were probably lost during the separation from the catalyst. Dihydroacetylferulic acid could then be used in polyesterification reactions both alone and with comonomers, the different results of which will be described in the following section.

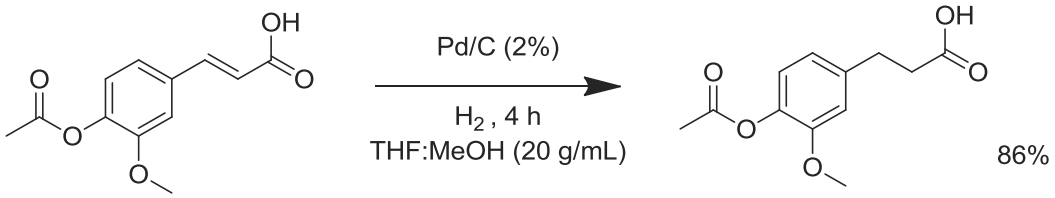

Scheme 105: Hydrogenation of acetylferulic acid

4.3 Polyesterification of ferulic acid and derivatives

Two main strategies were used to incorporate ferulic acid into a polyester, as shown in scheme 106. The first, again following the example of Mialon *et al.*, involved the polyesterification of dihydroacetylferulic acid with and without added comonomers first under N_2 atmosphere followed by a period under vacuum to remove by-products and increase the conversion.[160]

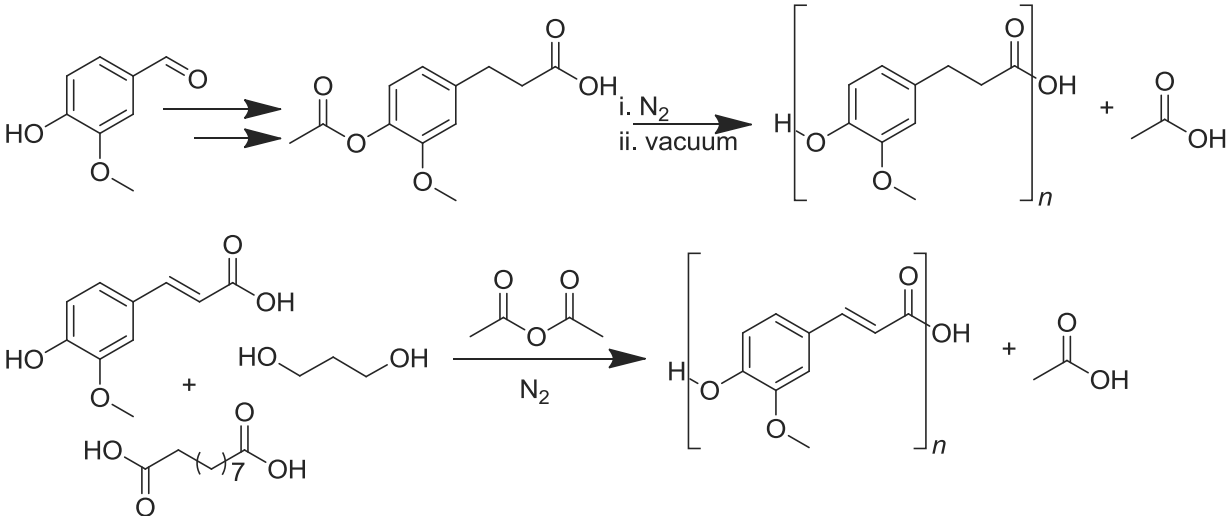

Scheme 106: Representation of two strategies for the polyesterification of ferulic acid derivatives

The second strategy consisted of the use of acetic anhydride as a condensation agent, following the example of Thi *et al.* amongst others.[153] Ferulic acid was reacted in an acetic anhydride solution with sebacic acid and 1,3-propanediol, and the effect of changing their respective ratios, the reaction time, the temperatures during the reaction and the work up methods was examined.

In order to determine their influence on the product composition, different factors such as the relative quantities of the monomers, reaction conditions and the presence of acetic anhydride were examined one by one.

4.3.1 Analysis methods

In each case, the products were analysed using a combination of NMR, mass spectrometry and size exclusion chromatography. The size exclusion chromatography was especially important as the different groups of peaks were used to identify the proportion of different degrees of reaction and the nature of the products. One of the main challenges that had to be solved was the lack of solubility of the product in common solvents. Several organic solvents including a range of fluorinated compounds were tested, but solubility was only observed in trifluoroacetic acid, hexafluoroisopropanol and pentafluorophenol. The first was selected despite the risk of breaking ester bonds introduced by its acidity due to the high price of the latter two.[XXXVII]

4.3.1.1 Size exclusion chromatography

The products were diluted at a concentration of 10 g/L in NMP and analysed at 50 °C to prevent precipitation in the column. Distinct peaks were then identified in the resulting chromatogram as shown in figure 50 and are reported separately with the corresponding retention time, weight and number average molecular weights and relative peak areas in %.

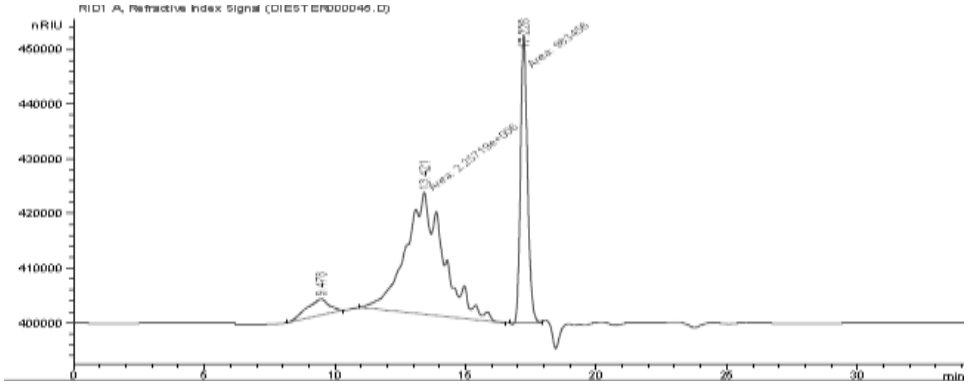

Figure 50: Example of SEC analysis in which three peaks were integrated separately

[XXXVII] See annexe for details of the solubility tests conducted.

The majority of the products examined contained two distinct peaks. One contained high weight average molecular weight products between 18 000 g/mol and 61 000 g/mol, which appeared after retention times of 6,7 min to 10,5 min. It only made up below 10 % of the total peak area in the majority of the products, with some exceptions where it had a proportion up to 46%.

The main peak appeared between 12 min and 15 min of retention time and made up 40% to 99% of the total peak area. It was found to contain products with weight average molecular weights between 1 300g/mol and 7 900 g/mol. Lastly, some samples also contained a third peak which appeared around 16 min of retention time and corresponded to oligomers between 800 g/mol and 1 000 g/mol.

4.3.1.2 NMR analysis

For the first group of product based on dihydroacetylferulic acid, NMR was just used to confirm the nature of the homopolymer product. For the second group of product based on ferulic acid, 1,3-propanediol and sebacic acid, however, the peak areas in ^{1}H NMR were also used to obtain an estimate of how much of each monomer was incorporated into the product.

The area of the CH_2 peaks of the linear chains of esterified 1,3-propanediol and sebacic acid and the area of the CH and CH_3 peaks of the aromatic ring of reacted ferulic acid were integrated and divided by the quantity of protons that correspond to each signal as well as by the quantity of protons present in each monomer. An average value was thus determined for each compound and compared with the average values of the other compounds.

In general, the ferulic acid peaks were used as a standard. Their integration was set to 10 and the other peaks are reported relative to this value.

4.3.1.3 Mass spectrometry

Electrospray ionisation mass spectrometry was also used to elucidate the structure of the products of the polyesterification reactions of ferulic acid with sebacic acid and 1,3-propanediol. The products were diluted in a 1:3 mixture of trifluoroacetic acid (TFA) and chloroform and analysed at low resolution.

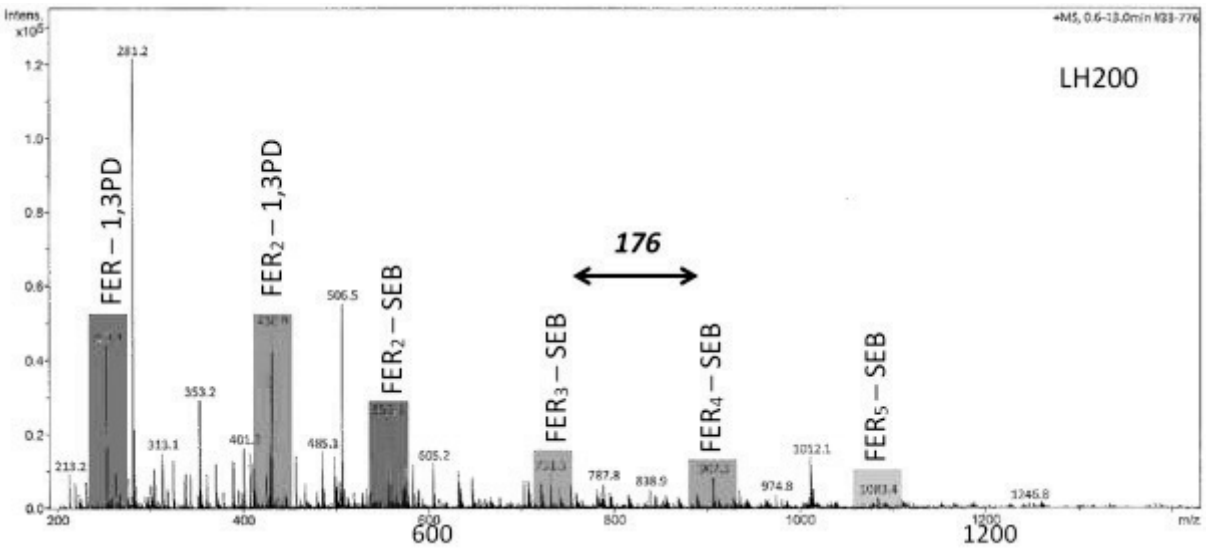

Figure 51: Mass spectrum of LH200

However, mostly products with a molecular mass below 1000 g/mol were detected in the analysis. Furthermore, a large variety of fragmentation products were observed, not all of which could be clearly identified. In figure 51, the mass spectrum of the reaction product LH200 is shown. Even though the SEC analysis revealed a weight average molecular weight of 2388 g/mol for the major peak, no peaks above the mass of 1246,8 g/mol were detected in the mass spectrum, and the majority actually lies below 600 g/mol.

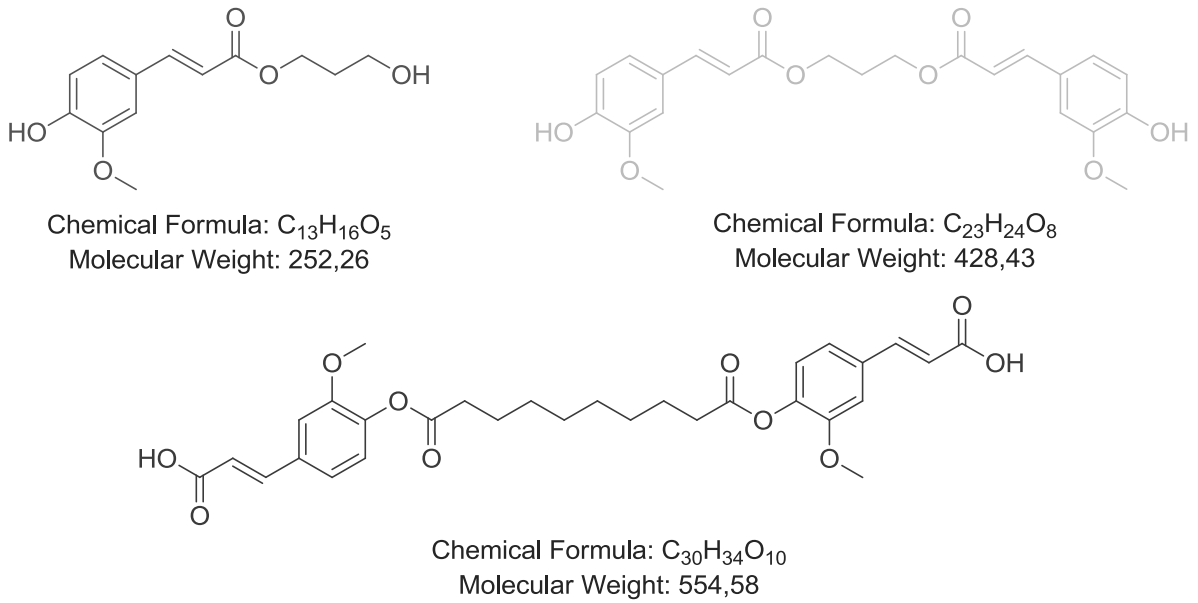

Scheme 107: Possible compounds observed in mass spectrometry

Despite the fact that the corresponding weights of all possible combinations of the three monomers and acetic anhydride, as well as some plausible fragments and combinations with the ions used were calculated, not all peaks could be assigned. Nevertheless, some were identified, such as the

combinations of ferulic acid with sebacic acid or 1,3-propanediol shown in scheme 107. A repeating distance of 176 between peaks, corresponding to the ferulic acid fragment, was also observed in several cases.

It should also be kept in mind that it is possible that the trifluoroacetic acid (TFA) is interfering with the mass spectroscopy results. As described for example by Mirza *et al.*, and Apffel *et al.*, the negative ions generated by the deprotonation of trifluoroacetic acid can pair with the positive ions generated in the ionisation used to analyse the products in the mass spectrometry.[255, 256] TFA can also interfere with the surface tension of the solution and cause in a suppression of certain signals, especially those with basic groups, as well as a lowering of the signal to noise ratio.

The mass spectrum was therefore mostly used as evidence for certain combinations of the monomers and the corresponding motives in the chain.

4.3.2 Polymerisation of dihydroacetylferulic acid

The polymerisation of dihydroacetylferulic acid alone and with comonomers was performed in two steps at 220 °C, first with nitrogen flow through the reaction mixture, then under vacuum. The product was purified by dissolving it in trifluoroacetic acid and dichloromethane and then precipitating it through the addition of methanol and dried before the yield was determined.

4.3.2.1 Homopolymerisation

In a first step, the influence of catalysts on the yield and molecular weight of the products was examined, as shown in scheme 108. Several catalysts already used for the reactivity study of guaiacol, such as butyl stannoic acid, DMAP, $Mn(OAc)_3.2H_2O$ and $Ti(OBu)_4$ were tested. $Zn(OAc)_2$ and a catalyst free reaction were also investigated.

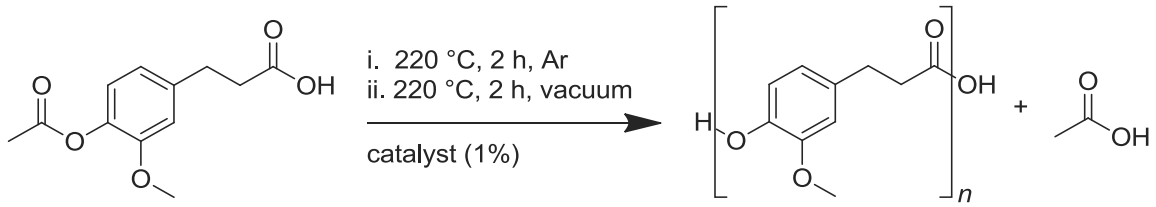

Scheme 108: Homopolymerisation of dihydroacetylferulic acid

While some differences in yield were observed between the different reactions, they could not be related to the catalyst with certainty, as a repetition of the reaction did not show the same results. Furthermore, the absence of a catalyst was not observed to significantly decrease the yield in either of the two runs, as shown in table 32.

Table 32: Weight yields of dihydroacetylferulic acid homopolymerisations with different catalysts

		yield 1		yield 2
catalyst	**reference 1**	**weight%**	**reference 2**	**weight %**
-	LH113	52	LH131	68
Fascat 4100	LH115	66	LH140	61
DMAP	LH118	74	LH133	68
$Mn(OAc)_3$	LH121	61	LH134	48
$Zn(OAc)_2$	LH145	57	-	-
$Ti(OBu)_4$	LH146	53	-	-

The differences between the results observed using SEC, shown in table 33, were somewhat clearer. Both the highest proportion of the medium molecular weight peak and the lowest number average molecular weight were observed for the catalyst free reaction. Nevertheless, the molecular weight was found to be above 3800 g/mol, so that the occurrence of polymerisation cannot be denied. Furthermore, the observation that the presence of a catalyst does not necessarily make a great difference that was drawn by comparing the yields was confirmed.

The highest proportion of large molecular weight products was observed when the $Ti(OBu)_4$ catalyst was added. It resulted in 12,3% of product with a weight average molecular weight of 39 531 g/mol, which is significantly larger than the proportion observed for all other reactions, which was between 0,7 % and 3,5 %.

Table 33: SEC analysis of dihydroacetylferulic acid homopolymerisations with different catalysts

		peak 1 (6,7 - 9,2 min)			peak 2 (12,2 - 13,2 min)		
catalyst	**reference**	**area**	$M_{\bar{n}}$	$M_{\bar{w}}$	**area**	$M_{\bar{n}}$	$M_{\bar{w}}$
		%	**g/mol**	**g/mol**	**%**	**g/mol**	**g/mol**
-	LH113	0,7	35916	36294	99,3	3873	5609
Fascat 4100	LH115	3,5	38295	38894	96,5	5524	7512
DMAP	LH118	1,1	36077	36363	98,9	5673	7868
$Mn(OAc)_3$	LH121	0,7	36851	37702	99,3	3915	4882
$Zn(OAc)_2$	LH145	1,0	36021	36281	99,0	5928	8312
$Ti(OBu)_4$	LH146	12,3	38508	39531	87,7	4179	6032

If each dihydroferulic acid unit is assumed to have a molecular weight of 178 g/mol, the first peak can be estimated to contain chains of approximately 200 to 220 units, while the second peak which represents the majority of the product, can be estimated to contain 20 to 35 units. Overall, polymerisation to a satisfying degree was observed in all samples, but the differences between samples were small.

4.3.2.1.1 Differential scanning calorimetry analysis

Differential scanning calorimetry was used to examine the thermal properties of the products. As shown in figure 52, no glass transitions could be detected. Instead, large peaks were observed between 150 °C and 250 °C, indicating a melting transition. The broad nature of the peak indicates that the mixture of molecular weights also corresponded to a range of different melting points.

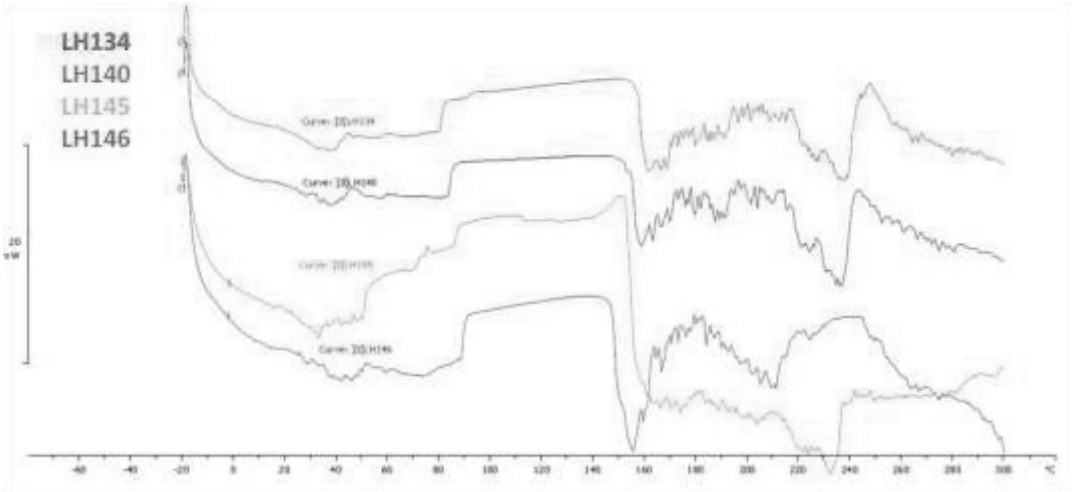

Figure 52: DSC curves (2nd heating, 20 K/min) obtained for the products LH134 - LH146

The points at 40 °C probably correspond to a transition caused by the evaporation of leftover dichloromethane in the products.

A more precise transition was observed for the product LH133, which was made using a DMAP catalyst. None of the products showed a glass transition. It can instead be assumed that they are to some part crystalline. This hypothesis was investigated in more detail by determining the melting points of the products.

4.3.2.1.2 Melting point analysis

The melting point analysis confirmed that all products were crystalline. It furthermore confirmed the presence of a range of molecular weights, as the melting occurred over the course of 4 °C to 20 °C, as shown in table 34. However, as for the yields, the reproducibility of the product melting points between two reactions was not very good.

While all products melted between 190 °C and 240 °C, the melting points were not necessarily closer together between two reactions in which the same catalyst was used than between two random reactions. Since the measurement was performed at a temperature gradient of 10 °C/min, a certain measurement error is possible. Nevertheless, the melting points, yields, and the fact that a similar

molecular weight was obtained with and without catalysts suggest that the catalyst used is not the main factor determining the properties of the reaction product.

Table 34: Melting points of dihydroacetylferulic acid polymers

		range 1		range 2
catalyst	**reference 1**	**°C**	**reference 2**	**°C**
-	LH113	222 - 228	LH131	206 - 211
Fascat 4100	LH115	235 - 243	LH140	195 - 215
DMAP	LH118	237 - 242	LH133	181 - 189
$Mn(OAc)_3$	LH121	236 - 240	LH134	218 - 231
$Zn(OAc)_2$	LH145	215 - 230	-	-
$Ti(OBu)_4$	LH146	190 - 201	-	-

4.3.2.2 Polymerisation of dihydroacetylferulic acid in the presence of other monomers

The product obtained from the homopolymerisation of dihydroacetylferulic acid was a fine, grey powder. Melting behaviour and therefore crystallinity was shown using both DSC and melting point analysis. This is not surprising considering the high proportion of aromatic rings in the product and the *para* substitution, which leads to high symmetry and consequently higher order in the chain. However, it is also not desirable if the product is to be used as a binder in coil coating applications.

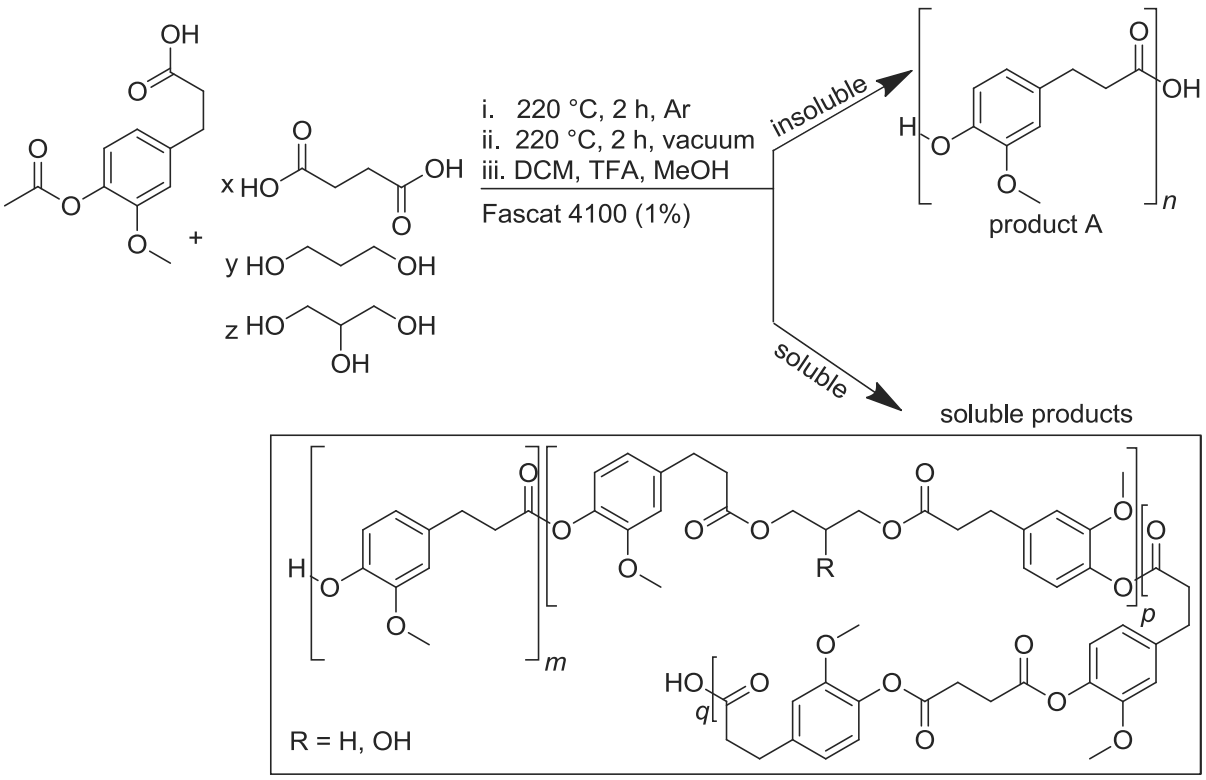

Scheme 109: Polymerisation of dihydroacetylferulic acid in the presence of other monomers

Therefore, succinic acid, 1,3-propanediol and glycerol were added to the reaction in order to introduce irregularities and linear chain segments into the polyester, and therefore to increase its flexibility and decrease its crystallinity. As shown in scheme 109, butylstannoic acid was used as the catalyst.

The effect of changing the quantities of the three non-aromatic monomers was tested, using a reaction procedure and work-up identical to that employed in the homopolymerisation. The work-up procedure involving the solubilisation in dichloromethane (DCM) and trifluoracetic acid followed by precipitation with methanol resulted in the separation of two product groups. The precipitate insoluble in methanol was identified by NMR ($CDCl_3$/TFA[d]) as the homopolymer containing only dihydroferulic acid units. Products of the reaction of ferulic acid with succinic acid, 1,3-propanediol and glycerol had a higher solubility in methanol and stayed in solution. Thus, they were separated from the homopolymer.

4.3.2.2.1 Analysis of the amounts of homopolymer obtained in each case

In figure 53, the yields of homopolymer product obtained after precipitation with methanol is shown against the total equivalents of other monomers added to the reaction with respect to dihydroacetylferulic acid. The yield clearly decreases with increasing amounts of succinic acid and 1,3-propanediol, indicating that the reaction with them is successful, creating more soluble products.

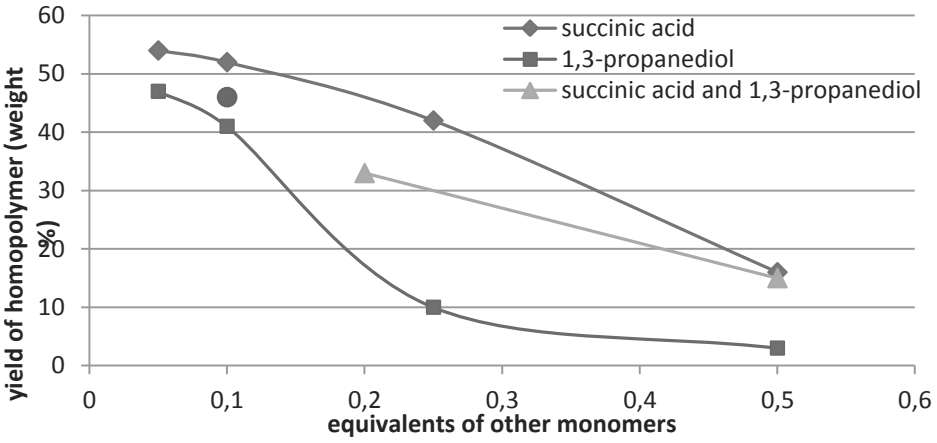

Figure 53: Homopolymer yield *vs.* equivalents of other monomers added to the reaction

The reaction with 1,3-propanediol is slightly more successful than that with succinic acid, possibly because the acid group is more reactive than the phenol group. The reaction with 0,1 equivalents of glycerol decreased the yield to 46%, which is between the yields of 52% and 41% observed for the reaction with 0,1 equivalents of succinic acid and 1,3-propanediol respectively.

4.3.2.2.2 Molecular weights of homopolymer products from the reaction with other monomers

As for the products obtained in the polymerisation reaction containing only dihydroacetylferulic acid, two main peaks after 8,5 – 9,0 min and 12,0 – 14,1 min were observed in the SEC analysism as shown in table 35. However, compared to the former, the molecular weights of the smaller, high molecular weight fraction were slightly higher, corresponding to up to 290 units of dihydroferulic acid. At the same time, the molecular weights of the medium fractions were slightly lower when succinic acid, 1,3-propanediol and glycerol were added to the reaction, corresponding only to 13 to 26 dihydroferulic acid units.

Table 35: Molecular weights of insoluble fraction recovered from reactions with different equivalents of succinic acid

		peak 1 (8,5 - 9,0 min)			peak 2 (12,20- 13,7 min)		
	equivalents	area	$M_{\bar{n}}$	$M_{\bar{w}}$	area	$M_{\bar{n}}$	$M_{\bar{w}}$
reference	succinic acid	%	g/mol	g/mol	%	g/mol	g/mol
LH148	0,05	10,9	39570	40406	89,1	4687	6393
LH147	0,1	6,5	42053	43254	93,5	3973	5634
LH149	0,25	5,8	50885	52690	94,2	3994	5421
LH150*	0,5	2,0	51464	53205	87,0	2355	2718

* third peak at 15,9 min, 11%, $M_{\bar{n}}$ = 840 g/mol and $M_{\bar{w}}$ = 845 g/mol

This trend is also confirmed when the different products of the reactions in which different amounts of succinic acid were added and compared with each other. The molecular weights of the high molecular weight fraction increase with increasing amounts of succinic acid, while the weights of the medium molecular weight fraction decrease.

The last reaction LH150, in which 0,5 equivalents of succinic acid were added, even resulted in 11% of oligomers of around 840 g/mol.

Table 36: Molecular weights of insoluble fraction recovered from reactions with different equivalents of 1,3-propanediol

		peak 1 (8,5 - 8,9 min)			peak 2 (13,0- 13,8 min)		
	equivalents	area	$M_{\bar{n}}$	$M_{\bar{w}}$	area	$M_{\bar{n}}$	$M_{\bar{w}}$
reference	1,3-propanediol	%	g/mol	g/mol	%	g/mol	g/mol
LH153	0,05	1,7	47803	48949	98,3	3704	4977
LH154	0,1	0,6	17450	17540	99,4	2956	3806
LH155	0,25	2,2	47122	48577	97,8	2684	3051
LH156	0,5	6,0	50282	55616	94,0	2395	2639

With the exception of the high molecular weight fraction of the reaction LH154, this trend is also reflected in the results of the reactions containing 1,3-propanediol, and in the reactions containing both 1,3-propanediol and succinic acid, shown in tables 36 and 37.

Table 37: Molecular weights of insoluble fraction recovered from reactions with both succinic acid and 1,3-propanediol and with glycerol

		reference	LH157	LH158	LH159
equivalents	succinic acid		0,1	0,25	-
	1,3-propanediol		0,1	0,25	-
	glycerol		-	-	0,1
peak 1 (8,7 min)	area	**%**	6,5	5,4	6,2
	$M_{\bar{n}}$	**g/mol**	51625	57960	51498
	$M_{\bar{w}}$	**g/mol**	53662	61373	54642
peak 2 (12,9- 13,7 min)	area	**%**	93,5	94,6	92,3
	$M_{\bar{n}}$	**g/mol**	3883	2648	4036
	$M_{\bar{w}}$	**g/mol**	4764	3220	5158
peak 3 (16 min)	area	**%**	-	-	1,5
	$M_{\bar{n}}$	**g/mol**	-	-	799
	$M_{\bar{w}}$	**g/mol**	-	-	806

The lower molecular weights of the major fraction could be due to reaction with succinic acid or 1,3-propanediol in such small amounts that the it is not visible in the NMR. It is possible that the reaction of the chain end with another monomer stops the chain growth because the reaction with another unit of dihydroacetylferulic acid is more favourable than that with a 1,3-propanediol or succinic acid ester. This would also explain the higher molecular weights of the smaller fraction.

4.3.2.2.3 Analysis of the soluble part of the product of the reaction of dihydroacetylferulic acid and 0,5 equivalents of 1,3-propanediol

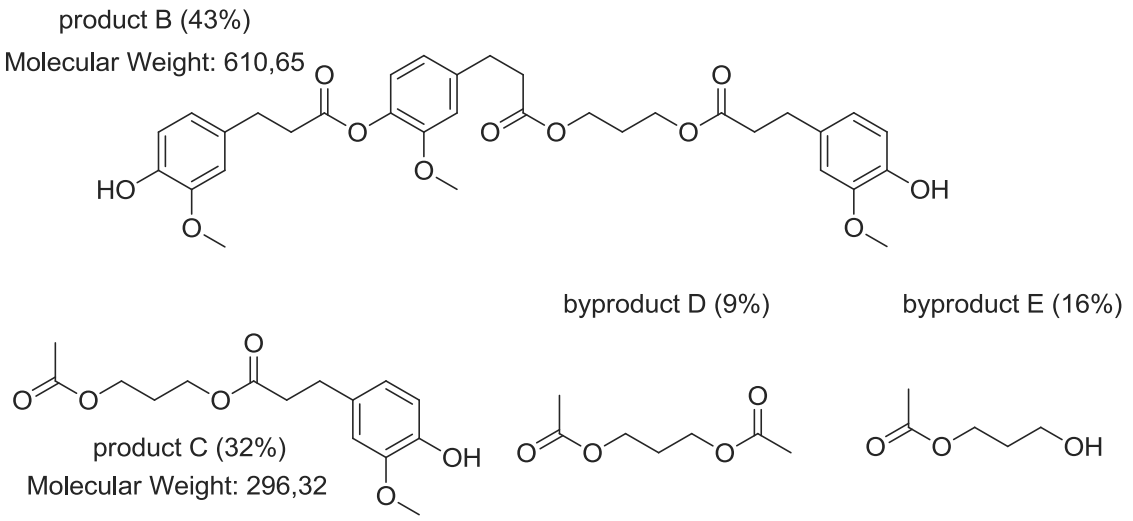

Scheme 110: Compounds identified in the soluble part of the reaction product of dihydroacetylferulic acid and 0,5 equivalents of 1,3-propanediol

Only one of the solutions left after purification was analysed because the majority had been discarded by the time the analysis of the precipitated products was finished. The solution was dried, but because only a small amount of product was recovered, no separation was performed. The products in scheme 110 were instead identified by NMR and their relative quantities were estimated.

The soluble fraction was found to contain only small molecules. The major component was the product of the esterification of one 1,3-propanediol unit with three dihydroferulic acid units. Smaller combinations and products of the reaction of 1,3-propanediol with the acetic acid liberated from the dihydroacetylferulic acid during esterification were also observed.

4.3.2.3 Insights from the replication and extension of dihydroacetylferulic acid polymerisation as proposed by Mialon et al.

The polymerisation of dihydroacetylferulic acid as described by Mialon *et al.* was successfully replicated in this work, and the molecular weight of the resulting polyesters, which was only calculated using end group analysis before, was confirmed with size exclusion chromatography. Little influence of the catalyst used in the reaction on the outcome was observed, and the crystallinity of the products was confirmed in DSC and by melting point analysis.

Unfortunately, the incorporation of other monomers into the polyester chain to reduce the crystallinity was not successful. The formation of the homopolymer product was still observed in all the reactions involving addition monomers, even though conversion with succinic acid, 1,3-propanediol and glycerol was evidenced by a decreasing yield. Furthermore, the homopolymer molecular weights were decreased through the presence of other monomers, possibly due to the creation of unreactive chain ends.

The reaction product of dihydroferulic acid with other monomers was found to be more soluble than the homopolymer, which is encouraging, but the one example examined by NMR only contained low molecular weight compounds. The lack of high molecular weight copolyester in the soluble fraction and the decreasing size of the homopolymer products in the presence of other monomers indicates that the reaction of dihydroacetylferulic acid with other monomers leads to a loss in polyesterification reactivity.

Therefore, instead of repeating the rest of the reaction to examine the soluble fractions in detail, it was decided to study the different aspects of the reaction between ferulic acid, sebacic acid and 1,3-propanediol. This study, which aims to tune the reactivity towards copolymerisation and the formation of more soluble products, is described in the following section.

4.3.3 Study of the copolymerisation of ferulic acid

In order to be able to control the polyesterification of ferulic acid to target different resin designs, various factors influencing the reaction were studied. Following the strategy of for example Thi *et al.*, acetic anhydride was added to the reaction to acetylate the phenol group and thus increase its reactivity to esterification.

The ferulic acid used was a mixture of cis- and trans- ferulic acid, because this is was available at a considerably lower price than pure trans-ferulic acid. For simplicity, however, the trans form will representatively be used in all schemes below.

First, the relative reactivity of the phenol group and the acid group compared to the alcohol and acid groups of 1,3-propanediol and sebacic acid was studied. Secondly, a variety of different reaction conditions were tested. The effect of changing the temperature and reaction time as well as the relative quantities of the different monomers was explored. Different purification methods and a variety of solvents for the work-up were also evaluated.

Lastly, the reaction was performed without acetic anhydride to define its importance for the reaction progress and the potential to minimise the quantity needed.

4.3.3.1 Relative reactivity of ferulic acid towards itself compared to towards other monomers

The reactivity of ferulic acid in an acetic anhydride solution towards other diols and diacids compared to the reactivity towards itself was tested by reacting it with different quantities of only one of the monomers. As the polymerisation of dihydroacetylferulic acid had still resulted in homopolymer product formation, this study was used to determine if the reaction with other monomers was possible, and to indicate possible sources of reactivity problems.

4.3.3.1.1 Reactivity towards 1,3-propanediol

First, 6 mmol of ferulic acid were reacted in an excess of acetic anhydride with 2 mmol, 4 mmol and 6 mmol of 1,3-propanediol, as shown in scheme 111.

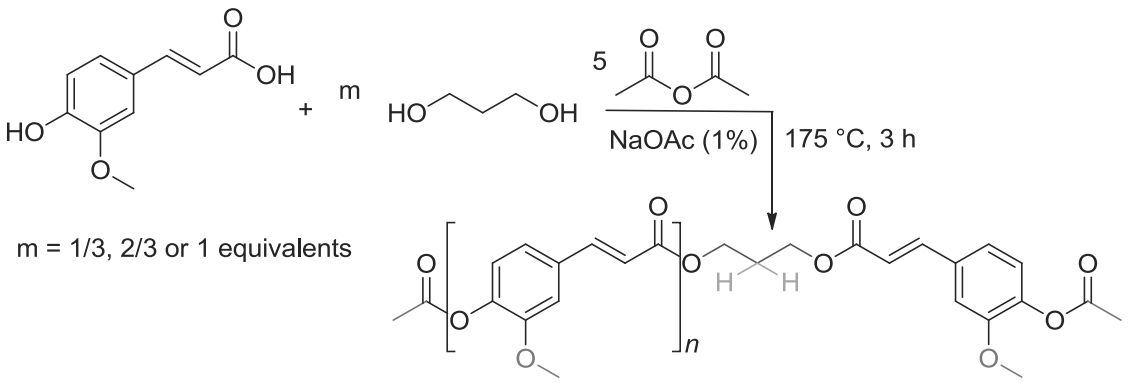

Scheme 111: Reaction of ferulic acid with 1,3-propanediol

Ethanol was used to separate the product from leftover starting material, and NMR and mass spectrometry were used to determine the nature of the product. In the NMR, signals corresponding to the combination of 1,3-propanediol with ferulic acid are visible as shown in figure 54 for the product of the reaction LH218, in which 4 mmol 1,3-propanediol, 2/3 equivalents of the amount of ferulic acid, were used.

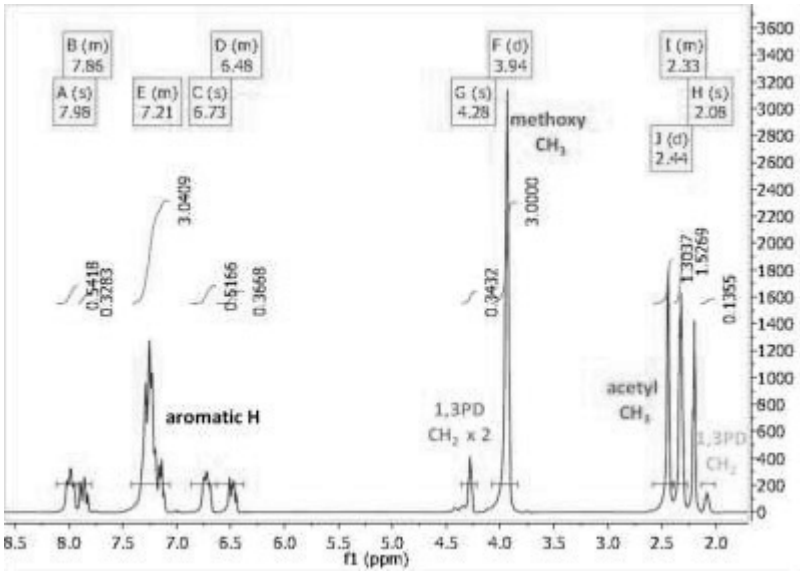

Figure 54: ^{1}H NMR ($CDCl_3$, TFA^d 3:1) of the product LH218 of ferulic acid and 2/3 equivalents of 1,3-propanediol

The peaks are however considerably smaller than those corresponding to the ferulic acid units, indicating that esterification between ferulic acid units has also taken place. While the 1,3-propanediol units make up about 10% of the product in LH218 according to the NMR, they are even smaller in the two other reactions LH216 and LH220, in which 2 mmol and 6 mmol 1,3-propanediol were used respectively.

This observation is confirmed by the mass spectrum of the different products. For all three reactions, combinations of ferulic acid and 1,3-propanediol but also products made up solely of ferulic acid

were detected. Below in scheme 112, some of the possible products which could correspond to the masses observed are shown.

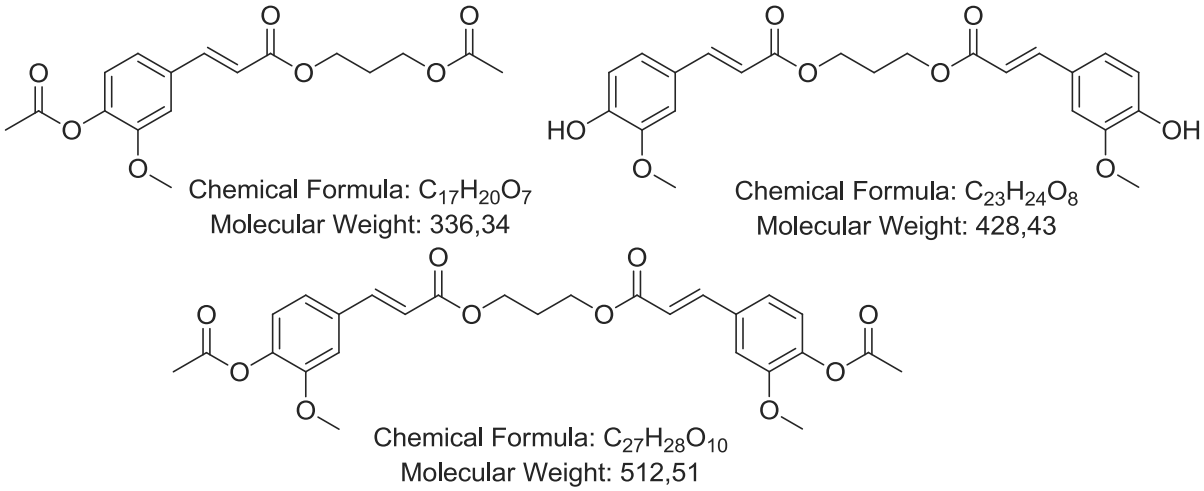

Scheme 112: Reaction products of ferulic acid with 1,3-propanediol observed in the mass spectrum

Both the acetylated form of ferulic acid and the phenol form were observed in the mass spectrum, as shown in scheme 113, though the removal of the acetyl group could be due to fragmentation during the analysis. The reaction of 1,3-propanediol with acetic anhydride was also confirmed by the presence of the resulting diester with a molecular weight of 160,17 g/mol.

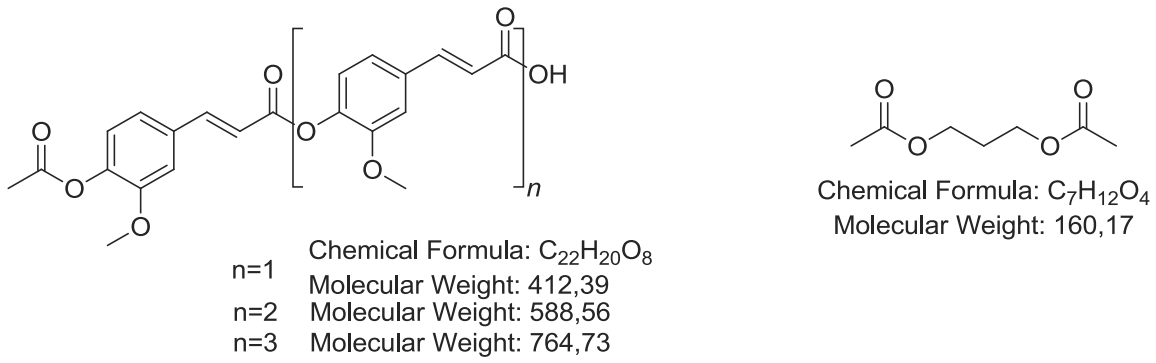

Scheme 113: Side products observed in the mass spectrum of the reaction of ferulic acid and 1,3-propanediol

The major peak in the mass spectrum of the ethanol solution was found at 359,1 g/mol. This corresponds to the sodium ion of the first product shown above with a molecular weight of 336,34 g/mol, which is formed from the reaction of 1,3-propanediol with ferulic acid followed by the esterification of each terminal alcohol with acetic anhydride.

The reaction was also repeated with 4 mmol of 1,2-propanediol instead of 1,3-propanediol, but no difference in result was observed.

Several fragments containing up to four units of ferulic acid were also observed in each mass spectrum. The larger NMR signals of the protons of the ferulic acid units and the presence of products containing only ferulic acid units in the mass spectrum indicate that the homopolymerisation of ferulic acid still takes place. In the reactions in which 4 mmol and 6 mmol of 1,3-propanediol was used, this means that the reaction of the ferulic acid with another ferulic acid phenol group took place despite an excess of 1,3-propanediol alcohol groups.

Possible explanations could either be a higher reactivity of the acetylated phenol group towards the acid, or the competition with the reaction of the 1,3-propanediol with the acetic anhydride. Nevertheless, the possibility to react ferulic acid with 1,3-propanediol was proven by the presence of NMR and mass spectrum peaks, though in smaller proportions than the reaction of ferulic acid with itself.

4.3.3.1.2 Reactivity towards sebacic acid

The reactivity of ferulic acid towards sebacic acid was tested using the same method as above, as shown in scheme 114. 6 mmol of ferulic acid were reacted with 2 mmol, 4 mmol and 6 mmol of sebacic acid and after washing with ethanol, the products were examined using NMR and mass spectrometry.

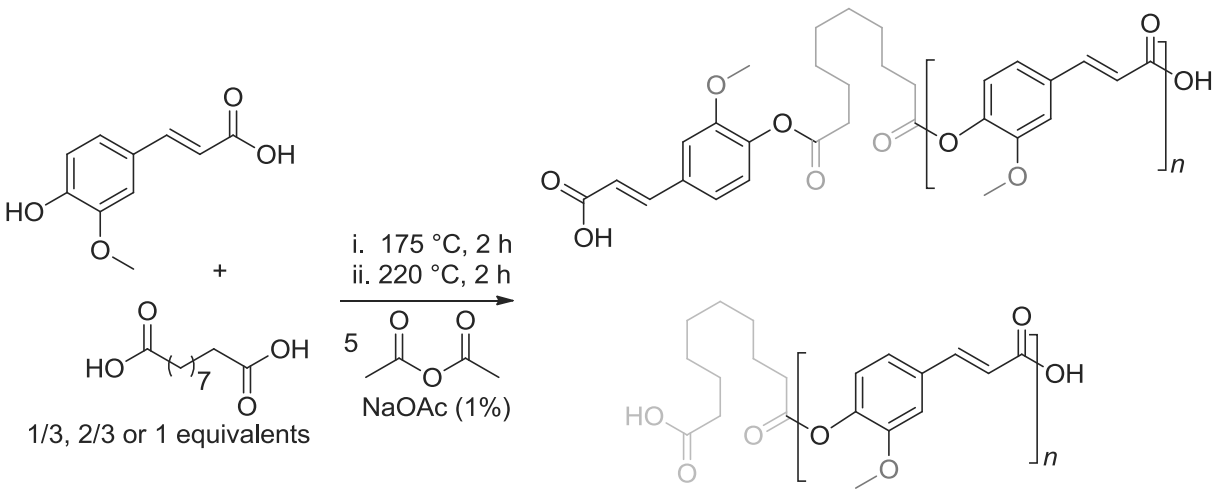

Scheme 114: Reaction of ferulic acid with different amounts of sebacic acid

Contrary to the presence of 1,3-propanediol in the product, sebacic acid peaks could be discerned very clearly in the NMR spectra. Two different groups of sebacic acid peaks, which could correspond to acid groups that had reacted twice and acid groups that had reacted only once, were observed as shown in figure 55 below. The peaks were much closer in size to those containing ferulic acid,

indicating that about two to three times as many ferulic acid groups as sebacic acid groups were incorporated into the product in total.

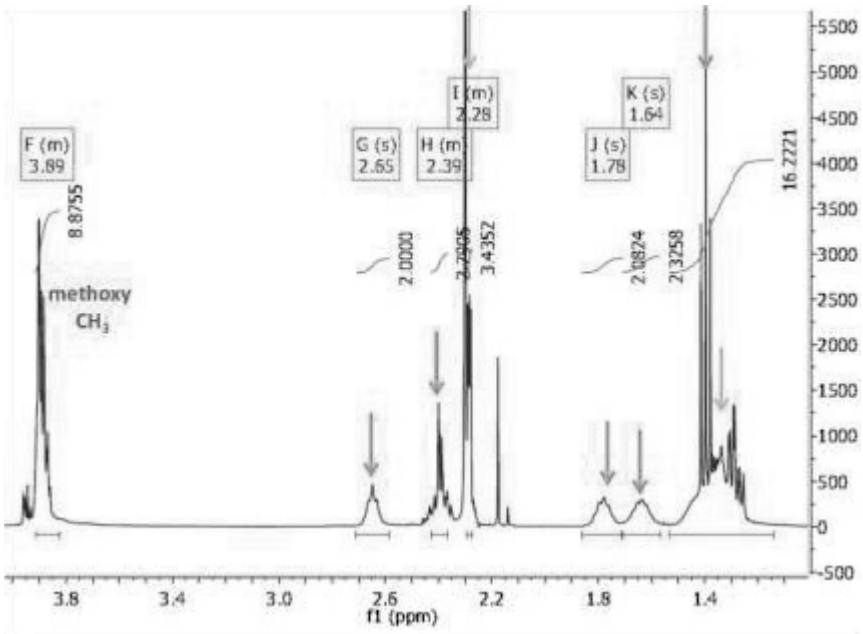

Figure 55: ^{1}H NMR of the product of the reaction of ferulic acid with 2/3 equivalents of sebacic acid LH222

This observation is also supported by the peaks observed in the mass spectrum. In all three reactions, a product at 555,2 g/mol corresponding to two ferulic acid and one sebacic acid units, as shown in scheme 115, was found.

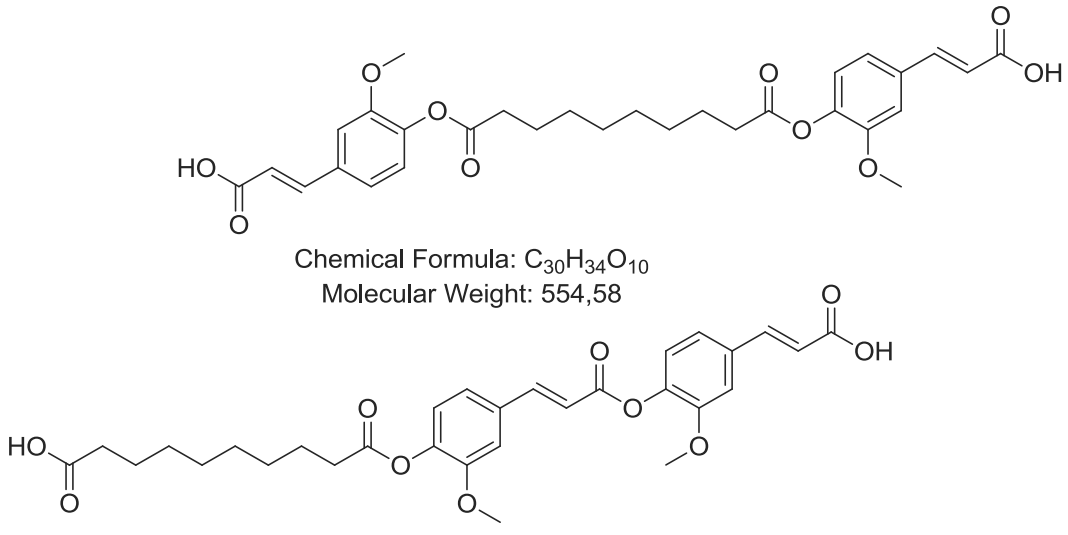

Scheme 115: Product of one sebacic acid and two ferulic acid units observed at 555 in the mass spectrum

Products corresponding to the combination of only ferulic acid were not observed except for in the mass spectrum of LH221, in which 1/3 equivalent of sebacic acid was used. The peak observed was at 413,1 and can be attributed to the combination of two ferulic acid units which are acetylated at the

OH group after the reaction with acetic anhydride. While it is hard to completely exclude the formation of any other products due to the multitude of fragmentation peaks observed in each spectrum, it is likely that there was considerably less formation of homopolymer products than in the 1,3-propanediol reactions, where the peaks were clearly visible.

Overall, it seems that the reaction of ferulic acid with both 1,3-propanediol and sebacic acid is possible, but that the reaction with sebacic acid is more competitive compared to the homopolymerisation reaction.

4.3.3.1.3 Reactivity with 1,3-propanediol or sebacic acid in the absence of acetic anhydride

Because competition between the reaction of 1,3-propanediol with acetic anhydride and ferulic acid was observed, the possibility of performing the reaction with 1,3-propanediol and sebacic acid without acetic anhydride was investigated.

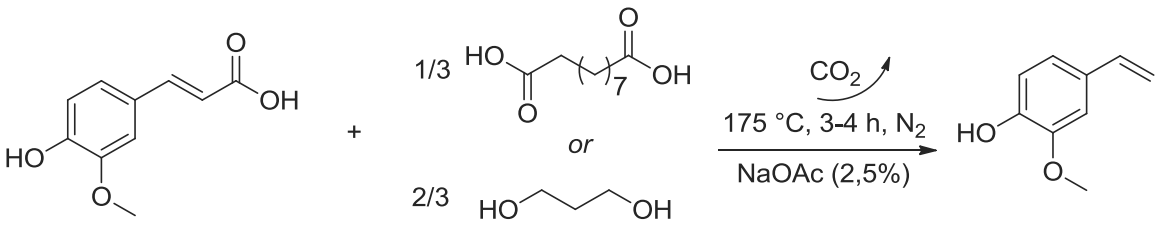

Scheme 116: Reaction of ferulic acid with 1,3-propanediol and sebacic acid in the absence of acetic anhydride

As shown in scheme 116, in both cases decarboxylation of ferulic acid was observed instead of the desired esterification. The decarboxylation product evaporated from the reaction and the yield was therefore not determined.

The reaction with 1,3-propanediol was repeated at 130 °C to avoid decarboxylation as shown in scheme 117, but only 20 – 30 % conversion was observed even after 10 h of reaction time. SEC analysis of the product showed a majority of polymer products of a low weight average molecular weight of 2211 g/mol, which could correspond to approximately 12 ferulic acid units and one 1,3-propanediol unit.

As both decarboxylation products were volatile, the reaction was again repeated without nitrogen flow to prevent their removal from the mixture and thus slow down their formation. Only a small increase in yield to 36% was observed as a result, and SEC analysis showed a decrease in weight average molecular weight to 1839 g/mol, which could correspond to 10 ferulic acid units with one 1,3-propanediol unit. Furthermore, the product colour changed from clear red to black due to the presence of air in the reaction.

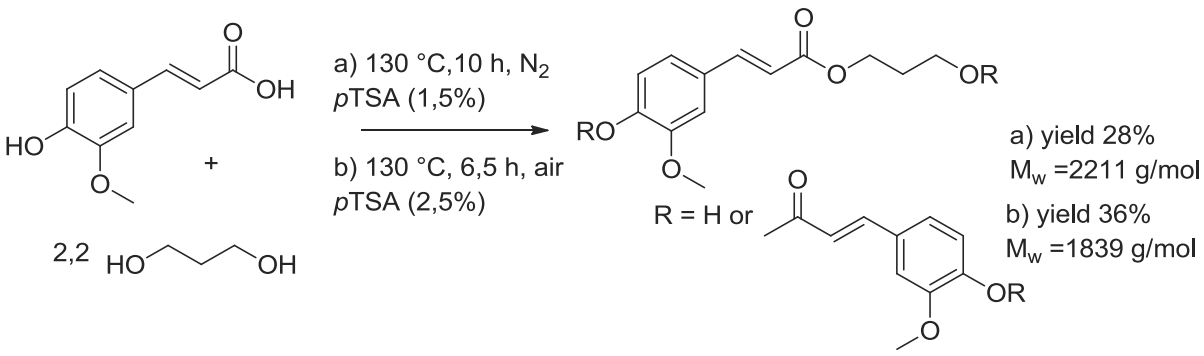

Scheme 117: Reaction of ferulic acid with 1,3-propanediol without acetic anhydride at 130 °C with and without nitrogen

Repeating the reaction of ferulic acid with sebacic acid was not possible at 130 °C because both reagents are solids at that temperature. It was therefore decided that the presence of acetic anhydride is necessary both to prevent decarboxylation, and therefore enable the reaction, and to dissolve the products at a suitable reaction temperature.

4.3.3.2 The effect of different monomer ratios

In order to determine an appropriate composition for a resin containing ferulic acid, three different ratios (x : y : z) of ferulic acid, sebacic acid and 1,3-propanediol were reacted together, as shown in scheme 118. To one equivalent of ferulic acid dissolved in 5 equivalents of acetic anhydride, 0,38 and 0,56 as well as 1 equivalents of sebacic acid and 1,3-propanediol were added. The reaction was heated starting at 175 °C and raised to 220 °C with a Vigreux column until most of the acetic anhydride had reacted or evaporated. Then, the heating was continued at 220 °C. Nitrogen was bubbled through the reaction to provide an inert atmosphere.

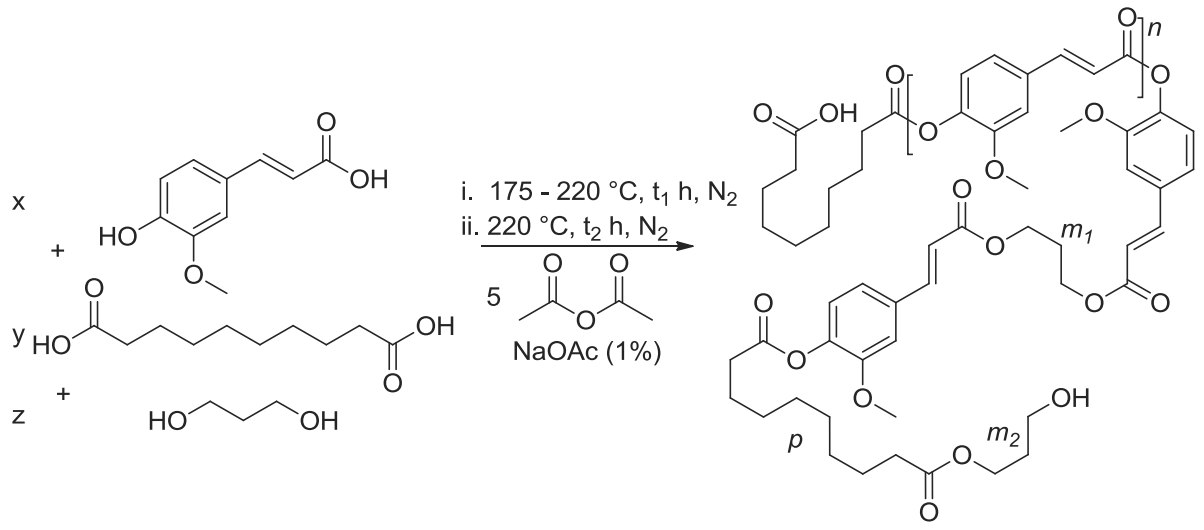

Scheme 118: Polyesterification of different levels of ferulic acid, sebacic acid and 1,3-propanediol

The reaction was generally stopped when stirring was no longer possible because the product had become solid. After separation of the products from the starting materials by dissolving everything in acetone followed by precipitation through the addition of ethanol, a yellow powder was recovered.

The target was to obtain an amorphous resin and not a powder. Therefore, each reaction was also repeated with an increased amount of 1,3-propanediol and therefore an overall excess of hydroxy groups compared to acid groups (7%), approaching the type of formulation used for the target resin.

Table 38: Results of the reaction of ferulic acid with different levels of sebacic acid and 1,3-propanediol and COOH=OH

	equivalents		yield	NMR peak area*			peak high $M_{\bar{n}}$	peak low $M_{\bar{n}}$
reference	**y (SEB)**	**z (1,3PD)**	**weight%**	**p (SEB)**	**m (1,3PD)**	**% m1**	**%**	**%**
LH205	1,00	1,00	28	4	2,2	60	19,2	80,8
LH200	0,56	0,56	41	3,8	1,4	70	7,0	93,0
LH208	0,38	0,38	78	3,4	1,3	69	1,2	89,0**

*if the ferulic acid peak is set to 10; **a 3rd peak at 18,5 min (265 g/mol) was observed

The products were analysed by NMR, mass spectrometry, SEC, DSC and melting point analysis to determine the reason for their consistency as well as possible routes to changing them to more suitable states. In table 38, the results of the analysis for the first three products, in which equivalent amounts of acid and alcohol groups were introduced into the reaction, are presented.[XXXVIII]

Table 39: Results of the reaction of ferulic acid with different levels of sebacic acid and 1,3-propanediol, excess OH

	equivalents		yield	NMR peak area*			peak high $M_{\bar{n}}$	peak low $M_{\bar{n}}$
reference	**y (SEB)**	**z (1,3PD)**	**weight%**	**p (SEB)**	**m (1,3PD)**	**% m1**	**%**	**%**
LH213	1,00	1,10	52	7,6	3,2	65	6,3	93,7
LH211	0,50	0,57	82	3,9	3,4	31	-	-
LH212	0,38	0,44	93	3,1	1,6	55	-	-

*if the ferulic acid peak is set to 10

The results for the reactions in which an excess of around 7% of alcohol groups from 1,3-propanediol was introduced are shown in table 39. SEC analysis was only performed on the sample in which 1 and 1,1 equivalents of sebacic acid and 1,3-propanediol were used respectively.

[XXXVIII] Sebacic acid (p) and 1,3-propanediol (m) peaks were compared to the ferulic acid peak, which was set to 10. m1% denotes the amount of 1,3-propanediol reacted twice. See annexe for a description of the SEC peaks.

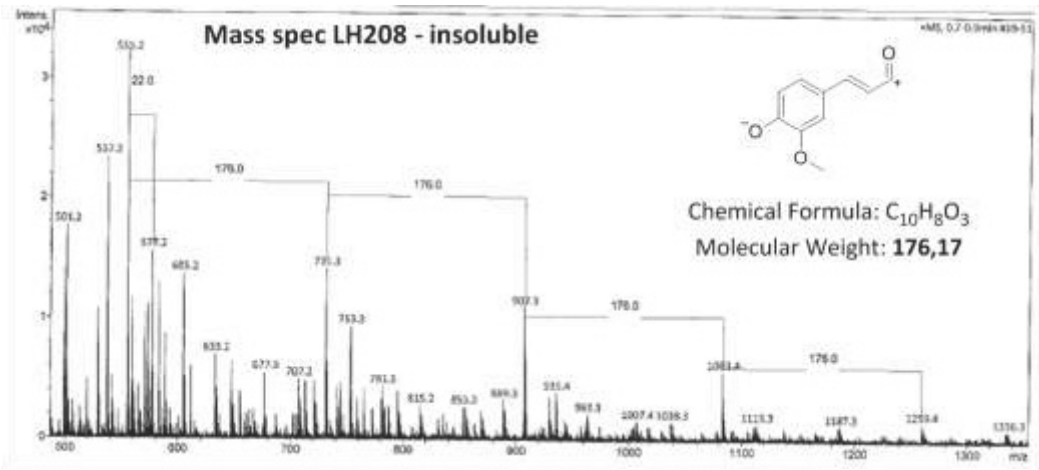

Figure 56: Mass spectrum of the insoluble product of LH208

In both the reactions with equivalent amounts of acid and hydroxy groups and those with an excess of hydroxy groups, the highest yields were obtained when the smallest amounts of sebacic acid and 1,3-propanediol were used. It can furthermore be observed that the amount of ferulic acid determined from the proportion of the peaks in the NMR was much larger than expected due to the amount of sebacic acid and 1,3-propanediol added to the reaction. The relative amounts detected in the NMR were only slightly larger for the reactions in which higher proportions of other monomers were introduced.

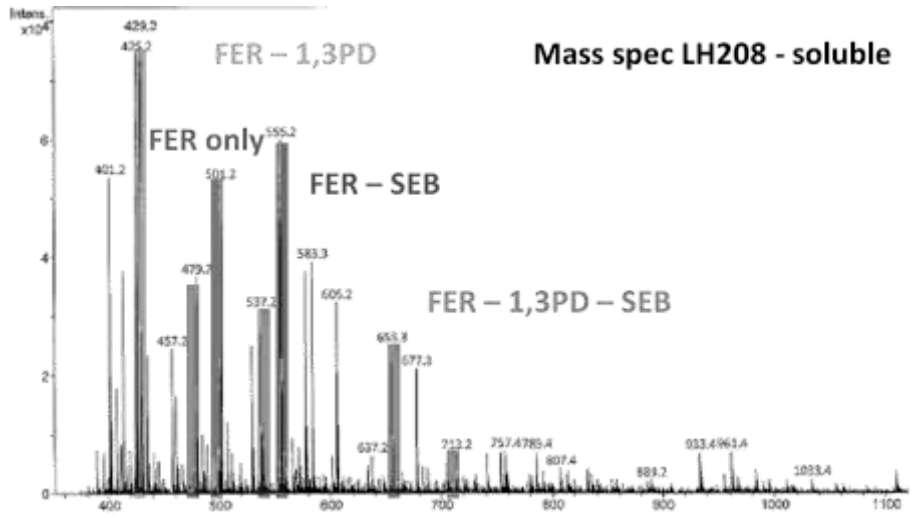

Figure 57: Mass spectrum of the soluble product of LH208

The disparity between the relative amounts of monomers added to the reaction and the NMR results as well as the decreasing yield can be explained by observation of the mass spectra. The mass spectra of the products of LH208, shown in figure 56, LH200 and LH205 all mainly show peaks corresponding to the reaction of ferulic acid with itself. After the peak corresponding to the reaction of one unit of

sebacic acid with two units of ferulic acid, a series of other peaks can be observed with a distance between peaks of 176, corresponding to the addition of more ferulic acid units to the chain.

On the other hand, analysis of the soluble fraction of LH208, shown in figure 57, reveals the presence of combinations of ferulic acid with 1,3-propanediol as well as of combinations of all three monomers. This suggests that in the reactions in which higher amounts of monomers were introduced, a larger amount of ferulic acid reacted with them and was thus extracted in the soluble fraction, decreasing the yield.

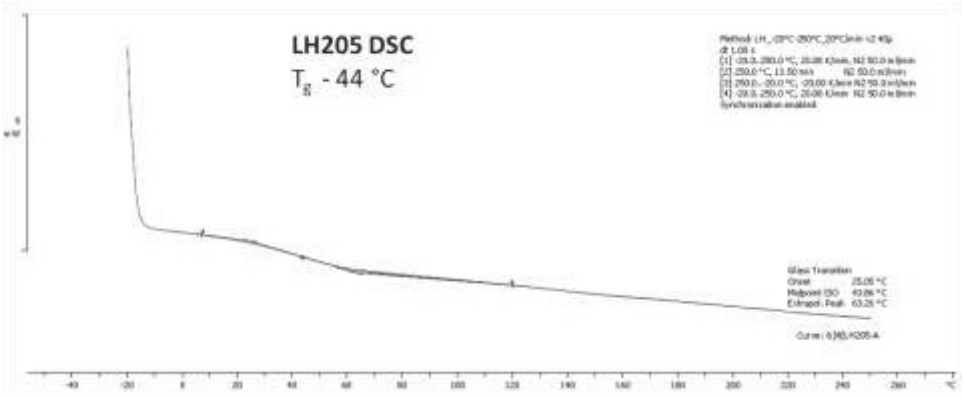

Figure 58: DSC curve for LH205 showing a glass transition

The only product for which a glass transition temperature was observed was LH205, which contained the least amount of 1,3-propanediol and sebacic acid and is shown in figure 58. All other five products showed flat curves in differential scanning calorimetry analysis.

Interestingly, the proportion of the high molecular weight peak observed in the SEC analysis increased for higher amounts of sebacic acid and 1,3-propanediol.

When comparing the products of the reactions in which equal amounts of acid and alcohol were used with those in which an excess of alcohols was used, several observations can be made. A higher incorporation of sebacic acid and 1,3-propanediol was observed in the NMR, and a lower proportion of the high molecular weight peak was seen in the one SEC analysis that was performed. Possibly due to the smaller ferulic acid content, the products could not be precipitated as easily with ethanol, and the acetone had to be evaporated in part to allow the separation to go ahead.

Table 40: Melting and decomposition temperatures of products with and without excess of OH

	reference	LH205	LH200	LH208	LH213	LH211	LH212
start of melting	**°C**	340		335	270	200	270
decomposition	**°C**	350-400	350-400			330	340

Also, more peaks corresponding to the incorporation of 1,3-propanediol and sebacic acid and overall smaller peak sizes were observed in the NMR spectra. While no glass transition was observed for any of the products from reactions with excess hydroxy groups, they melted at lower temperatures than their equivalents synthesised with equal amounts of acid and alcohols, as shown in table 40.

Overall, neither a change in ratio between the monomers used nor an excess of hydroxy group resulted in an amorphous product. The decrease in yield observed when higher amounts of 1,3-propanediol and sebacic acid were used, as well as the presence of low molecular weight combinations of all three monomers in the soluble fraction indicates that the reaction between the monomers is possible but does not go to completion.

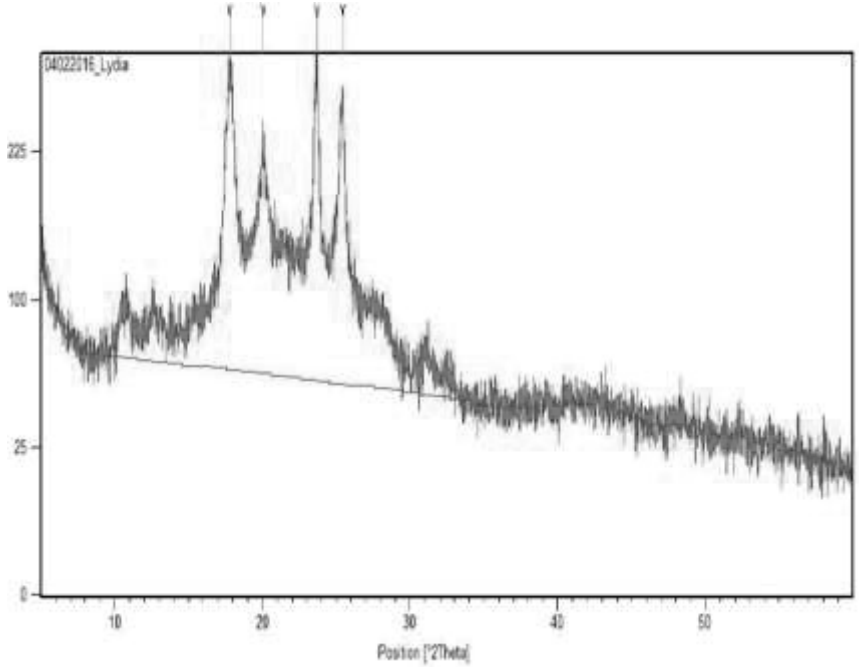

Figure 59: X-ray diffraction spectrum of LH200

Unfortunately, it was not possible to extend the reaction time to increase the completion of the polymerisation and the formation of higher molecular weight products incorporating all three monomer due to the consistency of the product, which was too hard to be stirred.

The powder nature and the melting points observed for some of the products indicate that this may be due to crystallinity in the polymer structure. An x-ray diffraction spectrum, obtained for one of the products, shown in figure 59, also displayed several peaks, indicating the presence of a regular crystal lattice.

Other reasons for the failure to form the desired amorphous polyester product with a composition corresponding to the starting materials introduced could be the loss of 1,3-propanediol through evaporation, competition between the ferulic acid phenol and 1,3-propanediol for the esterification with sebacic acid and a lack of reactivity or competing side reactions. In the following section,

different attempts made to counteract each of these factors and therefore to determine their individual relevance are described.

4.3.3.3 Changes in reaction conditions to increase the amount and degree of copolymerisation

Several measures were taken to test different theories for why the copolymerisation was not proceeding to a sufficient degree, and are presented in table 41. First, the 1,3-propanediol was replaced with 1,2-propanediol to decrease the symmetry of the polyester chain and reduce its crystallinity and therefore enable a longer reaction before hardening of the product.

For LH209, 0,56 equivalents of 1,2-propanediol and sebacic acid were used for one equivalent of ferulic acid. In all other reactions, 1 equivalent of sebacic acid and 1,1 equivalents of 1,3-propanediol were added.

The 1,2-propanediol reaction actually had to be stopped 1 hour after the Vigreux column was removed *vs.* 2,5 h in the identical reaction with 1,3-propanediol, which indicates higher crystallinity of the product. A much higher fraction of the high molecular weight peak was also observed. In the mass spectrum of the reaction, a higher amount of combinations of all three monomers was observed than when 1,3-propanediol was used.

Table 41: Results of different measures taken to improve the copolymerisation

		yield	**NMR peak area***			**peak high** $M_{\bar{n}}$	**peak low** $M_{\bar{n}}$
reference	**change**	**weight%**	**p (SEB)**	**m (1,3PD)**	**% m1**	**%**	**%**
LH209*	1,2PD	44	3	0,1	100	45,9	54,1
LH214	Fascat 4100	51	6,7	3,3	67	24,4	75,6
LH215	late addition of 1,3PD	38	4,1	3,3	61	-	-
LH223	Fascat 4100 and late addition of 1,3PD	40	5,6	3,8	66	10,8	89,2
LH225	Fascat 4100, late addition of 1,3PD, slow heating	48	10,9	12,3	59	-	-

*0,56 equivalents each of 1,2-propanediol and sebacic acid

In a second reaction, butylstannoic acid catalyst, which is often used in industrial polyesterification reactions despite its toxicity due to its efficiency, was added in addition to the sodium acetate. While this led to an increase in the high molecular weight peak, the incorporation of each monomer observed in the NMR did not change. The latter was also true for the reaction LH215, in which the 1,3-propanediol was only added after 2 h.

This indicates that neither an overall lack of reactivity, which should be remedied by the addition of a catalyst, nor the competition between the 1,3-propanediol and ferulic acid for the reaction with sebacic acid are causing the low levels of incorporation and undesirable product properties.

The most successful measure was the decrease of the heating rate. While the other reactions were heated to 175 °C from the beginning, LH225 was first heated to 155 °C for 3 h and then to 165 °C for 2 h before being raised to the same level as the other reactions. This doubled the incorporation of sebacic acid and tripled the incorporation of 1,3-propanediol observed in the NMR.

This could have two explanations. It is possible that the lack of incorporation of 1,3-propanediol and sebacic acid was due to a loss of the monomers through evaporation. While their boiling points were both more than 30 °C above the initial reaction temperature at 211 °C and 294 °C respectively, the flushing with nitrogen cause evaporation even at low temperatuers. The second explanation is that the reaction of ferulic acid with itself is more favourable, but needs higher temperatures than the reaction with the other monomers.

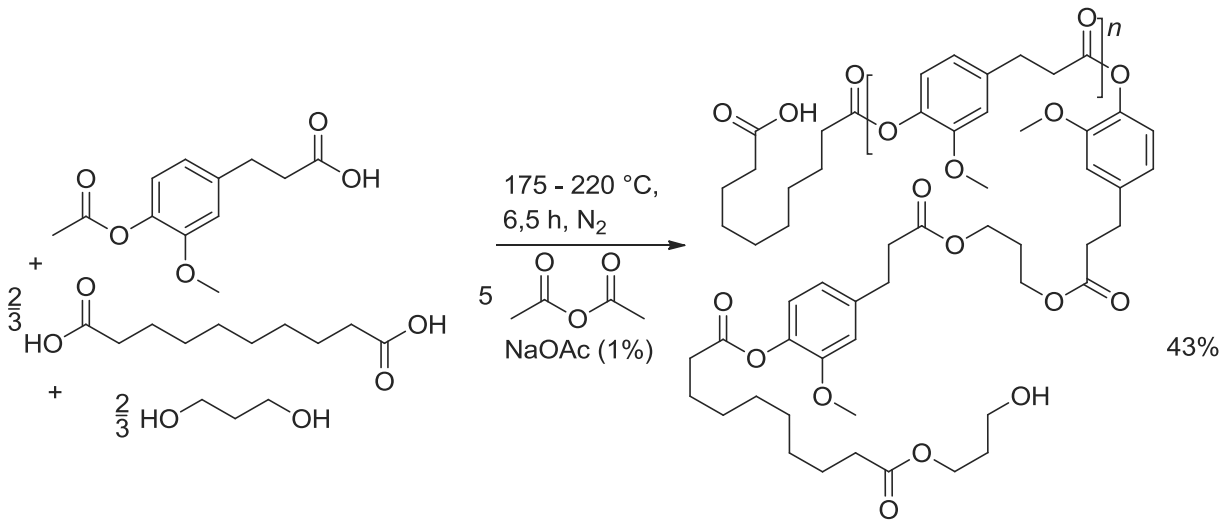

Scheme 119: Reaction LH229 with dihydroacetylferulic acid instead of ferulic acid

One reaction using dihydroacetylferulic acid instead of ferulic acid was also performed, as shown in scheme 119, to ensure that the lack of reactivity is not due to decarboxylation, which would occur much more easily on the conjugated carboxylic acid of ferulic acid. In the end, the reaction had to be stopped earlier and gave a lower yield compared to an identical reaction with ferulic acid. Therefore, it was concluded that decarboxylation was not the origin of the problem.

4.3.3.4 The use of solvent to increase the homogeneity and duration of the polymerisation

Because the reaction generally had to be stopped when stirring became impossible due to product consistency, and because low molecular weight fragments of combinations of all three monomers were observed in the mass spectra of the products as well as in the parts that were soluble in ethanol, the possibility to increase the reaction time by adding a solvent to enable the formation of higher molecular weight combinations of all monomers was investigated.

4.3.3.4.1 The choice of the solvent

In order to be suitable for the reaction, a solvent with a high boiling point to enable the high temperatures and with the capability to dissolve both the starting materials and the higher molecular weight products had to be found.

One possible candidate was *N*-methyl pyrrolidone (NMP), but due to its carcinogenic nature, several more benign alternatives were also tested. In scheme 120, the structures and boiling points of the eleven solvents tested are shown. They were chosen because they had been considered either internally in the lab or in the literature as more environmentally friendly alternatives to NMP.

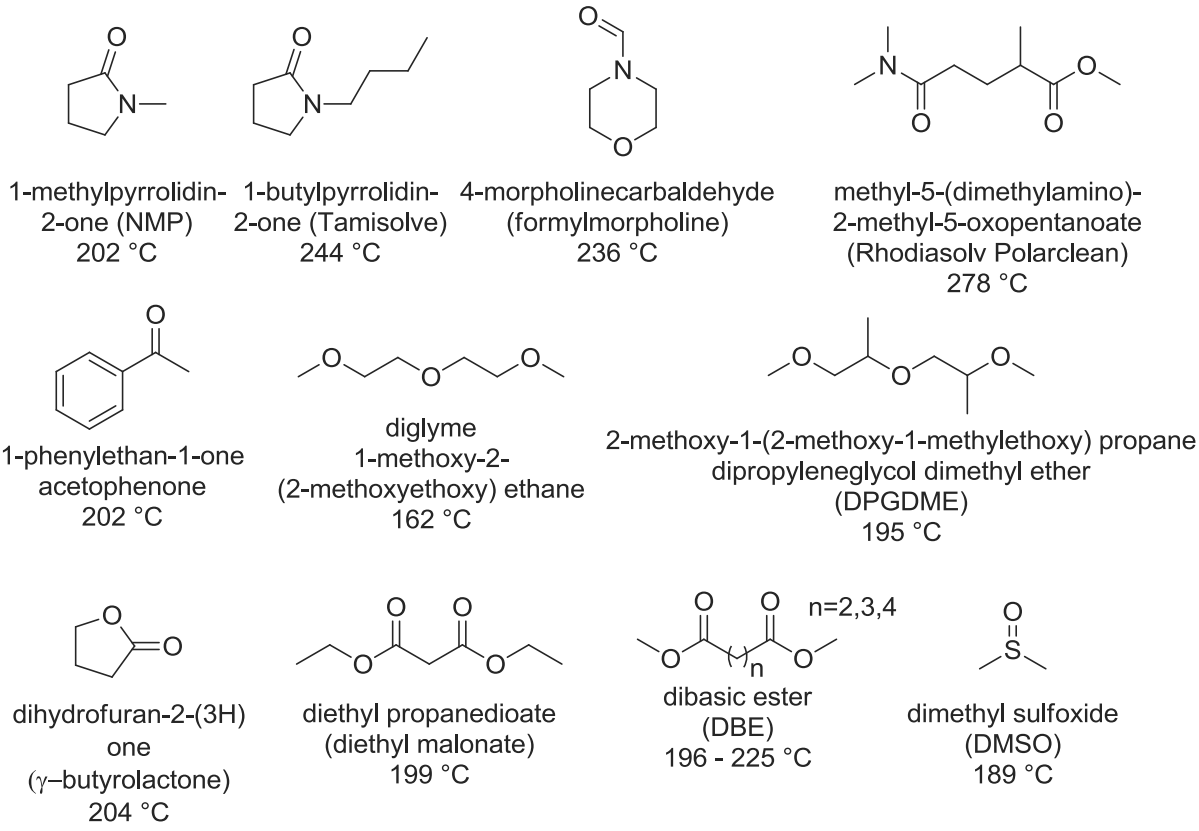

Scheme 120: Solvents and their boiling points tested for use in the polyesterification of ferulic acid

The solvents were added to a sample of the reaction product LH200 and first stirred at a concentration of 7 g/L for 19 – 20 h at room temperature. No dissolution was achieved; instead, the sample was suspended in all solvents.

The concentration was therefore decreased to 0,9 g/L, and the temperature was increased every 30 min from room temperature to 75 °C to 110 °C to 130 °C until dissolution was observed. In table 42, the lowest temperature at which LH200 was dissolved after 30 min of stirring or, where no dissolution was achieved, the observations made after 30 min at 130 °C, are presented.

Table 42: Solubility of LH200 at 0,9 g/L in NMP analogue solvents at different temperatures

	temperature	**observation**	
solvent	**°C**	**after 30 min**	**after cooling down**
NMP	110	dissolved	stays in solution
formylmorpholine	110		
Tamisolve	130	dissolved	stays in solution
Rhodiasolv Polarclean	130	partially dissolved, clearer suspension	precipitates
acetophenone	130		
γ-butyrolactone	130		
diglyme	130	not soluble, suspension	-
DPGDME	130		
diethyl malonate	130		
DBE	130		
DMSO	110	dissolved	becomes hazy, suspension

Four solvents capable of dissolving the sample of LH200 at a concentration of 0,9 g/L at high temperatures were found. Of those, it was decided that Tamisolve and formylmorpholine were the best choices due to their higher environmental compatibility compared to NMP and due to the fact that the product stayed in solution even after cooling down, contrary to DMSO. A series of reactions was therefore tested in Tamisolve solvent to explore the effect on the product properties.

4.3.3.4.2 Reactions in Tamisolve solvent

The reactions in Tamisolve were performed at a concentration of 1,6 – 2 g/L of solid material in the solvent, and with 1,2-propanediol instead of 1,3-propanediol, as shown in scheme 121. Additionally in all reactions except for the second reaction LH245, the temperature was raised slowly to enable the reaction of 1,2-propanediol and sebacic acid with ferulic acid prior to the reaction of ferulic acid with itself.

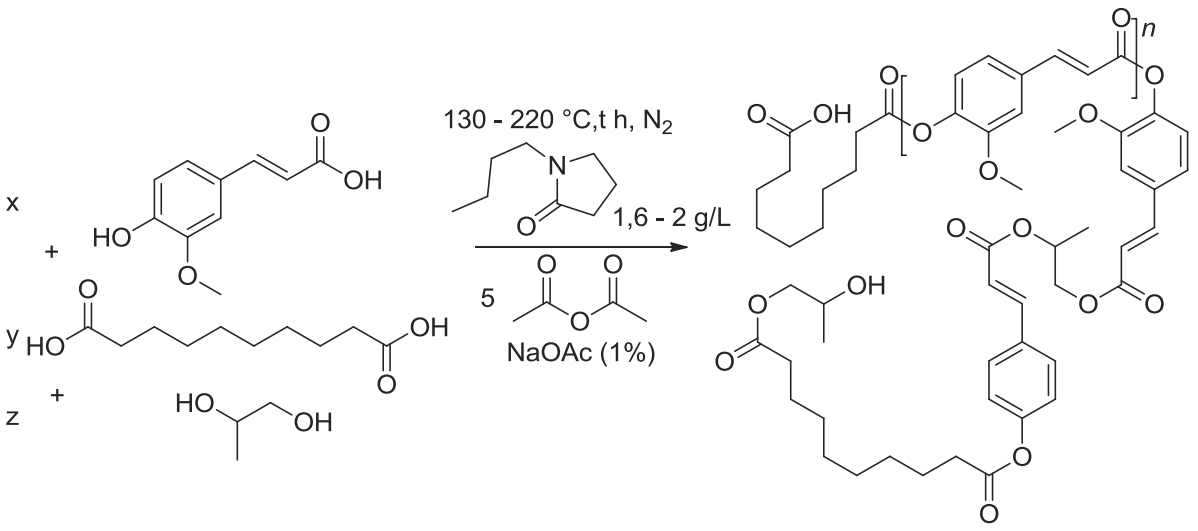

Scheme 121: Ferulic acid polymerisation with 1,2-propanediol and sebacic acid in Tamisolve

This method enabled much higher reactions times than had been reached without solvent. However, contrary to the example of LH209, in which 1,2-propanediol was also used and which resulted in a much higher fraction of high molecular weight product detected in SEC, the molecular weight distribution was very similar to that observed for the other products, as shown in table 43.

Table 43: Results of reactions in Tamisolve solvent

	equivalents		time t	yield	peak high $M_{\bar{n}}$	peak low $M_{\bar{n}}$	peak 835 g/mol
reference	**y (SEB)**	**z (1,3PD)**	**h**	**weight%**	**%**	**%**	**%**
LH244	0,27	0,27	17,5	22	2,9	97,1	-
LH245*	0,38	0,38	22	31	20,0	80,0	-
LH246	0,38	0,38	28	50	3,7	96,3	-
LH247	1,00	1,00	33	32	14,0	39,5	46,5

* the reaction was heated to 175 °C straight away instead of slow heating

It was difficult to determine whether the amount of incorporation of 1,2-propanediol and sebacic acid into the product has changed thanks to the presence of the solvent because the separation from the solvent proved to be very difficult. While it was in part evaporated by vacuum distillation, it was impossible to remove the Tamisolve completely after the end of the reaction. No precipitation was observed even when ethanol was added to the solution.

Because of the overlap of Tamisolve peaks in the NMR with those corresponding to reacted 1,2-propanediol and sebacic acid, the examination of the product composition with NMR was impossible. Analysis of the thermal behaviour using DSC, shown in figure 60, and melting point analysis was also not very fruitful.

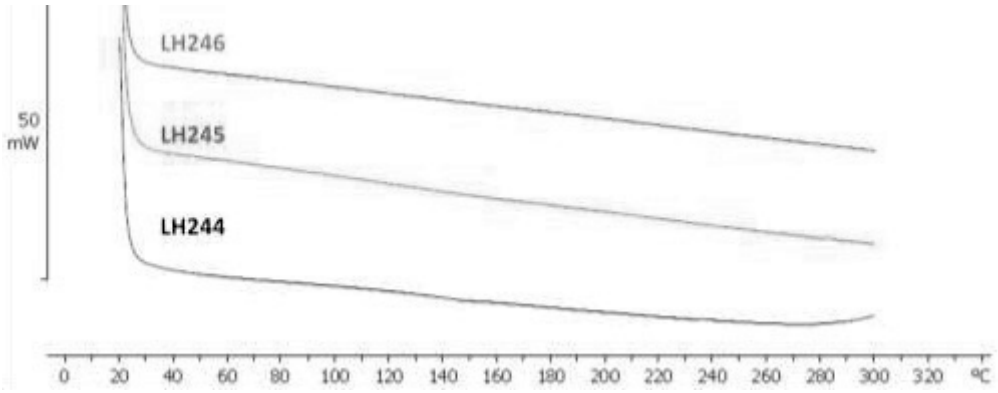

Figure 60: DSC curves of products synthesised with Tamisolve solvent

The product was however still a powder and no glass transition was visible in the DSC curves as for the other products formed. All decomposed before melting at 340 °C – 380 °C. Because no improvement was observed in the SEC analysis, DSC profiles and consistency of the products, and because the nature of the Tamisolve made the NMR analysis more difficult and the purification impossible, it was discarded as an option to improve the reaction outcome.

4.3.3.5 The importance and role of acetic anhydride

In order to fully elucidate the mechanism and obstacles towards copolymerisation during the reaction, several reactions were performed without acetic anhydride. Because decarboxylation was observed when ferulic acid was reacted without acetic anhydride, the reactions were conducted at 130 °C. An excess of 1,3-propanediol was used to enable stirring and homogenisation of the products. No purification was performed in order to be able to characterise all products at once.

Instead, three different yields are presented. The first corresponds to the relative amount of weight left in the flask after the reaction. While a certain weight loss due to water loss can be expected, the differences between the products nevertheless provide information about the amount of monomers evaporated during the reaction.

The amount of starting materials *vs.* reacted products still present afterwards was determined by NMR, and is shown as conversion. Lastly, the weight yield was multiplied with the conversion to obtain an approximation of the overall product yield.

The majority of the products had more promising consistencies than those obtained when acetic anhydride was used. Several resembled resins and had a clear aspect directly after the reaction, even though precipitation and phase separation was observed after several weeks probably due to the presence of the starting materials. Analysis with differential scanning calorimetry revealed glass transitions for the majority of the products, which are also reported below.

4.3.3.5.1 Catalyst study

Two different aspects of the reaction were studied. First, it was performed with 0,34 equivalents sebacic acid, 2,3 equivalents 1,3-propanediol and 3,5 mol% of *p*TSA, butylstannoic acid or no catalyst. The reaction with *p*TSA catalyst was repeated with one equivalent of sebacic acid and 4,7 mol% of catalyst, as shown in scheme 122.

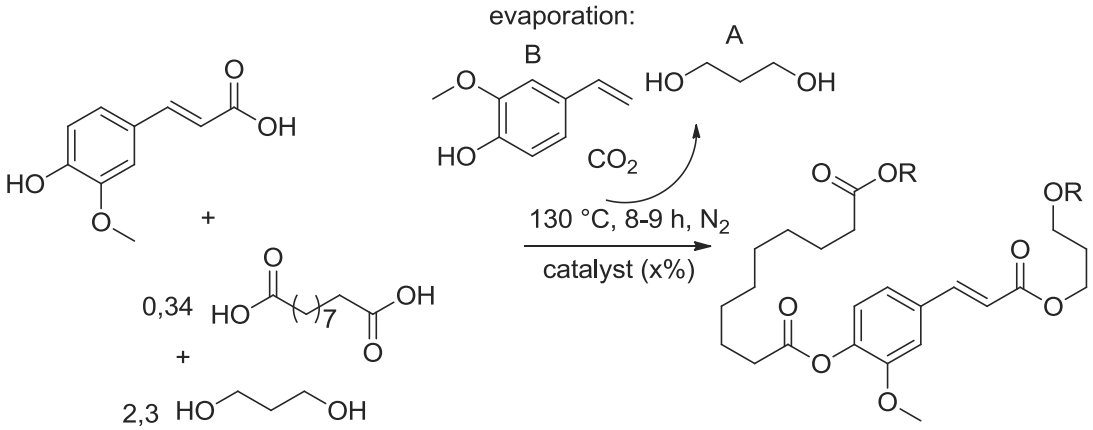

Scheme 122: Reaction of ferulic acid with 1,3-propanediol and sebacic acid without acetic anhydride - catalysis

Nitrogen was bubbled through the reaction, and the evaporation products were monitored. Despite the fact that the reaction was conducted 80 °C below the boiling point of 1,3-propanediol, evaporation was still observed in every reaction. In the reaction without catalyst and with a butylstannoic acid catalyst, a small amount (1-2%) of ferulic acid decarboxylation product (B) was also discovered.

Table 44: Results of catalyst study with ferulic acid, sebacic acid, 1,3-propanediol but no acetic anhydride

			yield $_{mass}$	**conversion**	**yield $_{overall}$**	**T_g onset**	**T_g midpoint**
reference	**catalyst**	**mol %**	**weight %**	**% NMR**	**product**	**°C**	**°C**
LH278	-	-	72	12	9	-	-
LH254	*p*TSA	3,5	52	20	10	1	8
LH274*		4,7	85	45	38	-62	-53
LH275	Fascat 4100	3,5	64	44	28	-12	-13

* using 1 equivalent of sebacic acid instead of 0,34

The highest mass yield and therefore the least evaporation were observed for the reaction LH274, in which the difference between acid and alcohol groups was smallest since a higher amount of sebacic acid was used. This reaction also showed the highest conversion and therefore the highest overall yield, as shown in table 44.

However, the SEC analysis revealed that only 41% of the product was polymerised to a number average molecular weight of 2233 g/mol, while the remaining 59% only had an average molecular

weight of 917 g/mol, as shown in table 45. This was also reflected in a very low glass transition temperature with a midpoint at -53 °C.

Table 45: SEC results for the catalyst study

	peak 1 (8 - 11 min)			peak 2 (14 - 15 min)			peak 3 (15 - 16 min)		
	$M_{\bar{n}}$	$M_{\bar{w}}$	area %	$M_{\bar{n}}$	$M_{\bar{w}}$	area %	$M_{\bar{n}}$	$M_{\bar{w}}$	area %
LH254	21089	22218	0,7	1626	2061	99,3	-	-	-
LH275	58487	60745	2,4	1142	1329	97,6	-	-	-
LH278	-	-	-				964	989	100,0
LH274	-	-	-	2233	2692	40,9	917	927	59,1

The second highest conversion and molecular weight was observed for the reaction with butylstannoic acid catalyst. The lowest molecular weight and overall yield were observed for the reaction in which no catalyst was used.

While a smaller proportion of the starting material was observed to evaporate in the absence of a catalyst, which could also be due to the fact that less water was lost, only 12% of the remaining material had been converted to an ester. SEC analysis revealed that the molecular weight of the product was below 1000 g/mol. This confirms the necessity to use a catalyst in the reaction, and the benefit of the other catalysts used.

Both products of the reactions LH254 and LH275 had glass transition temperatures and molecular weights which are not far from the target properties of resins.

4.3.3.5.2 Reaction atmosphere study

Because evaporation of 1,3-propanediol was observed in all reactions in the catalyst study described above, the second aspect which was examined was changes that could be made to the reaction vessel and atmosphere to better control the composition of the product.

As shown in scheme 123, a *p*TSA catalyst at 3,5% was used in all reactions and the ratio of ferulic acid, sebacic acid and 1,3-propanediol was kept at 1 : 0,34 : 2,3. Four different set-ups were tested. In the first reaction (LH276), the flask was filled with nitrogen and then closed, while in the second reaction, nitrogen was bubbled through for the duration of the reaction (LH277). In a third reaction (LH279), the flask was filled with nitrogen and closed for 14 h of reaction, and then opened with a nitrogen bubble for another 10 h. Finally, in the last reaction (LH280), the nitrogen bubble was followed by 1,5 h of vacuum.

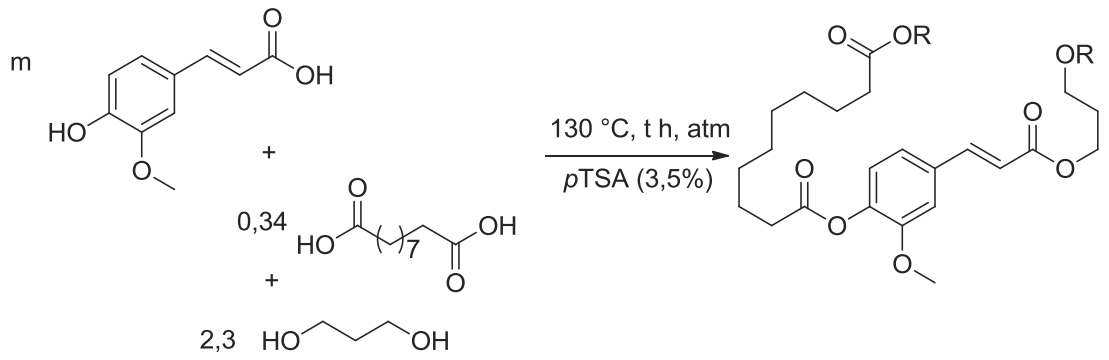

Scheme 123: Reaction of ferulic acid, sebacic acid and 1,3-propanediol without acetic anhydride - different atmospheres

The scale and overall reaction time was also varied as shown in table 46 below.

Interestingly, the yield was not improved by closing the reactor instead of bubbling nitrogen through it. In fact, the highest amount of product was lost in the closed reaction. Both yield and conversion were however increased when the reactor was closed for 14 h followed by bubbling nitrogen through it for 10 h.

Table 46: Results of different polyesterification set-ups without acetic anhydride

	m	time	atmosphere	yield $_{mass}$	conversion	yield $_{overall}$	T_g
reference	**mmol**	**h**		**weight %**	**% NMR**	**product**	**°C**
LH276	5,15	7,8	N_2 (closed)	48	52	25	-54
LH277	25,75	17,8	N_2 (bubble)	75	41	31	3
LH279	5,15	14 + 10	N_2 (closed) + N_2 (bubble)	84	83	70	5
LH280	25,75	24 + 1,5	N_2 (bubble) + vacuum	65	16	25	-7

The SEC analysis, shown in table 47, revealed however that the reaction product LH279 in which the reaction was closed still contained 26% of low molecular weight components of around 880 g/mol. Despite the fact that its molecular weight was overall significantly larger, the last reaction, in which 1,5 h of vacuum were used to remove volatile compounds and push the reaction further towards completion, had a lower glass transition temperature.

Table 47: SEC results for the study of different atmospheres

	peak 1 (8 - 11 min)			peak 2 (14 - 15 min)			peak 3 (15 - 16 min)		
reference	$M_{\bar{n}}$	$M_{\bar{w}}$	**area %**	$M_{\bar{n}}$	$M_{\bar{w}}$	**area %**	$M_{\bar{n}}$	$M_{\bar{w}}$	**area %**
LH279	20175	20568	1,2	2095	2836	72,8	881	884	25,9
LH280	26473	26890	2,2	1362	1654	97,8	-	-	-

Overall, with the exception of the first reaction which was closed for its entire duration, the reaction products again showed glass transition temperatures close to those that are targeted in the resin synthesis, as shown in figure 61.

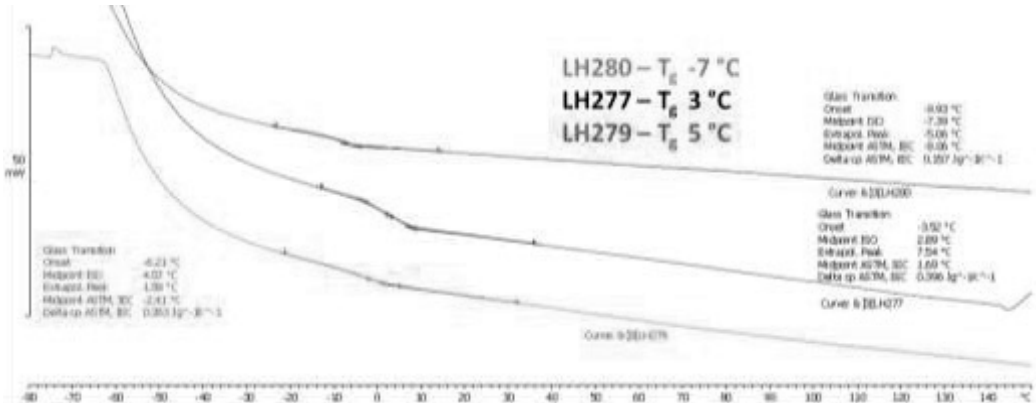

Figure 61: DSC curve examples of products made without acetic anhydride

4.3.3.6 Possibilities for the optimisation of the reaction design

Overall, the results of the polyesterification of ferulic acid with sebacic acid and 1,3-propanediol or 1,2-propanediol were promising. Molecular weights of several thousand g/mol were obtained and where no acetic anhydride was used in the reaction, partially amorphous products displaying glass transition temperatures not far from the target were observed.

However, the relative reactivity of the ferulic acid groups towards other ferulic acid molecules compared to their reactivity towards other monomers remains an unsolved problem. While ferulic acid is activated in the presence of acetic anhydride, leading to the formation of molecules with high molecular weights, the formation of homopolymers or of products with relatively low content of other monomer units is favoured.

These products were proven to be crystalline, which is not desirable for the use in paints, and their increased formation stops the progress of the reaction as it can no longer be stirred. While the incorporation of non ferulic acid units could be increased through slower heating and by increasing their relative amounts at the start of the reaction, no products that were not crystalline were obtained.

The addition of a butylstannoic acid catalyst and the addition of 1,3-propanediol later in the reaction as well as the replacement of 1,3-propanediol with 1,2-propanediol was not effective, either. Several solvents were investigated to enable continued reaction despite the crystalline nature of the product, but no significant changes in the nature of the product were observed. This suggests that the relative reactivity and not the limited reaction time is the most problematic obstacle.

The copolyesterification was found to be more successful in the absence of acetic anhydride. However, decarboxylation of the ferulic acid was also observed, limiting the reaction temperature to 130 °C. Furthermore, an excess of 1,3-propanediol had to be used in the absence of acetic anhydride to ensure homogenisation of the reaction, making it very difficult to precisely control the composition of the product. As a consequence, only low molecular weight products were obtained and the conversion to ester products was low despite long reaction times.

Possible solutions to this problem could be the addition of acetic anhydride after a certain reaction time without it. In order to better control the composition during the acetic anhydride free phase, the use of a less reactive solvent such as methoxypropyl acetate (MPA) could be tested. If the solvent doesn't have to be separated from the final product, and the incorporation of sebacic acid and 1,3-propanediol in the first step prevent the formation of crystalline, insoluble product, a larger choice of solvents may be suitable. In order to avoid waste, the minimum amount of acetic anhydride needed as well as a reactor structure that avoids excessive loss of the solvent also needs to be found.

In conclusion, this work provided interesting insights concerning the reaction and the problems that need to be solved to enable the copolyesterification of ferulic acid. While promising molecular weights and glass transition temperatures were observed, all obstacles could not yet be solved with the methods tested.

4.4 The potential of vanillin and vanillin derivatives as new monomers for polyester resins

The lack of reactivity of the vanillin phenol group was identified as a main obstacle for its incorporation into a polyester. It was attributed to the electronegative presence of the methoxy group discouraging the approach of acidic molecules for esterification. While no catalysts effective enough to overcome this factor could be identified, the problem was successfully solved by using anhydrides either as reaction substrates or as reactive solvents.

The Perkin reaction of vanillin, the hydrogenation of the product and the homopolymerisation of dihydroacetylferulic acid were also successfully replicated from the literature, and the molecular weight of the product was confirmed for the first time using SEC. Examination of the products revealed their crystalline nature, as well as little dependence of the yield and molecular weights on the catalysts used.

The introduction of the additional monomers succinic acid and 1,3-propanediol only resulted in lower homopolymer yields and the formation of low molecular weight combinations of all three monomers, but no high molecular weight copolymers were obtained.

The reason for this was investigated using ferulic acid, sebacic acid and 1,3-propanediol or 1,2-propanediol. It was discovered that at high temperatures and in the presence of acetic anhydride, the reaction of ferulic acid with itself is favourable to that with other monomers, especially 1,3-propanediol. Despite various changes made to the reaction procedure, no products incorporating enough of the comonomers to be amorphous were obtained when acetic anhydride was added to the reaction.

Without acetic anhydride, decarboxylation was observed at high temperatures and low temperatures resulted in incomplete reactions despite long durations. Nevertheless, the partial formation of polyesters with suitable glass transition temperatures was observed.

In conclusion, a variety of aspects of the incorporation of vanillin and derivatives was investigated, and valuable insights into obstacles and possible solutions were gained, even though no final resin product could be obtained yet. The synthesis and evaluation of resins based on more reactive and available monomers from renewable resources will be discussed in the following two chapters.

5 New biosourced polyester resins with a wide range of properties

While the supply of rigid biobased monomers may be limited, a selection of linear products with different chain lengths, functionalities and degree of branching is already widely commercially available. Monomers such as 1,2-propanediol, succinic acid and sebacic acid have been used in a large number of polyester products, even if their use in coil coating resins is mostly unexplored.

The properties of coil coating resins are determined by the choice of monomers used in the synthesis, but the composition, i.e. the relative amount of monomers incorporated in the resin, is just as important. Therefore, the qualitative and quantitative study of the effect that different biobased monomers create is worthwhile both to expand the space of biobased resins and to help target specific desirable properties.

Within the Sorago project, Arkema proposed a resin fully based on renewable monomers for use in coil coating products destined for interior applications. The rigidity was provided by isosorbide at a level of 30 mol%, and preliminary tests revealed insufficient weatherability for exterior applications. Nevertheless, the resin, which was adjusted to be suitable for application on a coil coating line, could be used as a basis to explore different changes to the composition while remaining in a formulation space likely to fit the purpose.

Compared to most purely petrol based monomers used in exterior coil coating products, isosorbide introduces additional susceptibility to degradation through the two ether linkages. They introduce polarity to the structure, which makes it more prone to hydrolysis, and also increase the liability to abstraction for neighbouring hydrogen atoms.

Therefore, the effect of isosorbide in a resin was compared to that of petroleum based phthalic anhydride, a rigidity inducing monomer used in some petroleum based formulation, which doesn't contain ether linkages but absorbs considerably more UV light. Partially biosourced resins based on phthalic anhydride, which are easier to synthesise due to the anhydride reactivity, were also used to evaluate ways to introduce rigidity and replace isosorbide with other biosourced monomers.

The solubility and viscosity of the modified formulations were characterised, and suitable resins were cured with melamine to examine their crosslinking behaviour. A relationship between formulation and mechanical properties as well as glass transition temperatures was established.

5.1 Resin design

The studied formulations were based on the fully biosourced resin proposed by Arkema for interior use. In order to be able to separate the effect of each monomer most effectively, changes were

made step by step, only replacing one monomer at a time. Most importantly, the main resin design parameters such as the ratio of acid and alcohol groups in the formulation and the functionality, which represents the number of functional groups per molecule and is used to determine the risk of gel formation, were kept constant.

5.1.1 Arkema's isosorbide resin for interior applications

The formulation of Arkema's resin was based on the currently used petroleum based resin. It contains phthalic anhydride as a rigidity inducing monomers, adipic acid as a linear acid, neopentyl glycol as a branched diol and trimethylol propane as a triol. The monomers were first replaced one by one with biosourced alternative, as shown in scheme 124, and then the relative quantities were adjusted until a resin with suitable viscosity and glass transition temperature for coil coating applications was created.

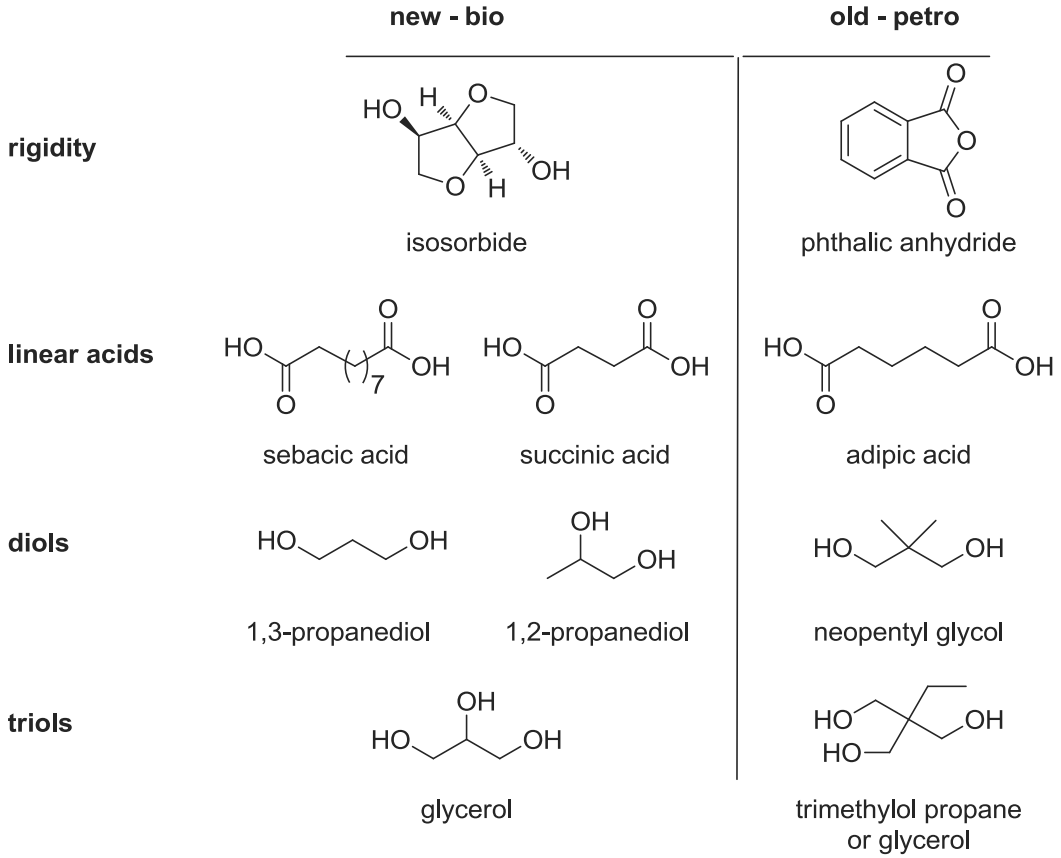

Scheme 124: Design of a biobased resin for the interior

Isosorbide (ISO) was used to provide rigidity instead of phthalic anhydride (PAN), and a mixture of the longer chain sebacic acid (SEB) and the shorter chain succinic acid (SUC) were used to replace adipic acid (ADI). Both 1,3-propanediol (1,3PD) and 1,2-propanediol (1,2PD) were tested as replacements for neopentyl glycol (NPG), and glycerol (GLY) was used to substitute trimethylol propane. The final formulation is shown in table 48 below.

Table 48: Formulation of biobased and petrosourced resins

Biobased resin		Petrosourced resin	
monomers	**mol%**	**monomers**	**mol%**
ISO	29,37	PAN	35,72
SUC	35,24	ADI	13,53
SEB	13,49		
1,2 PD	15,76	NPG	44,03
GLY	6,14	GLY	6,72

When comparing the formulations, we can see that slightly less isosorbide is necessary to maintain the glass transition temperature compared to the phthalic anhydride. Furthermore, the glycerol content was slightly reduced, and 1,2-propanediol was determined as the better replacement for neopentyl glycol.

5.1.2 Modification of the isosorbide based resins

Two sets of isosorbide based resins were synthesised. A possible chain composition is shown in scheme 125 below, but the order of the individual monomers is assumed to be random, so that many different arrangements are possible.

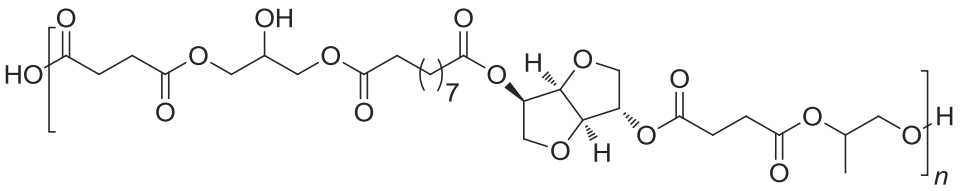

Scheme 125: Possible sequence in an isosorbide type polyester

5.1.2.1 Increased and decreased isosorbide content

The first set of isosorbide resins was synthesised to explore the effect isosorbide has on the resin properties. The quantity of isosorbide was varied between 19,37 mol% and 45,13 mol%. As described above, the ratio of acid to alcohol groups in the resin was kept constant, in this case at an excess of 1,115 alcohol groups per acid group. In order to achieve this, an equimolar amount of 1,2-propanediol was exchanged for isosorbide in the formulations. The relative amounts of all other monomers were kept constant at the level proposed by Arkema.

Table 49 below shows the different resins synthesised in this set, as well as their reference numbers, which will be used throughout the rest of the thesis. The resin containing 29,37 mol% isosorbide is equivalent to the resin proposed by Arkema for interior applications.

Table 49: Resins with different isosorbide contents

resin reference	isosorbide content	1,2-propanediol content	OH-value$_{theoretical}$
	mol%	mol%	mg$_{KOH}$/g
LH249	19,37	25,76	59,99
LH190	24,37	20,76	58,05
LH184	29,37	15,76	56,24
LH040	34,37	10,76	54,53
LH243	39,37	5,76	52,93
LH248	45,13	0	51,19

Due to the difference in weight between isosorbide and 1,2-propanediol, their theoretical hydroxy value, which is calculated from the amount of alcohol groups present per gram of resin, changes even though the molar amount of hydroxy groups is kept constant.[XXXIX]

5.1.3 Formulation of a partially biosourced resin

In order to study the effect of the isosorbide monomers, and to explore the effect of other monomers, a resin with an equivalent formulation but containing phthalic anhydride instead of isosorbide was designed.

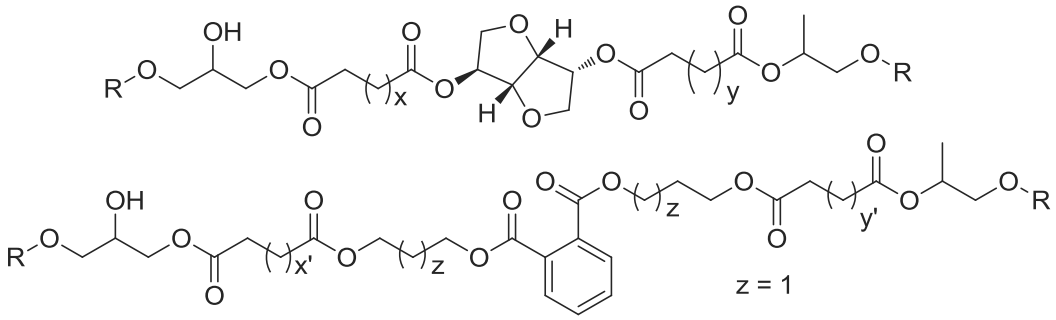

Scheme 126: Segments of isosorbide and phthalic anhydride resins illustrating the replacement of monomers

Table 50: Phthalic anhydride formulation equivalent to isosorbide resin

Monomer	mol %
PAN	29,37
SUC	10,77
SEB	8,60
1,2PD	15,76
GLY	6,14
1,3PD	29,37

Because phthalic anhydride reacts as the equivalent of two acids while isosorbide is a diol, a one to one replacement as such is not possible. Instead, the other acid and alcohol monomers were adjusted to keep the number of linear chain segments, denoted x,y and z below, constant and obtain two formulations as close to each other as possible, as illustrated in scheme 126.[XL]

[XXXIX] The possibility of keeping the hydroxy value constant was studied on several prototypes, but only LH168, which had a similar isosorbide content to LH040, was kept for further testing due to more promising properties. Details can be found in the annexe.

[XL] The exact process used to calculate the amount of different monomers is explained in the annexe.

The ratio of alcohol to acid groups was kept a 1,115 this way, as well as the resin functionality. The theoretical hydroxy value changed to 62,11 mg_{KOH}/g. The formulation is shown in table 50.

5.1.4 Single monomer modifications of the partially biosourced resin

Due to the higher reactivity and thermal stability of phthalic anhydride compared to isosorbide, the synthesis of phthalic anhydride based resins was both faster and crowned by a higher success rate. Therefore, it was decided to investigate the effect of the other biobased monomers by modifying the partially biobased formulation.

5.1.4.1 Changes in linear monomers

The phthalic anhydride based resin contains five biobased monomers, namely succinic acid, sebacic acid, 1,3-propanediol, 1,2-propanediol and glycerol. In order to evaluate the effect of each, five modified resins were synthesised. In order to maximise the comparability between the new resins, and to single out the effect of the monomer in question, the ratio of alcohol to acid groups and resin functionality was again kept constant, as shown in table 51.

Table 51: Composition of resins for the evaluation of the effect of each biobased monomer

resin composition	LH174	LH177	LH181	LH182	LH219
(mol%)	succinic acid	sebacic acid	1,3-propanediol	1,2-propanediol	glycerol
PAN	29,37	29,37	29,37	29,37	29,79
SUC	19,36	-	10,77	10,77	10,92
SEB	-	19,36	8,60	8,60	8,72
1,2PD	15,76	15,76	-	45,13	14,47
1,3PD	29,37	29,37	45,13	-	26,83
GLY	6,14	6,14	6,14	6,14	9,27

In the first four, one monomer was completely replaced by the other with identical functional groups. Succinic acid was completely replaced with sebacic acid and vice versa, and 1,2-propanediol was completely replaced with 1,3-propanediol and vice versa. In order to test the effect of glycerol, it was increased from 6,14 mol% to 9,27 mol%. The additional alcohol groups were compensated for by decreasing the amount of 1,2-propanediol and 1,3-propanediol present in the formulation, while keeping their ratio constant.

5.1.4.2 Increased and decreased phthalic anhydride content

In order to quantitatively compare the effect of isosorbide and phthalic anhydride as rigidity inducing monomers, a series of resins mirroring the resins with different quantities of isosorbide was created. Imitating the isosorbide resins, the quantity of phthalic anhydride was varied between 9,37 mol%

and 48,73 mol%, and the additional acid groups were compensated for with succinic acid and sebacic acid, while the ratio of the two monomers was kept constant, as shown in table 52.

The resin with 29,37 mol% of phthalic anhydride (LH189) represents the equivalent to the isosorbide resin proposed by Arkema for interior applications described in the section above. The resins were all crosslinked and tested for their film properties with the exception of LH239 and LH165, containing 9,37 mol% and 39,37 mol% of phthalic anhydride, due to the lack of capacity.

Table 52: Resins with decreased and increased phthalic anhydride content

resin reference	phthalic anhydride	succinic acid	sebacic acid	OH-value$_{theoretical}$
	mol%	mol%	mol%	mg$_{KOH}$/g
LH239	9,37	21,50	17,86	63,24
LH237	19,37	16,13	13,23	62,67
LH162	24,37	13,27	11,10	62,29
LH189	29,37	10,77	8,60	62,11
LH163	34,37	8,27	6,10	61,93
LH165	39,37	5,77	3,60	61,75
LH242	48,73	0	0	60,88

5.1.5 Mapping out the possibilities of partially biobased resins

After determining the effect achievable with each monomer, the design possibilities for partially biosourced resins were mapped out. Three different aspects were investigated. Firstly, different ways to maximise the glass transition temperature were tested. The results then served to determine the minimum amount of phthalic anhydride necessary for an acceptably rigid resin. Lastly, the possibility to incorporate other monomers into the resins was evaluated.

5.1.5.1 Maximising the glass transition temperature of partially biosourced resins

In order to maximise the glass transition temperature of the phthalic anhydride based resins and to test whether the observed effects of the monomers are additive, the changes that caused the largest increase in T_g were combined. Therefore, a resin in which both sebacic acid and 1,3-propanediol were completely replaced with succinic acid and 1,2-propanediol, as well as two resins with an increased phthalic anhydride content, in which either sebacic acid or 1,3-propanediol was replaced were synthesised, as shown in table 53.

The combination of an increased phthalic anhydride content with only succinic acid and 1,2-propanediol resulted in the formation of a gel. A similar resin was therefore synthesised in which sebacic acid was completely replaced by succinic acid, but some 1,3-propanediol was left in the formulation (LH199).

Table 53: Resins combining the changes with lead to an increased glass transition temperature

composition mol%	LH192	LH193	LH196	LH199	gel_{LH195}
PAN	29,37	34,37	34,37	34,37	34,37
SUC	19,36	8,27	14,36	14,36	14,36
SEB	-	6,10	-	-	-
1,2PD	45,13	45,13	15,76	25,76	45,13
1,3PD	-	-	29,37	19,37	-
GLY	6,14	6,14	6,14	6,14	6,14

5.1.5.2 Minimisation of phthalic anhydride content

The observations from the previous section were used to determine the minimum amount of phthalic anhydride necessary in the resin formulation. As phthalic anhydride represents the only petroleum sourced monomer in the formulation, its replacement with the other monomers is desirable. However, as its structure fulfils an important role in the resin, ways to substitute for the rigidity were explored.

Several prototypes, in which phthalic anhydride was gradually replaced by the other rigidity inducing monomers 1,2-propanediol and succinic acid were therefore synthesised, as shown in table 54. It was found that a decrease of phthalic anhydride down to 9,37 mol% could be compensated for in terms of glass transition temperature.

Table 54: Resins with minimised petro-sourced content

composition mol%	LH228	LH231	LH234	LH238	gel_{LH233}
PAN	24,37	19,37	14,37	9,37	14,37
SUC	24,36	29,36	30,36	35,36	34,36
SEB		-	4,00	4,00	-
1,2PD	45,13	45,13	45,13	45,13	45,13
GLY	6,14	6,14	6,14	6,14	6,14

Two resins (LH228 and LH231) were successfully synthesised with reduced phthalic anhydride content and without any 1,3-propanediol or sebacic acid. However when only 14,37% of phthalic anhydride were left in the formulation, a gel was formed. Therefore, the synthesis was repeated, reintroducing 4,00 mol% sebacic acid to replace 4,00 mol% of succinic acid. Two prototypes, one with and one without sebacic acid (LH231 and LH238) were selected to be tested for their film properties.

5.1.5.3 Incorporation of cyclohexanedicarboxylic acid

A series of prototypes in which phthalic anhydride was replaced with cyclohexanedicarboxylic acid (CHDA) was also prepared, as shown in table 55. They were based on the formulations containing the

minimum amount of phthalic anhydride acceptable. While cyclohexanedicarboxylic acid is a little less reactive than phthalic anhydride, it also has a much lower absorption of UV light due to its aliphatic nature and is often used to confer weatherability for exterior applications. Its higher price presents an additional incentive to minimise the amount of CHDA used to its petroleum based origin.

Table 55: Formulations of CHDA containing prototypes

composition mol%	LH265	LH272	gel_{LH270}	gel_{LH273}
CHDA	9,37	14,26	14,37	9,45
SUC	35,36	10,68	30,36	31,04
SEB	4,00	23,42	4,00	8,67
1,2PD	45,13	44,79	45,13	43,14
GLY	6,14	6,84	6,14	7,71

The one to one replacement of phthalic anhydride with cyclohexanedicarboxylic acid resulted in a drop of glass transition temperature from -5 °C to -12 °C. Therefore, different modifications were made to increase the level of rigid monomers. The increase of cyclohexanedicarboxylic acid or glycerol led to the formation of gels in the end of the reaction. Only the simultaneous increase of the level of cyclohexanedicarboxylic acid and sebacic acid was successful. Unfortunately, the additional sebacic acid resulted in a further drop of glass transition temperature to -33 °C, so that the first prototype, LH265, was selected for further examination of the film properties.

5.1.6 Transferring the results to improve isosorbide resins

In order to test the transferability of conclusions from a phthalic anhydride based system to an isosorbide based system and also the compatibility of isosorbide and phthalic anhydride, a last series of resins was synthesised as shown in table 56. The formulations were optimised reflecting the results both of the evaluation of suitability for coil coating applications and preliminary results of the weatherability tests which will be described in the following chapter.

Table 56: New isosorbide based prototypes

composition mol%	LH266	LH268	LH269	LH267
ISO	15,76	39,37	38,98	39,37
PAN	19,37	10,00	9,90	-
SUC	16,13	-	-	-
SEB	13,23	38,73	38,35	48,73
1,3PD	29,37	5,76	5,70	5,76
GLY	6,14	6,14	7,07	6,14

In a first attempt, similar amounts of isosorbide (15,76 mol%) and phthalic anhydride (19,37 mol%) were used in the formulation. However, the slow progress of the reaction necessitated a duration of 5 days, which led to an unacceptably dark colour of the resin.

Therefore, the amount of isosorbide was increased to around 39 mol%, keeping only around 10 mol% of phthalic anhydride in the formulation. While this increased the reaction kinetics considerably, a lack of reactivity of the hydroxy groups represented by an elevated hydroxy value was observed. Finally, the problem could be solved by increasing the level of glycerol. The resulting resin LH269 had a glass transition temperature of -2 °C and was selected as a prototype for further testing.

For comparison, the phthalic anhydride in the formulation was replaced by sebacic acid to give a fully biosourced prototype. Unfortunately, this resulted in a drop of the glass transition temperature to -15 °C and an increase in viscosity from 5 638 mPa*s at 66% concentration to 25 806 mPa*s at 66% concentration in methoxypropyl acetate (MPA) solvent.

5.2 Synthesis of fully and partially biobased resins

The apparatus used for the synthesis of the resins was newly assembled at the start of the project based on the apparatus used by Arkema. During the three years, it was progressively adjusted and improved. As explained in the introduction, isosorbide contains two hydroxy groups of different reactivity. While one is orientated towards the outside of the cavity and easily accessible, the other one is hydrogen bonded to the ether oxygen on the neighbouring ring.

The challenges encountered and conclusions drawn about the reaction both in terms of the glassware used and in terms of the behaviour of isosorbide are summarised in this section. The NMR analysis as well as the molecular weights of the synthesised resins will also be presented.

5.2.1 General description of the reaction procedure

In order to ensure complete esterification of both isosorbide hydroxy groups, the synthesis is performed in a two-step procedure, as also employed by Arkema. First, the isosorbide was reacted in an excess of succinic and sebacic acids. The temperature was kept under 180 °C until the first hydroxy group had reacted and then gradually raised up to 220 °C to react the second hydroxy group. The other diols and glycerol were only added once the hydroxy value had decreased to 0 mg_{KOH}/g.

The isosorbide was supplied in different forms. In the beginning, it was used in solid form, supplied either by Sigma Aldrich or Roquette. Later on, isosorbide from one of Arkema's plants was used, which was delivered in 80% purity as a water solution. This required an additional step in the synthesis: The liquid isosorbide solution was added to the reactor and heating as well as the nitrogen

flow was started, while succinic acid and sebacic acid were slowly added under stirring. The water was distilled off in its majority before the reaction was started.

All isosorbide reactions were performed in an azeotropic synthesis. This means that a methyl-isobutyl-ketone (MIBK) was added in 5 – 10% to the synthesis to facilitate the water removal. MIBK and water form a low boiling azeotrope containing 34,91% solvent which lowers the boiling point to 89 °C.[257]

The phthalic anhydride based resins were synthesised using a slightly different method. Firstly, all monomers were added in the beginning of the reaction. Secondly the azeotropic solvent was only added later. The reaction was started in the melt, i.e. solventless, and at around 150 °C. Instead of MIBK, xylenes were used as an azeotropic solvent, and added after about 5 h of reaction. Xylenes form an azeotrope with water containing 23,37% solvent and lower the boiling point of the mixture to 93 °C.[257]

Because different reaction procedures were employed for isosorbide and phthalic anhydride resins, the effect of the order of addition of monomers on the resin properties was examined. For both types of resins, slightly higher molecular weights were observed when the monomers were added at the same time or with a smaller delay. Only little effect on the viscosity or the glass transition temperature was detected, though, so that the study was not pursued any further.[XLI]

5.2.2 Challenges encountered during the resin synthesis

During the resin synthesis, several problems were encountered that can serve as a guide for future studies. Some resins had to be discarded because the final hydroxy value determined did not match the theoretically calculated target value. Evidence of evaporation of several monomers was found, and the hydroxy value was finally adjusted by compensating for the monomer loss by adding 1,2-propanediol shortly before the end of the synthesis.[XLII]

Colouration was also the reason several resins had to be discarded. Nitrogen flow and the duration of the reaction were identified as the origin of the problem, and isosorbide was found to be more prone to colouration than phthalic anhydride. However, no further correlation to the resin formulation could be established, and no colouration problems of the coating after curing were observed.[XLIII]

[XLI] Details of the prototypes synthesised and the reaction protocols used can be found in the annexe.
[XLII] Details concerning the hydroxy values and monomer loss observed for different types of resins as well as the methods employed for compensating for it can be found in the annexe.
[XLIII] For more details on the origins and the steps taken to avoid colouration of the resins, see annexe.

Several modifications were also made to optimise the polyesterification reactor in terms of stirring, heat distribution, the presence of oxygen and leaks.[XLIV]

A last challenge concerned the aspect of the resins after dilution. Despite the fact that the resins are all soluble in the solvent methoxypropyl acetate (MPA) which was used to dilute them in the end of the synthesis, they sometimes showed a hazy aspect after the addition of the solvent.[XLV]

The manner of solvent addition in the end of the reaction was identified as the root of the problem for other resins. In the end of the reaction, the resin is diluted from about 95% to around 70% concentration while it is still at a temperature around 130 °C to permit thorough mixing with the solvent. In the beginning, this was done by adding the solvent to the top of the reactor in several portions of 50 – 100 mL, so that the entire addition was finished after around 5 min.

However, clear resins such as LH162 shown in figure 62 below were only obtained after the addition was considerably slowed down. The temperature was decreased to below 120 °C, and the solvent addition was performed dropwise with increased stirring speed. The time of the solvent addition was thus increased to 30 – 45 min, depending on the batch size. The resin was allowed to cool down only gradually, and solvent addition was stopped to increase the temperature when the mixture showed signs of incompatibility. After this new procedure was implemented, and where no grease was used in the reactor, all products showed a clear aspect.

This indicates that the hazy aspect was a consequence of structural changes induced by the sudden presence of the solvent. It is likely that the addition of the solvent as well as the consequential temperature change caused some of the polymer chains to contract. This decreased their solubility and caused a more emulsion like behaviour through which light could not travel uninhibited. The contracted chains also cause regions of different polarity, so that when the hazy resins were applied for curing, craters formed on the film.

Figure 62: Example of clear and hazy resins due to reaction procedures

[XLIV] The nature of the different modifications is detailed in the annexe.
[XLV] One possible cause for the hazy aspect was also the contamination of the resins with grease, as described in the annexe.

The slower addition allowed time for the interaction between solvent molecules and polymer chains and lead to proper solubilisation of the resins.

This also explains why no hazy aspect was observed when the viscosity of the resin was tested by solubilisation of a small batch. In this case, the addition of the solvent was more gradual because the mixing was manually done with a spatula instead of a mechanical stirrer.

5.2.3 Resin characterisation

The success of the polyesterification was assessed using NMR spectroscopy and size exclusion chromatography. The conclusions drawn are presented in this section.

5.2.3.1 NMR characterisation of the resins

In order to understand the NMR spectra of isosorbide resins, the peaks of the isosorbide NMR first had to be assigned. Due to their chemical similarity, all proton signals can be found between 3,24 ppm and 5,11 ppm and all carbon signals can be found between 70,92 ppm and 87,82 ppm in DMSO[d] solvent. 2-dimensional NMR was therefore used to assign the different signals, as shown in figure 63.[XLVI]

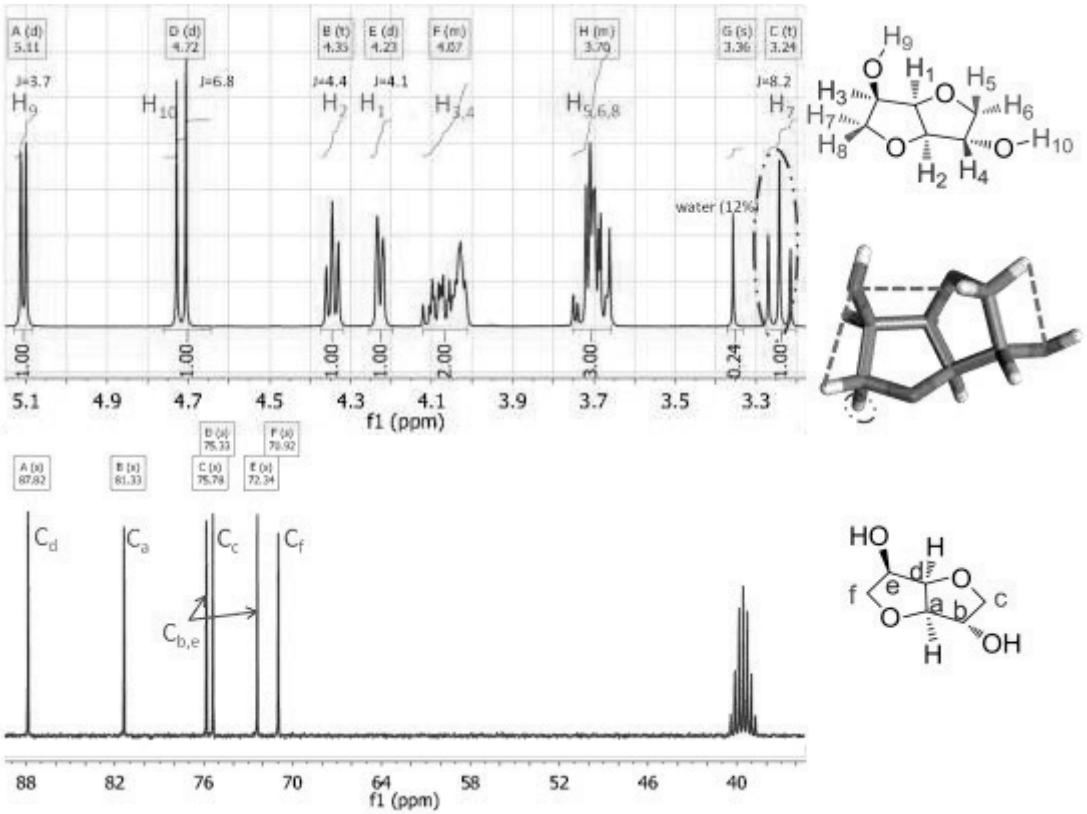

Figure 63: Assignment of isosorbide NMR signals

[XLVI] The different 2D spectra as well as an explanation for the peak assignments can be found in the annexe.

5.2.3.1.1 NMR of the isosorbide based resin LH184

The proton NMR of the polyester resin in figure 64 clearly shows the peaks of succinic acid and sebacic acid as well as the CH_3 peak corresponding to the 1,2-propanediol methyl group. The peaks are slightly shifted from their position in the monomers confirming that the polyesterification has indeed taken place.

The identification of esterified diols is difficult because the unreacted hydroxy protons, the protons of esterified glycerol and propanediol and all isosorbide peaks are located in the same area. They overlap and make it impossible to unambiguously identify or quantify specific protons. End group analysis, which is sometimes used to determine the degree of the polymerisation reaction and the polymer chain length, is therefore difficult.

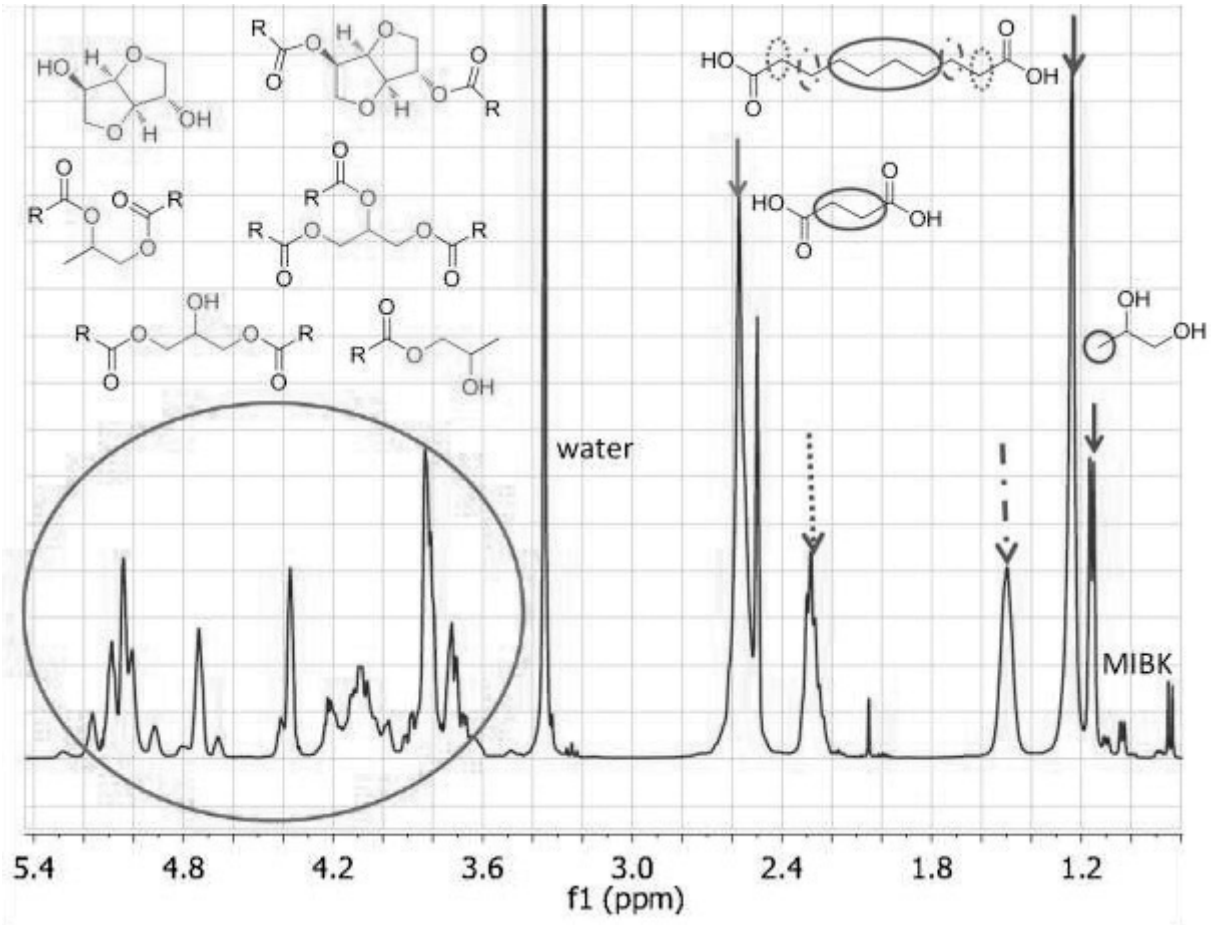

Figure 64: ^{1}H NMR of the isosorbide resin LH184

This is also reflected in the carbon NMR in figure 65. While the signals corresponding to the single monomers can still be recognised, numerous additional peaks, especially between 50 and 90 ppm, can be observed. These correspond to the different ester linkages that are formed between the different monomers, but are hard to assign due to their close proximity.

Small traces of the azeotropic solvent MIBK are visible in both the carbon and the proton NMR. Compared to the 12% present in isosorbide, the quantity of water has also clearly increased. This indicates that despite the high reaction temperature, not all the water produced in the esterification has evaporated, possibly because it is closely bound to the hydrophilic parts of the polymer chain.

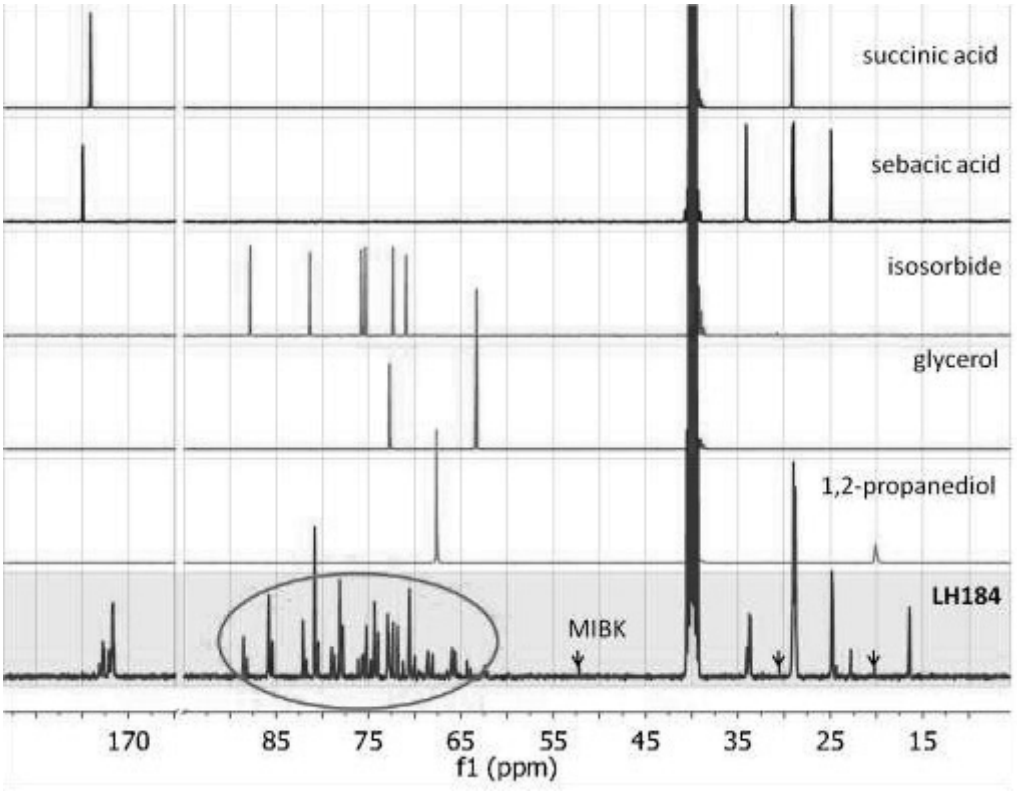

Figure 65: ^{13}C NMR of the isosorbide resin LH184

The DEPT analysis of the resin spectrum, shown in figure 66, shows that while several new CH_2 peaks from the esterification of 1,2-propanediol and glycerol are present, isosorbide has also reacted, resulting in numerous new CH peak shifts.

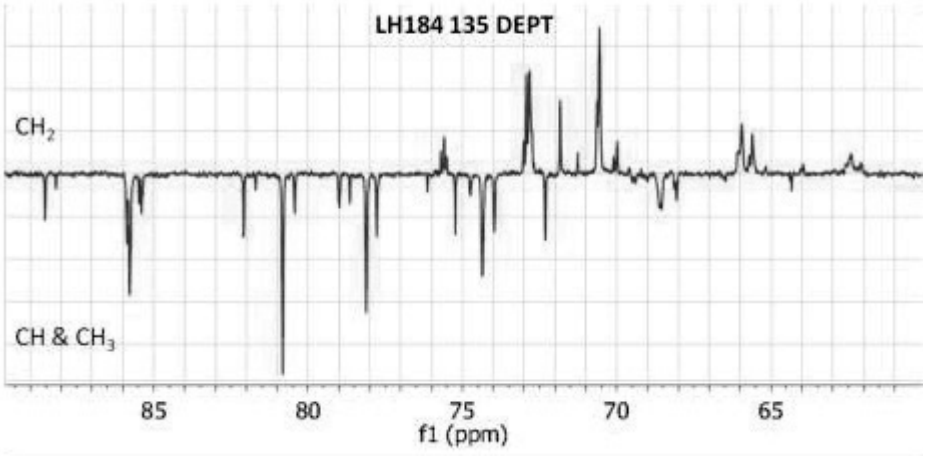

Figure 66: 135 DEPT NMR of the isosorbide resin LH184

5.2.3.1.2 Comparison of the NMR spectra of different isosorbide resins

In comparing the proton spectra of the resins containing 19,37 mol% to 45,13 mol% of isosorbide as in figure 67, no major differences in the signals can be detected. Different quantities of water and MIBK are left in the resins, but otherwise, the signal shape stays largely the same.

The decrease in quantity of 1,2-propanediol from 25,76 mol% (LH249) to 0 mol% (LH248) is reflected in the disappearance of the methyl peak at 1,16 ppm. The isosorbide protons are also more pronounced as the quantity of isosorbide in the resin increases.

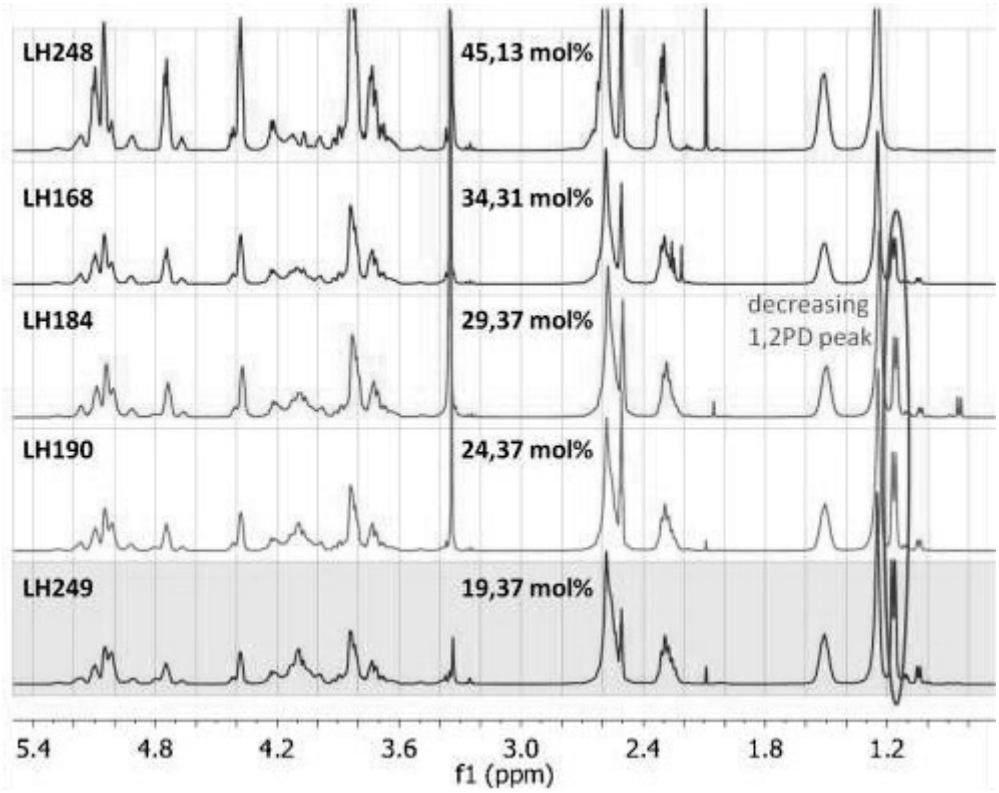

Figure 67: ^{1}H NMRs of the series of isosorbide resins

When comparing the absorption of the peaks which can be quantified with the amount of the corresponding monomer that was added in the formulation as in table 57, good agreement is obtained. The ratio of sebacic acid to succinic acid in the formulations is 0,38 : 1. It is slightly overestimated in the NMR from 0,40 : 1 to 0,43 : 1, which could be due to two factors. The lower boiling point of succinic acid, which is at 235 °C much closer to the maximum reaction temperature of 220 °C than that of sebacic acid, which boils only at 295 °C could be responsible for some succinic acid loss. A second reason could be an underestimation of the size of the succinic acid peak, which overlaps with the DMSO^{d} solvent peak.

The quantity of 1,2-propanediol is slightly underestimated in the NMR, which is consistent with the observation that some of it may evaporate from the reaction mixture due to the high temperature.

Again, the precision of the NMR measurements is limited by the overlap of the 1,2-propanediol signal with the neighbouring sebacic acid signal.

Table 57: Monomer ratios in isosorbide resins in the formulation compared to the NMR spectrum

	ratio :succinic acid in formulation		ratio :succinic acid in NMR		
resin	**sebacic acid**	**1,2-propanediol**	**sebacic acid**	**1,2-propanediol**	**water**
LH249	0,38	0,73	0,41	0,62	0,18
LH190	0,38	0,59	0,43	0,56	0,56
LH184	0,38	0,45	0,41	0,44	1,26
LH168	0,38	0,31	0,40	0,29	0,63
LH248	0,38	0,00	0,43	0,00	0,40

Unreacted and partially reacted 1,2-propanediol can also be seen in the NMR spectra in figure 68 slightly to the right of the reacted 1,2-propanediol peaks. It was not taken into account to calculate the ratio, and indicates that the addition of 1,2-propanediol to compensate for the hydroxy value has not led to a 100% incorporation into the resin.

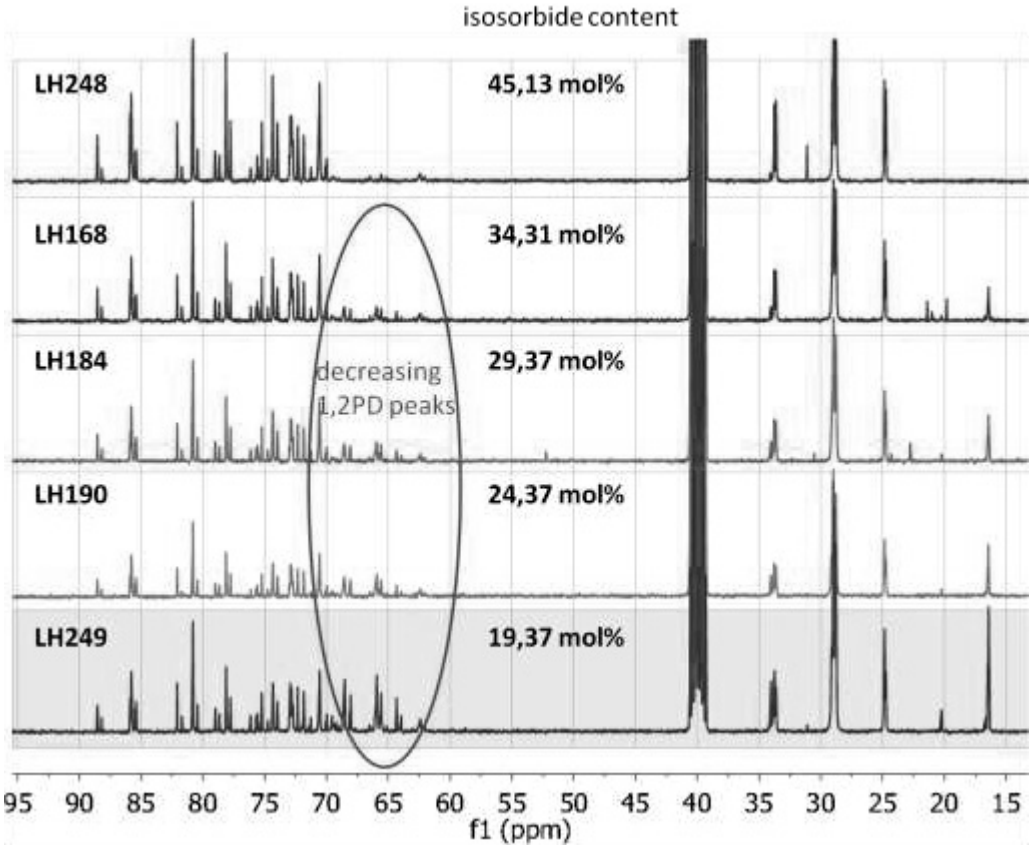

Figure 68: ^{13}C NMR of the series of isosorbide resins

The quantity of water present in the NMR spectrum varies from 18% to an alarming 126% of the amount of succinic acid in LH184. It definitely confirms the hydrophilic nature of at least part of the

resin. However, the hygroscopic nature of the DMSO[d] solvent could also account for some of the water as well as its relatively strong presence in the spectrum.

The disappearance of reacted 1,2-propanediol signals can also be observed in the carbon NMR spectra.

5.2.3.1.3 NMR of phthalic anhydride resins

Comparing the NMR of the phthalic anhydride resin LH189 with that of the isosorbide resin with an equivalent formulation, LH184, helps identify some of the peaks which were previously obscured by the isosorbide. The glycerol signals above 5 ppm are clearly visible, as well as a strong signal from 1,2-propanediol and 1,3-propanediol CH_2 an CH_3 peaks, as shown in figure 69. The peak corresponding to resident water is considerably smaller due to the more hydrophobic nature of the resin.

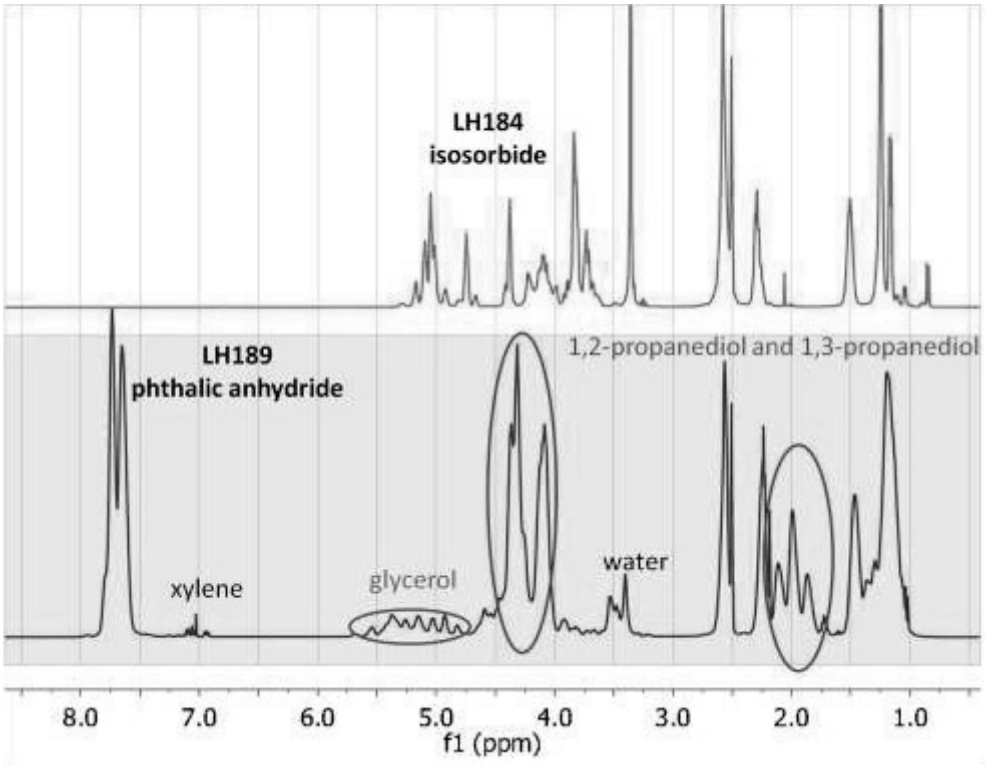

Figure 69: Comparison of the ^{1}H NMRs of an isosorbide and a phthalic anhydride based resin

In table 58, the relative size of the monomer signals relative to the glycerol signal is compared with the amount of each monomer added to the formulation. The amount of each monomer is slightly underestimated, with an average error of 6 - 12% because it was assumed that only two of the glycerol hydroxy protons had reacted. When the calculation is done assuming that all glycerol hydroxy groups have reacted, the quantities are overestimated by 12 – 18% instead. It can be concluded that a part of the glycerol hydroxy groups has been esterified.

Table 58: Monomer ratios of phthalic anhydride resins in the formulation compared to the NMR spectra

	ratio monomer : glycerol in formulation				ratio monomer : glycerol in NMR				
Resin	**PAN**	**SUC**	**SEB**	**1,2PD&1,3PD**	**PAN**	**SUC**	**SEB**	**1,2PD&1,3PD**	**water**
LH237	3,15	2,63	2,15	7,35	3,12	2,37	2,14	6,84	0,80
LH162	3,97	2,16	1,81	7,35	3,68	1,94	1,67	6,26	0,68
LH189	4,78	1,75	1,40	7,35	4,48	1,57	1,29	6,90	0,59
LH163	5,60	1,35	0,99	7,35	5,43	1,11	0,94	6,90	-
LH242	7,94	0,00	0,00	7,35	7,24	0,00	0,00	6,37	0,83

In the corresponding carbon NMR spectra in figure 70, it is possible to distinguish clearly between the succinic acid ester, phthalic anhydride ester and sebacic acid ester peaks. The variety of combinations from the three alcohol and three acidic monomers is reflected in the large amount of signals located around 60 ppm. This variety is considerably reduced in the spectrum of LH242, in which the only monomer with acid functionality used was phthalic anhydride. Therefore, only one type of ester could be formed from each alcoholic monomer.

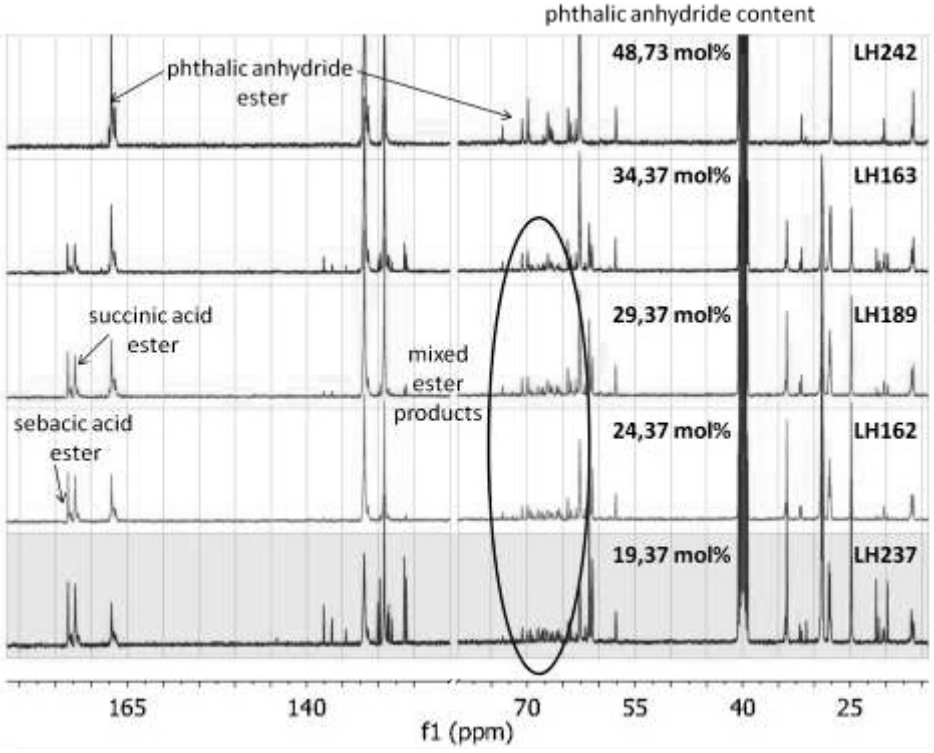

Figure 70: ^{13}C NMRs of phthalic anhydride based resins

5.2.3.2 Resin chain lengths

The size of the polyester chains in the different resins was determined by size exclusion chromatography. Due to the nature of step growth polymerisation and the different reactivities of the monomers present in the formulation, not all chains have the same length. Therefore, an average is used to describe their size. Below, the number average molecular weight, which is calculated as

$M_{\bar{n}}=\sum n_i M_i/\sum n_i$, and the weight average molecular weight, calculated as $M_{\bar{w}}=\sum n_i M_i^2/\sum n_i M_i$, will be discussed. Here, n_i is the number of molecules of weight i and M_i is their molecular mass. The ratio of $M_{\bar{w}}/M_{\bar{n}}$ is called polydispersity and is indicative of the variety of chain length present in the resin product.

Relatively little difference was observed between the number average molecular weights which were between 2 100 g/mol and 3 850 g/mol for all resins examined. The weight average molecular weights on the other hand displayed greater variations between 6 200 g/mol and 40 150 g/mol. Accordingly, a range of polydispersities were observed.

The highest weight average molecular weights also corresponded to the highest polydispersities.[XLVII] In comparing the molecular weights and polydispersities to the loss of diols observed and the point of addition of additional diol to compensate for this loss, no correlation was discovered.

5.2.3.2.1 Molecular weights of isosorbide resins

A theoretical estimation of the number average molecular weight can be made based on the reaction outcome, too. The number of molecules present in the reaction is estimated by subtracting the number of acid equivalents from the total number of moles, assuming that each acid group will connect two molecules and thus reduce the number of molecules by one. The end acid value, representing the unreacted acid groups, is then converted from mg_{KOH}/g to mol and added to the number of molecules. Finally, the molecular weight is determined by dividing the end weight of the product by the number of moles. This theoretical number average molecular weight is shown in table 59 and also discussed below.

Table 59: Molecular weights of isosorbide resins

isosorbide content		$M_{\bar{n}}$	$M_{\bar{w}}$	$M_{\bar{w}}/M_{\bar{n}}$	$M_{\bar{n}\ \text{theoretical}}$
mol%		**g/mol**	**g/mol**		**g/mol**
LH249	19,37	3750	31150	8,3	3039
LH190	24,37	3300	40150	12,2	2590
LH184	29,37	3600	29600	8,2	2956
LH168	34,31	3300	24400	7,4	2928
LH243	39,37	3400	36650	10,8	2928
LH248	45,13	3100	16450	5,3	2394

The experimentally determined number average molecular weights of isosorbide resins were in all cases slightly higher than the theoretical estimates, but follow the same trend. This could be due to

[XLVII] See annexe for a graph of the weight average molecular weights and the corresponding polydispersities.

the loss of diols, which reduces the possible number of chains formed, or due to differences in the response of the resin to that of the polystyrene standard used for calibration.

The weight average molecular weights are considerably higher than the number average molecular weights. The average is higher than that obtained with phthalic anhydride based resins. While lowest $M_{\bar{w}}$ was obtained with the highest quantity of isosorbide, no overall correlation between the chain length and isosorbide content was observed.

5.2.3.2.2 Influence of phthalic anhydride content on molecular weight

As for the isosorbide containing resins, the phthalic anhydride resin with the lowest molecular weight was obtained from the maximum amount of phthalic anhydride in the formulation. However, in the case of phthalic anhydride, a correlation between the amount of phthalic anhydride and the resulting chain length can be observed as shown in table 60. Overall, it seems that the presence of phthalic anhydride inhibits the growth of very long chains and decreases the polydispersity.

Table 60: Molecular weights of resins with different phthalic anhydride contents

phthalic anhydride content		$M_{\bar{n}}$	$M_{\bar{w}}$	$M_{\bar{w}}/M_{\bar{n}}$	$M_{\bar{n}\ theoretical}$
	mol%	**g/mol**	**g/mol**		**g/mol**
LH239	9,37	3850	17350	4,5	2840
LH237	19,37	3750	21250	5,7	2730
LH162	24,37	3400	17250	5,1	2883
LH183	29,37	3650	20350	5,6	3345
LH189	29,37	3300	15200	4,6	2949
LH163	34,37	2600	9150	3,5	2585
LH165	39,37	2600	9100	3,5	2705
LH242	48,73	2100	6200	2,9	2513

This trend was confirmed in the series of resins synthesised to explore the minimum necessary amount of phthalic anhydride shown in table 61. When phthalic anhydride was replaced by other rigid or glass transition temperature raising monomers such as succinic acid and 1,2-propanediol, an increase in molecular weight was observed.

Table 61: Minimised phthalic anhydride content with compensation using other monomers

phthalic anhydride content		$M_{\bar{n}}$	$M_{\bar{w}}$	$M_{\bar{w}}/M_{\bar{n}}$	$M_{\bar{n}\ theoretical}$
	mol%	**g/mol**	**g/mol**		**g/mol**
LH228	24,37	2800	12550	4,5	3610
LH231	19,37	2750	12350	4,5	2422
LH234	14,37	2950	14500	4,9	2627
LH238	9,37	3000	15050	5,0	2234

In this case, the trend of the calculated number average molecular weights did not correlate with the experimentally determined results. Overall, the weight average molecular weights observed were slightly lower than those of the resins with the same amount of phthalic anhydride in which the amount of non-aromatic rigid monomers was not increased.

5.2.3.2.3 Influence of other monomers on molecular weight

A series of resins was synthesised based on the phthalic anhydride resin LH189 in which one or more monomers were exchanged to explore the influence of each component in the formulation. The resin in which the sebacic acid was completely substituted by succinic acid (LH174) displayed a slightly lower molecular weight, as shown in table 62. The corresponding resin in which the succinic acid was completely substituted by sebacic acid (LH177), on the other hand, showed a slightly increased molecular weight. Both effects were predicted in the theoretical calculation of the number average molecular weight.

Conversely, an increased amount of 1,3-propanediol (LH181) decreased the chain length while an increased amount of 1,2-propanediol (LH182) increased it considerably. The latter is in contrast to the number average molecular weight predicted from calculations.

Table 62: Effect of different monomers on molecular weight

	resin description	$M_{\bar{n}}$	$M_{\bar{w}}$	$M_{\bar{w}}/M_{\bar{n}}$	$M_{\bar{n}\ theoretical}$
		g/mol	**g/mol**		**g/mol**
LH189	basis	3300	15200	4,6	2949
LH174	SUC only, no SEB	2950	11750	4,0	2853
LH177	SEB only, no SUC	3500	16900	4,8	3059
LH181	1,3PD only, no 1,2PD	2900	11750	4,1	2910
LH182	1,2PD only, no 1,3PD	3450	24650	7,1	2747
LH207	GLY 7,18 mol%	3750	37700	10,1	3368
LH204	GLY 8,22 mol%	3350	25650	7,7	3967
LH219 (SEC D)	GLY 9,27 mol%	-	30776	1,1	4286
LH192	high T_g prototype	2900	16800	5,8	2738
LH193	high T_g prototype	2750	11650	4,2	2892
LH196	high T_g prototype	2550	8650	3,4	2597
LH199	high T_g prototype	2650	9850	3,7	2603

A series of resins in which the glycerol content was increased from 6,14 mol% to up to 9,27 mol% showed higher molecular weights due to the reduction of monomers present at the same ratio of alcohols and acids. Contrary to the theoretical calculations, the higher glycerol content did not correlate with a higher molecular weight between the three resins.

Finally, the series of prototypes in which the quantity of all rigidity inducing monomers was increased to maximise the glass transition temperature was also examined. Generally, the number average molecular weight was close to that predicted from calculations. Three out of four prototypes also showed a decreased weight average molecular weight compared to LH189, suggesting that the introduction of rigidity into the polymer may somewhat hinder the formation of long chains.

The most common reason for which prototypes had to be discarded was high molecular weight. In the case of isosorbide resins, this caused viscosities far above the specification, and was mostly linked to the use of isosorbide monomer that had been stored for a long time.

For phthalic anhydride resins and cyclohexanedicarboxylic acid resins, gel formation was observed instead. The gel formation was linked to high resin functionality as well as to a lack of chain flexibility.[XLVIII]

5.2.4 Insights into the synthesis of biobased resins

Several general conclusions about the synthesis of biobased polyester resins were drawn and can serve as a guide for future work.

Firstly, the nature of the esterification reaction and order of the monomers was confirmed to be random, both by the fact that changing the order of addition of the monomers to the reaction mixture only had a very small effect on the resin properties and by the variety of the signals observed in the NMR spectrum. Unfortunately, the overlapping of these signals made the determination of chain lengths by end group analysis impossible, particularly where more isosorbide or more than two different diols were used in the formulation.

The theoretical calculation of number average molecular weights yielded results close to those obtained in experimental studies. However, polydispersities and therefore the weight average molecular weights were often significantly larger and probably better guides for the resin properties.

The high reaction temperatures were shown to cause evaporation of succinic acid, sebacic acid, isosorbide, phthalic anhydride and 1,2-propanediol by analysis of the composition of sublimation on the reactor wall, but the evaporation of glycerol and 1,3-propanediol is equally possible.

In general, isosorbide containing resins were found to have higher weight average molecular weights than their phthalic anhydride equivalents, even though no correlation could be established between

[XLVIII] Details on the formulation and study of isosorbide resins with high viscosities and resin formulations that resulted in gel formation can be found in the annexe.

the quantity of isosorbide used and the individual chain lengths. A significantly higher amount of water was also observed in the NMR spectrum of isosorbide resins.

5.3 Properties of biobased resins

A number of fully and partially biobased resins were synthesised. While their properties can provide interesting insights into the structure and reactivity of biobased monomers, as described in the sections above, only a few were selected for further evaluation as prototypes. These can be classed into two categories. Firstly, a series of prototypes was synthesised to examine the effect of each monomer on the film properties, to help the design of a resin suitable for exterior used. Secondly, several prototypes based on insights from the first series and assumptions based on previous experiences and literature knowledge were created as a preliminary proposition for the exterior paint. Below, the characterisations of these resins are summarised. Their viscosities, solubilities and glass transition temperatures will then be discussed.

5.3.1 Overview of prototypes selected for evaluation

The acid value and hydroxy value of the resins one day after their synthesis was completed, as well as their aspect and colour are detailed below. The weight average molecular weight was chosen as most indicative of the resin properties. An example of the four colours used in the descriptions is shown in figure 71.

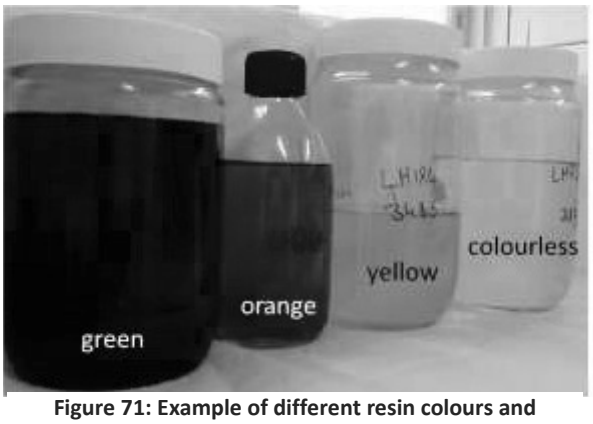

Figure 71: Example of different resin colours and descriptions used

5.3.1.1 Prototypes synthesised for the evaluation of each monomer's influence

As described in the beginning of the chapter, this series of prototypes was designed to generate insights about the effect of each monomer on the formulation, and to serve as guidance for the design of prototypes for a resin for exterior use. Therefore, changes were made to only one monomer in the formulation while keeping the rest as similar as possible.

5.3.1.1.1 Isosorbide

The prototypes shown in table 63 were synthesised gradually increasing the isosorbide content from the minimum of 19,37 mol% in LH249 to the maximum of 45,13 mol% in LH248. Three resins in which the isosorbide content was increased while the theoretical hydroxy value was kept constant were also examined.

Table 63: Characterisation of prototypes with different isosorbide contents

	acid value	OH value	$M_{\bar{w}}$	colour	aspect
resin	**mg_{KOH}/g**	**mg_{KOH}/g**	**g/mol**		
LH249	4,9	60,0	31150	yellow	clear
LH190	8,5	59,8	40150	yellow	clear
LH184	6,3	62,6	29600	yellow	clear
LH168	5,9	61,5	24400	yellow	clear
LH243	7,2	51,4	36650	yellow	
LH248	11,8	49,8	16450	orange	clear
LH038	7,8	82,8	-	yellow	hazy
LH067	7,1	57,9	6077	yellow	hazy
LH079	5,7	59,6	4639	orange	hazy

5.3.1.1.2 Phthalic anhydride

The phthalic anhydride content was varied from 9,37 mol% in LH239 to 48,72 mol% in LH242, as shown in table 64.

Table 64: Characterisation of prototypes with different phthalic anhydride contents

	acid value	OH value	$M_{\bar{w}}$	colour	aspect
resin	**mg_{KOH}/g**	**mg_{KOH}/g**	**g/mol**		
LH239	5,4	60,6	17350	colourless	clear
LH237	6,6	60,1	21250	yellow	clear
LH162	5,4	52,8	17250	colourless	clear
LH189	5,0	60,9	15200	colourless	clear
LH163	7,7	65,2	9150	yellow	clear
LH165	6,8	58,7	9100	yellow	clear
LH242	8,5	63,2	6200	yellow	clear

5.3.1.1.3 Other monomers

Table 65: Characterisation of prototypes in which other monomers were varied

	acid value	OH value	$M_{\bar{w}}$	colour	aspect
resin	**mg_{KOH}/g**	**mg_{KOH}/g**	**g/mol**		
LH174	4,5	62,3	11750	colourless	clear
LH177	5,4	56,5	16900	colourless	clear
LH181	5,2	60,8	11750	colourless	clear
LH182	6,4	63,2	24650	colourless	clear
LH219	6,9	62,2	30776	yellow	clear
LH204	5,6	61,5	37700	white	hazy
LH207	5,3	51,0	25650	white	hazy

The resins LH174, LH177, LH181 and LH182 were synthesised to test the influence of succinic acid, sebacic acid, 1,3-propanediol and 1,2-propanediol respectively. The influence of glycerol was tested

by varying the content from 9,27 mol% in LH219 to 7,18 mol% in LH207, which is increased compared to the 6,14 mol% usually used, as shown in table 65.

5.3.1.2 Possible propositions for an exterior applications resin

Three groups of prototype propositions were synthesised and studied. In the first and the second group consisted of partially biosourced resins based on phthalic anhydride, one with maximised glass transition temperatures and the other with minimised phthalic anhydride content. In the third group, isosorbide and cyclohexanedicarboxylic acid were used additionally to provide rigidity in the structure.

5.3.1.2.1 High rigidity prototypes

Table 66: Characterisation of high rigidity prototypes

	acid value	**OH value**	$M_{\overline{w}}$	**colour**	**aspect**
resin	**mg_{KOH}/g**	**mg_{KOH}/g**	**g/mol**		
LH192	5,4	58,8	16800	colourless	clear
LH193	5,4	60,7	11650	colourless	clear
LH196	6,8	61,2	8650	colourless	clear
LH199	6,8	64,7	9850	colourless	clear

The glass transition temperature of the first group of prototypes was raised by increasing the quantity of rigid monomers, namely phthalic anhydride, succinic acid and 1,2-propanediol, as shown in table 66. The two most promising prototypes (LH196 and LH199) were tested for their solubility in organic solvents by Activation.

5.3.1.2.2 Minimum phthalic anhydride content prototypes

Table 67: Characterisation of prototypes with minimised phthalic anhydride contents

	acid value	**OH value**	$M_{\overline{w}}$	**colour**	**aspect**
resin	**mg_{KOH}/g**	**mg_{KOH}/g**	**g/mol**		
LH228	5,7	62,1	12550	colourless	clear
LH231	7,2	60,3	12350	colourless	clear
LH234	5,6	68,4	14500	colourless	clear
LH238	8,9	69,7	15050	colourless	clear

The insights gained from the synthesis of the previous prototypes was used to minimise the phthalic anhydride content in the series of prototypes shown in table 67 while keeping the glass transition temperature at an acceptable level. While the phthalic anhydride content was decreased from 24,37

mol% in LH228 to 9,37 mol% in LH238, the amount of succinic acid and 1,2-propanediol in the formulation were increased as much as possible.

5.3.1.2.3 Other prototypes

A few different formulations, based on preliminary weatherability test results and literature studies were also proposed as shown in table 68. The phthalic anhydride in the formulations with minimised petroleum content was replaced by cyclohexanedicarboxylic acid for the resins LH265 and LH272, and isosorbide was reintroduced into the resin for LH266 – LH269.

Table 68: Characterisation of prototypes containing cyclohexanedicarboxylic acid or both isosorbide and phthalic anhydride

	acid value	**OH value**	$M_{\bar{w}}$	**colour**	**aspect**
resin	**mg_{KOH}/g**	**mg_{KOH}/g**	**g/mol**		
LH265	6,1	68,8	24854	colourless	clear
LH272	5,4	65,1	20200	colourless	clear
LH266	9,5	57,0	20884	green	-
LH268	19,9	39,2	22697	orange	clear
LH267	9,4	48,8	21200	yellow	clear
LH269	9,3	56,4	20680	orange	clear

5.3.2 Viscosity

The viscosity of the resin is an important factor determining its suitability for application on a coil coating line and the quality of the film formed after curing. After dilution to 65% with a solvent, it should be between 1000 mPa*s and 6000 mPa*s. After mixing with the other components of the paint, such as the melamine crosslinker, the final viscosity will then be adjusted to fit the specific application conditions. The different factors determining the viscosity such as the monomers used in the formulation, the molecular weight and the solvents used will be discussed below.

5.3.2.1 Dependence on solvent and concentration

The effect of small variations in concentration and different solvents was tested for the resin LH042, which was synthesised according to the same formula as the interior use resin proposed by Arkema and for example LH184. Different solvent systems recommended by Arkema were evaluated as shown in figure 72.

Very large differences were observed even for small variations in concentration. For example the increase in concentration from 68,1% to 69,0% in the Solvarex 9 / DBE solvent system caused the viscosity to change by 37% from 28 833 mPa*s to 39 533 mPa*s.

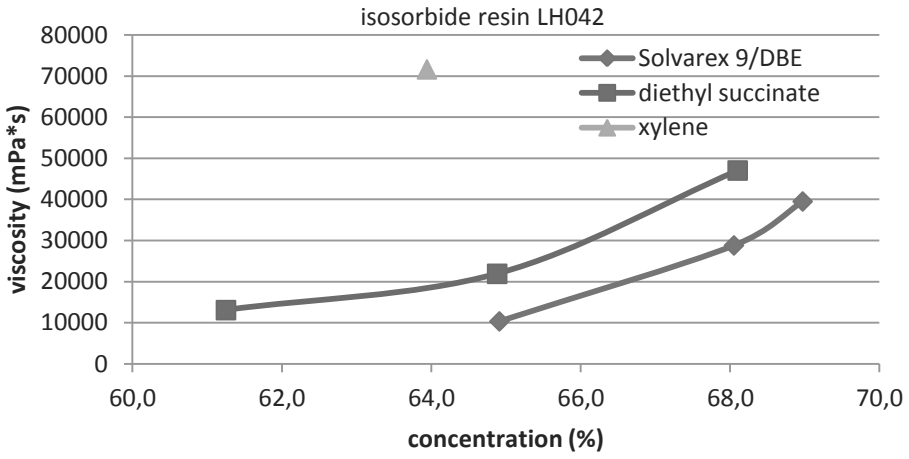

Figure 72: Viscosity dependence on solvent and concentration for LH042

The three solvent systems evaluated are shown in scheme 127 and 128. The first consisted of a 8:2 mixture of the Total solvent Solvarex 9 and dibasic ester solvents, which are also mixtures of several compounds. Solvarex 9 is a combination of aromatic compounds with an average of 9 carbon atoms such as 1,3,5-trimethyl benzene, toluene, xylenes and naphthalene. Dibasic ester is the trade name for a mixture of dimethyl adipate (10 – 25%), dimethyl glutarate (50 – 75%) and dimethyl succinate (19 – 30%).

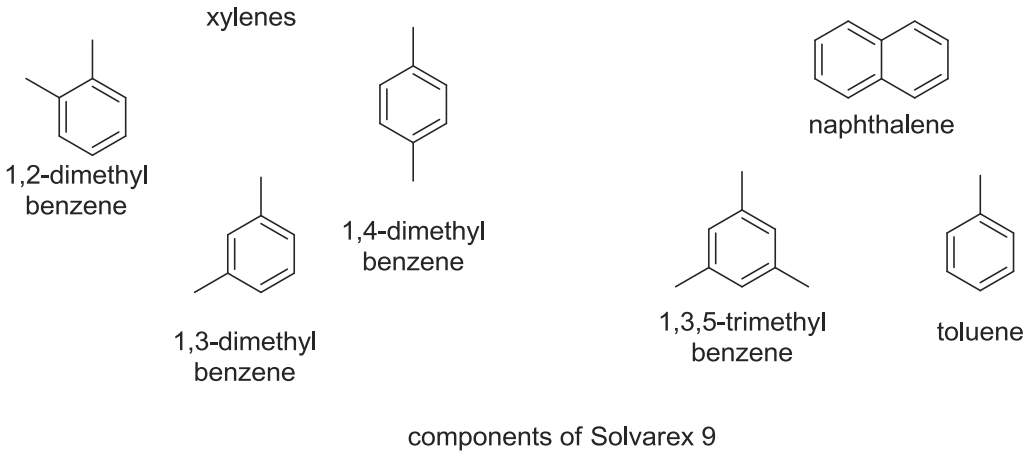

Scheme 127: Aromatic solvents used to dilute the resins

The second solvent system evaluated were xylenes, which refers to a mixture of 1,2-dimethyl benzene, 1,3-dimethyl benzene and 1,4-dimethyl benzene. Diethyl succinate was also tested as a solvent.

The difference in viscosity observed in the different solvents can be explained by their chemical similarity with the resin. Diethyl succinate is much more capable of bonding to the isosorbide based resins, due to the presence of ester bonds in both structures and also due to the polarity of the isosorbide ether groups. Therefore, the diethyl succinate can disrupt the intramolecular bonds

between different parts of the polymer chain, causing the resin to form extended coils. These can entangle and resist movement, causing a higher solution viscosity.

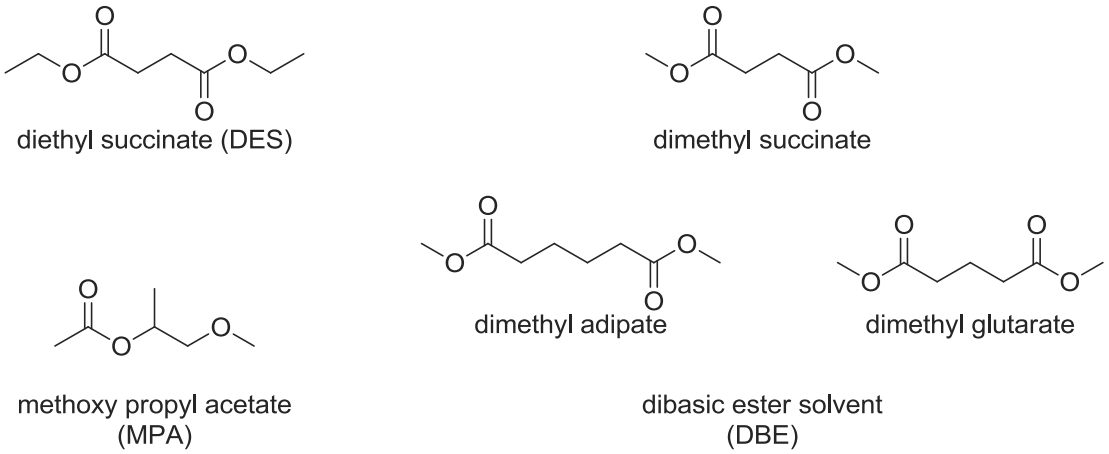

Scheme 128: Polar solvents used to dilute the resins

The Solvarex 9/dibasic ester mix only contains 20% of polar, esterified solvent. Therefore, its capability to disrupt the intramolecular bonds within resin chains is much smaller, and more chains are present in contracted coil structures, taking up less space and leading to a lower solution viscosity.

On the other hand, the xylenes have no chemical similarity to the resin, which does not contain any aromatic units. Therefore, they cannot interact with the resin very effectively. This leads to intermolecular bonds being formed between the resin chains, which are responsible for the high viscosity.

Overall, the viscosity of the resin diluted by these three solvent systems was significantly too high. The alternative solvent methoxypropyl acetate (MPA) was therefore used instead, giving much better results. While the resin viscosity of problematically viscous resins obtained in some cases could probably be lowered by the addition of a less polar solvent such as Solvarex 9, MPA was used in all cases to keep the results comparable.

The compatibility between resins and the different solvents were however used to modify the viscosity of some of the prototypes for exterior use, and will be discussed below in section 5.3.3.

The dependence of the viscosity on the resin concentration in MPA was examined for two phthalic anhydride based resins as shown in figure 73. The low viscosity of LH239 and LH242 at 65% concentration prompted the evaluation of the minimum solvent level still permitting to stay within the viscosity specifications.

LH239, a resin with only 9.37 mol% of phthalic anhydride, and LH242, a resin with 48,73 mol% phthalic anhydride, both displayed acceptable viscosities below 4000 mPa*s at concentrations of 69,9% and 69,5% respectively. While only a relatively small increase was observed for LH239 between concentrations of 65,3% and 69,9%, a large increase to 10 385 mPa*s was caused when the concentration was increased to 80,4%.

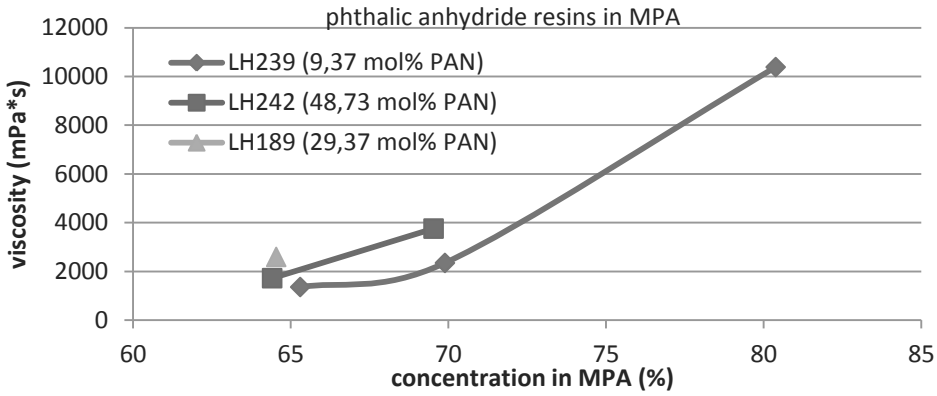

Figure 73: Viscosity dependence on concentration

All other resins tested equally displayed a non-linear dependence of the viscosity on the concentration. Estimating the viscosity at intermittent concentrations is therefore difficult, and the best compromise needs to be determined empirically.

5.3.2.2 Dependence on isosorbide and phthalic anhydride

The variation of viscosities between the resins with different phthalic anhydride and isosorbide content is shown in figure 74. While it is clear that the use of isosorbide raises the viscosity when it replaces phthalic anhydride, no further dependence on the presence of the monomers can be derived. The viscosity of the phthalic anhydride resins is fairly constant in between 1358 mPa*s and 2756 mPa*s, irrespective of the relative amounts of phthalic anhydride, succinic acid and sebacic acid.

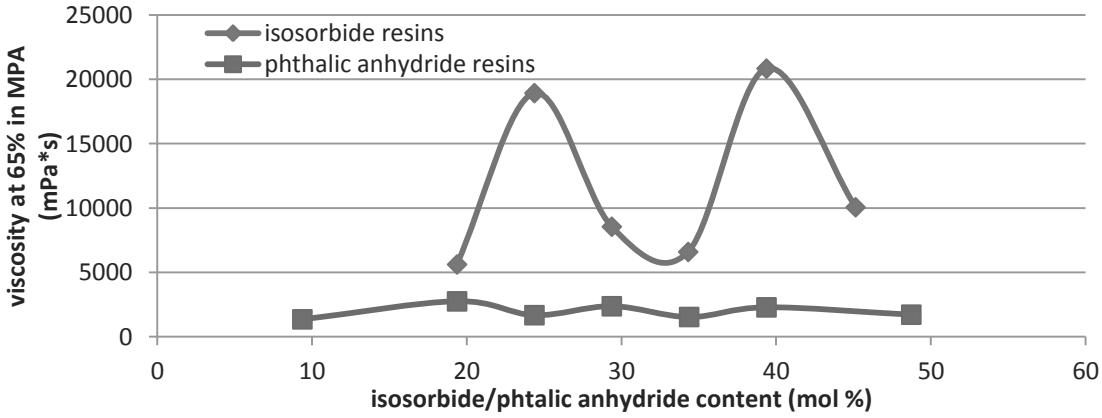

Figure 74: Viscosity dependence in MPA on isosorbide and phthalic anhydride content

The isosorbide resins display a greater variation in viscosity, but the two viscosity maxima of 18 934 mPa*s and 20 839 mPa*s can be attributed to the decrease of isosorbide quality after storage[XLVIII] and not the absolute amount of isosorbide in the resin.

5.3.2.3 Influence of other monomers

The impact of the other monomers on the viscosity was also tested. In figure 75, the viscosity difference compared to the resin LH202, which was a replica of the phthalic anhydride based basis resin LH189 containing 29,37 mol% phthalic anhydride, is shown. All viscosities were evaluated at around 65% concentration in MPA.

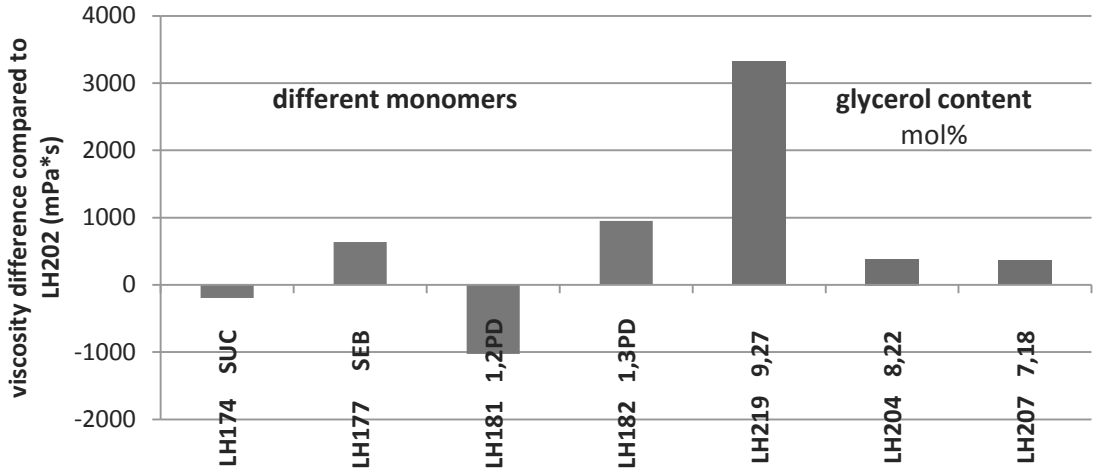

Figure 75: Viscosity dependence on different monomers

Increased glycerol content raised the viscosity in all three cases. However, as with the concentration, the dependence was not linear, and the increase from 8,22% to 9,27% is much more significant than that achieved between 6,14% and 7,18% and between 7,18% and 8,22%, as shown in table 69.

Table 69: Viscosites and molecular weights of resins in which different monomers were tested

		viscosity	concentration in MPA	$M_{\overline{w}}$
resin	**description**	**mPa*s**	**%**	**g/mol**
LH174	succinic acid	2397	64,5	11750
LH177	sebacic acid	3229	65,6	16900
LH181	1,2-propanediol	1567	65,9	11750
LH182	1,3-propanediol	3542	65,2	24650
LH219	glycerol 9,27 mol%	5915	65,0	30776
LH204	glycerol 8,22 mol%	2977	70,0	37700
LH207	glycerol 7,18 mol%	2958	68,7	25650

The addition of sebacic acid and 1,3-propanediol also caused an increase in viscosity, while succinic acid and 1,2-propanediol decreased it. It is however likely that this effect was caused by the

differences in molecular weight of the resins rather than the interaction between monomer units and solvent.

The resins LH177, LH182 and all resins with increased glycerol content have an elevated molecular weight as well as an elevated viscosity compared to the other two resins.

5.3.2.4 Influence of molecular weight on the viscosity

The molecular weight can have an influence on the viscosity because long chains can entangle more easily, which can impede individual motion and therefore increase the viscosity. Furthermore, shorter chain lengths correspond to a higher availability of polar end groups on the chains, if they correlate with lower polydispersity, which was the case here.

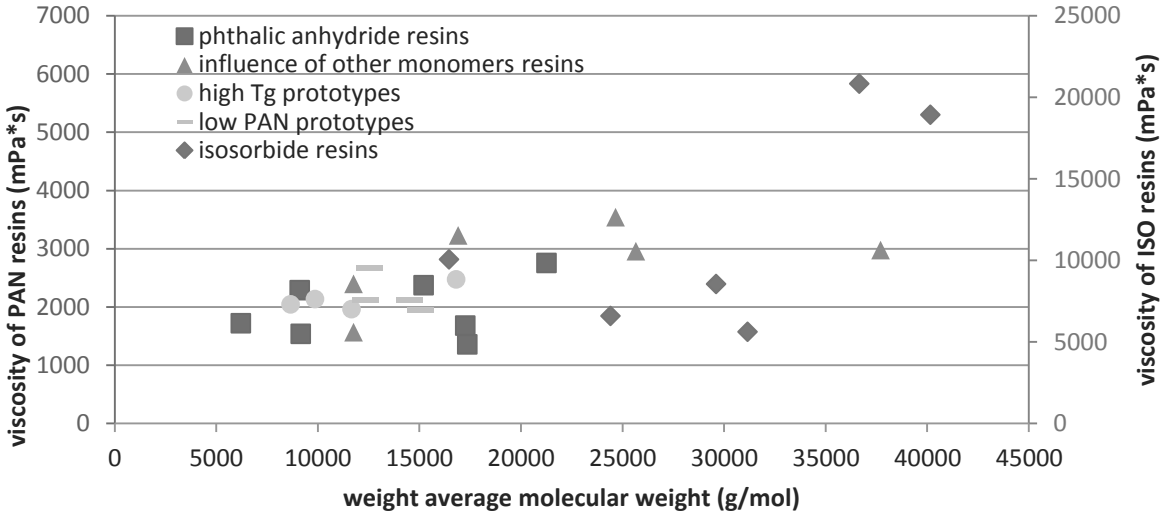

Figure 76: Relationship between the viscosity and the weight average molecular weight

In figure 76, the weight average molecular weights and viscosities of the different resin groups are shown. The highest viscosities also correspond to high weight average molecular weights. However, the correlation does not always apply. In several cases, lower molecular weight resins have slightly higher viscosities than other, higher molecular weight prototypes.

It can be concluded that the viscosity is determined by a combination of the molecular weight and the interaction between the resin components and the solvent. The effect of the molecular weight is therefore particularly obvious for large changes.

5.3.2.5 Viscosities of the three groups of prototypes

Overall, the synthesised prototypes had suitable viscosities when diluted to around 65% in MPA solvent, as shown in table 70. The prototypes based on phthalic anhydride in which the amount of

rigid comonomers was maximised either to increase the glass transition temperature or to be able to decrease the amount of phthalic anhydride all had low viscosities under 3000 mPa*s.

On the other hand, the addition of cyclohexanedicarboxylic acid in the resins LH265 and LH272 caused an increase of viscosity to 5618 mPa*s and 5629 mPa*s for the two prototypes. The prototypes containing both isosorbide and phthalic anhydride displayed viscosities between 3000 mPa*s and 6000 mPa*s.

Unfortunately, the new isosorbide prototype not containing phthalic anhydride had a viscosity of 25 806 mPa*s. This could be due both to the long storage of the isosorbide used in the synthesis, or to the formulation. Because of the high viscosity, this prototype was not used in further testing.

Table 70: Viscosities of resins synthesised as prototypes for the exterior

		viscosity	**concentration in MPA**
resin	**description**	**mPa*s**	**%**
LH192	high T_g	2474	63,2
LH193	high T_g	1963	64,7
LH196	high T_g	2045	65,4
LH199	high T_g	2136	64,5
LH228	minimised petro	2661	65,7
LH231	minimised petro	2113	64,5
LH234	minimised petro	2115	65,7
LH238	minimised petro	1950	65,7
LH265	CHDA	5618	65,1
LH272	CHDA	5629	64,9
LH266	ISO&PAN	3193	65,5
LH268	ISO&PAN	4835	66,4
LH269	ISO&PAN	5638	66,2
LH267	ISO new	25806	65,6

5.3.3 Solubility

The compatibility of the resins with different solvents can provide information both about their structure and about properties such as polarity and hydrogen bonding ability. Furthermore, a good understanding of the interactions can help the selection of suitable biosourced solvents and the optimisation of the paint viscosity.

Different aspects of the resin solubility were studied. The change in viscosity with different solvent systems was evaluated for a selection of phthalic anhydride based resins. Two of the evaluated prototypes were equally studied by Activation to determine their place in the Hansen solubility

space.[258] Lastly, the compatibility with solvents commonly added before the curing process was tested for a selection of resins.

5.3.3.1 Viscosity change in different solvent systems

The viscosity behaviour upon addition of a solvent other than methoxypropyl acetate was tested for a group of resin prototypes based on phthalic anhydride as shown in table 71 and 72. Four prototypes with an increased amount of rigid monomers, designed to reach a maximum glass transition temperature, as well as two prototypes containing 29,37 mol% and 34,37 mol% of phthalic anhydride were examined.

In a first test, the viscosity of the resin diluted to around 65% with either pure MPA or a mixture containing MPA and 44 – 65% of dibasic ester (DBE) solvent was evaluated. It was found that the addition of dibasic ester caused an increase in viscosity of 46% to 71% in each case.

This indicates that the dibasic ester interacts more strongly with the phthalic anhydride based resins than the methoxypropyl acetate. Of the prototypes tested, the smallest increase in viscositiy, of only 46%, was observed for the phthalic anhydride prototype LH210 designed to be equivalent to the isosorbide resin proposed by Arkema. This indicates that the increase either of the rigid monomers 1,2-propanediol and succinic acid increases the interaction with DBE. Unsurprisingly, the increase of succinic acid in the prototype LH192 caused the greatest increase of viscosity with 71%. The strong interaction between dibasic ester and high succinic acid content resins can be explained by the presence of disuccinate esters in both products.

Table 71: Viscosity change upon addition of DBE to the solvent system

		phthalic anhydride content	MPA		MPA + DBE		
			viscosity	conc.	viscosity	conc.	amount of DBE
resin	**description**	**mol%**	**mPa*s**	**%**	**mPa*s**	**%**	**%**
LH192	high T_g	29,37	2474	63,2	4234	63,8	63,8
LH193	high T_g	34,37	1963	64,7	2892	65,2	48,6
LH196	high T_g	34,37	2045	65,4	3254	65,6	44,6
LH199	high T_g	34,37	2136	64,5	3307	67,0	45,1
LH210	PAN basis	29,37	997	60,8	1457	60,8	64,5

The increase in phthalic anhydride seems to counteract the influence of 1,2-propanediol and succinic acid, since a smaller increase of viscosity is observed when all three monomers are present in larger quantities. This also indicates that the polarity of the monomers and not the rigidity of the structure is the governing factor for the solvent compatibility in this case.

The effect of replacing 46 – 56% of the MPA with the aromatic solvent system Solvarex 9 was also examined on three different prototypes. The prototype LH199 containing increased amounts of succinic acid, phthalic anhydride and 1,2-propanediol as well as a prototype equivalent to LH163, containing 34,37 mol% of phthalic anhydride and the phthalic anhydride basis prototype LH202, equivalent to LH210 and LH189, were tested.

Table 72: Viscosity change upon addition of Solvarex 9 to the solvent system

		phthalic anhydride content	MPA		MPA + Solvarex 9		
			viscosity	conc.	viscosity	conc.	amount of S9
resin	**description**	**mol%**	**mPa*s**	**%**	**mPa*s**	**%**	**%**
LH199	high T_g	34,37	2136	64,5	4523	64,1	49,6
LH201	increased PAN	34,37	1597	63,8	1411	62,9	55,6
LH202	PAN basis	29,37	2593	64,5	2437	64,1	46,3

A significant increase in viscosity was observed for the prototype LH199 containing a larger amount of rigid monomers. Contrarily, both other prototypes showed only a small decrease of 12% and 6% respectively for LH201 and LH202.

This indicates that the increase in rigid monomers also improved the resin compatibility with aromatic solvents. In this case, it seems more likely that the structure is the deciding factor rather than the polarity of the monomers, since the shorter distance between ester groups caused by the exchange of sebacic acid for succinic acid should actually increase the resin polarity.

On the other hand, the compatibility of the two latter phthalic anhydride resins with aromatic solvents seems to be on par or slightly lower than that with methoxypropyl acetate.

In general, it can be concluded that the viscosity can be adjusted by the introduction of dibasic ester and aromatic solvents in either direction, and that good solubility in aromatic solvents can be expected from phthalic anhydride based partially biosourced resins.

5.3.3.2 Hansen parameters of partially biosourced resins

The Hansen solubility parameters were used to examine the solubility of two partially biosourced resins. In table 73, their dispersion forces (δD), polarity (δP) and hydrogen bonding ability (δH) are shown.

Compared to the isosorbide resin, both LH196 and LH199 have larger solubility spheres, which is probably due to the added compatibility with aromatics caused by the presence of phthalic anhydride units. While the hydrogen bonding ability and polarity of LH199 is quite close to that of isosorbide, LH196 displays a significantly greater δH than the other resins. This is possibly due to the

greater steric availability of ester groups, which are somewhat sterically blocked by the isosorbide or 1,2-propanediol used in LH199 and in the Arkema resin.

Table 73: Hansen parameters for LH199 and LH196 in comparison

Resin	δD	δP	δH	Hansen sphere diameter
LH196	20,3	13	11,4	12,7
LH199	18,7	14,4	8	11,8
Petrosourced	17,9	12,7	4,3	12,5
Arkema isosorbide	16,7	14	8,5	8,9

Both resins were compatible with a range of biosourced solvent formulations prepared by Activation, also in accordance with the Hansen parameter based prediction. Their viscosities were within specifications, and the highest and lowest viscosities vaguely correlated to the highest and lowest similarity between the calculated Hansen parameters.[XLIX]

5.3.3.3 Compatibility with other paint components

In the paint formulation, the resin is mixed with melamine crosslinker, additives, additional solvents and pigments where a coloured coating is targeted. After addition of a fixed quantity of each component, the end viscosity is individually adjusted to match a process dependent target by adding more solvent. Additives are only added in small quantities, and pigments are dispersed, not dissolved, but the compatibility of the resin with additional solvents and with the crosslinker is important to produce a film with an even surface tension that will form a high quality film during the curing.

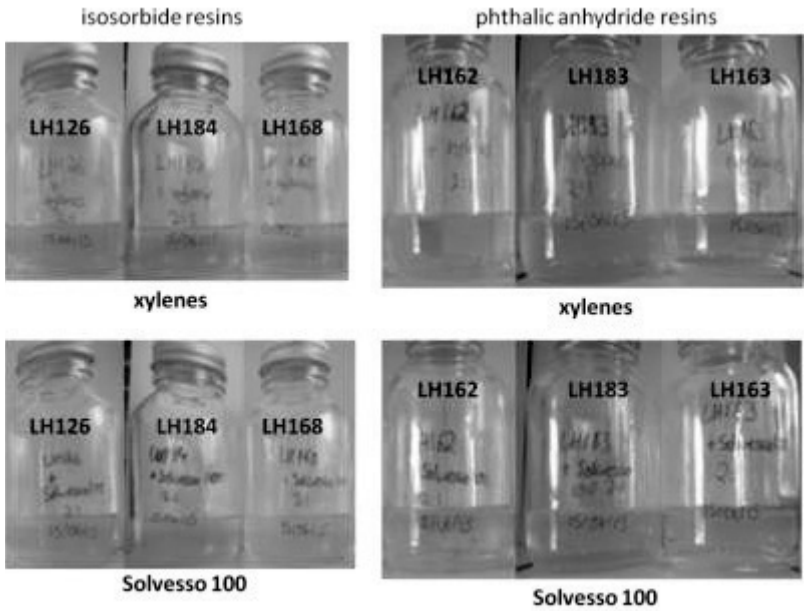

Figure 77: Compatibility of resins with aromatic solvents

The compatibility of a group of resins with melamine and three solvents generally added to the formulation by Beckers was therefore evaluated. Each of the substances was mixed with the resin in larger quantities than would usually be added and allowed to stand overnight.

[XLIX] See annexe for details on the methods and results of the Hansen parameter evaluation by Activation .

The appearance was then evaluated as shown in figure 77 and reported in table 74.

The group of resins tested contained three isosorbide and three phthalic anhydride based resins, with different quantities of isosorbide and phthalic anhydride respectively. Two resins, LH126 and LH183 had hazy aspects due to fast solvent addition in the synthesis. This did not change upon addition of melamine and the other solvents. However, the resins synthesised according to the same formula (LH190 and LH189) which had a clear appearance and were used to replace LH126 and LH183 for further tests confirmed that their hazy appearance was not due to incompatibility with the substances tested.

All resins showed good compatibility with melamine after mixing in a one to one weight ratio. No phase separation was observed after one night and with the exception of LH126 and LH183, all resin showed clear aspects.

Table 74: Compatibility of isosorbide and phthalic acid based resins with the paint formulation

isosorbide	mol%	aspect 65%	melamine	DBE	xylenes	Solvesso 100
LH126	24,37	hazy	hazy	clear	a little hazy	phase separation
LH184	29,37	clear	clear	clear	phase separation	phase separation
LH168	34,31	clear	clear	clear	phase separation	phase separation
phthalic anhydride	**mol%**	**aspect 65%**	**melamine**	**DBE**	**xylenes**	**Solvesso 100**
LH162	24,37	clear	clear	clear	clear	clear
LH183	29,37	hazy	hazy	clear	a little hazy	a little hazy
LH163	34,37	clear	clear	clear	clear	hazy

The solvents evaluated were xylenes, dibasic esters and Solvesso 100 which contains 99% aromatic compounds similar to those in Solvarex 9.They were added to the resins in a 2:1 ratio. In general, the isosorbide containing resins showed good solubility in the dibasic ester mixture, but phase separated when aromatic solvents were added. As suspected from the results of the Hansen solubility parameter study, the phthalic anhydride resins were more compatible with aromatic solvents and showed no phase separation.

Table 75: DBE addition necessary for isosorbide resins

		viscosity at 65%	DBE added
isosorbide content	**mol%**	**mPa*s**	**%**
LH249	19,37	5622	20
LH190	24,37	18934	23
LH126	24,37	3349	8
LH184	29,37	8553	22
LH168	34,31	6595	20
LH248	45,13	10063	20

The viscosity of the formulated resins was adjusted through the stepwise addition of dibasic ester (DBE) solvent as shown in table 75 and 76.[L]

Table 76: DBE addition necessary for phthalic anhydride resins

		viscosity at 65%	DBE added
phthalic anhydride content	**mol%**		
LH237	19,37	2756	10
LH162	24,37	1681	4
LH183	29,37	2706	9
LH189	29,37	2374	8
LH163	34,37	1539	0
LH242	48,73	1721	1

Overall, the amount of DBE necessary for the adjustment was greater on average for the isosorbide containing resins than for the phthalic anhydride containing resins, and correlates roughly with the viscosity displayed at 65% concentration.

Table 77: DBE addition necessary for other prototypes

1C	viscosity (65%)	+ DBE	2A	viscosity (65%)	+ DBE	2B	viscosity (65%)	+ DBE
resin	**mPa*s**	**%**	**resin**	**mPa*s**	**%**	**resin**	**mPa*s**	**%**
LH174	2397	1	LH192	2474	10	LH231	2113	10
LH177	3229	5	LH193	1963	3	LH238	1950	14
LH181	1567	1	LH196	2045	4	LH265	5618	15
LH182	3542	10	LH199	2136	3	LH269	5638	11
LH219	5915	27						

A similar correlation between the resin viscosity at 65% in MPA and the amount of DBE that had to be added to reach the target viscosity of the paint formulation was observed within the other prototype groups as shown in table 77. However, significantly less DBE had to be added for the resins LH265 and LH269, containing CHDA and a mix of phthalic anhydride and isosorbide, with 15% and 11%, compared to other prototypes based purely on phthalic anhydride or isosorbide, such as LH219 and LH249, which displayed similar viscosities at 65%.

5.3.4 Glass transition temperature

The glass transition temperature of the resins before curing is an important parameter for several reasons. Primarily, it depends on the chain mobility and structural rigidity of the resin, and is therefore a convenient way to characterise the polymer. Furthermore, it serves as an indication of

[L] See annexe for details of the viscosity measurement.

the glass transition temperature of the film after curing. The glass transition temperature after curing can be used to estimate the flexibility and resistance to deformation of the coating.

The glass transition temperature of a resin can be determined by differential scanning calorimetry (DSC). In the experiment, the heat flux necessary to increase the resin temperature is measured. As the heat capacity of the polymer changes at the glass transition temperature, a change in the curve gradient can be observed. Software is then used to determine the onset and midpoint of that change, and the midpoint is reported as the glass transition temperature. An example of the heat flux curves between -40 °C and 30 °C of the three resins LH269, LH268 and LH272 is shown in figure 78. The change in gradient is clearly visible.

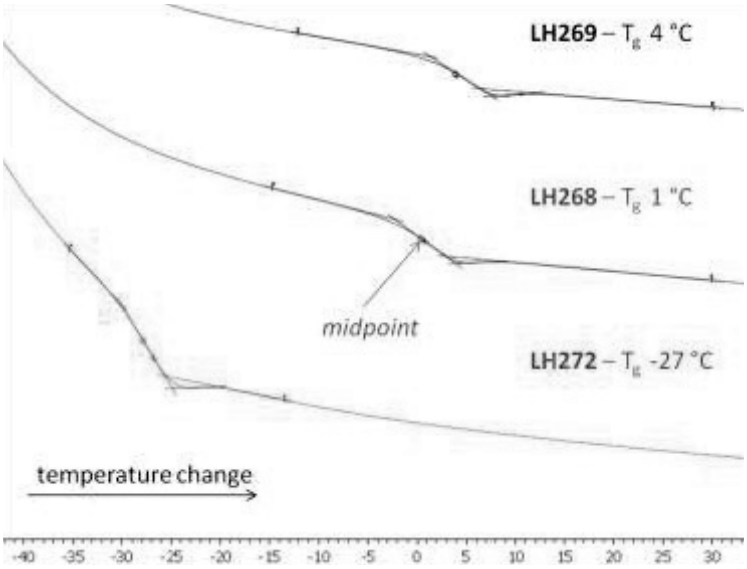

Figure 78: Differential scanning calorimetry curves used to determine the resin T_g

Generally, the resin temperature was once raised to 100 °C and cooled down to -50 °C before the curve used to determine the glass transition temperature was recorded.[LI]

5.3.4.1 Effect of isosorbide and phthalic anhydride on the resin glass transition temperature

A linear dependence of the glass transition temperature on the amount of both isosorbide and phthalic anhydride added in the formulation was observed as shown in figure 79. While the one to one replacement of isosorbide with phthalic anhydride led to lower glass transition temperatures, the general effect of increasing the phthalic anhydride was slightly stronger.

While adding 1 mol% of isosorbide to the formulation led to an approximate increase of the T_g of 1,3 °C, the same increase in phthalic anhydride led to an increase of 1,56 °C. The glass transition temperatures of resins containing 45,13 mol% isosorbide and 48,73 mol% phthalic anhydride were therefore quite close to each other at 31 °C and 27 °C.

[LI] The error in the glass transition temperature measurements was equally examined and found to be below 1 °C. Details on the process can be found in the annexe.

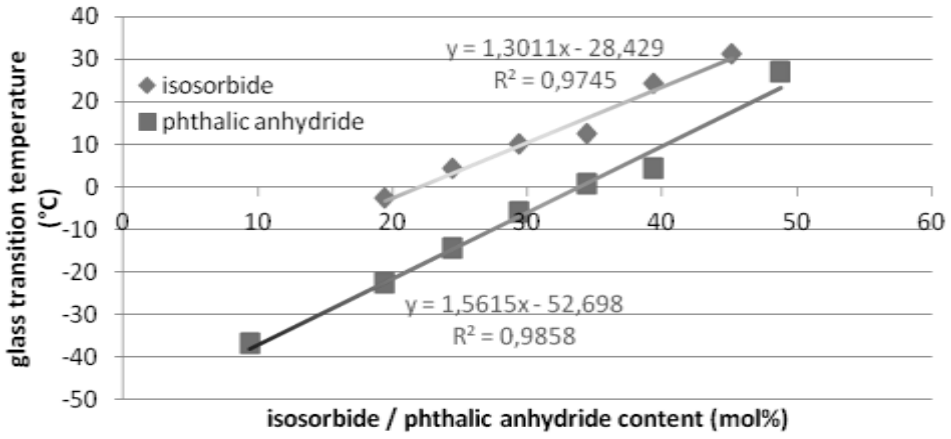

Figure 79: T_g *vs.* Isosorbide and phthalic anhydride content

5.3.4.2 Effect of other monomers on the glass transition temperature

The effect of the other monomers on the glass transition temperature was also studied. The change in T_g compared to LH189 is shown in figure 80. The changes caused by sebacic acid, 1,3-propanediol, 1,2-propanediol and succinic acid are shown in blue, and the changes caused by gradual increase in glycerol content are shown in green. The first group of prototypes, in which the changes which caused an increase in T_g were combined to induce maximum rigidity, are also included in purple.

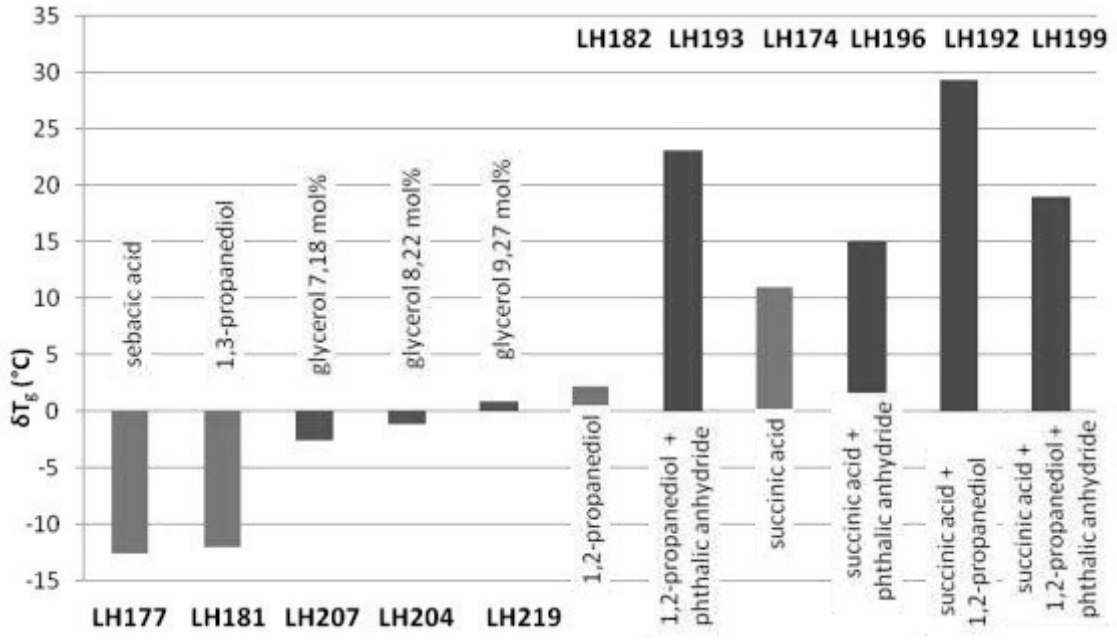

Figure 80: Change in T_g induced by different monomers

A significant decrease in glass transition temperature was observed for the replacement of succinic acid with sebacic acid and for the replacement of 1,2-propanediol with 1,3-propanediol. The increase of glycerol and the replacement of 1,3-propanediol with 1,2-propandiol, on the other hand, only

caused a very small change in glass transition temperature. The largest increase for a single monomer change was achieved by the replacement of sebacic acid with succinic acid.

The simultaneous increase of two monomers in the formulation did not have the same effect that could be expected from adding the changes observed after an individual increase of each. For example, the simultaneous replacement of 1,3-propanediol with 1,2-propanediol, which cause a 2 °C increase, and the increase of phthalic anhydride content from 29,37 mol% to 34,37 mol%, which cause a 7 °C increase, resulted in the overall increase of 23 °C in the resin LH193.

On the other hand, the simultaneous increase in phthalic anhydride content by 5%, which caused an increase in T_g of 9 °C on its own, with the replacement of sebacic acid with succinic acid, which caused an increase in T_g of 11 °C on its own, only resulted in an overall increase of 15 °C in the resin LH196. The highest glass transition temperature of 29 °C was obtained by combining the replacement of sebacic acid with the replacement of 1,3-propanediol in the resin LH192.

5.3.4.3 Relationship of the resin molecular weight and its glass transition temperature

The relationship of the glass transition temperature and the molecular weight can be described by the Flory-Fox equation.[259] It relates the T_g at any molecular weight to the maximum glass transition temperature which could be reached at infinite molecular weight ($T_{g\infty}$), the molecular weight and a constant K.

$$\textit{Flory-Fox equation}: T_g = T_{g\infty} - K/M_{\bar{n}}$$

This relationship leads to an asymptotic increase of the glass transition temperature as the molecular weight increases. The existence of this kind of relationship was also investigated for the different formulations. The glass transition temperatures plotted against the weight average molecular weights for the different resins are shown in figure 81. No correlation could be observed for the series of isosorbide resins or for the phthalic anhydride resins LH174, LH177, LH181, LH182 and LH207, LH204 and LH219, shown in green, in which the effect of other monomers were tested.

The resins with varying phthalic anhydride content show the opposite of the expected relationship. The fact that lower glass transition temperatures correspond to higher molecular weights is however more likely due to the fact that both lower molecular weights and high glass transition temperatures are linked to high phthalic anhydride content than to a direct correlation.

The only group of resins which follows the kind of trend described by the Flory-Fox equation are the prototypes with an increased amount of rigid monomers, who display a higher T_g with higher $M_{\bar{w}}$. Looking at the overall distribution of the resins on the graph, it is however clear that the molecular

weight cannot be used as a predictor for the glass transition temperature. The relationship between the number average molecular weight was also examined, and the same conclusion was reached.

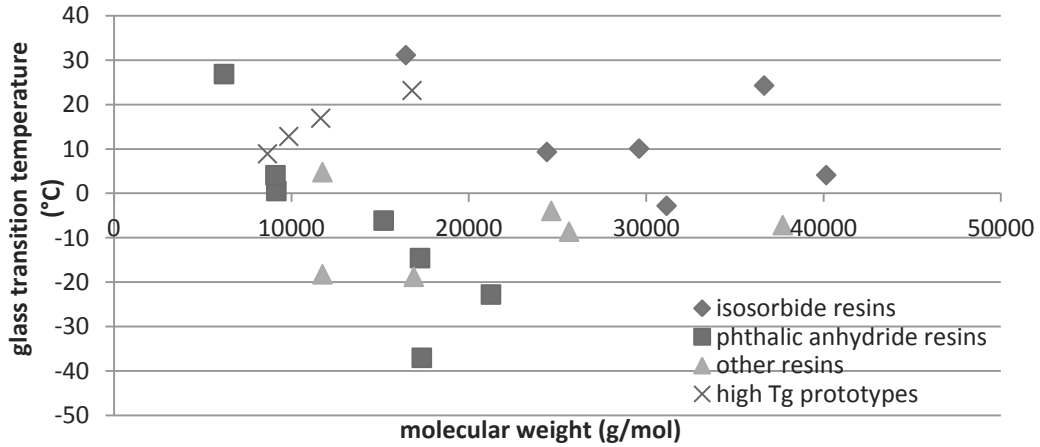

Figure 81: T_g *vs.* $M_{\overline{w}}$

The deviation from the relationship between molecular weight and glass transition temperature reported by Fox *et al.* is not really surprising, since the Flory-Fox equation is only valid for samples of different molecular weights of the same polymer. It does not take into account the chemical differences between resins, which can evidently have a much bigger impact on the glass transition temperature than the chain length. Furthermore, it is known that the Flory-Fox equation is most reliable for large number average molecular weights and narrow polydispersities, neither of which are given in this case.[LII]

5.3.4.4 Compensation for T_g decrease associated with the reduction of phthalic anhydride

In order to maximise the biosourced content of the resins, the amount of phthalic anhydride in the formulation needs to be reduced while compensating for the decrease of the glass transition temperature caused by the loss in rigidity. The simultaneous increase in 1,2-propanediol and succinic acid were found to cause a significant increase in T_g in the resin LH192. Therefore, a series of prototypes was made reducing the phthalic anhydride content stepwise while also increasing the amount of succinic acid and 1,2-propanediol.

The increase in rigidity through succinic acid and 1,2-propanediol was successful in increasing the glass transition temperature from -15 °C and -23 °C to 17 °C and 11 °C for resins containing 24,37 mol% and 19,37 mol% phthalic anhydride respectively.

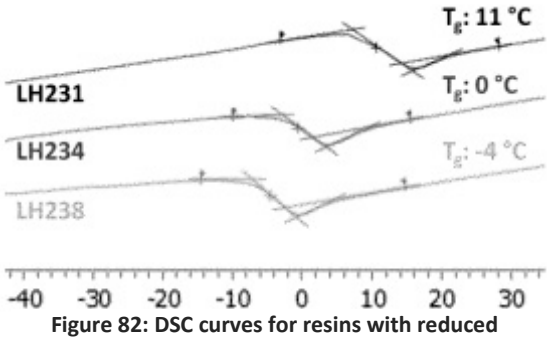

Figure 82: DSC curves for resins with reduced phthalic anhydride content

[LII] The glass transition temperatures of isosorbide resins in which the isosorbide content was increased while the hydroxy value was kept constant is presented in the annexe.

The 32 °C and 34 °C increase is even higher than that of 29 °C achieved for the resin containing 29,37 mol% phthalic anhydride.

Two more prototypes, LH234 and LH238, were synthesised in which the phthalic anhydride content was decreased even further to 14,37 mol% and 9,37 mol%. In their formulations, the 1,3-propanediol was completely replaced with 1,2-propanediol, but 4 mol% sebacic acid were added to prevent gel formation. Nevertheless, an increase in glass transition temperature from -37 °C to -4 °C for LH238 compared to LH239 also containing 9,37 mol% of phthalic anhydride was achieved, as shown in figure 82.

In conclusion, the petroleum based content of the resins could be reduced by over 60% while still maintaining an acceptable glass transition temperature. In table 78, the phthalic anhydride content for each resin in the series is shown both in terms of mol% and in terms of weight%. The two prototypes LH231 and LH238, one with and one without sebacic acid, were selected for further evaluation.

Table 78: Prototypes with reduced phthalic anhydride content

	phthalic anhydride content		T_g
resin	**mol%**	**weight%**	**°C**
LH228	24,37	34,42	17
LH231	19,37	27,75	11
LH234	14,37	20,22	0
LH238	9,37	13,38	-4

5.3.4.5 Glass transition temperatures of cyclohexanedicarboxylic acid and new isosorbide prototypes

A last group of prototypes was created by incorporating isosorbide or cyclohexanedicarboxylic acid into the formulation of the phthalic anhydride based resins described above. The petroleum based content and glass transition temperatures of the resulting resins are shown in table 79.

Table 79: Glass transition temperatures and petroleum based content of isosorbide and CHDA resins

	petrosourced content		T_g
resin	**mol%**	**weight%**	**°C**
LH265	9,37	15,22	-9
LH272	14,26	19,66	-27
LH266	19,37	22,85	-4
LH268	10,00	9,21	1
LH269	9,90	9,16	4
LH267	0,00	0,00	-16

The resins LH265 and LH269 were selected for further investigation because they presented the best compromise between low petroleum based content and high glass transition temperatures. In order to increase the low T_g of -9 °C of the CHDA based resin, another resin containing more CHDA was formulated. However, gel formation could only be prevented by also increasing the amount of sebacic acid, which largely offset the effect of the additional CHDA on the T_g in the resin LH272.

A similar conclusion was reached for the resin LH267, which contains 39,37 mol% of isosorbide but no succcinic acid or 1,2-propanediol. Again, the T_g raising effect of isosorbide was offset by the sebacic acid and 1,3-propanediol, leading to a glass transition temperature of -16 °C compared to 24 °C of the resin LH243 also containing 39,37 mol% of isosorbide.

Overall, it can be concluded that the presence of different aliphatic chain lengths in the case of succinic and sebacic acid and the presence or absence of a methyl branch in the case of 1,2-propandiol and 1,3-propanediol can influence the glass transition temperature to a similar degree as the amount of cyclic and aromatic monomers such as cyclohexanedicarboxlic acid, phthalic anhydride and isosorbide.

5.4 Properties of biobased melamine crosslinked polyester films

Five groups of resins were applied and cured with melamine crosslinker in the Beckers laboratory to evaluate their curing behaviour and the properties of the resulting films, which will be discussed in this section.

5.4.1 Summary of prototypes tested in application

The first three groups were designed to explore the effect of each monomer in the formulation on the overall film properties. Their characterisations are summarised below in table 80.

Table 80: Group 1A – Characterisation of resins with different quantities of isosorbide tested in application

	isosorbide content	$M_{\overline{w}}$	viscosity	conc. in MPA	T_g
resin	**mol%**	**g/mol**	**mPa*s**	**%**	**°C**
LH249	19,37	31150	5622	65,5	-3
LH190	24,37	40150	18934	66,1	4
LH184	29,37	29600	8553	65,4	10
LH168	34,31	24400	6595	64,7	9
LH248	45,13	16450	10063	66,1	31

Five different resins, from here on termed 1A, containing quantities of isosorbide from 19,37 mol% to a maximum of 45,13 mol% were tested. Equivalent phthalic anhydride resins (1B) with quantities of 19,37 mol% to a maximum of 48,73 mol% were also examined and are shown in table 81. When

comparing the resins containing a maximum amount of isosorbide and phthalic anhydride, the phthalic anhydride content is slightly higher due to the continued presence of glycerol in the formulation.

Table 81: Group 1B – Characterisation of resins with different quantities of phthalic anhydride tested in application

	phthalic anhydride content	$M_{\overline{w}}$	viscosity	conc. in MPA	T_g
resin	**mol%**	**g/mol**	**mPa*s**	**%**	**°C**
LH237	19,37	21250	2756	66,1	-23
LH162	24,37	17250	1681	65,3	-15
LH189	29,37	15200	2374	*65,0**	-6
LH163	34,37	9150	1539	64,9	1
LH242	48,73	6200	1721	64,4	27

* DBE solvent mixed with MPA solvent was used instead of pure MPA solvent to dilute LH189

Lastly, five different phthalic anhydride based resins with increased quantities of succinic acid, sebacic acid, 1,3-propanediol, 1,2-propanediol and glycerol (1C) compared to LH189 were also examined and are shown in table 82.

Table 82: Group 1C – Characterisation of resins for the examination of the effect of other monomers in the formulation used in application

		$M_{\overline{w}}$	viscosity	conc. in MPA	T_g
resin	**monomer tested**	**g/mol**	**mPa*s**	**%**	**°C**
LH174	succinic acid	11750	2397	64,5	5
LH177	sebacic acid	16900	3229	65,6	-19
LH181	1,3-propanediol	11750	1567	65,9	-18
LH182	1,2-propanediol	24650	3542	65,2	-4
LH219	glycerol 9,27 mol%	30776	5915	65,0	-5

The last two groups consisted of prototypes proposed for exterior coil coating application and are shown in table 83. The first group of prototypes (2A) contained resins in which the amount of rigid monomers was increased to reach high glass transition temperatures. They can also serve to examine the addition of the effects observed for the group of prototypes shown above.

Table 83: Group 2A – Characterisation of prototypes with a high glass transition temperature used in application

		$M_{\overline{w}}$	viscosity	conc. in MPA	T_g
resin	**description**	**g/mol**	**mPa*s**	**%**	**°C**
LH192	high Tg	16800	2474	63,2	23
LH193	high Tg	11650	1963	64,7	17
LH196	high Tg	8650	2045	65,4	9
LH199	high Tg	9850	2136	64,5	13

The last group of prototypes (2B) is a selection of the most promising monomers containing the minimum possible amount of phthalic anhydride, a mixture of phthalic anhydride and isosorbide or cyclohexanedicarboxylic acid, shown in table 84. Aside from the evaluation of their suitability for exterior coil coating, they also serve to explore changes that are possible to expand the space of biobased and partially biobased resins.

Table 84: Group 2B – Characterisation of other prototypes made to explore the possibilities for biobased resins used in application

		$M_{\overline{w}}$	viscosity	conc. in MPA	T_g
resin	**description**	**g/mol**	**mPa*s**	**%**	**°C**
LH231	reduced petro	12350	2113	64,5	11
LH238	reduced petro	15050	1950	65,7	-4
LH265	CHDA	32368	5618	65,1	-9
LH269	ISO/PAN	20680	5638	66,2	4

All prototypes shown in these five groups were not only characterised after application but also subjected to artificial weathering to examine their durability. The results concerning the first group of prototypes 1A, 1B and 1C for the examination of the effects of each monomer as well as the high T_g prototypes of the second group 2A will be discussed in chapter 6. The weatherability testing for the last group of prototypes 2B is still in progress.

5.4.2 Curing behaviour

The resins were cured with hexamethoxymethylmelamine resin (5-15%) in a formulation with additional solvents as well as a catalyst and flow additives onto a primer coated steel plate. The coating was crosslinked in an oven for 25 s at 320 – 340 °C to reach a peak metal temperature of 232 °C.

In the first round of applications, three more resins, described in table 85, were also tested. They were later replaced with the resins characterised above. After the synthesis of LH070, LH126 and LH183 was complete, the methoxypropyl acetate solvent added to dilute them was added too quickly, and their aspects became hazy.

Table 85: Characterisation of resins with hazy aspects replaced by other resins later

				$M_{\overline{w}}$	viscosity	conc. in MPA	T_g
resin	**replaced by**	**based on**	**mol%**	**g/mol**	**mPa*s**	**%**	**°C**
LH126	LH190	isosorbide	24,37	19050	3349	63,0	1
LH070	LH168	isosorbide	34,31	-	9090	66,7	12
LH183	LH189	phthalic anhydride	29,37	20350	2706	65,1	-4

After application to a primer coated steel plate, small holes were observed in the paint layers, which resulted in the appearance of craters in the coating after curing. The replacement of LH070, LH126 and LH183 with LH168, LH190 and LH189, which were based on the same formulation but to which the solvent was added more carefully so that their aspects were clear, improved the aspect of both the wet and the cured film.

The other resins, which had clear aspects at 65% concentration in MPA, also formed smooth wet films and craterless dried films. This suggests that incompatibility with the solvent system or incomplete solubilisation results in damage to the coating.

5.4.2.1 Creation of free films

Free films, i.e. cured coatings that can be completely separated from their support, are sometimes used for accelerated ageing tests, because they can be spectroscopically analysed without fear of noise from the support, and for dynamic mechanical analysis. They are obtained by curing the resin on a teflon surface coated with anti-adhesives.

Several unsuccessful attempts were made to obtain free films. In figure 83, the result for LH183, the coating of a resin with a hazy aspect, and LH184, the coating of a resin with a clear aspect, are shown. The craters caused by the uneven surface tension in LH183 are enlarged on the teflon surface, probably due to the lack of adhesion. They are so big that the resin is only gathered at the crater edge, and only a very limited amount of thin, clear film is obtained.

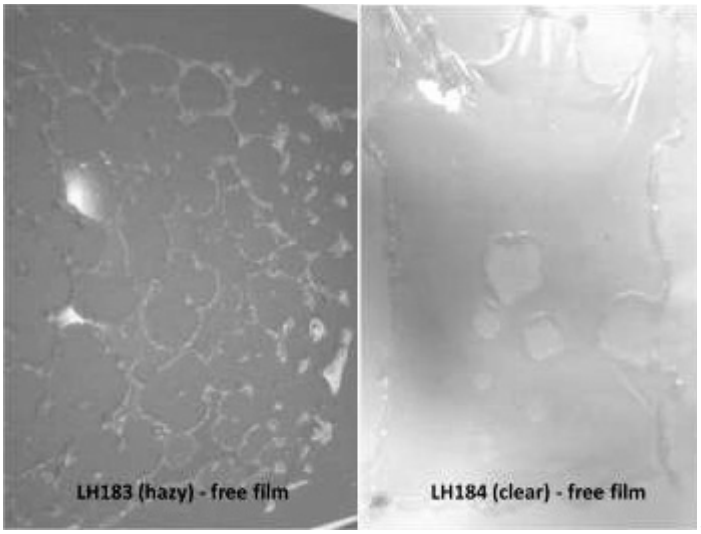

Figure 83: Free films made from LH183 and LH184

The result is markedly better with the clear resin LH184, but some craters are also formed. First of all, this indicates that some difference in surface tension still exists within the film, and that the compatibility between the solvent system and the resin may have to be optimised. Secondly, even though only a few craters are observed, they cannot be removed from the teflon plate as smoothly as the rest of the film, and leave behind microscopic or larger defects. This in turn markedly decreases the quality of the next film applied.

After two to three applications, the removal of the film in one piece becomes impossible, and little scraps are obtained instead. Therefore, the creation of free films was abandoned and all weathering tests and dynamic mechanical analysis measurements were performed on films on steel substrates.

5.4.2.2 Gloss

The gloss of the cured film was only measured for the first batch of resins tested in application. The gloss test measures the amount of light reflected at a 60° angle. If unevenness or cracks are present in the surface, the light is diffracted and the gloss is lowered.

Table 86: Gloss of isosorbide and phthalic anhydride based coatings

resin	**isosorbide content**	**Gloss 60° (%)**
LH126	24,37 mol%	97
LH184	29,37 mol%	90
LH070	34,31 mol%	87
LH168	34,31 mol%	91
resin	**phthalic anhydride content**	**Gloss 60° (%)**
LH162	24,37 mol%	95
LH183	29,37 mol%	92
LH163	34,37 mol%	98

All resins tested displayed good gloss properties within specifications, with reflections between 87% and 98%, as shown in table 86. This included even the resins which had shown a hazy aspect before applications and craters after curing.

The gloss of the resins directly after curing was therefore not further evaluated except for in the context of gloss retention measurements which were used as a measure of ageing. These are discussed in chapter 6.

5.4.2.3 Solvent rub test

The solvent rub test is a measure of the resistance to chemicals which can also indicate problems with the curing, as poorly crosslinked films are dissolved much easier. It is performed by rubbing a piece of cotton soaked in methyl ethyl ketone (MEK) solvent back and forth over the coating with a constant pressure. The amount of rubs necessary to damage the film is recorded.

All of the coatings tested resisted 100 rubs back and forth without any damage. Overall, the gloss measurement, the rub test and the visual assessment of the coatings suggests that the curing was successful and that all resins tested are suitable for application.

5.4.3 Mechanical properties

Three different approaches were used to evaluate the mechanical properties of the resins after curing. First, thermal analysis was used to determine their glass transition temperature and estimate their crosslinking density. Secondly, the μ-hardness test, which evaluates the response to stress and viscoelasticity, was performed. Last, traditional tests for identifying mechanical failure such as the T-

bend test, the Erichsen indentation test and the impact test were evaluated. The results and conclusions drawn relating to the resin composition are presented in this section.

5.4.3.1 Glass transition temperature evaluation after curing by DSC

The glass transition temperature of the cured film was determined by scraping off a small sample from the support and evaluating it in differential scanning calorimetry. In figure 84, the difference in T_g for each coating compared to the T_g of the corresponding resin before curing is shown. Interestingly, for the same quantity of isosorbide and phthalic anhydride present in the resin, the isosorbide resins show a larger increase in all cases.

Furthermore, all the changes which were made to the phthalic anhydride resin to explore the effect of single monomers, shown in green, led to a larger increase compared to the basis LH189. The largest increase of 40 °C was observed for the resin LH182, in which all 1,3-propanediol was replaced by 1,2-propanediol. The resin LH219, in which the amount of glycerol was increased from 6,14 mol% to 9,27 mol% compared to LH189, also showed an above average increase of 31 °C. This suggests that the curing is effective on previously not reacted secondary hydroxy groups.

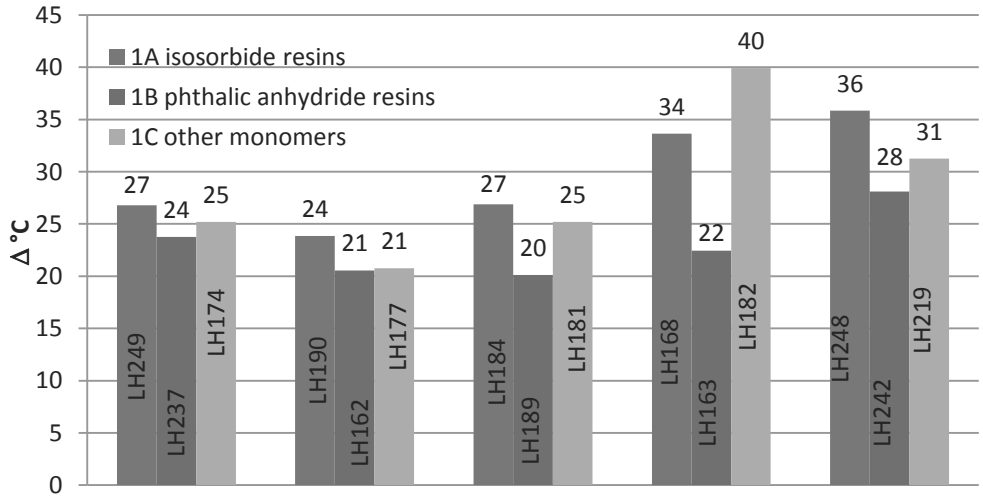

Figure 84: Increase in T_g after curing

The average increase observed in all examined coatings was 27 °C, with 29 °C for the isosorbide coatings (1A) and the high T_g prototypes (2A), and 28 °C for the coatings in which one monomer was modified (1C) and the last group of prototypes (2B). The lowest average of 23 °C was observed for the group of prototypes in which the quantity of phthalic anhydride was modified (1B). Both phthalic anhydride and isosorbide coatings show the largest increase of glass transition temperature for the prototype containing a maximum amount of either monomer. The difference to the pre-curing resin decreases initially as the amount of isosorbide and phthalic anhydride decrease, and then increases

again for the very low amounts. However, too few samples were examined to determine if this is random or a trend.

Overall, the absolute glass transition temperature of the isosorbide coatings is in all cases higher than that of the phthalic anhydride coatings, and a linear correlation can still be observed between the amount of isosorbide and phthalic anhydride added to the formulation and the final glass transition temperature reached, as shown in figure 85.

When targeting mechanical properties of the film, the aim is to reach a compromise between hardness, which can withstand minor impacts and keep the film flawless, and flexibility so that the coated metal sheets can be formed without damaging the paint. Therefore, the best way to evaluate the suitability of mechanical properties is by comparing them to those of the standard petroleum based film currently used for exterior applications.

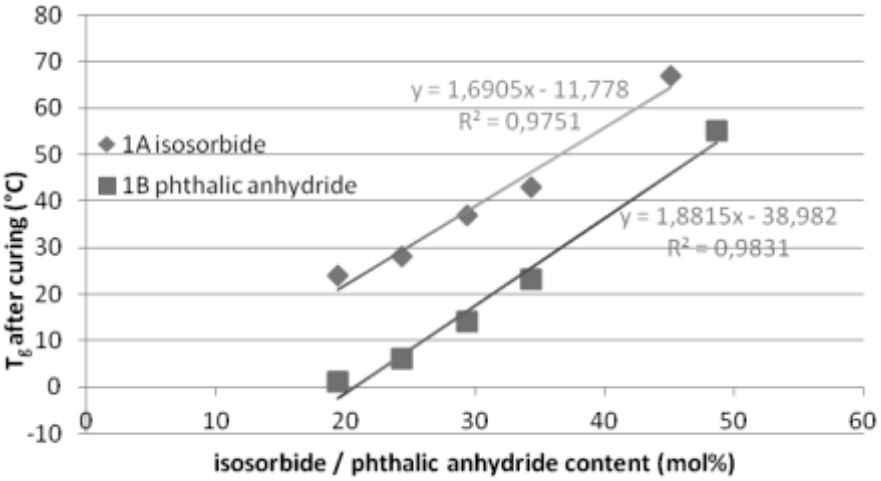

Figure 85: T_g after curing *vs.* isosorbide and phthalic anhydride content

The glass transition temperature of this standard resin after curing is 23 °C. Comparing the absolute values of the resins in the phthalic anhydride series (1B) and the isosorbide series (1A) shows that most isosorbide resins are slightly too rigid, while only the phthalic anhydride resins containing 34,37 mol% or more reached the required T_g.

Fortunately, the partially biosourced resins LH174, in which the sebacic acid was replaced with succinic acid, LH182, in which the 1,3-propanediol was replaced with 1,2-propanediol and LH219, in which the quantity of glycerol was increased, all have glass transition temperatures above that of the standard. It can be concluded that the modification of phthalic anhydride resin can easily be used to increase the glass transition temperature after curing to sufficient levels.

The group of prototypes with an increased amount of rigid monomers (2A) all showed a similar increase of glass transition temperature after curing between 27 °C and 30 °C, as shown in table 87.

The large increase observed for the resin LH182 where 1,3-propanediol was replaced with 1,2-propanediol was not mirrored in the resin LH193, in which 1,3-propanediol was replaced with 1,2-propanediol and the phthalic anhydride content was increased from 29,37 mol% to 34,37 mol%. Either the increase of phthalic anhydride counteracted the efficiency of the crosslinking and therefore the increase of T_g during the curing reaction, or it led to a more efficient conversion of secondary hydroxy groups in the first place.

Table 87: Glass transition temperatures after curing of third, fourth and fifth group of prototypes (1C, 2A and 2B)

group 1C	T_g	group 2A	T_g	group 2B	T_g
resins	°C	resins	°C	resins	°C
LH174	30	LH192	51	LH231	42
LH177	2	LH193	46	LH238	23
LH181	7	LH196	36	LH265	16
LH182	36	LH199	43	LH269	34
LH219	26				

In the last group of prototypes (2B), the suitability of the resin LH238, which contains only 9,37 mol% of phthalic anhydride, was confirmed as it reached a glass transition temperature of 23 °C after curing. The resin containing cyclohexanedicarboxylic acid only reached a T_g of 16 °C. While this is a little low compared to that of the standard, a slight deviation in either direction doesn't automatically exclude a resin, as the properties can still vary significantly due to other factors. Its suitability for coil coating purposes will be further evaluated in the other tests.

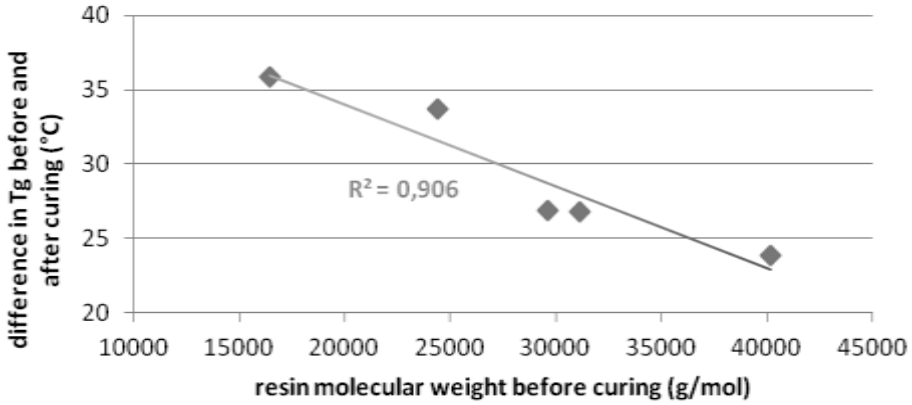

Figure 86: T_g increase after curing *vs.* $M_{\overline{w}}$ for isosorbide resins (1A)

When comparing the molecular weight of the resin before curing with the increase of the glass transition temperature after curing, a linear trend can be observed among the isosorbide coatings as shown in figure 86. The higher the molecular weight was before curing, the smaller is the increase

that can be achieved by crosslinking. This indicates that the increase in T_g is linked to the increase in molecular weight achieved by the crosslinking.

No similar correlation is discernible in the phthalic anhydride resins, which could be due to the fact that the differences observed in molecular weight for those prototypes are much smaller than the differences in molecular weight between the different isosorbide resins.

5.4.3.2 Dynamic mechanical analysis of the cured resins

An important property governing the behaviour of a coating is its crosslink density. It can be influenced by the quantity and type of melamine added to the paint formulation, by the efficiency of the catalyst, by the quantity and availability of hydroxy groups in the uncured resin and by the temperature and duration of the curing process. It affects the viscoelastic response to stress of the coating and thus its hardness and its flexibility. Therefore, it can be indirectly evaluated by mechanical tests such as the T-bend and the impact test, but separating the influence of the single monomers from that of the crosslinking density can be challenging.

A convenient and direct way to directly analyse the crosslinking density is by dynamic mechanical analysis (DMA). It evaluates the response to stress while slowly raising the temperature, and enables conclusions about the polymer network. If the overall density of the polymer film is known, conclusions can also be drawn about the size of the chain segments between crosslinking points. This is a good way to estimate the molecular weight of a crosslinked network. Size exclusion chromatography requires solubilisation of the sample, which is not possible for coatings without destroying the crosslinks, and mass spectrometry, which would be possible for example using matrix assisted laser desorption ionisation (MALDI), is significantly more expensive.

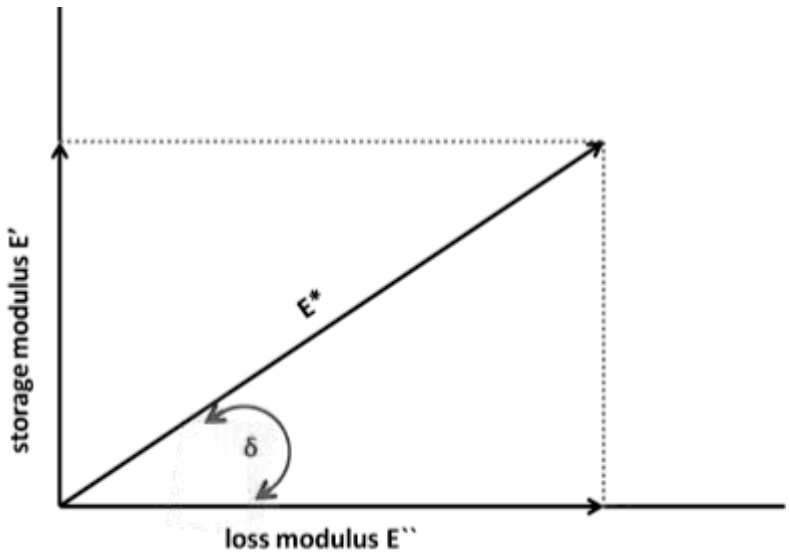

Figure 87: Vectorial representation of the dynamic modulus

In general, DMA is performed by applying a periodic force to the coating, and measuring its response over a range of temperatures. The strain experienced by the coating is out of phase with the strain applied by an angle termed δ because of the viscoelasticity of the polymer, and the time needed for the molecules to rearrange and relax.

The two waves of stress and strain can be represented as vectors with an angle corresponding to the phase lag between them, as shown in figure 87 above. Depending on the technique used, different types of moduli can be measured. The illustration above, which was taken from an article by Koleske, shows the complex tensile modulus, which is denoted as E*.[260] From the complex modulus and the angle δ, the storage modulus E' and the loss modulus E'' can easily be calculated. The ratio of the loss modulus and the storage modulus is equal to the tangent of the angle δ, and often used to characterise the measurement.

The storage modulus E', which is the first derivative of the complex modulus, represents the elastic response of the material, and is associated with the ability to store energy and release it upon deformation, and with the stiffness of the material. The loss modulus E'', or the second derivative of the complex modulus, represents the viscous response of the material and is associated with energy dissipation in the form of heat.

Depending on the type of sample that needs to be analysed, different measuring methods are used and different complex moduli are determined. A few of the different methods are illustrated in figure 88.[261] In order to measure the response of a coating on its steel substrate, the shear modulus was measured in this work by applying vertical motion parallel to the sample surface on a lever in contact with two samples of coating applied onto steel coupons, as illustrated in the bottom right.

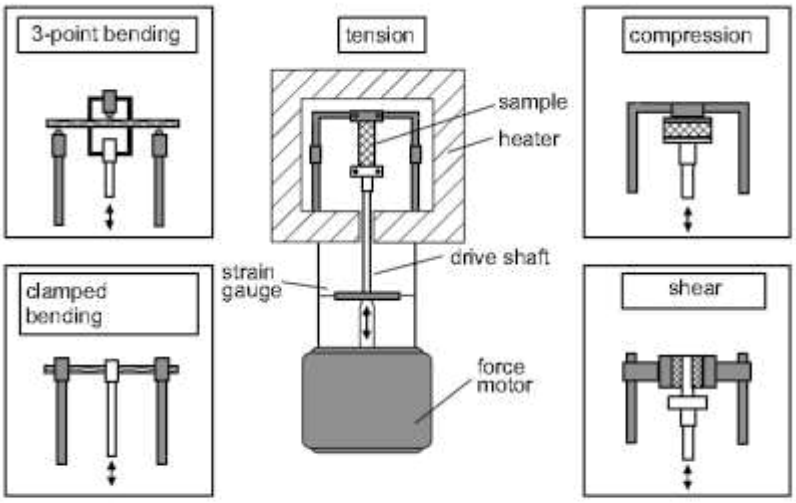

Fig. 6.6 Schematic design of a dynamic-mechanical analyzer under vertical load, and showing the various possible test arrangements

Figure 88: Illustration of different DMA measurement methods

The shear modulus, also called viscous modulus, is calculated in the same manner as the tensile modulus, and is usually denoted by G*, G' and G'' for the complex, storage and loss components.

The glass transition temperature can be observed in the response of the tangent of the angle δ (tanδ) or from its components, the storage and the loss modulus, to the change of temperature. The viscous response to the force, i.e. the loss modulus, is maximised when the timescale of the molecular motion is similar to the oscillation of the force.[261] In that case, the applied force is converted to deformations at the molecular scale with maximum efficiency. This occurs at the glass transition temperature, which can therefore be determined from the maximum of the loss modulus curve.

On the other hand, the storage modulus decreases rapidly when the glass transition temperature is approached, as the capability of the material to respond elastically decreases. As the tan δ is the ratio of the loss modulus and the storage modulus, it also reaches a peak near the glass transition temperature. However, the peak is shifted a few degrees up as the decrease of the storage modulus initially compensates for the increase of the loss modulus. The overall distance between the peak of the loss modulus and the peak of tan δ is influenced by the load applied to the material as well as by the frequency of the force application.

Other than to the glass transition temperature, DMA measurements have also been linked to a number of other coating mechanical properties, such as the scratch resistance by Schlesing *et al.*, the tensile strength by Buder-Stroisznigg *et al.*, failure stress and failure strain by Giannakopoulos *et al.* and the stone chip resistance by Lee *et al.* very recently.[262-266]

The minimum of the storage modulus curve is of particular interest to derive mechanical properties because it correlates to the crosslinking density of the network. The storage modulus decreases to a minimum after the glass transition temperature, which should theoretically be a plateau. However, due to the high temperatures, additional crosslinking can take place, increasing the minimum elastic response. Therefore, the minimum is usually taken to correspond to the original crosslinking density present in the coating.

Above the glass transition temperature, the coating approaches rubbery behaviour. Therefore, the kinetic rubber theory can be used to relate the storage modulus to the crosslinking density. The formula $\upsilon = G'_{min}/RT$ is used, where υ is the crosslinking density in mol/m^3, G'_{min} is the minimum of the shear storage modulus in Pa, R is the gas constant of 8,314 J/K*mol or 8,314 $m^3Pa/K*mol$ and T is the temperature at which the minimum occurred in K.[267, 268] If the tensile storage E' is measured, the relationship $\upsilon = E'_{min}/3RT$ is applied instead.

The crosslinking density thus obtained can be converted into the average size of the chain segments between crosslinks using the formula $M_c=\rho/\upsilon$, where ρ is the density of the coating in g/m^3 and M_c is the chain length obtained in g/mol.[267]

5.4.3.2.1 Glass transition temperatures obtained in DMA

All coatings in group 1, designed to determine the effect of the different monomers qualitatively and quantitatively, were analysed using dynamic mechanical analysis at laboratory of the CRM group in Liège, Belgium. The peak of the tan δ curve as well as of the G'' curve were determined and compared to the glass transition temperatures of the coatings that were found using DSC.

The fact that the DMA measurements were performed on the coatings together with the steel substrate introduces a risk of error, because the steel is much thicker and more rigid than the coating. In order to increase the response for the coating, four samples were measured simultaneously. Instead of one coated steel coupon, two, with the coating facing in the same direction, were inserted into the DMA machine. Furthermore, the measurement was repeated two to four times until good agreement between the response curves was observed. The average values from the measurements performed are reported in figure 89 and 90 below.

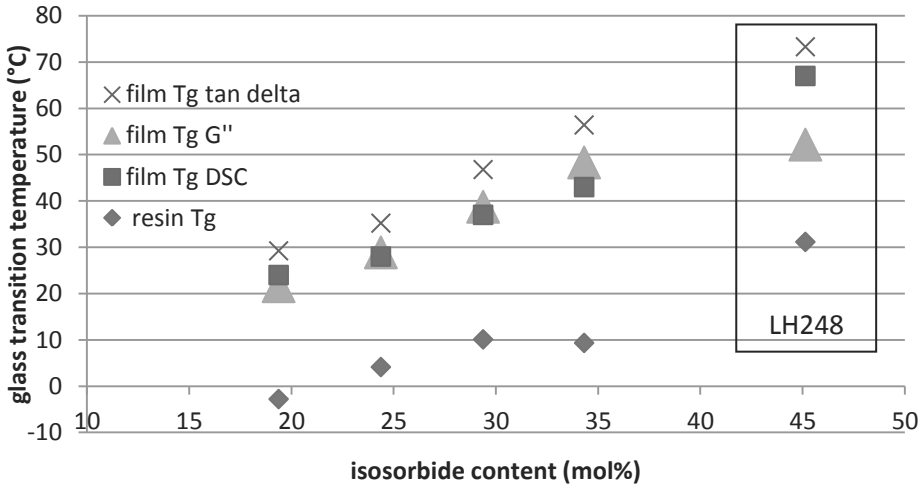

Figure 89: 1A isosorbide resin based coatings T_g's determined by different methods

In general, very good agreement was obtained between the maxima of the G'' loss modulus curve and the glass transition temperature determined by DSC. On average, the peak of the G'' curve was 4 °C higher than the glass transition observed in DSC. One exception was the measurement made for the isosorbide resin LH248, which contains the highest amount of isosorbide tested. In this case, the G'' maximum was 15 °C below the previously determined T_g. When comparing the determined values to the trend observed in the other resins containing less isosorbide, the G'' value is slightly below the expected value while the DSC value is slightly above it. Only the tan δ value seems to fit the trend.

Overall, we consider the DMA method validated by the agreement of the T_g values with the DSC measurements and the consistency of the trends with different isosorbide contents observed in the different measurement parameters.

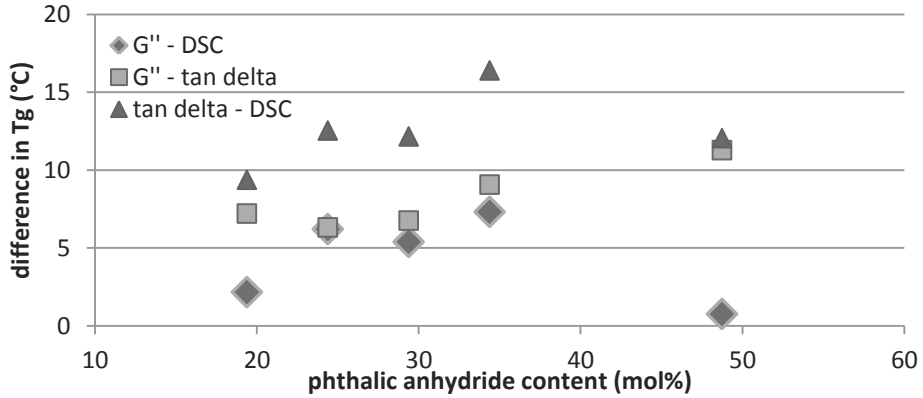

Figure 90: Difference in T_g's determined by different methods for phthalic anhydride resin based coatings (1B)

Concerning the phthalic anhydride coatings, the difference between tan δ and both the G'' maximum and the DSC transition seem to increase with increasing phthalic anhydride content. It is particularly remarkable in the difference between G'' and tan δ. This is also confirmed by the third group of resins, which all contain 29,37 mol% phthalic anhydride and in all of which a difference of 7 – 8 °C is observed between the G'' and tan δ maxima.

Since the tan δ value is calculated from the ratio of the loss modulus and the storage modulus, this suggests that the presence of phthalic anhydride in the formulation has an important impact on the energy distribution, and the relative amount of elastic and viscous deformation. The overall average values for the difference between G'' and tan δ observed in all resins is 9 °C, and the average difference between tan δ and the DSC T_g is 11 °C.

5.4.3.2.2 Crosslinking densities

Table 88: DMA measurements for isosorbide resin based coatings (1A)

	isosorbide content	T_g			crosslinking density		
		DSC	tan δ	G''_{max}	G'_{min}	υ	error (υ)
resin	**mol%**	**°C**	**°C**	**°C**	**°C**	**mmol/cm³**	**mmol/cm³**
standard	-	23	38	29	73	0,0270	0,0023
LH249	19,37	24	29	22	71	0,0670	0,0047
LH190	24,37	28	35	29	80	0,0576	0,1370
LH184	29,37	37	47	39	85	0,0906	0,0030
LH168	34,31	43	56	48	93	0,0592	0,0071
LH248	45,13	67	73	52	101	0,0599	0,0095

The crosslinking densities calculated from the minimum of the G' storage modulus curves are summarised in table 88, 89 and 90. The values are reported in mmol/cm^3 for better overview.

While the maxima of the tan δ curves and the G'' loss modulus curves were generally only a few degrees apart between repetitions of the measurement, the agreement of different values of the storage modulus minimum was not as good. The average absolute deviation from the average is therefore also shown to indicate the size of the measurement error. Relative to the average of the corresponding measurement, it ranges from 0,4% to 40%, with 11% on average.

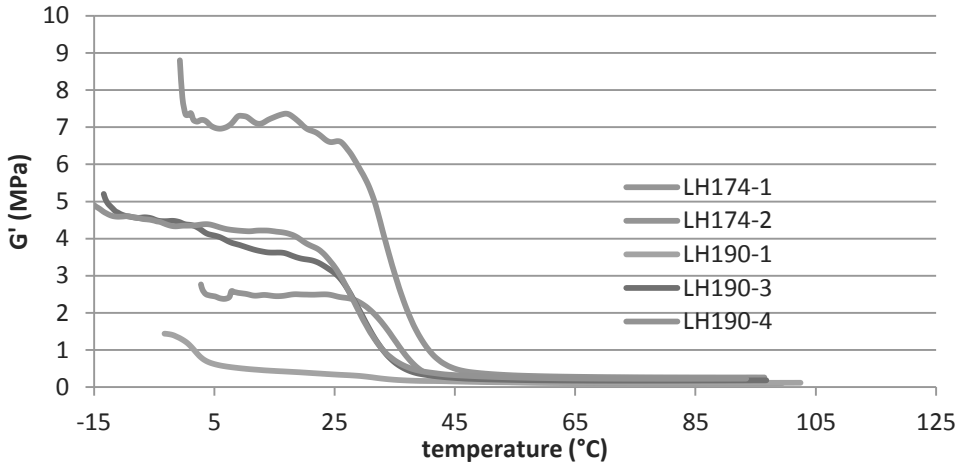

Figure 91: Storage modulus for curves with large error in the crosslinking density

This large uncertainty could be due to the nature of the measurement. As shown in figure 91 above for the two films LH190 and LH174, which displayed an error in the crosslinking density of 24% and 40% respectively, the storage modulus curves reach a very flat plateau after the glass transition temperature.

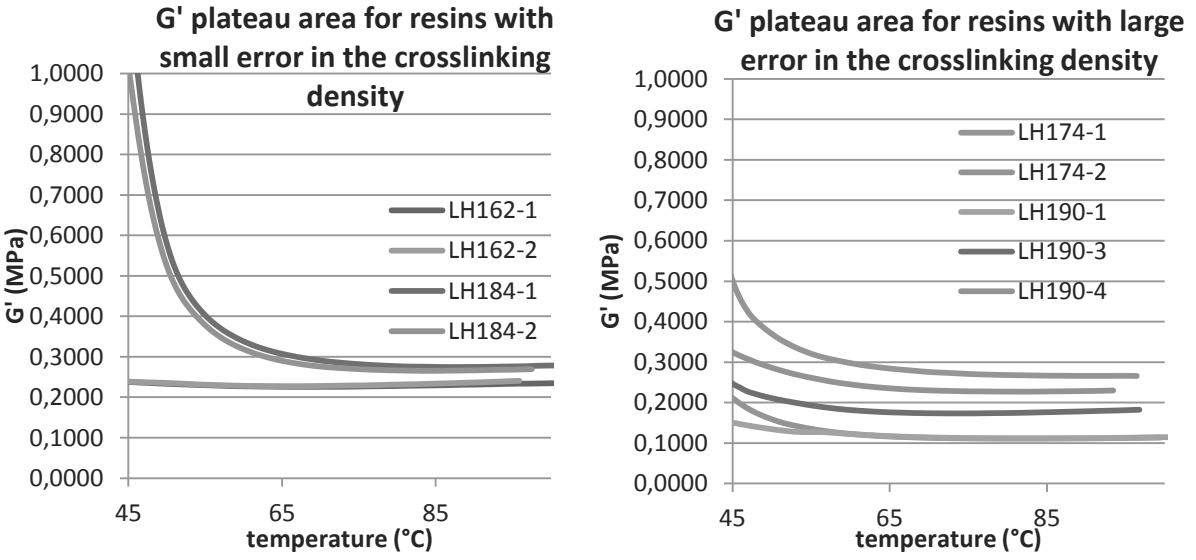

Figure 92: G' plateau area for resins with different errors in the crosslinking density

The variation that is caused by lower temperature or by additional crosslinking reactions only happens on the scale of 0,1 MPa. In figure 92, the plateau areas of the two resins shown above with a large error as well as that of the two resins LH184 and LH162, which displayed errors of only 3% and 0,4% respectively, and are shown in figure 93, are compared. It is therefore possible that the measurement of the different storage modulus minima is outside the sensitivity of the measurement. When comparing the overall curve of the large error films to those of the small error films, it does seem that the small errors also correspond to the better agreement of the overall curve.

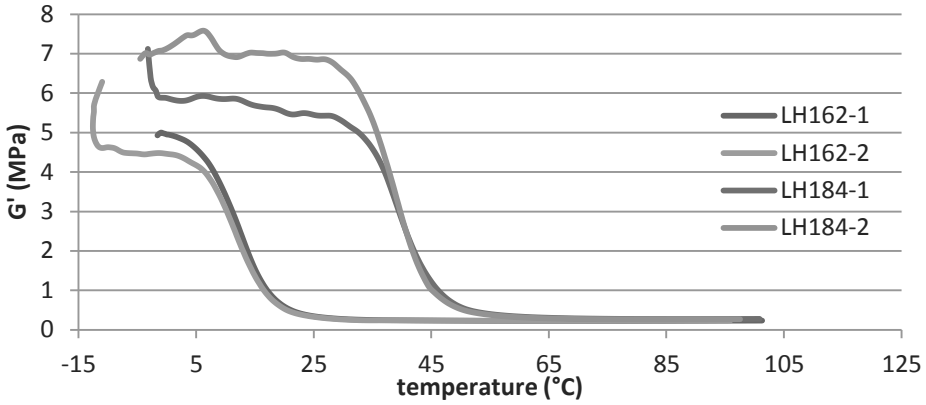

Figure 93: Storage modulus for curves with small error in the crosslinking density

Unfortunately, it was not possible to repeat the measurements often enough to confirm which of the measured minima corresponded to the real crosslinking density, and whether the variation is due to a lack of sensitivity or due to random errors. The values of crosslinking densities obtained should therefore be viewed as estimates of the real value.

The minimum of the storage modulus curves was observed between 43 °C and 60 °C after the glass transition. The average distance to the T_g of all measurements was 51 °C.

Table 89: DMA measurements for phthalic anhydride resin based coatings (1B)

	phthalic anhydride content	T_g			crosslinking density		
		DSC	tan δ	G''_{max}	G'_{min}	υ	error (υ)
resin	**mol%**	**°C**	**°C**	**°C**	**°C**	**mmol/cm³**	**mmol/cm³**
standard	-	23	38	29	73	0,0270	0,0023
LH237	19,37	1	10	3	46	0,0595	0,0018
LH162	24,37	6	19	12	67	0,0812	0,0003
LH189	29,37	14	26	19	73	0,0747	0,0018
LH163	34,37	23	39	30	90	0,0963	0,0085
LH242	48,73	55	67	56	100	0,0565	0,0079

Overall, all crosslink densities observed for the partially and fully biosourced coatings are higher than that observed in the standard coatings. No correlation between the quantity of isosorbide and

phthalic anhydride used could be detected. In the third group of coatings (1C), the lowest crosslinking densities are attributed to the films containing the resins LH182 and LH219, which contain increased amounts of 1,2-propanediol and glycerol respectively. This indicates that the relatively large increase in glass transition temperature compared to other coatings may not be due to additional crosslinking of the secondary hydroxy groups, but to a different mechanism.

Contrary to the increase of 1,3-propanediol, the increase of sebacic acid did not lead to higher crosslinking density. This suggests that the aliphatic chain length is not a vital factor in the development of the crosslinked network.

Table 90: DMA measurements of other monomer resin based coatings (1C)

	monomer added	T_g			crosslinking density		
		DSC	tan δ	G''_{max}	G'_{min}	υ	error (υ)
resin		°C	°C	°C	°C	mmol/cm³	mmol/cm³
standard	-	23	38	29	73	0,0270	0,0023
LH174	succinic acid	30	41	34	89	0,0627	0,0251
LH177	sebacic acid	2	15	7	68	0,0515	0,0052
LH181	1,3-propanediol	7	18	11	75	0,0684	0,0054
LH182	1,2-propanediol	36	48	40	86	0,0465	0,0037
LH219	glycerol 9,27 mol%	26	34	27	76	0,0421	0,0027

5.4.3.2.3 Calculation of the chain length between crosslinks

The average chain length between crosslinking points, M_c, can be calculated using the obtained crosslinking density υ in the formula $M_c=\rho/\upsilon$. For this, the density of the film, ρ, is needed. Two different ways were used to estimate the density. Firstly, the density ρ_1 was estimated from the weight and the thickness of the film on the steel substrate. Three different samples of coupons both with and without coating were weighed, and the average density was calculated based on the difference in weight and the average thickness of the film determined after the curing.

Table 91: Chain length between crosslinks for isosorbide resin based coatings (1A)

	isosorbide content	resin $M_{\bar{w}}$	υ	ρ_1	M_{c1}	ρ_2	M_{c2}
resin	mol%	g/mol	mmol/cm³	g/cm³	g/mol	g/cm³	g/mol
standard	-		0,0270	1,21	45156	1,15	42887
LH249	19,37	31150	0,0670	1,12	16782	1,15	17252
LH190	24,37	40150	0,0576	1,04	19790	1,15	21861
LH184	29,37	29600	0,0906	1,10	12134	1,15	12705
LH168	34,31	24400	0,0592	1,30	22280	1,15	19713
LH248	45,13	16450	0,0599	0,97	16662	1,15	19856

While this method yields coating specific results, a large error is also introduced with the uncertainty of the weighing measurement, especially because only small samples of 10 mm diameter could be tested. Another error is introduced by the natural variation of thickness of both the steel substrate and the film.

The second estimation was used for the density ρ_2. It is based on measurements made by the Beckers laboratory, which revealed the film density to usually be around 1,15 g/cm^3. The measurements were made over a much larger surface, and on a larger amount of samples, so the obtained density is likely to be more accurate. However, the measurements were made on a generic coating based on petroleum sourced monomers, so that a difference in density compared to the films used here is possible.

Table 92: Chain length between crosslinks for phthalic anhydride resin based coatings (1B)

	phthalic anhydride content	resin $M_{\bar{w}}$	υ	ρ_1	M_{c1}	ρ_2	M_{c2}
resin	**mol%**	**g/mol**	**mmol/cm^3**	**g/cm^3**	**g/mol**	**g/cm^3**	**g/mol**
standard	-		0,0270	1,21	45156	1,15	42887
LH237	19,37	21250	0,0595	1,93	32429	1,15	19335
LH162	24,37	17250	0,0812	2,43	29945	1,15	14156
LH189	29,37	15200	0,0747	1,61	21585	1,15	15402
LH163	34,37	9150	0,0963	0,96	10016	1,15	12045
LH242	48,73	6200	0,0565	3,24	58434	1,15	20757

The respective chain lengths calculated using the two different densities are shown as M_{c1} and M_{c2}. In general, the densities obtained for ρ_1 were commensurate with those obtained by Beckers with a few exceptions. However, further analysis for example of the densities of the resin before curing would be necessary to determine if the variation between ρ_1 and ρ_2 is due to the chemical and structural differences between the resins or the experimental error in determining ρ_1.

Table 93: Chain length between crosslinks for other monomer based coatings (1C)

		resin $M_{\bar{w}}$	υ	ρ_1	M_{c1}	ρ_2	M_{c2}
resin	**monomer added**	**g/mol**	**mmol/cm^3**	**g/cm^3**	**g/mol**	**g/cm^3**	**g/mol**
standard	-		0,0270	1,21	45156	1,15	42887
LH174	succinic acid	11750	0,0627	0,33	6296	1,15	21825
LH177	sebacic acid	16900	0,0515	1,56	30698	1,15	22560
LH181	1,3-propanediol	11750	0,0684	1,15	16974	1,15	16908
LH182	1,2-propanediol	24650	0,0465	1,22	26409	1,15	24894
LH219	glycerol 9,27 mol%	30776	0,0421	1,87	44612	1,15	27403

When comparing the calculated chain length between crosslinks obtained with either method shown in table 91, 92 and 93, with the weight average molecular weight of the resin before crosslinking, the small difference between the two values is conspicuous. The chain length between two crosslinking points, which would be expected to decrease by a factor of 2 by each crosslinking the resin chain experiences, is at most decreased by a factor of 2.44 for the smallest chains in the case of LH190, and in several cases actually increased compared to the resin molecular weight.

Several explanations are possible for this phenomenon. First of all, we can determine the theoretical amount of free hydroxy groups per polymer chain as proposed by Buder-Stroisznigg *et al.*, using the number average molecular weight and the end hydroxy value.[264] The hydroxy value of mg_{KOH}/g was converted to molKOH/g and then multiplied with the number average molecular weight. The results are shown in table 94 below.

Table 94: Average amount of free hydroxy groups per polymer chain before crosslinking

isosorbide group 1A	OH groups /chain	phthalic anhydride group 1B	OH groups /chain	other monomers group 1C	OH groups /chain
LH249	4,01	LH237	4,02	LH174	3,28
LH190	3,52	LH162	3,20	LH177	3,52
LH184	4,02	LH189	3,58	LH181	3,14
LH168	3,62	LH163	3,02	LH182	3,89
LH248	2,75	LH242	2,37	LH219	-

From the theoretical calculation, each polymer chain contains only between 2,75 and 4,02 free hydroxy groups on average. Two of the free hydroxy groups can be assumed to represent the chain ends. If the chain ends react with the crosslinker, this would result either in the same chain length between crosslinks as was present before the curing, or the prolongation of chains if the crosslinker molecule in question only reacts with one other hydroxy group. The crosslinking efficiency of hexamethyl methoxy melamine (HMMM) has been observed to average around the reaction of three out of six of the methoxy groups, so it is imaginable that a part of the crosslinker reacted only twice.

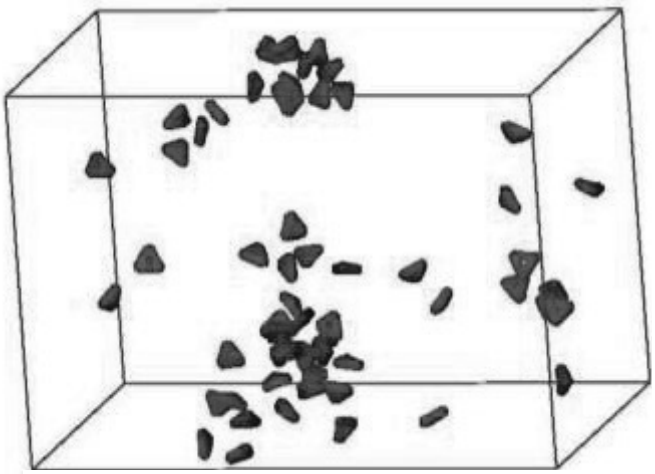

Figure 94: MARTINI coarse grained model based distribution of melamine in a paint (Rossi 2011)

Therefore, only 0,75 – 2,02 hydroxy groups are available per chain to cause a reduction of the chain length, which agrees well with the change in chain

length observed in the DMA analysis. The fact that the resins with a high weight average molecular weight, in which the proportion of end groups per chain is smaller, show the largest decrease in chain length also supports this hypothesis.

Another important factor for the network formation is the behaviour of the melamine crosslinker prior to curing. Rossi *et al.* studied the distribution of melamine in a polyester coating formulation using a computational model.[18] Each part of the resin chain as well as the melamine was represented by different types of beads in a coarse grain MARTINI based modelling approach. The authors found that the melamine has a tendency to form clusters in the resin space, as represented in figure 94 above.

This behaviour could cause the single resin chains to either be suspended between two melamine clusters, in which case their end groups are crosslinked but no further crosslinking occurs in the intermediate space, or crosslink multiple times with the same cluster by wrapping around it. This would mean that the chain length between two crosslinking points is either very long or very short, and could explain the large average.

5.4.3.2.4 Correlation of the crosslinking density with the molecular weight before curing

No correlation was observed between the molecular weight of the resin and the crosslinking density of the film after it was cured with melamine. This justifies the comparison of the resins with each other to determine the effect of the single monomers after curing despite their initial difference in molecular weight.

No correlation was equally observed when the calculated chain length between crosslinking points was compared to the molecular weight before curing for isosorbide containing films as shown in figure 95.

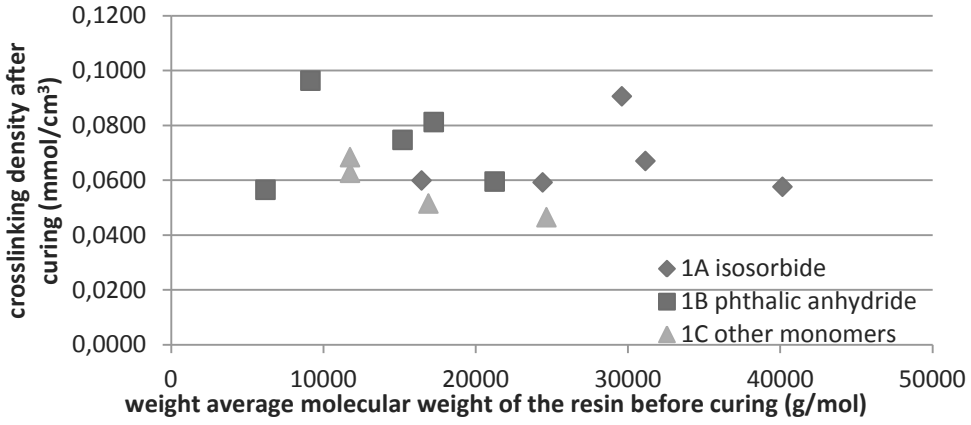

Figure 95: $M_{\overline{w}}$ before curing *vs.* crosslinking density after curing

When only phthalic anhydride containing films were examined, a vague correlation of the chain lengths between crosslinking points and the molecular weight of the resins before crosslinking could be possible as shown in figure 96. For both methods used to calculate these chain lengths, higher values are obtained for resins which had a higher molecular weight.

This could mean that for phthalic anhydride resins, the molecular weight influences the crosslinking behaviour. However, it can also be concluded that a large difference in $M_{\bar{w}}$ before curing only causes a small difference in chain length. The weight average molecular weight before curing is therefore not a useful parameter to characterise the crosslinking network reliably.

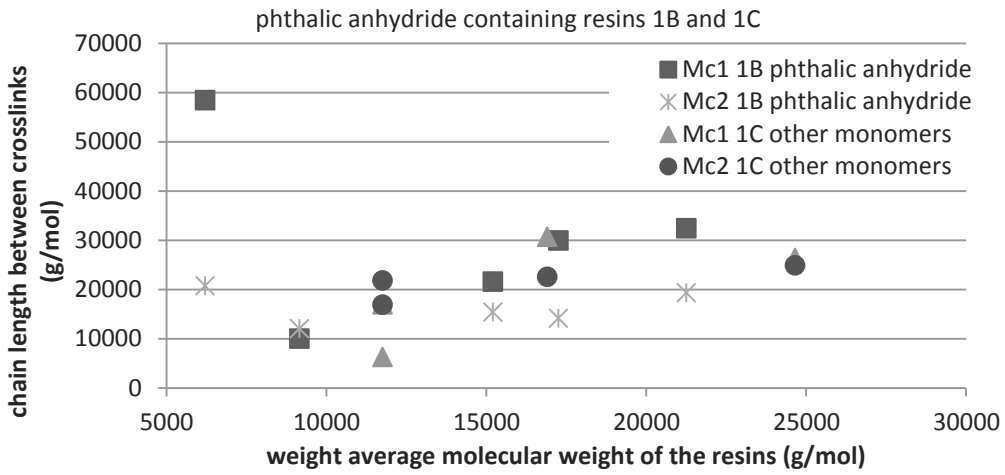

Figure 96: Chain length between crosslinks *vs.* $M_{\bar{w}}$ before curing

Lastly, in agreement with the results of Buder-Stroisznigg *et al.*, no correlation of the amount of hydroxy groups per chain and the end crosslinking density was observed.[264]

5.4.3.2.5 Influence of the crosslinking density on the glass transition temperature

No correlation between the coating glass transition temperature determined from the maximum of the loss modulus curve and the crosslinking density was observed as shown in figure 97. This is not necessarily due to the lack of influence of the crosslinking density on the film properties. It shows however clearly that the effect that the change in the formulation had on the glass transition temperature is much more important than that any difference in crosslinking densities could cause.

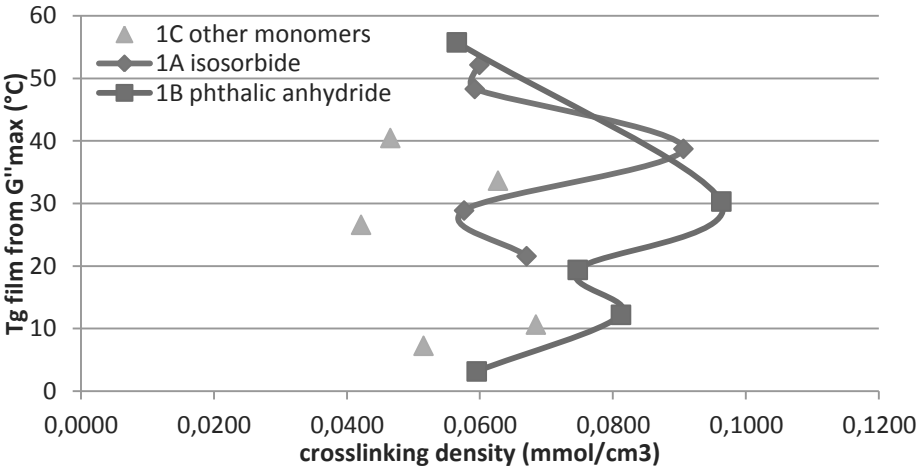

Figure 97: No correlation between glass transition temperature and crosslinking density

In conclusion, the dynamic mechanical analysis has validated the comparison of films based on different formulation despite their different molecular weights before curing. The results of the DMA have been validated by the proximity of the glass transition temperatures determined from the peak of the loss modulus curve with those determined in differential scanning calorimetry. While relatively large errors were observed between measurements of the crosslinking density, the determined values also fit well with the theoretical calculation of hydroxy groups available per polymer chain and the behaviour of the melamine crosslinker.

5.4.3.3 The µ-hardness indentation test

The µ-hardness indentation test is used to measure the viscoelastic response to stress of the crosslinked coating. A small pyramid is pushed into the coating surface with linearly increasing force until a 2 µm indentation is achieved, as shown in figure 98 below. The reached force is then maintained for 60 s, and the increase in the indentation is measured. This movement is termed creep 1 and represents the viscous movement of chains that occurs delayed to the actual application of stress. It is reported in % of the initial indentation.

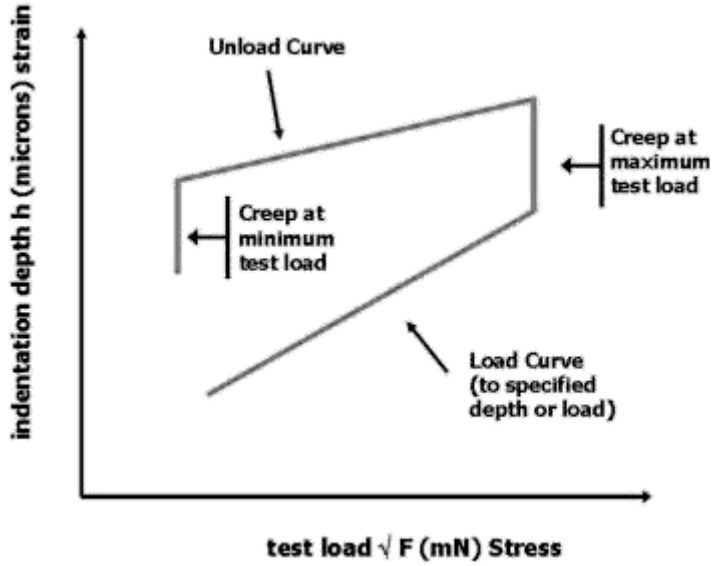

Figure 98: The µ-hardness indentation procedure

The stress is then relieved at the same rate as it was applied, and the pyramid is maintained in the end position for 60 s without any applied force. The reduction in indentation observed in this period is referred to

as creep 2 and also reported relative to the indentation.

The most important value derived from the μ-hardness test is the universal hardness, which is the ratio of the maximum test load applied and the indentation area achieved before creep occurs. The difference in indentation before and after creep allows the characterisation of the elastic and the viscous response to the force, and the indentation left after the load is relieved represents the plastic deformation.

The component of the energy applied that results in elastic deformation is reported as W_e relative to the total energy invested in the indentation. The ratio of the stress over the strain gives the Young's modulus, which is a measure of stiffness of the coating.

The measurement is repeated nine times in different positions for each sample, and an average is calculated. In addition to better reproducibility, the repetition is also performed to identify outliers, which can occur when the pyramid is placed on the edge of a depression in the surface. In this case, significantly less energy is needed for the indentation, as only one side of the pyramid is actually penetrating the coating. These kinds of outliers are more frequent for less regular surfaces, and are excluded from the calculation of the average.

The universal hardness is a measure of the overall resistance to deformation of the polymer network and is increased by monomer rigidity and by the structural rigidity achieved by crosslinking. Both the amount of creep and the plastic deformation are a measure of the capability of the chains to rearrange out of the way of the applied pressure. This capability is decreased through increasing crosslinking density.

The creep values, the relative amount of plastic deformation and the universal hardness are best assessed compared to the test values observed for the standard coating. A certain amount of hardness is desirable to protect the coating from deterioration upon small impacts, but very large hardness can lead to brittleness and cracking upon strain. Similarly, a certain amount of plastic deformation is necessary for the coating to enable its shaping together with the metal. High creep can lead to crawling of the paint away from the metal surface into its original shape, and overly large amount of plastic deformation can cause permanent damage upon low stress.

5.4.3.3.1 Universal hardness

The universal hardness H_{uk} reflects the resistance of the crosslinked network to deformation when stress is applied. High hardness can be beneficial as it means that the film surface will not easily be disturbed by small mechanical impacts, but can also correspond to high brittleness. The standard

coating is characterised by a universal hardness of 47 N/mm^2, which is lower than the hardness of the majority of coatings examined here.

In general, the μ-hardness test should be performed below the glass transition temperature of the coating to enable conclusions about the properties of the glassy network. In figure 99, a plot of the universal hardness results of the different groups of coatings relative to their glass transition temperatures is shown. It can be seen very clearly that the coatings whose glass transition temperatures are below 19 °C, at which the test was performed, show barely any resistance to deformation.

For all coatings with glass transition temperatures above 19 °C, a good correlation between the glass transition temperature and the resistance to deformation can be observed regardless of resin composition. The glass transition temperatures reported were determined by DSC.

The one outlier corresponds to the resin LH248, which contains a maximum amount of 45,13 mol% of isosorbide. The different behaviour can probably be attributed to the DSC measurement rather than to unusual behaviour. It was already observed in the comparison of DMA and DSC results that the glass transition temperature measured for LH248 in DSC did not correspond well to that measured in DMA. In contrast to the other resins measured, the DSC glass transition temperature was significantly above that measured from the maximum of the loss modulus curve. It is therefore possible that the glass transition temperature used to plot LH248 is slightly overestimated, which would place the actual point closer to those observed for other resins.

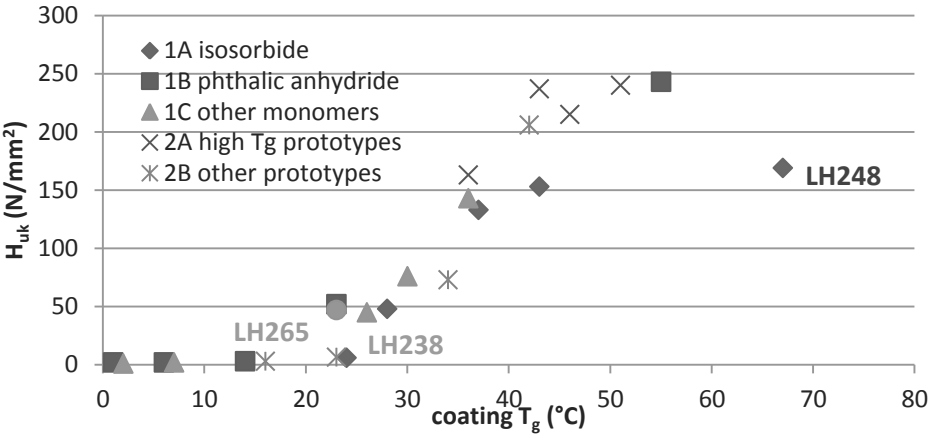

Figure 99: Glass transition temperatures and universal hardness

Of the new resins tested in the group of coatings 2B, LH265 and LH238 showed very low universal hardness of 3 N/mm^2 and 7 N/mm^2 respectively. This is considerably lower than the hardness of 47 N/mm^2 measured for the standard despite the fact that their glass transition temperatures of 16 °C and 23 °C are close to that of the standard which is 23 °C. This indicates a difference in overall

network structure which affects the universal hardness but not the glass transition temperature, i.e. the individual molecular motions.

For the remaining prototypes of group 2A and 2B, good and high hardness values were observed. Overall, most of the coatings tested were harder than the standard, and an increase in the hardness of LH265 and LH238 by small formulation modifications should be possible.

In figure 100, the dependence of the coating hardness on isosorbide and phthalic anhydride content is shown. For the same amount of isosorbide and phthalic anhydride present in the resin, the isosorbide coatings have a higher hardness in the majority of the coatings tested. On the other hand, when the increase of universal hardness is approximated with a linear equation, as shown above for those coatings whose glass transition temperatures are above the measurement temperature, the increase of phthalic anhydride causes a greater increase in hardness than the equivalent increase in isosorbide. This observation may however be misleading as only two phthalic anhydride containing coatings with glass transition temperatures above the measurement temperature were tested. The sample size is therefore insufficient to be certain.

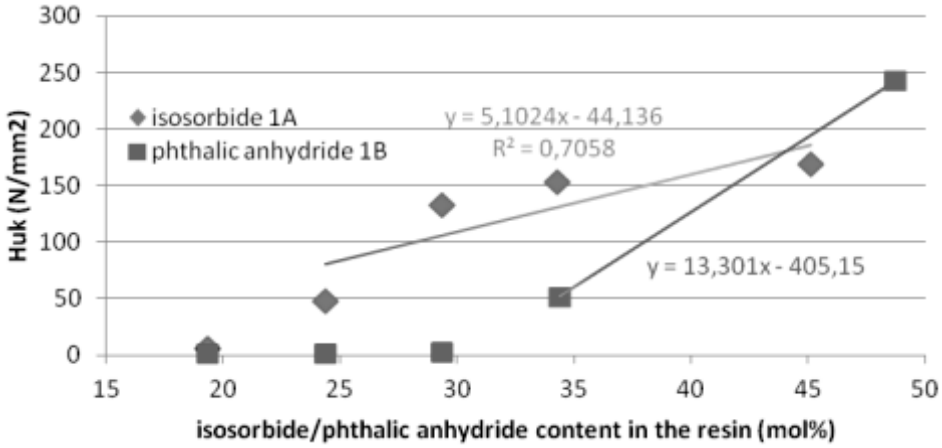

Figure 100: Increase in universal hardness with isosorbide and phthalic anhydride content (above T_g)

The dependence on the quantity of isosorbide and phthalic anhydride on the universal hardness cannot be completely separated from the glass transition temperature. The presence of either monomer impacts heavily on the glass transition temperature, so its increase naturally correlates with the increase in the monomer. The fact that overall, resins containing either monomer follow the same trend when the universal hardness is plotted against the T_g suggests however that the T_g may be the more important influence.

No correlation between the crosslinking density determined in dynamic mechanical analysis and the universal hardness was observed.

5.4.3.3.2 Elastic energy component

The elastic energy component of the material displacement work W_e represents the relative amount of energy invested in the deformation of the coating that didn't result in plastic deformation. It is reported as a percentage of the total energy invested and is a measure of the ability of the coating to recover from deformation. As with the universal hardness, a certain amount of elastic energy absorption is desirable because it means that small impacts will not damage the coating, but large elastic energy absorption can lead to undesirable properties such as poor formability. It is therefore best evaluated compared to the value measured for the standard coating, which was 4,6% in this case.

As in the case of the universal hardness, the elastic energy component W_e was found to strongly depend on the relationship of the coating glass transition temperature and the measurement temperature as shown in figure 101. Unsurprisingly, large W_e values are reported for those resins examined close to or above their T_g. For the phthalic anhydride resins, a decrease of W_e can be observed as the coating T_g approaches that of the measurement. Contrarily, the isosorbide coating containing the resin LH249 that was measured just above its T_g shows a very high W_e compared to the other isosorbide containing coatings.

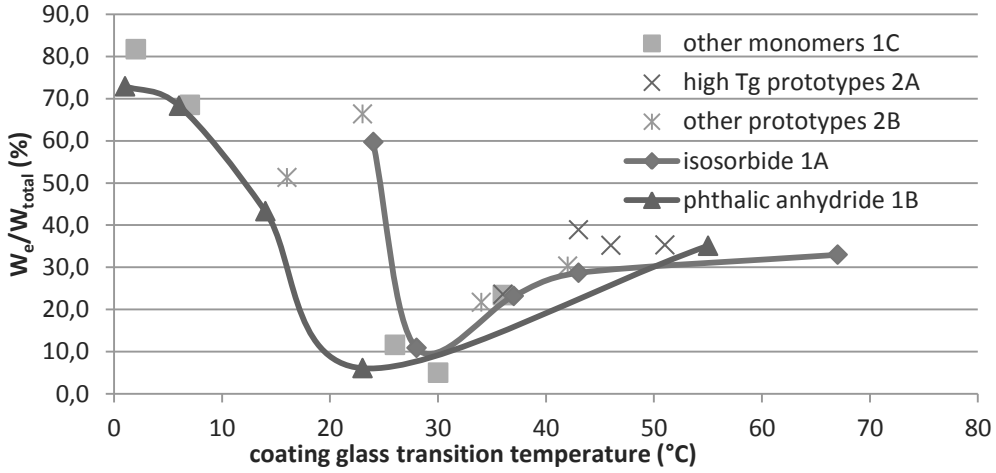

Figure 101: Elastic energy component *vs.* coating T_g

When the W_e is measured above the glass transition temperature of the coating, the values measured increase with increasing glass transition temperature and seem to again follow a similar trend regardless of the monomers used in the formulation.

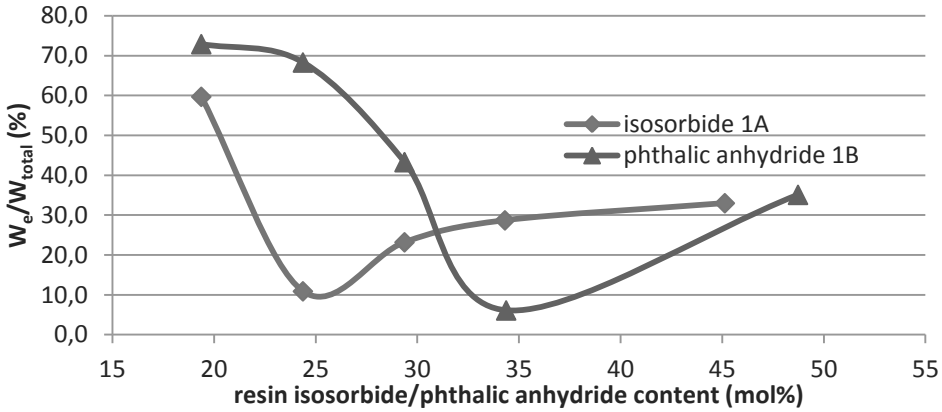

Figure 102: Elastic energy component W_e *vs.* isosorbide and phthalic anhydride content

When comparing the elastic energy components of coatings from resins containing the same amount of isosorbide and phthalic anhydride as in figure 102, the isosorbide resins show smaller elastic energy components where the phthalic anhydride resins were measured above their T_g but a higher elastic energy component when both coatings were measured above their T_g.

Regardless of the relation of the measurement temperature and the glass transition temperature or the resins used in the coating synthesis, no correlation could be established between the elastic energy component and the crosslinking density.

5.4.3.3.3 Creep 1

In contrast to the elastic energy component, the creep 1 value represents the part of the energy that was transformed into time delayed rearrangement of the chain, and therefore the mobility within the network. The value measured for the standard coating which can be used as comparison to judge the suitability of other prototypes was 107%.

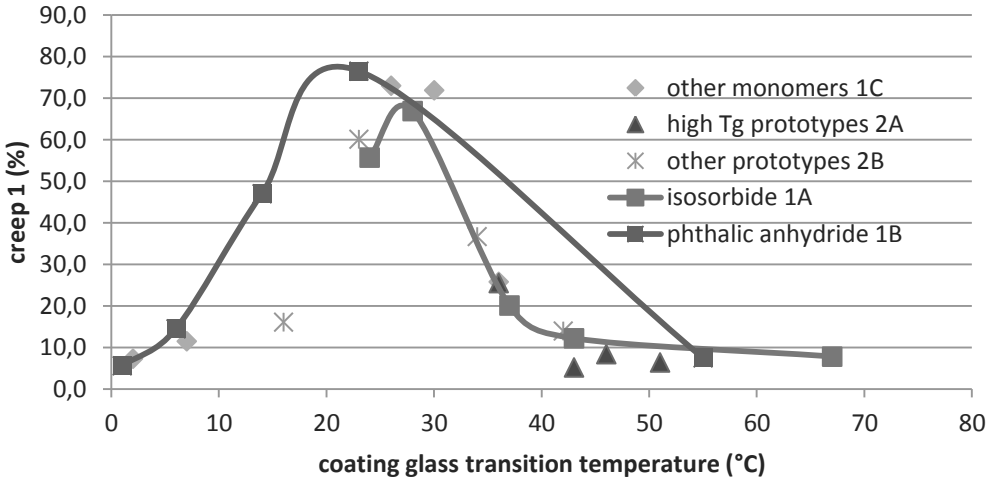

Figure 103: Creep 1 *vs.* coating T_g

The opposite trend compared to the elastic energy component is observed for the creep 1, as shown in figure 103. As for the elastic energy component, the values were strongly dependent on the coating glass transition temperature. However, in the case of creep, it was observed to increase as the coating glass transition temperature approached the measurement temperature, and then decrease with increasing glass transition temperatures.

Again, the glass transition temperature of the coating seems to be more relevant than its composition. Concerning the influence of isosorbide and phthalic anhydride, the opposite relationship is observed compared to the W_e values. For the coating from resins containing less than 25 mol% of either compound, the creep 1 observed for isosorbide is higher, for those coatings containing more than 25 mol% of either compound, the creep 1 observed for phthalic anhydride is higher.

No correlation between the creep 1 values with the crosslinking density, neither for measurements below nor above the glass transition temperature of the coating was observed.

5.4.3.3.4 Correlation between the μ-hardness test results and the network chain length

The lack of correlation between the crosslinking densities and the viscoelastic properties determined in the μ-hardness test could have two explanations. First of all, it is possible that the error in the crosslinking density calculated from the dynamic mechanical analysis results was too large, making the measurements inaccurate and meaningless for their properties.

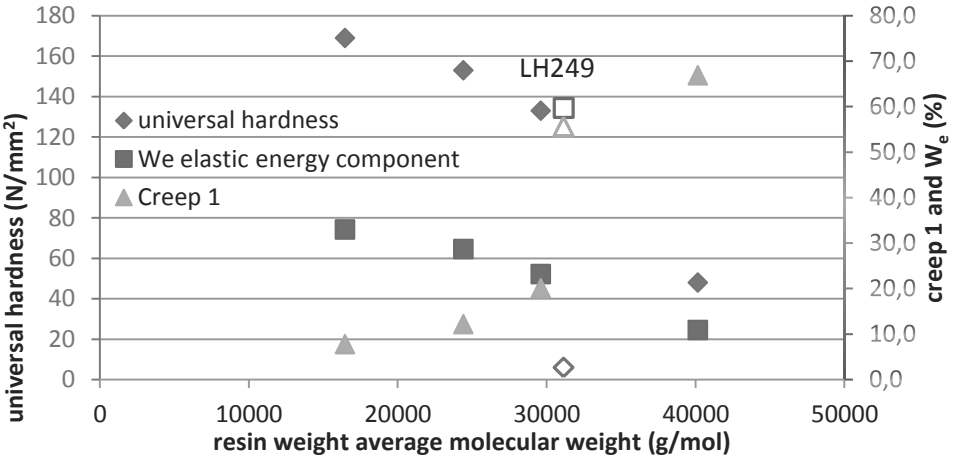

Figure 104: Isosorbide coating properties dependence on resin $M_{\bar{w}}$

The second possibility is that the glass transition temperature has such a strong influence on the results of the μ-hardness test that it overshadows any differences induced by the crosslinking density. Overall, the dependence of the universal hardness, elastic energy component and creep 1 on the glass transition temperature was observed to be greater than the dependence on the resin

formulation used in the coating. It can be concluded that the glass transition temperature is a useful parameter for the estimation of viscoelastic properties.

For the isosorbide resin containing coatings, a relationship between the μ-hardness properties and the resin weight average molecular weights was observed as shown in figure 104. Both the universal hardness and the elastic energy component decreased for increasing molecular weights, while the creep 1 measured increased for high resin molecular weights. The coating corresponding to a resin LH249 with a molecular weight of 31 150 g/mol shown without filling does not fit the trend as its glass transition temperature is too close to the measurement temperature of the μ-hardness test.

These trends were not mirrored in the other coating groups. No correlation between the universal hardness or the creep 1 and the resin molecular weights were observed for phthalic anhydride containing resins. For the elastic energy component, an increase with increasing molecular weight could be implied, as shown in figure 105 below.

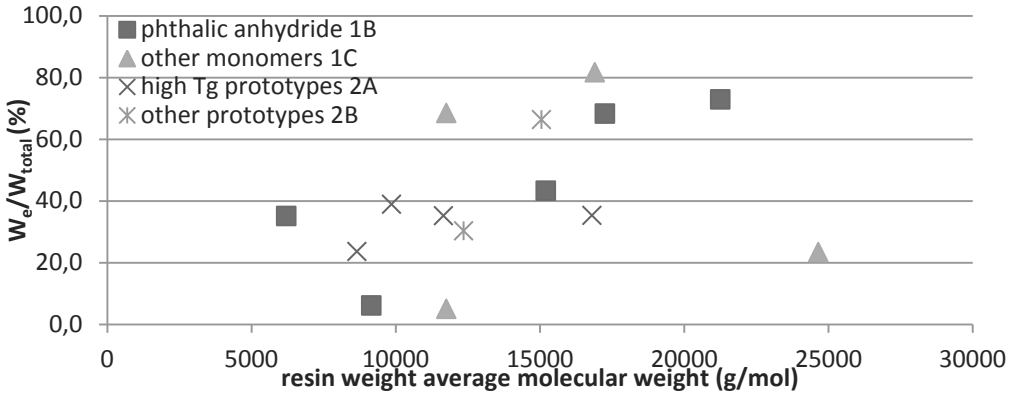

Figure 105: Correlation between resin $M_{\overline{w}}$ and elastic energy component W_e for phthalic anhydride containing coatings

The disagreement between the trends observed between different resin types indicates that the resin molecular weight is not causing the μ-hardness behaviour, but rather correlates with it coincidentally. In the case of both isosorbide and phthalic anhydride resins, lower molecular weights were observed with increasing isosorbide and phthalic anhydride content in the formulations. Due to the correlation between higher contents of rigid monomers and high glass transition temperatures, the lower molecular weights also correlate to high glass transition temperatures.

This is probably also the main cause for the correlation between the resins molecular weights and the μ-hardness properties. The illusion of a seemingly opposite relation between the phthalic anhydride resin coatings and the elastic energy component stems from the large amount of coatings measured above their glass transition temperature, where the behaviour is not governed by the same factors.

5.4.3.3.5 Creep 2 and Young's modulus

The creep 2 value represents the degree to which the coating recovered its original shape after the indentation force was completely relieved. As shown in table 95 - 99 below, the differences in the creep 2 values measured are not very significant.

Table 95: Isosorbide containing coatings 1A - µ-hardness results

isosorbide content		Tg DSC	H_{uk}	W_e/W_{total}	creep 1	creep 2	Young's modulus
resin	mol%	°C	N/mm^2	%	%	%	GPa
standard		23	47	4,6	107	-6,6	N/A
LH249	19,37	24	6	59,7	55,7	-4,2	0,0
LH190	24,37	28	48	10,9	66,9	-11,4	3,2
LH184	29,37	37	133	23,2	20,1	-10,0	4,3
LH168	34,31	43	153	28,7	12,2	-9,0	4,5
LH248	45,13	67	169	33,0	7,8	-8,9	4,6

While the standard had a creep 2 of -6,6%, the other coatings ranged between 0,3% and -14,4%. The highest values, between 0,3% and -0,2%, were observed for those coatings that were examined above their glass transition temperatures.

Some of the coatings with a low T_g, such as LH249, which displayed a universal hardness of only 6 N/mm^2, or LH238, which displayed a universal hardness of only 7 N/mm^2, displayed creep 2 values close to that of the standard at -4,2% and -4,5% respectively. The creep 2 value closest to the standard was observed for the resin LH193 at -7,6%.

Table 96: Phthalic anhydride series coatings 1B - µ-hardness results

phthalic anhydride content		Tg DSC	H_{uk}	W_e/W_{total}	creep 1	creep 2	Young's modulus
resin	mol%	°C	N/mm^2	%	%	%	GPa
standard		23	47	4,6	107	-6,6	N/A
LH237	19,37	1	2	72,9	5,6	0,2	0,0
LH162	24,37	6	2	68,3	14,5	0,1	0,0
LH189	29,37	14	3	43,3	47,0	-0,2	0,0
LH163	34,37	23	52	6,1	76,5	-10,3	N/A
LH242	48,73	55	243	35,1	7,5	-7,1	6,4

No clear correlation could be observed between the creep 2 values and the coating glass transition temperature. The resin LH193, which had the creep 2 behaviour closest to that of the standard, is quite far from the standard where the other parameters measured in the µ-hardness test are concerned. These facts and the small differences observed between the creep 2 of the different coatings indicate that creep 2 is not a very useful parameter for assessing the coating properties.

Table 97: Coatings for the assessment of other monomers 1C - µ-hardness results

resin	monomer added	T_g DSC	H_{uk}	W_e/W_{total}	creep 1	creep 2	Young's modulus
		°C	N/mm^2	%	%	%	GPa
standard		23	47	4,6	107	-6,6	N/A
LH174	succinic acid	30	76	5,0	71,9	-8,1	N/A
LH177	sebacic acid	2	1	81,7	7,3	0,0	0,0
LH181	1,3-propanediol	7	2	68,5	11,5	0,0	0,0
LH182	1,2-propanediol	36	143	23,4	25,8	-10,0	4,2
LH219	glycerol 9,27%	26	45	11,6	73,0	-13,4	2,8

The Young's modulus, which is the ratio of the stress applied and the strain experienced by the coating system, is a measure of the stiffness of the coating. Therefore, it naturally correlates well with both the glass transition temperatures observed for the coatings in DSC and the amount of rigid monomers such as isosorbide and phthalic anhydride present in the resins.

Table 98: Prototypes with high glass transition temperatures 2A - µ-hardness results

resin	description	T_g DSC	H_{uk}	W_e/W_{total}	creep 1	creep 2	Young's modulus
		°C	N/mm^2	%	%	%	GPa
standard		23	47	4,6	107	-6,6	N/A
LH192	high T_g	51	240	35,3	6,4	-8,3	6,3
LH193	high T_g	46	215	35,2	8,4	-7,6	5,5
LH196	high T_g	36	163	23,6	25,5	-9,7	4,8
LH199	high T_g	43	237	38,9	5,2	-14,4	5,8

No Young's modulus could be measured for the standard coating, so it cannot easily be evaluated. In general, the Young's modulus of all resins examined too close to or above their glass transition temperature was determined as 0, so it could serve as a good indication of the validity of the measurement.

Table 99: Coatings with reduced petroleum based content, CHDA and mixed isosorbide and phthalic anhydride 2B - µ-hardness results

resin	description	T_g DSC	H_{uk}	W_e/W_{total}	creep 1	creep 2	Young's modulus
		°C	N/mm^2	%	%	%	GPa
standard		23	47	4,6	107	-6,6	N/A
LH231	reduced petro	42	206	30,3	14,0	-11,3	5,5
LH238	reduced petro	23	7	66,4	60,1	-4,5	0,0
LH265	CHDA	16	3	51,3	16,1	0,3	0,0
LH269	ISO/PAN	34	73	21,7	36,7	-12,4	2,2

5.4.3.4 Mechanical quality assessment

The mechanical quality assessment tests evaluate the response of the coatings to stress that could realistically occur during their forming into the final shape and their use. The response is related to the coating hardness and flexibility, but gives a closer to real live result that can be viewed on its own. Comparison to a standard was nevertheless practiced because the tests were performed in a room that wasn't controlled for temperature or humidity.

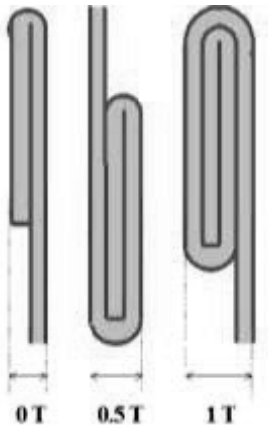

Figure 106: Degrees of T-bend

5.4.3.4.1 The T-bend test

In the T-bend test, the capability of the coating to endure shaping of the metal support is evaluated. The metal is bent around itself and the occurrence of cracks in the paint as well as the possibility to peel off some paint using a strip of adhesive tape is observed. The first bend at which no paint is removable by adhesive tape is reported as SD, and the first bend at which no cracks or other damages are observed is reported as SF.

Bends are counted in terms of thickness (T) of the metal. Each bend therefore counts 0,5T, without counting the first bend which is reported as 0T as shown in figure 106.

Different results were obtained for the standard in the three test series examined. The first test series, containing the isosorbide resins LH190, LH184 and LH168 as well as the phthalic anhydride resins LH162, LH189 and LH163 was performed in June 2015, at which time the temperature in the laboratory in Montbrison, France, was quite elevated around 30 °C. The standard resin was evaluated at 0T without paint peeling and at 1,5T without crack.

Table 100: T-bend test results of coatings with different isosorbide and phthalic anhydride contents 1A and 1B

isosorbide content	mol%	SD	SF	phthalic anhydride content	mol%	SD	SF
standard		0 - 0,5T	1,5T	**standard**		0 - 0,5T	1,5T
LH249	19,37	0,5T	1,5T	**LH237**	19,37	0,5T	1,5T
LH190	24,37	0,5T	1,5T	**LH162**	24,37	1,5T	2T
LH184	29,37	0T	1,5T	**LH189**	29,37	0,5T	1,5T
LH168	34,31	0,5T	1,5T	**LH163**	34,37	0T	2T
LH248	45,13	1T	2T	**LH242**	48,73	0,5T	1,5T

Contrarily, the second series of resins containing the coatings of the group 1C with the resins in which the other monomers were evaluated as well as the prototypes with an elevated glass

transition temperature of the group 2A, were tested in November 2015 at lower temperatures and the standard was instead evaluated at 0T without peeling and 2T without cracks.

The third evaluation which contained the coatings based on the resin LH249, LH248, LH237 and LH242 from the isosorbide and phthalic anhydride series 1A and 1B as well as the last prototype series 2B were evaluated in June 2016. In this series, the standard showed no peeling only after 0,5T and no cracks after 1,5T.

Table 101: T-bend results of coatings based on resins containing different other monomers 1C

resin	monomer tested	SD	SF
standard		0T	2T
LH174	succinic acid	0T	2T
LH177	sebacic acid	0T	2,5T
LH181	1,3-propanediol	0T	2,5T
LH182	1,2-propanediol	0T	1,5T
LH219	glycerol 9,27 mol%	0T	2,5T

With the exception of the coating based on the resin LH162, containing 24,37 mol% of phthalic anhydride, which only showed no peeling after 1,5T, the coatings performed at most 0,5T worse than the standard in each case, as shown in tables 100 - 102. No peeling (SD) was generally observed after 0T or 0,5T, and no cracks were observed between 1,5T and 2,5T. One coating based on the resin LH182 performed better than the standard in the same test, showing no cracks after 1,5T, 0,5T earlier than the standard. Several coatings showed a performance identical to that of the standard.

Table 102: T-bend results for prototypes 2A and 2B

resin	description	SD	SF	resin	description	SD	SF
standard		0T	2T	standard		0,5T	1,5T
LH192	high T_g	0T	2T	LH231	reduced petro	0,5T	1,5T
LH193	high T_g	0T	2,5T	LH238	reduced petro	0,5T	1,5T
LH196	high T_g	0T	2T	LH265	CHDA	0,5T	1,5T
LH199	high T_g	0T	2T	LH269	ISO/PAN	0,5T	1,5T

Overall, the performance of the coatings tested was good, i.e. within specifications, and only displayed small differences between the different samples. In the series of test conducted in November, for coatings of the group 1C, the poorer T-bend performance can be attributed to the resins with lower glass transition temperatures LH177, LH181 and LH219. In the case of LH177 and LH181, they contain increased amounts of the long linear aliphatic sebacic acid and 1,3 propanediol, which would usually be expected to induce greater flexibility into the resin structure.

Contrarily, in the coating group 1A based on isosorbide resins, the worst performance was observed for the resin LH248 containing the highest amount of isosorbide and the highest glass transition temperature. No differences in T-bend that could be explained either by the glass transition temperature or related to the individual monomers in the resins were observed within the other groups of coatings. Overall, no clear correlation between the formulation and the performance in the T-bend test could be established.

5.4.3.4.2 The Erichsen test and the impact test

The Erichsen test and the impact test are indentation tests that mirror the µ-hardness test on a larger scale. In the impact test, a ball is dropped onto the coating, while in the Erichsen test, it is slowly pressed into the back of the steel plate. In both cases, the damage to the paint in the deformation area is assessed.

The difference between the tests is linked to the time scale of the deformation. It occurs suddenly in the impact test, but more slowly during the Erichsen test. The network is therefore given more time for rearrangement in the latter, while in former, only the flexibility of the individual monomer can be used to avoid damage.

No differences between the coatings examined could be observed because no damage to the coating was caused by either indentation. To enable a differentiation, the impact was maximised in both tests. In the Erichsen test, the ball was pressed as far into the metal as the machine allowed, and the impact test was launched using the maximum ball weight from a maximum height. Neither escalation resulted in a change of the test results.

5.4.3.4.3 Pigmented coatings

The introduction of TiO_2 pigments into the coating formula can often weaken the mechanical performance as the pigments disrupt the polymer network. Five resins were formulated with pigments and the resulting mechanical properties were tested. The resins used were LH206 and LH203, which were synthesised according to the same formulas as the isosorbide based resins LH190 and LH168, and LH198, LH210 and LH201, which were synthesised according to the same formulas as the phthalic anhydride based resins LH162, LH189 and LH163.

As shown in table 103 below, the performance in the Erichsen indentation test was equivalent to that of the standard, showing no peeling of the paint and a few cracks. No damage to the coating was observed after an impact test of 15 J and 18 J for any of the coatings, which is better than the standard in the case of the 18 J test.

Table 103: Mechanical properties assessment for pigmented coatings

resin	equivalent to	phthalic anhydride / isosorbide content mol%	T-bend SD	T-bend SF	Erichsen 8mm	impact test 15 J	impact test 18 J	Clemen hardness kg
standard			1T	2T	NR/few C	NR/NC	NR/few C	3,1
LH206	LH190	ISO 24,37	1T	2,5T	NR/few C	NR/NC	NR/NC	3,6
LH203	LH168	ISO 34,31	1,5T	3T	NR/few C	NR/NC	NR/NC	3,6
LH198	LH162	PAN 24,37	1T	2T	NR/few C	NR/NC	NR/NC	2,9
LH210	LH189	PAN 29,37	1T	2T	NR/few C	NR/NC	NR/NC	3,2
LH201	LH163	PAN 34,37	1T	2T	NR/few C	NR/NC	NR/NC	3,4

*NR: no removal/peeling off of coating with an adhesive tape, NC: no cracks, fewC: few cracks

In the T-bend test, the phthalic anhydride resins performed equivalent to the standard while a slightly worse performance was detected in the isosorbide resins. This is in accordance with the Clemen hardness determined for the coatings. The Clemen hardness represents the scratch resistance of the coating, and was considerably higher for the isosorbide resins than for the standard. On the other hand, it was observed to increase with increasing phthalic anhydride content. It can be concluded that the phthalic anhydride resins result in more flexible coatings when used in pigmented formulations, while the isosorbide resins give greater hardness.

5.5 Possibilities for new biobased polyester resins and coatings

Based on the isosorbide resin for interior coil coating proposed by Arkema, several series of completely and partially biobased resins were synthesised. By varying the amounts of the biobased diols isosorbide, 1,2-propanediol, 1,3-propanediol, of glycerol and of the biosourced diacids succinic acid and sebacic acids, and by including the petroleum based compounds phthalic anhydride and cyclohexanedicarboxylic acid, the resin properties could be tuned within a wide range.

In a first series of resins, which will be further discussed in the following chapter, the monomers were modified one by one to establish their influence on the resin properties. Isosorbide resins were found to be more hydrophilic than their phthalic anhydride counterparts, and also displayed higher weight average molecular weights, viscosities and glass transition temperatures.

The phthalic anhydride resins on the other hand displayed more affinity towards aromatic solvents. For both groups of resins, a linear dependence of the glass transition temperature on the amount of isosorbide and phthalic anhydride both before and after curing was observed. Overall, the glass transition temperature was found to be a good indicator of coating properties such as the universal hardness, the elastic energy component and the creep behaviour.

A second series of resins containing different prototypes were also produced and examined for their mechanical properties. All coatings based on the new prototypes were within specifications, and in impact, Erichsen indentation, gloss and solvent rub test as good as the standard. Two phthalic anhydride resins whose Hansen solubility parameters were examined showed bigger solubility spheres than the standard and showed good compatibility with several partially biobased solvents proposed by Activation.

The glass transition temperature, and therefore the hardness and flexibility of the coating, was also modified through the amounts of 1,2-propanediol, succinic acid, sebacic acid, glycerol and 1,3-propanediol in the resin. This allowed a reduction of the petroleum based content to less than 10 mol%.

The molecular weights of the resins could not be estimated by NMR due to the overlapping of the end group peaks with other peak groups, but were successfully determined by SEC. They were found to impact slightly on the resin viscosity, but no links to other resin or coating properties were observed. The crosslinked coatings were analysed by dynamic mechanical analysis. While the results were validated by their agreement with DSC results and theoretical calculation, no link between the crosslinking density and other observed coating properties could be established.

Overall, a detailed understanding was built about the limits and possibilities of the examined biobased formulations. While some further modifications especially concerning the μ-hardness behaviour of the coatings may still be necessary, the impact of each monomer and the resulting properties are well established, and the coatings show promising suitability for the coil coating process and good mechanical properties.

The next chapter will be dedicated to the influence of each monomer on the weatherability of the coatings, and therefore their suitability for exterior application in comparison to the interior resin proposed by Arkema and the standard resin currently in use.

6 Structure – weatherability correlation for biobased monomers in melamine crosslinked polyester films

Many different factors influence and interact with each other to define the response of a coating to exterior forces, or its weatherability. This complexity, and the fact that most relevant studies have been conducted under the blanket of confidentiality, means that the relationship between monomers in the formulation and the degradation of the coating is not very well documented. Several theories exist, linking the UV absorption, the hydrophilicity and the liability of different functional groups to the damage, and are generally used to explain observed differences, but very little convincing evidence has been reported.

The most well researched degradation behaviour it that of polyethylene terephthalate (PET) and of polymer products intended for biodegradation. While some of the conclusions drawn from these studies can help to understand coating weatherability, the conditions used are in most cases not comparable.

Because the products examined are thermoplastic rather than thermosetting, and because of their use, the polymer structure and surface to bulk ratio is fundamentally different from that in a coating. Furthermore, hydrolytic degradation and the associated penetration of water and oxygen into the polymer structure is often considered as the main factor, especially where the biodegradation in nature is envisioned.

The main factors influencing the coating weatherability include also the absorption of UV light, the propagation mechanism of radicals formed and the liability of bonds to thermal degradation. All of these are highly specific to the monomers used in the resin, the fashion in which it was crosslinked and the structure of the surface resulting from the interaction of the resin, solvents and crosslinkers used.

As demonstrated in the previous chapter, even using only a limited number of biobased monomers, a wide variety of properties can be introduced to the resins and the corresponding coatings. This means that the suitability of the paint for the coil coating process will be adjustable once factors in the formulation or coating structure contributing to the degradation or enhancing the stability are identified. The weatherability is therefore the critical criterion for the design of a new biobased resin.

Weatherability tests were launched to determine the effect of each monomer in the resin formulation, and to identify degradation behaviour in a melamine crosslinked coating correctly representing the target product. The same principles as in chapter 5 were followed, varying the monomers in the formulation one by one, and avoiding the introduction of pigments to simplify the influences on the observations.

The coatings were aged in accelerated weathering cabinets, and examined on several different levels. Visual examination and measurements of the gloss retention over time were used to evaluate the customer relevant coating aspect. This was accompanied by several analytical techniques to enable linking the observations to the formulation and to elucidate deterioration mechanisms. The film thickness was evaluated to show erosion, and the μ-hardness test was repeated after weathering to indicate changes in the viscoelastic response. Furthermore, infrared and UV/Vis spectroscopy were employed to quantify the presence of different functional groups and the absorption of UV light.

The space in weathering cabinets was limited so that originally, only three coatings were used to quantify the effect of the isosorbide and phthalic anhydride each in the coatings. Because the results were ambiguous, additional tests were launched using the coatings based on resins LH249, LH248, LH237 and LH242, which contain minimum and maximum amounts of isosorbide and phthalic anhydride respectively. Unfortunately, at the time of writings, the tests were still in progress and could not be included in the final analysis.

In the following chapter, the different weathering procedures and evaluations will be discussed, and the results will be linked to the formulation and properties of the resins used. Particular emphasis will be placed on the infrared analysis, and the different observations made also in terms of methodology. The correlation of the results of different evaluation techniques will be addressed, and recommendations for the formulation of a resin for exterior use will be made based on the conclusions about the degradation mechanisms.

6.1 Test design

The weatherability tests were designed to determine the influence of each of the monomers in the formulation, shown in scheme 129, on the overall stability. Specific emphasis was placed on the monomers isosorbide and phthalic anhydride, which provide rigidity to the structure, and the effect of changing their quantities.

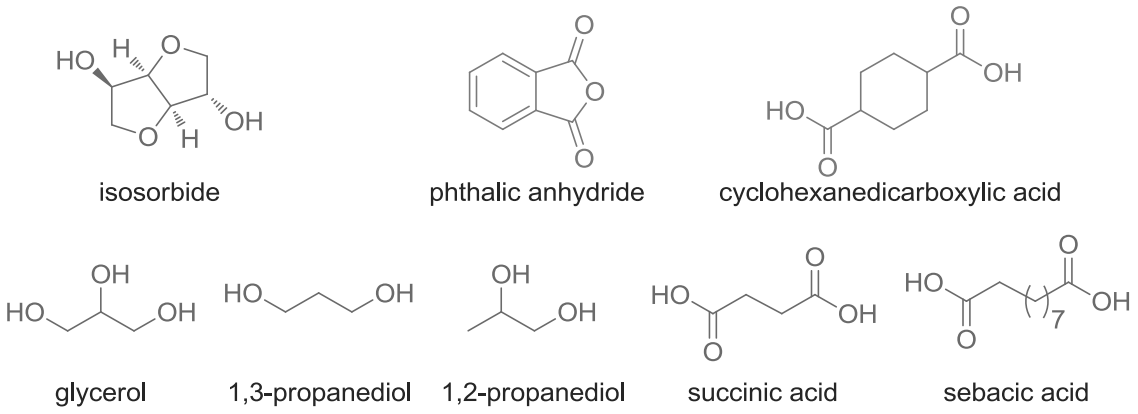

Scheme 129: Monomers used in the synthesis of the resins

In order to be as close to real conditions as possible, the coatings were exposed simultaneously to UV light, high temperatures and humidity. The weathering test conditions as well as the properties of the resins and coatings used in the tests are summarized below. Coatings for which the tests are still in progress are shown in grey.

6.1.1 Coatings designed to evaluate the effect of single monomers on weatherability

The first group of coating prototypes (1A) was designed to determine the influence of isosorbide on the weatherability, and is presented in table 104. Several reasons led to the suspicion that isosorbide introduced a higher susceptibility to degradation than the other monomers used.

Nagai *et al.* for example studied the degradation of a thermoplastic polyester-polyether film consisting of polybutylene terephthalate and polytetramethylene glycol. The study concluded that the degradation took place mainly in the polyether parts.[205] This could be explained in part by the increased susceptibility to abstraction of hydrogens adjacent to ether bonds compared to those adjacent to ester or alkane groups.[188]

Table 104: Isosorbide based coatings used in weatherability tests 1A

resin properties				film properties			
resin	isosorbide content	$M_{\overline{w}}$	viscosity*	T_g	crosslinking density	H_{uk}	W_e/W_{total}
	mol%	g/mol	mPa*s	°C	mmol/cm^3	N/mm^2	%
LH249	19,37	31150	5622	24	0,0670	6	60
LH190	24,37	40150	18934	28	0,0576	48	11
LH184	29,37	29600	8553	37	0,0906	133	23
LH168	34,31	24400	6595	43	0,0592	153	29
LH248	45,13	16450	10063	67	0,0599	169	33

* In MPA (65%)

In addition to the introduction of two ether bonds into the structure with every isosorbide molecule, the increase in polarity and hydrophilicity was also a cause for concern. The introduction of isosorbide and isomannide into a polyester structure was used for example by Okada *et al.* to increase the hydrolytic degradability.[212] The increase in hydrophilicity was confirmed in the NMR analysis of the resins described in the previous chapter (*5.2.3.1*), as considerably more water was detected in the isosorbide resins compared to the phthalic anhydride containing resins.

On the other hand, the isosorbide resins had higher weight average molecular weight and were found to result in considerably higher glass transition temperatures in the coating compared to their phthalic anhydride equivalents. The greater rigidity and steric bulk around the ester bond could also possibly prevent radical attack and propagation reactions.

In order to quantify the effect of isosorbide, three coatings based on resins with different isosorbide contents were subjected to weathering test, followed by two more coatings. Furthermore, coatings based on resins with similar formulations, but in which the isosorbide was replaced with phthalic anhydride, were also tested (1B) and are shown in table 105.

The aromatic moiety in phthalic anhydride is a much more effective chromophore than the other functional groups in the resin. This could also catalyse photolytic degradation. Osterhold *et al.* for example linked the increased aromatic content in a melamine crosslinked polyol clear coat to a higher increase of the glass transition temperature after weathering.[243]

Table 105: Phthalic anhydride based coatings used in weathering tests 1B

resin properties				film properties			
resin	phthalic anhydride content	$M_{\bar{w}}$	viscosity*	T_g	crosslinking density	H_{uk}	W_e/W_{total}
	mol%	g/mol	mPa*s	°C	mmol/cm^3	N/mm^2	%
LH237	19,37	21250	2756	1	0,0595	2	73
LH162	24,37	17250	1681	6	0,0812	2	68
LH189	29,37	15200	2374	14	0,0747	3	43
LH163	34,37	9150	1539	23	0,0963	52	6
LH242	48,73	6200	1721	55	0,0565	243	35

* In MPA (65%), except for LH189, which was measured in a mixture of MPA and DBE

On the other hand, Batista *et al.* observed greater stability in a melamine crosslinked polyester coating based on isophthalic acid than in two other films containing the aliphatic hexahydrophthalic and 1,4-cyclohexanedicarboxylic acids.[219] As with isosorbide, the presence of phthalic anhydride also has to be seen in terms of the structural and polarity changes and not only in terms of its UV absorption. For example, Siyab *et al.* postulated that the hydrophobicity of the aromatic ring can protect the coating from hydrolytic attack.[17]

Table 106: Coatings designed to test the effect of other monomers on the weatherability 1C

resin properties				film properties			
resin	monomer tested	$M_{\bar{w}}$	viscosity*	T_g	crosslinking density	H_{uk}	W_e/W_{total}
		g/mol	mPa*s	°C	mmol/cm^3	N/mm^2	%
LH174	succinic acid	11750	2397	30	0,0627	76	5
LH177	sebacic acid	16900	3229	2	0,0515	1	82
LH181	1,3-propanediol	11750	1567	7	0,0684	2	69
LH182	1,2-propanediol	24650	3542	36	0,0465	143	23
LH219	glycerol 9,27 mol%	30776	5915	26	0,0421	45	12

* In MPA (65%)

The change in quantity of isosorbide or phthalic anhydride had to be compensated for with other monomers to keep the ratio of acid and alcohol groups and the functionality constant. In order to be

able to separate the effect of the change in quantity of other monomers from those of isosorbide and phthalic anhydride, five additional resins in which the quantities of 1,2-propanediol, 1,3-propanediol, glycerol, succinic acid and sebacic acid were varied were tested in coating formulations (1C). They are shown in table 106.

This last series of coatings also permits conclusions about the effect of longer aliphatic chain length, from the comparison of succinic acid and sebacic acid, and of pendant methyl groups and secondary hydroxy groups, from the comparison of 1,2-propanediol, 1,3-propanediol and glycerol.

6.1.2 Coatings designed as prototypes and tested for their weatherability

Two series of resin prototypes for exterior use were synthesised and tested for their weatherability and are presented in table 107 and 108. In the first series, the glass transition temperature raising monomers, such as succinic acid, 1,2-propanediol and phthalic anhydride were used in increased quantities (2A).

Table 107: Prototypes with high glass transition temperatures used in weatherability testing 2A

resin properties				film properties		
resin	description	$M_{\bar{w}}$	viscosity	T_g	H_{uk}	W_e/W_{total}
		g/mol	mPa*s	°C	N/mm^2	%
LH192	high Tg	16800	2474	51	240	35
LH193	high Tg	11650	1963	46	215	35
LH196	high Tg	8650	2045	36	163	24
LH199	high Tg	9850	2136	43	237	39

* In MPA (65%)

These coatings can also be used to evaluate the effect of combining changes in monomers made in the second and the third series described above (1B and 1C), as well as the effect of high hardness and structural rigidity.

The last series of prototypes contains coatings based on resins in which the phthalic anhydride content was minimised as much as possible, one in which both isosorbide and phthalic anhydride were used, and one in which phthalic anhydride was substituted with the cycloaliphatic 1,4-cyclohexanedicarboxylic acid.

While these coatings are still being tested, they could reveal interesting information about the interaction between phthalic anhydride and isosorbide, and the possibility to boost the weatherability by using a cycloaliphatic compound in small quantities. As cyclohexanedicarboxylic acid has neither ether groups nor a high UV absorption as phthalic anhydride, it could help understand the role of both in the degradation of the coating.

Table 108: New prototypes with reduced phthalic anhydride content, cyclohexanedicarboxylic acid or mixed isosorbide and phthalic anhydride used in weatherabiltiy testing still in progress 2B

resin properties				film properties		
resin	description	$M_{\overline{w}}$	viscosity*	T_g	H_{uk}	W_e/W_{total}
		g/mol	mPa*s	°C	N/mm^2	%
LH231	reduced petro	12350	2113	42	206	30
LH238	reduced petro	15050	1950	23	7	66
LH265	CHDA	28642	5618	16	3	51
LH269	ISO/PAN	20680	5638	34	73	22

* In MPA (65%)

6.1.3 Paint formulation choices

The resins were cured in the paint formulation of the standard coating, most importantly with a hexamethoxymethylmelamine crosslinker.

Aside from the resin used in the paint, several other factors influence the properties of the crosslinked coating. As observed in a computer simulation by Rossi *et al.*, the melamine and therefore the resin are not distributed completely homogeneously in the coating, as the melamine can form clusters before the curing process starts.[18] The degree to which this occurs is very likely dependent on the interactions and compatibility of the melamine with the resin. Their interaction is also influenced by the solvents added, xylenes, Solvesso 100 and DBE, both in terms of compatibility and in terms of quantity.

Furthermore, the evaporation of the solvents is influenced by the strength of their interactions with the resin, while the density and quality of the polymer network formed is in turn dependent on the presence of solvents in the bulk and near the surface.

Ideally, the solvent mixture and quantity of melamine in the formulation could be adjusted for each resin formulation to give the same evaporation behaviour and interaction to yield equally crosslinked and structured coatings. However, these parameters are difficult to measure and are generally tuned empirically and gradually for each new formulation. Within the capabilities of the project, it was not possible to individually adjust each formulation.

However, with the exception of the viscosity dependent quantity of dibasic ester, the exact same ingredients were used to make each coating. One advantage of this strategy is that the quantities of the other components of the paint are similar in the coating, and can be assumed not to be the cause of the differences in weatherability.

It should however be kept in mind for the interpretation of the results that the differences in interactions of each resin with flow additives, melamine and solvent as well as the different amount

of dibasic ester present in the paint prior to curing could have influenced the surface and bulk structure of the coating and therefore its weatherability.

6.1.4 Accelerated weathering conditions

Due to time restraints and reproducibility, the weathering of the different coatings was performed in accelerated weathering cabinets of the Q-lab type, as shown in figure 107. The tests are referenced according to the temperature and radiation intensity used as Hot QUVa and QUVa, and are described below.

6.1.4.1 The Hot QUVa test

For the Hot QUVa test, the coatings were subjected to the maximum exposure to cover all types of degradation and estimate a worst case scenario. The exposure does not correspond to any norm but is used internally by Beckers to evaluate their products. The coatings aged in this manner were used for all evaluations described in this chapter unless otherwise stated.

Figure 107: Q-lab accelerated weathering cabinet

Specifically, the coatings were subjected to exposure cycles consisting of 8 h of irradiation at 78 °C followed by 4 h of darkness at 50 °C and at 100% humidity. The variation serves to mimic the change in day and night and causes condensation on the panels, and is repeated for a total duration of 2000 h with intermediate evaluation of the panel each 200 h or 500 h. As the name suggests, irradiation in the UVa region of the spectrum was used, generated by a mercury lamp at 0,89W/m^2/nm with a peak at 340 nm. The temperatures were adjusted at the panel.

6.1.4.2 The QUVa test

The QUVa test describes exposure according to the norm NF EN ISO 11507 and was performed to enable later comparison to coatings evaluated in other normed procedures. It is overall quite similar to the Hot QUVa test. The exposure cycles consist of 4 h at 60 °C instead of 8 h at 78 °C, followed also by 4 h in the darkness at 50 °C at 100% humidity. The same lamp was used but the radiation intensity was 0,80 W/m^2/nm.

The results of the QUVa test were only evaluated through the gloss retention of the panels, but comparison with the Hot QUVa results permit nonetheless to draw conclusions about the synergy of temperature and radiation in the degradation process.

6.1.4.3 Coating state during the weathering

In both tests, the temperature was varied, but kept above 50 °C at all times. This is considerably above the glass transition temperature of all coatings except for those containing the resins LH248, LH242 and LH192. Even they can be considered to have been exposed above their glass transition temperature in the Hot QUVa test for a part of the cycle.

Therefore, we can assume that the large difference in behaviour that was observed in the µ-hardness test (*5.4.3.3*) between resins with a glass transition temperature above and below 20 °C does not impact on the coating weatherability from these tests. It is likely to impact on the real life weatherability, when the coatings are regularly cooled to ambient temperature and will therefore undergo a thermal transition depending on their glass transition temperature more or less frequently. However, due to the conditions used in this case, the results obtained are assumed to be a valid reflection of the resin formulation rather than the relative position of the glass transition temperature with respect to ambient temperature.

6.1.4.4 Sample evaluation frequency and reproducibility

Three different batches of weatherability tests were launched. The first, including the coatings based on isosorbide and phthalic anhydride containing the resins LH190, LH184, LH168, LH162, LH189 and LH163 (1A and 1B), was weathered for 2000 h and samples were evaluated every 500 h. It is termed series 1.

The fact that only five readings were obtained made it difficult to identify outliers which could originate for example from measurement errors. Therefore, more frequent evaluations were made in the second series, series 2.

The second batch contained the coatings with the resins LH174, LH177, LH181, LH182 and LH219 in which the other monomers were evaluated (1C) as well as the first batch of prototypes (LH192, LH193, LH196 and LH199) with a high glass transition temperature (2A). This batch was weathered for 1920 h in total and evaluated every 192 h. It is referred to as series 2. In each series, a standard coating and a coating based on the interior resin proposed by Arkema were also included as references.

While there was not enough space to include replica of each coating, the repeated weathering of an identical standard coating permits to estimate the accuracy of the measurement.

The weathering of the third batch, including the coatings based on additional resins LH249, LH248, LH237 and LH242 containing isosorbide and phthalic anhydride (1A and 1B) as well as the last series

of prototypes (2B) is still in progress but is performed according to the same method as the second batch.

6.2 Direct assessment of weatherability

As briefly addressed in the introduction, a variety of methods exist to assess the weatherability of a coating. They generally represent a trade off between the relevance of the observation to consumers and the ease at which the findings can be related to the formulation. The directly consumer relevant methods used in this case include the measurement of the gloss retention, the evaluation of the film thickness after weathering, and images taken of the coating surface with an optical microscope.

The colour change in the coatings was also evaluated in the coatings but only results in relevant insights where pigments were used in the formulations. As tests with pigmented coatings are still in progress, these will not be discussed here.

For clear coats, which are pigment free and which were used for the majority of the evaluations, it can be assumed that the colour changes observed will be obscured by any type of pigment used in the same formulation.

6.2.1 Gloss retention

In the gloss retention assessment, the ability of the coating to reflect light at an angle equivalent to the its input is tested. As cracks and unevenness develop in the coating surface due to exposure, the light is increasingly scattered and less is reflected. The result is reported in % of the incident light and correlates well with the visual perception of a less shiny or glossy surface.

6.2.1.1 Performance of the standard coating

Below in figure 108, the performance of the standard coating in the two weathering tests is compared. Two observations can be made. Firstly, both series generally follow a smooth trend with the exception of the measurements after 384 h and 1920 h in the second series S2. Especially the low value of 85% gloss retention after 384 h which increases to 99% gloss retention again after 576 h proofs that erroneous measurement can occur and that the more frequent evaluation is justified to identify outliers.

Secondly, the performance of the coating in the second series is clearly worse than that in the first series. This could be attributed to several factors. First of all, it calls into question the accuracy of the measurement. However, the fact that the values of the second series are consistently lower than those of the first series indicates that the difference is not due to measurement error.

Two explanations are possible for a performance loss. The first is inherent to the measurement. It is possible that the more frequent removal of the coating from the high temperature weathering

cabinet for the purpose of measurement, and therefore its cooling below the glass transition temperature, causes increased strain to the polymer structure.

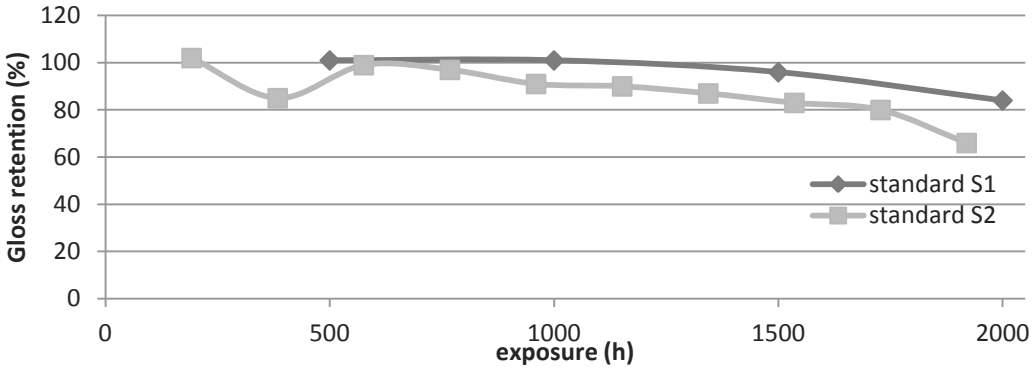

Figure 108: Gloss retention of standard coatings in the two weathering series

A second explanation lies in the storage of the paint. The formulation was prepared first in June 2015 for the weathering test, and stored until November 2015 to be reused for the second test. It is possible that upon storage, the homogeneity of the formulation has decreased, causing larger defects in the surface of the coating and therefore greater susceptibility to deterioration.

The validity of either hypothesis will be confirmed by the results of the third series of weathering tests, which was launched in the summer 2016. If the third standard performs even worse, we can conclude that the storage time impacted upon its performance. If it performs equal to the second series but worse than the first, we can conclude that the more frequent evaluation was causing the disparity.

Three coatings, based on the resins LH184, LH189 and LH181, which were formulated in June 2015 and November 2015 respectively, will also be tested in the third weatherability series to confirm whether the storage can have a negative impact on the coating quality.

Awaiting this result, each series of coatings will be evaluated in comparison to the standard launched under the same conditions.

6.2.1.2 Gloss retention of biobased coatings compared to the standard

In comparison to the standard, the coatings based on new completely biobased resins with isosorbide (blue) or partially biobased resins with phthalic anhydride (red) performed significantly worse. Below in figure 109, the result of the gloss retention test after exposure for 2000 h of the coatings tested in the first series is shown. The coating based on the interior resin by Arkema is shown in yellow.

The new coatings show a similar performance to the coating based on the resin proposed by Arkema, but only retain between 30% and 39% of the gloss in comparison to 84% retained by the standard

coating. The performance of the coatings containing higher levels of isosorbide and phthalic anhydride is slightly better than that of those containing less, but still in the same range.

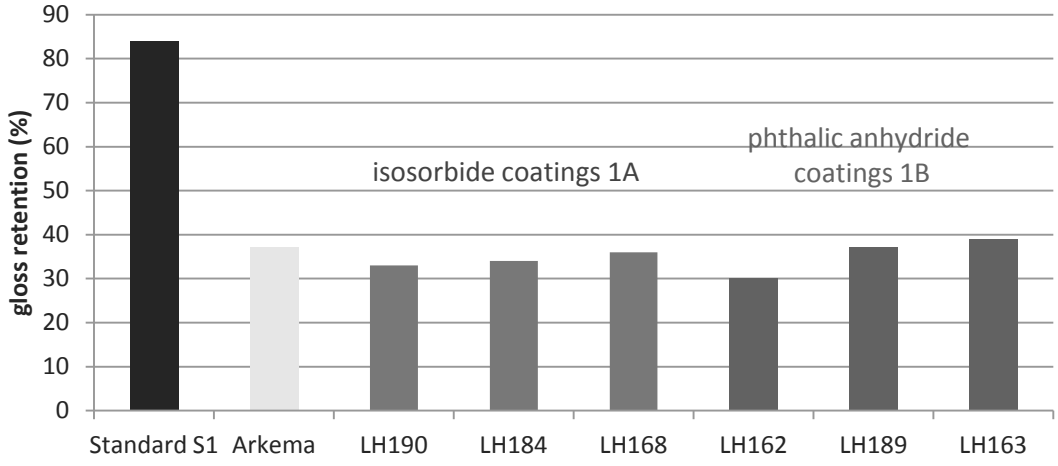

Figure 109: Gloss retention after 2000 h compared to the standard- series 1

The coatings tested in the second weathering series equally performed consistently worse than the standard. The standard in this series only retained 66% gloss after 1920 h of exposure. The results of the partially biobased resins are therefore not as far from the standard as in the first series. The overall gloss retention is only between 13% and 38%, as shown in figure 110.

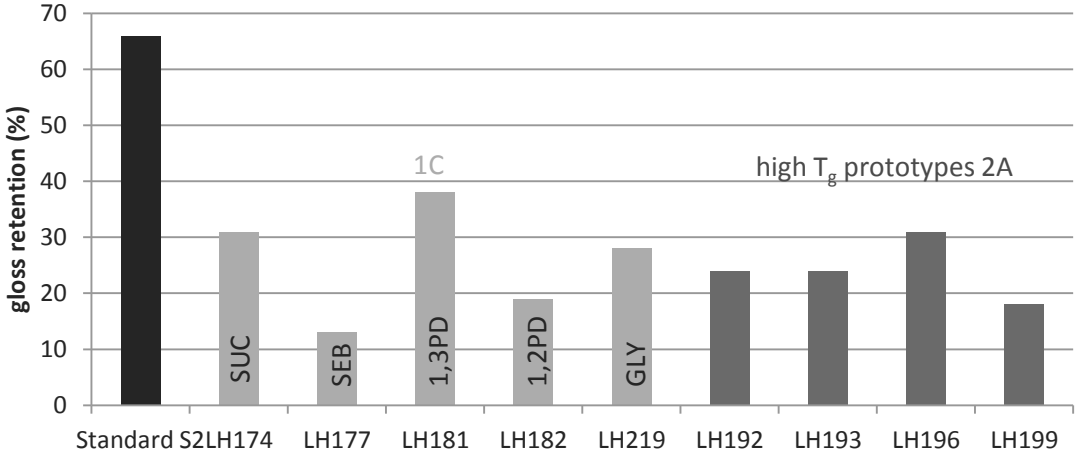

Figure 110: Gloss retention after 1920 h compared to the standard- series 2

The best gloss retention performance was shown by the coating based on the resin LH181, which contains only 1,3-propanediol and no 1,2-propanediol, while the worst gloss retention was shown by the coating based on the resin LH177. It contains only sebacic acid and no succinic acid.

These trends are reflected in the end results of the high T_g prototypes. The coating based on resin LH196, which contains no sebacic acid but 29,37 mol% of 1,3-propanediol and 34,37 mol% of phthalic anhydride retained the most gloss out of the four prototypes. The prototype based on the resin LH199, on the other hand, in which the 1,3-propanediol content was reduced to 19,37 mol% in

favour of more 1,2-propanediol, while the other monomers were kept at the same level as in the resin LH196, shows a smaller gloss retention.

6.2.1.3 Improvement of the gloss retention compared to Arkema's resin

Aside from determining the influence of each of the monomers on the weatherability, the main goal of the study was the improvement of the resistance to degradation of the final coating. The coatings tested in the first series showed a very similar performance to that of the coating based on the resin proposed by Arkema.

While the coatings in the second series also did not show any improvement compared to the coating based on Arkema's resin in absolute terms, as none showed gloss retention significantly above 37%, it is also interesting to compare the performance relative to the standard, as shown in figure 111.

Relative to the standard in series one, the Arkema resin based coating retained 44% of the gloss, while three coatings in the second series retained more compared to the standard of series two. The largest relative improvement was observed in the coating containing the resin LH181, which retained 58% of the gloss compared to the standard. However, the coatings based on resins LH174 and LH196 also caused a slight relative improvement, retaining 47% of the gloss.

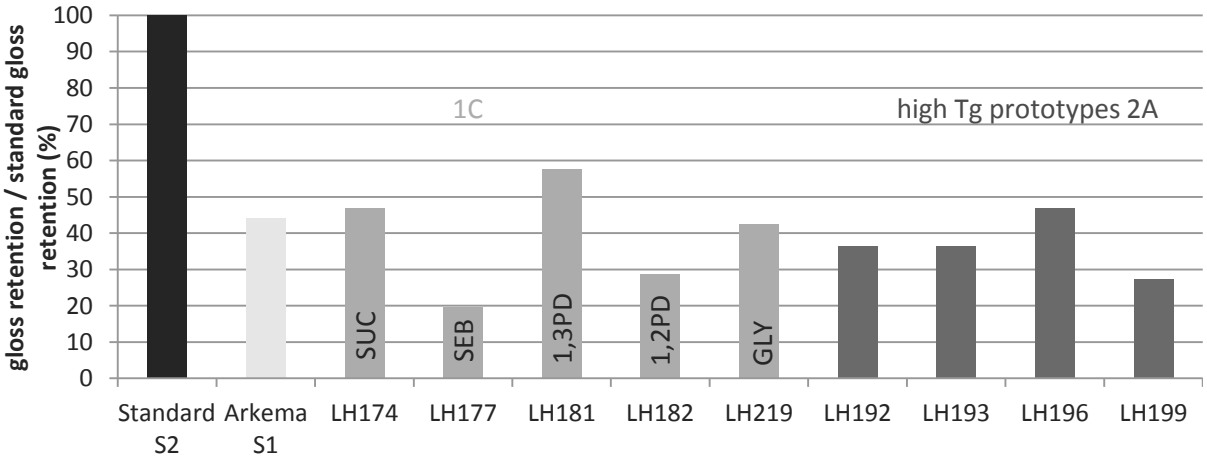

Figure 111: Gloss retention after 1920 h relative to the standard

While the bad performance compared to the standard and the small degree of improvement achieved relative to the Arkema resin coating are quite disappointing, the nature of the formulations needs to be kept in mind when evaluating the results. As the paint formulation was optimised for the standard, and is possibly to a degree incompatible with the biosourced resins, it is natural that the standard performs best.

It is very possible that the performance of the biobased resins can be significantly improved through adjustment of the solvent system and other ingredients present in the formulation. While the results

suggest that it may be difficult to achieve a weathering performance equivalent to that of the standard, it would be wrong to outright dismiss the potential of biobased resins.

The effect of the different changes made to the biobased resins on the coating weatherability will be discussed in the following sections to provide guidance for design routes that can lead to an improvement in weatherability.

6.2.1.4 The influence of isosorbide and phthalic anhydride on the gloss retention

The gloss retention determined after 2000 h correlates with the quantity of isosorbide in the resin that was used in each coating. However, the coatings are only within 3% from each other. Plotting the gloss retention against the exposure reveals a different picture. As shown in figure 112 below, the coating containing the smallest amount of isosorbide (LH190) displayed higher gloss retention than the two other coatings within the first 1500 h.

The differences observed between the different coatings diminish with increasing exposure time. It is possible that the presence of isosorbide initially causes faster degradation compared to the 1,2-propanediol present with which it was replaced, but that the effect becomes irrelevant with increasing deterioration, when other mechanisms take over. It is also possible that the measurement is not precise enough, and that the differences perceived between the coatings in the first three measurements are coincidental.

In order to clarify if the presence of isosorbide influences the weatherability, and the role it plays, two further coatings containing resins LH249 and LH248 containing 19,37 mol% and 45,13 mol% of isosorbide were launched in weatherability tests.

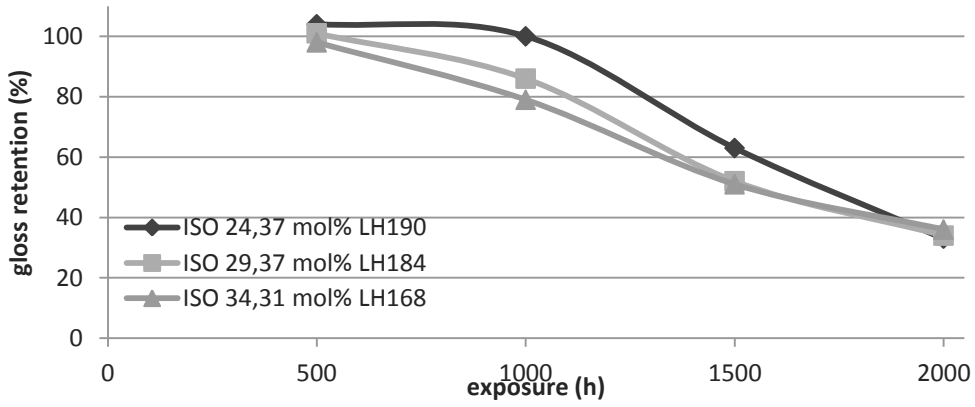

Figure 112: Gloss retention of isosorbide containing coatings over time (1A)

The data measured for the phthalic anhydride containing coatings was equally ambiguous, as shown in figure 113. The coating containing the resin LH163, with the highest amount of phthalic anhydride,

performed worse initially, but better than that containing LH162, with the smallest amount of phthalic anhydride after 1500 h and best after 2000 h.

As for the isosorbide containing coatings, two new coatings containing resin with 19,37 mol% and 48,73 mol% of phthalic anhydride were launched to clarify its effect.

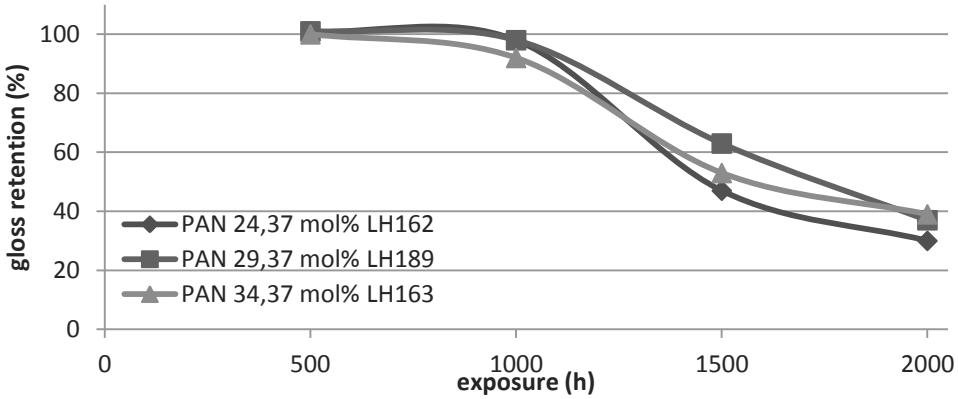

Figure 113: Gloss retention of phthalic anhydride containing coatings over time (1B)

Additional to the comparison of coatings containing different amounts of isosorbide and phthalic anhydride, we can also observe the effect of the replacement of one with the other, as shown in figure 114 - 116 below. Despite the fact that isosorbide and phthalic anhydride are two fundamentally different monomers, the differences caused by the replacement of one with the other in the resin are relatively small.

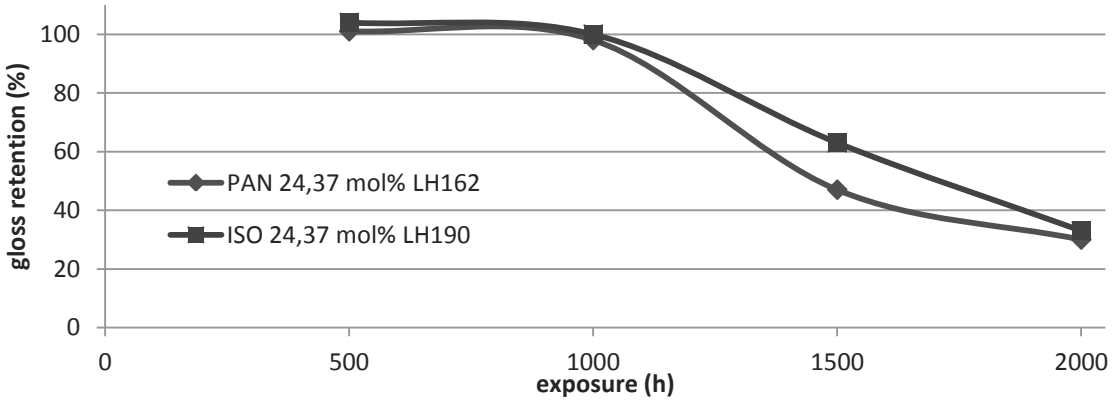

Figure 114: Gloss retention of coatings with resins containing isosorbide or phthalic anhydride - 24,37 mol%

The isosorbide containing coating performs slightly better in every assessment than the phthalic anhydride containing coating for the resins containing 24,37 mol% of each monomer, as shown above. However, the biggest difference is observed after 1500 h, and decreases before and after.

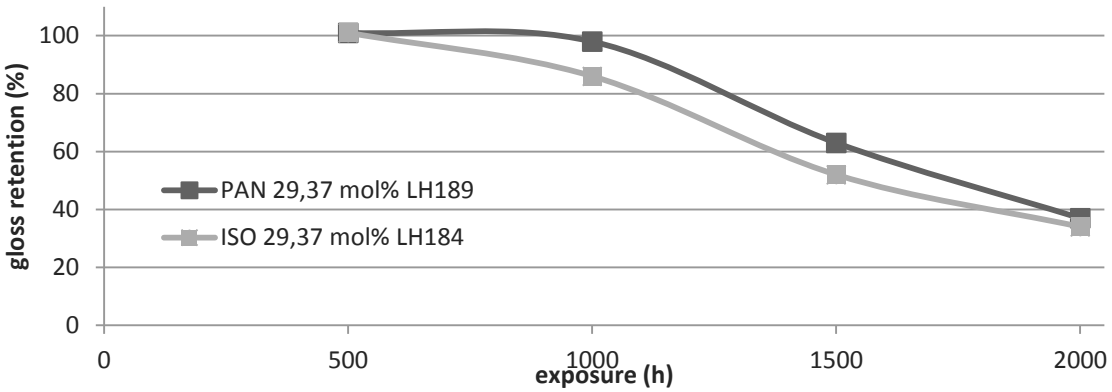

Figure 115: Gloss retention of coatings with resins containing isosorbide or phthalic anhydride - 29,37 mol%

Contrarily, for the resins containing between 29 mol% and 34 mol% of either monomer, the coatings containing phthalic anhydride perform better than those containing isosorbide. As between the different quantities, the differences seem to diminish after 2000 h of weathering.

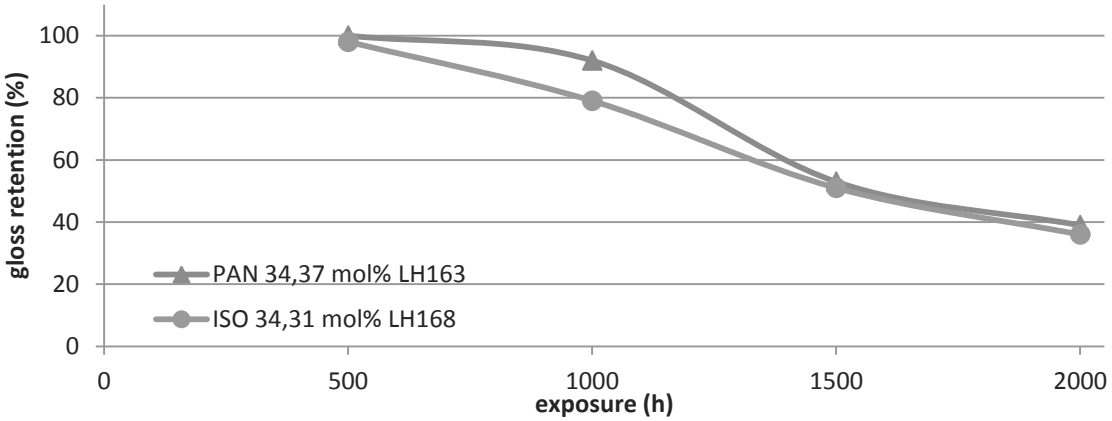

Figure 116: Gloss retention of coatings with resins containing isosorbide or phthalic anhydride - 34 mol%

This indicates that a degradation mechanism independent of the binder composition takes over after a certain degree of deterioration. Another possibility would be that the gloss retention measurement cannot distinguish degrees of degradation when less than 40% of light is reflected back. This theory and the results need to be confirmed but it is possible that the early measures of gloss retention results are more indicative of the relative performance of coatings to each other than those obtained after a maximum amount of weathering.

6.2.1.5 The influence of other monomers in the resin formulation on the gloss retention behaviour

The influence of other monomers on the coating weatherability was tested by modifying the formulation of the phthalic anhydride resin LH189, which contains 10,8 mol% of succinic acid, 8,6 mol% of sebacic acid, 29,4 mol% of 1,3-propanediol and 15,8 mol% of 1,2-propanediol. The succinic acid was completely replaced with sebacic acid and vice versa, and the same was done with the propanediols. In an additional resin, the glycerol content was raised from 6,1 mol% to 9,3 mol%.

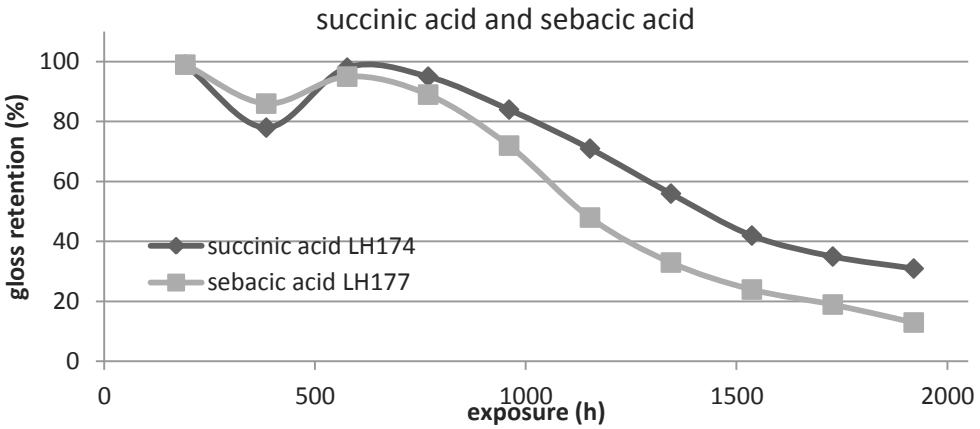

Figure 117: Gloss retention of coatings containing linear acids with different chain lengths

The gloss retention plots of the coatings incorporating these resins mostly reflect the conclusions that could be drawn from the comparison of the gloss retention after 1920 h. The succinic acid containing coating performs better than the sebacic acid containing coating, and the 1,3-propanediol containing coating performs better than the 1,2-propanediol containing coating, as shown in figure 117 and 118.

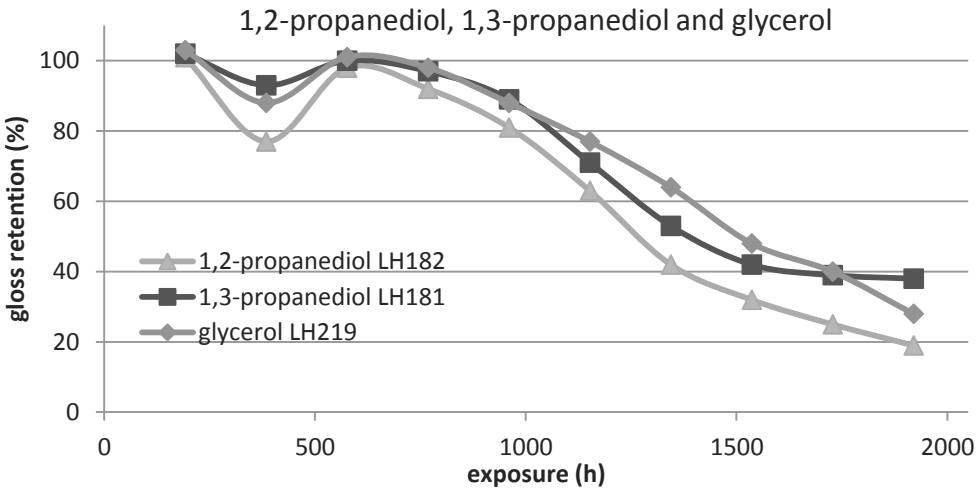

Figure 118: Gloss retention of different alcohol monomers

One exception is the coating with the increased glycerol content containing the resin LH219. While the end result suggests that its performance is approximately between that of the 1,2-propanediol containing coating and the 1,3-propanediol containing coating, the development over time actually shows that its performance is equal or slightly better than that of the 1,3-propanediol containing coating.

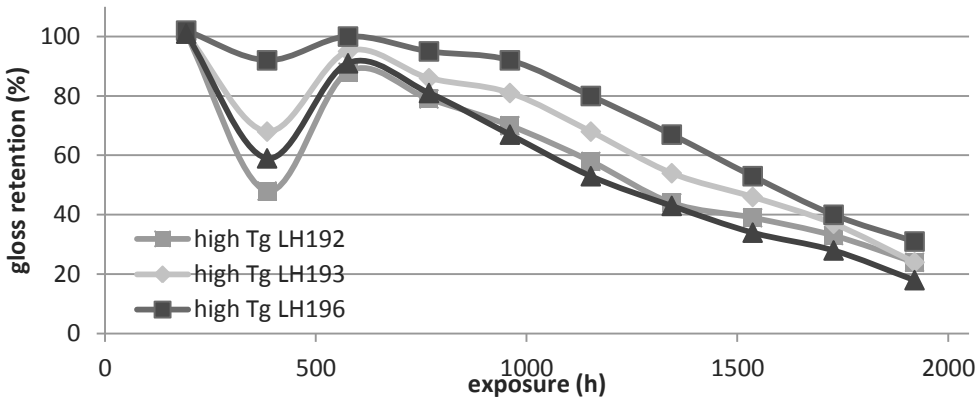

Figure 119: Gloss retention over time of high T_g prototypes 2A

The occurrence of faulty measurements is particularly obvious in the curves of gloss retention over time of the high T_g prototypes, as shown in figure 119. In all coatings measured for the second series, it is clear that the value measured after 384 h is too low. The accuracy of the last measurement after 1920 h for the high T_g prototypes is less obvious, but overall, the smooth trends indicate that confidence in the gloss retention values is justified. Of the four prototypes, LH196 showed the best performance.

Due to the fact that the coating containing the resin LH189 was weathered in a different series to the coatings containing its modified version, and due to the fact that the standard tested in each series showed different weatherability, the direct comparison of absolute results is not useful. Instead, the values were divided by the standard measured in their series, and plotted as percentages relative to that standard, as shown in figure 120.

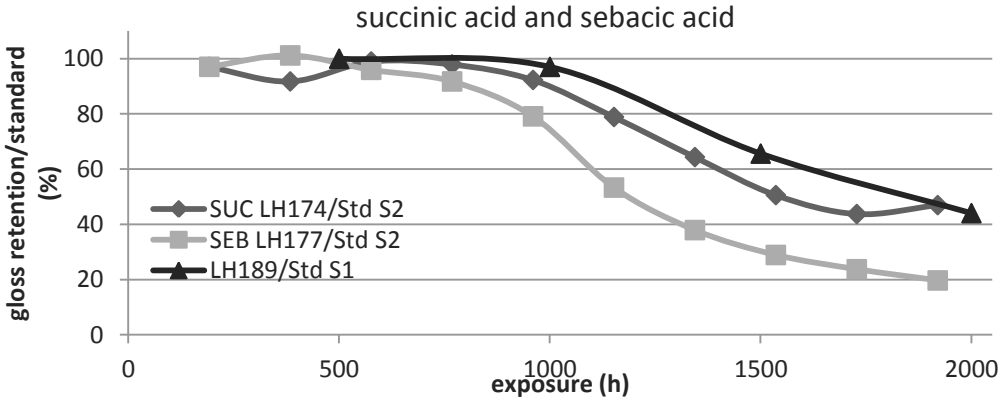

Figure 120: Gloss retention relative to the standard of coatings containing linear acids with different chain lengths

From the resin formulation, the weatherability of the coating containing the resin LH189 would be expected to average between those of the coatings containing the resins LH174 and LH177, as one contains more succinic acid and the other more sebacic acid. As shown above, it instead displays better weatherability than both.

The same observation was made for the resins in which the 1,2-propanediol or 1,3-propanediol content was increased. The coating containing the resin LH189 also performed better than both of these coatings, as shown in figure 121.

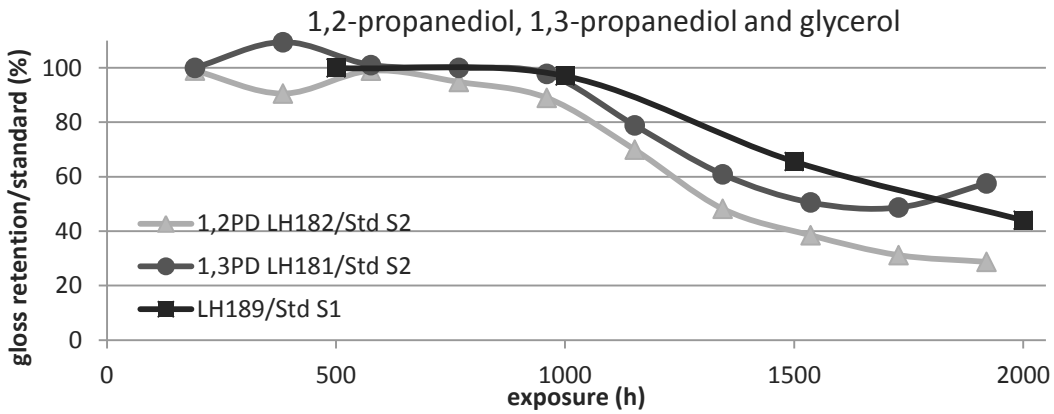

Figure 121: Gloss retention relative to standard of coatings with different diols

This could be due to two different reasons. A first possibility is that the coating containing LH189 is really more resistant to exposure, either due to structural factors or because monomer variety is better for gloss retention than the use of only a few monomers. The second possibility is that the division by the standard is not an adequate method to calibrate the gloss retention performance because it is affected by the changed evaluation procedure differently than the other resins.

6.2.1.6 Additive effect of monomer changes

When the glass transition temperatures of the resins of the high T_g prototype group (2A) were compared with the glass transition temperatures of the resins in which only a single change to the monomer composition was made (1C), it was observed that the combination of two changes, such as the increase of succinic acid and 1,2-propanediol, could lead to a higher increase in T_g than would be expected from adding the increase that each change caused.

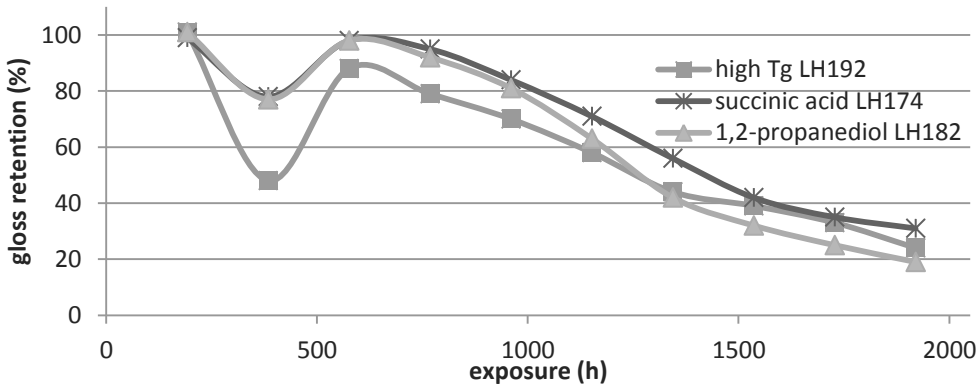

Figure 122: Comparison of gloss retention of LH192 (2A) with LH174 and LH182

In order to test if a similar effect can be observed in the gloss retention development upon exposure, the gloss retention of the coatings containing high T_g prototypes were compared to those of coatings containing resins to which similar changes were made.

The only prototype for which a direct comparison was possible is the coating containing the resin LH192, in which only succinic acid and 1,2-propanediol were used. Contrary to the effect on the glass transition temperature, in this case the former had an increasing effect on the gloss retention while the latter caused a decrease, as shown in figure 122.

The gloss retention of the coating containing LH192 is initially lower than that of both other coatings, which could possibly be due to a structural effect caused by the high rigidity. After 1344 h of exposure, however, the measurements lie between the other two curves, as it would be expected.

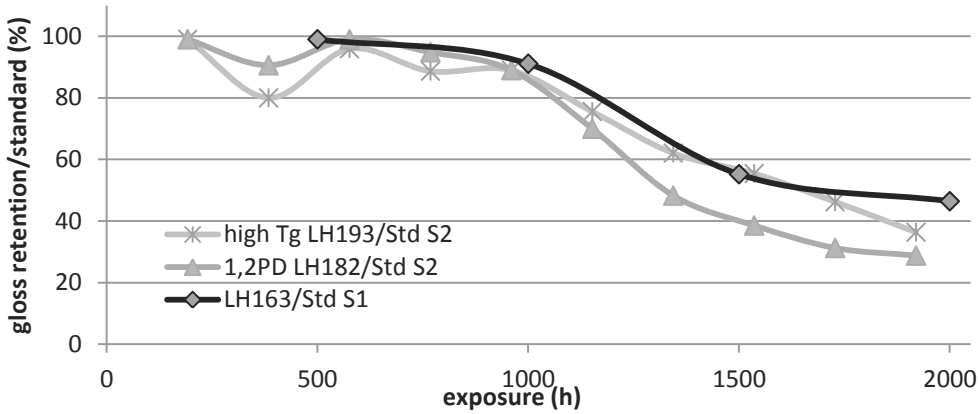

Figure 123: Comparison of relative gloss retention of LH193 (2A) with LH182 and LH163

The other prototypes, in which the amount of phthalic anhydride was increased to 34,37 mol% as in the resin LH163, need to be compared with a coating from the first series, which can only be done in relative terms. As shown in figure 123 above, the coating containing a resin in which the content of 1,2-propandiol and phthalic anhydride was increased shows a gloss retention in between the that of the coatings containing resins in which only one of the two monomers was increased for the majority of the measurements.

This is in agreement with the earlier observation that the increase in phthalic anhydride improves the gloss retention performance, while the increase in 1,2-propanediol worsens it.

In line with this, the coating containing the resin LH196, in which the amount of both phthalic anhydride and succinic acid were increased, which caused an improvement in gloss retention in the respective coatings with the resins LH163 and LH174, has a better gloss retention than both, as shown in figure 124, and the best result of all high T_g prototypes.

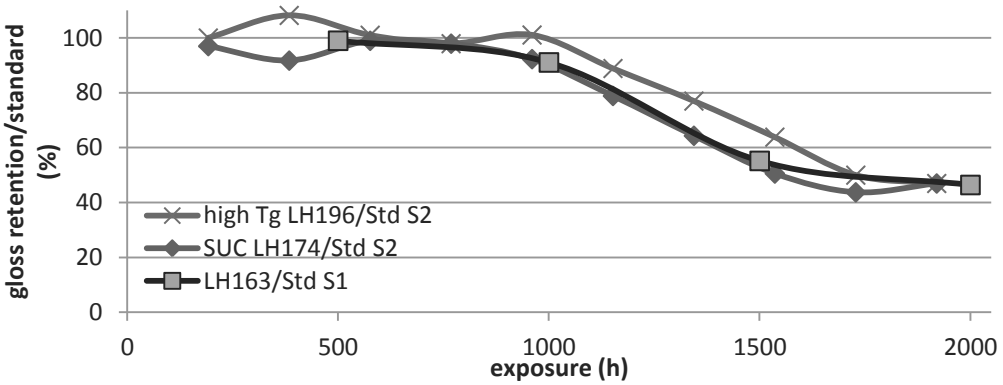

Figure 124: Comparison of relative gloss retention of LH196 with LH174 and LH163

It has to be kept in mind, however, that the values presented are extremely close, so that any conclusion from the comparison should be treated with caution.

6.2.2 Film thickness loss

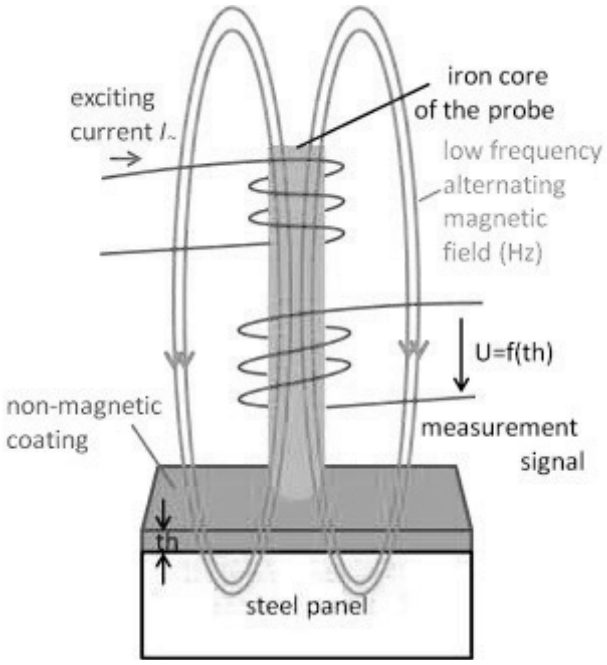

Figure 125: Determination of film thickness

The thickness of the coating can be determined for example using a Fischer permascope. As shown in figure 125, the iron probe of the instrument imposes an excitation current which generates a low frequency magnetic field. The strength of the magnetic field (U) corresponds to the distance between the probe and the base material. When the probe is placed onto the coating, the magnetic field signal can therefore be measured and converted to the coating thickness.[269]

In general, the thickness of the primer is measured before the top coat is applied, and then subtracted from the total coating thickness afterwards to determine the top coat thickness. In this work, coatings with thicknesses between 17 µm and 19 µm were used.

In order to increase the measurement accuracy, the thickness is generally determined by averaging 10 measurements performed in five predetermined locations. Since the thickness of the primer is known, the loss in topcoat thickness can equally be determined by measuring the coating thickness after weathering.

6.2.2.1 Influence of different monomers on film thickness loss

In figure 126 below, the loss in film thickness after exposure under Hot QUVa conditions for 2000 h is shown for the different prototypes. As indicated by the error bars, the standard deviation observed between the separate measurements was relatively large. Some trends can nevertheless be distinguished.

It should also be noted that the loss observed for some of the films, particularly the isosorbide containing coatings, makes up up to 72% of the original coating present. The hypothesis postulated above that the degradation mechanism changes after a certain degree of deterioration is strengthened through this observation. It is quite plausible that the behaviour of the coatings changes once more than 50% of their substance is lost.

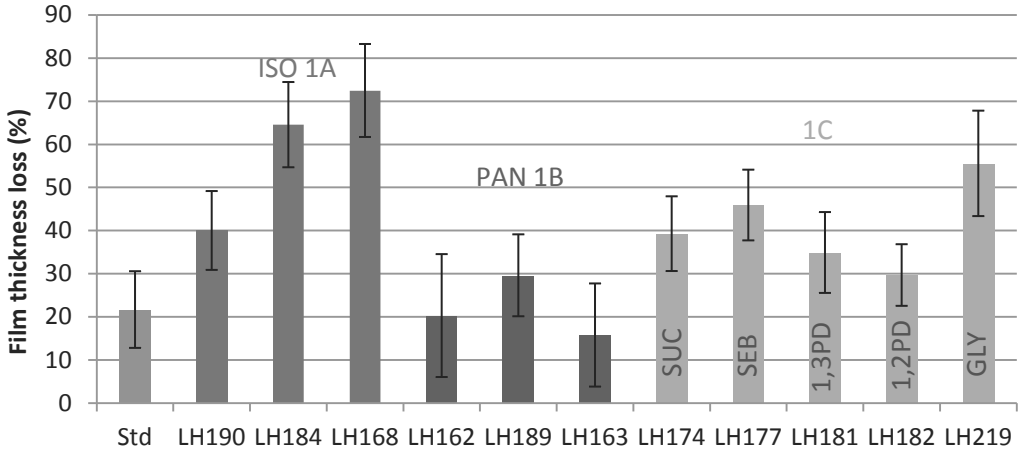

Figure 126: Relative film thickness loss – film thickness loss/original film thickness

First of all, the prototypes containing isosorbide experience significantly larger film thickness loss than those with an equivalent quantity of phthalic anhydride. Furthermore, the highest thickness loss is associated with the highest quantity of isosorbide, suggesting that the loss is proportional to the isosorbide present in the coating.

This could be explained by the erosion taking place when the coatings are exposed to humidity. If small fractions of the network are liberated through chain scission or hydrolysis, they can be dissolved in the water and separated from the coating. Since the isosorbide contains two ether links, it is considerably more hydrophilic than 1,2-propanediol and phthalic anhydride, and could increase both the susceptibility to hydrolysis and the solubility of broken off fragments in condensation water.

No correlation between the quantity of phthalic anhydride and the film thickness loss is observed. It does however reflect the gloss retention loss upon exposure, which was also greatest for the coating containing LH189 and smallest for the coating containing LH163 for the measurement after 1500 h of exposure.

Even though the coatings containing resins LH174, LH177, LH181, LH182 and LH219 (1C) were all formulated with 29,37 mol% phthalic anhydride like LH189, the film thickness loss is considerably higher than that of the coating LH189. This is in line with the gloss retention observed and could be attributed to the greater strain placed on the coatings by more frequent examinations.

Comparing these resins within each other, the largest loss is observed for the coating containing an increased amount of glycerol, while the smallest is observed for the coating containing an increased amount of 1,2-propanediol. The former could be due to the increased presence of free hydroxy groups near the middle of the chain. The secondary hydroxy groups on glycerol could increase the hydrophilicity of the middle of the chain, facilitating the breaking of the chain into two large parts rather than the breaking off of small end groups. The latter could be due to the steric hindrance imposed by the adjacent methyl groups to 1,2-propanediol ester links. This observation points towards hydrolysis rather than radical chain scission as the dominant mechanism of film thickness loss.

6.2.2.2 Correlation between film thickness loss and gloss retention

The film thickness loss results only correlate with the gloss retention results in the first series. Both put the three coatings containing different amounts of isosorbide and phthalic anhydride in the same order of weatherability.

However, the differences in the film thickness are significantly larger, and the performances of the coatings containing isosorbide and phthalic anhydride with respect to each other are very different. While all six coatings perform similar in gloss retention, the isosorbide containing coatings lose significantly more film thickness. Furthermore, while the gloss retention results suggested that both isosorbide containing coatings (1A) and phthalic anhydride containing coatings (1B) perform significantly worse than the standard, the phthalic anhydride coatings display a similarly small loss of film thickness to the standard.

Furthermore, the coating containing 1,2-propanediol, which showed worse gloss retention results than all other coatings in its series (1C), showed the smallest film thickness loss.

This disparity suggests that different degradation mechanisms may be prominent in the different coatings depending on the resin composition. It would be, for example, imaginable, that the isosorbide coatings experience significantly more water uptake due to their hydrophilicity, but either do not crack as a result, because the water can be accommodated through swelling, or that cracks are evened out through erosion.

Both the gloss retention and the film thickness are relevant to the coating performance. While a loss in gloss may be more immediately visible, a significant loss in coating thickness will reduce the ability of the paint to protect the metal from corrosion, which is its primary function. Considering the disparity observed between the results in this case, it would be recommendable not to conclude from good gloss retention result to little film thickness loss, but to always check both parameters.

6.2.3 Optical microscopy images

An optical microscope was used to obtain images of a selection of coatings before and after weathering. The sample was lit from the side and the colour and zoom were adjusted during the imaging process. In order to render the features of the coating surface more visible, the images were treated using Microsoft office picture manager software, and contrast, brightness and colour intensity were again changed.[LIII]

The images were obtained in 100 x zoom and are shown in figures 127 - 130. While it is difficult to quantify the degradation observed in the images, some observations can be made.

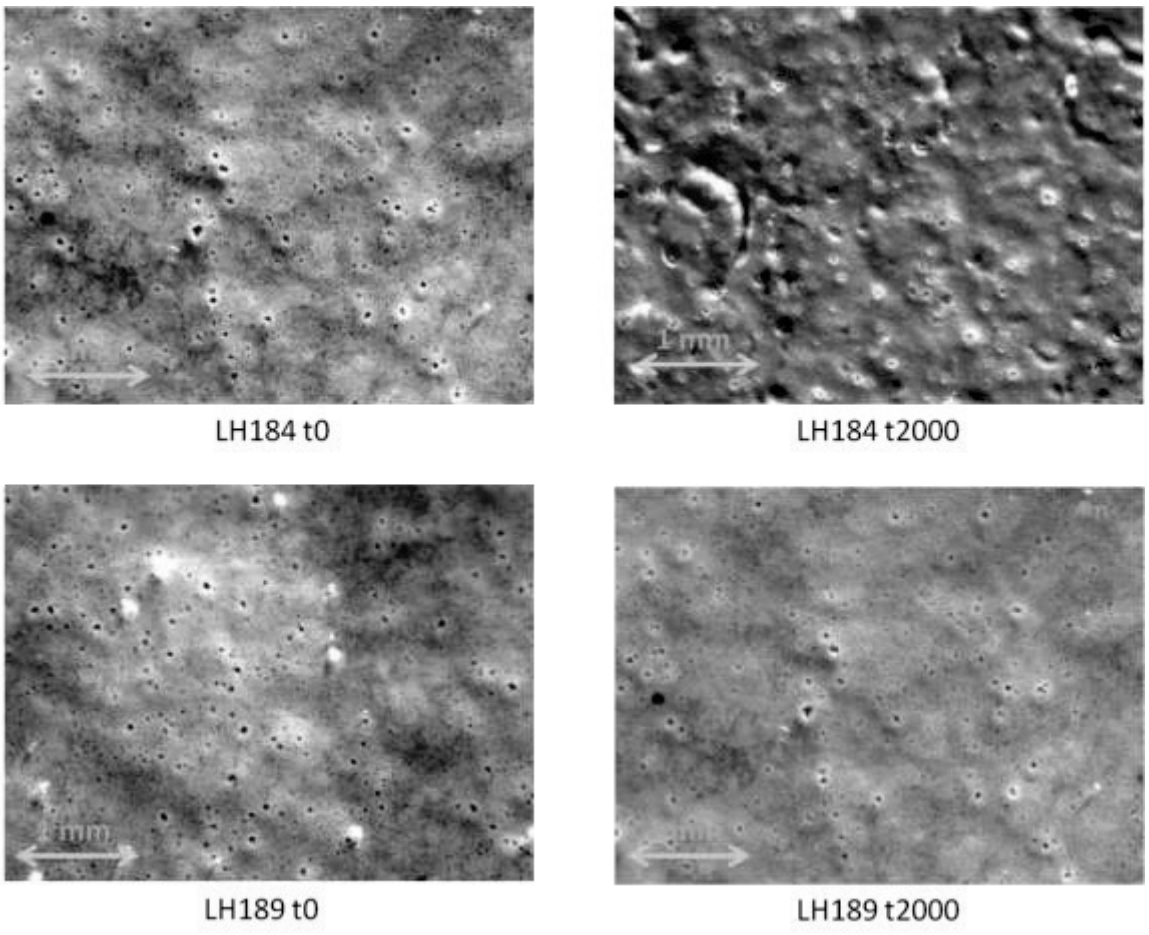

Figure 127: Optical microscopy images of LH184 and LH189 before and after weathering

[LIII] The original images can be found in the annexe.

In comparing the images of the coatings containing the resin LH184, with isosorbide, and the resin LH189, with phthalic anhydride, the degradation in the isosorbide containing coatings between t0 and t2000 is more visible. The surface of the phthalic anhydride containing coatings seems to be more even both before and after weathering, while several valleys are visible in the isosorbide coating after weathering.

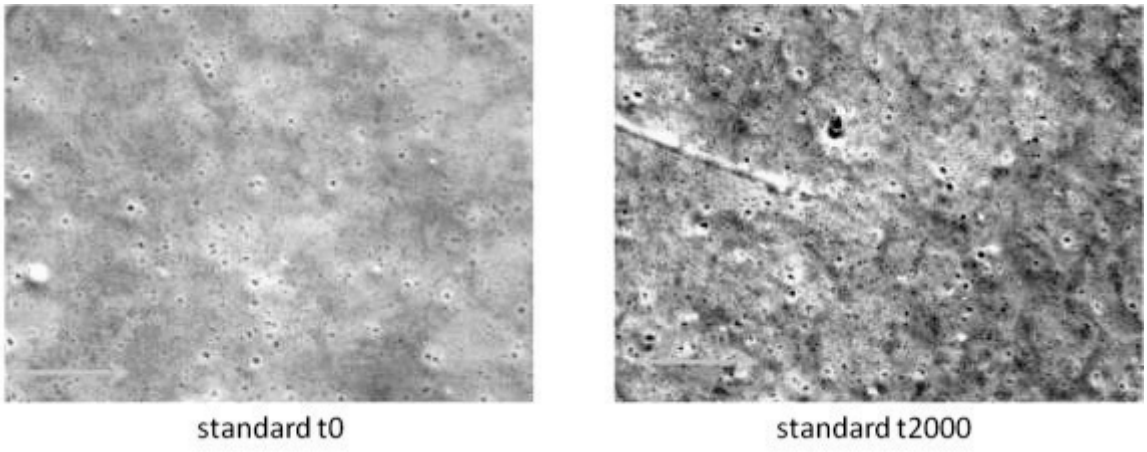

Figure 128: Optical microscopy images of standard coating before and after weathering

This is in line with the large degree of film thickness loss that was observed for isosorbide containing coatings but not for phthalic anhydride containing coatings. Comparing the standard coating with the coating containing LH189, the standard coating seems to be slightly smoother before weathering, but similar after 2000 h of exposure. This also correlates with the results of the film thickness evaluation.

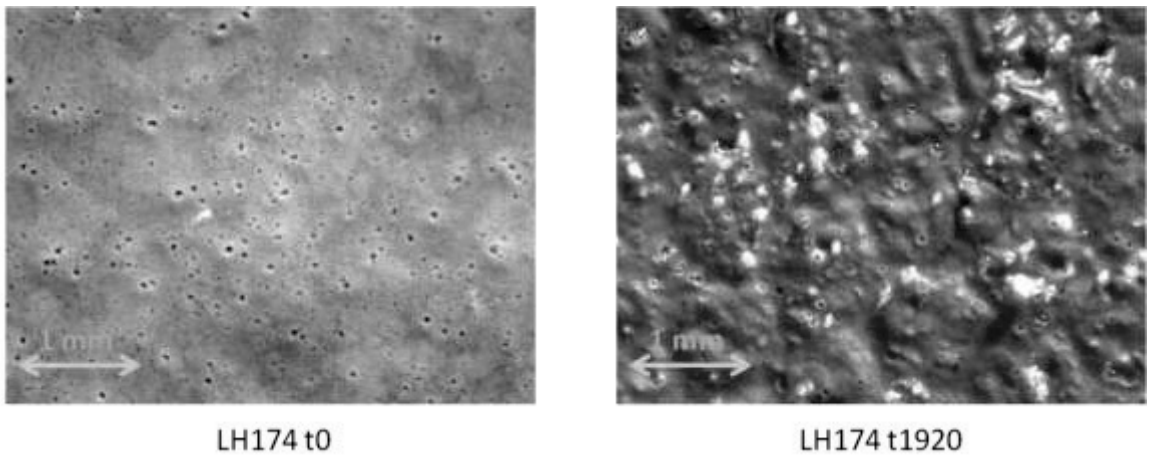

Figure 129: Optical microscopy image of LH174 containing coating before and after weathering

The behaviour of the coating containing the phthalic anhydride based resin LH174 in which the content of succinic acid was increased resembles the isosorbide containing coating LH184 more strongly than that of LH189. The coating surface after weathering looks smoother, but valleys and mountains are visible.

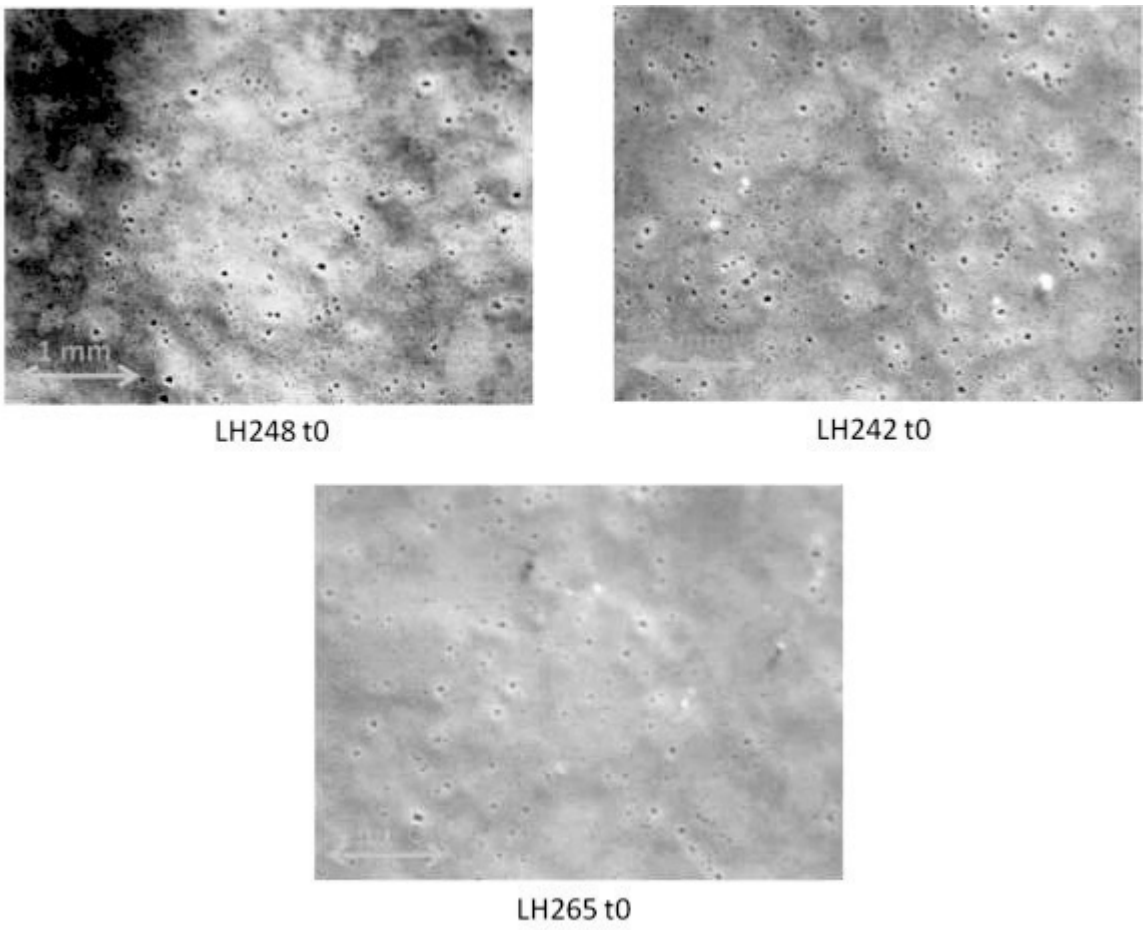

Figure 130: Optical microscopy image of coatings with isosorbide, phthalic anhydride and cyclohexanedicarboxylic acid at t_0

In general, we can observe slightly more and larger craters in the surface of most biobased coatings than in that of the standard. This is also confirmed in the images of the coatings based on isosorbide containing resin LH248 and phthalic anhydride containing resin LH242. The surface of the cyclohexanedicarboxylic acid based coating LH265 looks slightly smoother, which could indicate that the large amount of craters is indeed due to a lack of compatibility with the paint formulation designed for a resin based on cycloaliphatic monomers.

Overall, however, the quality of the images and the lack of quantification mean that they are not sufficient as a basis for conclusions and should be used only as supplementary illustrations.

6.2.4 Correlation between the crosslinking density and the weatherability

The standard coating has been determined to have a crosslinking density of 0,0270 mmol/cm^3 in dynamic mechanical analysis, as described in the previous chapter (*5.4.3.2.2*). This is considerably below the crosslinking densities calculated for the other coatings, which range from 0,0421 mmol/cm^3 to 0,0963 mmol/cm^3.

The larger distance between the crosslinking points could be a reasonable explanation for the different degree of degradation observed in the standard and the other prototypes. For the gloss retention observed after different times of exposure in the first coating series, no further correlation could however be discovered to the crosslinking density, as shown in figure 131.

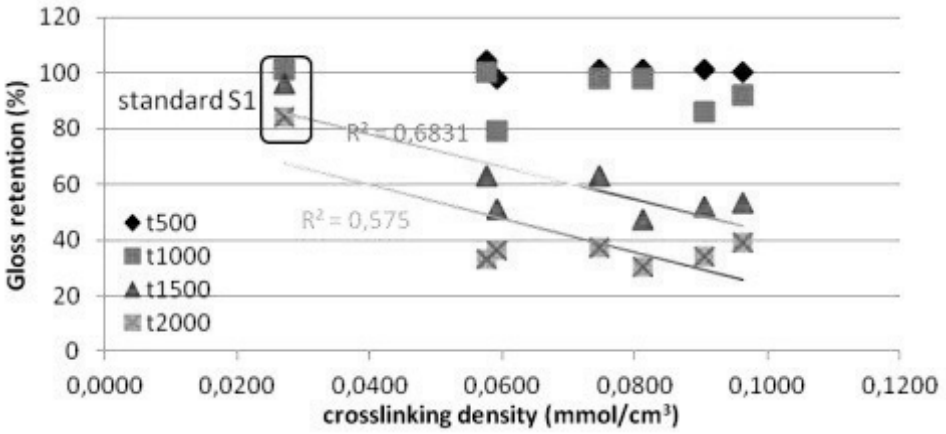

Figure 131: Crosslinking density *vs.* gloss retention series 1, no correlation observed

Interestingly, in the second series, the two coatings with the best end gloss retention other than the standard, containing the resins LH174 and LH181, also had the highest crosslinking density. Considering only the coatings containing the resins LH219, LH182 and LH177, a linear correlation between the crosslinking density and the gloss retention can be observed, as visible in figure 132.

This suggests that both very low and very high crosslinking densities can improve the gloss retention performance, but that medium crosslinking densities are problematic. The observation can only be partially confirmed for the first series, where only the resins with a crosslinking density above 0,800 mmol/cm^3 were examined.

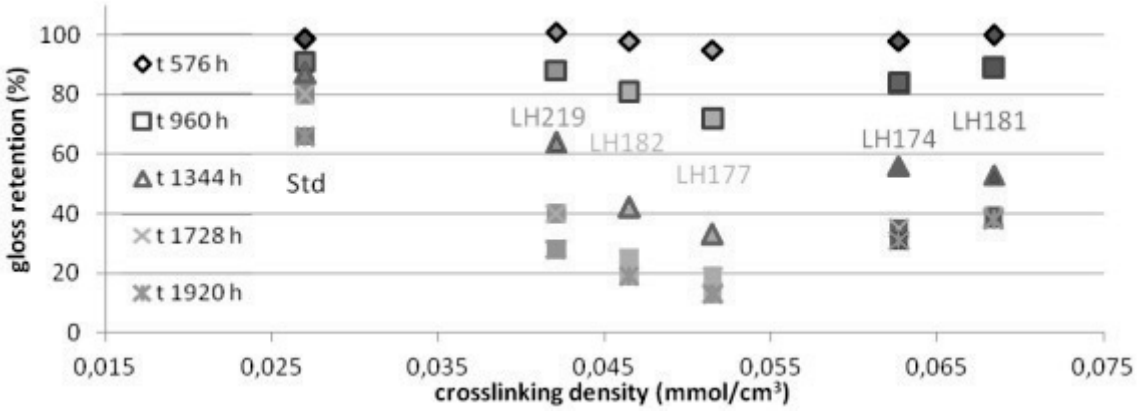

Figure 132: Crosslinking density *vs.* gloss retention series 2

A clearer correlation was observed between the crosslinking density of phthalic anhydride containing coatings and their film thickness loss. As shown in figure 133 below, the films with higher crosslinking

densities experienced considerably less loss than those with lower crosslinking densities. This correlation does not extend to the isosorbide containing coatings or the coating containing the resin LH182, in which the quantity of 1,2-propanediol was increased.

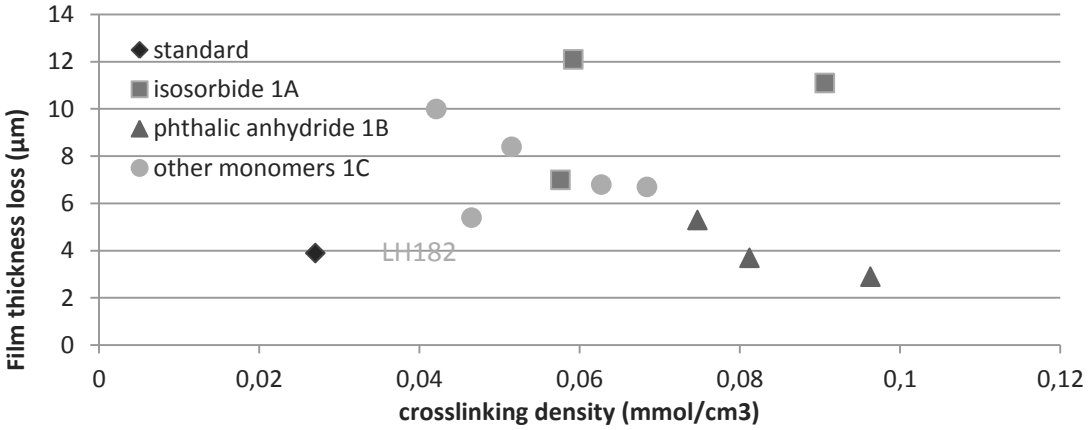

Figure 133: Crosslinking density *vs.* film thickness loss

Overall, it suggests that in the presence of hydrophilic groups such as isosorbide or methyl pendent groups providing steric hindrance in 1,2-propanediol have a greater influence on the acceleration or prevention of film loss than the crosslinking density. In the absence of such factors, however, the crosslinking density seems to be the deciding factor.

This rule does again not apply to the standard coating, which shows a lower film thickness loss than the majority of the biosourced resin based coatings. This indicates that another factor, either a greater hydrophobicity or a greater steric hindrance, governs the resistance to film thickness loss in the standard coating.

This last correlation also validates the crosslinking density results to a degree, which have not been linked to any other coating properties discussed above.

6.3 Spectroscopic assessment of the weatherability

The assessment of the visual qualities of the coatings as well as the evaluation of their response to mechanical stress described above can give a good picture of their behaviour upon weathering and the way the changes will be perceived by end users. Spectroscopic studies can, on the other hand, help to understand the changes at a molecular level. The response of the resins and coatings to radiation was used to provide a link between the observations made concerning the gloss retention, appearance and µ-hardness of the coatings and the formulations used for the resin syntheses, so that the conclusions can serve as a guide for the design of more durable resins.

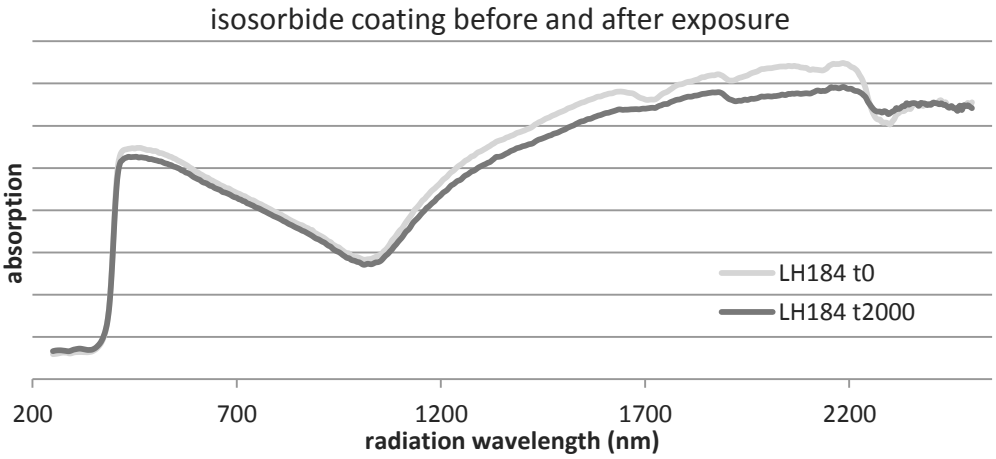

Figure 134: LH184 absorption of radiation from 250 nm – 2500 nm before and after weathering

In figure 134 above, the reflection spectrum of radiation from 250 nm to 2500 nm of an isosorbide based coating before and after weathering is shown. Two areas are of particular interest. First of all, the UV absorption, between 200 nm and 400 nm, can provide information about the capability to absorb UV light from the sun and therefore the liability of the coating to photolytic degradation. Furthermore, the change in absorption after weatherability can provide evidence of the degree of autocatalytic change in the structure, and the creation of new chromophores during the degradation.

Secondly, the absorption in the infrared region can provide information about the bonds formed in the crosslinking process, and the functional groups present before and after degradation. This can in turn be used to qualitatively and quantitatively characterise the changes occurring in the polymer network during exposure.

The detailed investigations of the UV region, performed with transition UV/Vis spectroscopy of the resins and their components, and the infrared region, performed using both attenuated total reflectance and photoacoustic methods, are discussed below.

6.3.1 Assessment of the capability to absorb UV light

While the most relevant UV absorption would be that of the crosslinked coating before and after weathering, access to a reflection spectrometer was limited. Furthermore, the coatings examined were formulated without pigments, but coated on top of a white primer containing TiO_2, so that the absorption of the TiO_2 pigments is likely dominate that of the coatings.

Therefore, only one spectrum of a cured coating was obtained. The other coatings were evaluated through the UV absorption of the corresponding resins, which could be measured with a traditional transition spectrometer.

While some differences in the UV absorption of the different resins were observed, they could not be correlated with their structure and composition. Furthermore, they were mostly in the low UV region, which is not the most relevant for weathering. From comparing the spectrum obtained in solution to that of the coating, it seems that the absorption is increased in the relevant region around 300 nm through the crosslinking. Overall, it was concluded that the UV absorption of the resins is probably not very relevant to the UV absorption of the coatings and therefore their weatherability, and that the measurement of UV absorption is not a very useful tool to distinguish different resins and to predict their performance.[LIV]

6.3.2 Infrared analysis of the coatings

Infrared analysis of the coatings was used to observe the change in the presence of different functional groups and to thus elucidate the mechanisms responsible for the degradation. First, the different peaks examined and their assignment to structural features in the coating will be explained.[LV]

Furthermore, a short explanation of the two techniques used to obtain the IR spectra, attenuated total reflectance (ATR) and photoacoustic spectroscopy (PAS), and the method of interpretation of the spectra chosen will be given. Finally, the changes in IR spectra observed upon weathering will be compared between coatings and to the standard to enable conclusions of which changes in formulation could lead to higher resistance to degradation.

6.3.2.1 Treatment of IR data

Several characteristic functional groups can be used to examine the degradation in the coatings. In figure 135 below, the fingerprint region of three resins based on phthalic anhydride, isosorbide and cyclohexanedicarboxylic acid is shown. The largest peak around 1740 cm^{-1} is attributed to the carbonyl stretching vibration of ester and acid groups, and is common to both the resins and the resulting coatings.

The main differences between the three resins are the two peaks at 1600 cm^{-1} and 1580 cm^{-1} corresponding to the phthalic anhydride aromatic ring present in LH163 and the absorption of the aliphatic ether at 1094 cm^{-1} present in the isosorbide containing LH184. Lastly, the peak around 1280 cm^{-1} corresponding to the ester and acid C-O stretching vibration is considerably broader in the resin LH163 containing phthalic anhydride than in the resins LH184 and LH265 containing isosorbide and cyclohexanedicarboxylic acid.

[LIV] See annexe for details on the UV absorption of monomers, solvents, resins as well as methods used and absorption coefficients calculated.
[LV] The methods used to make the different measurements comparable to each other are explained in the annexe.

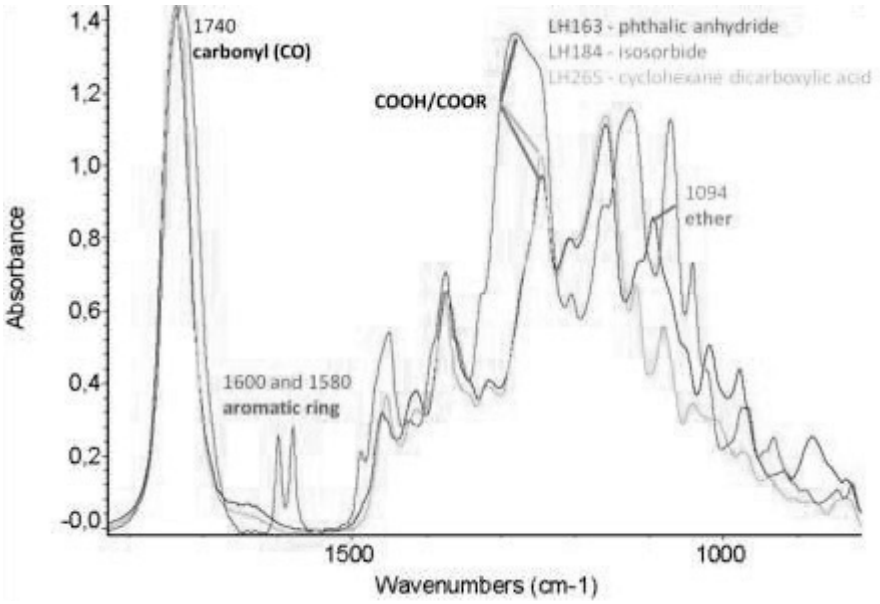

Figure 135: Comparison of IR fingerprint regions of resins based on different monomers

The other region of interest is between 2400 cm^{-1} and 3900 cm^{-1} and contains the C-H, N-H and O-H stretching vibrations. As shown in figure 136 below, the OH vibrations are very prominent in the resin. When it is formulated into the paint, a slight shift to lower wavenumbers can be observed due to the additional N-H groups present in the unreacted melamine.

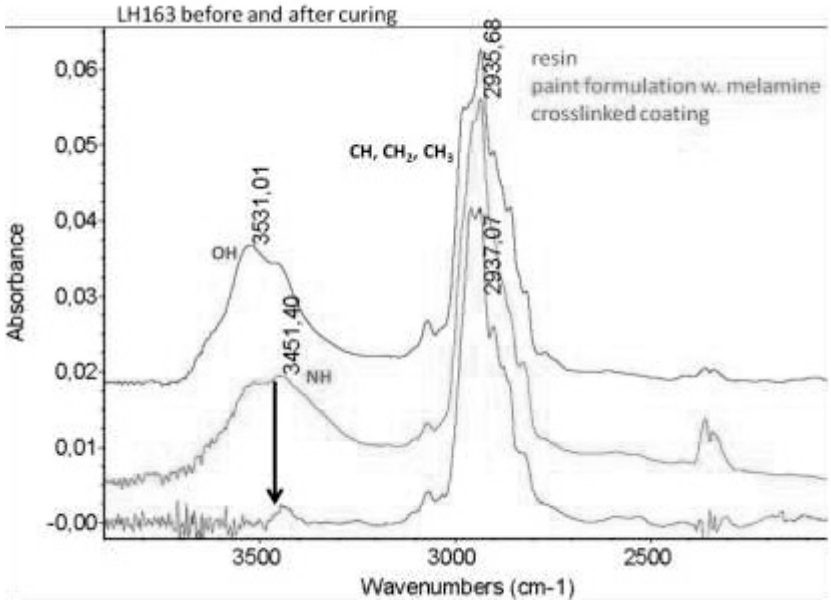

Figure 136: IR spectrum of a resin, paint and coating before weathering

After curing, the N-H and O-H vibrations disappear due to crosslinking, while the C-H vibration peak remains in similar intensity, as shown in figure 137. With ageing, the peak due to N-H and O-H stretching vibrations reappears as ester and resin melamine bonds are cleaved. It can therefore be used as a quantitative measure for the degradation process. A decrease in quality between the IR

spectra taken from liquid resin and paint formulation to those taken from the solid coating can furthermore be observed.

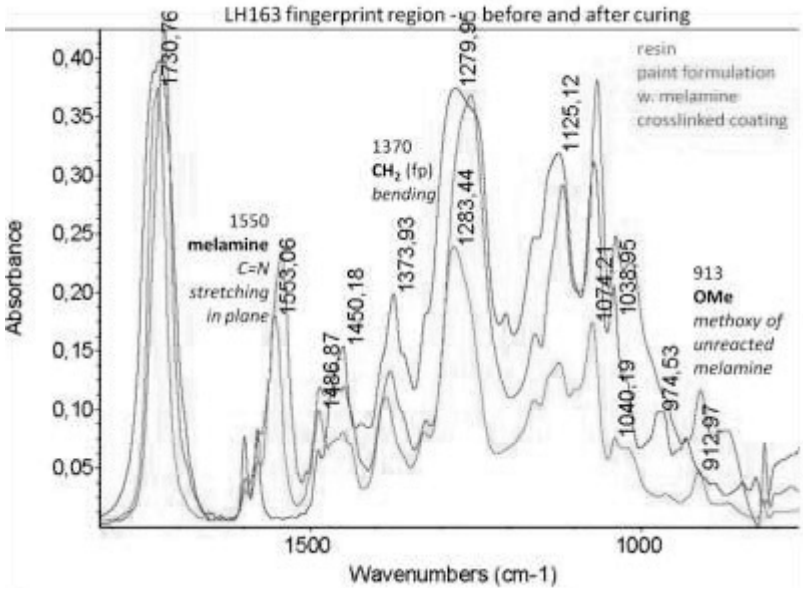

Figure 137: LH163 fingerprint region before and after curing

Absorptions of interest in the fingerprint region include the peak at 1550 cm^{-1}, which corresponds to the C=N stretching vibration in the aromatic melamine ring, the CH_2 bending vibration at 1370 cm^{-1} and the absorption of unreacted methoxy groups at 913 cm^{-1}, represented in scheme 130.

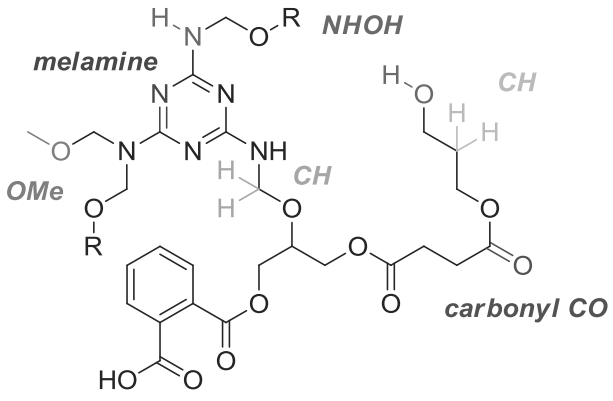

Scheme 130: Examples of functional groups observed in the IR in the resin structure

In order to quantify the presence of each functional group, the area of the each absorption was determined. For this, the "automatic smooth" function in the Omnic software was used. Furthermore, the baseline of each spectrum was adjusted to between 2400 cm^{-1} and 3950 cm^{-1} so that the spectrum was not in negative absorption at any point.

The areas integrated for each peak are shown exemplary for the spectrum of the coating based on the resin LH174 taken after 1536 h of exposure in figure 138. Both baseline and peak limits were chosen to comply with the standard procedure used by Beckers.

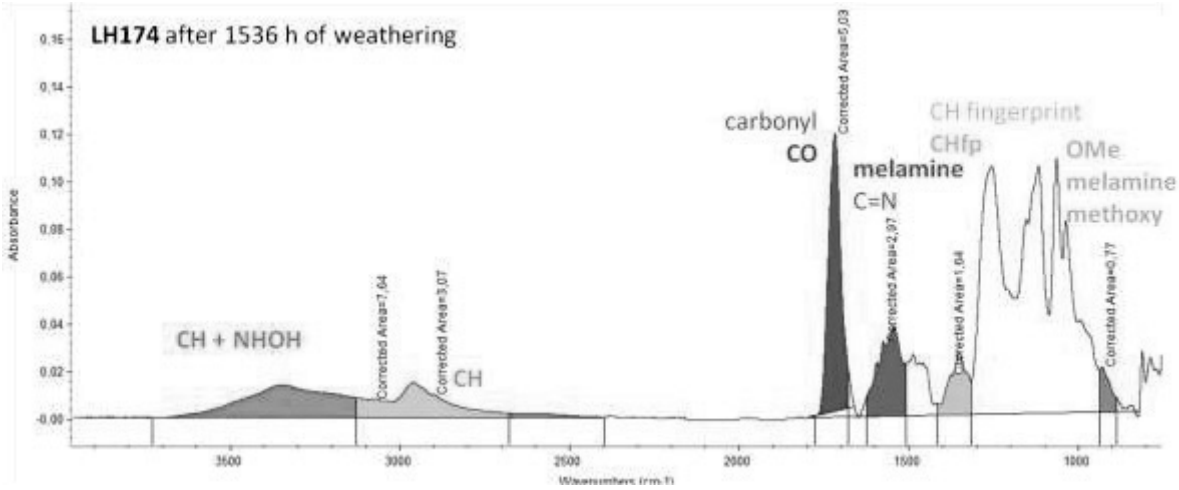

Figure 138: Peak integration on the example of the LH174 coating

Due to differences in the surrounding of each peak, the limits and baselines were slightly adjusted depending on the presence of isosorbide and phthalic anhydride and for the standard resin, which contains neither.[LVI]

In the following analysis, the absorption of the CH, CH_2 and CH_3 stretching around 2900 cm^{-1} will be referred to as CH, while the absorption in the fingerprint region corresponding to the CH_2 bending around 1380 cm^{-1} will be referred to as CHfp. The carbonyl absorption is referenced CO, the methoxy group stemming from unreacted melamine is called OMe and the combined absorption of N-H and O-H stretching vibrations is referred to as NHOH. The area of the NHOH peak was determined by subtracting the area of the CH peak from the surrounding absorption.

In order to compare the absorptions in separate spectra, normalisation of the amount of coating analysed is necessary. For this, C-H peaks adjacent to the peaks to be analysed or the carbonyl peak have been used as a standard in the literature. Upon examination of both methods, it was found that while the CH peaks are only stable during exposure for the standard resin, they change shape and increase in their absorption with respect to the carbonyl peak for the biobased resins, especially those containing isosorbide.

Furthermore, when the carbonyl peak was used for normalisation, the results were more consistent than when CH peaks were used. Its shape was also more similar between different coatings and over

[LVI] The exact wavenumbers of the integration and baselines are detailed in the annexe.

the exposure period. It was therefore decided to normalise all infrared spectra recorded using the attenuated total reflectance method with the carbonyl peak.

It should however be kept in mind that a distance of over 1000 cm^{-1} lay between the peaks assessed and the carbonyl in some cases. Because the coating thickness observed depends to a degree on the wavelength, this can mean that the depth used for normalisation was sometimes different to that assessed for the peak evaluated, which could induce an error in the results.

For the presentation of the results, it was decided to use absolute and not relative values. Relative values, which have been used in the literature, can be obtained by dividing the absorption through the value measured before exposure.[216, 219, 238] It was however found that this did not correctly represent the trend in the performances, and the risk of error associated with dividing all values by one measurement was judged too high.[LVII]

The difference in absorption before exposure was instead incorporated as a shift along the y-axis. Each value is presented as the absolute difference in absorption of the corresponding peak compared to the value measured before exposure was started, as shown in figure 139 below.

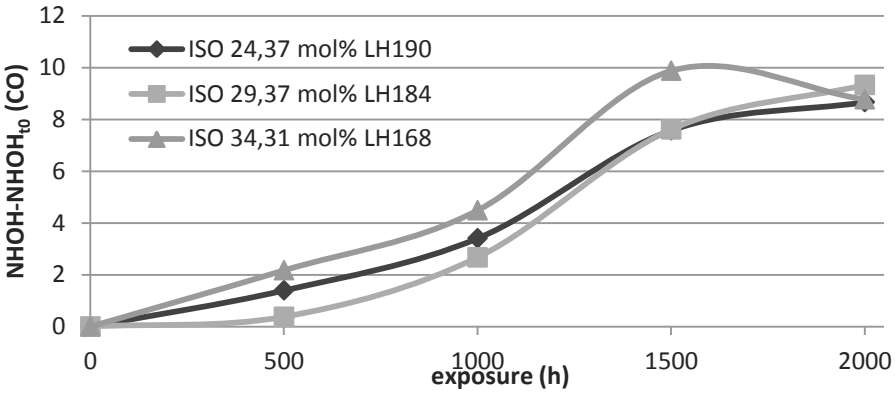

Figure 139: NHOH – NHOH$_{t0}$ of isosorbide coatings (1A)

In conclusion, the peak areas obtained in the infrared analysis of the coatings will be presented with respect to the carbonyl peak and as an absolute increase with respect to the value measured before exposure unless otherwise noted.[LVIII]

6.3.2.2 Different infrared measurement techniques

Two different techniques were used to obtain infrared spectra directly from the solid samples. While attenuated total reflectance (ATR) was used to follow the progress of the coatings over time, and therefore for the majority of the analysis, photoacoustic measurements (PAS) were also employed to supplement the data obtained.

6.3.2.2.1 Attenuated total reflectance IR spectroscopy

In order to obtain the spectrum using attenuated total reflectance, a crystal is brought into intimate contact with the sample. As shown in figure 140, infrared radiation is then shone onto the crystal, and the reflected light is observed.

The quality of the spectra depends largely on the quality of the contact of crystal and surface, and can therefore deteriorate if cracks develop on the surface, as is the case after long periods of weathering.

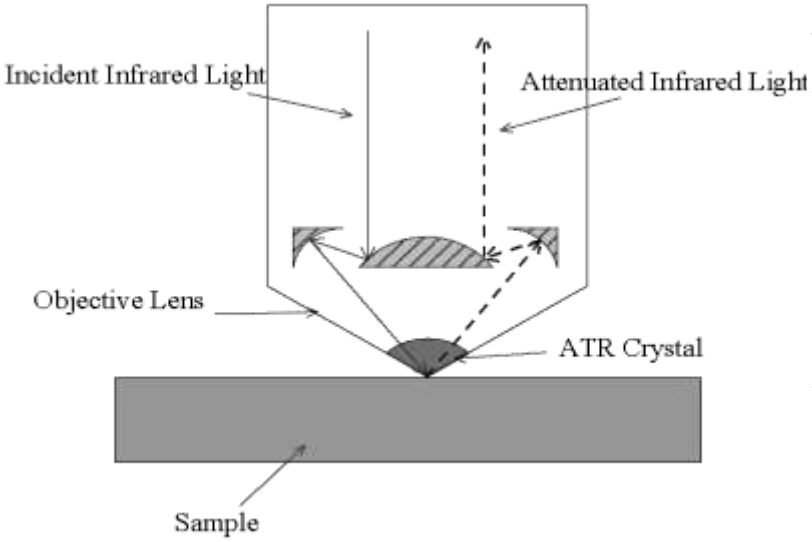

Figure 140: Attenuated total reflectance measurement method

The signal strength obtained with this technique is relatively low.

6.3.2.2.2 Photoacoustic IR spectroscopy

Photoacoustic IR spectroscopy (PAS) was used to complement the ATR results. It was not as readily available as the ATR, but it eliminated the dependence on contact and produced a significantly stronger signal.

PAS spectra were therefore obtained for all samples before and after 2000 h of exposure. The photoacoustic technique utilises the acoustic wave produced by the thermal changes which occur in the samples when they are submitted to IR radiation. The sample is placed in a helium gas chamber, and a microphone is used to pick up the pressure waves caused by thermal expansions and contractions, as shown in figure 141.

The penetration depth into the sample depends on its thermal conductivity, heat capacity, and density as well as on the infrared light frequency, and therefore varies for different wavenumbers. In contrast to the ATR measurements, which mainly capture the surface

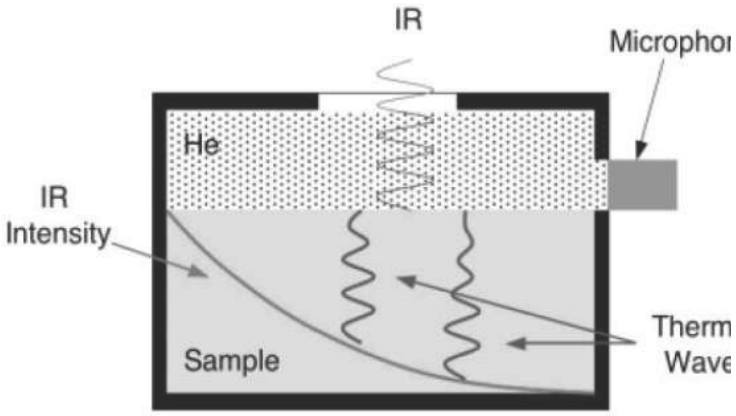

Figure 141: Photoacoustic spectroscopy method

[LVII] The different possible representations are shown in the annexe.
[LVIII] The original IR data before normalisation and transformation can be found in the annexe.

area, the PAS technique can penetrate the coating up to 15 µm deep.

One major disadvantage of the technique is that it is extremely sensitive to acoustic disturbances such as noise in the laboratory during the measurement.

The agreement between the results of the ATR and PAS measurements was found to be dependent on the normalisation method used. Due to the deeper penetration depth of PAS, the carbonyl was not suitable for normalisation of the methoxy and NHOH peaks that are far away from it. Good agreement was however obtained when nearby C-H peaks were used for normalisation instead for those two absorptions.[LIX] As no suitable reference exists for them, the CH peak and CHfp peak recorded using the PAS method will not be discussed.

6.3.2.3 Correlation of the IR spectra to the coating composition prior to exposure

The infrared spectra of the different coatings were found to be comparable.[LX] With the exception of the larger OMe peak corresponding to a lower crosslinking density in the standard coating, slightly larger NHOH peaks in isosorbide containing coatings and a larger CH peak in a coating containing an increased amount of sebacic acid, no differences that could be related to the resin composition were observed.

Especially the absorption corresponding to the melamine ring, but also most other peaks were found to be very similar, validating the chosen analytical method. This also suggests that any change observed during the weathering process can be assumed to be due to degradation and not artefacts due to different situations at the start.

6.3.2.4 Weathering behaviour observed in the infrared spectra

In the following section, the development of the different peaks observable in IR upon exposure and the differences in behaviour between different coatings will be discussed. In order to evaluate whether the trends observed constitute different behaviour or are just coincidental, the uncertainty associated with the results was first examined.

6.3.2.4.1 Uncertainty of IR results

Due to limits in the availability of weathering space, it was not possible to submit replicas of the different coatings to the exposure. However, the standard coating and the coating based on the resin for interior coatings proposed by Arkema were included in both series of coatings examined. The peak areas measured were therefore examined to provide an estimate of the associated experimental error.

[LIX] See annexe for details about the agreement between ATR and PAS measurements.
[LX] The absorptions at t_0 of the different coatings are analysed in the annexe.

In the gloss retention study, a larger degree of degradation was observed in the standard coating submitted to the second series of experiments compared to that submitted to the first series. This trend was not seen in the infrared results.

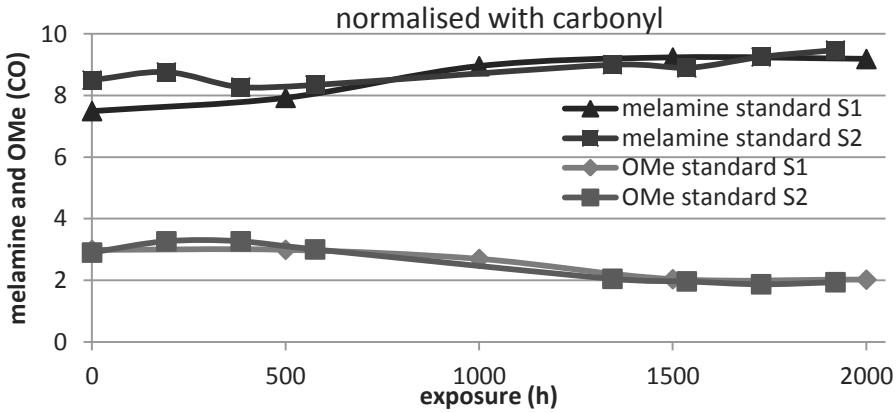

Figure 142: Reproducibility of melamine and OMe peaks in the standard coating

The end results as well as the development of the peaks in both series were very similar, as shown on the example of the respective melamine and methoxy group peaks in figure 142 above. This suggests that the impact the more frequent analysis had on the degradation merely concerned the surface but not the bulk, thus affecting the gloss retention without being visible in the sum of the functional groups.

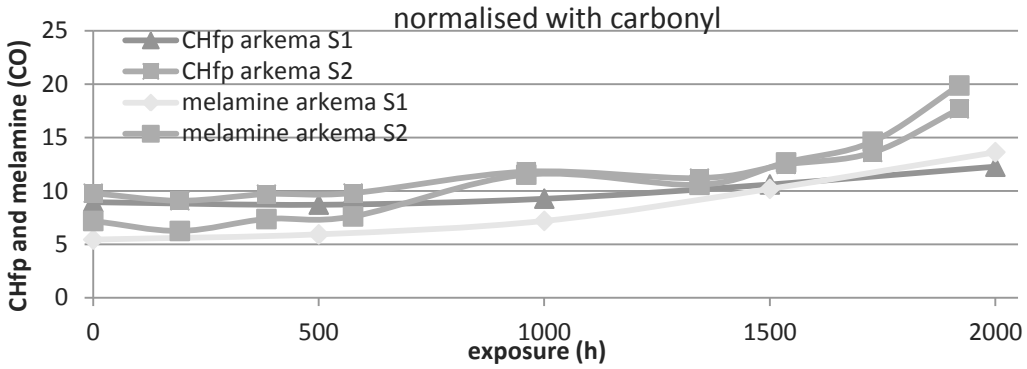

Figure 143: Reproducibility of CHfp and melamine peaks in the Arkema coating

The effect was however observed in some of the spectra of the Arkema coatings. Both the area of the CH fingerprint and of the melamine peak experienced a larger increase in the second than in the first series of tests, as shown in figure 143.

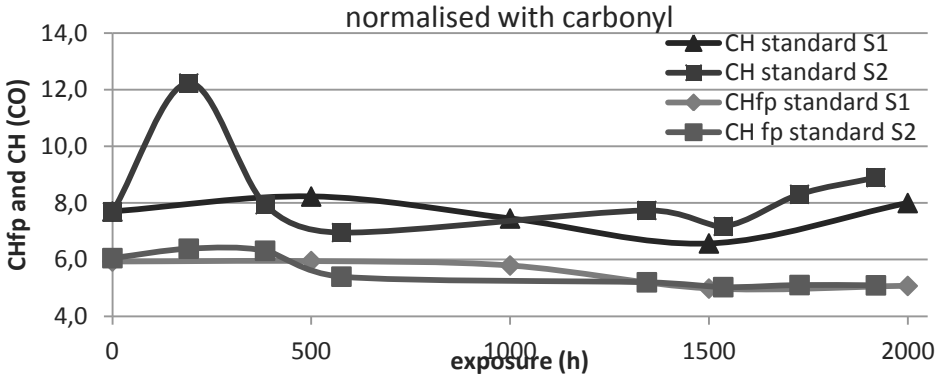

Figure 144: Reproducibility of the CH fingerprint and the CH peak in the standard coating

Some outliers were also observed, presumably due to experimental error. These can be seen as unproblematic if they are obvious outliers such as shown above in the case of the CH and CH fingerprint curves of the standard in figure 144, and don't influence the final result. If they occur however on the last measurement, they are difficult to distinguish from real developments. Two examples are shown in figure 145 in the NHOH curves of the standard and the Arkema coatings.

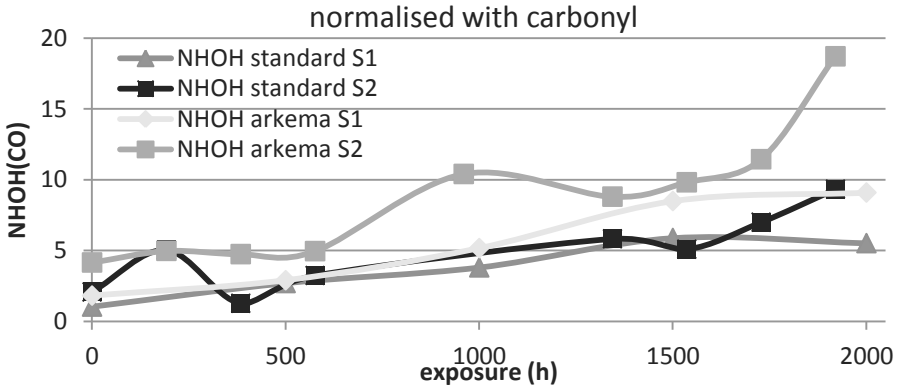

Figure 145: Reproducibility of NHOH peaks in standard and Arkema coatings

In both cases, the last measurement taken in the second series is significantly above that of the first series, despite the fact that the other measurements taken in both series were quite close to each other.

In conclusion, a relatively good agreement between the peak changes observed in two separate weathering series for the same coating was obtained. However, fairly large outliers were also observed in some cases. The evaluation of the entire series is therefore necessary to confirm any differences observed between coatings.

6.3.2.4.2 Development of the NHOH peak

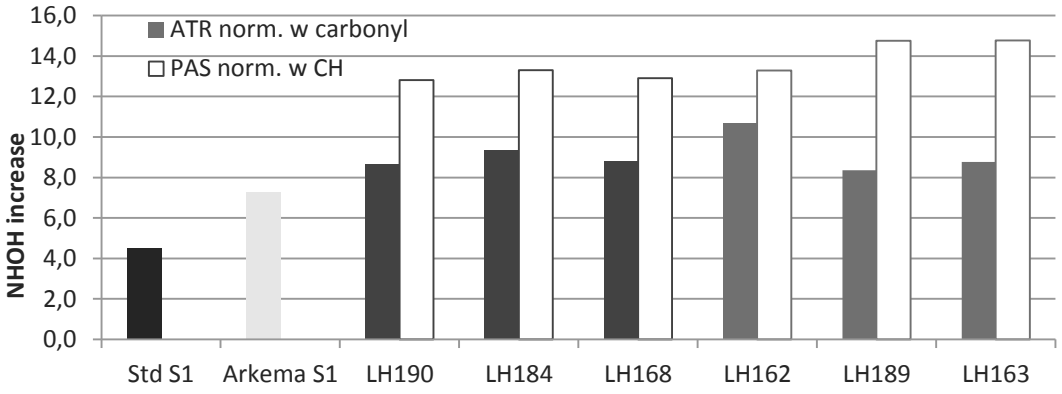

Figure 146: NHOH Δt_{2000}-t_0 peak increase series 1

The NHOH peak is taken to be the most important indicator for degradation, as it increases with the breaking of ester bonds, but also with the formation of peroxides and the breaking of melamine crosslinks.

In the first series, the NHOH peak of the biobased coatings was observed to increase by almost twice the amount observed in the standard coating, as shown in figure 146. The Arkema resin based coating performed slightly better than the new prototypes. The end result of the different biobased coatings was however very similar, which was confirmed both by the photoacoustic measurements and by the overall development of the absorption over time, as shown in figure 147.

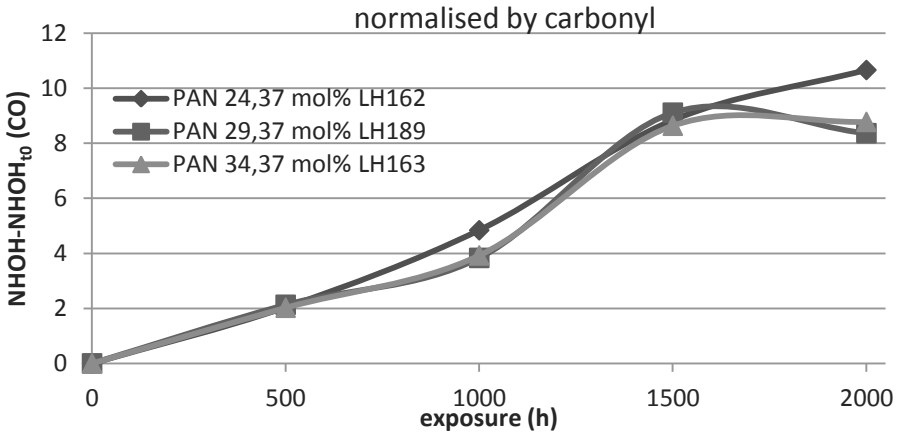

Figure 147: NHOH - $NHOH_{t0}$ peak increase over time series 1 phthalic anhydride coatings

The corresponding curves for the isosorbide coatings can be found above (*6.3.2.1, figure 139*). Both the much larger degradation compared to the standard and the similarity of the results obtained for all biobased coatings confirm the results of the gloss retention study.

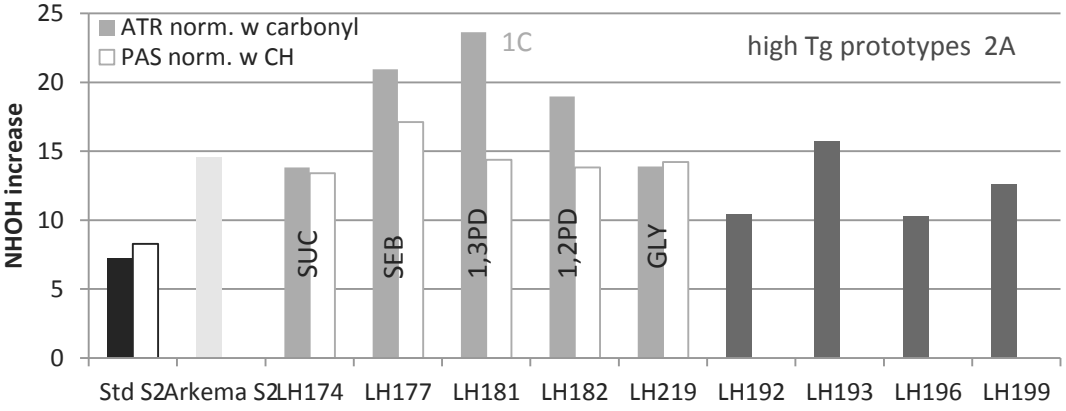

Figure 148: NHOH Δt_{1920}-t_0 peak increase series 2

Larger differences were observed in the ATR measurements of the second series of coatings, as shown in figure 148. With the exception of the coating containing the resin LH181 with an increased amount of 1,3-propanediol, which showed the best performance in the gloss retention measurements but the largest increase in NHOH peak, the ranking of the coatings corresponds to that obtained in the gloss retention evaluation.

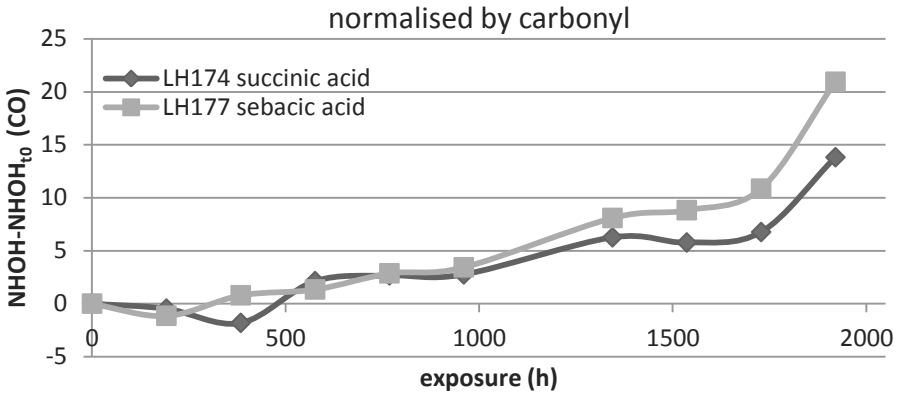

Figure 149: NHOH – $NHOH_{t0}$ peak increase over time series 2 coatings containing different diacids

The large differences are however not confirmed in the photoacoustic measurements. This suggests that they may be due to the deterioration of the surface rather than overall degradation, which would affect both gloss retention and ATR measurements, but not show as clearly in the PAS.

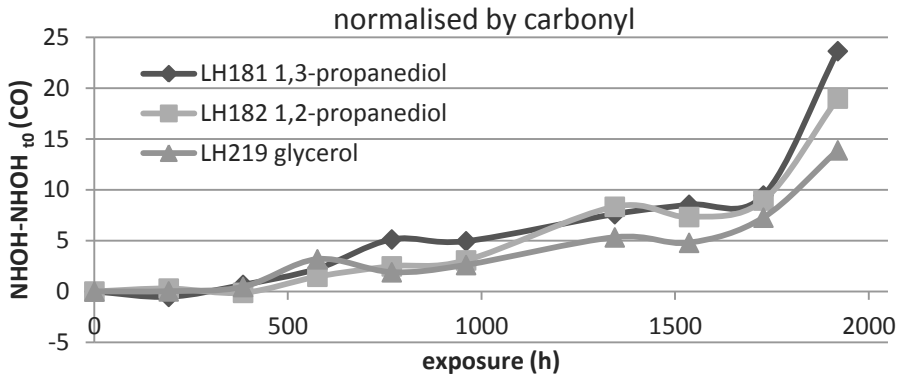

Figure 150: NHOH-NHOH$_{t0}$ increase over time for coatings containing different alcohols (series 2)

The better performance of succinic acid compared to sebacic acid, and the ranking of the coatings containing different alcohols in the order 1,3-propanediol<1,2-propanediol<glycerol is consistent over the weathering process, but more obvious after 1000 – 1500 h of exposure, as shown in figure 149 and 150.

Similarly, the development of the NHOH peak of the high T_g prototypes as shown in figure 151 is exactly the same until 1536 h of exposure, only differentiating them in the last two measurements.

Overall, it can be concluded that the degradation observed in the gloss retention measurements is at least in part due to mechanisms involving the formation of new N-H and O-H bonds. This mechanism is significantly more prominent in the biobased coatings than in the standard coatings, but not affected by different quantities of isosorbide and phthalic anhydride present.

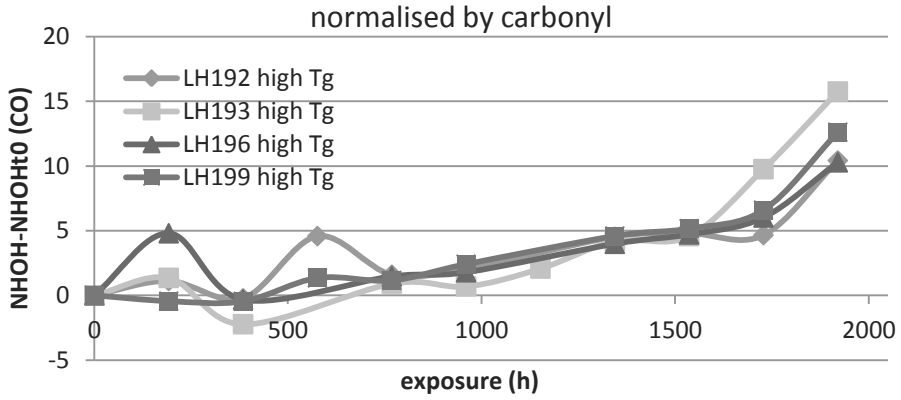

Figure 151: NHOH – NHOH$_{t0}$ peak increase over time for high T_g prototypes (2A)

While it proceeded relatively linearly over the course of the first series, an acceleration was observed in the last measurements of the second series, which caused a differentiation between the coatings examined. The result was not reflected in the PAS measurements, which could mean that it was either due to a measurement error or to a surface effect.

6.3.2.4.3 The development of CH-peaks

An increase of the peaks corresponding to the vibration of C-H bonds was observed upon exposure, leading to the choice of the carbonyl for normalisation. The CH fingerprint peak of the standard coating, which decreased after ageing, constituted the only exception to this, as shown in figure 152.

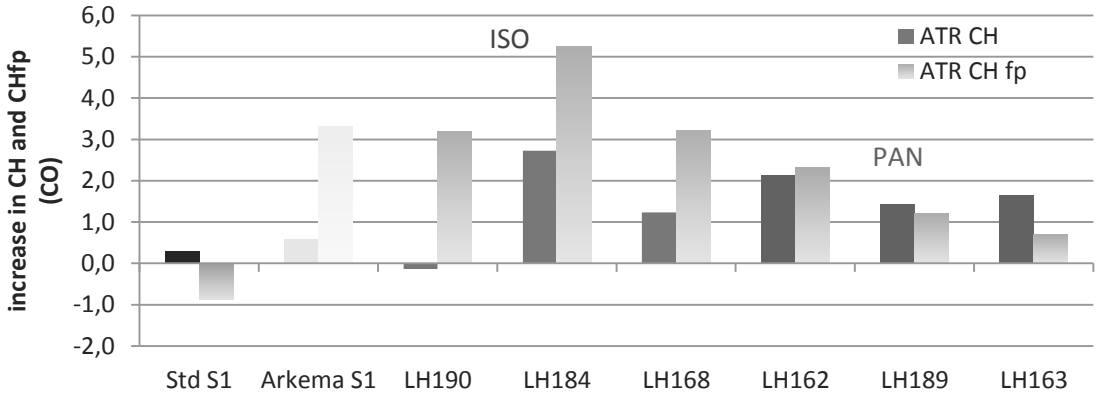

Figure 152: Increase in CH and CHfp Δt_{2000}-t_0 peaks series 1

In the first series, the largest increases in CH fingerprint peak were observed for the coatings containing isosorbide. Both CH fingerprint and CH peak increases varied a lot between the different isosorbide coatings, but no correlation with their isosorbide content could be detected.

The increase of both peaks was more constant for the phthalic anhydride coatings. Furthermore, a smaller increase in CH fingerprint was observed for the coatings containing more phthalic anhydride, as shown in figure 153. This trend was reflected in the majority of the measurements analysed, even though the progression of the corresponding curves was not linear, which could induce some doubt with respect to their accuracy.

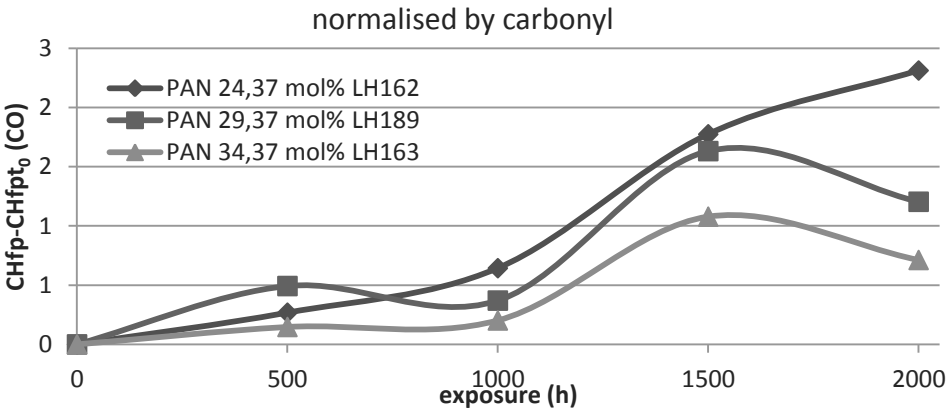

Figure 153: Increase in CHfp peaks over time CHfp-$CHfp_{t0}$ series 1 phthalic anhydride resins

As for the first series, a large increase in both CH and CH fingerprint absorption was observed for all biobased coatings in the second series. The largest increase corresponded to the coating containing

the resin LH177, as shown in figure 154. This coating also displayed the largest CH absorptions before weathering, which was attributed to the sebacic acid used in the resin.

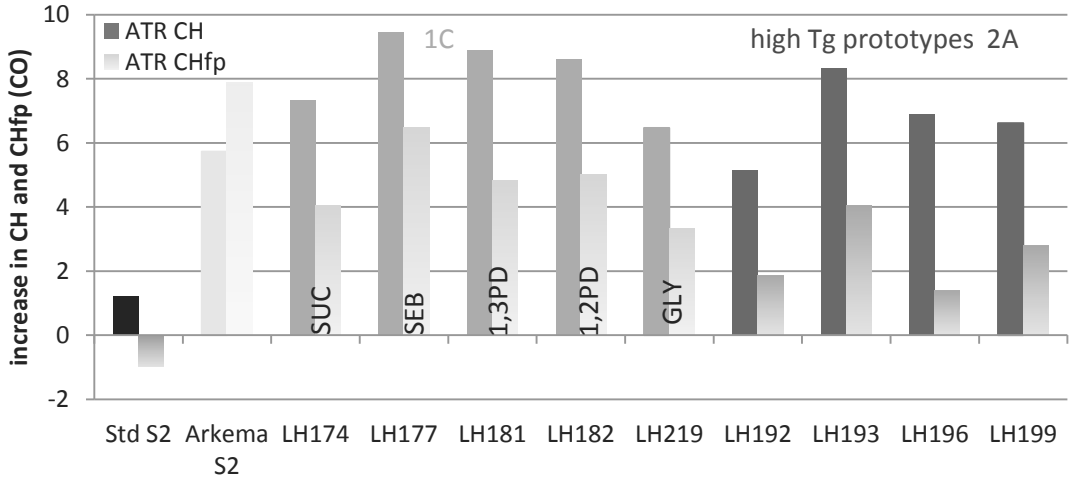

Figure 154: Increase in CH and CHfp peaks ATR Δt_{1920}-t_0 series 2

There are no degradation mechanisms which inherently cause an increase in C-H bonds. Two explanations for the observation are possible. The first possibility is that due to degradation induced polarity changes, such as the formation of denser crosslinking networks caused by the recombination of carbon based radicals, the C-H bonds have migrated closer to the surface while the C=O bonds used for normalisation have migrated away from it. The higher presence of C-H bonds in the area analysed by IR is therefore reflected as an increase in absorption.

The second possibility is that the concentration of carbonyls used for normalisation has decreased not only in the analysed area but in absolute terms. The breaking of chains near the chain end can cause the formation of short, hydrophilic fragments that can be eroded in the hydrolysis process. The occurrence of such erosion is confirmed by the overall film thickness loss discussed above.

Through the water originated erosion primarily of hydrophilic, and therefore carbonyl rich fragments, the overall quantity of carbonyls with respect to C-H bonds could be decreased. The normalisation using the carbonyl peak, which assumes that the quantity of carbonyls is constant, is therefore reflected as an increase in C-H bonds.

The accuracy of either hypothesis is difficult to prove. As discussed above (*6.3.2.2.1*), a change in C-H peak shape was observed in several spectra, making it a non-reliable option for normalisation of other peaks. Therefore, a way to normalise the carbonyl peaks and therefore to prove whether they decrease during the exposure remains to be found.

Nevertheless, it seems probable that C-H bond neutral degradation mechanisms, such as the homolytic cleavage of C-C bonds, and those potentially leading to the formation of small, erodible

fragments, such as hydrolytic degradation and decarboxylation, dominate over mechanisms such as peroxide formation and other processes which lead to the transfer of hydrogen atoms from C-H to O-H bonds and the associated intrinsic decrease in C-H bonds.

6.3.2.4.4 The development of the melamine peak

As detailed above, the melamine peak was measured between 1510 cm^{-1} and 1625 cm^{-1}. According to studies of the melamine IR absorptions published for example by Wang *et al.* and by Merline *et al.*, this area could contain two different absorptions.[270, 271] The main absorption, centred around 1525 - 1530 cm^{-1}, corresponds to the C=N stretching vibration and the NCN bending vibration.

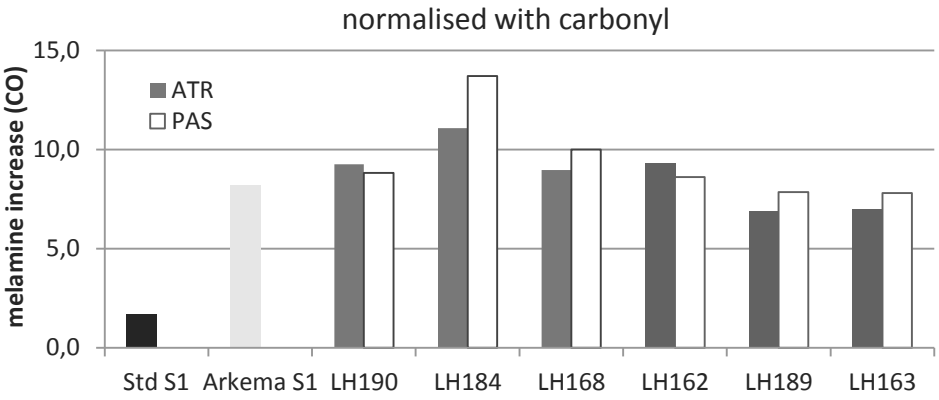

Figure 155: Melamine increase ATR and PAS series 1 Δt_{2000}-t_0

The second contribution, centred around 1625 cm^{-1}, is attributed to the N-H bond which can be formed once the link between the polyester and the melamine is broken, or if free methylol groups are removed. It could explain the increase in the melamine peak observed upon exposure in all coatings, shown in figure 155.

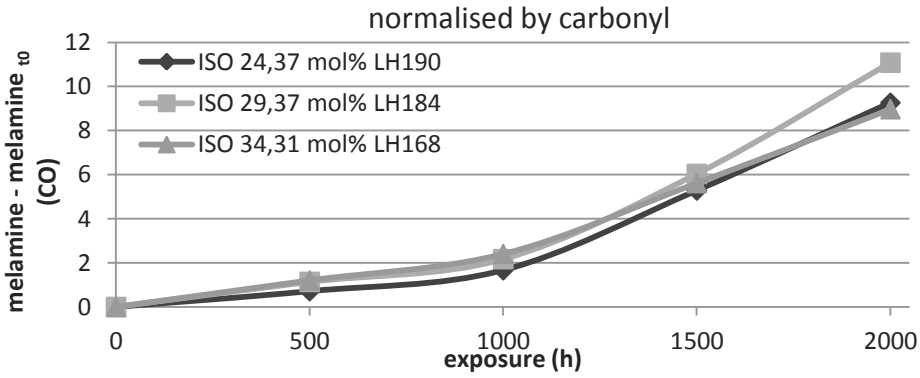

Figure 156: Melamine- melamine t_0 increase over time series 1 isosorbide resins

While the increase in melamine peak was significantly larger for the biobased coatings than for the standard coating, the behaviour amongst the biobased coatings was again very similar. While the increase was slightly larger overall for isosorbide based resins, barely any difference was observed

for different quantities of isosorbide, as shown in figure 156, or for different quantities of phthalic anhydride, as shown in figure 157.

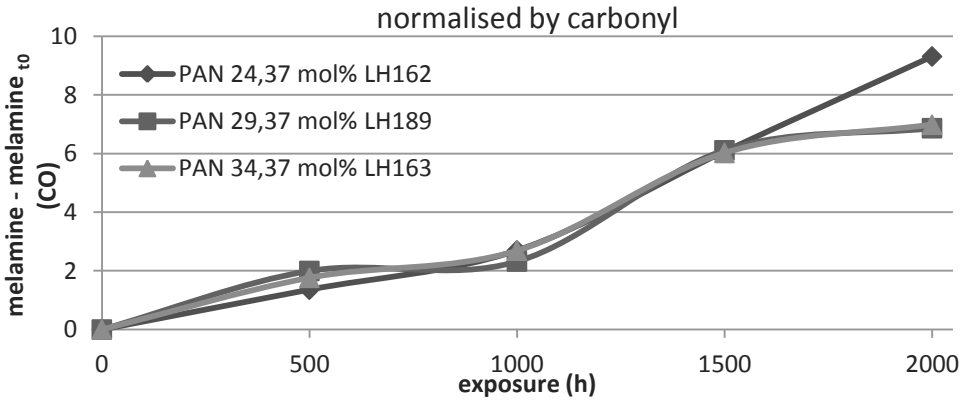

Figure 157: Melamine- melamine t_0 increase over time series 1 phthalic anhydride resins

For both series, the trends examined were confirmed by the photoacoustic measurements. One exception was the coating containing the resin LH219 with an increased amount of glycerol, which displayed the lowest increase of melamine in ATR but the highest in PAS, as shown in figure 158.

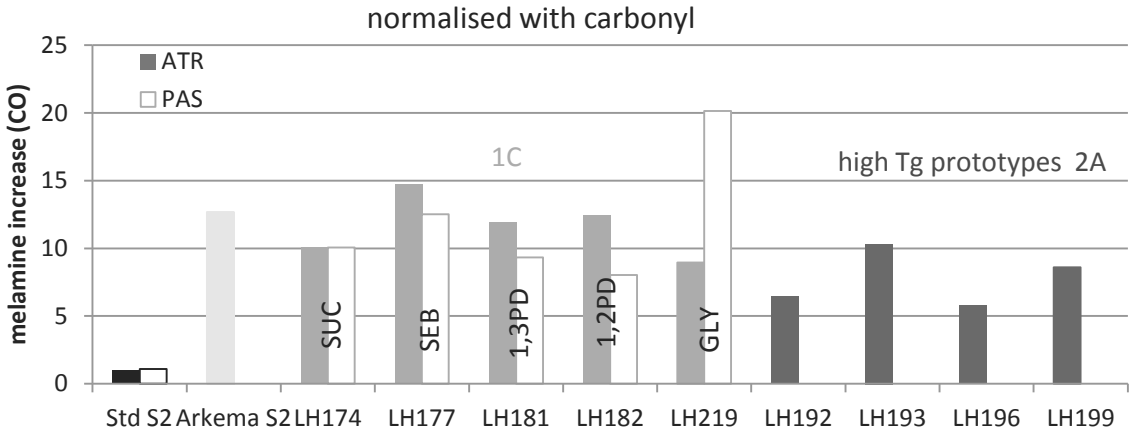

Figure 158: Melamine ATR and PAS series 2 Δt_{1920}-t_0 increase (1C, 2A)

Overall, the trends observed were confirmed by the curves showing the development of the melamine peak in each coating over different exposure lengths, shown in figure 159 – 161.

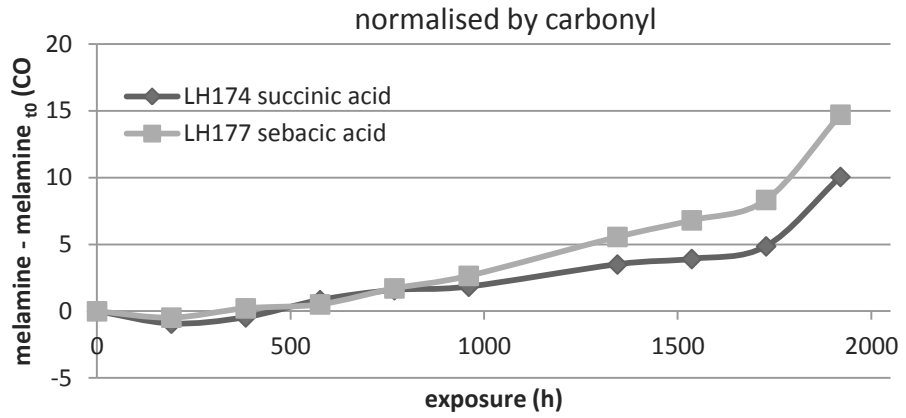

Figure 159: Melamine-melamine t_0 increase over time series 2 coatings containing different diacids

In general, the same resins which showed a large increase in NHOH absorption in the ATR measurement also showed a large increase in melamine absorption. This could be in part due to the fact that the N-H bond contributes to both peaks in bending and stretching vibrations respectively.

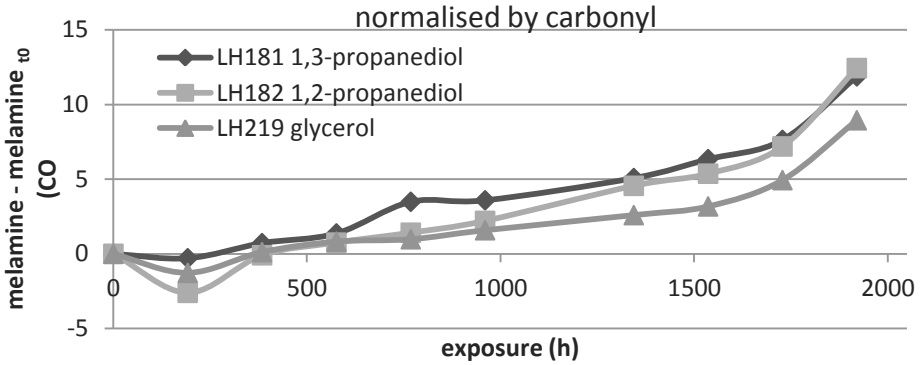

Figure 160: Melamine-melamine t_0 increase over time series 2 coatings containing different alcohols

Another possible explanation is the contribution of the carbonyl peak. As both peaks were normalised with the carbonyl peak, its decrease would cause an increase in the relative area of both other peaks. The fact that the curves of the melamine peak show an acceleration in their increase in the last three measurements, exactly as those of the NHOH peak, suggests that the carbonyl peak may be at least partially responsible for the observed trend.

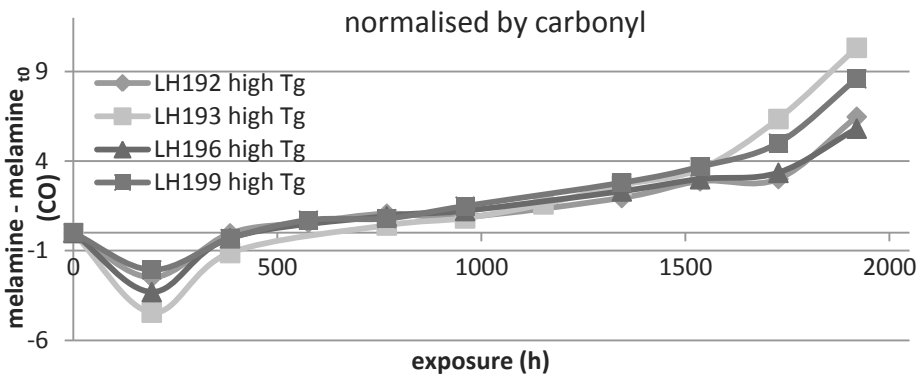

Figure 161: Melamine - melamine t_0 increase over time high T_g prototypes (2A)

However, a similar increase in melamine peak was also observed when the spectra were normalised using the CH fingerprint peak, as shown in figure 162. Interestingly, the increase observed relative to the CH fingerprint peak was very similar for biobased and standard coatings.

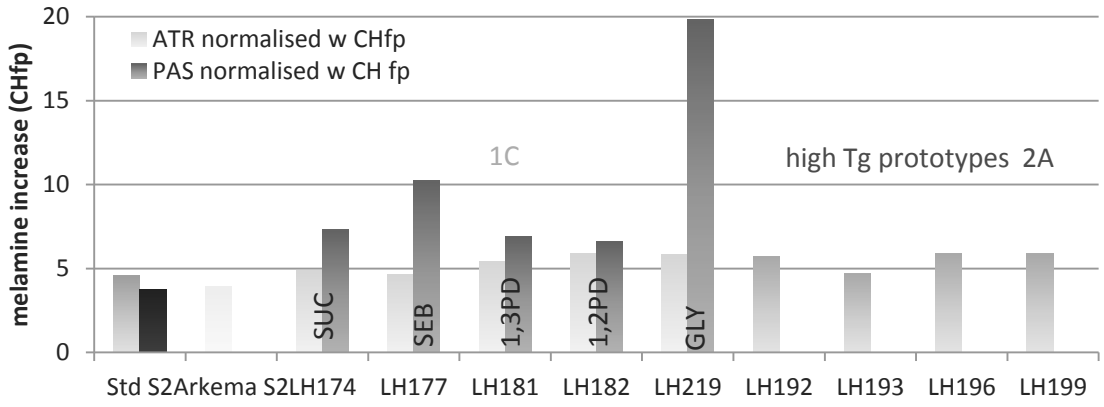

Figure 162: Melamine ATR and PAS series 2 Δt_{1920}-t_0 increase normalised with CHfp peak series 2

As with the C-H related peaks, an increase of melamine content in absolute terms is not likely. Instead, the increase in peak area can be attributed to the scission of melamine – resins bonds and the associated increase in N-H bending vibrations, the decrease of the carbonyl peak, the migration of melamine molecules closer to the surface or a combination of these phenomena.

6.3.2.4.5 The development of the methoxy group peak

A decrease in methoxy group absorption upon exposure was observed in all coatings examined, as shown in figure 163. In the first series of coatings examined, no difference between the development of the biobased and the standard coatings was found.

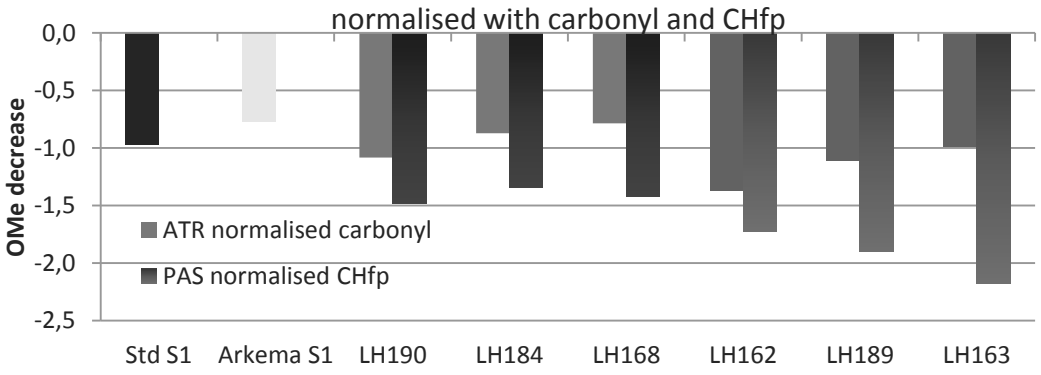

Figure 163: Methoxy group decrease ATR and PAS Δt_{2000}-t_0 series 1

While the ATR end measurements suggest that a larger decrease of methoxy groups correlates with a smaller amount of both isosorbide and phthalic anhydride present in the coatings, these observations were not confirmed by the development of the curves over the course of the exposure.

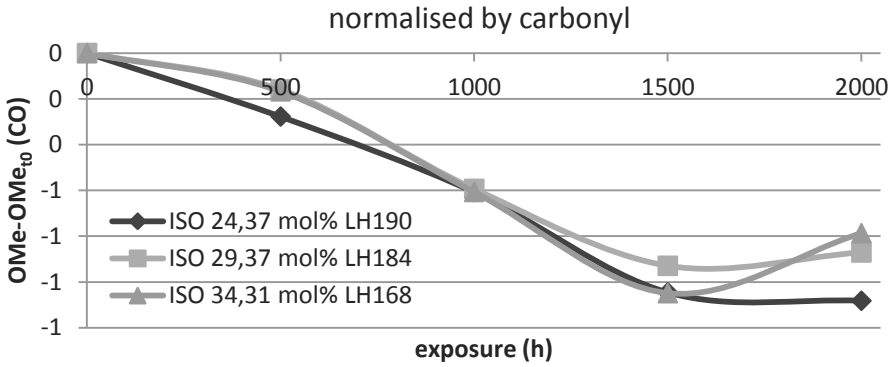

Figure 164: OMe decrease OMe - OMe t_0 over time series 1 isosorbide coatings

The curves of both the isosorbide and the phthalic anhydride containing coatings, shown in figure 164 and 165 respectively, suggest that the composition of the resin did not influence the development of the methoxy peak.

The majority of the coatings in the second series displayed a similar behaviour to that observed in the first series, i.e. a small decrease in methoxy peak size after the exposure, and are shown in figure 166. The PAS measurements normalised with the CH fingerprint peak were however somewhat higher, especially for the standard coating.

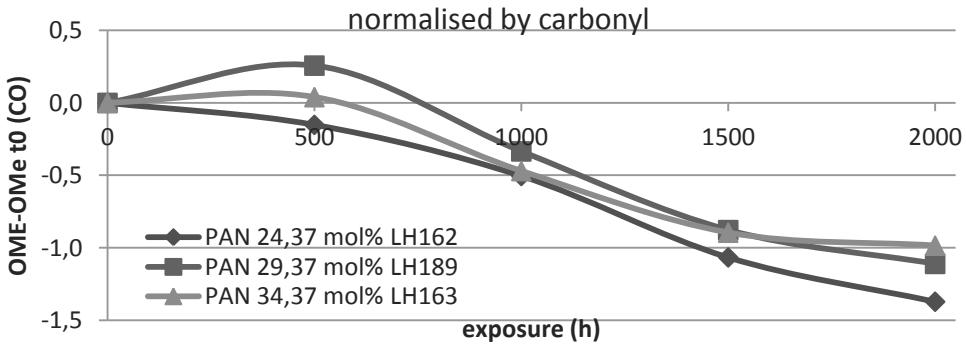

Figure 165: OMe decrease OMe-OMe t_0 over time series 1 phthalic anhydride coatings

The decrease in methoxy groups observed, which correspond to uncrosslinked melamine side chains, could indicate that late crosslinking is part of the ageing and degradation process.

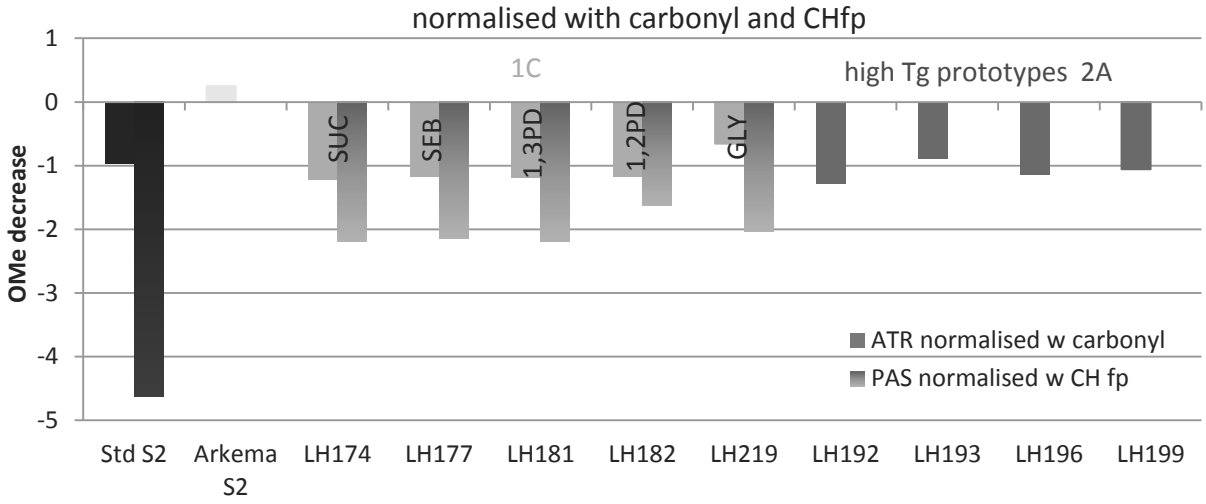

Figure 166: OMe decrease ATR and PAS Δt_{1920}-t_0 series 2

6.3.2.5 General insights about the use of IR analysis for the evaluation of weathering processes

The unambiguous interpretation of infrared spectra obtained of the weathered coatings is difficult for several reasons. The most important one which was observed in this study is that the chosen conditions largely determine the outcome.

One important factor, for example, is the normalisation method chosen to compare the spectra of different coatings with each other. It was found that the poor quality of the IR spectra and the change in their shape made the CH peaks unsuitable to be used as a reference in ATR. Unfortunately, the carbonyl peak is very far away from the other peak, and was therefore unsuitable as a reference in the PAS method, which can span almost the entire depth of the coating depending on the wavelength.

However, the choice of one or the other can largely change not only the degree of change in peaks observed but also their relative ranking in terms of degradation. Furthermore, an increase in C-H

groups relative to the carbonyl peak suggests that it probably decreases as well during the degradation.

Another important factor is the setting of the baseline. In this work, it was decided to keep the baseline relatively constant, ranging either from 2400 cm^{-1} to 3950 cm^{-1} for the interpretation of the CH peaks or from 825 cm^{-1} to 1800 cm^{-1} for the interpretation of the peaks in the fingerprint region. Another option, which was chosen for example by Zhang *et al.*, is to set the limits of the baseline directly adjacent to the peak.[216] As shown in figure 167 for the example of the NHOH peak and the CH peak, this leads to an integration solely of the area of the CH peak that is above the NHOH peak.

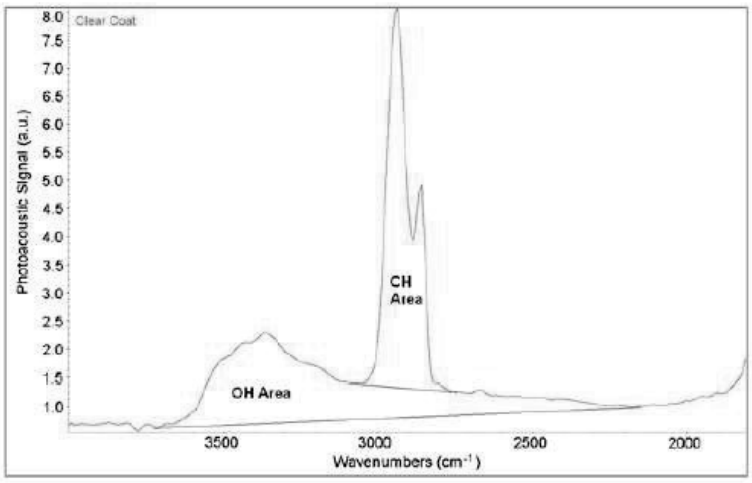

Fig. 3. Hydroxyl and hydrocarbon band area measurement in SSPA-FTIR spectra.

Figure 167: Baseline chosen by Zhang *et al.* (2012)

This decision can significantly change the result as demonstrated by the fact that Zhang *et al.* observed a loss of melamine of up to 20% while in this study, all coatings showed an increase of the same peak.

A second problem with the interpretation of IR data that was observed in this study is that the behaviour of the different coatings was largely identical in nature. All coatings showed an increase in NHOH absorption, C-H absorption and melamine peak as well as a decrease in terms of the methoxy peak.

As both absolute and relative quantities observed depend largely on the normalisation method and choice of baseline position, this makes differentiating qualitative observations difficult and any quantitative evaluation ambiguous.

Despite these uncertainties, the IR investigation and the methods chosen here were validated to a degree because both the ranking of the NHOH peaks and that of the melamine peaks agreed with the findings of the gloss retention study. The lack of differentiation of the biobased coatings in the first series could also be seen as a kind of validation. If it is assumed that the small differences made to the resin structure are not having an impact on the overall weatherability of the coating, the closeness of the results could be interpreted as great reproducibility.

6.4 Insights into the degradation mechanism

During the weathering tests, the coatings were exposed to cycles of UV light exposure, high humidity and high temperatures. Therefore, the amount of degradation cannot be directly attributed to photolytic, hydrolytic or thermal degradation. Nevertheless, the different performances in connection with the nature of the resin formulation as well as the differences between tests permit to draw conclusions about which degradation mechanisms are most prominent, and will be discussed in this section.

6.4.1 Bulk structural changes caused by exposure observed in the µ-hardness test

The µ-hardness test reflects the response of the polymer network to strain, and the results can be extrapolated to give information about the stiffness of the network and its capability to rearrange in response to stress, which is linked to the crosslinking density.

Table 109: µ-hardness results after weathering – isosorbide and phthalic anhydride coatings

1A	H_{uk}	W_e/W_{total}	Young's m.	1B	H_{uk}	W_e/W_{total}	Young's m.
resin	N/mm^2	%	GPa	resin	N/mm^2	%	GPa
LH190	168	26	5,9	LH162	101	33	2,3
LH184	250	30	7,5	LH189	106	27	3,0
LH168	262	32	8,0	LH163	227	31	6,2

6.4.1.1 Change in universal hardness, elastic energy component and Young's modulus

In comparing the results of the µ-hardness test that was performed on the unexposed coatings with those performed after the coatings were subjected to Hot QUVa weathering for 2000 h, we can draw conclusions about the effect that the weathering had on the structure. In table 109 above, the universal hardness, elastic energy component and Young's modulus measured for coatings based on resins containing different amounts of isosorbide and phthalic anhydride are shown.

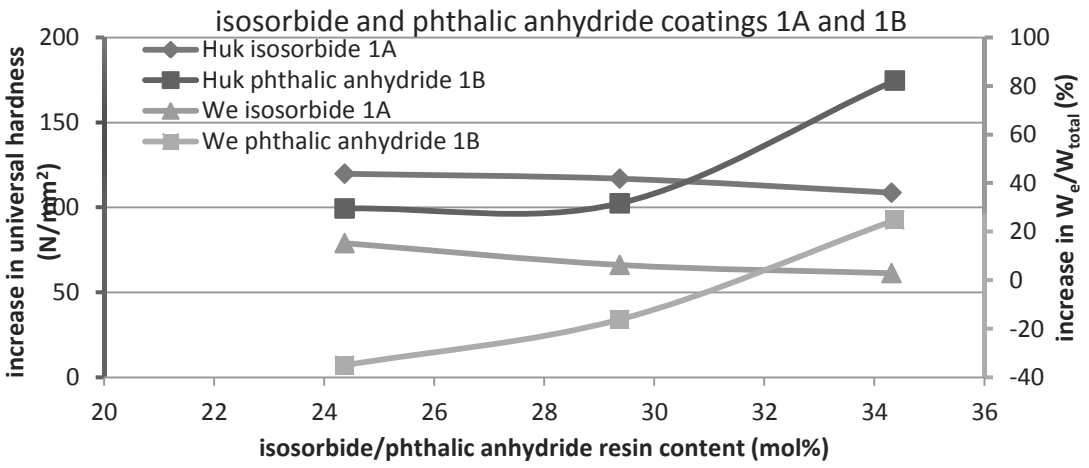

Figure 168: Difference in µ-hardness behaviour before and after weathering

In figure 168, the increase in the universal hardness compared to the measurements made before weathering are plotted against the quantity of isosorbide and phthalic anhydride present in the corresponding resins.

In all resins, an increase in universal hardness as well as stiffness represented by the Young's modulus was observed after weathering. This means that the network has become less flexible, suggesting that the crosslinking of chains dominated over chain scission experienced in the course of the degradation.

This also indicates that degradation caused by high temperature and UV light, which can lead to the formation of radicals and therefore to the creation of new links between the chains, was more important than hydrolytic degradation, which leads to the breaking of ester bonds and therefore a decrease in network connections.

This hypothesis is supported by the fact that the increase in hardness was larger for higher amounts of phthalic anhydride, the UV absorption of which could catalyse photolytic degradation and therefore crosslinking, as shown in figure 168. At the same time, it was slightly decreased for larger amounts of isosorbide, whose polarity and hydrophilicity could catalyse hydrolytic chain scission.

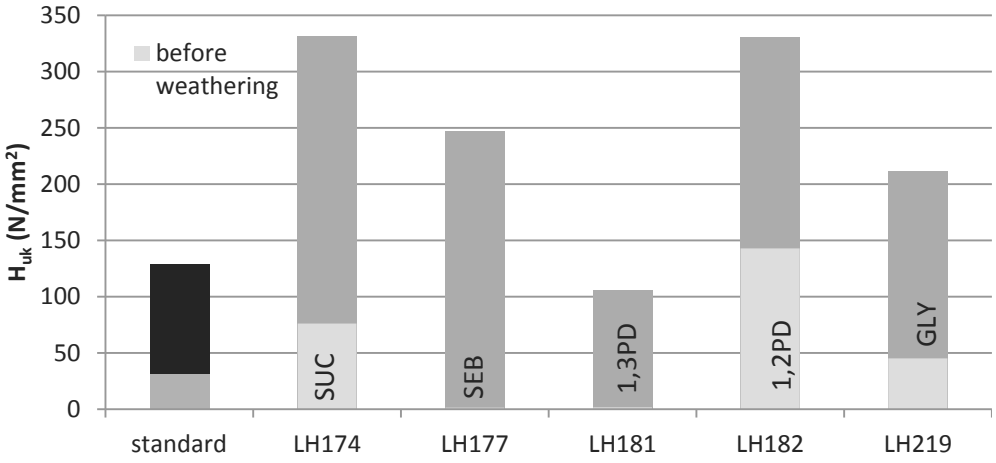

Figure 169: Universal hardness of biobased coatings before and after weathering (1C)

The increase in universal hardness was equally observed in the third group of coatings (1C) and in the standard resin, shown in figure 169 and table 110. However, the increase observed in all biobased coatings was larger than that of the standard, which was 98 N/mm^2, with the largest increase of 256 N/mm^2 measured in the coating containing the resin LH174 in which the content of succinic acid was increased.

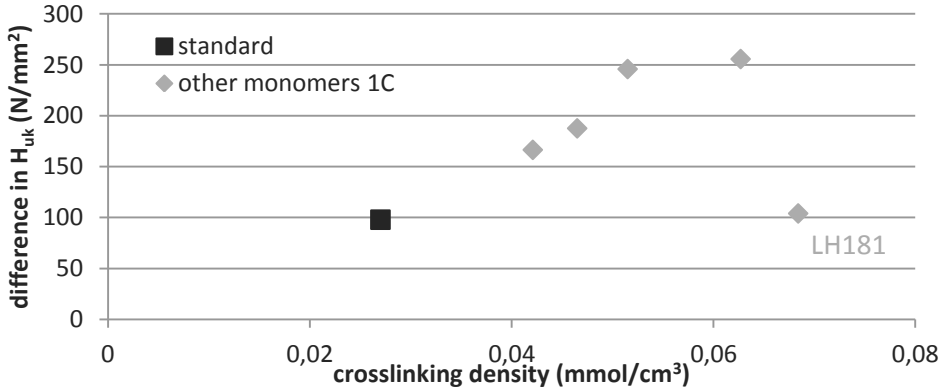

Figure 170: Difference in universal hardness *vs.* crosslinking density series 2 (standard and 1C)

With the exception of the coating containing the resin LH181, which had a high crosslinking density but a low T_g before weathering, a large increase in universal hardness also corresponded to higher crosslinking densities before exposure, as presented in figure 17. However, this relationship was only observed between the standard coating and the coatings containing resins in which non-rigid monomers were tested (1C). It did not extend to the coatings discussed above in which the quantity of phthalic anhydride or isosorbide was varied, possibly due to the different range of crosslinking densities.

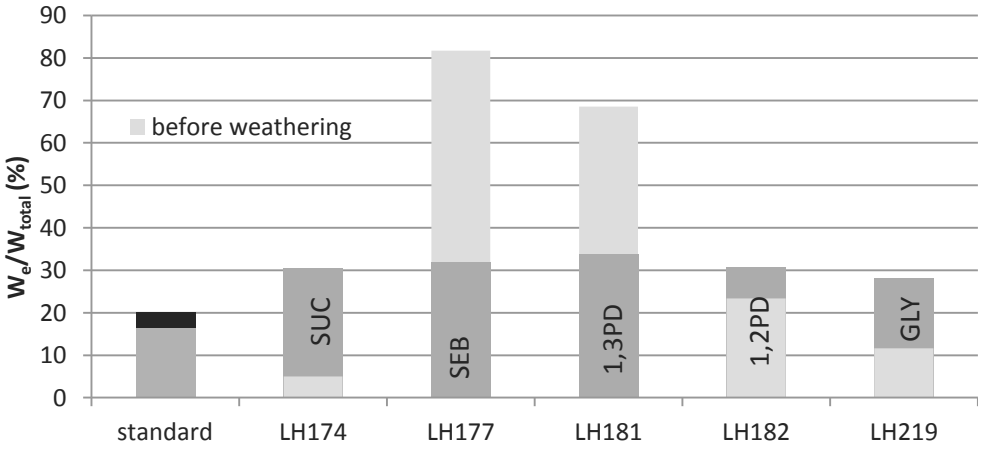

Figure 171: Elastic energy component series 2 before and after weathering (1C)

The elastic energy component of the coatings after weathering was equally found to increase, following the same trend as the universal hardness with regard to the quantity of isosorbide and phthalic anhydride in the corresponding resins, as shown in figure 171.

Exceptions to this were the coatings whose glass transition temperature was below that of the µ-hardness measurement before weathering, containing the resins LH162, LH189, LH177 and LH181. In the case of those coatings, the elastic energy component was observed to decrease considerably. It can be assumed both from the increase in universal hardness, from the increase in Young's modulus

and from the decrease in elastic energy that the glass transition temperature of those coatings was increased in the course of the exposure, and had reached a level above 20 °C after weathering.

Table 110: µ-hardness results after weathering – 1C and standard

		H_{uk}	W_e/W_{total}	creep 1	creep 2	Young's m.
resin	**monomer tested**	**N/mm²**	**%**	**%**	**%**	**GPa**
standard		129	20	27	-10,6	4,7
LH174	succinic acid	332	30	11	-14,8	10,1
LH177	sebacic acid	247	32	15	-18,7	6,5
LH181	1,3-propanediol	106	34	23	-20,8	3,0
LH182	1,2-propanediol	331	31	10	-14,7	10,1
LH219	glycerol 9,27 mol%	212	28	16	-14,7	6,7

No correlation between the µ-hardness results after weathering and the change in methoxy groups observed in IR could be found.

6.4.1.2 Change in creep behaviour

The creep 1 measurement, representing time delayed relaxation in response to the stress applied after it is no longer increased, and thus the slow rearrangement of chains, was decreased after weathering. Exceptions are again the coatings whose creep 1 response before weathering was skewed by the fact that the measurement was performed above their glass transition temperature, namely the coatings containing the resins LH162, LH177 and LH181.

The largest decrease in creep 1 was observed for the standard resin, which showed 121% before and only 27% after exposure. On the other hand, the creep 2, i.e. the slow recovery of the original shape of the coating time delayed after the stress is released, increased after the weathering for all coatings. Contrary to the observation made for the creep 1 value, the increase was smallest for the standard coating.

Its creep was increased by only -3,9% from -6,7% before weathering to -10,6% after weathering, while the increase observed by the other coatings ranged from -4,0% for the coating containing the resin LH190 to -22,0% for the coating containing the resin LH162. As with the elastic energy component, however, the disproportionately large increases in creep 2 can be explained by the fact that the measurement before exposure was performed at temperatures too high for the coatings.

In figure 172 – 174 below, the creep 1 development of isosorbide and phthalic anhydride containing coatings is plotted against time. One representative curve was selected out of the nine measurements obtained as described in the previous chapter to exemplify the nature of the values.

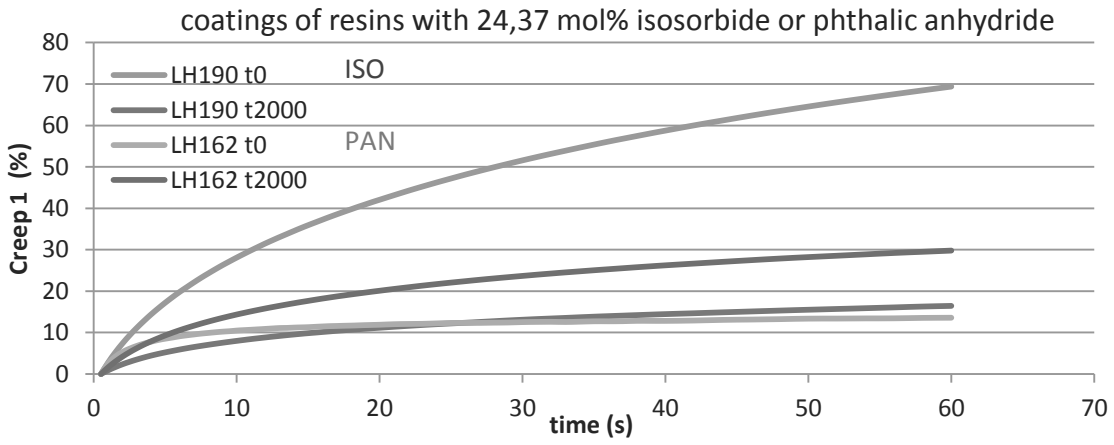

Figure 172: Creep 1 behaviour over time for LH190 and LH162 containing coatings before and after weathering

Several different phenomena can be observed. Firstly, some curves, such as that of the coatings containing the resins LH190 and LH163 before weathering, have clearly not reached the full extent of the creep, which would result in a flattening of the curve. We can therefore assume that the creep 1 values reported in some cases represent an underestimation of the creep possible. Unfortunately, the nature of the software made it impossible to continue the creep measurement for longer than 60 seconds.

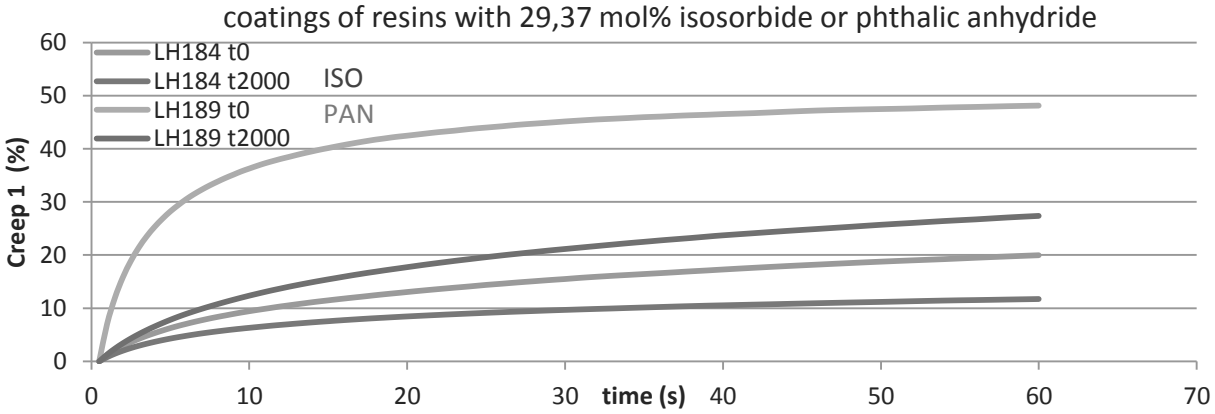

Figure 173: Creep 1 behaviour before and after weathering of LH184 and LH189 coatings

The exceptional behaviour of the coatings which were tested above their glass transition temperature is also reflected in the creep curves, for example in the coating containing the resin LH162. While all other coatings experience a decrease in creep after weathering, the t0 curve of this particular coating is actually below that recorded after weathering at t2000.

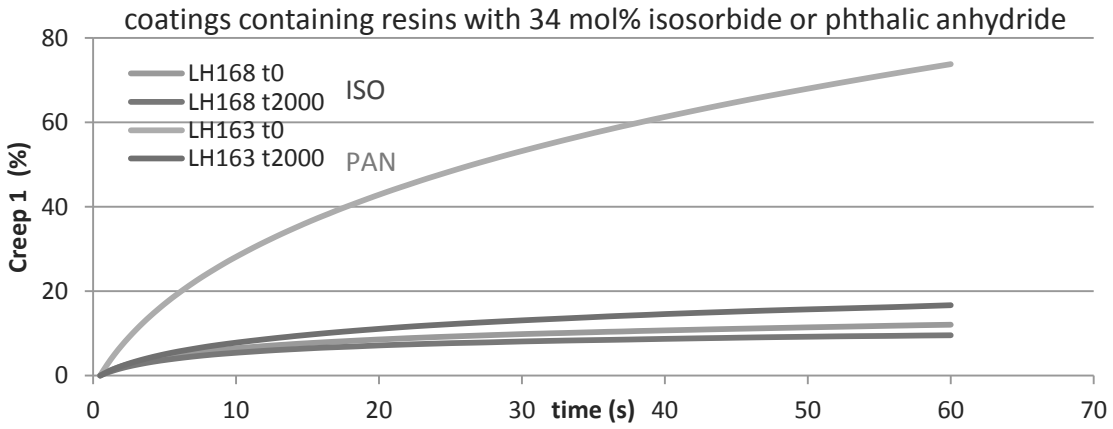

Figure 174: Creep 1 behaviour before and after weathering of LH168 and LH163 curves

In all cases except that of the coating containing the resin LH162 before weathering, the isosorbide containing coatings display lower creep than their phthalic anhydride containing equivalents. Furthermore, while the difference between the creep before and after weathering increases with increasing phthalic anhydride content, it markedly decreases with increasing isosorbide content. In the coating of the resin LH168, containing 34,31 mol% isosorbide, the difference in creep 1 behaviour is only barely visible.

Table 111: Creep measurements series 1

1A	creep 1	creep 2	creep 1: Δt2000-t0	1B	creep 1	creep 2	creep 1: Δt2000-t0
resin	%	%	%	resin	%	%	%
LH190	18	-15	-49	LH162	27	-22	12
LH184	13	-15	-7	LH189	29	-18	-18
LH168	9	-13	-3	LH163	16	-15	-60

This is also reflected in the average creep 1 and 2 values, shown in table 111. Overall, the development of the isosorbide and phthalic anhydride creeps upon exposure fits with the hypothesis that the presence of phthalic anhydride catalyses additional crosslinking, while the presence of isosorbide increases hydrolytic chain scission, thus reversing the overall effect of photolytic crosslinking.

In general, this, as well as the decrease in creep 1 and increase in creep 2 observed in almost all coatings, confirm the formation of additional crosslinks, which was indicated by the increase in the universal hardness and elastic energy component. The behaviour of the isosorbide resins furthermore reinforces the theory that both photolytic and hydrolytic degradation mechanisms are occuring.

6.4.2 Impact of photolytic degradation through the change caused by HALS

In order to increase the durability of polyester melamine coatings, hindered amine light stabilisers (HALS), which can trap radicals and therefore slow down the effect of photolytic degradations, are often added to the paint formula. Equivalent coatings to those tested in this work were created with HALS and subjected to identical conditions. The motivation was on the one hand to evaluate the potential improvements to their weatherability that can be achieved through formulation changes and on the other hand to quantify the degree of photolysis contributing to the overall degradation. Their performances were examined through their gloss retention and their IR spectra.

6.4.2.1 Gloss retention after the addition of HALS

The gloss retention after weathering could be significantly improved through the addition of HALS, as shown in figure 175, indicating that photolytic degradation plays an important role in the decrease of gloss retention. The final value was on average 47% above that measured for the coatings not containing HALS after Hot QUVa exposure.

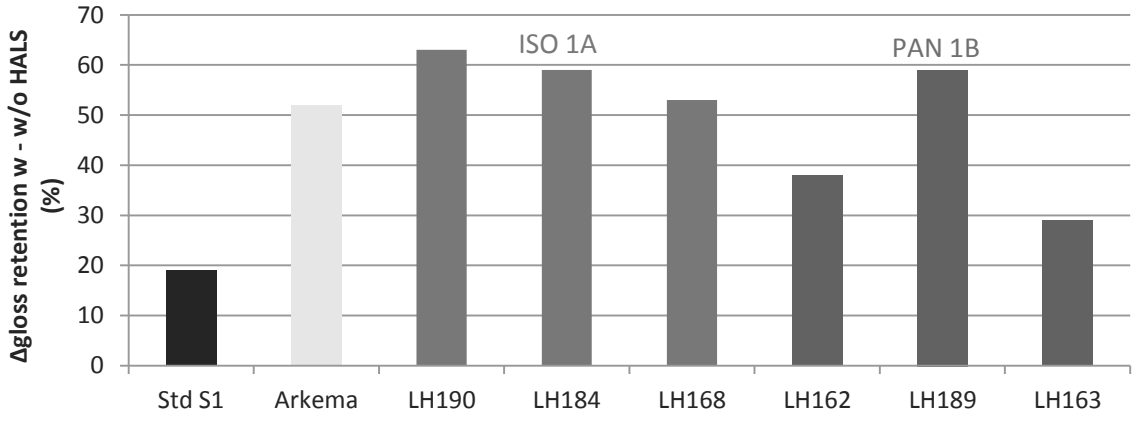

Figure 175: Increase in gloss retention after 2000 h by HALS series 1

The small increase observed for the standard coating is due to the fact that it already performed very well without HALS, and that an improvement above 100% is not possible. The measurement performed on the second series, shown in figure 180, in which the gloss retention of the standard was significantly lower than in the first series, improved by 35% after the addition of HALS and showed no loss of gloss retention even after 1920 h of exposure. This proves that compatibility between the standard coating and the HALS is not an issue.

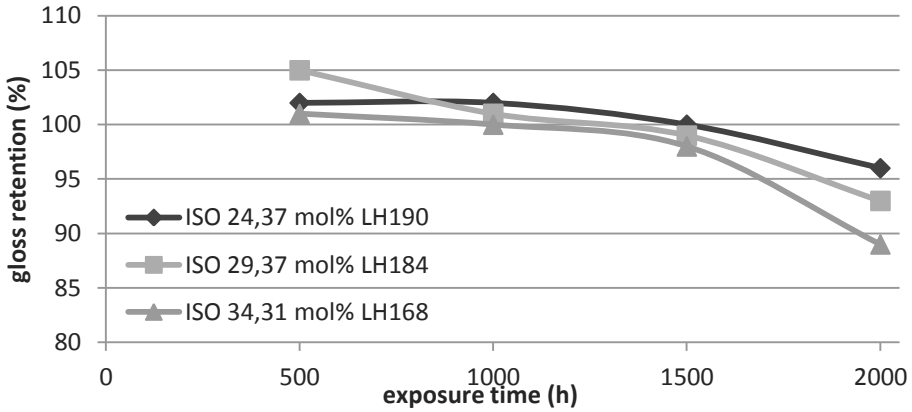

Figure 176: Gloss retention with HALS over time series 1 isosorbide coatings (1A)

In general, the isosorbide containing coatings profited more from the addition of HALS than the phthalic anhydride containing coating with an average improvement of 57% *vs.* 47%. The explanation can be found in the development of gloss retention over exposure time of each type of coating. Overall, the gloss retention changes very little in the first 1000 h of exposure, and then starts to decrease more rapidly, as shown in figure 176 - 179.

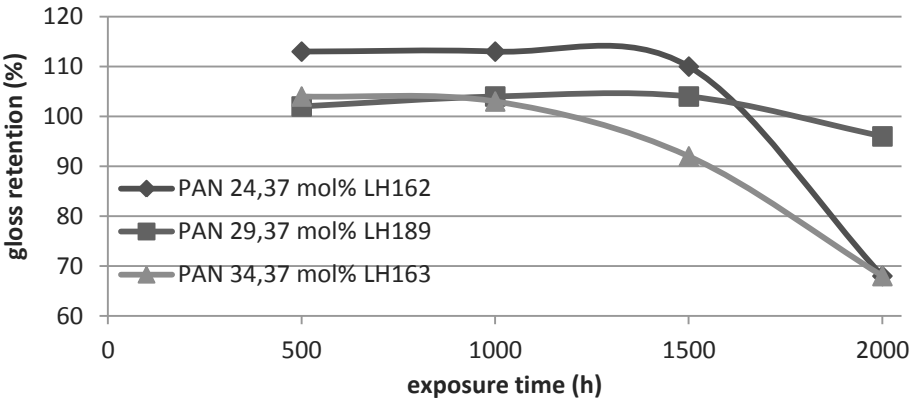

Figure 177: Gloss retention with HALS over time series 1 phthalic anhydride coatings (1B)

This behaviour is in line with observations made in the Beckers laboratory on previous studies, and is generally attributed to the loss of HALS activity. Hindered amine light stabilisers can regenerate after trapping a radical through the Denisov cycle and therefore deactivate photolytic degradation in above stoichiometric yields.[272] However, they can become deactivated themselves for a variety of reasons. These include the inability to complete the Denisov cycle, as well as the removal of the HALS from the coating for example through erosion.

Therefore, the addition of HALS generally only leads to an initial improvement in the weatherability, and is avoided in weatherability study as it necessitates longer exposures to observe any effects. It was therefore concluded that the presence of HALS is equally beneficial to the preservation of gloss

retention in coatings containing isosorbide and phthalic anhydride, but that their deactivation affects the phthalic anhydride containing coatings more quickly.

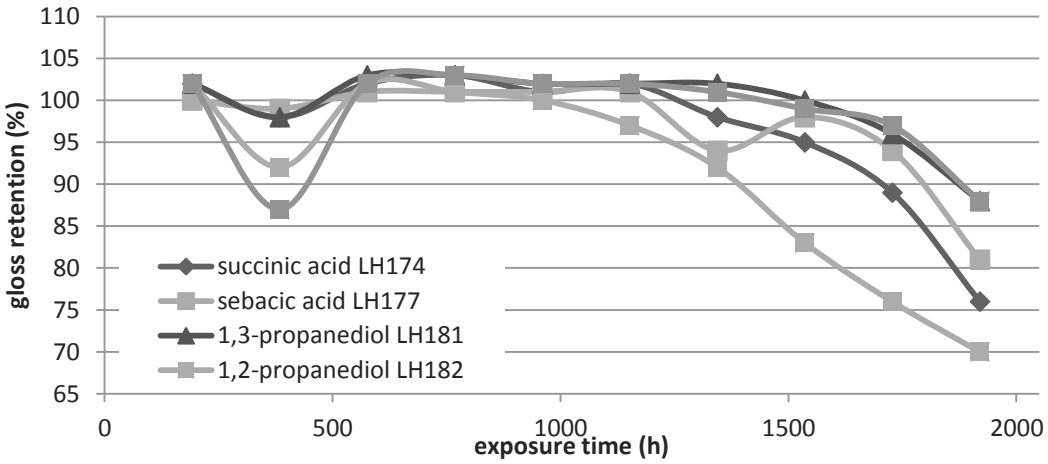

Figure 178: Gloss retention with HALS over time series 2 (1C)

A possible explanation for this behaviour can be derived from an observation made by Zhang *et al.* in a recent paper.[216] The authors found that the degradation in the melamine crosslinked polyester coating studied proceeded in several stages. In the first stage, the degradation was mainly caused by UV light, which penetrated the entire film. After 1000 h, however, the degradation was advanced enough for the moisture to penetrate the surface layer, and thus was accelerated by the synergetic effects between hydrolysis and photolysis.

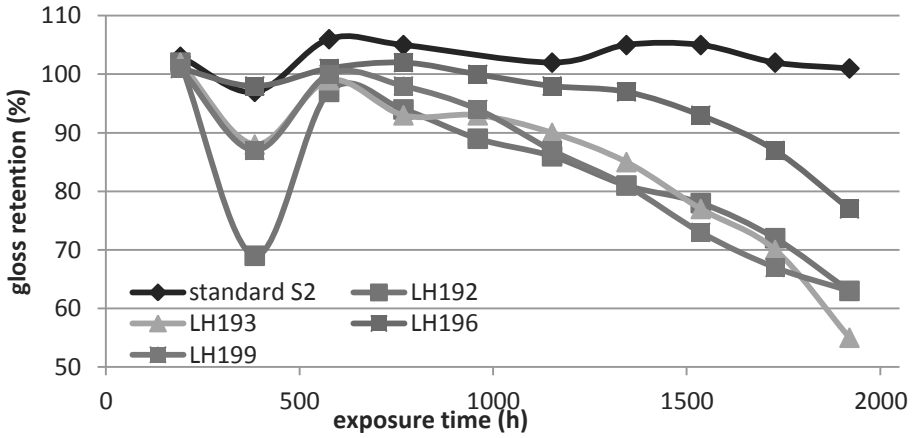

Figure 179: Gloss retention with HALS over time high T_g prototypes (2A)

If we therefore assume that the degradation in isosorbide containing coatings is significantly influenced by hydrolysis, due to their hydrophilic nature, while the degradation in phthalic anhydride coatings is governed by photolytic degradation due to the chromophore nature of the aromatic ring, we can rationalise their respective behaviour when formulated with HALS. The higher influence of

hydrolysis on the isosorbide coatings compared to the phthalic anhydrides coatings is confirmed for example by the increased film thickness loss observed in the former.

Once the HALS are deactivated, the degradation in phthalic anhydride containing coatings will begin in its full extend. On the other hand, the degradation in isosorbide coatings is delayed by the induction period necessary for the water to penetrate the coating surface, and its full extend is therefore not observed because the exposure was stopped after 2000 h.

This indicates that the degradation observed in the isosorbide coatings formulated without HALS is due to the collaborative effects of hydrolytic degradation and UV light and not possible in the absence of radical formation. Furthermore, it shows that a considerable improvement of the performance of isosorbide based coatings is possible through the addition of HALS.

Interestingly, the performance of the isosorbide containing coatings containing HALS as well as their relative improvement compared to the performance without HALS correlates to the amount of isosorbide present in the corresponding resins and was best for the coatings containing the least amount of isosorbide.

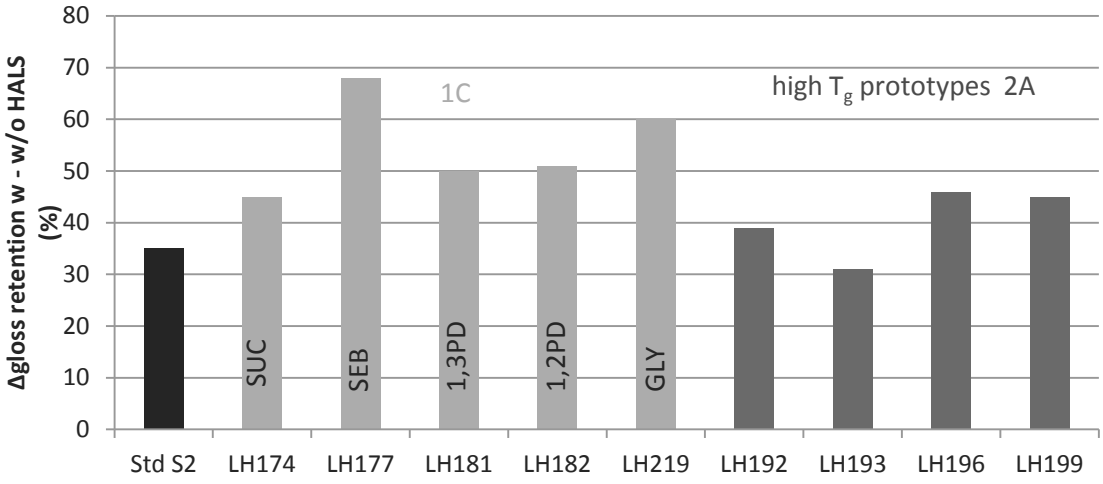

Figure 180: Increase in gloss retention through HALS after 1920 h series 2

Concerning the performance of coatings in which the amounts of monomers other than isosorbide or phthalic anhydride were changed, their behaviour unsurprisingly resembled that of the first series of phthalic anhydride containing coatings. The coating containing an increased amount of 1,2-propanediol, with the resin LH182, performed worst of all the coatings in the same series (1C) when HALS were added. At the same time, the coating containing the resin LH196, which contains the least amount of 1,2-propanediol of all the prototypes in the high T_g series (2A), performed best.

This could possibly be attributed to the tertiary hydrogen which is introduced with the 1,2-propanediol monomer, but not present in other monomers in the phthalic anhydride containing

formulations. Tertiary hydrogens are more susceptible to abstraction in radical reactions than secondary and primary hydrogens, and could therefore accelerate photolytic degradation. However, the improvement of performance observed upon the addition of HALS in the coatings containing the resins LH182 and LH196 did not differ significantly from the improvement observed in the other resins.

Interestingly, the largest improvement was observed for the coatings containing the resins LH177 and LH219, in which the amount of sebacic acid and glycerol was increased respectively.

Lastly, the deviation of results in the measurement after 384 h was observed in the second series for the HALS containing coatings as well as for those without HALS.

6.4.2.2 Infrared spectra after the addition of HALS

The spectra before exposure of the different coatings were largely identical with and without HALS.[LXI] After exposure, the isosorbide coatings performed better than the phthalic anhydride coatings when HALS were added, as observed in the gloss retention measurements. In figure 181, the absorptions of the NHOH peak with and without HALS are shown after 2000 h of exposure. The difference between the absorptions was larger for isosorbide containing coatings, and the absolute absorption after exposure was lower and closer to the standard than that measured for phthalic anhydride coatings.

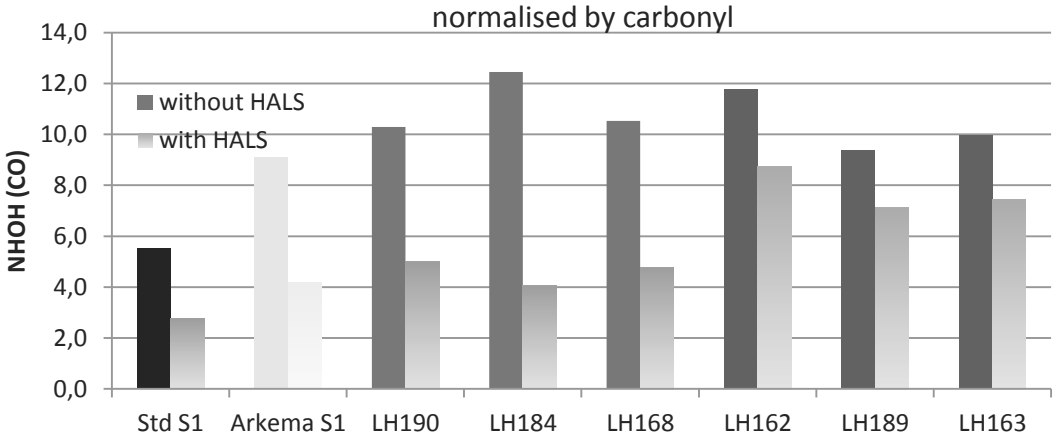

Figure 181: NHOH series 1 t_{2000} with and without HALS

In the second series, shown in figure 182, a larger difference between the NHOH absorption with and without HALS was observed also for the phthalic anhydride containing coatings. The end values were however, as for the first series, between 7 and 9 with respect to the carbonyl, and still higher than that measured for the isosorbide containing Arkema coating.

[LXI] See annexe for a more detailed description of the observations made concerning the IR spectra of coatings formulated with HALS before exposure.

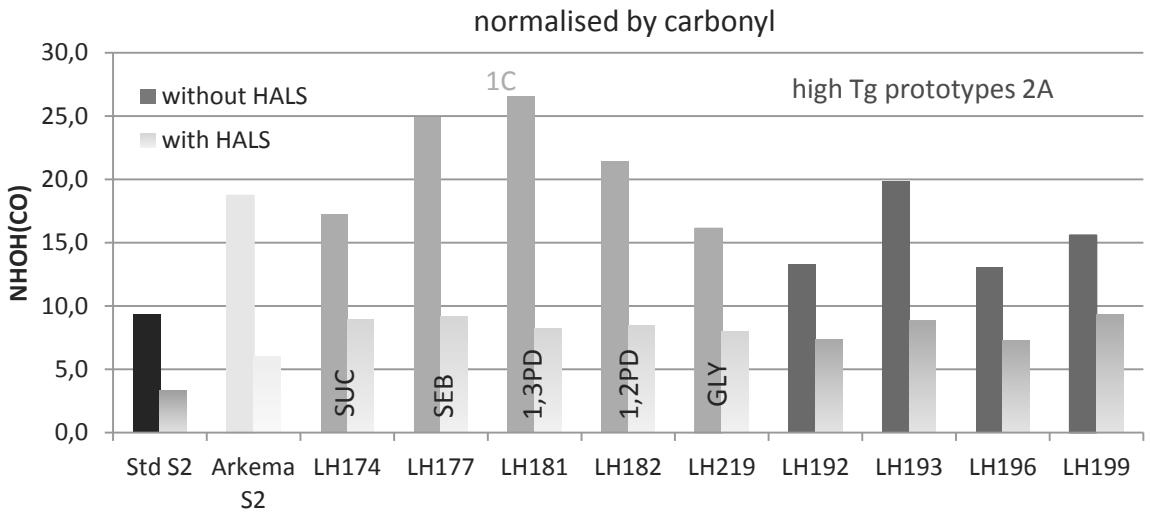

Figure 182: NHOH series 2 t_{1920} with and without HALS

This indicates that the larger degree of degradation observed for phthalic anhydride coatings as well as the standard coating was eliminated by the addition of HALS for coatings in the second series.[LXII]

Overall, we can conclude that the performance of all new biobased coatings can be significantly improved through the addition of hindered amine light stabilisers, and therefore that the creation of radicals plays a significant part in the degradation observed. The fact that the performance of isosorbide containing coatings is improved more than that of phthalic anhydride coatings through the addition of HALS in both gloss retention and infrared measurements furthermore indicates that the degradation mechanisms in terms of the influence of photolysis differ depending on the resin composition.

6.4.3 Impact of temperature through the difference between HotQUVa and QUVa

While the majority of the weatherability test analysis was performed on the coatings subjected to Hot QUVa conditions, their gloss retention was also evaluated after exposure to QUVa conditions. The main difference between the tests is, as the name suggests, the temperature. While in the Hot QUVa test, the coatings are subjected to an 8 hour cycle at 78 °C under UV light, under QUVa conditions, the temperature is only increased to 60 °C and the cycle only lasts 4 h.

Another difference lies in the intensity of the UV lamp, which is decreased from 0,89 W/m^2/nm in the Hot QUVa test to 0,80 W/m^2/nm in the QUVa test. Therefore, the effect of the decrease in temperature cannot be entirely separated from the reduction in the intensity and duration of the UV exposure. Nevertheless, the difference in temperature is more pronounced, as it doubles both in

[LXII] Details on the development of the other peaks upon exposure when HALS were added to the formulation can be found in the annexe.

exposure time and increases by 18 °C. Therefore, it is reasonable to assume that at least part of the degradation that is observed in the Hot QUVa test and not in the QUVa test is of thermal origin.

In figure 183 below, the gloss retention at the last measurement of the Hot QUVa test, which was taken after 2000 h for the first series of coatings (1A and 1B) and after 1920 h for the second series of coatings (1C) is compared with the gloss retention measured after 2000 h under QUVa conditions.

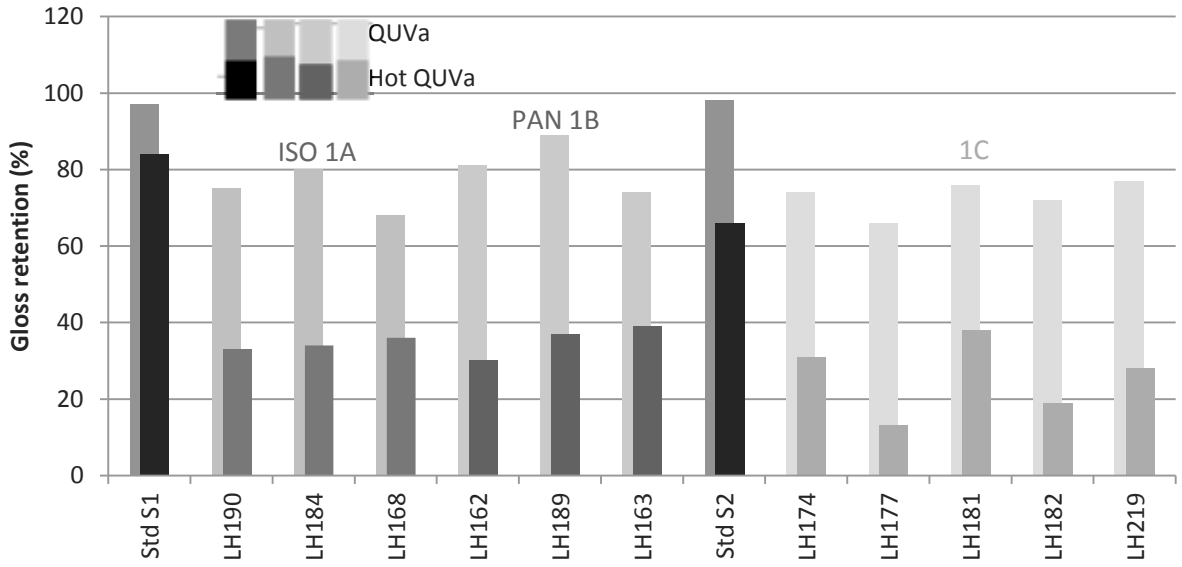

Figure 183: Gloss retention after 2000 h and 1920 h of HotQUVa and QUVa exposure

The gloss retention measured after the QUVa test is between 32% and 52% higher than that measured after the Hot QUVa test for all coatings, with the exception of the standard in the first series, which is due to its good performance in the Hot QUVa test rather than to the bad performance in the QUVa test. Therefore, it can be concluded that the temperature has a significant effect either causing or accelerating the degradation.

The isosorbide containing coatings perform slightly worse than the phthalic anhydride containing coatings, which could be due to the relatively increased exposure to high humidity, which makes up half of the time in the QUVa test in contrast to a third in the Hot QUVa test. While the phthalic anhydride coatings' performance increases by an average of 46% in the first series and 47% in the second, the isosorbide containing coatings only perform on average 40% better in the QUVa test.

The ranking of the different coatings of series one observed in the QUVa test does not correspond to that observed in the Hot QUVa test. Interestingly, despite the overall higher gloss retention, the differences between coatings containing different amounts of isosorbide and phthalic anhydride are more pronounced. No correlation was however observed between those amounts. In both cases, the coating with the resin containing 29,37 mol% of isosorbide or phthalic anhydride performs best, followed by the coating containing 24,37 mol%.

Contrarily, the ranking of the coatings of the second series, in which the quantities of succinic acid, sebacic acid, 1,3-propanediol, 1,2-propanediol and glycerol were varied, are the same in both Hot QUVa and QUVa tests. This could be due to the fact that the changes made in this series affected the overall structure more than either the UV absorption or the hydrophilicity of the coatings. The relative degradation of the second series of coatings was therefore not affected as much by the relative amount of UV light and humidity during the weathering.

The larger differences between the gloss retention after QUVa exposure and Hot QUVa exposure also correspond to the poorer performances in the Hot QUVa test. For example, the closest gloss retention in the two tests was observed for the coating containing the resin LH181, with only 38% difference, while the largest difference of 53% was observed for the coating containing the resin LH177.

Lastly, the standard of the second series performed equally as good as the standard of the first series in the QUVa test. Since the measurement frequency was not changed between the different series of QUVa tests, this indicates that this rather than the prolonged storage of the paint was responsible for its poorer performance measured in the gloss retention test. It could however also be due to the fact that virtually no degradation was observed in either coating in the QUVa test.

6.5 Structure-weatherability relationship

The weatherability tests were designed to yield information about the impact each of the monomers used in the resin had on the degradation behaviour of the resulting coating, and to provide guidance to which changes could be made to achieve better weatherability in a biobased coating to make it suitable for use on the exterior. The results are summarised in table 112 – 115.

The main method to assess the weatherability was the measurement of the gloss retention after exposure in a weathering cabinet. Unfortunately, all biobased and partially biobased coatings tested performed significantly worse than the standard coating currently used in exterior applications.

Table 112: Weathering test results of the standard coating (series 1)

		Change in		Gloss retention after 2000 h		
T_g	crosslinking density	H_{uk}	film thickness	Hot QUVa	HALS	QUVa
°C	mmol/cm^3	N/mm^2	µm	%	%	%
23	0,027	98	3,9	84	100	97

Nevertheless, thanks to the use of infrared spectroscopy, µ-hardness measurements and film thickness loss assessment, some conclusions about the causes of the higher degradation and the influence of the resin formulation on the weatherability could be drawn, and will be presented here.

6.5.1 The influence of isosorbide on the weatherability

Five resins containing different quantities of isosorbide from 19,37 mol% to 45,13 mol% were incorporated into coatings. The analysis of the coatings containing the resins with 19,37 mol% and 45,13 mol% is still ongoing to confirm the conclusions drawn from the analysis of the coatings containing resins with 24,37 mol% to 34,31 mol% isosorbide.

Nevertheless, the analysis of the three coatings revealed only small differences in degradation behaviour despite the replacement of the rigid diether in isosorbide with the simpler 1,2-propanediol, as shown in scheme 131. While at the start of the gloss retention measurements, the coatings containing smaller amounts of isosorbide performed slightly better, the differences decreased to reveal an almost identical performance after 2000 h of weathering.

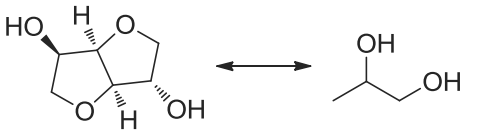

isosorbide 1,2 propanediol

Scheme 131: Monomer exchange in the different isosorbide resins

This was also reflected in the results of the gloss retention measurement of identical coatings to which hindered amine light stabilisers, which slow down the degradation process by trapping radicals, were added. In the coatings with HALS, the one containing the least amount of isosorbide again performed best.

This indicates that initially and in the absence of radical degradation, 1,2-propanediol confers greater resistance to exposure than isosorbide, but that the difference is eradicated once the degradation has processed past a certain level.

Table 113: Weathering test results isosorbide coatings (1A)

				Change in		Gloss retention after 2000 h		
isosorbide content		T_g	crosslinking density	H_{uk}	film thickness	Hot QUVa	HALS	QUVa
resin	mol%	°C	mmol/cm^3	N/mm^2	µm	%	%	%
LH190	24,37	28	0,0576	120	7,0	33	96	75
LH184	29,37	37	0,0906	117	11,1	34	93	80
LH168	34,31	43	0,0592	109	12,1	36	89	68

The film thickness loss observed in isosorbide containing coatings was equally greater for coatings containing larger amounts of isosorbide. Contrary to the other coatings examined, no link to the crosslinking density was found. Furthermore, the loss was considerably larger than that observed for phthalic anhydride coatings.

The main reason for a decrease in film thickness is the erosion of small fragments split off from the main network through chain scission, either caused by radical degradation or by hydrolysis. The dependence on isosorbide quantity and increase compared to phthalic anhydride containing coatings

indicates that the main process causing film thickness loss in this case was hydrolysis, accelerated by the hydrophilicity of the isosorbide motive.

While the universal hardness was found to increase after weathering for all isosorbide coatings, only small differences were found between the different quantities of isosorbide. This indicates that the higher degree of hydrolysis taking place in coatings containing more isosorbide affected mostly the surface and network chain ends, but not the bulk structure of the network. As the increase in universal hardness indicates that additional crosslinking has taken place, similar levels must mean that the hydrolysis taking place has not counteracted this process in the bulk.

Only a small decrease in universal hardness difference after exposure, as well as an increased similarity of the creep 1 curves before and after weathering with increased amounts of isosorbide attest to a small influence of the hydrolysis on the overall structure.

The infrared measurements largely confirmed the results of the gloss retention measurements. An increase in the NHOH peak area of each coating indicated that the degradation observed was either due to the breaking of crosslinks, creating free N-H bonds adjacent to the melamine molecules, or the breaking of ester bonds. The fact that the increase was so similar despite the different quantities of isosorbide and that an increase in the melamine peak, which incorporates the N-H bending vibration, was simultaneously observed, indicates that the breaking of melamine resin bonds are likely the main cause.

In addition to the increase in melamine and NHOH peaks, a C-H peak shape change was also observed for the isosorbide resins. This and the improvement caused by the addition of HALS, which was larger than that observed for comparable resins formulated with phthalic anhydride, suggests that a radical mechanisms involving the abstraction of hydrogen atoms from one carbon to another is also involved. As an overall increase of both C-H vibrations with respect to the carbonyl peak was also observed, it is likely that the abstraction of the hydrogen atoms occurred after homolytic cleavage resulting in carbon based and not oxygen based radicals.

In conclusion, higher quantities of isosorbide initially led to larger degradation, but did not influence the end result. The main degradation mechanisms causing an increase in NHOH bond and in gloss retention was attributed to the breaking of resin melamine bonds, which was not influenced by the quantity of isosorbide in the coating. Evidence of a second degradation mechanism, involving carbon based radicals, the abstraction of hydrogen atoms and the formation of new carbon – carbon bonds, which caused an overall increase of coating hardness, was also found. This mechanisms was equally not significantly influenced by the quantity of isosorbide present in the coating, but was found to be effectively stopped by the addition of HALS.

In coatings containing HALS, the use of isosorbide was found to cause greater stability compared to phthalic anhydride equivalents.

The most significant effect of isosorbide was detected in the film thickness loss measurements. However, it seems that while higher amounts of isosorbide cause higher levels of erosion, no impact was made on either the network structure or the network appearance.

6.5.2 The influence of phthalic anhydride on the weatherability

As for the isosorbide resins, no influence of the quantity of phthalic anhydride used in the resin, or its replacement with succinic acid and sebacic acid as shown in scheme 132, on the overall weatherability of the coatings as measured by the gloss retention was detected. Furthermore, no difference in gloss retention was observed when isosorbide was replaced by phthalic anhydride in the resin structure.

Therefore, no evidence of an impact of either the aromaticity or the hydrophobicity of phthalic anhydride on the gloss retention could be found. Compared to the isosorbide resins, the film thickness loss was considerably smaller. But despite the fact that the amount of coating eroded by humidity was comparable to that observed in the standard coating, the gloss retention results were much worse and in line with those of isosorbide coatings.

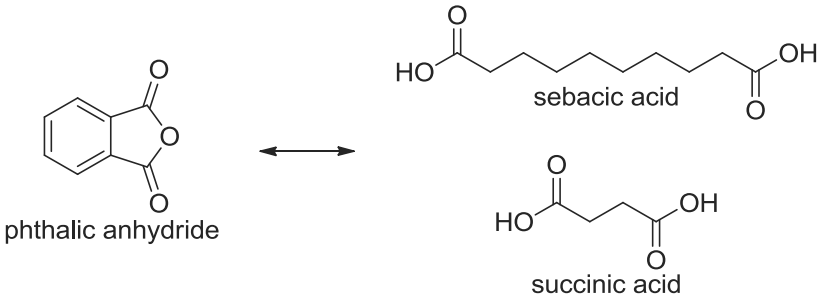

Scheme 132: Monomer exchange in the different phthalic anhydride resins

As in the isosorbide coatings, the results of the gloss retention measurements were confirmed by an increase in the NHOH peak in the infrared spectra. An increase in C-H bonds with respect to the carbonyl peak and of the melamine peak was equally observed, indicating that the degradation was caused to some degree by the breaking of melamine resins crosslinks as well as by carbon based radicals.

In contrast to the isosorbide coatings, the addition of HALS did not considerably improve the degradation after 2000 h. The gloss retention measurements over time revealed that the deactivation of HALS is followed by a steep decrease in gloss retention reaching the same level as was observed without them. The observation was confirmed by the NHOH levels observed in the infrared spectrum.

The most significant impact of the quantity of phthalic anhydride in the coatings was observed in the μ-hardness measurements. For several phthalic anhydride coatings, the universal hardness was found to correlate with the crosslinking density measured in the DMA after curing. A significantly

larger increase in universal hardness and elastic energy component was observed for coatings containing larger amounts of phthalic anhydride. This suggests that a larger degree of crosslinking has occurred in the coatings containing more phthalic anhydride. A larger change in creep 1 behaviour with increased phthalic anhydride content was also observed.

Table 114: Weathering test results phthalic anhydride coatings (1B)

				Change in		Gloss retention after 2000 h		
phthalic anhydride		T_g	crosslinking density	H_{uk}	film thickness	Hot QUVa	HALS	QUVa
resin	mol%	°C	mmol/cm^3	N/mm^2	µm	%	%	%
LH162	24,37	6	0,0812	99	3,7	30	68	81
LH189	29,37	14	0,0747	102	5,3	37	96	89
LH163	34,37	23	0,0963	175	2,9	39	68	74

This effect could be explained with the chromophore nature of phthalic anhydride. However, while phthalic anhydride as a monomer absorbs significantly more UV light than isosorbide, no evidence could be found of a dependence of the UV absorption of the corresponding resins on the phthalic anhydride content. The absorption also occured at wavelengths which are not part of the natural spectrum of the sun, and may therefore be irrelevant.

Lastly, the improvement in gloss retention observed for phthalic anhydride resins when the exposure was changed from the Hot QUVa to the QUVa protocol was larger than that observed for the isosorbide resins. This indicates that the phthalic anhydride is affected more than the isosorbide either by the higher temperature or by the higher intensity of the UV light.

Overall, the change of the biobased isosorbide monomer to the petroleum based phthalic anhydride did not result in an improvement in weatherability. While the µ-hardness change observed in the phthalic anhydride coatings was considerably larger and the film thickness loss was considerably smaller, neither affected on the end gloss retention performance.

6.5.3 The influence of other monomers on the weatherability

The influence of the other monomers used in the resin formulation, namely 1,2-propanediol, 1,3-propanediol, succinic acid, sebacic acid and glycerol, on the weathering performance was significantly greater than that observed for either isosorbide or phthalic anhydride.

While part of this may be due to the more frequent evaluation, which was done every 192 h instead of every 500 h, the results were confirmed in the infrared spectrum, in which no difference between the two standard coatings was observed. The fact that large differences in performance were observed when the relatively similar 1,2-propanediol, 1,3-propanediol and glycerol or succinic acid

and sebacic acid were exchanged as shown in scheme 133 indicates that overall structural features rather than individual functional groups are determining the degree of degradation.

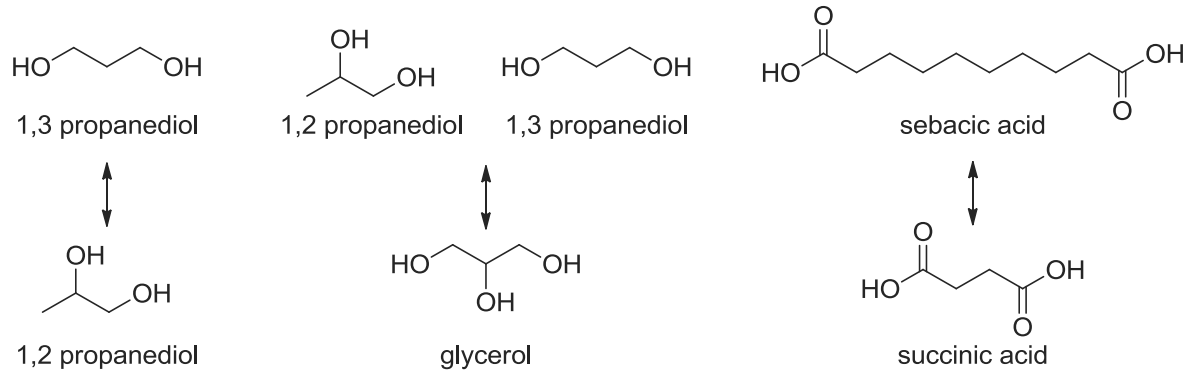

Scheme 133: Monomer exchanges in other resins

The coating containing only succinic acid performed better than the coating containing only sebacic acid in the gloss retention measurements. The infrared measurements confirmed that a larger increase in NHOH groups occurred in the sebacic acid containing coating. Furthermore, a larger absorption of C-H bonds and a larger increase of C-H bonds after weathering were detected for the sebacic acid coating.

The film thickness loss was larger for the sebacic acid coating than for the succinic acid coating, as well. Interestingly, while the ranking of the five coatings stayed the same whether Hot QUVa or QUVa weathering was used, the improvement in gloss retention was largest for the sebacic acid coating, indicating that it was affected by the temperature or the more intense UV radiation more than the others. The fact that the sebacic acid coating performed slightly better than the succinic acid coating when HALS were added to the formulation indicates that the decrease in UV radiation intensity may have caused the improvement in the QUVa weathered samples.

Table 115: Weathering test results for coatings in which other monomers were tested (1C)

				Change in		Gloss retention (2000 h)		
monomer tested		T_g	crosslinking density	H_{uk}	film thickness	Hot QUVa	HALS	QUVa
resin	mol%	°C	mmol/cm^3	N/mm^2	µm	%	%	%
LH174	SUC	30	0,0627	256	6,8	31	76	74
LH177	SEB	2	0,0515	246	8,4	13	81	66
LH181	1,3PD	7	0,0684	104	6,7	38	88	76
LH182	1,2PD	36	0,0465	188	5,4	19	70	72
LH219	GLY 9,27	26	0,0421	167	10,0	28	88	77

Overall, the lowering of the available C-H groups in the structure when sebacic acid was replaced with succinic acid caused an improvement of the gloss retention due to a decrease in radical degradation. However, both coatings in which the relative amounts of succinic and sebacic acid were

changed performed worse than that in which a mixture of both was used. This suggests that next to the nature of the monomers used, the overall resin properties affect the weatherability in such a way that the use of a mixture of monomers good and bad for degradation is beneficial.

The effect of replacing 1,2-propanediol with 1,3-propanediol and of replacing both with glycerol was less clear. While the 1,3-propanediol coating performed better than all others in the gloss retention, it also showed a greater increase in NHOH peaks than the 1,2-propanediol coating. The coating in which the content of glycerol was increased showed a better gloss retention than the other two for the majority of the measurements but was slightly worse than the 1,3-propanediol coating in the last measurement.

In terms of film thickness loss, the performance of the 1,2-propanediol coating was best, while the coating containing larger amounts of glycerol showed significantly more loss than the others. On the other hand, the coating with 1,3-propanediol showed both the least increase of universal hardness after weathering and the least improvement when the weathering protocol was changed from Hot QUVa to QUVa.

This indicates that the change from 1,2-propanediol to 1,3-propanediol could have increased the vulnerability of the melamine resin crosslinks, because it changed the nature of the free hydroxy groups in the resin from secondary to primary hydroxys. This would explain the larger increase in NHOH peak for the 1,3-propanediol coating. Similarly, the higher susceptibility to bond scission at resin melamine and resin ester bonds could explain the higher degree of hydrolysis and therefore film thickness loss, as well as counteract the radical crosslinking and therefore the increase in μ-hardness.

As the gloss retention of the 1,3-propanediol coating was nevertheless better than that of the other coatings, this suggests that an additional factor to the NHOH peak and the nature of the monomers determines the degree of gloss retention.

Like the isosorbide coatings, all five coatings examined in the second series profited considerably from the addition of HALS, but the differences observed between the coatings were also less pronounced. This suggests that the differences induced by the change in 1,3-propanediol, 1,2-propanediol, succinic acid, sebacic acid and glycerol were at least in part due to radical degradation mechanisms.

6.5.4 Other parameters influencing the weatherability

Neither a change in the isosorbide quantity nor in the phthalic anhydride quantity was found to achieve an improvement in weatherability. Even though coatings free of each of the monomers

succinic acid, sebacic acid, 1,2-propanediol and 1,3-propanediol were prepared, none of them showed a performance even nearly as good as that of the standard coating.

This suggests that something other than the nature of the monomers is determining the degradation behaviour. While the melamine has been found to provide a weak link for degradation, the same quantity was used in all of the coatings, so that it can also be excluded as a cause.

The overall polarity as well as UV absorption of the coating would be significantly changed by the quantities of isosorbide and phthalic anhydride, as would be the stiffness of the network. Both are therefore unlikely to be the origin of the bad performance.

Two important factors which cannot be excluded at this time are the overall compatibility with the paint formulation and the crosslinking density of the network. Solvent system, melamine type and flow additives have been designed to fit the standard coating and it is possible that they are not as miscible with the biobased resins proposed.

In order to keep the coatings comparable, a large amount of monomers and formulation parameters was nevertheless kept constant between the different resins, and it is possible that the compatibility problems would be common to them all. One marked difference between the standard resin and all proposed biobased resin was the difference in glass transition temperature between the resin before curing and the coating afterwards. The glass transition temperature of the standard only increased by 7 °C after crosslinking, while that of the biobased prototypes increased by 27 °C on average.

This difference is also reflected in a much lower crosslinking density determined for the standard coating in DMA measurements. While no clear correlation could be established between the crosslinking density and the overall performance, it is possible that the difference in resin composition caused a difference in interaction with the solvent system and that the different interaction with the solvent system subsequently caused a difference in crosslinking density.

The microscopic images of the coatings before weathering as well as the craters observed in the formation of free films suggest that differences in surface tension or evaporation behaviour in the wet coating may cause unevenness in the cured film to a larger degree in the biobased coating than in the standard coating.

A correlation was also established for several of the phthalic anhydride containing resins between the crosslinking density and the film thickness loss, and the gloss retention was observed to be higher for coatings with either very high or very low crosslinking densities, so that the importance of the parameter cannot be completely denied.

6.5.5 Ways to improve coating weatherability

An increased amount of isosorbide in the coating accelerates hydrolysis, as was evidenced by the film thickness loss. On the other hand, an increased amount of phthalic anhydride causes a larger amount of radically generated crosslinks, as proven by the increase in universal hardness and elastic energy component. Nevertheless, neither had an impact on the overall gloss retention performance, or the amount of NHOH bonds measured in the infrared spectrum.

The replacement of sebacic acid with succinic acid resulted in a better coating performance compared to the replacement of succinic acid with sebacic acid, but not compared to the use of a mixture of both. Furthermore, the use of 1,3-propanediol instead of 1,2-propanediol resulted in a better gloss retention but a higher film thickness loss and increase in NHOH bonds.

A possible reason is that the parts of the coating affected by hydrolysis are eroded away, and that another factor, such as the overall crosslinking density or the evenness of the surface created by good compatibility with the paint formulation, is more important for the overall weatherability.

In order to create a biobased coating with sufficient weatherability for use in exterior applications, three different strategies could be used. The first could be to imitate the crosslinking behaviour and network properties of the standard coating. A biobased resin with a lower hydroxy value which produces a coating with a glass transition temperature only a few degrees higher should be tested.

While the exact reason for the difference in degradation behaviour between the standard coating and the biobased coating is not clear, the glass transition temperature difference achieved by curing and the much lower crosslinking density of the standard coating are the most obvious differences and should be addressed.

Secondly, the paint formulation needs to be adjusted. While this is impractical for a whole series of resins, at least one formulation compatible with a phthalic anhydride resin and one compatible with an isosorbide resin should be created. The use of aromatic solvents should probably be avoided for the latter, but several suitable alternatives are proposed by Beckers. The change of the MPA solvent to something more compatible with the resins should also be considered.

Once the paint formulation and the resin parameters and crosslinking behaviour are adjusted, the other conclusions drawn from this study can then be used to optimise the degradation behaviour. Depending on whether the radical degradation or the hydrolysis shows to be a problem, phthalic anhydride can be used to replace isosorbide and 1,2-propanediol can be used to replace 1,3-propanediol.

Further insights can also be expected from the analysis of the other coatings currently under exposure, both concerning the role of isosorbide and phthalic anhydride (1A and 1B), and concerning potential directions for the development of new prototypes, such as the combination of isosorbide and phthalic anhydride and the incorporation of cyclohexanedicarboxylic acid.

6.5.6 Potential of biobased resins for use in exterior coatings

The main change made when replacing petroleum based resin with biobased resin is the use of biobased monomers in the resin synthesis instead of petroleum based monomers. In this work, it was found that their poor performance in weatherability studies is in all likelihood not due to the nature of any single monomer, but to overall structural features such as their compatibility with the paint formulation and their crosslinking density.

As these are challenges that are not inherent to their biobased nature, it is very likely that they can be addressed and solved. Furthermore, in this work, the influence of six biobased monomers on resin and coating properties were thoroughly examined, and it was found that adjustment of the properties in a wide range covering different viscosities, glass transition temperatures, hardness values and creep behaviours is possible.

Therefore, it can be concluded that biobased monomers have a huge potential for the use in resins and that the development of a coating for exterior application based on biosources is definitely within the realm of the possible.

7 Experimental

7.1 General information

Starting materials were purchased from Sigma Aldrich, Alfa Aesar or Acros Organics, with the exception of isosorbide, which in the majority donated by Roquette and Arkema. Starting materials and solvents were used without further purification.

Nuclear magnetic resonance spectra were recorded on a Bruker AV 300, Bruker AV 400 or Bruker AV 500 Avance III spectrometer in deuterated DMSO or in a 3:1 mixture of deuterated chloroform and deuterated trifluoroacetic acid. Chemical shifts are reported in parts per million (ppm) downfield to tetramethylsilane and the residual solvent signal was used as a reference (DMSO: 2.500 ppm in a proton spectrum, 39.52 ppm in a carbon spectrum; $CDCl_3$: 7.260 ppm in a proton spectrum, 77.16 ppm in a carbon spectrum). Peaks are reported in the format: *Chemical shift, multiplicity (s = singlet, d = doublet, t = triplet, q = quadruplet and m = multiplet), J coupling constant (Hz), number of protons, assignment* for proton spectra and *chemical shift, assignment* for carbon spectra.

Mass spectra were acquired on a Thermofinnigan LCQ Advantage spectrometer in low resolution mode using electrospray ionisation (ESI-MS). UV/Vis spectra of the coatings were recorded on a PerkinElmerLambda 950 UV/Vis reflection spectrometer. All other UV/Vis spectra were recorded on a Shimadzu UVmini-1240 machine. Melting points were measured on a Büchi melting point B-540 apparatus, and measurements were taken at a temperature gradient of 10 K/min.

The infrared spectra of the resins and paint formulations were taken on a Nicolet Avatar 370DTGS spectrometer. The infrared spectra of the coatings were taken on an attenuated total reflection Thunderdome PE 1600 spectrometer and on a Thermo Nicolet iS10 photo acoustic spectrometer. The data was analysed using OMNIC software.

The glass transition temperatures of all uncrosslinked products were determined using differential scanning calorimetry on a Mettler Toledo DSC1 calorimeter. Unless stated otherwise, after an isothermal segment at 150 °C (5 min), the temperature was decreased to -50 °C and then raised to 100 °C at a heating rate of 20 K/min. The glass transition temperature of crosslinked products (films) were determined in the LTD Beckers laboratory using differential scanning calorimetry on a Mettler Toledo DSC1 star system calorimeter. The film was scratched off the support, heated from 25 °C to 125 °C at 2 K/min and then cooled down to -30 °C at 2 K/min. The glass transition temperature was determined using the final heating process which went from -30 °C to 125 °C at 10 K/min.

The molecular mass of the polymers were determined by size exclusion chromatography on four different machines, as detailed in the table below.

The first group (A) was analysed in the C2P2 laboratory on a triple detection Viscotek by Malvern Instrument equipped with a refractive index detector, static diffusion of RALS (90°) and LALS (7°) light and a viscosimetric detector. The samples were analysed at 35 °C in THF at a concentration of 2,5 mg/mL and at a flow rate of 0,9 mL/min. The injection volume used was 100 µL. A precolumn of the type PLgel Olexis Guard (7,5*50 mm) and three columns installed in series of the type PLgel Olexis Guard (7,5*50mm) were used for the separation. A standard calibration with polystyrene and the Malvern Instrument “OmniSEC” software were used for the interpretation.

The second group (B) was analysed in the Arkema laboratory on a Waters SEC System apparatus equipped with a Waters 2414RI refractive index detector. The samples were analysed at 35 °C in THF stabilised with BHT purchased from Fisher at a concentration of 12,5mg/mL and at a flow rate of 1 mL/min. Four Agilent columns of the "low molecular weight" set containing two columns of the type mixed D (ref. 1110-6504), one column of 100 Å (ref. 1110-6520) and one column of 50 Å (ref. 1110-6515) of the size 7,8 mm*300 mm were used for the separation. The injection volume used was 50 µL. A standard calibration with polystyrene and the software EMPOWER were used for the interpretation.

The third group (C) was analysed in the IMP laboratory on a WATERS size exclusion chromatography apparatus equipped with a refractive index detector. The samples were analysed at 35 °C in hexafluoroisopropanol (HFIP) at a concentration of 5 mg/mL at a flow rate of 0,3 mL/min. One precolumn and three columns in series of the types Acquity APC XT450, Acquity APC XT125 and Acquity APC XT45 were used for the separation. The injection volume used was 20 µL. EMPOWER 3 software was used for the interpretation.

All other products were analysed in our own laboratory on a Agilent 1260 Infinity apparatus equipped with an Agilent refractive index detector which was set to 55 °C. The samples were analysed at 50 °C in *n*-methyl pyrrolidone (NMP) solvent at a concentration of 10 mg/mL at a flow rate of 0,2 mL/min. A MesoPore column of the size 300*7,5 mm (ref. 1113-6325) was used for separation. A standard calibration with polystyrene and the SEC Agilent software were used for the interpretation.

Group A	Group B	Group C
LH059, LH067, LH072, LH075, LH077, LH079, LH094, LH105, LH107, LH109, LH112, LH116, LH117, LH119, LH120, LH122, LH123, LH127, LH128, LH152, LH161, LH200, LH229, LH230	LH126, LH162, LH163, LH165, LH168, LH174, LH177, LH181, LH182, LH183, LH184, LH185, LH186, LH189, LH190, LH192, LH193, LH196, LH198, LH199, LH201, LH202, LH203, LH206, LH207, LH210	LH200

7.2 Vanillin derivatives

7.2.1 Product purification and NMR analysis – General remarks

The reactivity of vanillin was studied using vanillin and also guaiacol as a model compound. Various catalysts, substrates and conditions were screened. In some cases, a simple work-up such as washing the product with $NaHCO_3$ and water, or removal of byproducts under reduced pressure was performed. However, this was often not very successful in separating the starting materials from the products. Since the aim was a screening and not the synthesis of new compounds, the purification was not further pursued with other methods which would take more time such as column chromatography.

Similarly, when the polyesterification reactions of ferulic acid and dihydroacetylferulic acid were studied, NMR analysis of the product mixture rather than the separation of all different components was used to determine degree of success of the reaction. The different peaks were assigned by comparison with the starting material spectra and using online NMR database based prediction tools to the best of knowledge and ability.[273] However, due to interactions with the strongly acidic solvent

(deuterated trifluoroacetic acid) and overlap between starting material and product peaks, it is possible that the peaks reported here differ slightly in ppm from what they would be if the product was completely pure. Furthermore, the identity of almost identical peaks in ^{13}C spectrum (less than 0,5 ppm difference) was only confirmed with HSQC where this added value to the understanding of the results.

7.2.2 Evaluation of the reactivity of the phenol group towards esterification

7.2.2.1 Catalysts

The below catalysts were used in the experiments described hereafter and abbreviated as shown:

Catalysts tested for phenol esterification

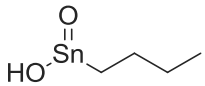	$BiCl_3$	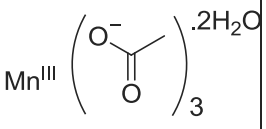	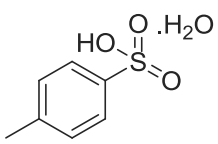	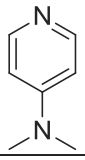	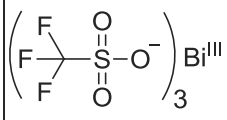
Fascat 4100	**$BiCl_3$**	**$Mn(OAc)_3$**	***p*TSA**	**DMAP**	**$Bi(OTf)_3$**
butyl stannoic acid	bismuth chloride	manganese acetate dihydrate	*p*-toluene-sulfonic acid monohydrate	dimethyl-amino-pyridine	bismuth triflate

*7.2.2.2 **Vanillin acetate** (LH062)*

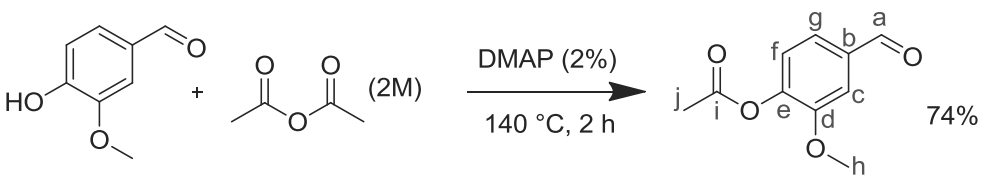

In a round bottom flask fitted with a reflux condenser, 1,52 g of vanillin (10 mmol) and 0,24 g of DMAP catalyst (5%) were diluted in 5 mL of acetic anhydride (2 M). The mixture was heated in a preheated sandbath to 140 °C for 2 h while stirring magnetically. The excess acetic acid and acetic anhydride were then removed by distillation under reduced pressure (44 °C, 20 mbar). Diethyl ether (10 mL) was added and the product was washed with water (3 x 10 mL) and dried over $MgSO_4$. The excess solvent was removed using a rotary evaporator to give a yellow oil (?) (1,44 g, 74 %).

^{1}H NMR (300 MHz, DMSO) δ 9.96 (s, 1H, $C_a\underline{H}O$), 7.60 (d, *J* = 1.7, 1H, $Ar_c\underline{H}$), 7.57 (dd, *J* = 8.0, 1.8, 1H, $Ar_g\underline{H}$), 7.34 (d, *J* = 7.9, 1H, $Ar_f\underline{H}$), 3.87 (s, 3H, Ar-$OC_h\underline{H_3}$), 2.30 (s, 3H, $C_j\underline{H_3}COOAr$); **^{13}C NMR (75 MHz, DMSO)** δ 192.36 (C_aHO), 168.58 (C_iOOAr), 152.03 (C_{arom}), 144.72 (C_{arom}), 135.53 (C_{ar}), 124.12 ($CH_{arom.}$), 124.00 ($CH_{arom.}$), 112.26 ($CH_{arom.}$), 56.37 (Ar-$O\underline{C_h}H_3$), 20.70 ($\underline{C_j}H_3COOAr$).

7.2.2.3 ***General procedure*** *for evaluating the reactivity of vanillin and vanillin derivatives towards succinic acid (LH018 A – D):*

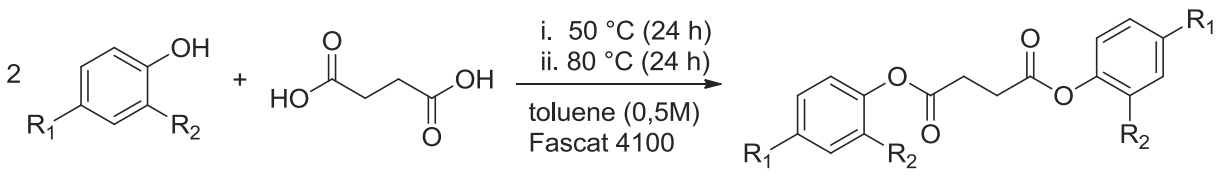

In order to evaluate the reactivity of vanillin and related compounds towards succinic acid, four test reactions were run and their progress was followed using ^{1}H NMR and TLC. Each aromatic compound (2 mmol) was placed in an open reaction tube (10 mL) together with 0,30 g succinic acid (1 mmol), 0,005 g butyl stannoic acid catalyst and 2 mL toluene. The reactions were heated in a sandbath to 50 °C for 24 h, then to 80 °C for 24 h, while stirring magnetically.

Conditions:

Compound	R_1	R_2	Result
Phenol	-H	-H	no reaction
Guaiacol	-H	$-OCH_3$	no reaction
Hydroxybenzaldehyde	-C=O	-H	no reaction
Vanillin	-C=O	$-OCH_3$	no reaction

7.2.2.4 Procedure for test of vanillin reactivity towards hexanoic acid: LH020

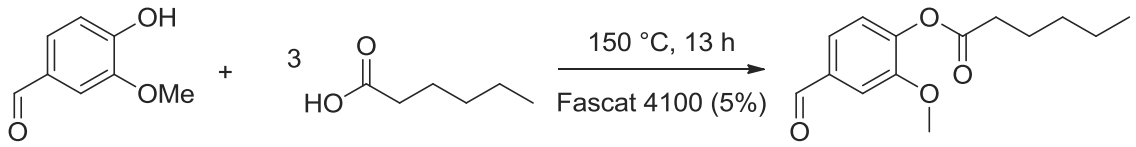

In a 150 mL round bottom flask, 1,52 g of vanillin (10 mmol) were mixed with 3,48 g of hexanoic acid (30 mmol) and 0,10 g of butylstannoic acid catalyst (0,5 mmol) and heated to 150 °C for 13 h. The product mixture was tested with ^{1}H NMR and thin liquid chromatography, but no products were observed.

7.2.2.5 Guaiacol hexanoate

7.2.2.5.1 Procedure I: Acid

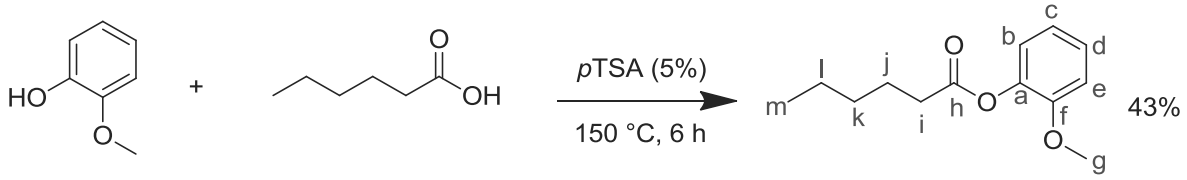

In 10 mL reaction tubes, 0,25 g guaiacol (2 mmol) and 0,23 g hexanoic acid (2 mmol) were mixed with 0,02 g *p*-toluene sulfonic acid (0,1 mmol) and heated while stirring magnetically in a preheated sand bath at 160 °C for 6 h to give a yield of 43% of guaiacol hexanoate determined by in situ NMR of the product mixture.

^{1}H NMR (300 MHz, DMSO) δ 7.21 (ddd, *J* = 8.2, 7.3, 1.7, 1H, Ar_cH), 7.09 (dd, *J* = 8.3, 1.4, 1H, Ar_bH), 7.05 (dd, *J* = 7.9, 1.7, 1H, Ar_dH), 6.95 (dd, *J* = 7.4, 1.5, 1H, Ar_eH), 3.75 (s, 3H, Ar-$OC_g\underline{H_3}$), 2.53 (t, *J* = 7.3, 2H, $C_i\underline{H_2}COOAr$), 1.72 – 1.58 (m, 2H, $C_j\underline{H_2}CH_2COOAr$), 1.41 – 1.30 (m, 4H, CH_3-$C_l\underline{H_2}$-$C_k\underline{H_2}$), 0.90 (t, *J* = 5.2, 3H, $C_m\underline{H_3}CH_2$).

7.2.2.5.2 Procedure II: (LH023) Methyl ester

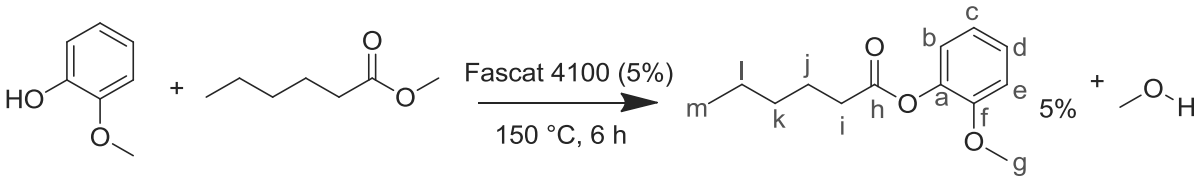

In 10 mL reaction tubes, 0,25 g guaiacol (2 mmol) and 0,26 g methyl hexanoate (2 mmol) were mixed with 0,02 g butylstannoic acid (0,1 mmol) and heated while stirring magnetically in a preheated sand bath at 150 °C for 6 h to give a yield of 5% of guaiacol hexanoate determined by in situ NMR of the product mixture. (NMR – see procedure I)

7.2.2.6 ***General procedure*** *for the evaluation of catalysts and conditions for the reaction of guaiacol with hexanoic acid:*

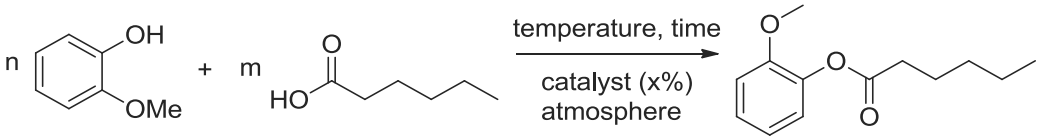

Guaiacol was mixed with hexanoic acid (1 – 100 equivalent) and a catalyst (0,5 or 5 %) in a 50 mL round bottom flask or 10 mL reaction tube. The flask was closed with a septum, leaving only a needle as outlet for water, or flushed with argon gas and then equipped with and argon balloon. The reaction was heated and reaction progress was monitored with thin liquid chromatography. In the end of the reaction, a sample of the product mixture was analysed with ^{1}H NMR to determine the result.

Conditions:

Conditions for the reaction of guaiacol and hexanoic acid

	n	**m**	**time**	**temp.**	**catalyst**	**x**	**atm**	**yield**
	mmol	**equiv.**	**h**	**°C**		**mol %**		**%**
LH022	10	3	8	150	Fascat 4100	5	air	no reaction
LH024	2	1	6,5	150	$Mn(OAc)_3$	5	air	no reaction
LH026	2	1	23	150	$Mn(OAc)_3$	5	Ar	no reaction
LH024	2	1	6,5	150	$BiCl_3$	5	air	no reaction
LH026	2	1	23	150	$BiCl_3$	5	Ar	no reaction
LH024	2	1	6,5	150	$Bi(OTf)_3$	5	air	37
LH025	2	1	6,5	150	*p*TSA	5	air	43
LH025	2	1	6,5	150	DMAP	5	air	no reaction
LH176	20	1,1	3	140	DMAP	5	air	no reaction
LH029	2	1	24	150	DMAP	5	Ar	15
LH029 10	2	10	24	150	DMAP	5	Ar	no reaction

	n	m	time	temp.	catalyst	x	atm	yield
	mmol	equiv.	h	°C		mol %		%
LH028 10a	0,2	10	24	150	$BiCl_3$	5	Ar	no reaction
LH028 10b	0,2	10	24	150	$BiCl_3$	5	Ar	no reaction
LH028 100	0,2	100	24	150	$BiCl_3$	5	Ar	n/a
LH027 10	0,2	10	24	150	$Bi(OTf)_3$	5	air	30
LH027 100	0,2	100	24	150	$Bi(OTf)_3$	5	air	n/a
LH041-A	12	1	2	120	Fascat 4100	0,5	air	no reaction
LH041-B	12	1	2	120	$Mn(OAc)_3$	0,5	air	no reaction
LH041-C	12	1	2	120	Fascat 4100	0,5	air	no reaction
LH046-A	12	1	2	150	$Mn(OAc)_3$	0,5	air	no reaction
LH046-B	12	1	2	150	Fascat 4100	0,5	air	no reaction

n/a: no reaction observed as hexanoic acid peak obscures all others in NMR

7.2.2.7 ***General procedure*** *for the reactivity study of guaiacol towards methyl hexanoate*

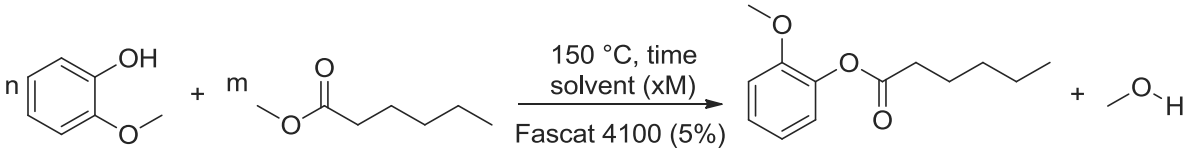

In 10 mL reaction tubes, guaiacol (2 mmol) and methyl hexanoate (1 equivalent) were mixed with butylstannoic acid (5%) and heated at 150 °C while stirring magnetically in a preheated sand bath together with xylenes solvent or without solvent. The reaction progress was monitored using thin liquid chromatography. Where solvent was used, distillation under reduced pressure (100 – 120 °C, 20 mbar) was used to separate it from the product. ^{1}H NMR was used to determine the result.

Conditions:

Conditions for the transesterification of methyl hexanoate with guaiacol

	n	m	time	solvent	concentration x	yield
	mmol	equivalents	h		M	%
LH023	2	1	5,5	-	-	5
LH030-C	2	1	48	-	-	24
LH033-B	2	1	20	xylenes	0,5	83

7.2.2.8 Guaiacol acetate

7.2.2.8.1 Procedure I: (LH050) Anhydride

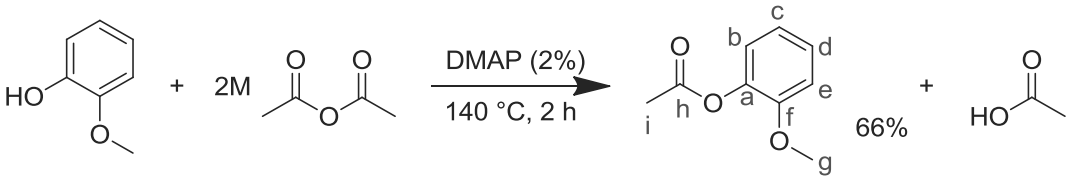

In a 50 mL round bottom flask, 1,24 g of guaiacol and 0,02 g of DMAP catalyst (0,2 mmol) were dissolved in 5 mL acetic anhydride and placed in a preheated sand bath (140 °C). The reaction

mixture was heated at reflux for 2 h and stirred magnetically. Excess acetic anhydride and acetic acid byproduct were removed by distillation under reduced pressure (20 mbar, 40 °C). The reaction product was purified by dissolving it in diethyl ether (20 mL) and washing it with water (3 x 10 mL). It was then dried over $MgSO_4$ and the solvent was removed using a rotary evaporator to give 1,10 g of brown oil (66%).

^{1}H NMR (300 MHz, $CDCl_3$) δ 7.20 (ddd, *J* = 8.3, 7.3, 1.8, 1H, Ar_cH), 7.04 (dd, *J* = 7.8, 1.7, 1H, Ar_bH), 7.00 – 6.90 (m, 2H, Ar_dH and Ar_eH), 3.83 (s, 3H; Ar-OC_gH_3), 2.32 (s, 3H, C_iH_3COOAr); **^{13}C NMR** – see procedure II below.

7.2.2.8.2 Procedure II: (LH173) Acid

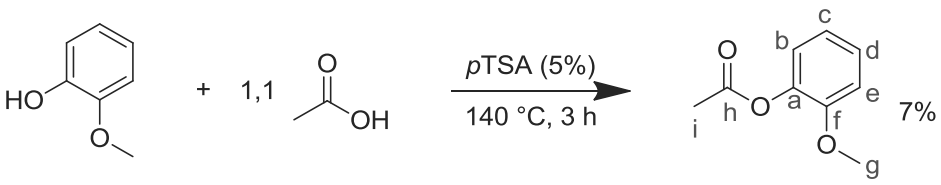

In a 50 mL round bottom flask, 2,48 g of guaiacol (20 mmol) was mixed with 1,32 g of acetic acid (22 mmol) and 0,19 g of *p*-TSA catalyst (1 mmol). The flask was equipped with a Vigreux column and placed in a preheated oil bath and the reaction was heated to 140 °C for 3 h while stirring magnetically. Unreacted acetic acid was then removed by distillation under reduced pressure (60 °C, 20 mbar). The product was purified by dissolving it in ethyl acetate (20 mL) and washing it three times with $NaHCO_3$ solution (sat., in water). It was then dried over Na_2SO_4, filtered and the solvent was removed using a rotary evaporator to give 2,02 g of pink powder which was found to still contain starting material. The purity was estimated using ^{1}H NMR (10 %) and the yield was calculated to be 7% (0,22 g).

^{1}H NMR – see procedure I; **^{13}C NMR (75 MHz, DMSO)** δ 168.87 (C_hOOAr), 151.27 (C_{arom}), 139.76 (C_{arom}), 127.17 (CH_{arom}), 123.13 (CH_{arom}), 120.83 (CH_{arom}), 112.93 (CH_{arom}), 55.83 (Ar-OC_gH_3), 20.52 (C_iH_3COOAr).

7.2.2.9 Guaiacol nonanoate: example LH175

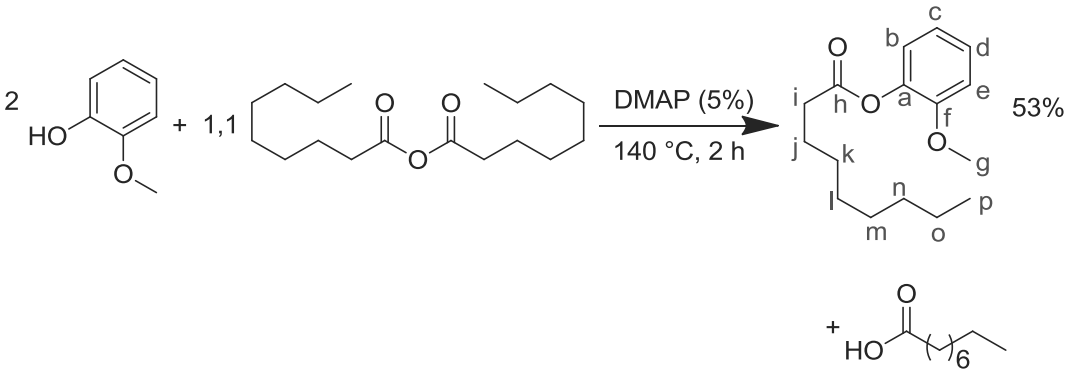

In a 50 mL round bottom flask equipped with a Vigreux column, 2,48 g of guaiacol (20 mmol) was reacted with 3,28 g of nonanoic anhydride (11 mmol) and 0,12 g of DMAP catalyst (1 mmol). The flask was placed in a preheated oil bath and heated to 140 °C for 3 h while it was stirred magnetically. After cooling, the product was dissolved in ethyl acetate (20 mL) and washed repeatedly with water (2 x 10 mL), $NaHCO_3$ (sat. in water, 3 x 10 mL), and water (3 x 10 mL). Brine (2 mL) was added to

improve phase separation. After washing, the ethyl acetate was removed using a rotary evaporator to give 4,95 g of product. The purity was determined by ^{1}H NMR to be 57%, corresponding to a yield of 53% (2,62 g).

^{1}H NMR (300 MHz, DMSO) δ 7.21 (ddd, *J* = 8.2, 7.4, 1.7, 1H, Ar_cH), 7.12 – 6.99 (m, 2H, Ar_bH and Ar_dH), 6.98 – 6.91 (m, 1H, Ar_eH), 3.75 (s, 3H, Ar-$OC_g\underline{H_3}$), 2.59 – 2.48 (m, 2H, $C_i\underline{H_2}COOAr$), 1.75 – 1.63 (m, 2H, $C_j\underline{H_2}$), 1.30 (s, 10H, $C_{k,l,m,n,o}\underline{H_2}$), 0.91 (t, *J* = 3.3, 3H, $C_p\underline{H_3}$); **^{13}C NMR (75 MHz, DMSO)** δ 171.04 (C_hOOAr), 151.20 (C_{arom}), 139.78 (C_{arom}), 126.79 (CH_{arom}), 122.82 (CH_{arom}), 120.53 (CH_{arom}), 112.74 (CH_{arom}), 55.60 (Ar-$O\underline{C_g}H_3$), 33.47 (C_iH_2), 31.60 (C_jH_2), 29.12 (C_kH_2), 29.04 (C_lH_2), 28.70 (C_mH_2), 24.81 (C_nH_2), 22.41 (C_oH_2), 13.96 ($CH_2\underline{C_p}H_3$).

7.2.2.10 ***General procedure*** *for catalyst study for the model reaction of guaiacol with acetic acid*

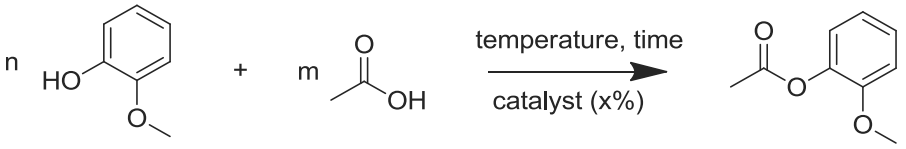

In 50 mL round bottom flask equipped with a Vigreux column, guaiacol was mixed with catalyst (5 - 20%) and acetic acid (1,1 - 175 equivalents) and heated while stirring magnetically. The reaction process was monitored by thin liquid chromatography. In order to purify the product, excess acetic acid was removed by distillation under reduced pressure (60 - 100 °C, 20 mbar). The product mixture was further diluted in ethyl acetate and washed with $NaHCO_3$ (sat.) and water. The solvent was removed using a rotary evaporator, and the result was examined by ^{1}H and ^{13}C NMR.

Conditions:

	n	m	time	temp.	catalyst	x	yield
	mmol	equiv.	h	°C		mol%	%
LH036-A	2	2	24	100	Fascat 4100	5	no reaction
LH036-B	2	10	24	100	Fascat 4100	5	no reaction
LH048	10	175	2	120	$Mn(OAc)_3$	4	no reaction
LH054	10	175	4	135	$Mn(OAc)_3$	4	31
LH049	1	53	1,3	120	$BiCl_3$	20	no reaction
LH169	20	1,1	3	140	$Mn(OAc)_3$	5	no reaction
LH171	20	1,1	3	140	$Bi(OTf)_3$	5	no reaction
LH172	20	1,1	3	140	DMAP	5	no reaction
LH173	20	1,1	3	140	*p*TSA	5	7

7.2.2.11 ***General procedure*** *for the catalyst study on the reaction of guaiacol with anhydrides:*

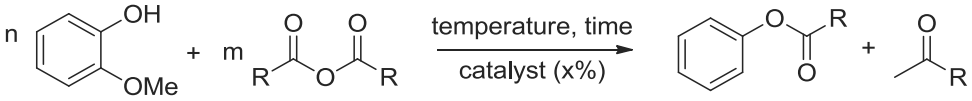

Guaiacol was mixed with catalyst (2 – 5%) and the anhydride (0,5 – 5,3 equivalents) in a round bottom flask equipped with a Vigreux column where acetic anhydride was used. The reaction mixture was heated while stirring magnetically, and the reaction progress was monitored using thin liquid chromatography. Where appropriate, the byproducts were removed by distillation under reduced

pressure (60 °C, 20 mbar) and the product was purified by diluting it in diethyl ether and washing it with $NaHCO_3$ (sat.) and water. The result was determined by ^1H NMR.

Conditions:

Conditions and results for the esterification of guaiacol with anhydrides

	R - group	n	m	time	temp.	catalyst	x	yield
		mmol	equiv.	h	°C		mol%	%
LH023	C_8H_{17}	4	0,5	5,5	150	Fascat 4100	5	no reaction
LH030-B	C_8H_{17}	4	0,5	48	150	Fascat 4100	5	65
LH175	C_8H_{17}	20	0,55	3	140	DMAP	5	53
LH036-C	CH_3	2	0,5	24	100	Fascat 4100	5	no reaction
LH050	CH_3	10	5,3	2	140	DMAP	2	66
LH052	CH_3	10	1,1	24	50	DMAP	2	no reaction

7.2.2.12 General procedure for reaction of guaiacol and citric acid

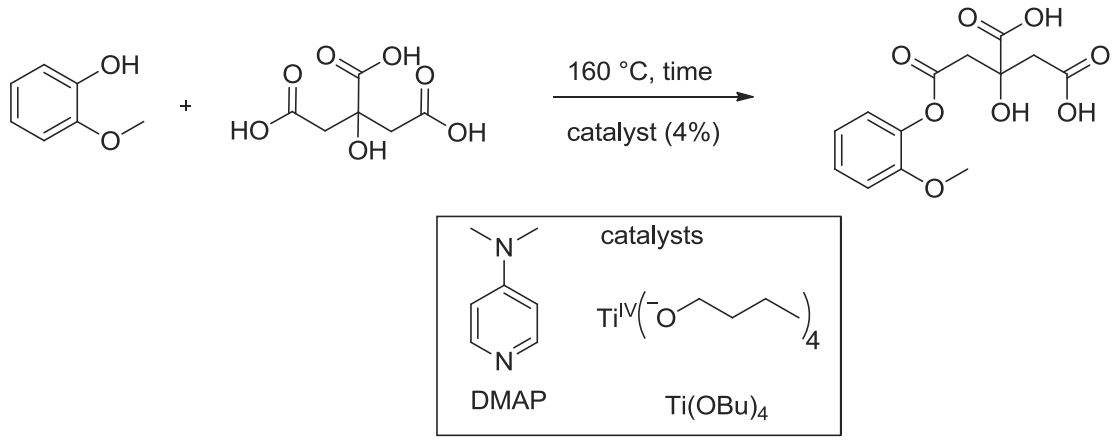

In a 50 mL round bottom flask equipped with a Vigreux column, guaiacol (10 mmol) was mixed with citric acid and a catalyst. The mixture was heated in an oil bath while stirring magnetically. The reaction progress was followed using thin liquid chromatography, and the result was examined using ^1H and ^{13}C NMR. Various degradation products as described by Wyrzykowski *et al.* and Barbooti *et al.* were observed, but no esterification product could be identified.[250, 251]

Conditions:

Conditions used for the reaction of citric acid with guaiacol

	catalysts	time	yield
		h	%
LH051	DMAP	1	no product
LH055	DMAP, $Ti(OBu)_4$	2	no product
LH056	$Ti(OBu)_4$	2	no product

7.2.3 Transformation of vanillin for further reactions

7.2.3.1 Perkin reaction: example LH143

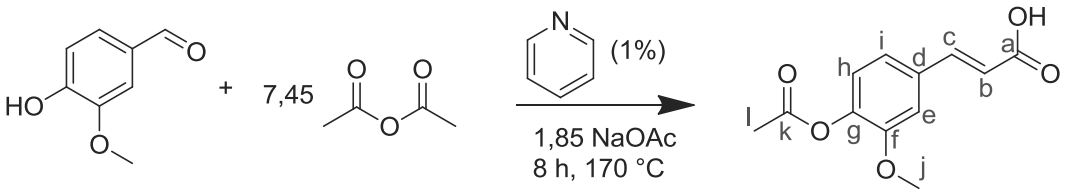

The Perkin reaction was conducted following the procedure published by Fosdick et al.[161] In a 100 mL round bottom flask, 15 g of vanillin (98,59 mmol) and 15 g of sodium acetate (182,86 mmol) were mixed. 75 mL acetic anhydride (734,65 mmol) and 0,075 mL pyridine catalyst (1 %) were added, and the mixture was heated at 170 °C in a preheated oil bath while stirring magnetically for 8 h. The product was poured over crushed ice (50 g) and heated at 130 °C while stirring until complete dissolution was achieved. The product was recrystallised in the refrigerator over night, filtered and washed with water. The thus obtained product was recrystallised again from dilute acetic acid (50 mL, 0,2 g/mL), filtered and dried on a rotary evaporator to give a yellow powder (12,43 g, 53%).

^{1}H NMR (300 MHz, DMSO) δ 12.38 (s, 1H, $C_aOO\underline{H}$), 7.58 (d, J = 16.0, 1H, $C_b\underline{H}COOH$), 7.47 (d, J = 1.7, 1H, $Ar_e\underline{H}$), 7.26 (dd, J = 8.2, 1.8, 1H, $Ar_i\underline{H}$), 7.11 (d, J = 8.1, 1H, $Ar_h\underline{H}$), 6.59 (d, J = 16.0, 1H, Ar-$C_c\underline{H}$), 3.82 (s, 3H, Ar-OC_j $\underline{H_3}$), 2.26 (s, 3H, $C_l\underline{H_3}COOAr$); **^{13}C NMR (75 MHz, DMSO)** δ 168.43 (C_aOOH), 167.62 ($CH_3\underline{C_k}OOAr$), 151.16 (C_{arom}), 143.37 (Ar-$\underline{C_c}H$), 140.82 (C_{arom}), 133.27 (C_{arom}), 123.21 ($CH_{arom.}$), 121.37 ($CH_{arom.}$), 119.54 ($\underline{C_b}HCOOH$), 111.84 ($\underline{C}H_{arom.}$), 55.99 (C_jH_3), 20.41 (C_lH_3).

The reaction procedure was varied as described in the following scheme and table:

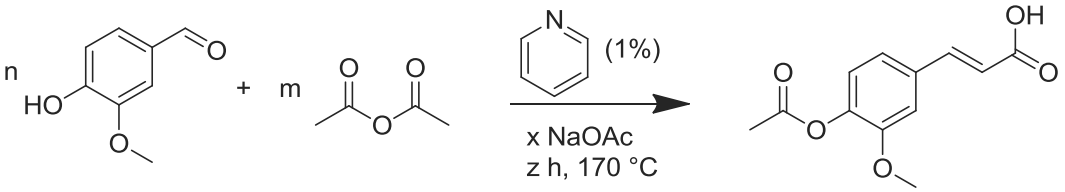

7.2.3.2 Conditions: Optimisation of Perkin reaction

	n	m	x	z time	yield
	g	equivalents	equivalents	h	%
LH064	2	7,45	1,85	2,75	25
LH073	4	7,45	1,85	6	4
LH080	4	7,45	1,85	6	18
LH086	4	7,45	1,85	6	6
LH089	4	7,45	1,85	7	27
LH093	4,56	1,5	2	6,5	0
LH099	12	7,45	1,85	6,5	33
LH101	12	7,45	1,85	6,25	35
LH106	12	7,45	1,85	8	27
LH111	12	7,45	1,85	7,5	49
LH129	12	7,45	1,85	8	35

	n	m	x	z time	yield
	g	equivalents	equivalents	h	%
LH136	15	7,45	1,85	8	51
LH138	15	7,45	1,85	8	36
LH141	15	7,45	1,85	7	38
LH143	15	7,45	1,85	8	53

7.2.3.3 ***Propane-1-ol-3-ferulate*** *(LH104)*

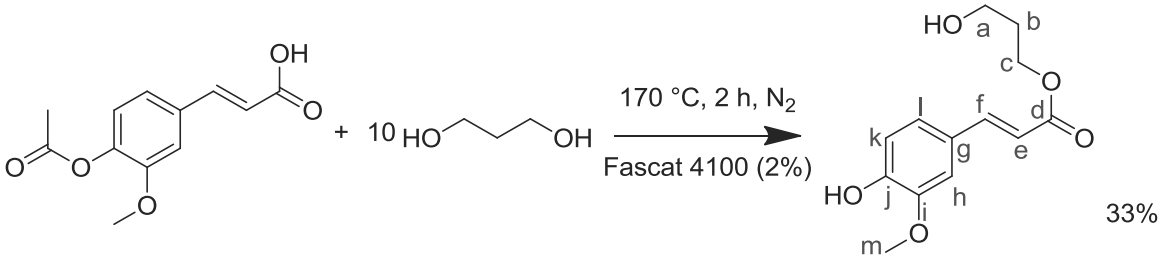

In a 50 mL round bottom flask, 1,18 g of acetylferulic acid (5 mmol) were mixed with 0,02 g of butylstannoic acid catalyst (2%) and diluted in 3,81 g of 1,3-propanediol (50 mmol), acting as a solvent and reagent. The flask was closed with a septum and equipped with a needle connected to a vacuum line and an open needle for gas outlet. It was placed in a preheated oil bath and heated to 170 °C for 2 h while stirring magnetically and bubbling N_2 through the reaction mixture. The resulting black oil was dissolved in dichloromethane (50 mL) and washed with water (2 x 20 mL). The organic phase was dried on a rotary evaporator and further purified using column chromatography with an ethyl acetate and cyclohexane eluant (1:1). After the solvent was removed on a rotary evaporator, a yield of 0,42 g (33%) was obtained.

^{1}H NMR (300 MHz, DMSO) δ 7.56 (d, *J* = 15.9, 1H, C_eHCOOR), 7.29 (d, *J* = 1.5, 1H, Ar_hH), 7.10 (d, *J* = 8.2, 1H, Ar_kH), 6.80 (t, *J* = 10.5, 1H, Ar_lH), 6.45 (d, *J* = 15.9, 1H, Ar-C_fH), 4.64 (s, 1H, OH), 4.20 (t, *J* = 6.5, 2H, $C_c\underline{H_2}OCO$), 3.82 (s, 3H, Ar-$OC_m\underline{H_3}$), 3.54 (t, *J* = 6.2, 2H, $C_a\underline{H_2}OH$), 1.80 (p, *J* = 6.4, 2H, $CH_2C_b\underline{H_2}CH_2$); **^{13}C NMR (75 MHz, DMSO)** δ 167.05 ($\underline{C_d}OOR$), 149.54 (C_{arom}), 148.19 (C_{arom}), 145.15 (Ar-$\underline{C_f}H$), 125.92 (C_{arom}), 123.27 (CH_{arom}), 115.80 ($\underline{C_e}HCOOR$), 114.80 (CH_{arom}), 111.33 (CH_{arom}), 61.44 ($\underline{C_c}H_2OCO$), 57.68 (Ar-$O\underline{C_m}H_3$), 55.86 ($\underline{C_a}H_2OH$), 31.90 (C_bH_2).

7.2.3.4 Hydrogenation of acetylferulic acid:

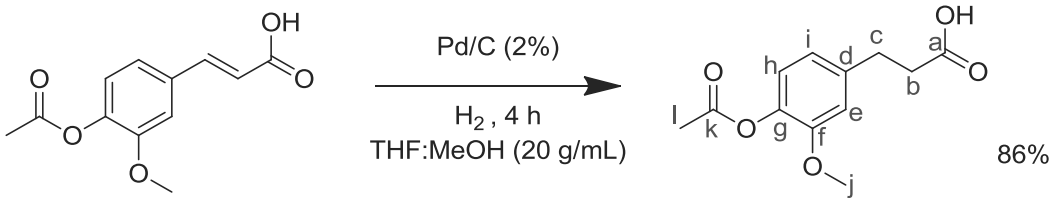

The hydrogenation of acetylferulic acid obtained from the Perkin reaction on vanillin was performed according to a procedure described by Mialon et al.[159] Acetylferulic acid (4,6 g) was dissolved in 23 mL THF (65%) and methanol (35%) and Pd/C (10%, 0,46 g) catalyst was added. The mixture was reacted in an autoclave and under H_2 (5 bar) for 4 h at room temperature, stirring magnetically. After all the hydrogen had reacted, the reaction mixture was filtered through celite and dried over $MgSO_4$. The remaining solvent was removed in a rotary evaporator, and the product was dissolved in THF (5

mL) and precipitatedt with hexane (20 mL) while being cooled with ice. The purified product was filtered and dried using a rotary evaporator to give a white / greyish powder (4.0 g, 86%).

^{1}H NMR (300 MHz, DMSO) δ 12.16 (s, 1H, $C_aOO\underline{H}$), 7.00 (d, J = 1.8, 1H, $Ar_e\underline{H}$), 6.95 (d, J = 8.0, 1H, $Ar_h\underline{H}$), 6.79 (dd, J = 8.1, 1.9, 1H, $Ar_i\underline{H}$), 3.75 (s, 3H, Ar-$OC_j\underline{H_3}$), 2.82 (t, J = 7.7, 2H, $C_b\underline{H_2}COOH$), 2.56 (t, J = 7.6, 2H, Ar-$C_c\underline{H_2}$), 2.23 (s, 3H, $C_l\underline{H_3}COOAr$); **^{13}C NMR (75 MHz, DMSO)** δ 174.02 (C_aOOH), 168.81 ($CH_3\underline{C_k}OOAr$), 150.72 (C_{arom}), 140.04 (C_{arom}), 137.69 (C_{arom}), 122.58 ($CH_{arom.}$), 120.20 ($CH_{arom.}$), 112.94 ($\underline{C}H_{arom.}$), 55.71 (C_jH_3), 35.37, 30.42 (Ar-$\underline{C_c}H_2$ and $\underline{C_b}H_2COOH$), 20.45 (C_lH_3).

7.2.4 Polymerisation of dihydroacetylferulic acid

7.2.4.1 Polydihydroferulic acid (LH118)

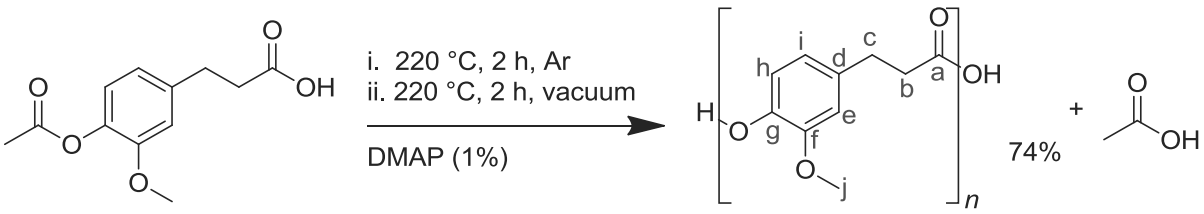

Dihydroacetylferulic acid was polymerised according to the procedure published by Mialon *et al.*[159] In a 10 mL reaction tube, 1 g of dihydroacetylferulic acid (4,23 mmol) obtained from transformation of vanillin as described above, was mixed with 5,6 mg DMAP catalyst (1%). The tube was flushed with argon, closed with a septum and equipped with an argon balloon. It was then heated in a preheated oil bath to 220 °C for 2 h while stirring magnetically. The tube was then connected to a vacuum line and the reaction was continued at 220 °C for 2 h under vacuum (5 mbar). After cooling down, the product was dissolved in a 3 : 4 mixture of trifluoroacetic acid and dichloromethane (7 mL), cooled with ice and precipitated by adding 10 mL methanol. The solvent was removed by vacuum filtration and dried overnight with a vacuum line (5 mbar) to obtain 0,60 g of a grey powder (74%).

^{1}H NMR (500 MHz, DMSO)* δ 7.05 (s, 1H, Ar_eH), 6.93 (d, *J* = 8.0, 1H, Ar_hH), 6.87 (d, *J* = 8.3, 1H, Ar_iH), 3.76 (s, 3H, Ar-$OC_j\underline{H_3}$), 3.01 (t, *J* = 7.3, 2H, $C_b\underline{H_2}$COOR), 2.92 – 2.89 (m, 2H, Ar-$C_c\underline{H_2}$); **^{13}C NMR (126 MHz, DMSO)*** δ 169.65 ($\underline{C_a}$OOR), 150.34 (C_{arom}), 138.60 (C_{arom}), 137.78 (C_{arom}), 121.78 (CH_{arom}), 119.78 (CH_{arom}), 113.27 (CH_{arom}), 55.54 (Ar-$O\underline{C_i}H_3$), 34.09, 29.56 (Ar-$\underline{C_c}H_2$ and $\underline{C_b}H_2$COOR).

*NMR was performed at 125 °C to achieve complete solubilisation in DMSO[d].

*7.2.4.2 **General procedure** for the polyesterification of dihydroacetylferulic acid*

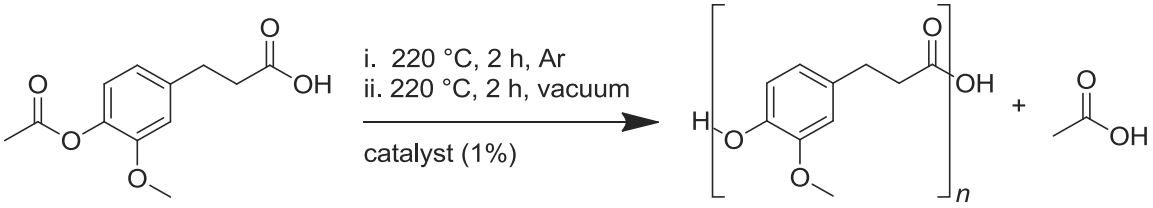

Dihydroacetylferulic acid was polymerised according to the procedure published by Mialon et al.[159] In a 10 mL reaction tube, 1 g dihydroacetylferulic acid (4,23 mmol) obtained from transformation of vanillin as described above, was mixed with catalyst (1%). The tube was flushed with argon, closed with a septum and equipped with an argon balloon. It was then heated in a preheated oil bath to

220 °C for 2 h while stirring magnetically. The tube was then connected to a vacuum line and the reaction was continued at 220 °C for 2 h under vacuum (5 mbar). After cooling down, the product was ground in a mortar and dissolved in a 1:3 mixture of trifluoroacetic acid and dichloromethane (8 mL), heating to 35 °C if necessary. The solution was then cooled with ice and precipitated by pouring it into methanol (30 - 50 mL). The solvent was removed by vacuum filtration and the solid product was ground with a spatula and dried overnight with a vacuum line (5 mbar). It was analysed by ^{1}H and ^{13}C NMR in a mixture of deuterated trifluoracetic acid and deuterated chloroform (1 : 3).

Conditions:

	catalyst	yield
		weight%
LH113	-	52
LH131	-	68
LH115	Fascat 4100	66
LH140	Fascat 4100	61
LH118	DMAP	74
LH133	DMAP	68
LH121	$Mn(OAc)_3$	61
LH134	$Mn(OAc)_3$	48
LH145	$Zn(OAc)_2$	57
LH146	$Ti(OBu)_4$	53

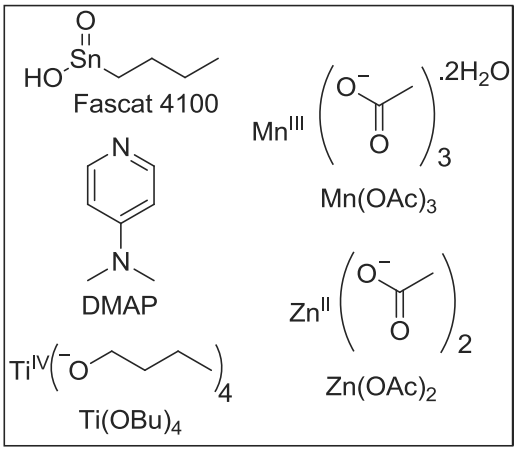

7.2.4.3 Reaction of dihydroacetylferulic acid with 1,3-propanediol (LH156-LH155-G)

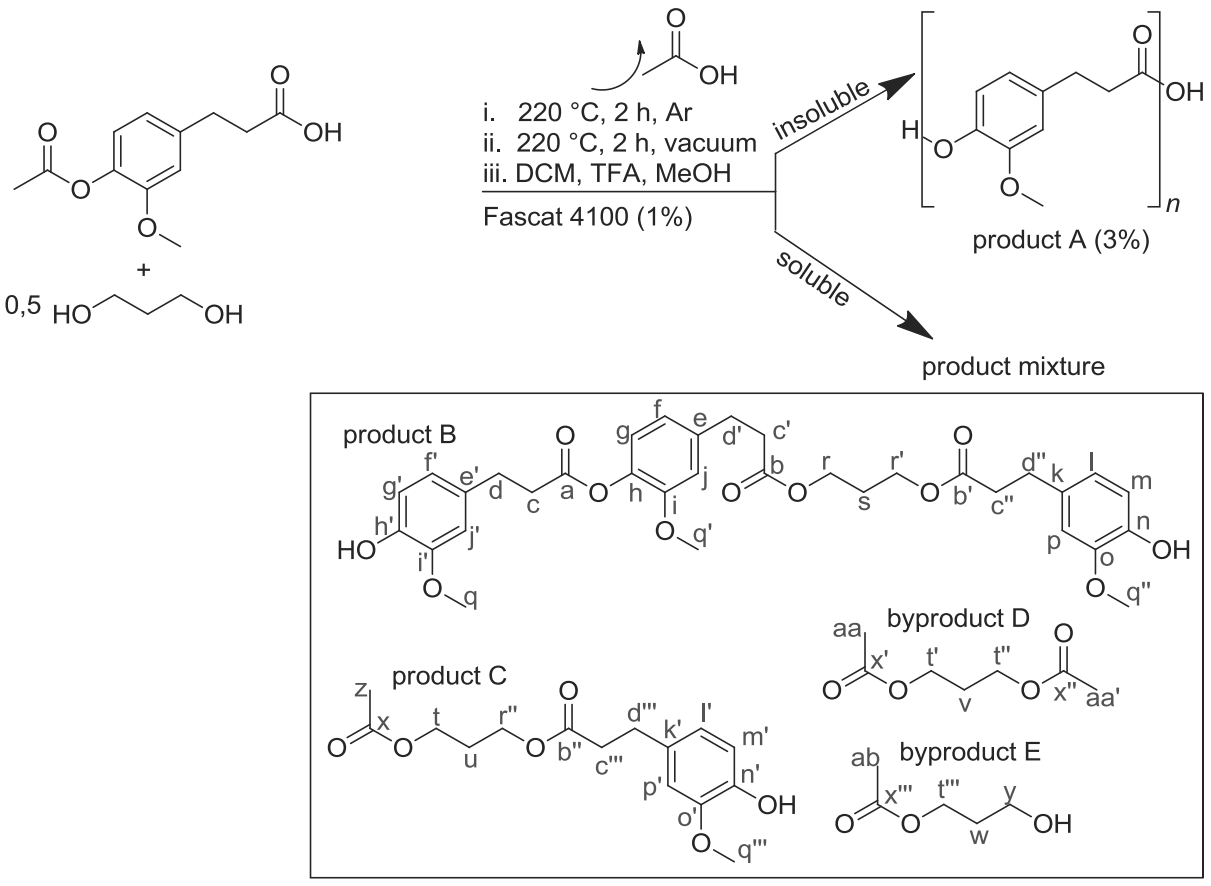

In a 10 mL reaction tube, 1,01 g dihydroacetylferulic acid (4,24 mmol) was mixed with 0,16 g 1,3-propanediol and 8,8 mg butylstannoic acid catalyst (1%). The tube was flushed with argon, closed with a septum and equipped with an argon balloon. It was then heated in a preheated oil bath to 220 °C for 2 h while stirring magnetically. The tube was then connected to a vacuum line and the reaction was continued at 220 °C for 2 h under vacuum (5 mbar). After cooling down, the product was ground in a mortar and dissolved in a 1:3 mixture of trifluoroacetic acid and dichloromethane (8 mL). The solution was then cooled with ice and a solid was precipitated by pouring it into methanol (30 -50 mL). The solid, polydihydroferulic acid (product A) was separated from the solvents by vacuum filtration, ground and dried overnight on a vacuum line to give 0,03 g of a grey powder (3%) which was analysed by ^{1}H and ^{13}C NMR. The soluble products (product B, C and byproducts D,E) were dried on a rotary evaporator and analysed with ^{1}H, ^{13}C, DEPT and HSQC NMR to illuminate its composition. It was found to contain 43% of product B, 32% of byproduct C, 16% of byproduct E and 9% of product D.

Product A: see above for NMR, same as LH118

7.2.4.3.1 Product B:

^{1}H NMR (300 MHz, DMSO) δ 6.77 (dd, *J* = 4.4, 1.8, 3H, $Ar_{j,j',p}H$), 6.67 (d, *J* = 7.9, 3H, $Ar_{g,g',m}H$), 6.62 – 6.53 (m, 3H, $Ar_{f,f',l}H$), 4.52 – 4.34 (m, 4H, $COOC_r\underline{H_2}CH_2C_{r'}\underline{H_2}OOC$), 3.74 (s, 9H, Ar-$OC_{q,q',q''}\underline{H_3}$), 2.73 (q, *J* = 7.3, 6H, $C_{c,c',c''}\underline{H_2}COOR$), 2.56 (t, *J* = 7.5, 6H, Ar-$C_{d,d',d''}\underline{H_2}CH_2$), 1.99 (dd, *J* = 8.3, 4.1, 2H, C_sH_2); **^{13}C NMR (75 MHz, DMSO)** δ 174.10 ($\underline{C_{b,b'}}OOCH_2$), 172.95 ($\underline{C_a}OOAr$), 147.58 ($C_{arom}$), 147.55 ($C_{arom}$), 144.94 ($C_{arom}$), 144.85 ($C_{arom}$), 131.87($C_{arom}$), 131.49 ($C_{arom}$), 131.43 ($C_{arom}$), 120.41 ($CH_{arom}$), 115.45 ($CH_{arom}$), 115.43 ($CH_{arom}$), 112.57 ($CH_{arom}$), 112.52 ($CH_{arom}$), 65.69 ($COO\underline{C_{r,r'}}H_2CH_2$), 55.60 (Ar-$O\underline{C_{q,q',q''}}H_3$), 35.89, 30.22 ($\underline{C_{c,c',c''}}H_2COOR$ and Ar-$\underline{C_{d,d',d''}}H_2CH_2$), 27.19 ($CH_2\underline{C_s}H_2CH_2$).

7.2.4.3.2 Product C:

^{1}H NMR (300 MHz, DMSO) δ 6.77 (dd, *J* = 4.4, 1.8, 1H, $Ar_{p'}H$), 6.67 (d, *J* = 7.9, 1H, $Ar_{m'}H$), 6.62 – 6.53 (m, 1H, $Ar_{l'}H$), 4.52 – 4.34 (m, 2H, $COOC_{r''}\underline{H_2}$), 4.13 – 3.98 (m, 2H, $CH_3COOC_t\underline{H_2}$), 3.74 (s, 3H, Ar-$OC_{q'''}\underline{H_3}$), 2.73 (q, *J* = 7.3, 2H, $C_{c'''}\underline{H_2}COOR$), 2.56 (t, *J* = 7.5, 2H, Ar-$C_{d'''}\underline{H_2}CH_2$), 1.70 (s, 2H, C_uH_2), 1.10 (s, 3H, $OOCC_z\underline{H_3}$); **^{13}C NMR (75 MHz, DMSO)** δ 174.10 ($\underline{C_{b''}}OOR$), 172.44 ($CH_3\underline{C_x}OOR$), 147.55 (C_{arom}), 144.85 (C_{arom}), 131.40 (C_{arom}), 120.41 (CH_{arom}), 115.43 (CH_{arom}), 112.52 (CH_{arom}), 65.55, 60.46 ($RCOO\underline{C_{r''}}H_2$ and $CH_3COO\underline{C_t}H_2$), 55.60 (Ar-$O\underline{C_{q'''}}H_3$), 35.60, 30.22, 30.13 (Ar-$\underline{C_{d'''}}H_2CH_2$, $\underline{C_{c'''}}H_2COOR$ and $CH_2\underline{C_u}H_2CH_2$), 21.36 ($\underline{C_z}H_3COOR$).

7.2.4.3.3 Byproduct D:

^{1}H NMR (300 MHz, DMSO) δ 4.13 – 3.99 (m, 4H, $COOC_{t',t''}\underline{H_2}$), 1.89 – 1.77 (m, 2H, $CH_2C_v\underline{H_2}CH_2$), 1.04 – 0.98 (m, 6H, $C_{aa,aa'}\underline{H_3}COOR$); **^{13}C NMR (75 MHz, DMSO)** δ 172.44 ($CH_3\underline{C_{x',x''}}OOR$), 60.82 ($COO\underline{C_{t',t''}}H_2$), 27.19 ($CH_2\underline{C_v}H_2CH_2$), 20.30 ($\underline{C_{aa,aa'}}H_3COOR$).

7.2.4.3.4 Byproduct E:

^{1}H NMR (300 MHz, DMSO) δ 4.13 – 3.99 (m, 2H, $COOC_{t'''}\underline{H_2}$), 2.46 (d, *J* = 7.3, 2H, C_yOH), 2.22 – 2.10 (m, 2H, $CH_2C_w\underline{H_2}CH_2$), 1.27 (m, 3H, $C_{ab}\underline{H_3}COOR$); **^{13}C NMR (75 MHz, DMSO)** δ 172.44 ($CH_3\underline{C_{x'''}}OOR$), 60.82 ($COO\underline{C_{t'''}}H_2$), 30.08 ($\underline{C_y}OH$), 27.77 ($CH_2\underline{C_w}H_2CH_2$), 20.30 ($\underline{C_{ab}}H_3COOR$).

7.2.4.4 General procedure for the polymerisation of dihydroacetylferulic acid in the presence of other monomers:

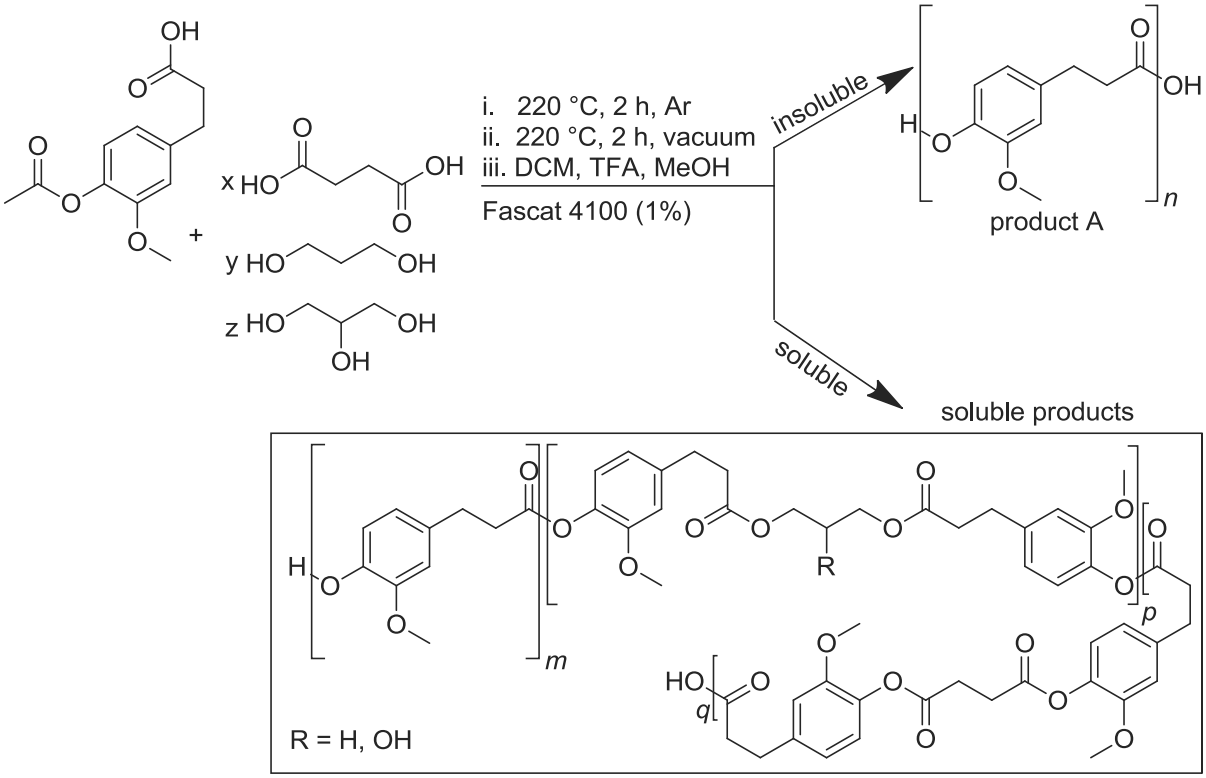

In a 10 mL reaction tube, 1 g dihydroacetylferulic acid (4,23 mmol) was mixed with catalyst (1%) and 1,3-propanediol (0,05 - 0,5 equivalents) and/or succinic acid (0,05 - 0,5 equivalents) or glycerol (0,1 equivalents). The tube was flushed with argon, closed with a septum and equipped with an argon balloon. It was then heated in a preheated oil bath to 220 °C for 2 h while stirring magnetically. The tube was then connected to a vacuum line and the reaction was continued at 220 °C for 2 h under vacuum (5 mbar). After cooling down, the product was ground in a mortar and dissolved in a 1:3 mixture of trifluoroacetic acid and dichloromethane (8 mL), heating to 35 °C if necessary. The solution was then cooled with ice and precipitated by pouring it into methanol (30 -50 mL). The solvent was removed by vacuum filtration and the solid product was ground with a spatula and dried overnight with a vacuum line (5 mbar). It was analysed by ^{1}H and ^{13}C NMR in a mixture of deuterated trifluoracetic acid and deuterated chloroform (1:3). The soluble condensation products of dihydroferulic acid and the other monomers present in the reaction was not recovered in most cases, and the yield was therefore estimated as the difference in yield of product A to that usually obtained in the reaction (64% on average).

Conditions:

	succinic acid x	**1,3-propanediol y**	**glycerol z**	**yield product A insoluble**	**estimated yield soluble products**
	equivalents	**equivalents**	**equivalents**	**weight %**	**weight %**
LH148	0,05	-	-	54	10
LH147	0,1	-	-	52	12
LH149	0,25	-	-	42	22

LH150	0,5	-	-	16	48
LH153	-	0,05	-	47	17
LH154	-	0,1	-	41	23
LH155	-	0,25	-	10	54
LH156	-	0,5	-	3	61
LH157	0,1	0,1	-	33	31
LH158	0,25	0,25	-	15	49
LH159	-	-	0,1	46	18

7.2.5 Reactions using ferulic acid

A mixture of cis- and trans-isomers of ferulic acid was used as purchased from Sigma Aldrich. Below, only the trans- form is shown, but it can be assumed that a mixture was present in starting materials and products in each case.

7.2.5.1 Reaction of ferulic acid with 1,3-propanediol (LH218)

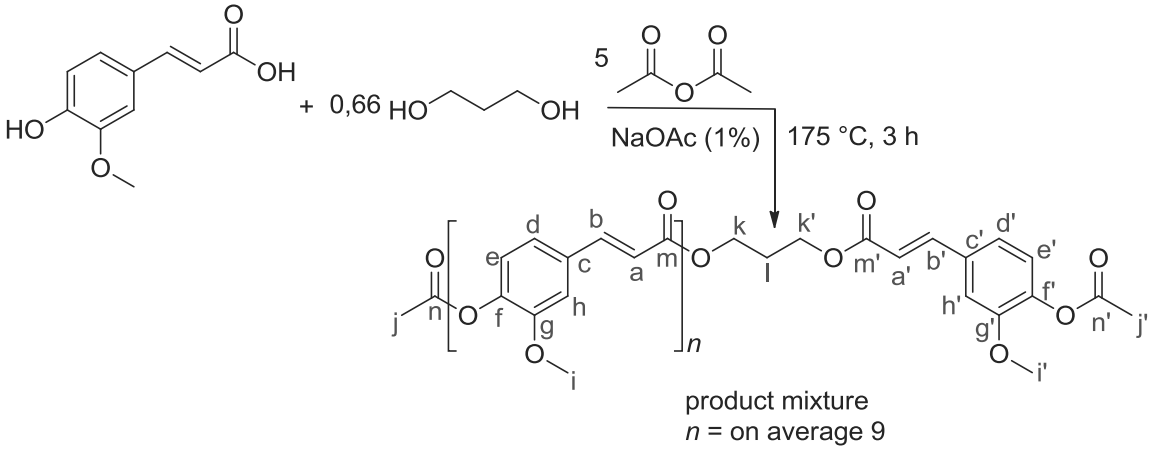

In a 25 mL round bottom flask, 1,17 g ferulic acid (6 mmol) and 4,9 mg sodium acetate catalyst (1%) were diluted in 3,06 g acetic anhydride (30 mmol) and 0,30 g 1,3-propanediol (4 mmol). The flask was placed into an oil bath and heated to 175 °C for three hours while stirring. The resulting mixture was too hard to stir, so ethanol was added (10 mL) and the product was dissolved by stirring at room temperature (3 h). The solvent was removed by vacuum filtration and the product was dried overnight with a vacuum line (5 mbar) to give 1,02 g of grey powder (69%). Low resolution mass spectrometry, ^{1}H and ^{13}C NMR were used to determine the nature of the product mixture. The integration due to repeating units are not reported below, but the relative sizes of peaks due to the ferulic acid and the 1,3-propanediol units indicate that they are present in approximately 10:1 quantities.

^{1}H NMR (400 MHz, $CDCl_3$ and TFA[d] (3:1)) δ 7.98 (s, 1H, C_{a}HCOOAr), 7.92 – 7.79 (m, 1H, $C_{a'}$HCOOCH$_2$), 7.42 – 7.06 (m, 6H, Ar$_{d,d',e,e',h,h'}$H), 6.73 (s, 1H, C_{b}HCHCOOAr), 6.63 – 6.37 (m, 1H, $C_{b'}$HCHCOOCH$_2$), 4.28 (s, 4H, COOC$_{k,k'}$H$_2$), 3.94 (d, *J* = 2.7, 6H, Ar-OC$_{i,i'}$H$_3$), 2.44 (s, 3H, C_{j}H$_3$), 2.33 (s, 3H, $C_{j'}$H$_3$), 2.08 (s, 2H, CH$_2$C$_l$H$_2$CH$_2$); **^{13}C NMR (101 MHz, $CDCl_3$ and TFA[d] (3:1))** δ 176.02 ($C_{m'}$OOCH$_2$), 173.29, 167.83, 167.80 (CH$_3$C$_n$OOAr, C_{m}OOAr and CH$_3$C$_{n'}$OOAr), 151.46, 151.30 (Ar-C_{b}H and Ar-$C_{b'}$H), 148.51 (C_{arom}), 148.47 (C_{arom}), 141.75 (C_{arom}), 133.57 (C_{arom}), 133.44 (C_{arom}), 123.60, 123.40 (C_{a}HCOOAr and $C_{a'}$HCOOCH$_2$),

122.35 (CH_{arom}), 122.30 (CH_{arom}), 116.53 (CH_{arom}), 116.36 (CH_{arom}), 112.26 (CH_{arom}), 112.22 (CH_{arom}), 62.76 ($COO\underline{C}_{k,k'}H_2CH_2$), 56.18, 56.15 (Ar-O$\underline{C}_iH_3$ and Ar-O$\underline{C}_{i'}H_3$), 27.44 ($CH_2\underline{C}_lH_2CH_2$), 20.84, 20.72 ($\underline{C}_iH_3COOAr$ and $\underline{C}_{i'}H_3COOAr$).

7.2.5.2 General procedure for the reaction of ferulic acid with 1,3-propanediol or 1,2-propanediol

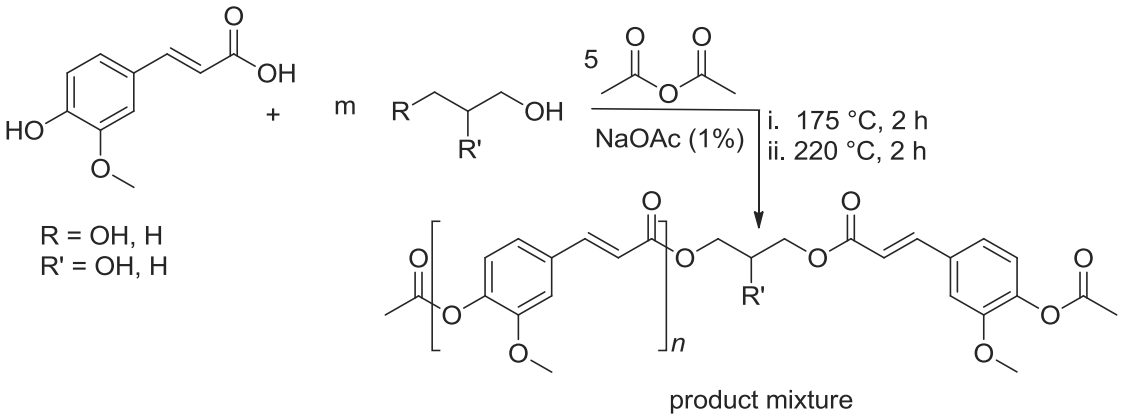

In a 25 mL round bottom flask, 1,17 g ferulic acid (6 mmol) and 4,9 mg sodium acetate catalyst (1%) were diluted in 3,06 g acetic anhydride (30 mmol) and 1,3-propanediol (2 – 6 mmol) or 1,2-propanediol (4 mmol). The flask was placed into an oil bath and heated to 175 °C for two hours while stirring, and then to 220 °C for 2 h or until stirring was no longer possible due to product consistency. Ethanol (10 - 20 mL) was added to the resulting mixture and the product was dissolved by stirring at room temperature. The solvent was removed by vacuum filtration and the product dried overnight with a vacuum line (5 mbar). Low resolution mass spectrometry, ^{1}H and ^{13}C NMR were used to determine the nature of the product mixture. Where appropriate, the ethanol soluble fraction was dried on a rotary evaporator and analysed by ^{1}H, ^{13}C NMR, low resolution mass spectrometry and size exclusion chromatography.

Conditions:

		R	R’	m	yield	yield of dried EtOH soluble fraction where recovered
	diol used			**mmol**	**weight %**	**g**
LH216	1,3-propanediol	-OH	-H	2	59	-
LH218	1,3-propanediol	-OH	-H	4	69	-
LH220	1,3-propanediol	-OH	-H	6	57	-
LH235	1,3-propanediol	-OH	-H	4	70	0,50
LH236	1,2-propanediol	-H	-OH	4	70	0,56

7.2.5.3 Reaction of ferulic acid with sebacic acid (LH222)

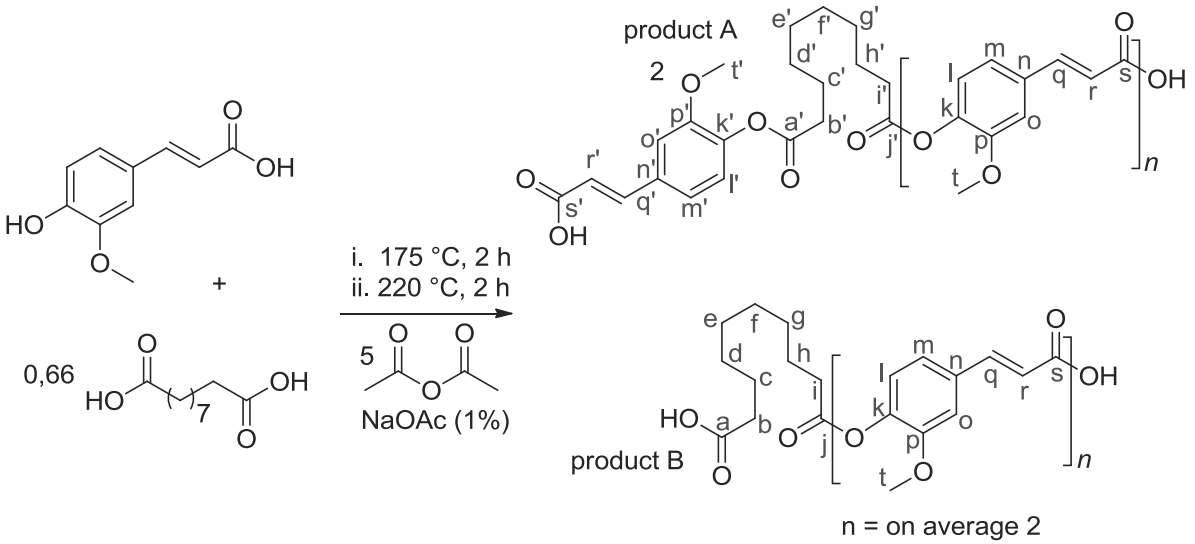

In a 25 mL round bottom flask, 1,17 g ferulic acid (6 mmol), 4,9 mg sodium acetate catalyst (1%) and 0,81 g sebacic acid (4 mmol) were diluted in 3,06 g acetic anhydride (30 mmol). The flask was placed into an oil bath and heated to 175 °C for two hours while stirring, and then to 220 °C for 2 h or until stirring was no longer possible due to product consistency. Ethanol (20 mL) and acetone (5 mL) were added to the resulting mixture and the product was dissolved by stirring at room temperature (48 h). The acetone was removed on a rotary evaporator and the ethanol was removed by vacuum filtration. The product was then dried overnight on a vacuum line (5 mbar). Low resolution mass spectrometry, ^{1}H and ^{13}C NMR were used to determine the nature of the product mixture. As for LH218, the integration due to repeating units is not reported. The relative peak sizes indicate that there are approximately two ferulic acid units for every sebacic acid units, and approximately twice as much of product A than of product B.

7.2.5.3.1 Product A:

^{1}H NMR (400 MHz, $CDCl_3$ and TFA^{d} (3:1)) δ 7.99 – 7.86 (m, 1H, $C_r\underline{H}COOAr$), 7.76 (ddd, *J* = 25.6, 16.0, 10.5, 1H, $C_{r'}\underline{H}COOH$), 7.38 – 7.00 (m, 6H, $C_{l,m,o,l',m',o'}H_{arom}$), 6.65 (ddd, *J* = 32.0, 18.3, 13.8, 1H, Ar-$C_q\underline{H}CHCOOAr$), 6.55 – 6.27 (m, 1H, Ar-$C_{q'}\underline{H}CHCOOH$), 3.91 – 3.82 (m, 6H, Ar-$OC_{t,t'}\underline{H}_3$), 2.29 – 2.27 (m, 4H, $OOCC_{b',i'}\underline{H}_2$), 1.32 – 1.24 (m, 12H, $C_{c',h'}\underline{H}_2$, $C_{d',g'}\underline{H}_2C_{e',f'}\underline{H}_2$); **^{13}C NMR (101 MHz, $CDCl_3$ and TFA^{d} (3:1))** δ 177.90 ($\underline{C}_{s'}OOH$), 173.07, 172.01, 166.92 ($\underline{C}_{i'}OOAr$, $\underline{C}_{a'}OOAr$ and $\underline{C}_sOOAr$), 151.53, 151.41 (Ar-$\underline{C}_{q'}H$ and Ar-$\underline{C}_qH$), 148.30 (C_{arom}), 147.94 (C_{arom}), 141.86 (C_{arom}), 141.79 (C_{arom}), 133.40 (C_{arom}), 133.18 (C_{arom}), 123.56, 123.42 ($\underline{C}_{r'}HCOOH$ and $\underline{C}_rHCOOAr$), 122.18 (CH_{arom}), 122.11 (CH_{arom}), 116.52 (CH_{arom}), 116.45 (CH_{arom}), 112.02 (CH_{arom}), 111.95 (CH_{arom}), 56.16, 56.12 (Ar-$O\underline{C}_{t'}H_3$ and Ar-$O\underline{C}_tH_3$), 34.77 ($\underline{C}_{b',l'}H_2COOAr$), 30.95, 29.15 ($C_{d',g'}H_2$ and $C_{c',h'}H_2$), 24.60 ($C_{e',f'}H_2$).

7.2.5.3.2 Product B:

^{1}H NMR (400 MHz, $CDCl_3$ and TFA^{d} (3:1)) δ 7.98 – 7.87 (m, 1H, $C_r\underline{H}COOAr$), 7.25 – 7.01 (m, 3H, $C_{l,m,o,l',m',o'}H_{arom}$), 6.72 – 6.60 (m, 1H, Ar-$C_q\underline{H}CHCOOAr$), 3.93 – 3.82 (m, 3H, Ar-$OC_{t,t'}\underline{H}_3$), 2.72 – 2.58 (m, 2H, $ArOOCC_i\underline{H}_2$), 2.43 – 2.36 (m, 2H, $HOOCC_b\underline{H}_2$), 1.84 – 1.71 (m, 2H, $C_h\underline{H}_2$), 1.70 – 1.57 (m, 2H, C_cH_2), 1.50 – 1.21 (m, 8H, $C_{g,d}\underline{H}_2$, $C_{e,f}\underline{H}_2$); **^{13}C NMR (101 MHz, $CDCl_3$ and TFA^{d} (3:1))** δ 174.65, 173.07, 169.75 (C_jOOAr, C_aOOH and C_sOOAr), 151.53 (Ar-$\underline{C}_qH$), 148.30 (C_{arom}), 141.86 (C_{arom}), 133.40 (C_{arom}), 123.56 ($\underline{C}_rHCOOAr$), 122.16 (CH_{arom}), 116.52 (CH_{arom}), 112.02 (CH_{arom}), 56.07 (Ar-$O\underline{C}_tH_3$), 34.28, 34.03

(C_iH_2COOAr and C_bH_2COOH), 30.76, 30.56, 29.08, 28.99 (C_cH_2, C_hH_2, C_dH_2 and C_gH_2), 25.02, 24.99 (C_fH_2 and C_eH_2).

7.2.5.4 ***General procedure*** *for the reaction of ferulic acid with sebacic acid*

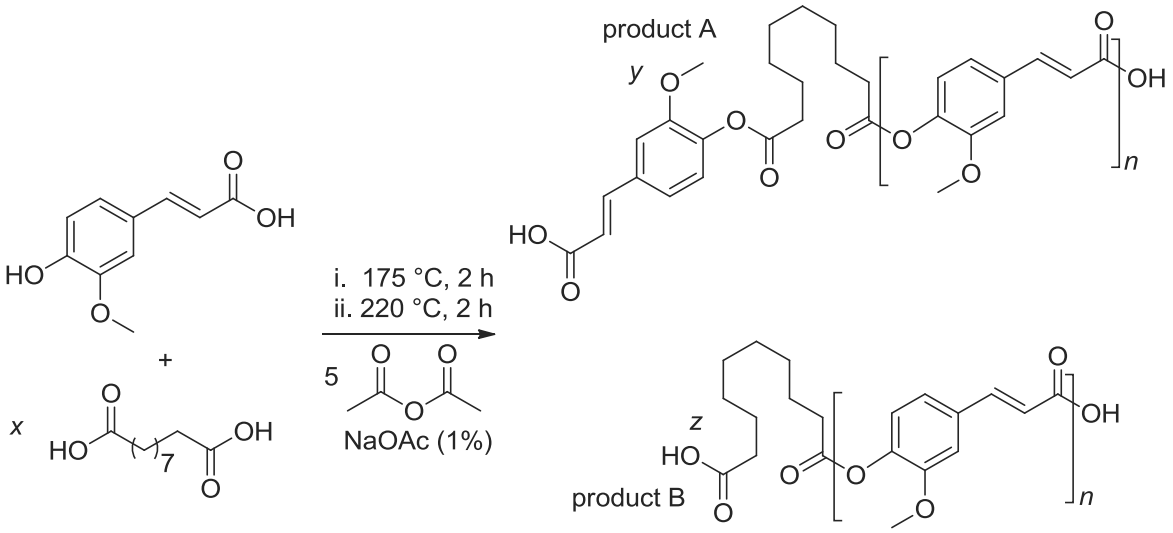

In a 25 mL round bottom flask, 1,17 g ferulic acid (6 mmol), 4,9 mg sodium acetate catalyst (1%) and sebacic acid (2 – 6 mmol) were diluted in 3,06 g acetic anhydride (30 mmol). The flask was placed into an oil bath and heated to 175 °C for two hours while stirring, and then to 220 °C for 2 h or until stirring was no longer possible due to product consistency. Ethanol (10 - 20 mL) and acetone (0 – 5 mL) were added to the resulting mixture and the product was dissolved by stirring at room temperature. The solvent was removed by vacuum filtration and the product washed with ethanol before being dried overnight with a vacuum line (5 mbar). Low resolution mass spectrometry, ^{1}H and ^{13}C NMR were used to determine the nature of the product mixture. The results are discussed in the results and discussion section.

Conditions:

	***x* - quantity sebacic acid**	***y/z***	**yield**
	mmol	**%**	**weight %**
LH221	2	28	49
LH222	4	69	22
LH226	6	0	28

7.2.5.5 Polymerisation of ferulic acid with 1,3-propanediol and sebacic acid

The reaction procedure was inspired by the "solvent polymerisation" method used to make liquid crystalline polymers based on ferulic acid as published for example by Du *et al.* and Matsusaki *et al*.[145, 155] In a 250 mL three necked round bottom flask equipped with a mechanical stirrer and a Vigreux column and connected to a vacuum line, 12,62 g ferulic acid (65 mmol), 5,06 g sebacic acid (25 mmol) and 53,3 mg sodium acetate catalyst (1%) were diluted in 1,90 g 1,3-propanediol (25 mmol) and 33,18 g acetic anhydride (5 equivalents). The flask was purged with nitrogen (3 times) and placed in an oil bath which was then heated to 175 °C. Nitrogen was bubbled through the reaction mixture, which was stirred mechanically. After 90 min, no more reflux of acetic anhydride or acetic

acid was visible, so the Vigreux column was removed and the temperature was raised to 185 °C. After 2 h, stirring was no longer possible due to product consistency, so the reaction mixture was cooled down and acetone (80 mL) was added to aid removal from the flask. After stirring for 2 h, the mixture was transferred to a beaker, ethanol (50 mL) was added to decrease solubility and the solid part was removed with vacuum filtration. This was repeated twice until no more precipitate was observed. The solid fraction was ground in a mortar and dried overnight under vacuum to obtain 12,74 g of a fine yellow powder. The remaining fraction was dried on a rotary evaporator to obtain a sticky yellow gum. This was further purified using a Soxhlet extractor (250 mL ethanol, overnight). The thus washed fraction was dried under vacuum to give 2,55 g of yellow powder (total insoluble yield: 78%). The ethanol soluble fraction was dried on a rotary evaporator to give 3,03 g of brown oil (17% of overall product obtained). Both soluble and insoluble products were analysed by ^{1}H and ^{13}C NMR as well as low resolution mass spectrometry.

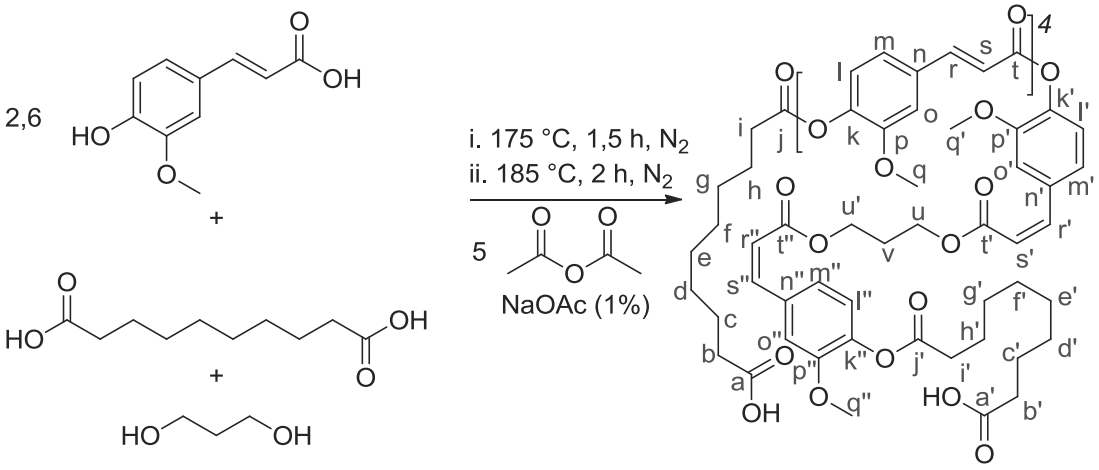

7.2.5.5.1 Insoluble fraction:

^{1}H NMR (300 MHz, $CDCl_3$ and TFA[d] (3:1)) δ 7.93 (ddd, *J* = 24.6, 15.9, 7.0, 6H, $C_{s,s',s''}\underline{H}COOR$), 7.45 – 7.02 (m, 18H, $Ar_{l,l',l'',m,m',m'',o,o',o''}H$), 6.82 – 6.41 (m, 6H, Ar-$C_{r,r',r''}H$), 4.33 – 4.17 (m, 4H, $COOC_{u,u'}\underline{H_2}$), 3.94 (t, *J* = 6.6, 18H, Ar-$OC_{q,q',q''}H_3$), 2.71 (s, 4H, $C_{b,b'}\underline{H_2}COOH$), 2.45 (d, *J* = 3.9, 4H, $C_{i,i'}H_2COOAr$), 2.13 – 2.02 (m, 2H, $CH_2C_v\underline{H_2}CH_2$), 1.83 (s, 4H, $C_{c,c'}H_2$), 1.70 (s, 1H, $C_{h,h'}H_2$), 1.34 (dd, *J* = 19.5, 12.9, 16H, $C_{d,d',f,f',e,e',g,g'}H_2$); **$^{13}C$ NMR (75 MHz, $CDCl_3$ and TFA[d] (3:1))** δ 176.24 ($C_{a,a'}OOH$), 173.72, 173.62, 168.13 (C_tOOAr, $C_{t',t''}OOR$ and $C_{j,j'}OOAr$), 151.46, 151.35, 151.27 (Ar-$C_{r'}H$, Ar-C_rH and Ar-$C_{r''}H$), 148.72 (C_{arom}), 148.64 (C_{arom}), 141.87 (C_{arom}), 141.82 (C_{arom}), 141.78 (C_{arom}), 133.68 (C_{arom}), 133.56 (C_{arom}), 123.65, 123.46 ($C_{s',s''}HCOOR$ and $\underline{C_s}HCOOAr$), 122.49 (CH_{arom}), 122.42 (CH_{arom}), 122.39 (CH_{arom}), 116.53 (CH_{arom}), 112.42 (CH_{arom}), 112.34 (CH_{arom}), 112.26 (CH_{arom}), 62.70 ($COO\underline{C_{u,u'}}H_2$), 56.23, 56.14 (Ar-$OC_qH_3$ and Ar-$OC_{q',q''}H_3$), 34.43, 34.12 ($\underline{C_{i,i'}}HCOOAr$ and $\underline{C_{b,b'}}H_2COOH$), 29.20, 29.13, 29.05 ($C_{c,c'}H_2$, $C_{h,h'}H_2$, $C_{d,d',g,g'}H_2$), 25.72, 25.06, 24.72 ($C_{f,f'}H_2$, C_vH_2 and $C_{e,e'}H_2$).

7.2.5.5.2 Soluble fraction:

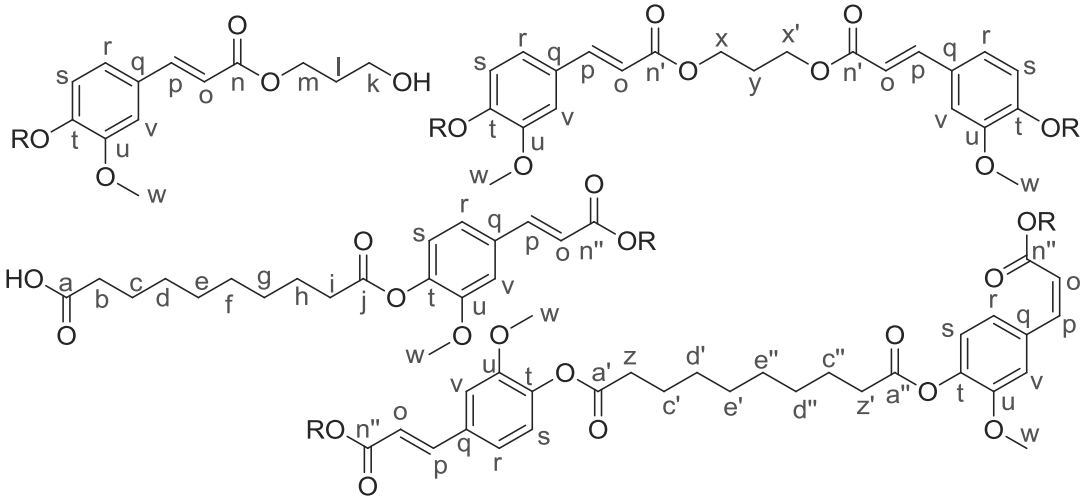

^{1}H NMR (300 MHz, $CDCl_3$ and TFA^{d} (3:1)) δ 7.79 – 7.59 (m, 1H, C_oHCOOR), 7.17 – 6.87 (m, 3H, $Ar_{r,s,v}H$), 6.45 – 6.21 (m, 1H, Ar-C_pH), 4.35 – 4.23 (m, 2H, $COOC_m\underline{H_2}$), 4.10 (dt, *J* = 14.4, 6.7, 4H, $COOC_{x,x'}H_2$), 3.77 – 3.74 (m, 3H, Ar-OC_wH_3), 3.69 (d, *J* = 7.1, 2H, C_kH_2OH), 2.54 (td, *J* = 7.4, 3.6, 2H, C_bH_2COOH), 2.32 (dd, *J* = 7.5, 3.6, 2H, C_iH_2COOAr), 2.28 (d, *J* = 1.6, 4H, $C_{z,z'}H_2COOAr$), 2.08 – 1.98 (m, 2H, $CH_2C_y\underline{H_2}CH_2$), 1.99 (s, 2H, $CH_2C_l\underline{H_2}CH_2$), 1.76 – 1.61 (m, 2H, C_cH_2), 1.60 – 1.42 (m, 2H, C_hH_2), 1.21 (dddd, *J* = 13.1, 12.2, 8.8, 5.7, 20H, $C_{c,c',c'',h,d,d',d'',g,e,e',e'',f}H_2$); **^{13}C NMR (75 MHz, $CDCl_3$ and TFA^{d} (3:1))** δ 181.78, 178.27, 177.82, 175.14, 173.09, 172.57 (C_jOOAr, $C_{n''}OOAr$, C_aOOH, $C_{n'}OOR$, $C_{a,a'}OOAr$ and C_nOOR), 151.52 (Ar-C_pH), 148.18 (C_{arom}), 141.78 (C_{arom}), 133.47 (C_{arom}), 123.37 (C_oCOOR), 122.12 (CH_{arom}), 116.51 (CH_{arom}), 112.08 (CH_{arom}), 64.87, 62.57 ($COO\underline{C_m}H_2$ and $COO\underline{C_{x,x'}}H_2$) , 59.25 ($C_kH_2OH$), 56.01 (Ar-$OC_wH_3$), 34.73, 34.56, 34.26, 34.00 ($\underline{C_i}H_2COOAr$, C_lH_2, $\underline{C_b}H_2COOH$ and $C_{z,z'}H_2COOAr$), 29.12, 29.05, 28.98, 27.53 (C_hH_2, C_cH_2, C_yH_2 and $C_{c',c''}H_2$), 25.00, 24.98, 24.92, 24.65, 24.63 ($C_{e,f}H_2$, $C_{d',d''}H_2$, C_gH_2, C_dH_2 and $C_{e',e''}H_2$).

7.2.5.6 ***General procedure*** *for the polymerisation of ferulic acid with 1,3-propanediol and sebacic acid:*

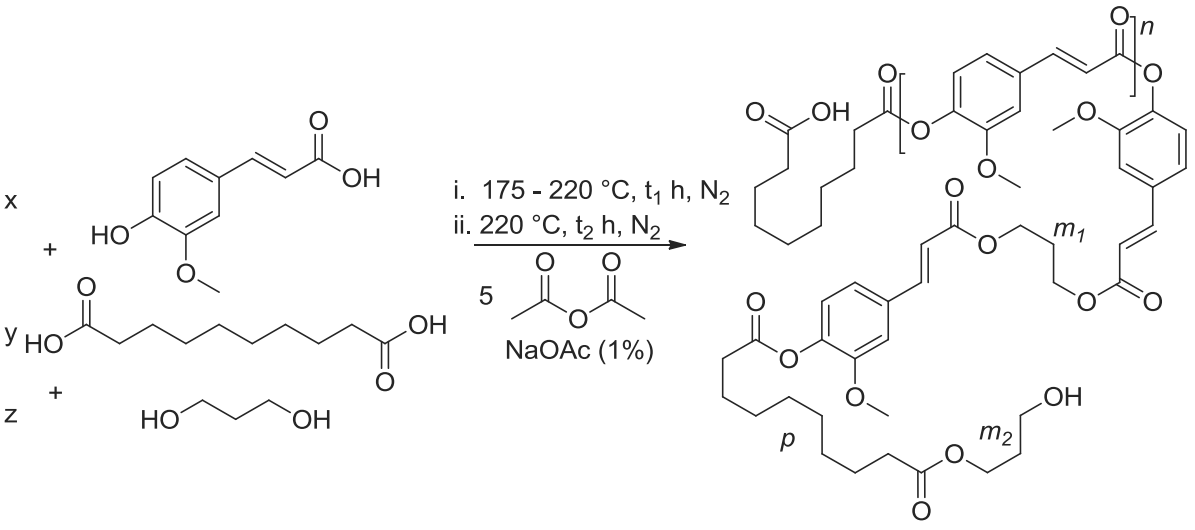

The reaction procedure was inspired by the "solvent polymerisation" method used to make liquid crystalline polymers based on ferulic acid as published for example by Du *et al* and Matsusaki *et al*.[145, 155] In a 250 mL three necked round bottom flask equipped with a mechanical stirrer and a Vigreux column and connected to a vacuum line, ferulic acid (2,78 - 185 mmol), sebacic acid (0,38 – 1

equivalents) and sodium acetate catalyst (1%) were diluted in 1,3-propanediol (0,38 – 1,1 equivalents) and acetic anhydride (5 equivalents). The flask was purged with nitrogen (3x) and placed in an oil bath which was then heated to 175 °C. Nitrogen was bubbled through the reaction mixture, which was stirred mechanically. The temperature was gradually increased until up to 220 °C until no more acetic acid or acetic anhydride reflux was observed (reaction time 1). Then the Vigreux column was removed and the reaction temperature kept at 220 °C. When stirring was no longer possible due to product consistency (after reaction time 2), the reaction mixture was cooled down and acetone was added to aid removal from the flask. The mixture was stirred at room temperature until a reasonable degree of dissolution was achieved and then transferred to a beaker. Ethanol was added to decrease solubility and the solid part was removed with vacuum filtration and washed with more ethanol. Depending on product consistency and solubility, it was further purified using work-up procedures II-V. All final products were dried overnight under vacuum (5 mbar).

7.2.5.6.1 Work-up methods:

I. The product was purified as described above, no further purification was performed.

II. Where it was not possible to filter the product / acetone / ethanol mixture, the solvents were removed on a rotary evaporator, and the product was washed with ethanol in a Soxhlet extraction instead (30 mL, 30 h).

IIb. After a part of the product had precipitated, the part remaining in solution could no longer be filtered. It was dried and washed with ethanol in a Soxhlet extraction.

III. When no precipitation upon the addition of ethanol was observed, the majority of the acetone was removed on a rotary evaporator. More ethanol was added and the product was stirred at room temperature until a good dispersion was observed. The precipitated product was then filtered off and further washed with ethanol.

IV. Instead of acetone, only ethanol (20 mL) was added to the batch after the reaction finished. The mixture was stirred for two nights and separated by vacuum filtration, and washed further with ethanol (3 x 5 mL).

V. Before the work-up was started, the solvent separated from the product by distillation under reduced pressure (20 mbar, 110 °C – 350 °C). The resulting product was then dissolved in acetone and precipitated with ethanol, followed by filtration, as described in procedure I.

7.2.5.6.2 Conditions and results:

	x	y	z	time 1	time 2	work-up	yield	monomer ratio			
	mmol	equiv.	equiv.	h	h	method	%	n : m : p			$\%m_1$
LH200	90	0,56	0,56	2,5	2,5	I	41	10	1,4	3,8	70
LH205	30	1	1	2	2	II	28	10	2,2	4,0	60
LH208	65	0,38	0,38	1,5	2	IIb	78	10	1,3	3,4	69
LH209[a]	45	0,56	0,56	2,5	1	I	44	10	0,1	3,0	100
LH211	70	0,5	0,57	2,5	4,25	III	82	10	3,4	3,9	31
LH212	80	0,38	0,44	3	1	III	93	10	1,6	3,1	55
LH213	50	1	1,1	8,5	0	III	52	10	3,2	7,6	65
LH214[b]	50	1	1,1	6,5	0,2	III	51	10	3,3	6,7	67
LH215[c]	50	1	1,1	6	0,5	IIb	38	10	3,3	4,1	61

LH217[d]	50	1	0,78	7	0,2	III	54	10	2,8	7,6	46
LH223[b,c]	50	1	1,1	8	0,2	III	40	10	3,8	5,6	66
LH225[b,c,e]	50	1	1,1	22,5	2,5	III	48	10	12,3	10,9	59
LH229[f]	2,78	0,67	0,67	6,5	0	IV	43	10	-	4,9	-
LH230	2,78	0,67	0,67	4	0	IV	75	10	2,6	4,1	49
LH244[a,e,g]	185	0,27	0,27	17,5	0	V	22	-	-	-	-
LH245[a,g]	32,5	0,38	0,38	22	0	IIb	31	-	-	-	-
LH246[a,e,g]	32,5	0,38	0,38	28	0	I	50	-	-	-	-
LH247[a,e,g]	30	1	1	33	0	V	32	-	-	-	-

Deviations from the general procedure: **a)**1,2-propanediol was used instead of 1,3-propanediol; **b)**In addition to NaOAc (1%), butylstannoic acid catalyst (1%) was also added to the reaction mixture; **c)**1,3-propanediol was not present in the reaction mixture when heating was started, it was added after: 1.75 h (LH215), 2 h (LH223), 6 h (LH225), **d)**Glycerol (0,15 equivalents) was added to the reaction mixture in addition to 1,3-propanediol; **e)**The reaction mixture was heated more slowly in the beginning of the reaction: 155 °C - 3 h, 165 °C - 2 h, then 175 °C (LH225); 130 °C – 2 h, 140 °C – 1,5 h, 150 °C – 1 h, 160 °C – 2 h, then 170 °C (LH244); 140 °C – 1,5 h, 150 °C – 8 h, then 175 °C (LH246); 145 °C – 6 h, then 170 °C (LH247); **f)**Dihydroacetylferulic acid was used instead of ferulic acid; **g)**Tamisolve solvent (200 mL – LH244; 50 mL – LH245, LH246, LH247) were added to the reaction mixture, and it was stirred magnetically. Due to the overlapping of tamisolve signals with the aliphatic product peaks, the ratio of different monomers in the product could not be determined in these cases.

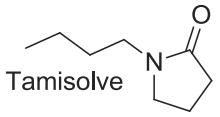

7.2.5.6.3 Average product composition:

The average product composition was determined from ^{1}H NMR by comparing the peak area of the aromatic hydrogens (s,r,v; 7.17 – 6.87) and the methoxy group CH_3 (w; 3.69) to that of the CH_2 group adjacent to the free acid group of a reacted sebacic acid monomer (b,) and the CH_2 groups in the middle of a sebacic acid monomer (d,e,f,g) and to the CH_2 groups in α- and β- position to the ester group on monoreacted 1,3-propanediol (m, l) and on twice reacted 1,3-propanediol (x,y).[LXIII]

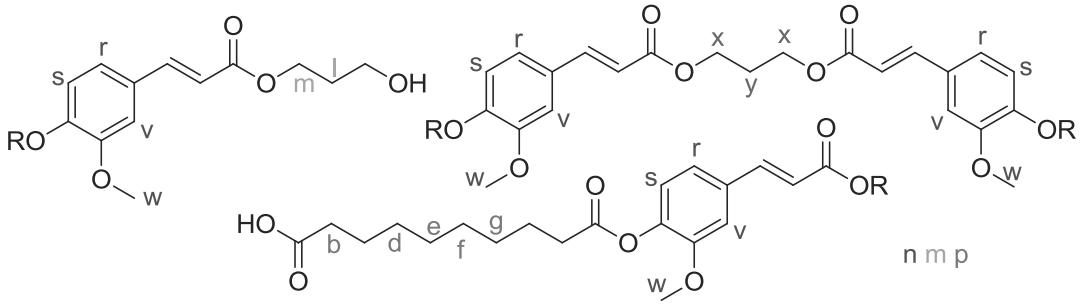

$$\%\,m1 = \frac{1}{2}\left(\frac{\frac{x}{4}}{\frac{x}{4}+\frac{m}{2}} + \frac{\frac{y}{2}}{\frac{y}{2}+\frac{l}{2}}\right)$$

$$n = \frac{1}{2}\left(\frac{r,s,v}{3} + \frac{w}{3}\right) \quad m = \frac{x,m}{4} * \%m1 + \frac{x,m}{2} * (1 - \%m1) \quad p = \frac{1}{2}\left(\frac{b}{2} + \frac{d,e,f,g}{8}\right)$$

[LXIII] See annexe for an example of one of the NMR spectra used for calculation.

7.2.5.7 Reaction of ferulic acid with 1,3-propanediol, 175 °C (LH250)

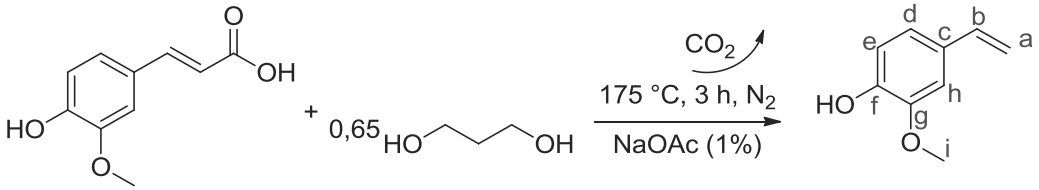

In a 25 mL round bottom flask closed with a septum connected to a nitrogen line and equipped with a needle used as a nitrogen outlet, 1,17 g ferulic acid (6 mmol), 0,3 g 1,3-propanediol (4 mmol) and 4,9 mg sodium acetate catalyst (1%) were heated to 175 °C for 3 h while bubbling nitrogen through the reaction mixture and stirring magnetically. A liquid was observed to evaporate and condense at the nitrogen outlet. This was found to be a mixture of 1,3-propanediol and the decarboxylation product of ferulic acid, 4-vinyl guaiacol (boiling point: 224 °C). This mixture was equally found to be the major component of the reaction mixture remaining in the flask.

^{1}H NMR (300 MHz, DMSO) δ 7.04 (d, *J* = 1.8, 1H, Ar$_h$H), 6.85 (dd, *J* = 8.1, 1.8, 1H, Ar$_d$H), 6.73 (d, *J* = 8.1, 1H, Ar$_e$H), 6.60 (dd, *J* = 17.6, 10.9, 1H, Ar-C$_b$H), 5.62 (dd, *J* = 17.6, 1.0, 1H, HC$_a$H), 5.06 (dd, *J* = 10.9, 0.9, 1H, HC$_a$H), 3.79 (s, 3H, Ar-OC$_i$H$_3$); **^{13}C NMR (75 MHz, DMSO)** δ 147.77 (C$_g$), 146.78 (C$_f$), 136.77 (Ar-C$_b$H), 128.90 (C$_{arom}$), 119.59 (CH$_{arom}$), 115.45 (CH$_{arom}$), 110.98 (C$_a$H$_2$), 109.63 (CH$_{arom}$), 55.61 (Ar-OC$_i$H$_3$).

7.2.5.8 Reaction of ferulic acid with sebacic acid at 175 °C (LH251)

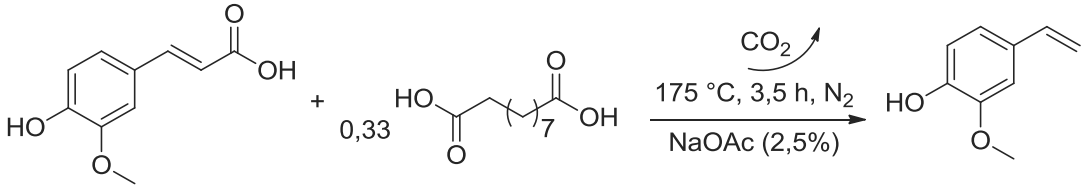

In a 25 mL round bottom flask closed with a septum connected to a nitrogen line and equipped with a needle used as a nitrogen outlet, 1,17 g ferulic acid (6 mmol), 0,40 g sebacic acid (2 mmol) and 12 mg sodium acetate catalyst (2,5%) were heated to 175 °C for 3,5 h while bubbling nitrogen through the reaction mixture and stirring magnetically. A liquid was observed to evaporate and condense at the nitrogen outlet. It was found to be the decarboxylation product of ferulic acid, 4-vinyl guaiacol by ^{1}H NMR. The reaction mixture was found to be unreacted sebacic acid and 4-vinyl guaiacol.

NMR: see above LH250

7.2.5.9 Reaction of ferulic acid with 1,3-propanediol at 130 °C (LH253)

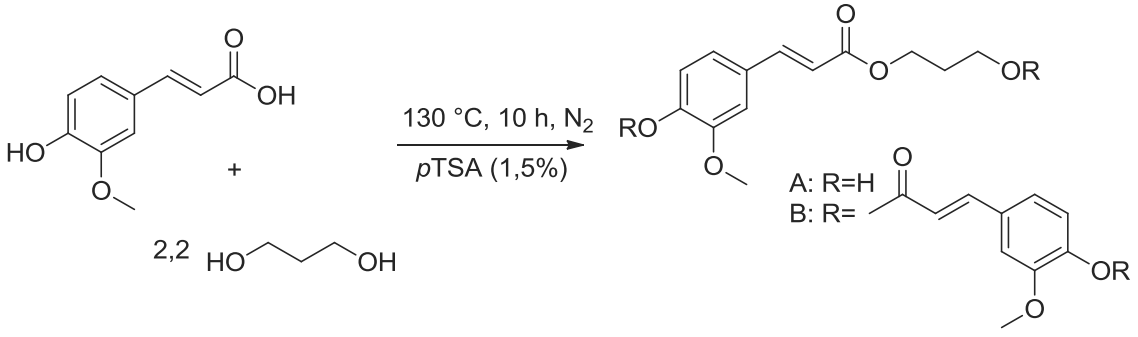

In a 25 mL round bottom flask closed with a septum connected to a nitrogen line and equipped with a needle used as a nitrogen outlet, 1 g ferulic acid (5 mmol), 0,42 g 1,3-propanediol (5,5 mmol) and 12 mg of *p*-toluene sulfonic acid catalyst (1,5%) were heated to 130 °C for 1 h while bubbling nitrogen through the reaction mixture and stirring magnetically. A liquid was observed to evaporate and condense at the nitrogen outlet and identified as 1,3-propanediol using ^{1}H NMR. 0,42 g 1,3-propanediol (5,5 mmol) were then added, and the reaction was continued for 9 h, and left to cool down. 0,8509 g of red, clear, viscous product (46%) were recovered. Analysis by ^{1}H and ^{13}C NMR revealed that about 28 % of the ferulic acid and 21 % of the 1,3-propanediol present in the product mixture had been converted to the ester.

For NMR of the products A and B, see above (LH104 – monoester; LH200 – diester)

7.2.5.10 Reaction of ferulic acid with 1,3-propanediol at 130 °C without nitrogen (LH258)

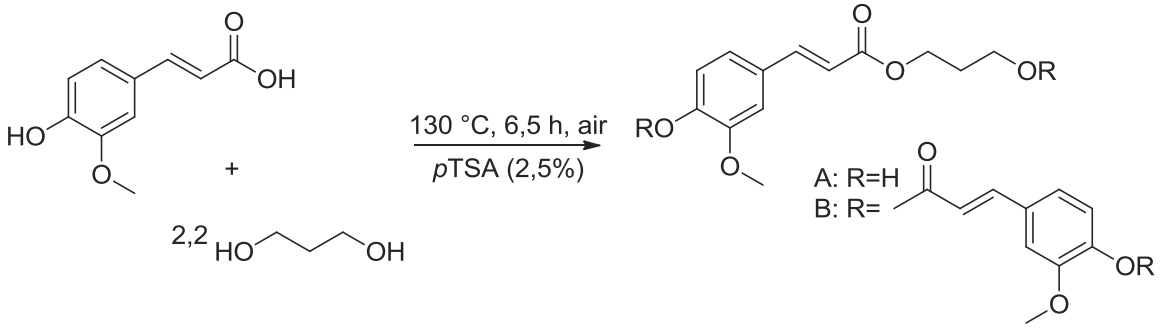

In a 25 mL round bottom flask closed with a septum in which a needle was inserted to provide an outlet for byproducts, 1 g ferulic acid (5 mmol), 0,84 g 1,3-propanediol (11 mmol) and 21 mg *p*-toluene sulfonic acid catalyst (2,5%) were heated to 130 °C for 6,5 h while stirring magnetically. The product was left to cool down, and 1,41 g of a clear, black, viscous gum (77%) was recovered. Analysis by ^{1}H and ^{13}C NMR revealed that 36% of the ferulic acid had been converted to an ester. Other than the darker colour of the product, no new byproducts caused by the interaction with oxygen at a concentration above 1% were observed.

For NMR of the products A and B, see above (LH104 – monoester; LH200 – diester)

7.2.5.11 Reaction of ferulic acid with 1,3-propanediol and sebacic acid at 130 °C (LH254)

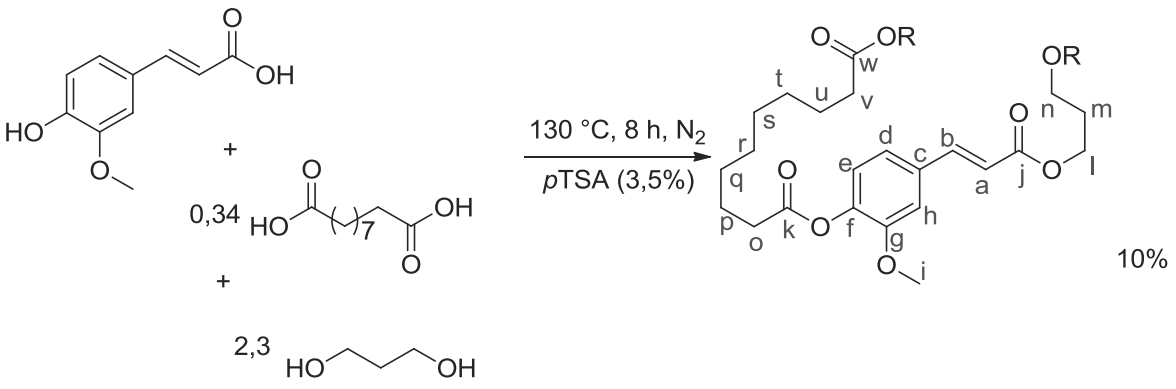

In a 25 mL round bottom flask closed with a septum connected to a nitrogen line and equipped with a needle used as a nitrogen outlet, 1 g ferulic acid (5 mmol), 0,89 g 1,3-propanediol (11,7 mmol), 0,35 g sebacic acid (1,7 mmol) and 31 mg *p*-toluene sulfonic acid catalyst (3,5%) were heated to 130 °C for

8 h while bubbling nitrogen through the reaction mixture and stirring magnetically. A liquid was observed to evaporate and condense at the nitrogen outlet and identified as 1,3-propanediol using ^{1}H NMR. 1,15 g red, clear, viscous product (52%) were recovered and examined using ^{1}H and ^{13}C NMR. It was found that about 80% of starting material remained unreacted. Traces of ester product (20%) were also identified.

^{1}H NMR (300 MHz, DMSO) δ 7.51 – 7.38 (m, 1H, Ar-$C_b\underline{H}$), 6.69 (s, 3H, $Ar_{e,d,h}\underline{H}$), 6.40 – 6.13 (m, 1H, $C_a\underline{H}COOR$), 4.44 – 4.25 (m, 2H, $COOC_lH_2$), 3.80 (s, 3H, Ar-OC_iH_3), 3.71 (s, 2H, C_nH_2COOR), 2.06 – 1.55 (m, 18H, $C_{m,o,p,q,r,s,t,u,v}H_2$); **^{13}C NMR (101 MHz, DMSO)** δ 168.14, 166.84 ($\underline{C_k}OOAr$ and C_jOOR), 145.27 (C_{arom}) 145.02 (C_{arom}), 130.23 (Ar-$\underline{C_b}H$), 127.67 (C_{arom}), 125.87 (CH_{arom}), 122.87 (CH_{arom}), 114.60, 114.35 ($\underline{C_a}HCOOR$ and C_hH_{arom}), 66.70 (C_lH_2), 61.17 (C_nH_2), 57.90 (Ar-OC_iH_3), 32.81, 31.82, 31.59, 30.70 ($\underline{C_{v,o}}H_2COOR$, $C_{p,u}H_2$, $C_{q,t}H_2$ and C_mH_2), 27.79 ($C_{r,s}H_2$).

7.2.5.12 ***General procedure I*** *for the reaction of ferulic acid with 1,3-propanediol and sebacic acid at 130 °C: test different catalysts*

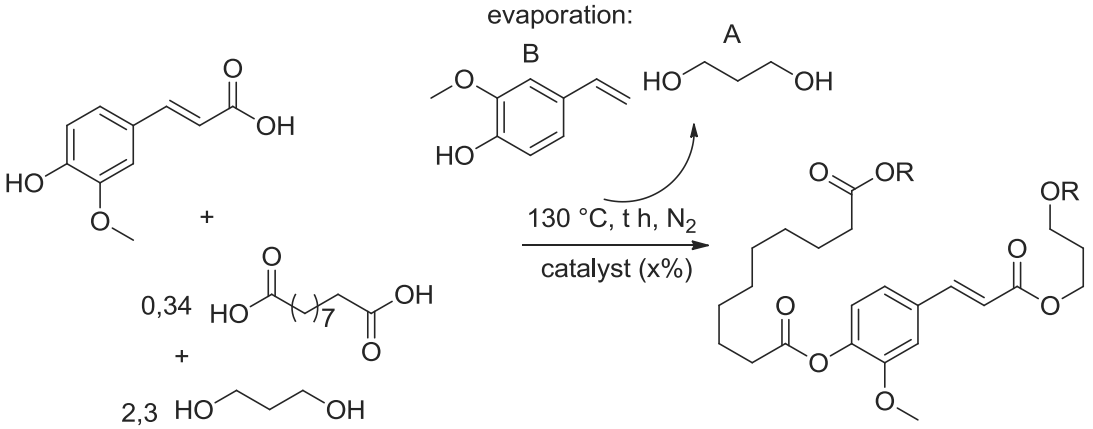

In a 25 mL round bottom flask closed with a septum connected to a nitrogen line and equipped with a needle used as a nitrogen outlet, 1 g ferulic acid (5 mmol), 0,89 g 1,3-propanediol (11,7 mmol), 0,35 g sebacic acid (1,7 mmol) and a catalyst were heated to 130 °C while bubbling nitrogen through the reaction mixture and stirring magnetically. Where a liquid was observed to evaporate and condense at the nitrogen outlet, it was examined using ^{1}H NMR. After cooling down, the product was examined by ^{1}H and ^{13}C NMR to determine the conversion of starting material to ester product.

Conditions:

			time	evaporation	yield[a]	conversion[b]	$yield_{overall}$[c]
	catalyst	**mol %**	**h**		**weight %**	**% NMR**	**%**
LH254	*p*TSA	3,5	8	A	52	20	10
LH275	Fascat 4100	3,5	8,25	A,B (0,8%)	64	44	28
LH278	-	-	8,5	A,B (1,4%)	72	12	9
LH274[d]	*p*TSA	4,7	8,25	A	85	45	38

a) yield: mass of reaction mixture recovered / total mass of monomers; b) conversion: % of product in NMR vs. starting material; c) yield: weight% recovered * conversion % from NMR; d) one equivalent of sebacic acid was used.

7.2.5.13 ***General procedure II*** *for reaction of ferulic acid with 1,3-propanediol and sebacic acid at 130 °C: test different atmospheres*

In order to test different reaction procedures, ferulic acid was mixed with 0,34 equivalents sebacic acid and 2,3 equivalents 1,3-propanediol. The mixture was heated in an oil bath and stirred magnetically. An inert atmosphere was maintained using a nitrogen balloon, by bubbling a constant nitrogen stream through the reaction mixture, or by connecting the flask to a vacuum line (5 mbar). Where the quantity permitted it, samples of the reaction mixture were taken and checked in an acid value titration, as described below, to check the reaction progress. The composition of the product was determined using ^{1}H and ^{13}C NMR.

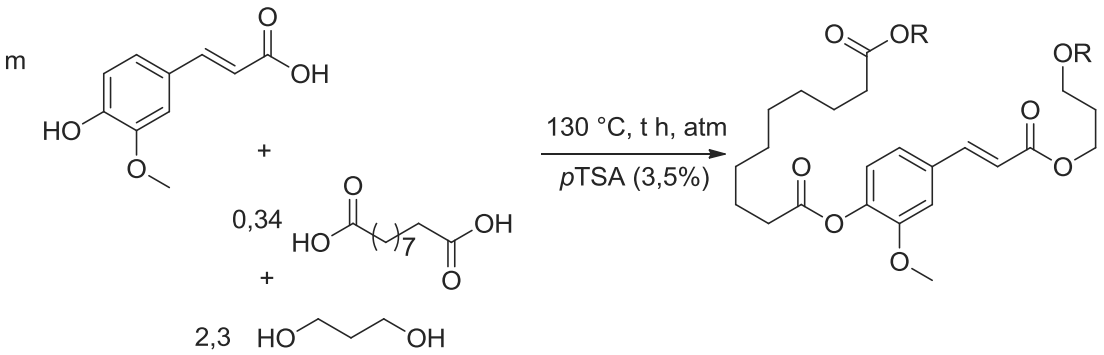

Conditions:

	m	time	atmosphere	yield[a]	conversion[b]	$yield_{overall}$[c]
	mmol	h		weight %	% NMR	%
LH276	5,15	7,75	N_2 (closed)	48	52	25
LH277	25,75	17,75	N_2 (bubble)	75	41	31
LH279	5,15	14 + 10	N_2 (closed) + N_2 (bubble)	84	83	70
LH280	25,75	24 + 1,5	N_2 (bubble) + vacuum	65	16	25

a) yield: mass of reaction mixture recovered / total mass of monomers; b) conversion: % of product in NMR vs. starting material; c) yield: weight% recovered * conversion % from NMR.

7.2.5.14 Acid value titration – ferulic acid reactions

A sample of the reaction mixture (20 – 50 mg) was taken and dissolved in a solvent mixture (75% xylenes, 25% isospropanol, 1% phenolphthalein indicator) by stirring at room temperature. It was then titrated with a potassium hydroxide solution (0.01M). A colour change from colourless to pink should indicate the change of the pH from neutral to basic. However, a change from colourless to pink was observed immediately after the titration was started. This was followed soon by a change to bright yellow. The bright yellow colour produced by the mixing of phenolphthalein and ferulic acid derivatives was so intense that the following colour change to pink could not be attributed to a precise amount of solution added. Acid value titration using this method was therefore determined to be unsuitable for the determination of the reaction progress in this type of reaction.

7.3 Resins

7.3.1 General resin synthesis

The resins were synthesised according to the general procedures described below:

7.3.1.1 ***Synthesis procedure I****: Isosorbide resins using neat isosorbide*

Isosorbide polyesterification – first step

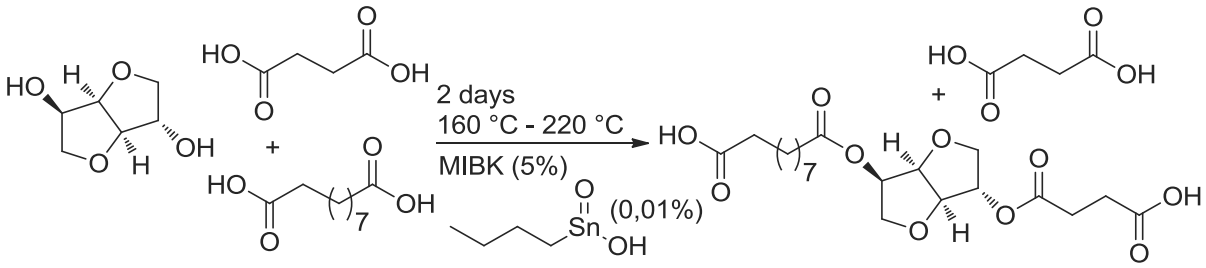

Procedure used for: *LH011, LH016, LH031, LH034, LH037, LH038, LH039, LH040, LH042, LH043, LH044, LH045, LH047, LH057, LH059, LH067, LH070, LH075, LH077, LH079, LH126, LH184, LH185, LH186, LH188, LH190, LH203, LH206, LH243, LH266*

Isosorbide is added to the round bottom flask together with all other monomers with acid functionality, butylstannoic acid catalyst (0,01%) and azeotropic solvent methyl isobutyl ketone (MIBK) (10%). The flask is connected to the reactor which consists of a thermocouple immersed in the reaction mixture, a steel tube connected to a nitrogen line, a mechanical stirrer and an opening for taking samples. Furthermore, it is connected to a Vigreux column on top of which a Dean-Stark trap fitted with a thermometer and connected to a jacketed coil condenser was placed. The top of the reactor is fitted with a gas bubbler filled with silicon oil to observe the gas flow and ensure air tightness. A schematic of the reactor is shown below.

The nitrogen flow is started and the sample is heated to 160 °C using a heating nest connected to a proportional – integral – derivative temperature controller (PID). The PID can be set to the desired temperature and regulates the heating input while taking into account the current batch temperature as well as the response to previous heating processes, thus permitting to minimise any errors. Two PIDs were used in the different syntheses, either a WEST P6100 Z2210 or a MC810B MKII digital temperature controller by Electrothermal. The batch is stirred mechanically as soon as its consistency permits it.

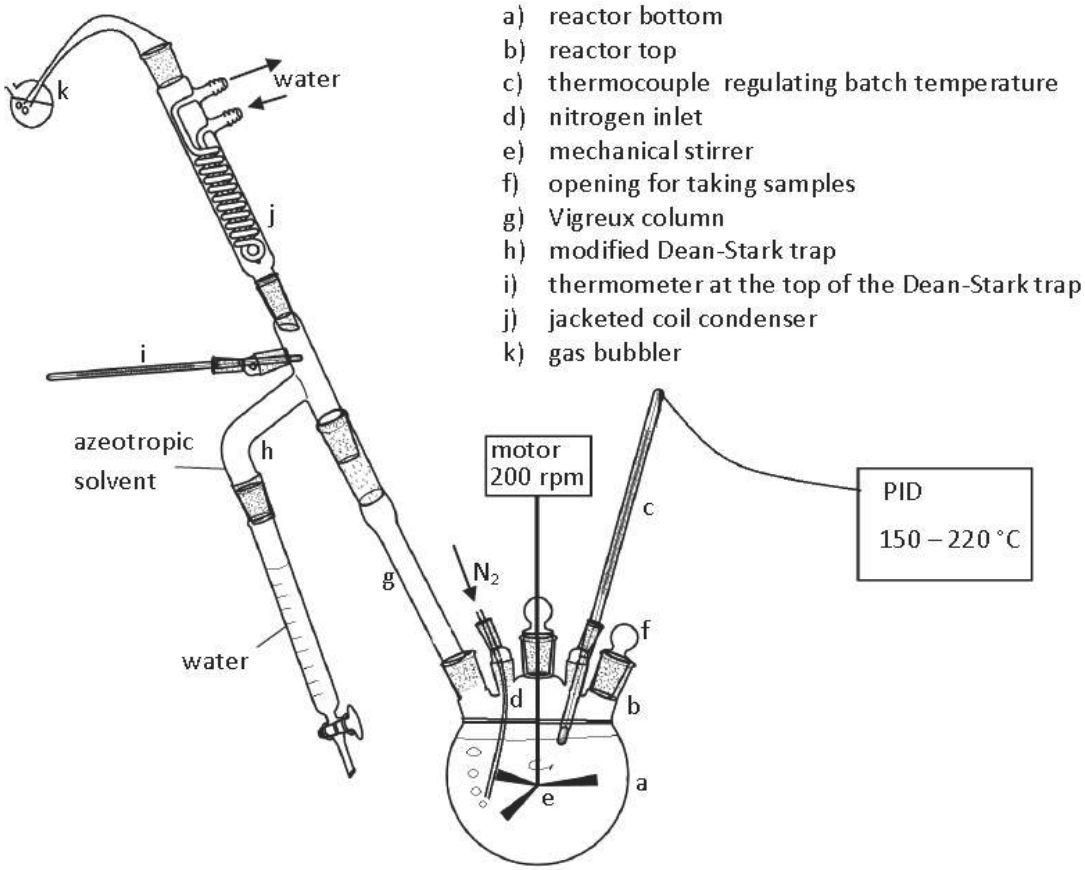

The water produced in the reaction is removed together with the azeotropic solvent, which gather as the bottom and top phase respectively in the Dean-Stark trap. The solvent level in the batch is kept at approximately 5% by adding additional solvent at the top of the reactor when constant reflux in the condenser cedes. Water is removed from the Dean-Stark trap from time to time to prevent it from falling back into the reactor. When the water level in the Dean-Stark trap is not rising anymore, the temperature of the batch is raised in 5 – 10 °C steps until 220 °C are reached.

Isosorbide polyesterification – second step

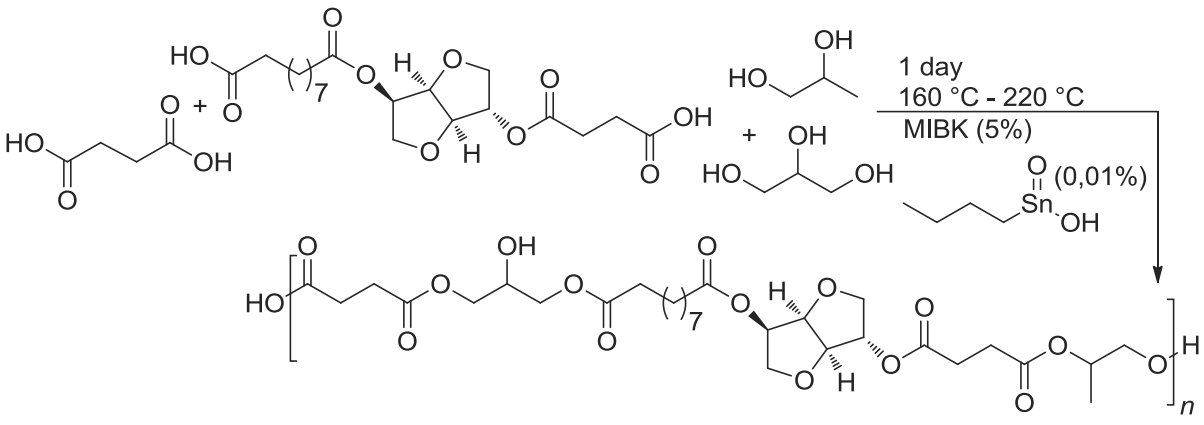

Acid value titration is used to determine the progress of the reaction. When all of the isosorbide has reacted, the batch is cooled down to 150 °C and the other diols and triols are added while stirring. The reaction is then continued as before.

When an acid value of 40 – 25 is reached, the hydroxy value is determined by reverse titration. If it is found to be lower than the theoretical value, the batch is cooled down to 150 °C and additional diol is added to compensate for the difference in hydroxy groups. The reaction is then continued at 220 °C.

In the end of the reaction, the viscosity and acid value are checked every 1 – 2 hours until an acid value of 10 or lower is reached. A neat sample of 1-5 g for measurement of the glass transition temperature is taken and the batch is cooled down to 120 °C. The Dean – Stark trap and the gas bubble are removed and methoxy propyl acetate (MPA) solvent is added slowly using a dropping funnel. When the product is diluted to approximately 70 % of dry content, it is transferred to a glass jar. After cooling down overnight, its dry content is determined and adjusted to the desired level of 65%.

*7.3.1.2 **Synthesis procedure II**: Isosorbide resins using isosorbide diluted in water*

Procedure used for: *LH166, LH168, LH248, LH249, LH262, LH263, LH267, LH268, LH269*

Isosorbide diluted to 80 % in water is added to the round bottom flask together with butylstannoic acid catalyst (0,01%) and azeotropic solvent MIBK (20%). The flask is connected to the reactor which consists of a thermocouple immersed in the reaction mixture, a steel tube connected to a nitrogen line, a mechanical stirrer and an opening for taking samples. Furthermore, it is connected to a Dean-Stark trap fitted with a thermometer and a jacketed coil condenser. The top of the reactor is fitted with a gas bubbler filled with silicon oil to observe the gas flow and ensure air tightness.

The mixture is stirred and flushed with nitrogen for 15 minutes, then heated to 105 °C using a heating nest controlled by a PID. At 40 – 60 °C, the monomers with acid functionality are slowly added. The temperature is maintained until all water has been distilled and collected in the Dean – Stark trap. The Vigreux column is added to the reactor and the batch is heated to 160 °C. For the rest of the reaction, an identical procedure as described in "**synthesis procedure I**" is followed.

*7.3.1.3 **Synthesis procedure III**: Resins not containing isosorbide*

Scheme: Phthalic anhydride resin polymerisation

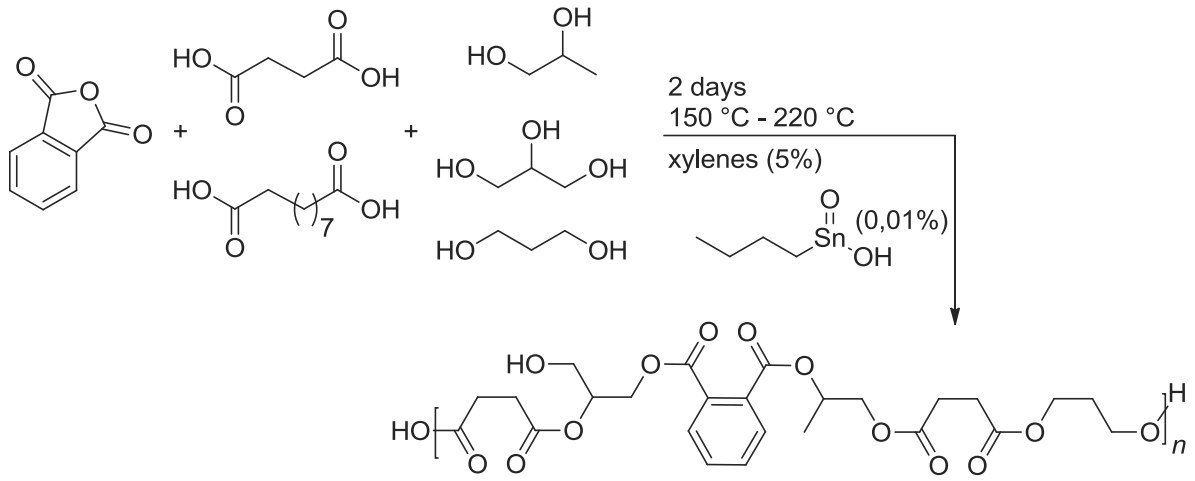

Procedure used for: *LH008, LH009, LH010, LH085, LH112, LH119, LH127, LH128, LH152, LH161, LH162, LH163, LH164, LH165, LH167, LH174, LH177, LH181, LH182, LH183, LH189, LH192, LH193, LH194,*

LH195, LH196, LH197, LH199, LH204, LH219, LH228, LH231, LH233, LH234, LH237, LH238, LH239, LH242, LH259, LH260, LH261, LH264, LH265, LH270, LH272, LH273

All monomers are added to the round bottom flask together with butylstannoic acid catalyst (0,01%). The flask is connected to the reactor which consists of a thermocouple immersed in the reaction mixture, a steel tube connected to a nitrogen line, a mechanical stirrer and an opening for taking samples. Furthermore, it is connected to a Vigreux column on top of which a Dean-Stark trap fitted with a thermometer and connected to a jacketed coil condenser was placed. The top of the reactor is fitted with a gas bubbler filled with silicon oil to observe the gas flow and ensure air tightness.

The nitrogen flow is started and the sample is heated to 150 °C using a heating nest connected to a PID. The batch is stirred mechanically as soon as its consistency permits it. The water produced in the reaction is gathered in the Dean – Stark trap. When the water level stops rising, the temperature is raised gradually by 5 – 10 °C until 220 °C. At around 180 °C, xylenes are added to help the water removal by creating an azeotrope. The solvent level is kept at around 5% from then on by adding additional solvent at the top of the reactor when constant reflux in the condenser cedes. Water is removed from the Dean-Stark trap from time to time to prevent it from falling back into the reactor.

Acid value titration is used to determine the progress of the reaction. When an acid value of 40 – 25 is reached, the hydroxy value is determined by reverse titration. If it is found to be lower than the theoretical value, the batch is cooled down to 150 °C and additional diol is added to compensate for the difference in hydroxy groups. The reaction is then continued at 220 °C.

In the end of the reaction, the viscosity and acid value are checked every 1 – 2 hours until an acid value of 10 or lower is reached. A neat sample of 1-5 g for measurement of the glass transition temperature is taken and the batch is cooled down to 120 °C. The Dean – Stark trap and the gas bubble are removed and MPA solvent is added slowly using a dropping funnel. When the product is diluted to approximately 70 % of dry content, it is transferred to a glass jar. After cooling down overnight, its dry content is determined and adjusted to the desired level of 65%.

*7.3.1.4 **Synthesis procedure IV**: Addition of 1,2-propanediol and glycerol before complete reaction of isosorbide*

Procedure used for: *LH072, LH123*

The synthesis is set-up and started as described in **synthesis procedure I**. Isosorbide is reacted with succinic acid and sebacic acid until an excess of hydroxy equivalents of about 50 mg_{KOH}/g and an acid value around 50 mg_{KOH}/g above the acid value corresponding to a complete reaction of the isosorbide is reached. The batch is then cooled down to 150 °C and the glycerol and 1,2-propanediol are added while stirring. The reaction is then continued as described in **synthesis procedure I**.

*7.3.1.5 **Synthesis procedure V**: Late addition of phthalic anhydride and glycerol*

Procedure used for: *LH0198, LH202, LH210, LH201*

The linear monomers (succinic acid, sebacic acid, 1,2-propanediol and 1,3-propanediol) are added to the round bottom flask together with butylstannoic acid catalyst (0,01%). The flask is connected to the reactor as described in **synthesis procedure III**.

The nitrogen flow is started and the sample is heated to 150 °C using a heating nest connected to a PID. The batch is stirred mechanically as soon as its consistency permits it. The water produced in the reaction is gathered in the Dean – Stark trap. When the water level stops rising, the temperature is raised gradually by 5 – 10 °C until 220 °C. Acid value titration is used to follow the progress of the reaction. When an acid value below 10 is reached, the reaction is cooled down to 160 °C, and the other monomers (phthalic anhydride and glycerol) are added while stirring. The reaction is continued by raising the temperature gradually, as before.

When the water level in the Dean – Stark stops rising, xylenes are added to create an azeotrope. The solvent level is kept at around 5% from then on by adding additional solvent at the top of the reactor when constant reflux in the condenser cedes. Water is removed from the Dean-Stark trap from time to time to prevent it from falling back into the reactor.

When an acid value of 40 – 25 is reached, the hydroxy value is determined by reverse titration. If it is found to be lower than the theoretical value, the batch is cooled down to 150 °C and additional diol is added to compensate for the difference in hydroxy groups. The reaction is then continued at 220 °C.

In the end of the reaction, the viscosity and acid value are checked every 1 – 2 hours until an acid value of 10 or lower is reached. A neat sample of 1-5 g for measurement of the glass transition temperature is taken and the batch is cooled down to 120 °C. The Dean – Stark trap and the gas bubble are removed and MPA solvent is added slowly using a dropping funnel. When the product is diluted to approximately 70 % of dry content, it is transferred to a glass jar. After cooling down overnight, its dry content is determined and adjusted to the desired level of 65%.

7.3.2 Acid value titration

Acid value titration was used to determine the progress of the reaction. As hydroxy groups are present in excess in the reaction mixture, the amount of free acid groups is indicative of the time left before completion.

A sample of reaction mixture (1 – 2 g) was dissolved in 20 mL solvent – indicator mixture (butanol 75%, xylenes 25%, phenolphthalein 0.1%). It was titrated with 0.1M KOH (3,30g KOH in 500 mL ethanol) until a basic pH was reached, indicated by the change of the colourless solution to bright pink.

The acid value is expressed in mg_{KOH}/g_{sample} and calculated by the following formula:

$$AV\ (mg_{KOH}/g_{sample}) = \frac{\text{volume titrated (mL)} * 0{,}1\ \text{(mol /L)} * 56{,}1\ \text{(g/mol)}}{\text{mass sample (g)}}$$

7.3.3 Hydroxy value titration

The hydroxy value titration is used to determine if diols have been lost during the reaction. Two samples (2-3 g) are dissolved in pyridine (10 mL) and the free hydroxy groups are acetylated using acetic anhydride (10 mL of 10 % solution in pyridine) and DMAP catalyst (5 mL of 2 % solution in pyridine) as shown in the scheme below.

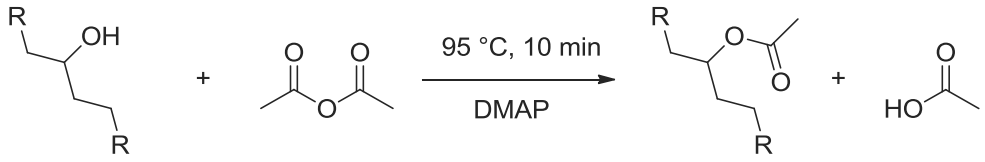

After heating to 95 °C for 10 min, the excess acetic anhydride is converted to acetic acid by adding water (10 mL). The products are diluted (butanol 66%, toluene 34%) and titrated using 0.5 M KOH (33,0 g KOH in 1 L ethanol) until a basic pH is reached, indicated by the change of the colourless solution to bright pink.

A reference sample containing only pyridine (10 mL) and acetic anhydride (10 mL of 10 % solution in pyridine) is also prepared and treated in the same way as the other samples. The amount of excess hydroxy groups present can be calculated from the difference in titration volume needed for the sample and the reference.

The hydroxy value is expressed in mg_{KOH}/g_{sample} and the excess amount of hydroxy groups compared to acid groups is calculated by the following formula:

$$\text{OHV } (mg_{KOH}/g_{sample}) = \frac{(\text{volume titrated reference (mL)} - \text{volume titrated sample(mL)}) * 0{,}5\ (\text{mol/L}) * 56{,}1\ (\text{g/mol})}{\text{mass sample (g)}}$$

In order to calculate the absolute amount of hydroxy groups present, the hydroxy value calculated above is added to the acid value determined beforehand.

7.3.4 Viscosity measurement

As the viscosity increases with the chain length, it can be used as an indicator to determine the progress of the reaction. The viscosity is generally measured at 65% dry content.

The viscosity was measured using the “Noury” or “falling sphere” method. A 20 – 30 g sample was taken from the reaction and diluted to 65% by addition of MPA solvent following by vigorous stirring with a spatula. When homogeneity was achieved, the product was transferred to a test tube which was closed and placed in a water bath at 25 °C. After 20 minutes, a steel ball of 2 mm diameter was dropped in the middle of the test tube and the time it needed to fall 104 mm was measured with a stop watch. The time in seconds corresponds to the viscosity of the sample in Poise, or in 100 mPa*s.

This measurement was repeated six times for viscosities below 6 000 mPa*s, and three times for viscosities above 6 000 mPa*s, and the average value was reported.

7.3.5 Determination of dry content

It is necessary to know the exact weight of the sample in both acid and hydroxyl value titrations, and the concentration of the sample for the viscosity measurement. All of these can be calculated by measuring the dry content.

A sample (0,95 – 1,05g) was placed in an aluminium cup and spread out with a paper clip. It was then placed in an oven (150 °C, 1 h). The difference in weight was determined and used to calculate the dry content according to the following equation:

$$\text{Dry content } (\%) = 100 * \frac{\text{weight after drying (g)}}{\text{weight before drying (g)}}$$

7.3.6 Resin formulation

7.3.6.1 Functionality and r0

In order to achieve good properties in a resin, certain principles as postulated by Patton should be observed.[274] Firstly, in order to achieve an optimum molecular weight, the ratio of hydroxy equivalents to acid equivalents should be higher than 1 but below 1,3. This ratio is reported as r_0 from here on.

Secondly, the formulation should be adjusted to avoid the formation of a gel. The point of gelation, which is defined as the point at which the chain length reaches infinity, and at which the resin becomes useless and its removal from the reactor highly problematic, can be estimated from the functionality of the monomers, as in the amount of acid and hydroxy equivalents present.

In order to do so, the reaction progress, P, is expressed in terms of the molecules in the system at the beginning of the reaction, m_0, and at reaction progress P, m_p. The amount of functional groups reacted is $2(m_0-m_p)$, as for each disappearing molecule, two groups have reacted. The amount of functional groups present in the beginning is $F_{av}*m_0$. F_{av} is the average functionality of the system, or the average amount of functional groups per molecule e_0/m_0. Therefore, the reaction progress can be expressed as shown in the following equation:

$P=2(m_0-m_p)/m_0F_{av}$ or $P=(2/F_{av})-(k*m_p/m_0F_{av})$

The amount of molecules becomes fewer as the reaction progresses, and at the gel point m_p/m_0 is so small that the second term in the second formula goes towards zero and $P=2/F_{av}$.

As the amount of acid and alcohol groups is not exactly stochiometric in the present system, an adjustment is made to F_{av}. The maximum amount of functional groups that can react is limited by those groups which are not in excess, so $F_{av}=e_0/m_0$ is replaced by $F_{av}=2e_A/m_0$. Here, e_A is the number of the underrepresented functional groups, i.e. the acid equivalent, and exactly twice their number can react. Therefore, the reaction progress at which gelation occurs for a non-stochiometric system can be calculated using the equation:

$P=2/2e_A/m_0=m_0/e_A$

The rule for the formulation that can be derived is that m_0/e_A should be higher than 1, i.e. gelation cannot occur before the reaction is complete, or that e_D/m_0 should be lower than 1, or indeed that $2e_A/m_0$ should be lower than 2. Of course, the formulation should not be too far from this value either, as then the molecular weight will be too low because the reaction won't be sufficiently complete. The value of twice the equivalents of acid groups per molecule at the beginning of the reaction, $2e_A/m_0$, will be expressed at F_n, or functionality from now on.

7.3.6.2 Theoretical hydroxy value

The theoretical hydroxy value quoted in the following is the value that should be reached in the end of the reaction, at an acid value 0. It can be calculated by subtracting the total amount of acid equivalents at the start of the reaction, e_A, from the total amount of hydroxy equivalents, e_{OH}.

Excess equivalents of OH = $e_{OH} - e_A$

Hydroxy value at acid value 0 (mg_{KOH}/g) = 56,1* excess equivalents OH (mol) * 1 000 / final mass (g)

The final mass of the resin can be calculated by calculating the amount of water released from the reaction. For this, the amount of acidic monomers is the limiting factor, and it is assumed that one water molecule is released for each acid group and 0.5 for each anhydride group. The total weight of water thus produced is then subtracted from the total weight of monomers at the start of the reaction.

Water produced (g) = ($n_{anhydrides}$ (mol) +2 $n_{diacids}$ (mol))* 18 (g/mol)

Final mass (g) = Σ monomers (g) – water produced (g)

Therefore, the value can be calculated using the following equation:

$Hydroxy_{theoret.}$ = 56,1*1 000 * (e_{OH} –e_A)/(Σ monomers – ($n_{anhydrides}$+$n_{diacids}$)*18)

This value also corresponds to the excess of hydroxy groups present in the reaction at any time, as for each equivalent of hydroxy groups that reacts, one acid equivalent reacts. The difference (e_{OH}-e_A) stays therefore constant, and so does the theoretical hydroxy value.

7.3.6.3 Monomer abbreviations

The following abbreviations are used to represent the monomers in the formulation:

Abbreviation	**Monomer**	**Alternative name**
CHDC	1,4-cyclohexanedicarboxylic acid	
GLY	glycerol	1,2,3 propanetriol
ISO	isosorbide	1,4 dianhydrosorbitol
PAN	phthalic anhydride	
1,2PD	1,2-propanediol	propylene glycol
1,3PD	1,3-propanediol	trimethylene glycol
SEB	sebacic acid	decanedioic acid
SUC	succinic acid	butanedioic acid

7.3.7 Overview of resin formulations[LXIV]

resin description (main monomer)		name	page annexe
Different quantity of isosorbide used in weathering tests		LH249	105
		LH190	106
		LH184	106
		LH168	106
		LH248	106
Different quantity of phthalic anhydride used in weathering tests		LH237	107
		LH162	107
		LH189	107
		LH163	107
		LH242	108
Effect of succinic acid, sebacid acid, 1,2-propanediol, 1,3-propanediol and glycerol on a phthalic anhydride based resin used in weathering tests		LH174	108
		LH177	108
		LH181	108
		LH182	109
		LH219	109
Repeated synthesis of weathering test resins to have a larger quantity to be tested at Beckers	Isosorbide type	LH206	109
		LH262	109
		LH203	110
		LH263	110
	Phthalic anhydride type	LH198	110
		LH210	110
		LH201	110
	Linear monomers type	LH260	111
		LH264	111
Increased isosorbide content to increase the T_g while keeping the hydroxy value constant		LH067	112
		LH070	112
		LH077	112
		LH079	112
Increased isosorbide content, not compensating for the hydroxy value		LH040	113
Reference for increased isosorbide content tests		LH075	113
Phthalic anhydride resins with increased T_g through increased amount of phthalic anhydride, succinic acid and 1,2-propanediol		LH192	113
		LH193	113
		LH196	114
		LH199	114
Prototype for exterior	Isosorbide & phthalic anhydride based	LH269	114
	Minimised phthalic anhydride content	LH231	114
		LH238	115
	Cyclohexanedicarboxylic acid	LH265	115
Isosorbide resin used for solvent tests		LH042	115
Addition of 1,2-propanediol and glycerol before isosorbide was		LH072	115

[LXIV] The exact formulations of the different resins can be found in the annexe in the order given here.

completely reacted		LH123	116
Different phthalic anhydride and isosorbide contents, not used in weathering tests due to lack of space	Isosorbide based	LH243	116
	Phthalic anhydride based	LH239	116
		LH228	116
		LH165	117
Resins not used because of their T_g, viscosity or colour	Isosorbide based	LH186	118
		LH166	118
		LH267	118
	Isosorbide & phthalic anhydride based	LH266	118
	Cyclohexanediocarboxylic acid based	LH272	119
Resins not used because their aspect was hazy	Isosorbide based	LH126	119
		LH059	119
	Phthalic anhydride based	LH152	119
		LH161	120
		LH183	120
		LH204	120
		LH207	120
Resins not used because their hydroxy value did not correspond to the theoretical hydroxy value	Isosorbide based	LH188	121
		LH034	121
		LH037	121
		LH044	121
		LH045	121
		LH057	122
	Isosorbide & phthalic anhydride based	LH268	122
	Phthalic anhydride based	LH128	122
		LH127	122
		LH202	123
		LH119	123
		LH167	123
		LH194	117
		LH197	117
		LH234	117
Gels	Phthalic anhydride based	LH195	123
		LH233	123
		LH259	124
		LH261	124
	Cyclohexanedicarboxylic acid based	LH270	124
		LH273	124

7.4 Film preparation

7.4.1 Clear coat varnish preparation

Two different types of formulations were prepared for testing. Firstly, for the mechanical tests, weathering tests and dynamic mechanical analysis, a hindered amine light stabiliser free clear coat varnish paint was prepared.

In addition to the resin (40 – 50%), which was used dilute at 65% dry content in MPA, the paint formulation contained a HMMM melamine resin (5 - 15%), and a mixture of solvents (30 – 40%) containing dibasic ester solvent, xylenes and naphtha 100 solvent, which consist of heavy aromatics.

This mixture was stirred mechanically (1400 rpm, 10 min) before flow additives (0,1 – 2%) were added. After stirring mechanically again (1400 rpm, 5 min), a catalyst mixture for crosslinking containing *p*-toluene sulfonic acid (0,1 – 2%) was added and the final mixture was stirred again (1400 rpm, 5 min). The product was then placed into a fridge to adjust the temperature to 20 °C. When this was achieved, viscosity was tested using a flow cone type viscometer, and dibasic ester solvent was added until a flow time of 100 – 110 s, which corresponds approximately to 450 – 500 mPa*s, was reached.

A variation of these formulations was prepared by adding hindered amine light stabilisers (HALS) to each batch, and used in weathering tests for comparison.

7.4.2 Coating application – supported films

The paint was applied on a chrome free panel made from galvanised steel coated with a melamine crosslinked polyester resin based primer of the type AG1122DE of approximately 10 * 15 cm. The panel had been cleaned with isopropanol, dried in an oven (320 °C, 30 s) and the exact thickness (17 - 20 µm) of the primer had been determined with a Fisher Permascope. An RD Specialties draw down bar (26 – 36 G) was used to apply the paint to the panel and it was cured in an oven (320 – 340 °C) to a peak metal temperature of 232 °C (dwelling time: 25 s). The coated panel was cooled down by placing it into a water bath for a few seconds and dried using pressurised air flow. The coating thickness (17 – 19 µm) was determined with a Fisher Permascope according to the norm ISO 2808.

7.4.3 Coating application – free films

In order to obtain a free film not attached to the panel, the paint was applied on a Teflon panel coated with an anti-adhesive substance previously cleaned with isopropanol and dried in an oven (320 °C, 30 s) using an RD specialties draw down bar (36 G). It was cured in an oven (320 °C) to a peak metal temperature of 232 °C (dwelling time: 17 s), cooled by placing it into a water bath for a few seconds and dried using pressurised air flow. It was then peeled from the panel with the help of a letter opener. The resulting film on the Teflon panel displayed craters (diameter: 0,5 – 2 cm) in the first applications, and due to small imperfections introduced on the panel with the letter opener and wear of the anti-adhesive coating, it became increasingly difficult to remove the film in one piece after each application. The free films were therefore to the most part recovered as small scraps, and could not be used for weathering tests or infrared analysis.

7.4.4 Resin compatibility tests with formulation ingredients

The compatibility of the resin with the other components that were present in more than 5 weight % in the clear coat formulation was tested. In a glass bottle, the resin was mixed with the melamine resin (1:1 in weight) and with each solvent (2:1 in weight) separately. The mixture was stirred and left overnight. The compatibility was determined failed if phase separation or a hazy aspect was observed the next day, and a pass if a clear aspect and only single phase were present.

7.4.5 Solubility tests

The Hansen parameters of the resins were determined by testing their solubility in 48 common organic solvents. In a 4 mL vial, 700 mg of resin and 1 mL of solvent were placed on a tube roller for two days. A score was assigned to the solubility depending if the resin was completely soluble (score: 1) or if the phase separation, solid residue or a hazy aspect was observed (score: 0). The results were evaluated with HSPiP software.

7.5 Coating characterisation and performance tests

7.5.1 T-bend test

The formability of the coating as well as its resistance to cracks and delamination are tested with the T-bend test, according to an internal Beckers standard. The ability of the coating to be bent around its own thickness (T) is examined. With the coating on the outside, the panel is bent to an approximately 100° angle using the machine schematically depicted below. Afterwards, the slightly bent panel is pressed together with two metal plates to achieve a 180° angle. The paint on the outside of the bent is then examined with a PEAK magnifying glass (x10) for cracks. An adhesive tape is applied to the edge and pulled off, and the paint is examined for delamination. If cracks or delamination is observed, the procedure is repeated and the panel is bent around itself again, this time in a slightly smaller angle. This is repeated until neither cracks not delamination are observed, and the lowest bend without damage is reported in terms of T, where each bend counts for 0,5 T as shown in the picture on the right.

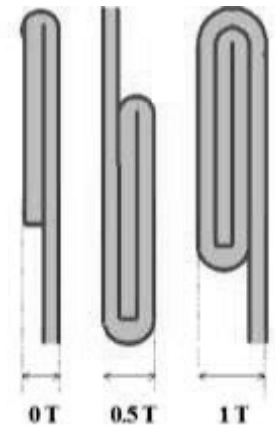

7.5.2 Impact test

The film was also tested for its resistance to rapid deformation in the impact test according to the ECCA norm T-5 1985 using a machine conform with the norm ASTM D2794. A 1 kg steel ball with a diameter of 15,87 mm was dropped from the height of 92 cm onto the panel with the coating facing down to achieve an impact of 18 J. The hemispherical deformation was then examined for cracks using a PEAK magnifying glass (x10). A scotch tape was also applied to the coated side of the deformation and pulled off, and the paint was examined for delamination. The result was rated from

0 – 4, where 0 represents no damages, 1 – 3 represent increasing amount of cracks, and 4 means delamination.

7.5.3 Erichsen indentation test

The resistance to slow deformation was tested using an Erichsen testing machine according to the norm NF EN ISO 1520 (T30-019). A greased, ball shaped indenter with a diameter of 20 mm +/- 0,3 mm was slowly forced at the speed of 12 +/- 1mm/min into the uncoated back side of the panel up to an indentation of 7 mm. As in the impact test, the coating on the hemispherical deformation is then examined using a PEAK magnifying glass (x10) for cracks and delamination, and reported with a grade from 0 – 4.

7.5.4 Clemen hardness

The Clemen hardness was tested by evaluating the resistance of the coating to scratches induced by tungsten carbide balls. It was conducted according to the norm NF EN 13523-12.

7.5.5 Rub test

The solvent resistance of the coating is examined in the MEK rub test according to the norm NF EN 13523-11. A piece of cotton is soaked in methyl ethyl ketone (MEK) solvent (2-butanone) and rubbed back and forth on a fixed, coated panel, exerting exactly 2 kg of pressure on the coating, until damage such as a significant colour change is observed. This is continued for up to 100 times, when the solvent resistance is considered to be sufficient and 100 is noted as the result even if no damage was observed.

7.5.6 Gloss

The gloss of the fresh coatings was measured with a Trigloss gloss metre using a photo electric cell. A beam of light was projected onto the surface at a 60° angle and the intensity of the reflection at 60° in the opposite direction was measured by a photo-electric cell. The ratio of the intensities is reported in gloss units. The measurement was repeated three times on different locations on the coating, and the average was reported.

Measurement of gloss was also used to quantify the weathering resistance (weathering protocol detailed below). In this case, a BYK device was used, and the ratio of gloss after and before weathering was reported in %, and in accordance with the norm EN13523-2.

7.5.7 Microhardness

The degree of resistance of the coating to penetration was evaluated according to the norm ISO 14577-1 on a Fisher Hardness Tester H100. The coating was penetrated by a diamond square based Vickers pyramid (apex angle: 136°) to a depth of 2 µm in 60 s, and the mechanical resistance at the moment of equilibrium between stress and strain was measured. The maximum force used was 100 mN. The pyramid was then removed again, reversing the force used for the indentation, during 60 s. A creep time of 60 s before and after unloading was allowed, and the creep in both directions as well as the elastic and plastic components of the deformations were determined, as illustrated in the graph below.

The measurement was repeated 9 times and an average value was reported. The temperature of the room during the measurement was between 19 °C and 20 °C.

The universal hardness (HU_k) can be calculated from the following equation, where F (N) is the applied force, V is a geometry factor calculated for the Vickers pyramid which equals 26,43 and h_r' is the indentation depth of 0,002 mm.

HU_k (N/mm^2) = F (N) / V*(h_r'(mm))^2

Due to a calibration mistake, the measurement result can be assumed to be around 20 mN too high, i.e. a measurement of 200 – 215 mN actually corresponds to 190 mN.

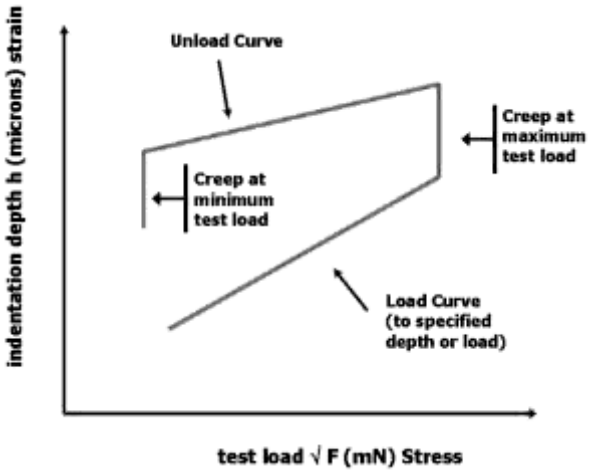

7.5.8 DMA

In order to perform the dynamic mechanical analysis, coupons of a diameter of 10 mm were stanced out of the centre region of the coated panel (at least 2 cm distance to any edge) while the uncoated side was facing up. In order to maximise the response, two coupons were stacked on top of each other, with the coating facing the same way, when placed in the DMA machine, so that each measurement was made on a total of 4 coupons. The measurements were performed on a DMA/SDT A961e apparatus. The response was measured on a temperature ramp starting from -15 °C or 0°C, depending on the expected T_g, and ending at 100 °C. The temperature was raised at 2 °C per minute. The measurements were made for a displacement of 1 µm at a frequency of 1 Hz and an applied force of 5N.

7.6 Weathering tests

The films were weathered in a QUVa and a Hot QUVa environment separately, and their resistance was assessed with infrared spectroscopy, gloss retention measurements and colour change measurements.

7.6.1 Exposure procedures

7.6.1.1 Hot QUVa

The supported films were placed in a Q-lab Hot QUVa exposure cabinet of 2000 h or 1920h and taken out for analysis every 500 h and 192 h respectively. A seven day cycle of UV light and humidity was alternated with a seven days prohesion cycle. A mercury lamp with an emission peak at 340 nm was used to provide UV light at an intensity of 0,89 W/m^2/nm. During the exposure cycle, 8 h of UV light at 78 °C were alternated with 4 h at 50 °C and 100% humidity in darkness. During the prohesion cycle, 1 h in fog at 25 °C were alternated with 1 h drying at 35 °C. The temperatures were determined at the panel.

7.6.1.2 QUVa

The supported films were placed in a Q-lab QUVa exposure cabinet for 2000 h in total, and assessed after 1200 h and 2000 h according to the norm NF EN ISO 11507. Exposure to UV light and humidity was alternated in 4 h alternating cycles. During the former, a mercury lamp with an emission peak at 340 nm was used to provide UV radiation with an intensity of 0,80 W/m^2/nm at 60 °C. During the latter, the panels were exposed to 100 % humidity at 50 °C in darkness.

7.6.2 Analysis techniques

7.6.2.1 Optical microscope

Images of the coatings were obtained on an Olympus BX6 microscope with a 100 x magnification. It was lit from the side, and an RT colour spot camera was used to take the picture.

7.6.2.2 Colour change

The colour change was determined in accordance with the norm EN13523-3 using a BYK device, and reported along the black and white axis (∆L*), the green and red axis (∆a*) and the blue and yellow axis (∆b*), which are shown in the figure on the right. The total colour change, ∆E, can be calculated from the formula below.

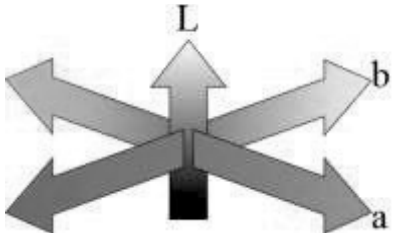

$$\Delta E^* = \sqrt{(\Delta L^{*2} + \Delta a^{*2} + \Delta b^{*2})}$$

7.7 Acknowledgements

The following experimental work was performed fully or in part by other people. The NMR spectra were measured at the “Centre Commun de RMN”. Many of the NMR spectra on the AV 400 spectrometer were measured by Anne Baudouin, all of the spectra on the AV 500 spectrometer were measured by Bernard Fenet, and the NOESY spectrum on the AV 300 spectrometer was measured by Christophe Gilbert. The mass spectra were all measured in the “Centre Commun de spectrométrie de masse – Lyon 1”. The size exclusion chromatography measurements were conducted in the C2P2 institute by Olivier Boyron and Manel Taam (Group A), at Arkema by Stephane Poirier (Group B), in the IMP institute by Marion Colella (Group C) and by Catherine Goux-Henry (all others). The solubility tests to determine the Hansen parameters of the resins were conducted at Activation by Yoann Yoyard and Jérome Monbrun. The preparation and application of films and the test of their mechanical qualities was conducted at Beckers (Savigneux) together with Jean-Dominique Paoli. The weathering of the films and their analysis afterwards was conducted at Beckers (Savigneux) by Jean-Dominique Paoli. The microhardness tests, determination of the glass transition temperature of the applied films, recording of the photo acoustic IR spectra, UV/Vis reflection measurements, optical microscopy and film thickness loss measurements were conducted at the Beckers Long Term Development Centre (Liverpool) by or with the help of James Maxted, Chris Lowe, Alan Butchart, Jean-Dominique Paoli and their coworkers. The dynamic mechanical analysis of the films was conducted at the CRM group together with Florence Avril and Nathalie Leclercq.

8 References

1. Mialon, L.; Pemba, A. G.; Miller, S. A., Biorenewable polyethylene terephthalate mimics derived from lignin and acetic acid. *Green Chemistry* **2010,** *12* (10), 1704-1706.
2. Sudip, S. Coil coatings market to reach US$ 6.27 Billion by 2023 - Global industry analysis 2016. http://www.prnewswire.com/news-releases/coil-coatings-market-to-reach-us627-billion-by-2023---global-industry-analysis-size-share-growth-trends-and-forecast-2015---2023-tmr-573726581.html (accessed 06.09.2016).
3. Latieule, S. Les peintures industrielles biosourcées au coeur de SOragO 2013. http://formule-verte.com/les-peintures-industrielles-biosourcees-au-coeur-de-sorago/ (accessed 06.09.2016).
4. Arkema's International website. http://www.arkema.com/en/arkema-group/profile/ (accessed 06.09.2016).
5. Activation - Creative Chemistry and Technology. http://www.activation.fr/cms/index.php/en/ (accessed 06.09.2016).
6. Beckers. http://www.beckers-group.com/index.php?id=55 (accessed 06.09.2016).
7. Prospa - Industrial paints. http://www.prospa.fr/?p=0&lg=en (accessed 06.09.2016).
8. Arcelor Mittal - transforming tomorrow. http://corporate.arcelormittal.com/ (accessed 06.09.2016).
9. CREIDD; UTT Project Sorago. http://creidd.utt.fr/fr/projets/sorago.html (accessed 06.09.2016).
10. Oldring, P. K. T.; Deligny, P.; Limited, S. T.; Tuck, N., *Resins for Surface Coatings: Alkyds & polyesters*. Wiley: 2000.
11. Brock, T.; Groteklaes, M.; Mischke, P., *European Coatings Handbook*. Curt R. Vincentz Verlag, Hanover, 2000.
12. Holmberg, K., *High Solids Alkyd Resins*. Taylor & Francis: 1987.
13. Introduction to Coil Coating. European Coil Coating Association. http://www.prepaintedmetalacademy.eu/temp/textbook/module_16.pdf.
14. Introduction to Organic Coatings. European Coil Coating Association. http://www.prepaintedmetalacademy.eu/temp/textbook/module_146.pdf.
15. Bretton, C., Sustainable Innovation in Coil Coating. In *Advancement for Metal Buildings congress*, European Association for Panels and Profiles: Dublin, Ireland, 2013.
16. European Coil Coating Association collection. http://www.creativebuilding.eu/prg/collection.pl (accessed 06.09.2016).
17. Siyab, N.; Tenbusch, S.; Willis, S.; Lowe, C.; Maxted, J., Going Green: making reality match ambition for sustainable coil coatings. *Journal of Coatings Technology and Research* **2016,** *13* (4), 629-643.
18. Rossi, G.; Giannakopoulos, I.; Monticelli, L.; Rostedt, N. K. J.; Puisto, S. R.; Lowe, C.; Taylor, A. C.; Vattulainen, I.; Ala-Nissila, T., A MARTINI Coarse-Grained Model of a Thermoset Polyester Coating. *Macromolecules* **2011,** *44* (15), 6198-6208.
19. Yokozawa, T.; Ajioka, N.; Yokoyama, A., Reaction Control in Condensation Polymerization. In *New Frontiers in Polymer Synthesis*, Kobayashi, S., Ed. Springer Berlin Heidelberg: 2008; Vol. 217, pp 1-77.
20. Hansen Solubility Parameters in Practice. http://www.hansen-solubility.com/ (accessed 21.09.2016).
21. *Plastic waste: Ecological and human health impacts - Science for environment policy*; European Commission - DG Environment News Alert Service: 2011.
22. Paszun, D.; Spychaj, T., Chemical recycling of poly(ethylene terephthalate). *Industrial & Engineering Chemistry Research* **1997,** *36* (4), 1373-1383.
23. Al-Sabagh, A. M.; Yehia, F. Z.; Eshaq, G.; Rabie, A. M.; ElMetwally, A. E., Greener routes for recycling of polyethylene terephthalate. *Egyptian Journal of Petroleum* **2016,** *25* (1), 53-64.
24. Park, S. H.; Kim, S. H., Poly (ethylene terephthalate) recycling for high value added textiles. *Fashion and Textiles* **2014,** *1* (1), 1-17.
25. Nikles, D. E.; Farahat, M. S., New Motivation for the Depolymerization Products Derived from Poly(Ethylene Terephthalate) (PET) Waste: a Review. *Macromolecular Materials and Engineering* **2005,** *290* (1), 13-30.
26. Kobayashi, S.; Uyama, H., Enzymatic Polymerization to Polyesters. In *Biopolymers Online*, Wiley-VCH Verlag GmbH & Co. KGaA: 2005.
27. Kobayashi, S., Lipase-catalyzed polyester synthesis – A green polymer chemistry. *Proceedings of the Japan Academy. Series B, Physical and Biological Sciences* **2010,** *86* (4), 338-365.
28. Tan, G. Y. A.; Chen, C. L.; Li, L.; Ge, L.; Wang, L.; Razaad, I. M. N.; Li, Y.; Zhao, L.; Mo, Y.; Wang, J. Y., Start a Research on Biopolymer Polyhydroxyalkanoate (PHA): A Review. *Polymers* **2014,** *6* (3), 706-754.
29. Braunegg, G.; Lefebvre, G.; Genser, K. F., Polyhydroxyalkanoates, biopolyesters from renewable resources: Physiological and engineering aspects. *Journal of Biotechnology* **1998,** *65* (2–3), 127-161.

30. Bugnicourt, E.; Cinelli, P.; Lazzeri, A.; Alvarez, V., Polyhydroxyalkanoate (PHA): Review of synthesis, characteristics, processing and potential applications in packaging. *Express Polymer Letters* **2014,** *8* (11), 791-808.
31. La Mantia, F. P.; Morreale, M., Green composites: A brief review. *Composites Part A: Applied Science and Manufacturing* **2011,** *42* (6), 579-588.
32. Dicker, M. P. M.; Duckworth, P. F.; Baker, A. B.; Francois, G.; Hazzard, M. K.; Weaver, P. M., Green composites: A review of material attributes and complementary applications. *Composites Part a-Applied Science and Manufacturing* **2014,** *56*, 280-289.
33. Dale, B. E.; Kim, S., Biomass Refining Global Impact–The Biobased Economy of the 21st Century. In *Biorefineries-Industrial Processes and Products*, Wiley-VCH Verlag GmbH: 2005; pp 41-66.
34. Kamm, B.; Kamm, M.; Gruber, P. R.; Kromus, S., Biorefinery Systems – An Overview. In *Biorefineries-Industrial Processes and Products*, Wiley-VCH Verlag GmbH: 2005; pp 1-40.
35. Corma, A.; Iborra, S.; Velty, A., Chemical routes for the transformation of biomass into chemicals. *Chemical Reviews* **2007,** *107* (6), 2411-2502.
36. Gandini, A.; Belgacem, M. N., Chapter 1 - The State of the Art. In *Monomers, Polymers and Composites from Renewable Resources*, Belgacem, M. N.; Gandini, A., Eds. Elsevier: Amsterdam, 2008; pp 1-16.
37. Kamm, B.; Kamm, M., Principles of biorefineries. *Applied Microbiology and Biotechnology* **2004,** *64* (2), 137-145.
38. Lindblad, M.; Liu, Y.; Albertsson, A.-C.; Ranucci, E.; Karlsson, S., Polymers from Renewable Resources. In *Degradable Aliphatic Polyesters*, Springer Berlin Heidelberg: 2002; Vol. 157, pp 139-161.
39. Saha, B. C., Commodity chemicals production by fermentation: An overview. *ACS Symposium Series* **2003,** *862* (Fermentation Biotechnology), 3-17.
40. foodnavigator.com Rhodia compares chemical routes in vanillin production. http://www.foodnavigator.com/Market-Trends/Rhodia-compares-chemical-routes-in-vanillin-production.
41. Borges da Silva, E. A.; Zabkova, M.; Araujo, J. D.; Cateto, C. A.; Barreiro, M. F.; Belgacem, M. N.; Rodriques, A. E., An integrated process to produce vanillin and lignin-based polyurethanes from Kraft lignin. *Chemical Engineering Research & Design* **2009,** *87* (9A), 1276-1292.
42. Borregaard Smart Vanillin. http://www.sustainablevanillin.com/nature.html (accessed 17.08.).
43. Li, K.; Frost, J. W., Synthesis of Vanillin from Glucose. *Journal of the American Chemical Society* **1998,** *120* (40), 10545-10546.
44. Gandini, A., Furans as offspring of sugars and polysaccharides and progenitors of a family of remarkable polymers: a review of recent progress. *Polymer Chemistry* **2010,** *1* (3), 245-251.
45. Gandini, A.; Belgacem, M. N., Furans in polymer chemistry. *Progress in Polymer Science* **1997,** *22* (6), 1203-1379.
46. Gandini, A.; Silvestre, A. J. D.; Neto, C. P.; Sousa, A. F.; Gomes, M., The Furan Counterpart of Poly(ethylene terephthalate): An Alternative Material Based on Renewable Resources. *Journal of Polymer Science Part a-Polymer Chemistry* **2009,** *47* (1), 295-298.
47. de Jong, E.; Dam, M. A.; Sipos, L.; Gruter, G. J. M., Furandicarboxylic Acid (FDCA), A Versatile Building Block for a Very Interesting Class of Polyesters. In *Biobased Monomers, Polymers, and Materials*, American Chemical Society: 2012; Vol. 1105, pp 1-13.
48. Gandini, A.; Belgacem, M. N., Chapter 6 - Furan Derivatives and Furan Chemistry at the Service of Macromolecular Materials. In *Monomers, Polymers and Composites from Renewable Resources*, Elsevier: Amsterdam, 2008; pp 115-152.
49. Moreau, C.; Belgacem, M. N.; Gandini, A., Recent catalytic advances in the chemistry of substituted furans from carbohydrates and in the ensuing polymers. *Topics in Catalysis* **2004,** *27* (1-4), 11-30.
50. Sigma Aldrich catalogue. http://www.sigmaaldrich.com/catalog/product/aldrich/722081?lang=fr&region=FR (accessed 18.08.2016).
51. Alfa Aesar Catalogue. https://www.alfa.com/de/catalog/H28718/ (accessed 18.08.2016).
52. Belgacem, M. N.; Gandini, A., Chapter 3 - Materials from Vegetable Oils: Major Sources, Properties and Applications. In *Monomers, Polymers and Composites from Renewable Resources*, Elsevier: Amsterdam, 2008; pp 39-66.
53. Sharmin, E.; Zafar, F.; Akram, D.; Alam, M.; Ahmad, S., Recent advances in vegetable oils based environment friendly coatings: A review. *Industrial Crops and Products* **2015,** *76*, 215-229.
54. Seniha Güner, F.; Yağcı, Y.; Tuncer Erciyes, A., Polymers from triglyceride oils. *Progress in Polymer Science* **2006,** *31* (7), 633-670.
55. Derksen, J. T. P.; Petrus Cuperus, F.; Kolster, P., Renewable resources in coatings technology: a review. *Progress in Organic Coatings* **1996,** *27* (1–4), 45-53.

56. Sharma, V.; Kundu, P. P., Condensation polymers from natural oils. *Progress in Polymer Science* **2008,** *33* (12), 1199-1215.
57. Castor Oil.In, Sebacic acid. http://www.castoroil.in/castor/castor_seed/castor_oil/sebacic_acid/sebacic_acid.html (accessed 18.08.2016).
58. Meier, M. A. R.; Metzger, J. O.; Schubert, U. S., Plant oil renewable resources as green alternatives in polymer science. *Chemical Society Reviews* **2007,** *36* (11), 1788-1802.
59. Bao, Y.; He, J.; Li, Y., Facile and efficient synthesis of hyperbranched polyesters based on renewable castor oil. *Polymer International* **2013,** *62* (10), 1457-1464.
60. Vilela, C.; Silvestre, A. J. D.; Meier, M. A. R., Plant Oil-Based Long-Chain C26 Monomers and Their Polymers. *Macromolecular Chemistry and Physics* **2012,** *213* (21), 2220-2227.
61. Noreen, A.; Zia, K. M.; Zuber, M.; Ali, M.; Mujahid, M., A critical review of algal biomass: A versatile platform of bio-based polyesters from renewable resources. *International Journal of Biological Macromolecules* **2016,** *86*, 937-949.
62. Zia, K. M.; Zia, F.; Zuber, M.; Rehman, S.; Ahmad, M. N., Alginate based polyurethanes: A review of recent advances and perspective. *International Journal of Biological Macromolecules* **2015,** *79*, 377-387.
63. Roesle, P.; Stempfle, F.; Hess, S. K.; Zimmerer, J.; Río Bártulos, C.; Lepetit, B.; Eckert, A.; Kroth, P. G.; Mecking, S., Synthetic Polyester from Algae Oil. *Angewandte Chemie International Edition* **2014,** *53* (26), 6800-6804.
64. Zamora, F.; Hakkou, K.; Muñoz-Guerra, S.; Galbis, J. A., Hydrolytic degradation of carbohydrate-based aromatic homo- and co-polyesters analogous to PET and PEI. *Polymer Degradation and Stability* **2006,** *91* (11), 2654-2659.
65. Roquette corporate website, Roquette reinforces its position as world leader in isosorbide. http://www.roquette.com/topic_id=11189/article_id=8959/ (accessed 19.08.2016).
66. Zia, K. M.; Noreen, A.; Zuber, M.; Tabasum, S.; Mujahid, M., Recent developments and future prospects on bio-based polyesters derived from renewable resources: A review. *International Journal of Biological Macromolecules* **2016,** *82*, 1028-1040.
67. Noordover, B. A. J., Polyesters, Polycarbonates and Polyamides Based on Renewable Resources. In *Renewable Polymers*, John Wiley & Sons, Inc.: 2011; pp 305-354.
68. Caliendo, H. Five major U.S. brands collaborating on plant-based PET. http://www.plasticstoday.com/five-major-us-brands-collaborating-plant-based-pet/69477799417544 (accessed 19.08.2016).
69. Schut, J. H. The race to 100% bio PET. (accessed 19.08.2016).
70. Peters, M. W.; Taylor, J. D.; Jenni, M.; Manzer, L. E.; Henton, D. E. Integrated Process to Selectively Convert Renewable Isobutanol to P-Xylene - US20110087000. http://www.google.com/patents/US20110087000.
71. Lin, Z.; Nikolakis, V.; Ierapetritou, M., Alternative Approaches for p-Xylene Production from Starch: Techno-Economic Analysis. *Industrial & Engineering Chemistry Research* **2014,** *53* (26), 10688-10699.
72. Le procède isobutène. http://www.global-bioenergies.com/le-groupe/procede-isobutene-petrole-ressources-renouvelables/ (accessed 19.08.2016).
73. Smith, P. B., Bio-Based Sources for Terephthalic Acid. *Green Polymer Chemistry: Biobased Materials and Biocatalysis* **2015,** *1192*, 453-469.
74. Tachibana, Y.; Kimura, S.; Kasuya, K.-i., Synthesis and Verification of Biobased Terephthalic Acid from Furfural. *Scientific Reports* **2015,** *5*.
75. Williams, C. L.; Chang, C.-C.; Phuong, D.; Nikbin, N.; Caratzoulas, S.; Vlachos, D. G.; Lobo, R. F.; Fan, W.; Dauenhauer, P. J., Cycloaddition of Biomass-Derived Furans for Catalytic Production of Renewable p-Xylene. *American Chemical Society Catalysis* **2012,** *2* (6), 935-939.
76. Wang, B.; Gruter, G. J. M.; Dam, M. A.; Kriegel, R. M. Process for the preparation of benzene derivatives from furan derivatives-WO2014065657A1. http://www.google.com/patents/WO2014065657A1?cl=en.
77. Harmsen, P. F. H.; Hackmann, M. M.; Bos, H. L., Green building blocks for bio-based plastics. *Biofuels, Bioproducts and Biorefining* **2014,** *8* (3), 306-324.
78. Jacquel, N.; Freyermouth, F.; Fenouillot, F.; Rousseau, A.; Pascault, J. P.; Fuertes, P.; Saint-Loup, R., Synthesis and Properties of Poly(butylene succinate): Efficiency of Different Transesterification Catalysts. *Journal of Polymer Science Part a-Polymer Chemistry* **2011,** *49* (24), 5301-5312.
79. Zhou, X.-M., Synthesis and characterization of polyester copolymers based on poly(butylene succinate) and poly(ethylene glycol). *Materials Science and Engineering: C* **2012,** *32* (8), 2459-2463.
80. Yokohara, T.; Yamaguchi, M., Structure and properties for biomass-based polyester blends of PLA and PBS. *European Polymer Journal* **2008,** *44* (3), 677-685.

81. Xu, Y.; Xu, J.; Liu, D.; Guo, B.; Xie, X., Synthesis and characterization of biodegradable poly(butylene succinate-co-propylene succinate)s. *Journal of Applied Polymer Science* **2008,** *109* (3), 1881-1889.
82. Umare, S. S.; Chandure, A. S.; Pandey, R. A., Synthesis, characterization and biodegradable studies of 1,3-propanediol based polyesters. *Polymer Degradation and Stability* **2007,** *92* (3), 464-479.
83. Tsai, C.-J.; Chang, W.-C.; Chen, C.-H.; Lu, H.-Y.; Chen, M., Synthesis and characterization of polyesters derived from succinic acid, ethylene glycol and 1,3-propanediol. *European Polymer Journal* **2008,** *44* (7), 2339-2347.
84. Tachibana, Y.; Masuda, T.; Funabashi, M.; Kunioka, M., Chemical Synthesis of Fully Biomass-Based Poly(butylene succinate) from Inedible-Biomass-Based Furfural and Evaluation of Its Biomass Carbon Ratio. *Biomacromolecules* **2010,** *11* (10), 2760-2765.
85. Teomim, D.; Nyska, A.; Domb, A. J., Ricinoleic acid-based biopolymers. *Journal of Biomedical Materials Research* **1999,** *45* (3), 258-267.
86. Guo, B.; Chen, Y.; Lei, Y.; Zhang, L.; Zhou, W. Y.; Rabie, A. B. M.; Zhao, J., Biobased Poly(propylene sebacate) as Shape Memory Polymer with Tunable Switching Temperature for Potential Biomedical Applications. *Biomacromolecules* **2011,** *12* (4), 1312-1321.
87. Brioude, M. d. M.; Guimaraes, D. H.; Fiuza, R. d. P.; Prado, L. A. S. d. A.; Boaventura, J. S.; Jose, N. M., Synthesis and characterization of aliphatic Polyesters from glycerol, by-product of biodiesel production, and adipic acid. *Materials Research* **2007,** *10* (4), 335-339.
88. Kricheldorf, H. R.; Behinken, G., Biodegradable hyperbranched aliphatic polyesters derived from pentaerythritol. *Macromolecules* **2008,** *41* (15), 5651-5657.
89. Celli, A.; Marchese, P.; Sullalti, S.; Berti, C.; Barbiroli, G.; Commereuc, S.; Verney, V., Preparation of new biobased polyesters containing glycerol and their photodurability for outdoor applications. *Green Chemistry* **2012,** *14* (1), 182-187.
90. Barrett, D. G.; Merkel, T. J.; Luft, J. C.; Yousaf, M. N., One-Step Syntheses of Photocurable Polyesters Based on a Renewable Resource. *Macromolecules* **2010,** *43* (23), 9660-9667.
91. Dai, J.; Ma, S.; Liu, X.; Han, L.; Wu, Y.; Dai, X.; Zhu, J., Synthesis of bio-based unsaturated polyester resins and their application in waterborne UV-curable coatings. *Progress in Organic Coatings* **2015,** *78*, 49-54.
92. Teramoto, N.; Ozeki, M.; Fujiwara, I.; Shibata, M., Crosslinking and biodegradation of poly(butylene succinate) prepolymers containing itaconic or maleic acid units in the main chain. *Journal of Applied Polymer Science* **2005,** *95* (6), 1473-1480.
93. Atta, A. M.; Elsaeed, A. M.; Farag, R. K.; El-Saeed, S. M., Synthesis of unsaturated polyester resins based on rosin acrylic acid adduct for coating applications. *Reactive & Functional Polymers* **2007,** *67* (6), 549-563.
94. Atta, A. M.; Nassar, I. F.; Bedawy, H. M., Unsaturated polyester resins based on rosin maleic anhydride adduct as corrosion protections of steel. *Reactive & Functional Polymers* **2007,** *67* (7), 617-626.
95. Dutta, N.; Karak, N.; Dolui, S. K., Synthesis and characterization of polyester resins based on Nahar seed oil. *Progress in Organic Coatings* **2004,** *49* (2), 146-152.
96. Alam, M.; Akram, D.; Sharmin, E.; Zafar, F.; Ahmad, S., Vegetable oil based eco-friendly coating materials: A review article. *Arabian Journal of Chemistry* **2014,** *7* (4), 469-479.
97. Xia, Y.; Larock, R. C., Vegetable oil-based polymeric materials: synthesis, properties, and applications. *Green Chemistry* **2010,** *12* (11), 1893-1909.
98. Miao, S.; Wang, P.; Su, Z.; Zhang, S., Vegetable-oil-based polymers as future polymeric biomaterials. *Acta Biomaterialia* **2014,** *10* (4), 1692-1704.
99. Johansson, K.; Johansson, M., The effect of fatty acid methyl esters on the curing performance and final properties of thermally cured solvent-borne coil coatings. *Progress in Organic Coatings* **2007,** *59* (2), 146-151.
100. Janvier, M. Thesis: Les isohexides comme nouvelle plateforme biosourcée pour l'organocatalyse. 2015.
101. Che, P. H.; Lu, F.; Nie, X.; Huang, Y. Z.; Yang, Y. L.; Wang, F.; Xu, J., Hydrogen bond distinction and activation upon catalytic etherification of hydroxyl compounds. *Chemical Communications* **2015,** *51* (6), 1077-1080.
102. Kricheldorf, H. R., ''Sugar diols'' as building blocks of polycondensates. *Journal of Macromolecular Science-Reviews in Macromolecular Chemistry and Physics* **1997,** *C37* (4), 599-631.
103. Fenouillot, F.; Rousseau, A.; Colomines, G.; Saint-Loup, R.; Pascault, J. P., Polymers from renewable 1,4:3,6-dianhydrohexitols (isosorbide, isomannide and isoidide): A review. *Progress in Polymer Science* **2010,** *35* (5), 578-622.
104. Galbis, J. A.; García-Martín, M. G., Synthetic Polymers from Readily Available Monosaccharides. In *Carbohydrates in Sustainable Development II*, Rauter, A. P.; Vogel, P.; Queneau, Y., Eds. Springer Berlin Heidelberg: 2010; Vol. 295, pp 147-176.

105. Braun, D.; Bergmann, M., Polymers from 1,4/3,6-dianhydrosorbitol. *Journal für Praktische Chemie/Chemiker-Zeitung* **1992,** *334* (4), 298-310.
106. Storbeck, R.; Rehahn, M.; Ballauff, M., Synthesis and properties of high-molecular-weight polyesters based on 1,4:3,6-dianhydrohexitols and terephthalic acid. *Die Makromolekulare Chemie* **1993,** *194* (1), 53-64.
107. Storbeck, R.; Ballauff, M., Synthesis and thermal analysis of copolyesters deriving from 1,4:3,6-dianhydrosorbitol, ethylene glycol, and terephthalic acid. *Journal of Applied Polymer Science* **1996,** *59* (7), 1199-1202.
108. Moens, L. Polyesters for coatings with good flexibility, manufactured from renewable resources and/or recycled materials and manufacture thereof and coating compositions therefrom. EP2325229A1, 2011.
109. Farrugia, V. M.; Sacripante, G. G.; Zwartz, E. G.; Hawkins, M. S.; Zhou, K. Preparation of bio-based amorphous polyester resins. DE102011003584A1, 2011.
110. Jacquel, N.; Saint-Loup, R.; Pascault, J.-P.; Rousseau, A.; Fenouillot, F., Bio-based alternatives in the synthesis of aliphatic-aromatic polyesters dedicated to biodegradable film applications. *Polymer* **2015,** *59*, 234-242.
111. Duan, R. T.; He, Q. X.; Dong, X.; Li, D. F.; Wang, X. L.; Wang, Y. Z., Renewable Sugar-Based Diols with Different Rigid Structure: Comparable Investigation on Improving Poly(butylene succinate) Performance. *American Chemical Society Sustainable Chemistry & Engineering* **2016,** *4* (1), 350-362.
112. Feng, X.; Saini, P.; Busto, G.; East, A.; Hammond, W.; Jaffe, M., Isosorbide containing polyesters: Homopolymers and copolymers. *Abstracts of Papers of the American Chemical Society* **2012,** *244*.
113. Yoon, W. J.; Oh, K. S.; Koo, J. M.; Kim, J. R.; Lee, K. J.; Im, S. S., Advanced Polymerization and Properties of Biobased High T-g polyester of Isosorbide and 1,4-Cyclohexanedicarboxylic Acid through in Situ Acetylation. *Macromolecules* **2013,** *46* (8), 2930-2940.
114. Noordover, B. A. J.; Duchateau, R.; van Benthem, R. A. T. M.; Ming, W.; Koning, C. E., Enhancing the functionality of biobased polyester coating resins through modification with citric acid. *Biomacromolecules* **2007,** *8* (12), 3860-3870.
115. Kricheldorf, H. R.; Chatti, S.; Schwarz, G.; Kruger, R. P., Macrocycles 27: Cyclic aliphatic polyesters of isosorbide. *Journal of Polymer Science Part a-Polymer Chemistry* **2003,** *41* (21), 3414-3424.
116. Kricheldorf, H. R.; Weidner, S. M., High Tg copolyesters of lactide, isosorbide and isophthalic acid. *European Polymer Journal* **2013,** *49* (8), 2293-2302.
117. Habeych, D. I.; Juhl, P. B.; Pleiss, J.; Vanegas, D.; Eggink, G.; Boeriu, C. G., Biocatalytic synthesis of polyesters from sugar-based building blocks using immobilized Candida antarctica lipase B. *Journal of Molecular Catalysis B-Enzymatic* **2011,** *71* (1-2), 1-9.
118. Okada, M.; Tachikawa, K.; Aoi, K., Biodegradable polymers based on renewable resources. III. copolyesters composed of 1,4 : 3,6-dianhydro-D-glucitol, 1,1-bis(5-carboxy-2-furyl)ethane and aliphatic dicarboxylic acid units. *Journal of Applied Polymer Science* **1999,** *74* (14), 3342-3350.
119. Besse, V.; Auvergne, R.; Carlotti, S.; Boutevin, G.; Otazaghine, B.; Caillol, S.; Pascault, J.-P.; Boutevin, B., Synthesis of isosorbide based polyurethanes: An isocyanate free method. *Reactive and Functional Polymers* **2013,** *73* (3), 588-594.
120. Noordover, B. A. J.; Heise, A.; Malanowski, P.; Senatore, D.; Mak, M.; Molhoek, L.; Duchateau, R.; Koning, C. E.; van Benthem, R., Biobased step-growth polymers in powder coating applications. *Progress in Organic Coatings* **2009,** *65* (2), 187-196.
121. Noordover, B. A. J.; van Staalduinen, V. G.; Duchateau, R.; Koning, C. E.; van Benthem, R.; Mak, M.; Heise, A.; Frissen, A. E.; van Haveren, J., Co- and terpolyesters based on isosorbide and succinic acid for coating applications: Synthesis and characterization. *Biomacromolecules* **2006,** *7* (12), 3406-3416.
122. van Haveren, J.; Oostveen, E. A.; Micciche, F.; Noordover, B. A. J.; Koning, C. E.; van Benthem, R. A. T. M.; Frissen, A. E.; Weijnen, J. G. J., Resins and additives for powder coatings and alkyd paints based on renewable resources. *Journal of Coatings Technology and Research* **2007,** *4* (2), 177-186.
123. Feng, X.; East, A.; Hammond, W.; Ophir, Z.; Zhang, Y.; Jaffe, M., Thermal analysis characterization of isosorbide-containing thermosets. *Journal of Thermal Analysis and Calorimetry* **2012,** *109* (3), 1267-1275.
124. Hong, J.; Radojcic, D.; Ionescu, M.; Petrovic, Z. S.; Eastwood, E., Advanced materials from corn: isosorbide-based epoxy resins. *Polymer Chemistry* **2014,** *5* (18), 5360-5368.
125. Gioia, C.; Vannini, M.; Marchese, P.; Minesso, A.; Cavalieri, R.; Colonna, M.; Celli, A., Sustainable polyesters for powder coating applications from recycled PET, isosorbide and succinic acid. *Green Chemistry* **2014,** *16* (4), 1807-1815.
126. Lorenzini, C.; Renard, E.; Bensemhoun, J.; Babinot, J.; Versace, D.-L.; Langlois, V., High glass transition temperature bio-based copolyesters from poly(3-hydroxybutyrate-co-3-hydroxyvalerate) and isosorbide. *Reactive & Functional Polymers* **2013,** *73* (12), 1656-1661.

127. Lorenzini, C.; Versace, D. L.; Renard, E.; Langlois, V., Renewable epoxy networks by photoinitiated copolymerization of poly(3-hydroxyalkanoate)s and isosorbide derivatives. *Reactive & Functional Polymers* **2015,** *93*, 95-100.
128. Noordover, B. A. J.; Haveman, D.; Duchateau, R.; van Benthem, R.; Koning, C. E., Chemistry, Functionality, and Coating Performance of Biobased Copolycarbonates from 1,4:3,6-Dianhydrohexitols. *Journal of Applied Polymer Science* **2011,** *121* (3), 1450-1463.
129. Jasinska, L.; Koning, C. E., Waterborne Polyesters Partially Based on Renewable Resources. *Journal of Polymer Science Part a-Polymer Chemistry* **2010,** *48* (24), 5907-5915.
130. Sadler, J. M.; Toulan, F. R.; Nguyen, A.-P. T.; Kayea, R. V., III; Ziaee, S.; Palmese, G. R.; La Scala, J. J., Isosorbide as the structural component of bio-based unsaturated polyesters for use as thermosetting resins. *Carbohydrate Polymers* **2014,** *100*, 97-106.
131. Fonseca, A. C.; Lopes, I. M.; Coelho, J. F. J.; Serra, A. C., Synthesis of unsaturated polyesters based on renewable monomers: Structure/properties relationship and crosslinking with 2-hydroxyethyl methacrylate. *Reactive and Functional Polymers* **2015,** *97*, 1-11.
132. Ma, S. Q.; Webster, D. C.; Jabeen, F., Hard and Flexible, Degradable Thermosets from Renewable Bioresources with the Assistance of Water and Ethanol. *Macromolecules* **2016,** *49* (10), 3780-3788.
133. Smiga-Matuszowicz, M.; Janicki, B.; Jaszcz, K.; Lukaszczyk, J.; Kaczmarek, M.; Lesiak, M.; Sieron, A. L.; Simka, W.; Mierzwinski, M.; Kusz, D., Novel bioactive polyester scaffolds prepared from unsaturated resins based on isosorbide and succinic acid. *Materials Science & Engineering C-Materials for Biological Applications* **2014,** *45*, 64-71.
134. Kricheldorf, H. R.; Berghahn, M.; Probst, N.; Gurau, M.; Schwarz, G., Cholesteric and photoreactive polyesters. *Reactive & Functional Polymers* **1996,** *30* (1-3), 173-189.
135. Llevot, A.; Grau, E.; Carlotti, S.; Grelier, S.; Cramail, H., From Lignin-derived Aromatic Compounds to Novel Biobased Polymers. *Macromolecular Rapid Communications* **2016,** *37* (1), 9-28.
136. Fache, M.; Boutevin, B.; Caillol, S., Vanillin, a key-intermediate of biobased polymers. *European Polymer Journal* **2015,** *68*, 488-502.
137. Offenhauer, R. D., The direct esterification of phenols. *Journal of Chemical Education* **1964,** *41* (1), 39.
138. Brown, J. S.; Glaser, R.; Liotta, C. L.; Eckert, C. A., Acylation of activated aromatics without added acid catalyst. *Chemical Communications* **2000,** (14), 1295-1296.
139. Stanzione, J. F., III; Giangiulio, P. A.; Sadler, J. M.; La Scala, J. J.; Wool, R. P., Lignin-Based Bio-Oil Mimic as Biobased Resin for Composite Applications. *American Chemical Society Sustainable Chemistry and Engineering* **2013,** *1* (4), 419-426.
140. Harvey, K. A.; Xu, Z.; Whitley, P.; Jo Davisson, V.; Siddiqui, R. A., Characterization of anticancer properties of 2,6-diisopropylphenol–docosahexaenoate and analogues in breast cancer cells. *Bioorganic & Medicinal Chemistry* **2010,** *18* (5), 1866-1874.
141. Gowda, S.; Lokanatha Rai, K. M., Manganese(III) acetate as catalyst for the direct acetylation of alcohols with acetic acid. *Journal of Molecular Catalysis A: Chemical* **2004,** *217* (1–2), 27-29.
142. Mohammadpoor-Baltork, I.; Khosropour, A. R.; Aliyan, H., A convenient and chemoselective acetylation and formylation of alcohols and phenols using acetic acid and ethyl formate in the presence of Bi(III) salts. *Journal of Chemical Research* **2001,** *2001* (7), 280-282.
143. Varala, R.; Nasreen, A.; Adapa, S. R., Ruthenium(III) acetylacetonate [Ru(acac)3] — An efficient recyclable catalyst for the acetylation of phenols, alcohols, and amines under neat conditions. *Canadian Journal of Chemistry* **2007,** *85* (2), 148-152.
144. Jin, X. M.; Carfagna, C.; Nicolais, L.; Lanzetta, R., Synthesis, characterization, and in-vitro degradation of a novel thermotropic ternary copolyester based on p-hydroxycinnamic acid. *Macromolecules* **1995,** *28* (14), 4785-4794.
145. Matsusaki, M.; Kishida, A.; Stainton, N.; Ansell, C. W. G.; Akashi, M., Synthesis and characterization of novel biodegradable polymers composed of hydroxycinnamic acid and D,L-lactic acid. *Journal of Applied Polymer Science* **2001,** *82* (10), 2357-2364.
146. Matsusaki, M.; Thi, T. H.; Kaneko, T.; Akashi, M., Enhanced effects of lithocholic acid incorporation into liquid-crystalline biopolymer poly(coumaric acid) on structural ordering and cell adhesion. *Biomaterials* **2005,** *26* (32), 6263-6270.
147. Dong, W.; Li, H.; Chen, M.; Ni, Z.; Zhao, J.; Yang, H.; Gijsman, P., Biodegradable bio-based polyesters with controllable photo-crosslinkability, thermal and hydrolytic stability. *Journal of Polymer Research* **2011,** *18* (6), 1239-1247.
148. Kaneko, T.; Matsusaki, M.; Hang, T. T.; Akashi, M., Thermotropic liquid-crystalline polymer derived from natural cinnamoyl biomonomers. *Macromolecular Rapid Communications* **2004,** *25* (5), 673-677.

149. Kaneko, T.; Kaneko, D.; Wang, S., High-performance lignin-mimetic polyesters. *Plant Biotechnology* **2010,** *27* (3), 243-250.
150. Kaneko, T., High-performance functional ecopolymers based on flora and fauna. *Chemical Record* **2007,** *7* (4), 210-219.
151. Kaneko, T.; Tran, H. T.; Matsusaki, M.; Akashi, M., Biodegradable LC oligomers with cranked branching points form highly oriented fibrous scaffold for cytoskeletal orientation. *Chemistry of Materials* **2006,** *18* (26), 6220-6226.
152. Kaneko, T.; Thi, T. H.; Shi, D. J.; Akashi, M., Environmentally degradable, high-performance thermoplastics from phenolic phytomonomers. *Nature Materials* **2006,** *5* (12), 966-970.
153. Thi, T. H.; Matsusaki, M.; Shi, D.; Kaneko, T.; Akashi, M., Synthesis and properties of coumaric acid derivative homo-polymers. *Journal of Biomaterials Science-Polymer Edition* **2008,** *19* (1), 75-85.
154. Thi, T. H.; Matsusaki, M.; Hirano, H.; Kawano, H.; Agari, Y.; Akashi, M., Mechanism of High Thermal Stability of Commercial Polyesters and Polyethers Conjugated with Bio-Based Caffeic Acid. *Journal of Polymer Science Part a-Polymer Chemistry* **2011,** *49* (14), 3152-3162.
155. Du, J.; Fang, Y.; Zheng, Y., Synthesis, characterization and biodegradation of biodegradable-cum-photoactive liquid-crystalline copolyesters derived from ferulic acid. *Polymer* **2007,** *48* (19), 5541-5547.
156. Sun, H.; Kanehashi, S.; Tsuchiya, K.; Ogino, K., Synthesis and Characterization of Biobased Polyesters Derived from Vanillin-based Schiff Base and Cinnamic Acid Derivatives. *Chemistry Letters* **2016,** *45* (4), 439-441.
157. Nagata, M., Synthesis, characterization, and hydrolytic degradation of copolyesters of 3-(4-hydroxyphenyl) propionic acid and p-hydroxybenzoic acid, vanilic acid, or syringic acid. *Journal of Applied Polymer Science* **2000,** *78* (14), 2474-2481.
158. Wilsens, C. H. R. M.; Noordover, B. A. J.; Rastogi, S., Aromatic thermotropic polyesters based on 2,5-furandicarboxylic acid and vanillic acid. *Polymer* **2014,** *55* (10), 2432-2439.
159. Mialon, L.; Miller, S. A. Poly(dihydroferulic acid) a biorenewable polyethylene terephthalate mimic derived from lignin and acetic acid. WO2011143379A2, 2011.
160. Mialon, L.; Miller, S. A. Biorenewable thermoplastic polyesters derived from dihydroferulic acid and production methods. US20130137847A1, 2013.
161. Fosdick, L. S.; Starke, A. C., Some alkamine esters of 4-acetylferulic and 3,4-dimethoxycinnamic acids. *Journal of the American Chemical Society* **1940,** *62*, 3352-3355.
162. Kricheldorf, H. R.; Stukenbrock, T., New polymer syntheses .92. Biodegradable, thermotropic copolyesters derived from beta-(4-hydroxyphenyl)propionic acid. *Macromolecular Chemistry and Physics* **1997,** *198* (11), 3753-3767.
163. Kricheldorf, H. R.; Lohden, G., Whisker .11. Poly(ester-amide)s derived from vanillic acid and 4-aminobenzoic acid. *Polymer* **1995,** *36* (8), 1697-1705.
164. Ouimet, M. A.; Griffin, J.; Carbone-Howell, A. L.; Wu, W.-H.; Stebbins, N. D.; Di, R.; Uhrich, K. E., Biodegradable Ferulic Acid-Containing Poly(anhydride-ester): Degradation Products with Controlled Release and Sustained Antioxidant Activity. *Biomacromolecules* **2013,** *14* (3), 854-861.
165. Nagata, M.; Hizakae, S., Synthesis and properties of biodegradable copolymers based on 4,4 '-(adipoyldioxy)dicinnamic acid, 1,6-hexanediol, and poly(ethylene glycol)s. *Journal of Polymer Science Part a-Polymer Chemistry* **2003,** *41* (19), 2930-2938.
166. Nagata, M.; Sato, Y., Biodegradable elastic photocured polyesters based on adipic acid, 4-hydroxycinnamic acid and poly(epsilon-caprolactone) diols. *Polymer* **2004,** *45* (1), 87-93.
167. Nagata, M.; Hizakae, S., Synthesis and characterization of photocrosslinkable biodegradable polymers derived from 4-hydroxycinnamic acid. *Macromolecular Bioscience* **2003,** *3* (8), 412-419.
168. Mialon, L.; Vanderhenst, R.; Pemba, A. G.; Miller, S. A., Polyalkylenehydroxybenzoates (PAHBs): Biorenewable Aromatic/Aliphatic Polyesters from Lignin. *Macromolecular Rapid Communications* **2011,** *32* (17), 1386-1392.
169. Kreye, O.; Oelmann, S.; Meier, M. A. R., Renewable Aromatic–Aliphatic Copolyesters Derived from Rapeseed. *Macromolecular Chemistry and Physics* **2013,** *214* (13), 1452-1464.
170. Bock, L. H. Polyesters made from dibasic acids derived from vanillin. US2662871, 1953.
171. Bock, L. H.; Anderson, J. K., Linear polyesters derived from vanillic acid. *Journal of Polymer Science* **1955,** *17* (86), 553-558.
172. Lange, W.; Kordsachia, O., Preparation and properties of polyesters from vanillin and syringic aldehyde. *Holz als Roh- und Werkstoff* **1981,** *39* (3), 107-12.
173. Erä, V.; Hannula, J., Polyesters from vanillin. Synthesis and characterization. *Paperi ja Puu* **1974,** *56* (5), 489-496.
174. Pang, C.; Zhang, J.; Wu, G.; Wang, Y.; Gao, H.; Ma, J., Renewable polyesters derived from 10-undecenoic acid and vanillic acid with versatile properties. *Polymer Chemistry* **2014,** *5* (8), 2843-2853.

175. Pang, C.; Zhang, J.; Zhang, Q.; Wu, G.; Wang, Y.; Ma, J., Novel vanillic acid-based poly(ether-ester)s: from synthesis to properties. *Polymer Chemistry* **2015,** *6* (5), 797-804.
176. Llevot, A.; Grau, E.; Carlotti, S.; Greliera, S.; Cramail, H., Renewable (semi)aromatic polyesters from symmetrical vanillin-based dimers. *Polymer Chemistry* **2015,** *6* (33), 6058-6066.
177. Pion, F.; Ducrot, P.-H.; Allais, F., Renewable Alternating Aliphatic-Aromatic Copolyesters Derived from Biobased Ferulic Acid, Diols, and Diacids: Sustainable Polymers with Tunable Thermal Properties. *Macromolecular Chemistry and Physics* **2014,** *215* (5), 431-439.
178. Fache, M.; Darroman, E.; Besse, V.; Auvergne, R.; Caillol, S.; Boutevin, B., Vanillin, a promising biobased building-block for monomer synthesis. *Green Chemistry* **2014,** *16* (4), 1987-1998.
179. Krause, F. Development of monomers from vanillin for polyesters as well as biologically degradable polyester materials. 2012.
180. Schwolow, C. Consideration of the Tishchenko reaction on vanillin derivatives for the synthesis of polyesters. 2013.
181. Hansen, C. A.; Frost, J. W., Deoxygenation of Polyhydroxybenzenes: An Alternative Strategy for the Benzene-Free Synthesis of Aromatic Chemicals. *Journal of the American Chemical Society* **2002,** *124* (21), 5926-5927.
182. Gioia, C.; Banella, M. B.; Vannini, M.; Celli, A.; Colonna, M.; Caretti, D., Resorcinol: A potentially bio-based building block for the preparation of sustainable polyesters. *European Polymer Journal* **2015,** *73*, 38-49.
183. Nemilov, V. E.; Orlova, T. V.; Chulkova, Y. S., Kinetics of polycondensation of betulin with adipic acid. *Russian Journal of Applied Chemistry* **2005,** *78* (7), 1162-1165.
184. Tator, K. B., Coating Deterioration. In *ASM Handbook Protective Organic Coatings*, K.B.Tator, Ed. ASM International: 2015; Vol. 5B, pp 462-473.
185. Shah, A. A.; Hasan, F.; Hameed, A.; Ahmed, S., Biological degradation of plastics: A comprehensive review. *Biotechnology Advances* **2008,** *26* (3), 246-265.
186. Okada, M., Chemical syntheses of biodegradable polymers. *Progress in Polymer Science* **2002,** *27* (1), 87-133.
187. *European Coil Coating Association, Coil Coating - Sustainable Business*; prepaintedmetal.eu: 2012.
188. Wicks, Z. W.; Jones, F. N.; Pappas, S. P., Exterior durability: I. *Journal of Coatings Technology* **1999,** *71* (888), 53-55.
189. Singh, B.; Sharma, N., Mechanistic implications of plastic degradation. *Polymer Degradation and Stability* **2008,** *93* (3), 561-584.
190. Rabek, J. F., *Photodegradation of polymers: physical characteristics and applications*. Springer: 1996.
191. Carlsson, D. J.; Wiles, D. M., *Degradation*. Wiley Interscience: 1986; Vol. 4.
192. Overberger, C. G.; Salamone, J. C.; Šebenda, J., Organic Chemistry of Synthetic High Polymers. Robert W. Lenz. Interscience (Wiley), New York, 1967. xvi + 837 pp., illus. $15. *Science* **1968,** *159* (3820), 1224-1224.
193. Commission International d'Eclairage (CIE, I. C. o. I., International lighting vocabulary. In *Pub CIE 17*, 1970.
194. Celina, M. C., Review of polymer oxidation and its relationship with materials performance and lifetime prediction. *Polymer Degradation and Stability* **2013,** *98* (12), 2419-2429.
195. Jones, T. E.; McCarthy, J. M., Statistical study of hydrolytic stability in Amine-neutralized waterborne polyester resins as a function of monomer composition. *Journal of Coatings Technology* **1995,** *67* (844), 57-65.
196. Perera, D. Y., Physical ageing of organic coatings. *Progress in Organic Coatings* **2003,** *47* (1), 61-76.
197. Jacques, L. F. E., Accelerated and outdoor/natural exposure testing of coatings. *Progress in Polymer Science* **2000,** *25* (9), 1337-1362.
198. Q-LAB Accelerated Weathering Testing and Corrosion Chambers. http://www.q-lab.com/en-gb (accessed 08.11.2016).
199. Zhu, Z.; Kelley, M. J., IR spectroscopic investigation of the effect of deep UV irradiation on PET films. *Polymer* **2005,** *46* (20), 8883-8891.
200. Pohl, H. A., The Thermal Degradation of Polyesters. *Journal of the American Chemical Society* **1951,** *73* (12), 5660-5661.
201. Launay, A.; Thominette, F.; Verdu, J., Hydrolysis of poly(ethylene terephtalate). A steric exclusion chromatography study. *Polymer Degradation and Stability* **1999,** *63* (3), 385-389.
202. Sammon, C.; Yarwood, J.; Everall, N., An FT–IR study of the effect of hydrolytic degradation on the structure of thin PET films. *Polymer Degradation and Stability* **2000,** *67* (1), 149-158.
203. Carroccio, S.; Rizzarelli, P.; Puglisi, C.; Montaudo, G., MALDI investigation of photooxidation in aliphatic polyesters: Poly(butylene succinate). *Macromolecules* **2004,** *37* (17), 6576-6586.
204. Shigemoto, I.; Kawakami, T.; Taiko, H.; Okumura, M., A quantum chemical study on the thermal degradation reaction of polyesters. *Polymer Degradation and Stability* **2012,** *97* (6), 941-947.

205. Nagai, Y.; Ogawa, T.; Nishimoto, Y.; Ohishi, F., Analysis of weathering of a thermoplastic polyester elastomer II. Factors affecting weathering of a polyether-polyester elastomer. *Polymer Degradation and Stability* **1999,** *65* (2), 217-224.
206. Malanowski, P.; Huijser, S.; van Benthem, R. A. T. M.; van der Ven, L. G. J.; Laven, J.; de With, G., Photodegradation of poly(neopentyl isophthalate) part I: Laboratory and outdoor conditions. *Polymer Degradation and Stability* **2009,** *94* (11), 2086-2094.
207. Malanowski, P.; van Benthem, R. A. T. M.; van der Ven, L. G. J.; Laven, J.; Kisin, S.; de With, G., Photodegradation of poly(neopentyl isophthalate). Part II: Mechanism of cross-linking. *Polymer Degradation and Stability* **2011,** *96* (6), 1141-1148.
208. Malanowski, P.; Huijser, S.; Scaltro, F.; van Benthem, R. A. T. M.; van der Ven, L. G. J.; Laven, J.; de With, G., Photodegradation of poly(neopentyl terephthalate). *Progress in Organic Coatings* **2012,** *74* (1), 165-172.
209. Commereuc, S.; Askanian, H.; Verney, V.; Celli, A.; Marchese, P., About Durability of Biodegradable Polymers: Structure/Degradability Relationships. In *Modern Trends in Polymer Science-Epf 09*, Stelzer, F.; Wiesbrock, E., Eds. 2010; Vol. 296, pp 378-387.
210. Commereuc, S.; Askanian, H.; Verney, V.; Celli, A.; Marchese, P.; Berti, C., About the end life of novel aliphatic and aliphatic-aromatic (co)polyesters after UV-weathering: Structure/degradability relationships. *Polymer Degradation and Stability* **2013,** *98* (7), 1321-1328.
211. Celli, A.; Marchese, P.; Sullalti, S.; Berti, C.; Commereuc, S.; Verney, V., New polymers from renewable resources: synthesis, characterization, and photodurability of aliphatic polyesters containing glycerol. *Journal of Biotechnology* **2010,** *150*, S206-S206.
212. Okada, M.; Okada, Y.; Aoi, K., Synthesis and degradabilities of polyesters from 1,4/3,6-dianhydrohexitols and aliphatic dicarboxylic-acids. *Journal of Polymer Science Part a-Polymer Chemistry* **1995,** *33* (16), 2813-2820.
213. Lukey, C. A., The use of chemiluminescence analysis to measure hydroperoxide levels in photo-oxidised polyester/melamine surface coatings. *Progress in Organic Coatings* **2001,** *41* (1?3), 129-134.
214. Gamage, N. J. W.; Hill, D. J. T.; Lukey, C. A.; Pomery, P. J., Factors affecting the photolysis of polyester-melamine surface coatings. *Polymer Degradation and Stability* **2003,** *81* (2), 309-326.
215. Binns, M. R.; Lukey, C. A.; Hill, D. J. T.; Odonnell, J. H.; Pomery, P. J., A new technique for the study of reactive species generated during the initial-stages of polymer photodegradation. *Polymer Bulletin* **1992,** *27* (4), 421-424.
216. Zhang, W. R.; Zhu, T. T.; Smith, R.; Lowe, C., A non-destructive study on the degradation of polymer coating I: Step-scan photoacoustic FTIR and confocal Raman microscopy depth profiling. *Polymer Testing* **2012,** *31* (7), 855-863.
217. Biggs, S.; Lukey, C. A.; Spinks, G. M.; Yau, S. T., An atomic force microscopy study of weathering of polyester/melamine paint surfaces. *Progress in Organic Coatings* **2001,** *42* (1-2), 49-58.
218. ATLAS Heraeus suntest. http://atlas-mts.com/products/product-detail/pid/237/ (accessed 08.11.2016).
219. Batista, M. A. J.; Moraes, R. P.; Barbosa, J. C. S.; Oliveira, P. C.; Santos, A. M., Effect of the polyester chemical structure on the stability of polyester-melamine coatings when exposed to accelerated weathering. *Progress in Organic Coatings* **2011,** *71* (3), 265-273.
220. Sullivan, C. J.; Cooper, C. F., Polyester weatherability - Coupling frontier molecular-orbital calculations of oxidative stability with accelerated testing. *Journal of Coatings Technology* **1995,** *67* (847), 53-62.
221. Narayan, R.; Chattopadhyay, D. K.; Sreedhar, B.; Raju, K.; Mallikarjuna, N. N.; Aminabhavi, T. M., Degradation profiles of polyester-urethane (hydroxylated polyester/diphenylmethane diisocyanate) and polyester-melamine (hydroxylated polyester/hexamethoxymethyl-melamine) coatings: An accelerated weathering study. *Journal of Applied Polymer Science* **2005,** *97* (3), 1069-1081.
222. Narayan, R.; Chattopadhyay, D. K.; Sreedhar, B.; Raju, K.; Mallikarjuna, N. N.; Aminabhavi, T. M., Degradation profiles of polyester-urethane (HP-MDI) and polyester-melamine (HP-HMMM) coatings: A thermal study. *Journal of Applied Polymer Science* **2005,** *97* (2), 518-526.
223. Broido, A., A simple, sensitive graphical method of treating thermogravimetric analysis data. *Journal of Polymer Science Part A-2: Polymer Physics* **1969,** *7* (10), 1761-1773.
224. Coats, A. W.; Redfern, J. P., Kinetic Parameters from Thermogravimetric Data. *Nature* **1964,** *201* (4914), 68-69.
225. Chang, W. L., Decomposition behavior of polyurethanes via mathematical simulation. *Journal of Applied Polymer Science* **1994,** *53* (13), 1759-1769.
226. Lukey, C. A.; Hill, D. J. T.; Pomery, P. J., UV photolysis of melamine formaldehyde crosslinkers. *Polymer Degradation and Stability* **2002,** *78* (3), 485-490.

227. Zhang, W. R.; Hinder, S. J.; Smith, R.; Lowe, C.; Watts, J. F., An investigation of the effect of pigment on the degradation of a naturally weathered polyester coating. *Journal of Coatings Technology and Research* **2011,** *8* (3), 329-342.
228. Mielewski, D. F.; Bauer, D. R.; Gerlock, J. L., The role of hydroperoxides in the photooxidation of cross-linked polymer-coatings. *Polymer Degradation and Stability* **1991,** *33* (1), 93-104.
229. Bauer, D. R., Kinetics of photooxidation and photostabilization in crosslinked polymer coatings. *Polymer Degradation and Stability* **1995,** *48* (2), 259-267.
230. Bauer, D. R.; Gerlock, J. L.; Mielewski, D. F., Photodegradation and photostabilization in organic coatings containing a hindered amine light stabilizer .6. ESR measurements of nitroxide kinetics and mechanism of stabilization. *Polymer Degradation and Stability* **1990,** *28* (2), 115-129.
231. Bauer, D. R.; Gerlock, J. L.; Mielewski, D. F.; Peck, M. C. P.; Carter, R. O., Photo-stabilization and photo-degradation in organic coatings containing a hindered amine light stabilizer .4. Photo-stabilization and photo-degradation in organic coatings containing a hindered amine light stabilizer .4. Photo-initiation rates and photooxidation rates in unstabilized coatings. *Polymer Degradation and Stability* **1990,** *27* (3), 271-284.
232. Bauer, D. R.; Gerlock, J. L.; Mielewski, D. F.; Peck, M. C. P.; Carter, R. O., Photostabilization and photodegradation in organic coatings containing a hindered amine light stabilizer .5. Infrared spectroscopic measurements of hindered amine effectiveness. *Polymer Degradation and Stability* **1990,** *28* (1), 39-51.
233. Mitra, S.; Ahire, A.; Mallik, B. P., Investigation of accelerated aging behaviour of high performance industrial coatings by dynamic mechanical analysis. *Progress in Organic Coatings* **2014,** *77* (11), 1816-1825.
234. Nichols, M. E.; Gerlock, J. L.; Smith, C. A., Rates of photooxidation induced crosslinking and chain scission in thermoset polymer coatings .1. *Polymer Degradation and Stability* **1997,** *56* (1), 81-91.
235. Richaud, E.; Gilormini, P.; Coquillat, M.; Verdu, J., Crosslink Density Changes during the Hydrolysis of Tridimensional Polyesters. *Macromolecular Theory and Simulations* **2014,** *23* (5), 320-330.
236. Mallon, P. E.; Li, Y.; Zhang, R.; Chen, H.; Wu, Y.; Sandreczki, T. C.; Jean, Y. C.; Suzuki, R.; Ohdaira, T., Durability of polymeric coatings: effects of natural and artificial weathering. *Applied Surface Science* **2002,** *194* (1–4), 176-181.
237. Nichols, M. E.; Gerlock, J. L., Rates of photooxidation induced crosslinking and chain scission in thermoset polymer coatings - II. Effect of hindered amine light stabilizer and ultraviolet light absorber additives. *Polymer Degradation and Stability* **2000,** *69* (2), 197-207.
238. Zhang, Y.; Maxted, J.; Barber, A.; Lowe, C.; Smith, R., The durability of clear polyurethane coil coatings studied by FTIR peak fitting. *Polymer Degradation and Stability* **2013,** *98* (2), 527-534.
239. Larche, J. F.; Bussiere, P. O.; Wong-Wah-Chung, P.; Gardette, J. L., Chemical structure evolution of acrylic-melamine thermoset upon photo-ageing. *European Polymer Journal* **2012,** *48* (1), 172-182.
240. Lee, S.; Nguyen, T.; Byrd, E.; Martin, J., Quantitative study of water transport during the hydrolysis of polymer coatings exposed to water vapor. *Journal of Materials Research* **2003,** *18* (9), 2268-2275.
241. Nguyen, T.; Martin, J.; Byrd, E., Relating laboratory and outdoor exposure of coatings: IV. Mode and mechanism for hydrolytic degradation of acrylic-melamine coatings exposed to water vapor in the absence of UV light. *Journal of Coatings Technology* **2003,** *75* (941), 37-50.
242. Nguyen, T.; Gu, X.; Vanlandingham, M.; Byrd, E.; Ryntz, R.; Martin, J. W., Degradation modes of crosslinked coatings exposed to photolytic environment. *Journal of Coatings Technology and Research* **2013,** *10* (1), 1-14.
243. Osterhold, M.; Glockner, P., Influence of weathering on physical properties of clearcoats. *Progress in Organic Coatings* **2001,** *41* (1-3), 177-182.
244. Maetens, D., Weathering degradation mechanism in polyester powder coatings. *Progress in Organic Coatings* **2007,** *58* (2-3), 172-179.
245. Gerlock, J. L.; Bauer, D. R., Electron-spin-resonance measurements of free-radical photoinitiation rates by nitroxide termination. *Journal of Polymer Science Part C-Polymer Letters* **1984,** *22* (8), 447-455.
246. Estácio, S. G.; Cabral do Couto, P.; Costa Cabral, B. J.; Minas da Piedade, M. E.; Martinho Simões, J. A., Energetics of Intramolecular Hydrogen Bonding in Di-substituted Benzenes by the ortho−para Method. *The Journal of Physical Chemistry A* **2004,** *108* (49), 10834-10843.
247. Velavan, R.; Sureshkumar, P.; Sivakumar, K.; Natarajan, S., Vanillin-I. *Acta Crystallographica Section C-Crystal Structure Communications* **1995,** *51*, 1131-1133.
248. Groom, C. R.; Bruno, I. J.; Lightfoot, M. P.; Ward, S. C., The Cambridge Structural Database. *Acta Crystallographica Section B-Structural Science Crystal Engineering and Materials* **2016,** *72*, 171-179.
249. Xu, S.; Held, I.; Kempf, B.; Mayr, H.; Steglich, W.; Zipse, H., The DMAP-Catalyzed Acetylation of Alcohols—A Mechanistic Study (DMAP=4-(Dimethylamino)pyridine). *Chemistry – A European Journal* **2005,** *11* (16), 4751-4757.

250. Barbooti, M. M.; Al-Sammerrai, D. A., Thermal decomposition of citric acid. *Thermochimica Acta* **1986,** *98*, 119-126.
251. Wyrzykowski, D.; Hebanowska, E.; Nowak-Wiczk, G.; Makowski, M.; Chmurzyński, L., Thermal behaviour of citric acid and isomeric aconitic acids. *Journal of Thermal Analysis and Calorimetry* **2011,** *104* (2), 731-735.
252. Choi, Y. H.; Kim, H. K.; Linthorst, H. J. M.; Hollander, J. G.; Lefeber, A. W. M.; Erkelens, C.; Nuzillard, J.-M.; Verpoorte, R., NMR Metabolomics to Revisit the Tobacco Mosaic Virus Infection in Nicotiana tabacum Leaves. *Journal of Natural Products* **2006,** *69* (5), 742-748.
253. Kita, Y.; Akai, S.; Ajimura, N.; Yoshigi, M.; Tsugoshi, T.; Yasuda, H.; Tamura, Y., Facile and efficient syntheses of carboxylic anhydrides and amides using (trimethylsilyl)ethoxyacetylene. *J. Org. Chem.* **1986,** *51* (22), 4150-8.
254. Sharma, V.; Kelly, G. T.; Watanabe, C. M. H., Exploration of the Molecular Origin of the Azinomycin Epoxide: Timing of the Biosynthesis Revealed. *Organic Letters* **2008,** *10* (21), 4815-4818.
255. Apffel, A.; Fischer, S.; Goldberg, G.; Goodley, P. C.; Kuhlmann, F. E., Enhanced sensitivity for peptide-mapping with electrospray liquid-chromatography mass-spectrometry in the presence of signal suppresion due to trifluoroacetic acid-containing mobile phases. *Journal of Chromatography A* **1995,** *712* (1), 177-190.
256. Mirza, U. A.; Chait, B. T., Effects of anions on the positive-ion electrospray-ionization mass-spectra of peptides and proteins. *Analytical Chemistry* **1994,** *66* (18), 2898-2904.
257. VLE-Calc - vapor-liquid equilibrium calculator. http://vle-calc.com/azeotrope.html?numOfC=2&compnames=1&Comp1=124&Comp2=4&Comp3=2.
258. Hansen, C. M., *Hansen Solubility Parameters: A User's Handbook, Second Edition*. CRC Press: 2007.
259. Fox, T. G.; Flory, P. J., 2nd-order transition temperatures and related properties of polystyrene .1. Influence of molecular weight. *Journal of Applied Physics* **1950,** *21* (6), 581-591.
260. Koleske, J. V., Mechanical Properties of Solid Coatings. In *Encyclopedia of Analytical Chemistry*, John Wiley & Sons, Ltd: 2006.
261. Ehrenstein, G. W.; Riedel, G.; Trawiel, P., Dynamic Mechanical Analysis (DMA). In *Thermal Analysis of Plastics*, Carl Hanser Verlag GmbH & Co. KG: 2004; pp 236-299.
262. Spinks, G. M.; Liu, Z. Z.; Brown, H.; Swain, M.; See, H.; Evans, E., Paint layer thermomechanical properties determined by in situ dynamic mechanical analysis in 3-point bending. *Progress in Organic Coatings* **2004,** *49* (2), 95-102.
263. Schlesing, W.; Buhk, M.; Osterhold, M., Dynamic mechanical analysis in coatings industry. *Progress in Organic Coatings* **2004,** *49* (3), 197-208.
264. Buder-Stroisznigg, M.; Wallner, G. M.; Strauss, B.; Jandel, L.; Lang, R. W., Structure-property correlations of flexible clear coats. *Progress in Organic Coatings* **2009,** *65* (3), 328-332.
265. Giannakopoulos, I.; Taylor, A. C., A modelling study of the visco-elastic behaviour of polyester-based coil coatings. *Progress in Organic Coatings* **2013,** *76* (11), 1556-1566.
266. Lee, Y.-H.; Kim, H.-J., Effect of cycloaliphatic structure of polyester on the formability and stone-chip resistance for automotive pre-coated metals. *Progress in Organic Coatings* **2016,** *99*, 117-124.
267. Hill, L. W., Calculation of crosslink density in short chain networks. *Progress in Organic Coatings* **1997,** *31* (3), 235-243.
268. Nielsen, L. E., Cross-linking effect on physical properties of polymers. *Journal of Macromolecular Science-Reviews in Macromolecular Chemistry* **1969,** *C 3* (1), 69-&.
269. FischerTechnology Probes for coating thickness measurements. http://www.fischer-technology.com/fileadmin/user_upload/default/Brochures/en-gb/BROC_Probes_902-111_en.pdf (accessed 07.10.2016).
270. Wang, Y.-L.; M. Mebel, A.; Wu, C.-J.; Chen, Y.-T.; Lin, C.-E.; Jiang, J.-C., IR spectroscopy and theoretical vibrational calculation of the melamine molecule. *Journal of the Chemical Society, Faraday Transactions* **1997,** *93* (19), 3445-3451.
271. Merline, D. J.; Vukusic, S.; Abdala, A. A., Melamine formaldehyde: curing studies and reaction mechanism. *Polymer Journal* **2013,** *45* (4), 413-419.
272. Gryn'ova, G.; Ingold, K. U.; Coote, M. L., New Insights into the Mechanism of Amine/Nitroxide Cycling during the Hindered Amine Light Stabilizer Inhibited Oxidative Degradation of Polymers. *Journal of the American Chemical Society* **2012,** *134* (31), 12979-12988.
273. Ecole polytechnique federale de Lausanne, I. o. C. S. a. E., NMR database.
274. Patton, T. C., *Alkyd Resin Technology: Formulating Techniques and Allied Calculations*. Interscience Publishers: 1962.

9 Thank you

First of all, I would like to express my appreciation to the members of the jury for accepting to evaluate my work. I would also like to thank my supervisor, Prof. Bruno Andrioletti, for giving the opportunity to participate in such an interesting and enjoyable project, for his guidance and for the confidence he had in my work throughout the three years. To Dr. Cathy Goux-Henry, I am also extremely grateful for her availability and kind council during these three years, and for fighting the battle to obtain appropriate equipment at my side.

I would also like to thank Alice Peyrard and Yuhang Ji for their contribution to the development of terephthalic acid esterification catalysts, and their enthusiasm for the project. Thank you also to current and previous members of the CASYEN group Laurent Copey, Raphaelle Kieffer, Marine Blain and Charles Guerin, particularly for many lunch breaks which are probably the main reason I now understand French. I am especially grateful to Zhan Zhang for making the last year so much more enjoyable than it would have been without her and our tea breaks.

Furthermore, I would like to thank the Beckers company for making the weathering tests possible, and especially Jean-Dominique Paoli, for teaching me how to make and analyse coatings, and for his contribution to the experiments, without which the weatherability analysis would not have been possible. Thank you also to Dr. James Maxted, Dr. Chris Lowe and Alan Butchart for their help and advice.I am equally grateful to Dr. Florence Avril, Nathalie Leclercq and the CRM group for letting me use their DMA machine and for helping me interpret the results. I would also like to thank Frank Cogordan and Hervé Ozeray for teaching me resin synthesis and being available for my questions especially in the beginning of the project. Thank you also to Stephane Poirier, Olivier Boyron and Manel Taam for their help and support with DSC and SEC analysis.

In general, I would like to express my gratitude to the members of the Sorago project, specifically Dr. Didier Verchere, Dr. Eric Chevet, Dr. Fanny Langevin, Dr. François Taconnet, Dr. Jérome Monbrun, Dr. Murielle Moneron, Dr. Vivien Henryon and Annie Leal Meza for their support during the project and for giving me the opportunity to be part of such an interesting collaboration.

Many people have also contributed to this PhD in non-scientific ways. I would like to first of all thank Cécile, Laurent, Stephanie, Sylvain, Jérome and Lucas, even though he doesn't know it yet, for showing me how awesome French people and the French way of life can be. Thank you also for accepting me with open arms into your group and for the beautiful memories of my time here that I will take with me where ever I go. For their moral and social support I would furthermore like to thank Nadja, Daniel, Michael, Eka, Horst, Sarah, Gwen, Wenjun, Florian and Erna.

Most importantly, I am grateful to Harald and Alexandra, for believing in me and helping me to believe in myself. I am grateful to Ina and Juliane, for being the best reason to get up on a Monday morning. And I am grateful to Niall. You are and will always be my number one Hermi crab. You all make my life so much richer and I could never have finished the PhD without you.